U.S. Department of Energy
Office of Freedom Car and Vehicle Technologies
1000 Independence Avenue S.W.
Washington, DC 20585-0121

FY 2003

Progress Report for Automotive Lightweighting Materials

Energy Efficiency and Renewable Energy
Office of Freedom Car and Vehicle Technologies
Advanced Materials Technologies

Edward Wall — Program Manager, OFCVT
Rogelio Sullivan — Materials Technologies Team Leader
Joseph Carpenter — Technology Area Development Manager

April 2004

This report was prepared as an account of work sponsored by an agency of the United States Government. Neither the United States government nor any agency thereof, nor any of their employees, makes any warranty, express or implied, or assumes any legal liability or responsibility for the accuracy, completeness, or usefulness of any information, apparatus, product, or process disclosed, or represents that its use would not infringe privately owned rights. Reference herein to any specific commercial product, process, or service by trade name, trademark, manufacturer, or otherwise, does not necessarily constitute or imply its endorsement, recommendation, or favoring by the United States Government or any agency thereof. The views and opinions of authors expressed herein do not necessarily state or reflect those of the United States Government or any agency thereof.

CONTENTS

1. INTRODUCTION 1

2. AUTOMOTIVE ALUMINUM R&D 7

A. Active Flexible Binder Control System for Robust Stamping 7
B. Warm Forming of Aluminum—Phase 2 17
C. Electromagnetic Forming of Aluminum Sheet 27
D. Aluminum Automotive Closure Panel Corrosion Test Program 35
E. Development of the Infrared Thermal Forming Process for Production of Aluminum Vehicle Components 41

3. ADVANCED MATERIALS DEVELOPMENT 49

A. Low-Cost Powder Metallurgy for Particle-Reinforced Titanium Automotive Components 49
B. Low-Cost Cast Aluminum Metal Matrix Composites 51
C. Structural Cast Magnesium Development 57
D. Magnesium Powertrain Cast Components 65
E. Low-Cost Titanium Evaluation 75
F. Structural Reliability of Lightweight Glazing Alternatives 85

4. POLYMER COMPOSITES R&D 93

A. Development of Manufacturing Methods for Fiber Preforms 93
B. Composite-Intensive Body Structure Development for Focal Project 3 101
C. High-Volume Processing of Composites 107
D. Thermoplastic Composite Sheet Manufacturing: Study of Thermoplastic Powder-Impregnated Composite Manufacturing Technology 113

5. LOW-COST CARBON FIBER 121

A. Low-Cost Carbon Fibers from Renewable Resources 121
B. Low-Cost Carbon Fiber Development Program 131
C. Microwave-Assisted Manufacturing of Carbon Fibers 141

6. RECYCLING 149

A. Recycling of Polymer Matrix Composites 149
B. Recycling Assessments and Planning 155

7. ENABLING TECHNOLOGIES 159

A. Durability of Carbon-Fiber Composites 159
B. Low-Cost Test Methods for Advanced Automotive Composite Materials; Creep Compression Fixture 167

C. Intermediate-Rate Crush Response of Crash Energy Management Structures 173
D. Composite Crash Energy Management 181
E. Energy Absorption in Adhesively Bonded Composites 189
F. Long-Life Electrodes for Resistance Spot Welding of Aluminum Sheet Alloys and Coated High-Strength Steel Sheet 195
G. Plasma Arc Welding of Lightweight Materials 209
H. Performance Evaluation and Durability Prediction of Dissimilar Material Hybrid Joints 219
I. Joining of Dissimilar Metals for Automotive Applications: From Process to Performance 229
J. Application of Thread-Forming Fasteners in Net-Shaped Holes 243
K. Nondestructive Evaluation Tools for Evaluation of Laser-Welded Metals 251
L. Inspection of Spot Welds Using an Ultrasonic Phased Array 259
M. Technical Cost Modeling 269
N. Springback Compensation in Advanced Sheet Forming Materials 273

8. HIGH-STRENGTH STEELS 279

A. Modeling of High-Strain-Rate Deformation of Steel Structures 279
B. Enhanced Forming Limits 289
C. High-Strength Steel Stamping Project 295
D. High-Strength Steel Joining Technologies Project 299
E. Sheet Steel Fatigue Characterization 307
F. Strain Rate Characterization 311
G. Advanced High-Strength Steel Tailor-Welded Blank Project 319
H. Tribology 323
I. Lightweight Front Structures 329

Appendix A. ACRONYMS AND ABBREVIATIONS 335

1. INTRODUCTION

Automotive Lightweighting Materials R&D

As a major component of the U.S. Department of Energy's (DOE's) Office of FreedomCAR and Vehicle Technologies Program (FCVT), Automotive Lightweighting Materials (ALM) focuses on the development and validation of advanced materials and manufacturing technologies to significantly reduce automotive vehicle body and chassis weight without compromising other attributes such as safety, performance, recyclability, and cost.

The specific goals of ALM are

1. By 2006, develop and validate advanced material technologies that will be needed to meet FCVT goals:
   - Enable significant reductions in the weight of body and chassis components and vehicle weight (50% reduction in weight of components and 40% reduction in vehicle weight relative to 1997 baseline five-passenger vehicle)
   - Exhibit performance, reliability, and safety characteristics comparable to those of conventional vehicle materials
   - Be cost-competitive, on a life-cycle basis, with costs of current materials
2. In support of the FreedomCAR goals, by 2010, develop and validate advanced material technologies that will
   - Enable reductions in the weight of body and chassis components by at least 60% and vehicle weight by 50% (relative to 1997 comparative vehicles)
   - Exhibit performance, reliability, safety, and recyclability characteristics comparable to those of conventional vehicle materials
   - Be cost-competitive, on a life-cycle basis, with costs of current materials

ALM is pursuing five areas of research: cost reduction, manufacturability, design data and test methodologies, joining, and recycling and repair. The single greatest barrier to use of lightweight materials is their high cost; therefore, priority is given to activities aimed at reducing costs through development of new materials, forming technologies, and manufacturing processes. Priority lightweighting materials include advanced high strength steels (AHSSs), aluminum, magnesium, titanium, and composites such as metal-matrix materials and glass- and carbon-fiber-reinforced thermosets and thermoplastics. The inclusion of AHSSs is an example that explains the use of the term "lightweighting," as opposed to just "lightweight," in order not to imply focus just on lower-density materials.

Collaboration and Cooperation

ALM collaborates and cooperates extensively in order to identify and select its research and development (R&D) activities and to leverage those activities with others. The primary interfaces have been and still are with the Big Three domestic automotive manufacturers, namely the FreedomCAR Materials Technical Team, the Automotive Composites Consortium (ACC), and the United States Automotive Materials Partnership (USAMP). This collaboration provides the means to determine critical needs, to identify technical barriers, and to select and prioritize projects. Other prominent partners include such organizations as the Aluminum Association, the American Iron and Steel Institute, the American Plastics Council, the Vehicle Recycling Partnership, the Society for the Advancement of Material and Process Engineering

(SAMPE), the International Magnesium Association, the International Titanium Association, and the Auto Parts Rebuilders Association. ALM also coordinates its R&D activities with entities of other U.S. and Canadian federal agencies. Interactions with the DOE Industrial Technologies Program (ITP), FCVT's High-Strength Weight Reduction (HSWR) Materials effort, and the Department of Natural Resources of Canada (NRCAN) are especially important by virtue of overlaps of interest in lightweight materials, and lightweighting

Project Selection and Stages

In cooperation with USAMP and the FreedomCAR Materials Technical Team, a procedure has been established to help facilitate the development of projects to help move high-risk leveraged research to targeted research projects that eventually migrate to the original equipment manufacturers (OEMs) as application engineering projects. Technology research projects are assigned to one of three phases: concept feasibility, technical feasibility, and demonstrated feasibility. Projects are guided to meet the requirements of each phase before they are allowed to move on to the next phase. The phases are defined as follows.

Concept Feasibility. Concept feasibility projects should contain a specific idea to address a need or to create something new. Projects are usually exploratory, small in monetary requirements, and short in duration. Projects should provide a yes/no answer to the value of the idea. All projects are required to have a detailed research plan, budget, and timing. These projects are typically less than $200,000 and have a duration of 1–2 years. They can be ended before proceeding to technical feasibility if there is a lack of technical progress or if the preliminary business case turns out to be unfavorable. Successful concept feasibility projects can develop into technical feasibility projects.

Technical Feasibility. Technical feasibility projects should continue research development for ideas with proven merit or potential. These projects should identify the key barriers in implementing the technology and focus on overcoming them. Technical feasibility projects should have well-defined OEM/industry supplier participation and pull. They are usually larger, longer-term projects than concept feasibility projects, with research investment typically in the 1 to 2 million dollar range and a length of 2–3 years. Technical feasibility projects can be ended before proceeding to demonstrated feasibility if there is a failure to overcome the key barriers to implementation or if the cost or business case does not develop as favorably as initially assessed.

Demonstrated Feasibility. Technology projects that need larger-scale validation may become demonstrated feasibility projects. Not all technical feasibility projects will need a demonstration or validation program. These projects are few in number, are much larger in scale, and may involve component or system fabrication and testing. Support and leverage from the OEMs/industry is a key requirement for these projects.

Stage progression for project selection.

Once selected, R&D projects are pursued through a variety of mechanisms, including cooperative research and development agreements (CRADAs), cooperative agreements, university grants, R&D subcontracts, and directed research. This flexibility allows the program to select the most appropriate partners to perform critical tasks. ALM efforts are conducted in partnership with automobile manufacturers, materials suppliers, national laboratories, universities, and other nonprofit technology organizations. These interactions provide a direct route for implementing newly developed materials and technologies. Laboratories include Argonne National Laboratory (ANL), Lawrence Berkeley National Laboratory (LBNL), Lawrence Livermore National Laboratory (LLNL), Los Alamos National Laboratory (LANL), Oak Ridge National Laboratory (ORNL), Pacific Northwest National Laboratory (PNNL), and Sandia National Laboratories (SNL). PNNL manages the Northwest Alliance for Transportation Technologies, drawing on expertise and developments in the Northwest. ANL oversees recycling efforts, and ORNL provides overall technical management, including management for the DOE cooperative agreement with USAMP.

Research areas and responsible organizations

Coordinated area	Organization
Production and fabrication of aluminum	The Aluminum Association, HSWR, ITP, Natural Resources of Canada (NRCAN)
Production and fabrication of magnesium	International Magnesium Association, NRCAN, HSWR
Recycling, reuse, repair of automotive parts and materials	Auto Parts Rebuilders Association, ITP, Vehicle Recycling Partnership, American Plastics Council
Fabrication of steel and cast iron	American Iron and Steel Institute, Auto/Steel Partnership, HSWR
Fundamental materials research	DOE Office of Energy Research, National Science Foundation
High-volume composite processing	Department of Commerce—National Institute of Standards and Technology's Advanced Technology Program
Materials research for defense applications	Department of Defense
Materials research for space applications	National Aeronautics and Space Administration
Crashworthiness	Department of Transportation
International vehicle material R&D	International Energy Association
Production and fabrication of titanium	International Titanium Association
Production and fabrication of composites	American Plastics Council

FY 2003 Accomplishments

Fiscal year (FY) 2003 was in the latter part of a second ALM phase that is running between about FY 2000 and FY 2004/5. In the first phase, between about FY 1994 and FY 2000, the ALM showed that

- Glass-fiber-reinforced polymer-matrix-composite (PMC) automotive structures could be manufactured at about the same cost as structures made of currently used steels, but they

could not meet the Partnership for a New Generation of Vehicles goal of 40% overall vehicle weight reduction.
- Acceptable automotive structures made of aluminum could achieve the Partnership for a New Generation of Vehicles weight reduction goal, but at a slight cost premium.

In its Ultralight Steel Autobody (ULSAB) program, which ran chronologically parallel to and independently of ALM's first phase, the steel industry showed that a body-in-white (BIW) could be produced using lower-strength HSSs that would be cost-neutral with (or cost even less than) current steels; but the BIW could not meet the PNGV weight reduction goal. The current second phase is focused on carbon-fiber-reinforced PMCs and magnesium and on manufacturing and recycling automotive components; some of the earlier efforts on aluminum and AHSSs are also being advanced. Some of the technologies developed by ALM and in the ULSAB are already on production vehicles and it is now apparent that aluminum, PMCs and the AHSSs are serious technical and economic contenders for eventually replacing some or all of the current steels when the market conditions are right.

To meet the goals set forth for the program, ALM is developing materials and material processing technologies; validating these technologies through fabrication and evaluation of representative, nonproprietary test components; and developing adequate design data to facilitate their beneficial application. The research is balanced between nearer-term objectives and longer-term, higher-risk research. As the technical barriers are removed, the technology is made available to industry. Because of the broad area of research and the limited resources, projects have been selected to overcome the most significant barriers within the technical areas that the materials community considers higher-risk but that, if successfully developed, would result in significant progress toward ALM's goals.

During 2003, the Test Machine for Automotive Crashworthiness (TMAC) for Intermediate Rate Crush Studies was installed and dedicated at the National Transportation Research Center (NTRC) in Knoxville, TN. This unique machine will permit, for the first time, progressive crush experiments at high-strain-force levels and constant intermediate velocities. The data obtained from the tests are critical for the development of predictive crash models. In addition, outside users may gain access to the machine as part of the NTRC User Facility Program. Activities in this task will focus on working with users to execute small to moderate-size projects. It is expected that the user will supply specimens and fixturing and participate with ORNL in test execution. Because of its complex nature, operation of the machine will be restricted to specifically trained ORNL personnel.

Metallic tubes tested in the TMAC demonstrate the conventional folding pattern associated with plastic hinge formation.

Short welding electrode life is a barrier to the implementation of new lightweight materials, including galvanized steels and aluminum alloys, in automotive applications. ORNL, in collaboration with Edison Welding Institute and the Big Three automotive companies, has developed a model to predict the deterioration of

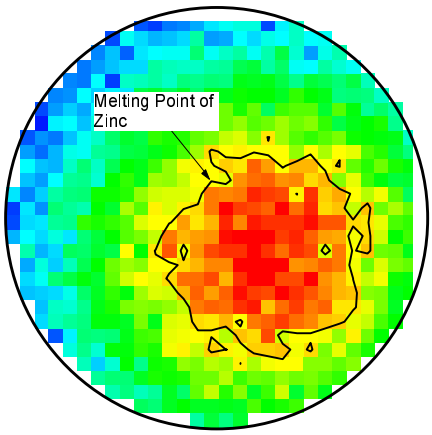

Schematic illustration of temperature distribution on the face of a copper resistance welding electrode. Regions in excess of the zinc melting point will experience accelerated degradation.

resistance-spot-welding electrodes through mechanical deformation and chemical attack. The model will allow industry to evaluate standard electrode materials, as well as new materials, under practical industrial conditions. The methodologies will lead to extended life of the existing electrodes and development of new long-life electrodes.

Significant advances were made in developing the technologies necessary to reduce the cost of carbon fiber to levels acceptable to industry, thereby enabling a cost-effective potential reduction in vehicle weight of 50%. Scientific development of the technologies to convert textile grade polyacrylonitrile (PAN) into carbon fiber was completed. This technology alone, if the engineering development phase is completed, can reduce the price of carbon fiber from $7 per pound to below $5 per pound. In addition, initial development of lignin-based precursors was concluded with a demonstration of a small composite made from carbon fibers produced from lignin. The next phase will consist of scaling up the technology to tow-size fiber bundles. This technology has the potential to reduce the carbon fiber price to $2.50–$3.50 per pound.

The automotive industry depends heavily on resistance spot welds in the manufacture of vehicles. However, the most common methods for monitoring spot welding integrity in manufacturing operations are pry checks and physical teardown, during which spot welds are pried apart and visually inspected or measured with calipers. For several obvious reasons, these methods do not provide the necessary information in a timely, cost-effective fashion. Lawrence Berkeley National Laboratory is working closely with automotive manufacturers to develop a nondestructive system that is sufficiently fast, accurate, robust, and cost-effective to be suitable for on-line inspection of spot welds in automotive components. Work to date demonstrates that characterization of spot welds is possible using ultrasonic phased-array technology. The advantages of the phased-array probes include the ability to perform high-resolution scans with increased detection capabilities, less sensitivity to probe placement, and the ability to inspect a wide array of welds with a single probe. The remaining research challenge is to refine the techniques so that they are suitable for large-scale manufacturing applications.

Significant progress was made in developing the technologies necessary to build a composite-intensive BIW. Initial molding trials were successfully completed for the inner and outer portions of the B-pillar portion of the design from the body side. This project addresses many challenging issues, including liquid molding of variable thickness sections (1.5–8.0 mm) at high volume fractions of reinforcing fibers. In addition to successfully molding several panels, researchers developed methods for joining the inner and outer sections of the panel. The bonded assemblies exhibited good dimensional control.

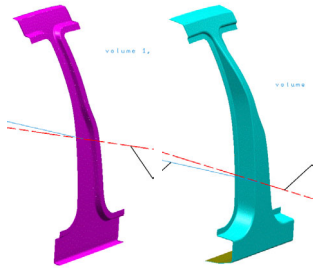

B-pillar test section, inner (left) and outer.

Future Direction

In FY 2002 and FY 2003, the Partnership for a New Generation of Vehicles was replaced by the FreedomCAR and Hydrogen Fuels Initiative, which has a 2012 goal of cost-neutral structures contributing to a fuel-cell-powered vehicle weighing 50% less than comparable vehicles of the mid-1990s. Thinking and planning on what will replace the current efforts in FY 2005 and beyond continues; but the process has already shown that a major role of lightweighting should be to reduce by as much as possible the required size of the fuel-cell propulsion system, which is expected to be heavier and more costly (at least initially) than the internal-combustion-engine propulsion system it replaces. Therefore, the focus of the second phase on materials with the greatest potential weight reductions turns out to be serendipitous for the third phase; thus technical-feasibility work is likely to continue along these lines. Base-technology, concept-feasibility, and demonstrated-feasibility work may also be considered.

Joseph A. Carpenter
Technology Area Development Manager
Office of FreedomCAR and Vehicle Technologies
Energy Efficiency and Renewable Energy

2. AUTOMOTIVE ALUMINUM R&D

A. Active Flexible Binder Control System for Robust Stamping

Project Leader: Tom Balun
Ford Motor Company
Vehicle Operations General Office, C290, 17000 Oakwood Blvd.
Dearborn, MI 48121
(313) 322-4951; fax: (313) 845-2647; e-mail: tbalun@ford.com

Project Administrator: Mahmoud Y. Demeri
FormSys Inc.
40180 Woodside Drive South
Northville, MI 48167
(734) 462-2742; fax: (734) 462-2742; e-mail: mdemeri@formsysinc.com

Technology Area Development Manager: Joseph Carpenter
(202) 586-1022; fax: (202) 586-1600; e-mail: joseph.carpenter@ee.doe.gov
Field Technical Manager: Philip S. Sklad
(865) 574-5069; fax: (865) 576-4963; e-mail: skladps@ornl.gov

---

Contractor: U.S. Automotive Materials Partnership
Contract No.: DE-FC05-95OR22910

Objective

- Develop and demonstrate, on an industrial scale, an optimized closed-loop flexible binder control system that can be installed in presses to improve the quality, reduce the variability, and maintain the accuracy of stampings made from aluminum alloys and ultra-high-strength and stainless steels. The system will also reduce the cost of developing and setting production tools.

Approach

- Conduct open-loop control demonstration of flexible binder technology.
- Develop methodology and guidelines for designing and building flexible binders.
- Develop computer simulation and process optimization capabilities for flexible binders.
- Develop a closed-loop flexible binder control system with appropriate sensors.
- Demonstrate closed-loop control of the flexible binder system on an industrial part.
- Evaluate technical and economic feasibility of flexible binder technology.

Accomplishments

- Conducted tests in a mechanical press to confirm the hydraulic reconfiguration necessary to obtain satisfactory closed-loop control in the hydraulic actuators of the Erie Binder Control Unit.

- Showed that the nonlinear control algorithm that has been validated in simulations and experimental tests provides effective closed-loop pressure control for constant and ramp step pressure profiles on a reconfigured cylinder from the Erie Unit.
- Began building a new tooling and binder control system at the University of Stuttgart (IFU). The tooling is based on a die design that included many features of automotive stampings (Hishida Die). The binder control system has special valves and controls for use in a mechanical press.
- Evaluated two methods, adaptive simulation (AS) and optimization (OPT), to predict feasible/optimum variable blank holder force (BHF) profiles for conical cup and rectangular pan drawing. Predictions were successfully verified by experimental results.
- Used AS and OPT methods to predict the variable BHF profiles for conical cups, rectangular pans, a tapered non-axisymmetric pan (Hishida part), and an S-rail. Experiments have also been conducted to verify the predicted optimum blank holder force profiles.
- Verified that variable BHF profiles improved the formability of conical cup drawing by about 9% compared with constant BHF profiles. Showed the importance of using results from AS as an initial guess for OPT in reducing the number of iterative simulation runs and computation time.
- Transferred the DOE-owned Binder Control Erie Unit to the U.S. Automotive Materials Partnership for use in the project.

Future Direction

- Retrofit the Erie Binder Control Unit with a digital dSPACE real-time controller system to achieve hydraulic pressure control on all 26 cylinders in a mechanical press environment. Use the unit to conduct trials on a General Motors (GM) liftgate to determine the benefits of using flexible binder control technology in sheet metal stamping.
- Set up and conduct trials on the new IFU flexible binder control system to determine the benefits of using flexible binder control systems in improving the part quality and consistency in automotive stampings.
- Conduct experiments to determine the critical sidewall wrinkle amplitude predicted by PAM-STAMP (i.e., amplitude of 1.21 mm). The critical sidewall wrinkle amplitude would greatly affect the prediction of variable BHF profiles in AS and OPT.
- Develop a method for determining initial guesses for BHF for use in predicting BHF profiles using AS or OPT. (The BHF profiles predicted by both AS and OPT depend on the initial guess for the BHF.)
- Evaluate the fatigue properties and determine stress concentrations and allowable stresses in flexible binders.

Introduction

Significant weight saving can be achieved by replacing parts made from mild steel with those made from lightweight materials (aluminum and magnesium alloys) and high specific strength materials (ultra-high-strength and stainless steels). Such materials are less formable than mild steel, and parts made from them lack dimensional control because of the significant amount of springback that they produce after forming.

Traditional stamping leaves no flexibility in the stamping process for using difficult-to-form materials and for responding to process variations (lubrication, material, die wear, blank placement) that can lead to stamping inconsistencies or even failure. It has been found that failure by wrinkling or tearing is

highly dependent on the magnitude and trajectory of the binder force. Recently, dynamic variation of the binder force during the forming stroke has been shown to affect formability, strain distribution, and springback. Optimal forming trajectories can be obtained under constant and variable binder force conditions, but there is no guarantee that process variables will remain constant during the stamping process. Specifying a binder force trajectory is not easy because the part shape changes during forming. Also, stresses in the part cannot be determined because the coefficient of friction is not a controllable quantity and it varies from location to location. Therefore, the forming process must be controlled, and a closed-loop system with an appropriate local control parameter (friction, draw-in) must be used to track a predetermined optimum control parameter trajectory.

Flexible binder control technology will be used in conjunction with innovative tool designs and closed-loop control to produce robust processes for stamping aluminum and high-strength-steel automotive panels. The focus of the project is on implementing binder and feedback process control in the stamping industry to increase the robustness of the forming process and improve the quality and consistency of stampings. This technology will use computer simulation and process optimization to predict optimum binder force trajectories that can be entered into programmable hydraulic cushions to control binder actions in mechanical and hydraulic presses.

Open-Loop Control Demonstration of Flexible Binder Control Technology

A two-path approach has been adopted for this task. The first one is to retrofit the existing Erie Unit with the appropriate real-time control system to achieve hydraulic pressure control in all 26 cylinders in a mechanical press environment. The unit will then be used as planned in conjunction with the liftgate tooling. The second path is to have IFU build a more robust and industrially oriented smaller unit.

Retrofit the Existing Erie Binder Control Unit

A single hydraulic cylinder test was conducted on a full-scale mechanical press at TDM in Warren, MI. The cylinder represented the force actuation component of a flexible binder unit. The objectives were to validate the mathematical models developed to represent the dynamics of the system and to validate the proposed nonlinear control strategy described in previous reports. A special hydraulic unit was constructed for this purpose. Figure 1 shows the single cylinder test setup in a mechanical press.

The tests showed that the mathematical model represented the dynamics of the system with good accuracy, and the closed-loop control results showed tracking performance within 10% of the commanded value in the critical operating range.

Figure 1. Single-cylinder test setup.

Tests were also conducted to confirm the hydraulic reconfiguration necessary to obtain satisfactory closed-loop pressure control in the hydraulic actuators of the Erie unit. The tests were conducted in a mechanical press with a peak ram speed of about 620 in./min.

The primary hydraulic problem observed was pressure spikes in the cylinder caused by the rod-side flow (upper and lower lines in Figure 2). Cylinder hydraulics were reconfigured to divert the rod-side flow directly to the tank. The reconfiguration eliminated the problem, and the pressure dynamics of the reconfigured system were close to the dynamics predicted by the mathematical model of the system. The nonlinear control algorithm that had been validated in previous simulations and tests was shown to provide effective closed-loop pressure control for constant and ramp-step pressure profiles on the reconfigured cylinder from the Erie unit.

Build a New Binder Control Unit

The new IFU unit will have only ten cylinders to accommodate a generic tool that captures the main features of industrial stampings. It will have state-of-the-art cylinders, valves, and controls and will accommodate three types of sensors for use in closed-loop control of the binder in a mechanical press environment. User interface with the system will be through a touch screen by which individual cylinder pressure may be selected. Figure 3 shows the IFU unit after the integration of a new valve block. The diagram gives the overall dimensions of the unit and shows the pyramidal pattern of the lower flexible binder and the lightweight structure of the upper binder.

Proportional valves are used to control pressure during the forming process. Initial pressure control tests on the valves showed good performance as indicated by a position control value of ±0.2 mm and a pressure change speed of 2000 bar/s.

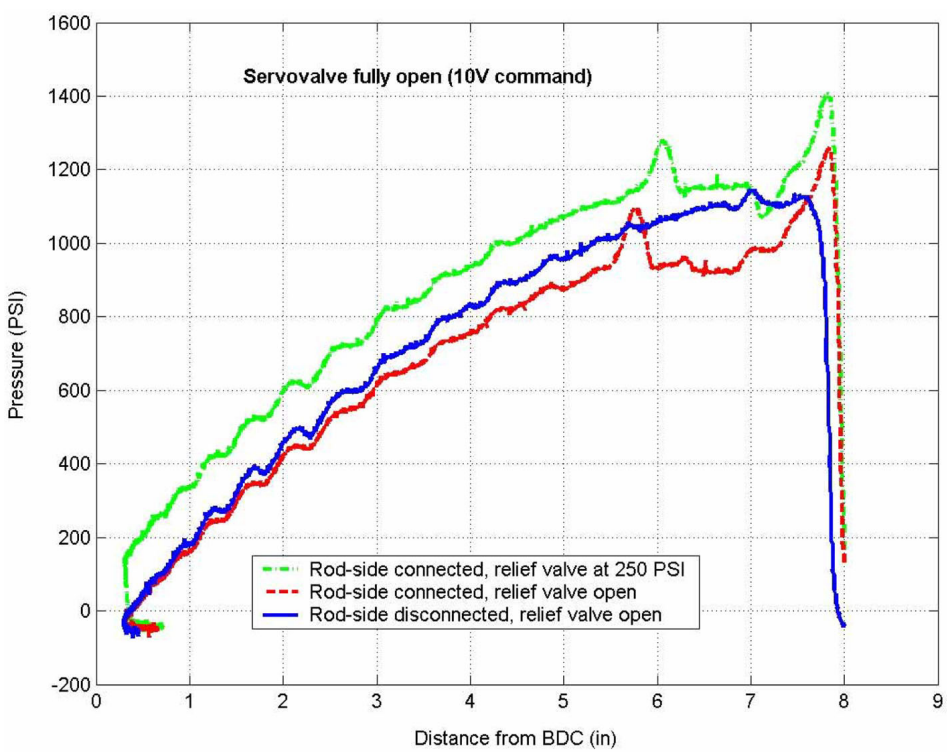

Figure 2. Open-loop pressure response showing pressure spikes due to rod-side flow.

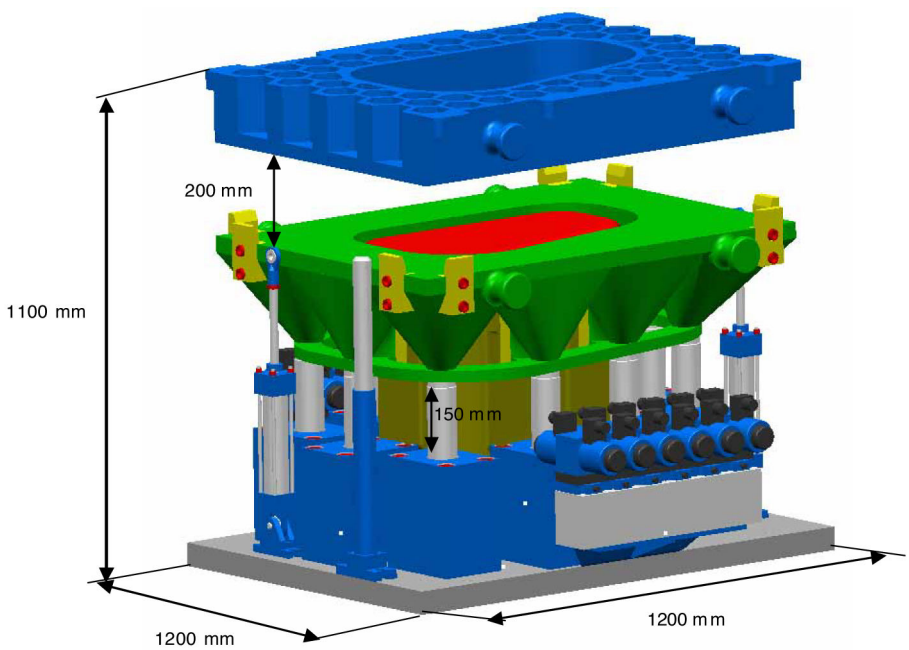

Figure 3. IFU binder control unit.

The closed-loop control system will automatically ensure that the desired binder forces are applied to the part by an electro-hydraulic actuation system during the forming process. The feedback control system will compensate for minor disturbances in the forming system caused by friction variation, inconsistent material properties, sheet thickness variation, die alignment problems, ram tilt, tool wear, blank placement, and press table deflection.

Feedback measurements will be used to modulate the binder force in real-time to keep optimum binder force trajectories for each cylinder in the control unit on target. The difference between the input signal and the output response will be fed to the controller to reduce the error and bring the output of the process to a desired value. One control strategy that can be used would have the following scenario:

- Finite-element method (FEM) produces an optimum material flow/friction trajectory.
- Sensor measures actual material flow/friction.
- Controller manipulates binder to achieve material flow/friction compliance.

In a closed-loop system, there is no need to determine in advance the binder forces needed to make a successful part because the system will modulate the forces based on measurements of the control parameter (material flow/friction).

IFU acquired the ten hydraulic cylinders, servo valves, and valve blocks; finished casting and manufacturing the punch, blank holder, die ring, and base plate for the Hishida die; acquired the sensors; and finished the development of the control system with the touch screen. The components are scheduled for assembly by the end of 2003, and unit testing is scheduled for the first quarter of 2004. The unit will be shipped to TDM in April for setup and testing in May–June of 2004.

Computer Simulation and Process Optimization Capabilities for Flexible Binders

BHF plays a key role in the sheet stamping process by applying a restraining force on sheet material to suppress wrinkles and eliminate splits. Many studies have pointed out that blank holder profiles that

can be varied in time and in space increase the formability of the stamping parts. Two methods for predicting feasible/optimum variable BHF profiles, AS and OPT were applied to determine the variable BHF profiles.

AS is used in this study to "optimize" the stamping process by automatically adjusting the process parameters (i.e., BHF profiles) within a single FE simulation. The strategy in AS is to monitor/identify defects (i.e., wrinkle and split) and promptly correct them by adjusting the relevant process parameters during the simulation run.

OPT involves minimizing the value of a certain objective (also called cost) function, subject to some constraints (thinning and wrinkling limits). The objective function depends on parameters called design variables. The problem is to determine the value of these design variables so that the objective function is a minimum.

This study used AS and OPT to predict the variable BHF profiles for conical cups, rectangular pans, a tapered non-axisymmetric pan (Hishida part), and an S-rail. Experiments were also conducted to verify the predicted optimum BHF profiles.

Conical Cups

Figure 4 shows a conical cup formed by optimum constant BHF of 26 tons (255 kN). The formed cup showed visible necking at a forming depth of 43 mm. Figure 5 shows a conical cup formed by optimum variable

Figure 4. Cup formed with optimum constant BHF. The cup showed visible necking at 43 mm.

Figure 5. Cup formed with optimum variable BHF. There is no visible necking at 47 mm.

BHF. The formed cup did not have any visible necking at a forming depth of 47 mm. This proves that optimum variable BHF profiles improve the formability of drawn cups compared with those drawn by optimum constant BHF profiles.

Rectangular Pans from DP600

AS and OPT were also used to predict the optimum BHF profiles for rectangular pan drawing. Although the BHF profiles predicted by AS and OPT for pan drawing of 50- and 90-mm depths are different, they form good parts with almost identical thinning distributions. The results lead to the conclusion that the rectangular pan allows a large forming window. Considering the computation time required, in this case study, the application of AS to determine an optimum BHF profile seems to be more efficient than OPT.

AS requires only one simulation run to result in a feasible variable BHF profile; OPT needs many more iterative simulation runs to result in an optimum variable BHF profile. In this study, the BHF profile from AS was applied as an initial guess for OPT. The result was a reduced number of iterative simulation runs, which decreased the total computation time.

In view of the simulation results, these conclusions can be stated:

- AS and OPT successfully predicted feasible/optimum variable BHF profiles

for rectangular pan drawing. In the simulation, improvement was obtained on overall thinning distribution of the part formed with the predicted variable BHF profile compared with a part formed with a constant BHF (408 kN).

- Feasible BHF profiles predicted by AS can be used as initial guesses for OPT. This reduces the number of iterative simulation runs and decreases total computation time. The combination of AS and OPT can lead to prediction of optimum BHF profiles for general stamping parts with fewer simulation runs than required using OPT alone.

Non-Axisymmetric Pans from AA5182-O and AA6111-T4

AS and OPT codes were updated to handle the IFU Hishida geometry for detecting sidewall and flange wrinkle. Constant and variable BHF profiles for the part were predicted using AS and OPT codes coupled with FE modeling. Materials used were 1.15-mm AA5182-O and 1.0-mm AA6111-T4 aluminum sheets. The blank shape was selected based on experiments conducted at IFU. Figure 6 shows the dimensions of the blank and locations for monitoring sidewall wrinkles.

The FE model used for simulating the IFU-Hishida die drawing process with AA5182-O material is shown in Figure 7. The blank was modeled using free mesh with 4-node shell elements. The flow stress of the sheet material was obtained using tensile test and then curve-fitted to power law. ALCAN conducted the tensile tests for GM, which provided the material properties of the material. Hill's 1990 yield criterion was used in the FE simulations. The anisotropy constants in Hill's 1990 yield criterion were obtained using tensile test data and biaxial test data from literature. A coulomb friction coefficient of 0.08 was used at all the tool-sheet interfaces.

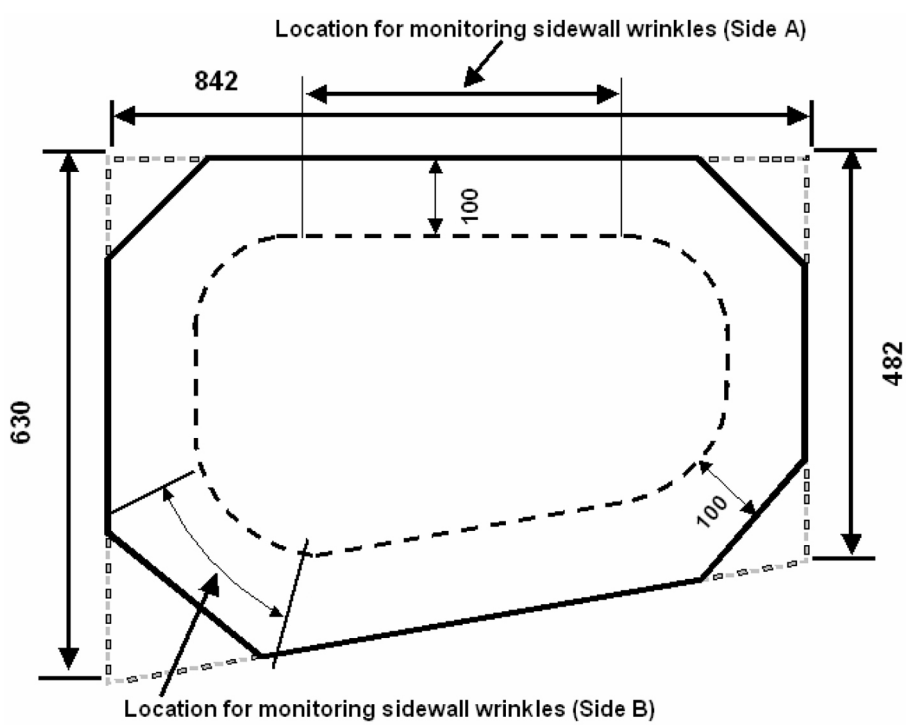

Figure 6. Dimensions of the blank used in the FE simulation and locations for monitoring sidewall wrinkles.

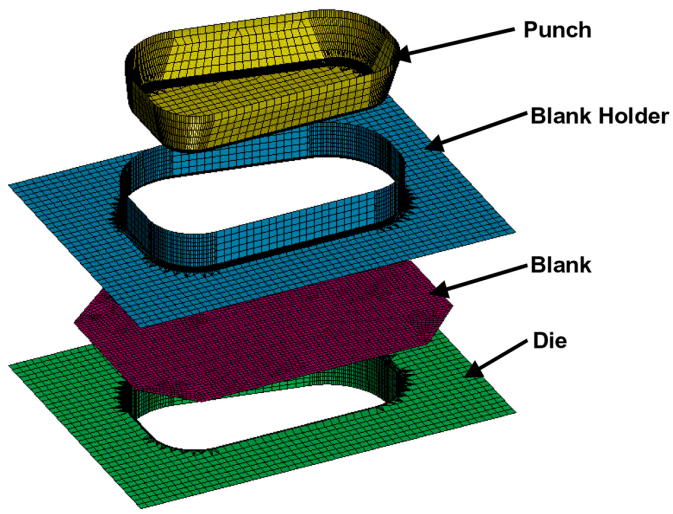

Figure 7. Schematic of the FE model used for IFU-Hishida die drawing simulations.

During FE simulation of the process, the BHF was varied using AS and OPT strategies to predict time varying and/or constant BHF profiles to form a given part with a desired quality (thinning and wrinkling). Currently, thinning and wrinkling are the only parameters used to monitor part quality. Wrinkling in the FE simulation is detected both in the flange and in the sidewalls. It was observed that the wrinkle amplitudes were more sensitive to BHF at the long sides of the pan than at the short sides and corners.

Thinning distributions along two sections were compared for the three different BHF profiles predicted by FE simulations: constant BHF obtained from OPT, variable BHF obtained from OPT, and variable BHF obtained from AS.

A comparison of thinning distribution obtained for three different BHFs along one section is shown in Figure 8. Results show that using variable BHF profiles results in a slight improvement in thickness distribution compared with constant BHF. The improvement could be due to the insensitivity

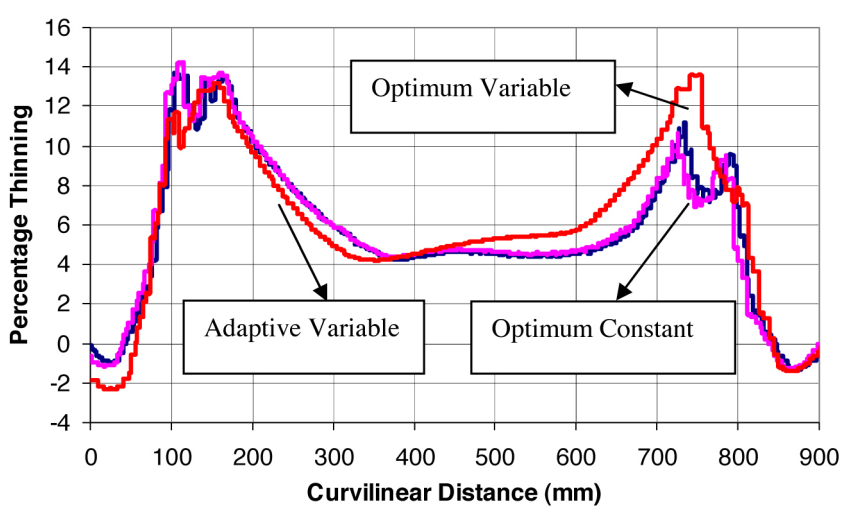

Figure 8. Comparison of thinning distribution predicted by FE simulation along a section for three different BHF profiles obtained from OPT and AS for AA5182-O.

of thickness variation to the time-varying BHF for this tapered pan geometry drawn to a height of 60 mm. Forming pans to a greater depth (greater than 60 mm) may show improvement in formability with the use of variable BHF.

Major conclusions drawn from the IFU-Hishida part study are these:

- Optimum constant and variable BHF were predicted using AS and OPT.
- Thinning decreased from 14.6% to 13.5% for variable BHF from AS compared with optimum constant for material AA5182-O.
- Thinning decreased from 13.5% to 12.0% for variable BHF from AS compared with optimum constant for material AA6111-T4.
- Optimum variable BHF did not improve formability for both the materials. More control points are needed in the B-spline to describe complex-shape BHF trajectories with compromise on simulation time. A variable BHF profile predicted by AS could be used to decide the number of control points and initial guess for OPT.
- Adaptive variable BHF resulted in slightly more uniform thickness distribution compared with optimum constant BHF.
- In this geometry, the effect of variable BHF (variations in stroke) was not significant, because little reduction in thinning was observed using variable BHF compared with constant.

S-Rail

Springback is a major problem in the stamping industry, especially in high-strength and/or low-modulus materials such as aluminum alloys and high-strength steels. Locking the material during the final stages of the forming cycle has been shown to significantly reduce springback. Therefore, there is a need to determine optimal BHF profiles for stamping sheet metal parts.

AS and OPT techniques coupled with the FE method were applied to predict constant and time-varying BHF profiles for the S-rail to minimize springback in the part. The material used was 0.92-mm-thick AA6111-T4. The FE model used for simulating the S-rail part is shown in Figure 9. The blank was modeled using free mesh with 4-node shell elements. Material properties of the sheet material AA6111-T4 were obtained using tensile tests from GM. During FE simulation of the process, the BHF was varied using AS and OPT strategies to

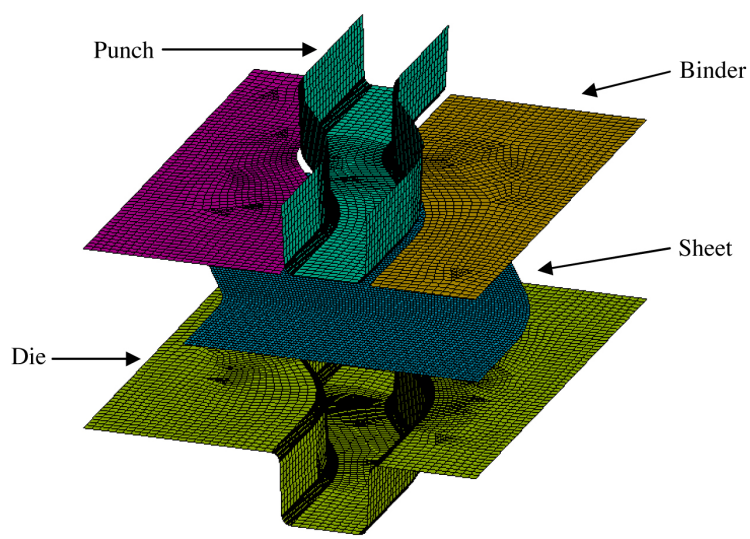

Figure 9. Schematic of the FE model used for the S-rail part simulations.

predict time-varying and/or constant BHF profiles to form parts with the desired quality (thinning and wrinkling) and minimum springback.

In this study, variable and constant BHF were predicted for the S-rail part for two cases:

- minimize thinning and avoid wrinkling without considering springback, and
- minimize springback and thinning and avoid wrinkling.

Wrinkling in the FE simulation was detected in both the flange and the side walls of the S-rail. Figure 10 shows the location of side wall wrinkles in the part simulation.

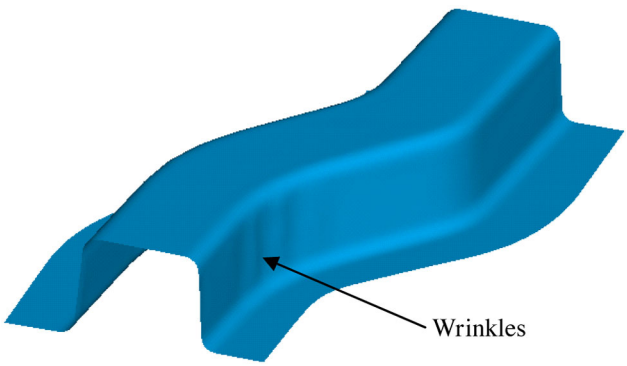

Figure 10. Location for side wall wrinkle monitoring in the S-rail part.

Results show that using variable BHF from AS resulted in a decrease in maximum thinning from 34% to 17% compared with the constant optimum BHF, although variable BHF from OPT resulted in a decrease in maximum thinning from 34% to 20% compared with constant BHF.

Major conclusions from the S-rail study are these:

- Optimum constant and variable BHF were predicted using OPT and AS with and without springback control.
- Springback in the part during forming was quantified using the ratio of the internal moment to internal force (ν) based on the mechanics of springback and results from past research. This ratio was used in OPT and AS as an index for springback in the part.
- The 37-mm-deep S-rail part could not be formed without wrinkling and excessive thinning using constant and variable BHF profiles from AS and OPT. Beyond a depth of 32 mm, maximum thinning in the part increased rapidly and would result in failure. Therefore, the S-rail part of 30-mm depth was considered for further analysis to predict constant and variable BHF.
- Thinning decreased from 34% to 17% for variable BHF from AS without springback control compared with optimum constant without springback control for a 30-mm-deep S-rail part.
- Thinning decreased from 34% to 20% for optimum variable BHF from AS without springback control compared with optimum constant without springback control for a 30-mm-deep S-rail part.
- Two OPT methodologies were implemented to predict variable BHFs that reduce springback in the part. For the S-rail geometry, variable BHF predicted by both the methods could not improve springback in the part because thinning in the part reached a maximum allowable limit of 20% even without springback control.
- Springback control based on post-stretching was implemented using AS. Post-stretching was initiated when the amount of stroke available (λ) was equal to one-half of the die corner radius (2.5 mm). Variable BHF with springback control predicted by AS resulted in a 50% reduction in springback compared with variable BHF without springback control.
- Variable BHF from AS performed better than OPT because, in OPT, the shape of the curve is restricted by number control points used to generate the B-spline that represents the BHF. More control points in the B-spline would increase the complexity of the curve at the expense of computing time.

B. Warm Forming of Aluminum—Phase 2

Project Leader: Suresh Rama
DaimlerChrysler Corporation
2730 Research Drive
CIMS 463-00-00
Rochester Hills, MI 48309
(248) 838-5356; fax: (248) 838-5338; e-mail: scr4@daimlerchrysler.com

Project Administrator: Constance J. S. Philips
National Center for Manufacturing Sciences
3025 Boardwalk
Ann Arbor, MI 48108-3266
(734) 995-7051; fax: (734) 995-1150; e-mail: conniep@ncms.org

Technology Area Development Manager: Joseph Carpenter
(202) 586-1022; fax: (202) 586-1600; e-mail: joseph.carpenter@ee.doe.gov
Field Technical Manager: Philip S. Sklad
(865) 574-5069; fax: (865) 576-4963; e-mail: skladps@ornl.gov

---

Contractor: U.S. Automotive Materials Partnership
Contract No.: DE-FC05-02OR22910

Objective

- Develop and demonstrate a production process for the warm forming (WF) of aluminum for automotive body structures, and measure the economic feasibility of the WF process in a mass production environment.

Approach

- Establish a warm-forming process in a laboratory environment with the application of new processes on a variety of aluminum sheet alloys. Balance alloy and lubricant development with continuing evaluation of commercial alloys, along with process modeling, design, and demonstration.
- Develop full-size demonstration of WF process and run tests in a production environment. Integrate a blank preheater, blank transfer mechanism, lubricant application system, WF press with a modified thermal profile controller, and lubricant removal step into production trials. Conduct production feasibility tests of the WF process at standard rates for current forming processes.
- Create a technical cost model that can generate cost comparisons between a warm-formed aluminum door inner and a same or similar door inner manufactured using conventional forming processes in steel and aluminum.
- Improve the formability of aluminum through development of enabling process advancements:
  - Establish the degree of improvement in formability of production-grade, commercial aluminum alloys.

  - Develop a cleanable lubricant suitable for use in a WF process.
  - Optimize the temperature distribution of the die.
  - Evaluate rapid heating systems for blanks.
  - Optimize the process design and layout.
  - Apply the results of the cost model to optimize process design.
- Demonstrate the manufacturing feasibility and economic feasibility for a new mass production process such as the WF process.
- Define the process flow.
- Develop and apply a technical cost model that allows comparison of a product made in the WF process with a comparable component fabricated from aluminum/steel with deep draw using current processes.

Accomplishments

- Completed the technical cost model and used model in current research work.
- Made progress toward identification of suitable aluminum material from candidate commercial alloys in laboratory-based WF process studies.
- Studied custom-formulated 5000 series aluminum alloys in laboratory formability tests in 2002 with inconclusive results.
- Used technical cost model data to show that material cost had highest impact on process costs. Therefore in 2003, formability studies were redirected to focus on commercially available 5000 series alloys to avoid the cost impact of expensive additives in custom alloys. WF process feasibility will be directly affected by the ability to use commercially available alloys.
- Made positive progress toward identification of a suitable lubricant through extensive laboratory-based studies.
- Made positive progress in the thermal analysis of the die through a heat transfer analysis of the WF dies to be used in the WF process scale-up. Objectives of this analysis include:
  - determine optimal ("good") heater layout, spacing, and size to achieve optimum temperature distribution over the die surface,
  - determine consequent die distortion effect,
  - develop guidelines for heating scheme for WF tooling for practical use in mass production, and
  - identify process parameters through this model including the time necessary for the top insert surface to reach an average temperature suitable for WF; heat expansion of the insert top surface in width, height, and thickness; and the temperature/distortion change after heating step is complete.

Future Direction

- Finish thermal studies and thermal models.
- Finish lubricant studies, and select the lubricant formulation for use in production demonstration.

- Investigate continuous cast aluminum materials for WF, compare to 5XXX series aluminum performance, and select an alloy for use in production demonstration.
- Decide on blank heating system to be used in production demonstration.
- Set up at contractor's site for production scale-up and demonstration.
- Employ the technical cost model to compare costs of WF process and alternative processes.

Introduction

In a quest to improve fuel economy, the automobile manufacturers have been seriously looking at aluminum to lightweight their vehicles. Because aluminum costs more than steel and because most automotive-grade aluminum alloys have limited formability, a cost penalty is associated with their use. The challenges include

- transferring steel-based designs for aluminum due to reduced formability,
- sliver management in trimming aluminum panels,
- difficulty in forming sharp-edge contours,
- hard-to-achieve deeper draws, and
- appearance problems in most 5000-series aluminum panels.

Warm Forming of Aluminum, Phase 2, was initiated after the initial technical feasibility of forming complex shapes at elevated temperatures was demonstrated. It is a 4-year development and demonstration program to establish the "production" feasibility of WF aluminum alloy blanks into automotive panels, such as shown in Figure 1, and to fully demonstrate a WF process for cost-effectively manufacturing aluminum automotive panels with deep draw.

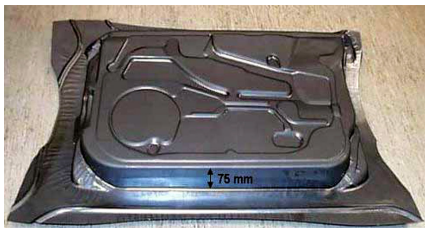

Figure 1. Dodge Neon door inner representing body panel with deep draw requirements.

The main purpose of this project is to focus on the following objectives:

- Develop and demonstrate a WF process including the materials, equipment, and heating processes that can cost-effectively expand the forming limits of aluminum sheet.
- Develop a technical cost model for the WF process that will help assess the economic feasibility of the warm forming process specific to component design.

The major enabling process improvements to make WF a production-capable process are the following:

- use of a high-temperature lubricant that has good lubricity at WF conditions and also is easy to wash off for automotive painting,
- managing temperature distribution on the die surface during the forming operation,
- effective preheating methods for blanks, and
- any improvement in alloy chemistry for improving the sheet fabrication at material supplier to reduce costs.

Phase 2 Detail

- ***Technical cost model:*** Camanoe Associates developed a very detailed cost model based on the process sequence agreed on by the project team. The sequence was established based on several discussions and data obtained from various testing from prior years. It was found that the

material cost accounted for more than 70% of the cost of the product, and thus a new direction in alloy development/selection was identified.

- ***Alloy selection:*** In 2003, this task, which was assigned to the University of Michigan, focused on improving the sheet fabrication process for WF-capable aluminum sheet at reduced costs. Because material costs are the largest cost factor of a warm-formed part cost, the efforts at the University of Michigan were redirected toward analyzing the warm formability of commercially available alloys.
- ***Lubricant selection***: The performance of various lubricants under different temperatures was evaluated through two major test methods: Tribotester at General Motors and lab-scale WF of pans at the University of Michigan. Lubricant formulations and cleanability evaluations were conducted at Fuchs laboratories.
- ***Die thermal analyses:*** University of Michigan's S. Wu Manufacturing Center is performing detailed finite-element analyses (FEAs) for investigating the temperature profiles on the stamping die and blanks for Neon door inners. Data about the geometry and heater locations on the die were obtained from computer-aided design (CAD) models of the die provided by Sekely Industries.
- ***Blank heating:*** Preliminary evaluation of infrared (IR) heating for heating blanks was investigated at the University of Michigan. The results will assist the team in determining if IR or another heating method is the best preheat method for large volume production.
- ***Alloy fabrication:*** With the focus on the investigation of warm formability of commercially available aluminum alloys, no additional custom alloys will be specified for fabrication by Pechiney Rolled Products. Pechiney continues to supply 5000 series aluminum sheet for these formability studies.
- ***Full-scale process demonstration:*** Once the individual component processes are validated at laboratory level for technical and economic feasibility, a full-scale WF demonstration using the Dodge Neon door inner stamping dies will be conducted. The work is currently planned to be conducted at Sekely Industries in 2004, press time and other scale-up variables considered. Additional suppliers may be considered for participation in the system integration and process demonstration if their resources would allow a full-scale process demonstration inclusive of a material flow process.
- ***Postprocess inspection and material analyses:*** Coupons from warm-formed parts will be cut out, and the materials properties will be evaluated by one of the original equipment manufacturers (OEMs). The typical properties to be evaluated will include strength, distortion, and corrosion.

Phase 2 Accomplishments

Technical cost model analyses—At the start of the year, the WF Project core team, consisting of the representatives from DaimlerChrysler, Ford, and GM, reviewed the results of the technical cost model and redirected the course of research and development for 2003. The technical cost model was developed by Camanoe Associates. One of the main components of the cost model is the process sequence. The project team agreed on a process sequence that would be suited for a high-volume production WF process, including the process steps, blank lubrication, blank preheating, warm forming, and cleaning. Using strawman example rates for labor, maintenance, and overheads, the technical cost model was shown to be able to generate a comprehensive cost breakdown for a Dodge Neon door inner panel if it were to be mass produced (250,000/year) using the identified WF process sequence.

The material cost accounts for more than 70% of the final product cost of the Dodge Neon door inner panel. Minimizing material cost in the WF process became critical. The original direction of developing new WF alloys by modifying the alloy chemistry of certain 5000 series alloys was only contributing more expense to the material cost component. Therefore, the core team decided to focus on commercially available 5000 series alloys, specifically 5182 and 5754 at oxygen and hydrogen tempers. It is desirable to add continuous cast sheet products to the alloy study if suitable material can be located at an economical price. Pechiney Rolled Products provided the project with the necessary amounts of 5182 and 5754 in both oxygen and hydrogen tempers.

Blank preheating and IR heater studies—The laboratory IR heater system was delivered to University of Michigan and integrated to work with the lab-scale WF press. The setup of the IR heater system included a control panel that later was modified to provide direct adjustable control over the conveyer belt speed. At this time, the distance between the heating lamps and the sheet is determined to be 5 in. since the entire system is 66 cm long, the heat loss from the inlet and exit of the heater is significant. Insulation at the entry and exit was added to contain the heat within the furnace so that the IR lamps can effectively heat the sheet (blank). Several tests were performed to study the effect of IR heat on WF process and microstructure.

Trials with the IR heater showed a relatively slow heat-up time. This is shown in Figure 2 where the time to heat the sheet to 300°C was approximately 3 min at an oven temperature of 400°C. To achieve production-level process times, a very long oven would be required for the blanks to reach the target temperature prior to reaching the press. This type of heater system would both be impractical and not cost-effective for the forming process.

In an effort to decrease heating time, several experiments were conducted at

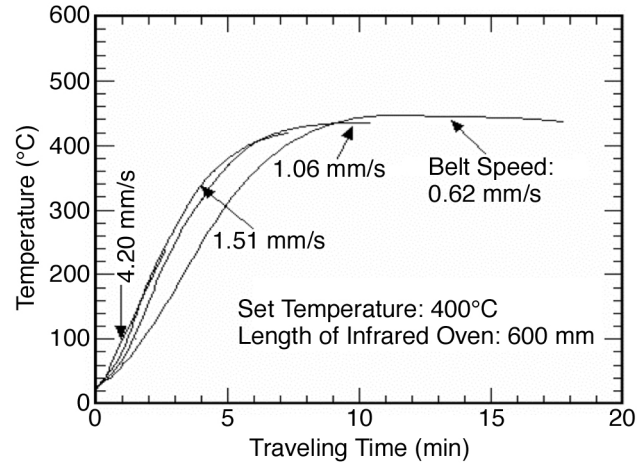

Figure 2. Sheet temperature as a function of time for three different belt speeds at an oven set temperature of 400°C.

higher set temperatures. The time vs temperature plots for heating trials at 800°C and 900°C are shown in Figures 3 and 4, respectively. Time to reach 300°C for these trials was closer to 35 and 25 s for the two oven set temperatures, respectively. This represents a significant improvement over the previous results at a set temperature of 400°C.

Photomicrographs of the material after heating to certain times indicate the materials become fully recrystallized at 76 and 50 s for the two set temperatures (see Figures 3 and 4). Recrystallization prior to forming is required to attain maximum formability. Material cost savings can be attained by using "hardened sheets" such as these instead of having the sheet batch-annealed at the aluminum manufacturing facility.

While these trials demonstrated that an IR oven is capable of supplying ample heating for the WF process, it does not appear to be the best solution. Significant overheating appears to be necessary to achieve production feasible heat-up times. Additionally, overheating presents the risk of melting the sheet if the conveyer system were to stop for any period of time. Additionally, highly emissive aluminum requires significant energy from the IR heater to reach target temperatures. For these reasons, the team decided to use a conduction heater, which is

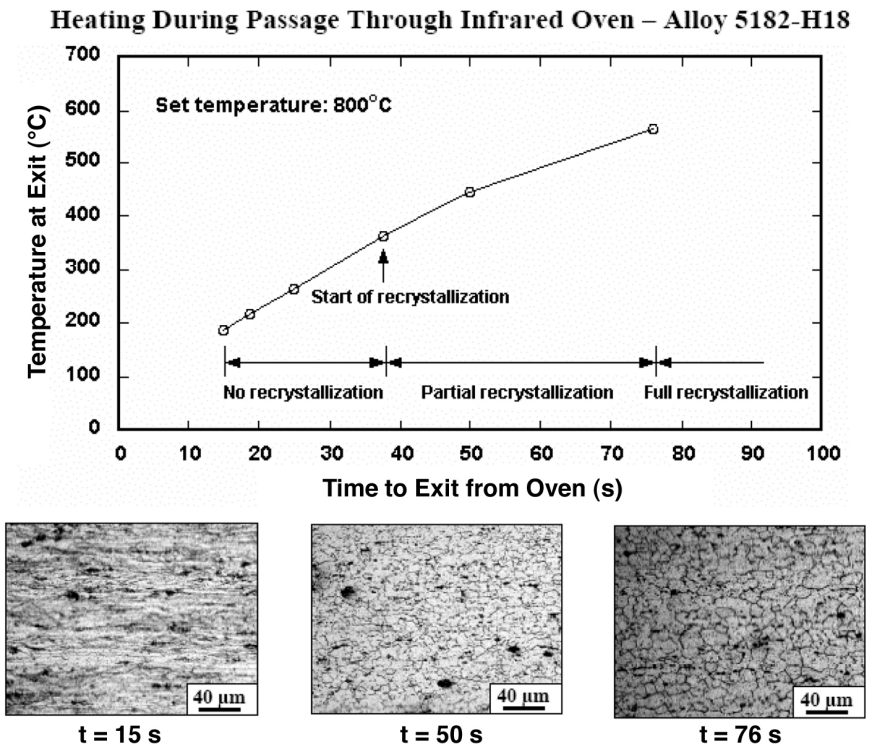

Figure 3. Sheet temperature as a function of time at an oven set temperature of 800°C. Note from the micrographs that full recrystallization occurs at approximately 76 s of heating time.

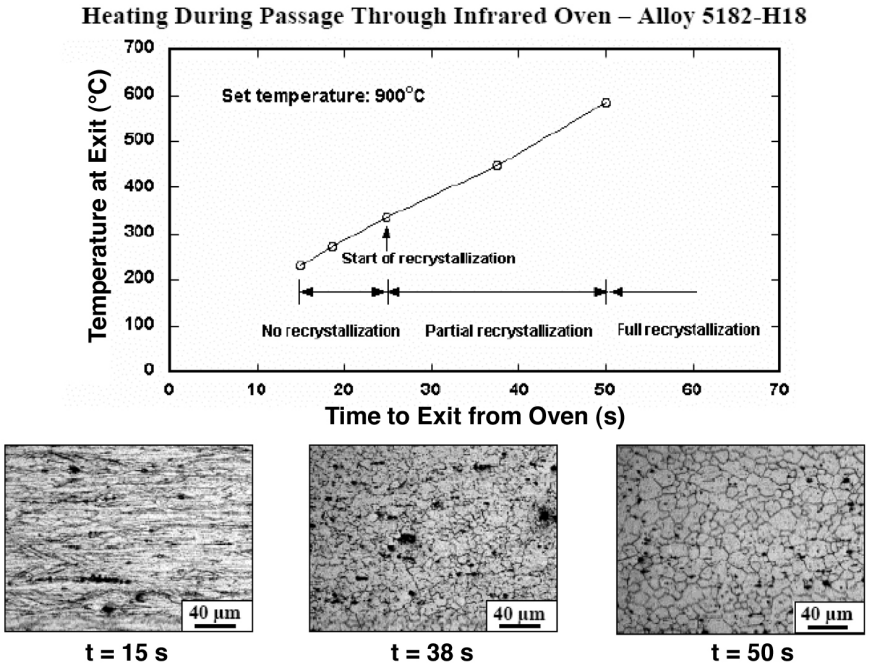

Figure 4. Sheet temperature as a function of time at an oven set temperature of 900°C. Note from the micrographs that full recrystallization occurs at approximately 50 s of heating time.

thought to be a more cost-effective and robust method of heating aluminum sheet, in the scale-up of the WF process. Preliminary tests indicate that forming temperatures can be reached within seconds with this type of heater.

Lubrication studies—Lubrication formulations and their effect on the formability of aluminum under various temperatures were studied by Fuchs Lubricants and GM. GM and Fuchs previously completed formability tests using Fuchs LN1184 and LN1169 lubricants at 215°C, 260°C, and 315°C, examining the lubricant layer after forming, drawing behavior due to lubricant/temperature effectiveness, and length of the wear scar and compared these test results with results of dry forming. Findings confirmed that cup depths are a function of temperature and lubricant. Higher formability is found with some lubricants at certain temperatures, but cleanability can be worsened at increased temperatures. See Figure 5 for a visual of the cleanability issues posed by a lubricant.

In 2003 Fuchs performed room temperature screening of several new candidate lubricants, and GM performed high-temperature testing. Cleanability is still a major issue in lubricant selection. The experimental setup at the University of Michigan used for the studies conducted by GM is shown in Figure 6.

Figure 5. Lubricant cleanability issues postforming at varying temperatures readily apparent on these sample parts.

Figure 6. Punch and die setup at University of Michigan for lubricant studies conducted by GM.

Lubricant work then focused on trying to improve other previously developed lubricants produced by Fuchs. These included the following:

- SJA216 Base—thermally stable soap with a wetting agent,
- SJA216 BN—SJA216 Base + BN as solid lubricant, and
- SJA216 LN—Previously tested LN1184 + BN as solid lube.

These lubricants were evaluated using the following methods:

- pin on disc friction test at room temperature at Fuchs,
- cleanability testing after thermal exposure at Fuchs,
- ring on plate tribotester at GM under two temperature conditions, 250°C and 350°C, and
- pan die forming at University of Michigan at three preheat temperatures, 215°C, 260°C, and 315°C.

Two important results from this work follow.

The results shown in Figure 7 demonstrate that for the base lubricant, the coefficient of friction decreased with increasing temperature. More importantly, the addition of BN to the base lubricant increased the coefficient of friction. The BN additions were made anticipating a reduction in coefficient of friction and improved elevated temperature stability. Neither effect was observed in the present study. This suggests that different additions such as graphite and molybdenum disulfide might be better for this application.

The pan die forming results are summarized in Figure 8. These results again show that that the addition of BN to the base lubricant decreases the effectiveness of the lubricant, in this case by decreasing the forming depth achievable at each temperature. There appears to be an optimum forming temperature around 250°C; however, the heating time and forming time (2–3 min) were longer than would be expected for a production system. This difference could lead to breakdown of the lubricant prior to forming and thus give a lower pan depth.

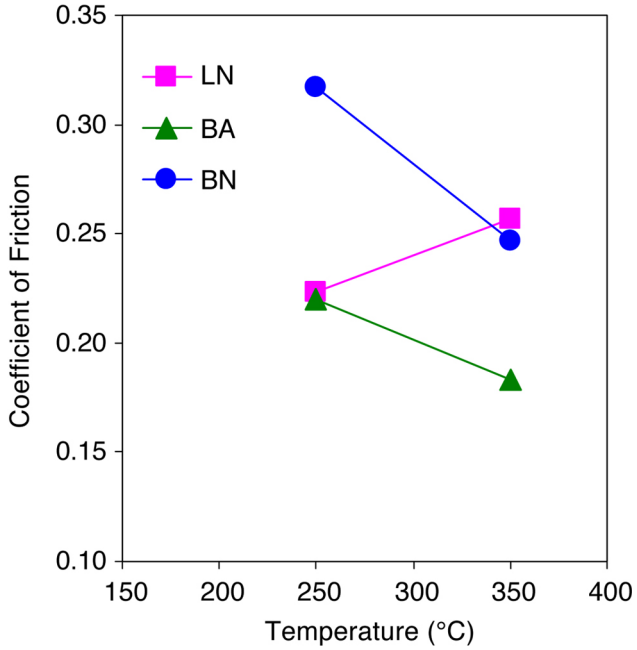

Figure 7. The effect of temperature on coefficient of friction during ring on plate tribotesting in three different lubricants. Plate material AA5083.

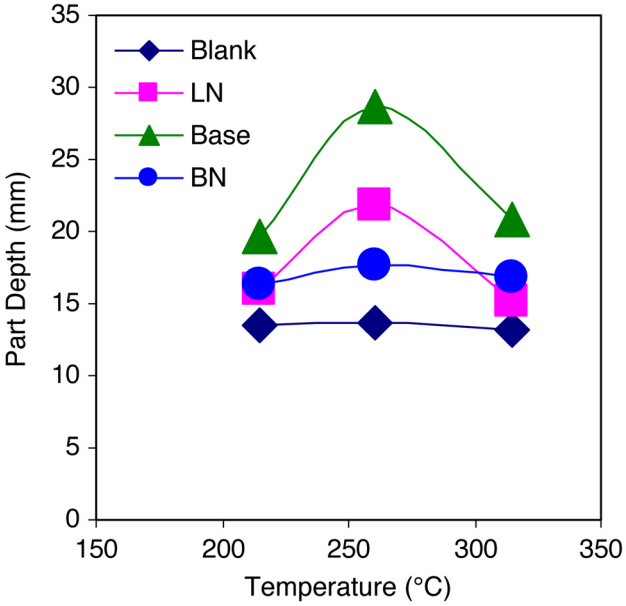

Figure 8. The effect of temperature on the pan die forming depth for a variety of lubricant systems.

This inconsistency in preheat and forming time can also explain why the friction coefficient data in Figure 7 showed the coefficient of friction decrease with increasing temperature; the data in Figure 8 show a reduction in formability with increasing temperature.

In 2004 lubricant studies will continue to evaluate alternate additives to the Fuchs base material, rapid preheating with the IR furnace to better control the thermal cycle in the process, valuation of the lubricants using a novel friction testing system at Ford, and evaluation of selected lubricant(s) on large-scale forming trials.

Die and blank thermal analyses—Positive progress has been made in the thermal analysis of the WF dies through a heat transfer analysis of the dies to be used in the WF process scale-up. A preliminary FEA model to study the heat-up and cooling of formed parts and die components was defined by S. M. Wu Manufacturing Research Center, University of Michigan. The FEA model was then used to examine the effects of air vs water cooling on simple deep draw parts, the loss of temperature during sheet material transfer from preheater to die, and heat

distortion effects on die and insert surfaces over time. Such information will be considered in the final process layout design.

Six parts (insert, low holder, blank, upper holder, punch, and base) make up this complex die-punch process. Heat fluctuation values for the die upper holder and insert were determined by a preliminary die heat transfer study. As part of this study, a three-dimensional sectional analysis of the die was done, and a simulation of the full stamping process was made.

Figure 9 graphically depicts the simulated process as well as the components of the die tooling and the thermal profiles of the tooling during the different WF process steps.

Blank distortion due to die thermal variances was also studied. The applied heat flux on the die during the heating stage caused die expansion. This expansion irregularity on the die surface was relatively small, and further expansion of the die during processes after heating was negligible. The formed blank continuously shrank due to spring-back for 27 h (see Figure 10).

Technical cost model completion— Iterative versions of the strawman cost model were reviewed during this report period. Various views of product and process cost can be generated by the model, including graphical displays; this feature allows flexibility in process design, materials selection (end product and process), labor, energy, machinery/equipment, tooling, overhead elements, facility and maintenance costs. Figures 11 and 12 contain two output

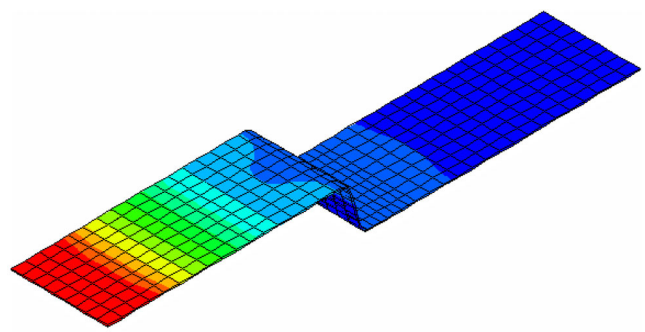

Figure 10. Blank deformation after WF.

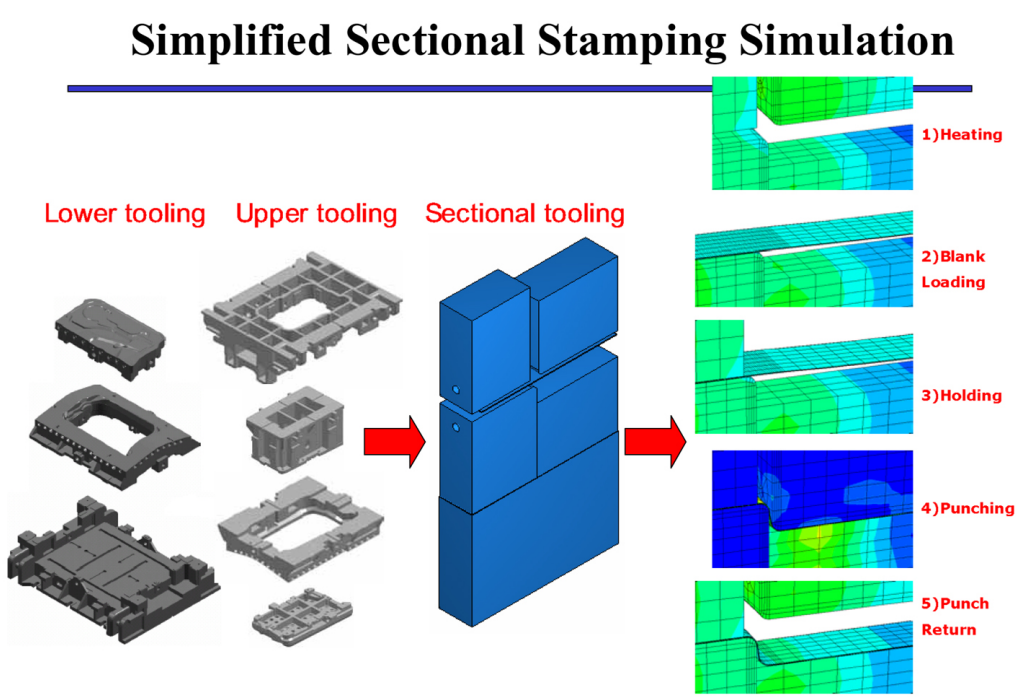

Figure 9. Dodge Neon door inner panel stamping die components sectioned and profiled to show thermal and vertical displacement data.

Breakdown by Cost Element		
Material	$21.66	74.8%
Process Material	$1.36	4.7%
Labor	$1.17	4.1%
Energy	$2.08	7.2%
Main Machine	$0.92	3.2%
Tooling	$0.81	2.8%
Overhead Labor	$0.65	2.2%
Building	$0.13	0.4%
Maintenance	$0.19	0.6%
TOTAL	**$28.98**	

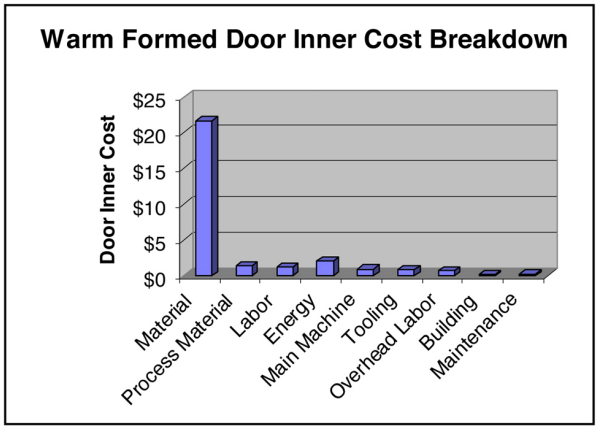

Figure 11. Example product cost display using strawman data inputs.

Breakdown by Process Step		
Material	$21.66	74.8%
Blanking	$0.79	2.7%
Lubrication	$0.82	2.8%
IR Heating	$1.20	4.1%
Forming	$2.43	8.4%
Cleaning	$2.07	7.1%
TOTAL	**$28.98**	

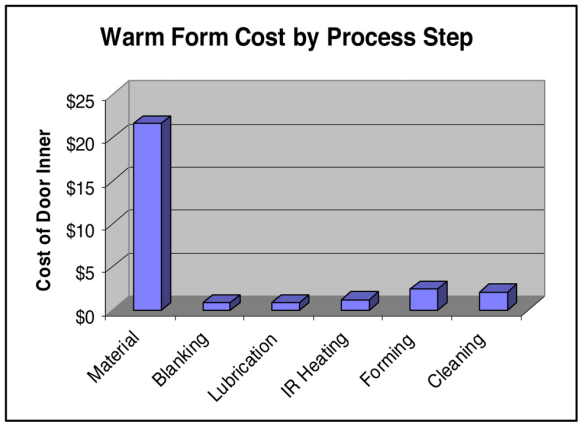

Figure 12. Example process cost display using strawman data inputs.

examples showing part and process costs in table and graphic forms. Strawman example data were used to generate these data for sample presentation purposes. The individual OEMs are now able to apply the technical cost model in their own proprietary planning using their confidential data as inputs. OEM confidential data and proprietary use of the technical cost model will not be shared among the team.

Future Work

- Finish thermal studies and thermal models of the entire die to gain a better understanding of what temperature set points need to be maintained for a more uniform temperature distribution on the die surfaces.
- Perform additional lubricant studies and finalize the formulation options with limitations identified through laboratory testing and scale-up demonstrations.
- Investigate the WF of continuous cast aluminum sheets, and additionally, magnesium sheet formability using the same process infrastructure.
- Finalize the blank heating system specification to be used in production scale-up and demonstration.
- Set up at contractor's site for production scale-up and demonstration.
- Apply the technical cost model to generate costs for comparing the WF process with known alternative processes using the strawman format.

C. Electromagnetic Forming of Aluminum Sheet

Richard W. Davies, Principal Investigator
Pacific Northwest National Laboratory
P.O. Box 999, Richland, WA 99352
(509) 376-5035; fax: (509) 376-6034; e-mail: rich.davies@pnl.gov

Sergey Golovashchenko, Technical Coordinator
Ford Motor Company
Ford Research Laboratory, Dearborn, MI 48121-2053
(313)-337-3738; fax: (313) 390-0514, email: sgolovas@ford.com

Technology Area Development Manager: Joseph A. Carpenter
(202) 586-1022; fax: (202) 586-1600; e-mail: joseph.carpenter@ee.doe.gov
Field Technical Manager: Philip S. Sklad
(865) 574-5069; fax: (865) 576-4963; e-mail: skladps@ornl.gov

Participants
Vladimir Dmitriev, EMF R&D, Ford Motor Company
Dwight Rickel, EMF System Development, Los Alamos National Laboratory
James Sims, Coil Durability, Materials, and Design, Los Alamos National Laboratory
Andy Sherman, EMF R&D, Ford Motor Company
Jeffrey Johnson, EMF System and Control, Pacific Northwest National Laboratory
Gary Van Arsdale, EMF System Design and Metal Forming, Pacific Northwest National Laboratory
Nick Bessonov, EMF Simulations, University of Michigan–Dearborn
Nick Klymyshyn, Computational Mechanics, Pacific Northwest National Laboratory
Dick Klimisch, Project Coordinator and Material Supply, Aluminum Association
Roy Cooper, Oxford Automotive Company, EMF Industrial Embodiment

---

Contractor: Pacific Northwest National Laboratory
Contract No.: DE-AC06-76RL01830

Objective

- Develop electromagnetic forming (EMF) technology that will enable the economic manufacture of automotive parts made from aluminum sheet.

Approach

- Establish analysis methods for forming system design.
- Develop durable actuators (coils).
- Analyze industrial embodiment of the EMF process.

Accomplishments

- Completed a literature search for information on EMF, coil materials, and coil design/durability.

- Completed design and assembly of a 150-kJ pulsed power unit (Figure 1) at Los Alamos National Laboratory (LANL).
- Tested Ford Motor Company's integrated forming coil system for high-volume automotive stamping.
- Used LANL's literature review of patents, relevant coil materials, and the design of EMF coils.
- Installed the 150 kJ pulsed power supply at Pacific Northwest National Laboratory (PNNL), demonstrated operation, and installed automated computer control system capable of automated cyclic testing and sheet metal forming.
- Completed fabrication of an experimental apparatus to evaluate coil durability.
- Established a Cooperative Research and Development Agreement (CRADA) that includes Ford, PNNL, and Oxford Automotive.
- Performed cyclic testing of an EMF coil assembly for durability assessment and achieved more than 1400 cycles.
- Developed conceptual layouts for industrial embodiment of EMF process.
- Demonstrated ability to improve formability of aluminum sheet by a factor of 2–3 times over conventional forming.

Future Direction

- Increase the cyclic testing rate to better evaluate the thermal characteristics of the current industrial coil assembly.
- Continue to evaluate the durability of the Ford-PNNL coil assembly design through high-rate cyclic testing.
- Further develop modeling capabilities that can assist in the design of EMF systems.
- Continue to investigate the industrial embodiment of EMF systems for automotive manufacturing.

Introduction

In the EMF process, a transient electrical pulse of high magnitude is sent through a specially designed forming coil by a low-inductance electric circuit. During the current pulse, the coil is surrounded by a strong transient magnetic field. The transient nature of the magnetic field induces current in a nearby conductive workpiece that flows opposite to the current in the coil. The coil and the workpiece act as parallel currents through two conductors to repel one another. The force of repulsion can be very high—equivalent to surface pressures on the order of tens of thousands of pounds per square inch. Thin sheets of material can be accelerated to high velocity in a fraction of a millisecond.

A recent interest in understanding the EMF of metals has been stimulated by the desire to use more aluminum in automobiles. The high workpiece velocities achievable using this forming method enhance the formability of materials such as aluminum. Also, the dynamics of contact with the forming die can help reduce or mitigate springback, an undesired effect that cannot be avoided in other forming techniques such as stamping. The commercial application of this process has existed since the 1960s. The large majority of applications have involved either the expansion or compression of cylinders (tubes). The forming of sheet

materials is considerably more complex and has received relatively little attention.

Project Deliverables

At the end of this program, methods and data to assist the economical design of EMF sheet forming systems will be documented. This will include (1) materials information and design methods for durable coils, (2) coil durability test data for selected materials and design concepts, (3) dynamic and hybrid formability data, (4) methods for modeling the forming process, and (5) concepts for the industrial implementation of the technology in an automotive manufacturing environment.

Approach

This project will address three main technical areas. The first technical area involves establishing analysis methods for designing forming systems. These methods will be based on developed knowledge of forming limits and relations between electrical system characteristics and deformation response for specific aluminum alloys of interest. The second area of technical challenge is coil durability. Existing knowledge of EMF and relevant knowledge from pulsed power physics studies will be combined with thermo-mechanical analyses to develop durable coil designs that will be tested experimentally. Until a more thorough understanding is achieved of economic factors determining required durability, a nominal level of 100,000-cycle coil life will be the goal for this project. The third technical area involves the industrial embodiment of the EMF process. In this project, EMF is expected to be hybridized with conventional sheet metal stamping. Different approaches to hybridization will be analyzed for issues affecting economical implementation in a modern stamping plant. Different system concepts will be developed and studied. Existing knowledge of the EMF process and technical achievements in this project will be combined to establish a methodology for designing hybrid forming systems that can be readily integrated into modern manufacturing facilities for the economic production of automotive sheet aluminum components. Some of the project focus areas and results are discussed in the following sections.

EMF System Commissioning

Initial testing and trials of the new EMF system at PNNL were conducted in September and October 2001. The trials consisted of assembling the new EMF power supply system, load cables, and inductive load coil. The apparatus used to conduct the experiments is illustrated in Figure 1. The figure shows the four parallel coaxial conductors connected between the power supply and the EMF coil. Figure 2 is an enlarged view of the single-turn coil. The coil used was a single-turn, low-inductance aluminum alloy coil made from AA6061-T6. Also shown in Figure 2 are multiple sheets of Mylar sheeting and G10 (glass fiber composite) insulating materials. Not shown in the figure are the coil containment shroud and associated supports. The experiments involved multiple cycles of charging and discharging of the capacitor bank through the load coil at various known energy levels. The capacitor bank was controlled via the custom system developed for the unit. The

Figure 1. Photograph of the capacitor bank and load cables connected to the forming coil.

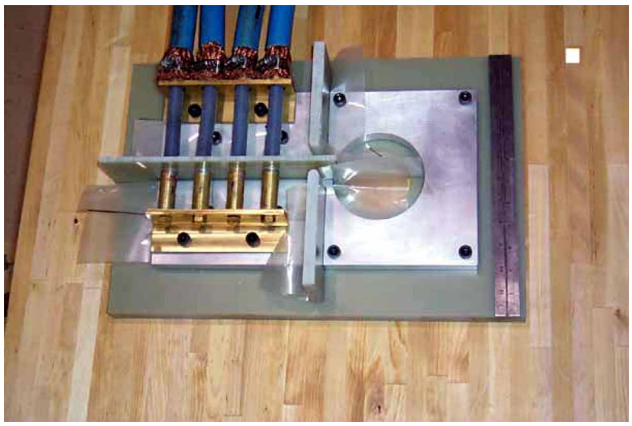

Figure 2. Photograph of the single-turn forming coil and the load cable connections.

sequence of testing consisted of charging the capacitor bank, isolating the charging power supply, triggering (releasing) the capacitor charge, and monitoring the response of the system. The system response was recorded using a high-speed digital oscilloscope. Figure 3 illustrates the typical response of the system during a 15-kJ discharge of the capacitor bank. This figure shows that the half-current (measuring half the total system current) of the system is approximately 86 kA, so that a total current of approximately 172 kA passed through the load

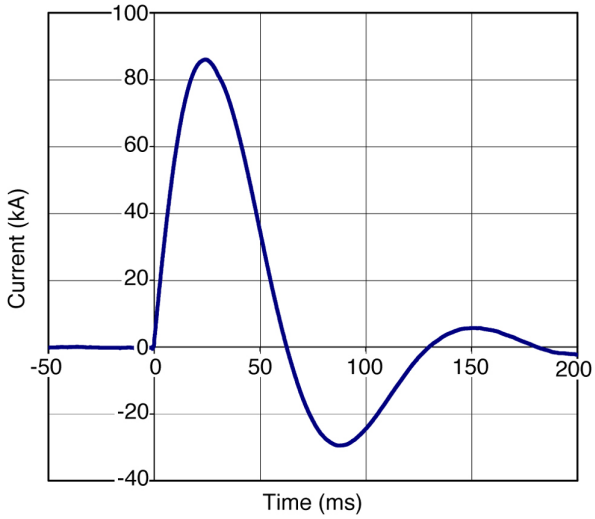

Figure 3. The current waveform that resulted during the initial system trials at PNNL. System charged to ~15 kJ, single turn coil, no ring suppression, half current plotted.

coil. The system rise time was shown to be approximately 26 ms. This EMF system has been commissioned and demonstrated with an automated cyclic testing during sheet metal forming. During the first half of FY 2003, the EMF capacitor bank has been demonstrated at current levels in excess of 225 kA. The system has also been cycled several thousands times at high current levels, while supporting our coil durability experimental work. The custom-designed control system was also successfully demonstrated in automated cyclic loading operating modes.

Coil Design Concepts and Durability

During EMF, the high-intensity electromagnetic forces are applied to the turns of the coil. The coil, insulators, and support structure must resist these forces, as well as related thermal cycles, without significant permanent deformation or material failure. In contrast to typical cylindrical coils, sheet forming will require coils with general three-dimensional (3-D) shapes that are inherently less resistant to forces induced during forming. The key issues involve materials selection and design. Materials must be selected for both electrical conductivity and mechanical properties, and they must lend themselves to manufacturing. Materials may also need to be compatible with the presence of coolants and the forces generated during hybrid forming that combine conventional stamping and EMF. The design must integrate these elements, while delivering the primary function of a spatial and temporal load distribution that achieves the desired deformations. Coil systems will have to be low-cost, modular, and durable (nominally 100,000 cycles) if they are to be relevant to automotive manufacturing.

During the second quarter of FY 2002, LANL generated a technical report containing a conceptual coil design to perform in a high-volume manufacturing system. This particular design is considered modular and would likely require multiple coils to execute

any singular forming operation. This modular coil approach may require further study of coil-to-coil interaction and durability before it can be commercially implemented. In contrast, Ford Motor Company designed an integrated forming coil system for high-volume automotive stamping of complex components. This Ford-designed system has evolved into the system currently being tested for high-cycle forming trials at PNNL. This design integrates features that enhance the stiffness and durability of the coil during cyclic forming operations.

Beyond these trials on the Ford-designed coil system, PNNL has developed a system to evaluate these potential coil materials under high-cycle EMF conditions. PNNL has designed and fabricated a coil durability test apparatus, which was used early in the project for EMF testing. Figure 4 is a photograph of the coil configuration that is part of the apparatus (copper alloy shown). Removed from this coil photograph (for clarity) are insulating sheets of Mylar that retard cross-coil sparking. This coil is connected to the EMF capacitor bank and control system via cables that connect on the bottom side of the coil shown. This coil is designed to be placed in close proximity to a stationary aluminum alloy plate and subject to cyclic pulse loading at different power levels and frequencies to determine the number of cycles to failure. The objective was to make coils from multiple materials and compare the coil durability across several samples from each population. This early work has evolved into testing of a full-scale coil assembly at PNNL.

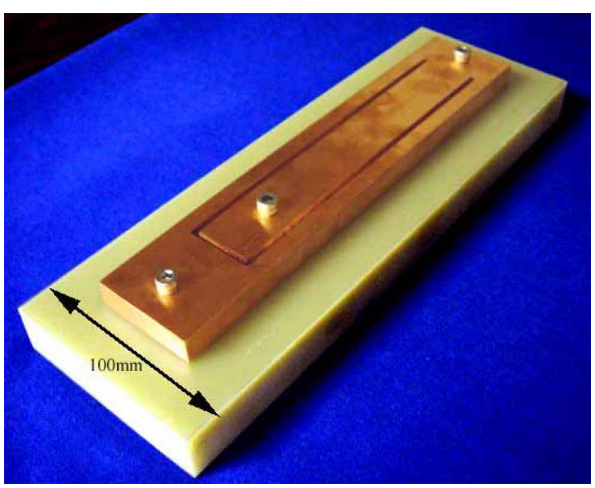

Figure 4. Photograph of the coil system originally used for testing different candidate coil materials.

Coil Durability Experiments

During the first half of FY 2003, PNNL evaluated the performance of the latest coil assembly designed and fabricated under this project. The experiments consisted of evaluating the forming effectiveness, measuring the coil's thermal characteristics, and starting durability tests under cyclic loading of the coil system. Figure 5 shows a photograph of the Ford- and PNNL-designed coil assembly. Figure 6 shows photographs of the forming die used and the resulting formed aluminum sheet after testing. In this figure, the coil is directly below the aluminum sheet and the holes in the die are 3 in. in diameter. After a single EM pulse through the coil, the system forms three domes as shown in Figures 6 and 7. These forming experiments were conducted to learn the necessary pulse magnitude to effectively form aluminum

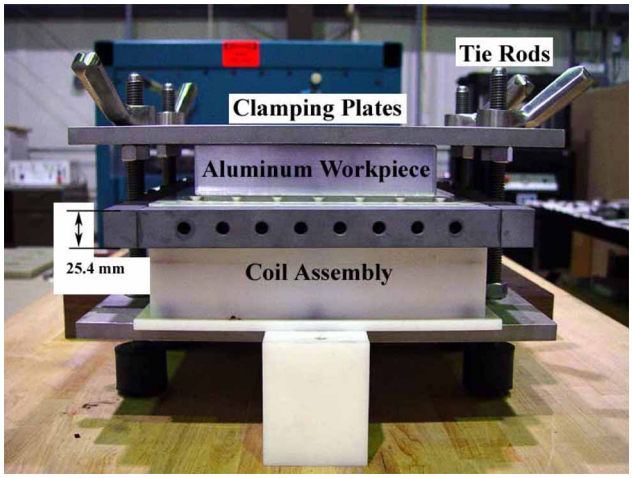

Figure 5. Photograph of the Ford- and PNNL-designed coil assembly. This assembly is currently undergoing cyclic testing at PNNL and has achieved more than 1400 cycles with no signs of coil degradation.

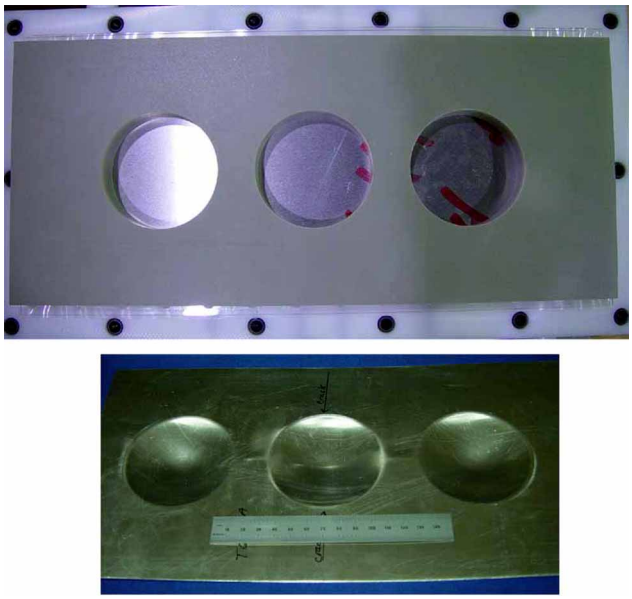

Figure 6. (top) Top view of the glass fiber-reinforced plastic tooling on the coil assembly with aluminum sheet metal between the coil and the tool. (bottom) Photograph of the deformed sheet after one EM pulse through coil.

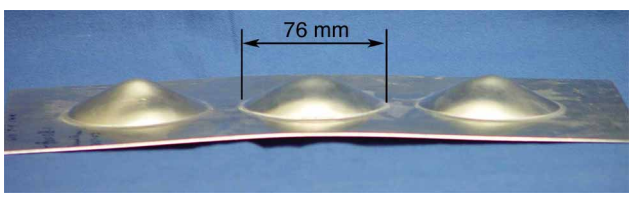

Figure 7. A formed aluminum sheet after a single EMF operation.

sheet. Subsequent to determining this critical EM pulse magnitude, PNNL initiated cyclic loading experiments on the coil system to determine the thermal and mechanical characteristics of the coil assembly to determine long-term durability. This assembly, which is currently undergoing cyclic testing at PNNL, has achieved more than 1400 cycles with no signs of coil degradation. These experiments are ongoing.

Formability of Aluminum during EMF

Ford Motor Company has conducted laboratory experiments to investigate the formability of aluminum alloy sheet during EMF. These laboratory experiments included free forming of domes and forming of sheet metal into v-shaped die cross-sections. Figure 8 includes a cross section through a v-shaped forming die showing the coil, die, and the workpiece before and after deformation. This figure also shows the results of a typical strain grid analysis and the two to three times improvement in formability under these forming conditions. However, the experimental data have shown that the formability is sensitive to the shape of the die being used to evaluate the formability. Further investigation may be required in this area to better define the forming limits of the material under the varying biaxial and triaxial states of stress that develop during EMF.

Numerical Simulation of EMF Process

The EMF process is challenging to simulate because of the need to simultaneously model electromagnetic, thermal, and elastic-plastic deformation of materials. Many of the commercial research codes have serious limitations as well as an inability to accurately predict the results of EMF processes. This project has focused on integrating portions of existing commercial research codes to accurately predict the important characteristics of a 3-D EMF process. The current work involves collaboration with Dr. Bessonov in cooperation with the University of Michigan at Dearborn. Figure 9 illustrates an example of a two-dimensional simulation of EMF of aluminum sheet into a conical die with a fully coupled electromagnetic-elastic plastic model. These models are currently being extended for use as a fully 3-D numerical simulation approach. This work is ongoing.

Industrial Embodiment

Oxford Automotive is conducting an ongoing study into the industrial embodiment of the EMF process, which is designed to analyze the potential methods to incorporate EMF into the highly integrated manufacturing of automobiles. The study is investigating integration into conventional sheet

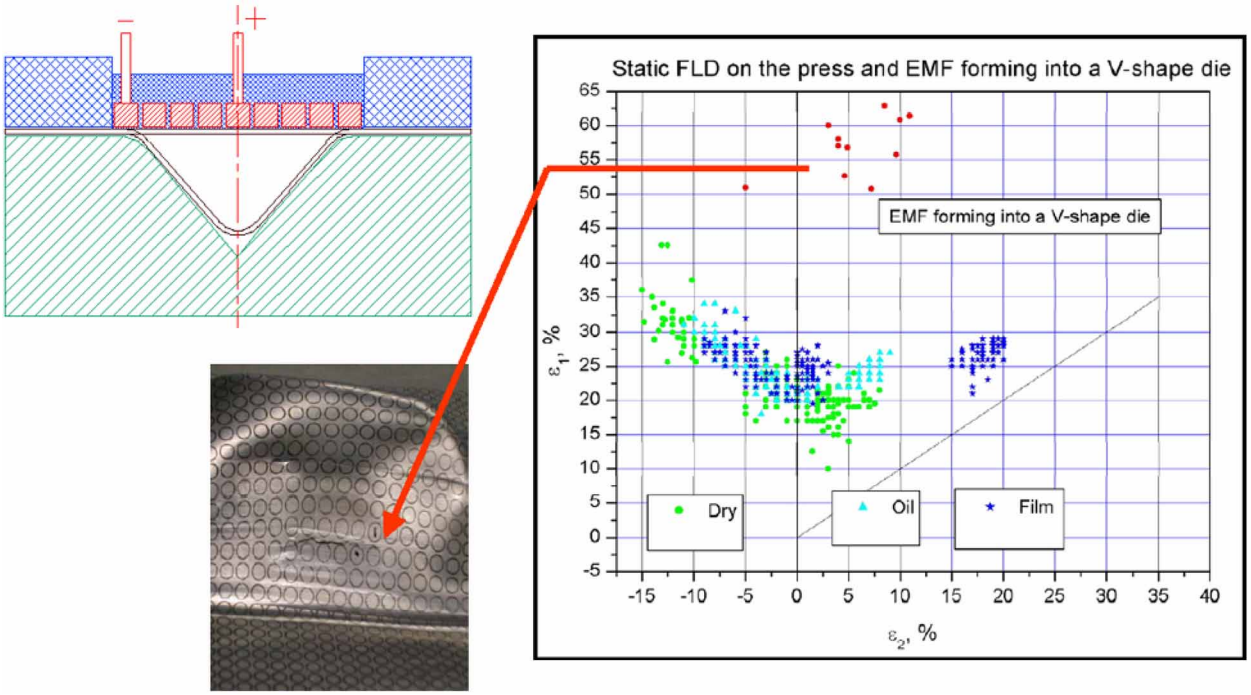

Figure 8. (Upper left) A cross-section through a v-shaped die showing the coil, die, and workpiece before and after deformation. (right) Strain grid formability data showing the improvement in aluminum formability under these forming conditions.

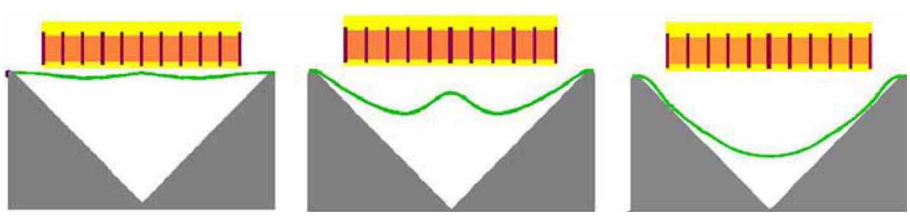

Figure 9. Example of a two-dimensional simulation of EMF of aluminum sheet into a conical die with a fully coupled electromagnetic-elastic plastic model. *Source:* Produced by Dr. Bessonov in cooperation with University of Michigan–Dearborn.

metal stamping production facilities and the potential to create an entirely new and separate production line based on EMF technology for aluminum alloy sheet. To date, several variations have been identified and are currently undergoing detailed study. Figure 10 shows a conceptual industrial embodiment of the EMF process as produced by Oxford. The system shown involves an EMF station located in conjunction with conventional mechanical presses. In the scenario shown in Figure 10, the EMF system would be used as a separate forming station to perform a restrike function. This restrike operation would be employed to increase deformation in local regions that require greater formability than conventional stamping will permit.

Conclusions

Technical feasibility of EMF for aluminum sheet in an automotive application has

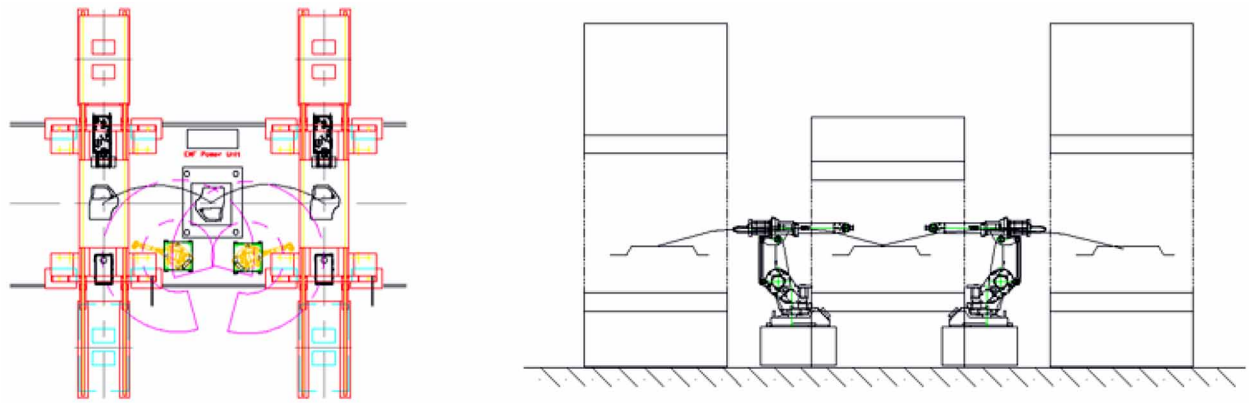

(a) Plan view of robotic transfer (b) Side view of robotic transfer

Figure 10. Conceptual industrial embodiment of the EMF process. The system shown involves an EMF station located in conjunction with conventional mechanical presses.

been demonstrated, during both this project and prior U.S. Council for Automotive Research projects. The durability of relevant coils systems and methods for the economical design, construction, and implementation of forming systems are yet to be demonstrated. There is also a need for additional dynamic formability data for relevant aluminum alloys. This project targets these issues. Progress has been made in assessing the current state of knowledge for materials, coil design, formability, and system design. Also, a pulsed power system has been designed and fabricated to serve in experimental testing of coil systems. This project has also shown that EMF can be performed using aluminum sheet while achieving intermediate coil life (~1400 cycles). As this project progresses, a balanced combination of analysis and experiment will be applied to demonstrate more durable coil systems that meet the performance requirements of automotive manufacturing.

D. Aluminum Automotive Closure Panel Corrosion Test Program

Project Co-Chair: Tracie Jafolla
General Motors Corporation
Mail Code 483-370-101
3300 General Motors Road
Milford, MI 48380-3726
(248) 676-7014; fax: (248) 685-5279; e-mail: tracie.l.jafolla@gm.com

Project Co-Chair: Greg Courval
Alcan International
P.O. Box 8400
Kingston, Ontario K7L 5L9
(613) 541-2233; fax: (613) 541-2134; e-mail: greg.courval@alcan.com

Technology Area Development Manager: Joseph Carpenter
(202) 586-1022; fax: (202) 586-1600; e-mail: joseph.carpenter@ee.doe.gov
Field Technical Manager: Philip S. Sklad
(865) 574-5069; fax: (865) 576-4963; e-mail: skladps@ornl.gov

---

Contractor: U.S. Automotive Materials Partnership
Contract No.: DE-FC05-020R22910

Objective

- Develop a cosmetic corrosion test for finished aluminum autobody panels, which provides a good correlation with lab testing and field performance.

Approach

- Define test matrix.
- Specify and obtain materials.
- Specify phosphate and paint system.
- Pretreat and paint test specimens.
- Conduct laboratory corrosion testing.
- Perform outdoor exposure, test track, and in-service testing.
- Evaluate test data according to defined procedures.
- Revise second iteration of testing based upon initial data.

Accomplishments

- Initiated laboratory, outdoor exposure, test track and in-service testing.
- Completed the first round of lab testing.

- Progressed with statistical analysis of the extent of corrosion on lab samples.
- Progressed with corrosion product analysis to support field—lab correlation.

Future Direction

- Complete analysis of lab test data from the first iteration
- Complete the corrosion product analysis study on lab test samples
- Progress toward second iteration of lab tests

Background

In the previous annual report, a description of the lab, test track, outdoor exposure, and in-service tests was provided as well as some general background on aluminum corrosion mechanisms. In this year's report, the focus will be on data analysis from the first iteration of lab tests, which have been completed.

Panel Evaluation

Goals of Analysis

The evaluation of the corrosion test panels is critical for the Aluminum Automotive Closure Panel Corrosion Test Program. The goal is to correlate accelerated testing to in-service performance. However, the method used to date for evaluation has been a visual inspection that is highly operator, or evaluator, dependent. The team has sought a more robust method for evaluation that is more quantitative. The Atlas Vieew system has provided a good method for this evaluation that eliminates the variations from one operator to the next. It is hoped that this technique will eliminate much of the "art" associated with visual evaluation and provide more consistency to corrosion test results.

Atlas Vieew

The Vieew technique is a digital image analysis method that can measure the maximum creepback from the scribe, the average creepback about the scribe, and the area affected by corrosion around the scribe line. The system uses direct light to identify the areas affected by corrosion. Panels analyzed by the system must be flat to eliminate errors associated with shadows. Figure 1

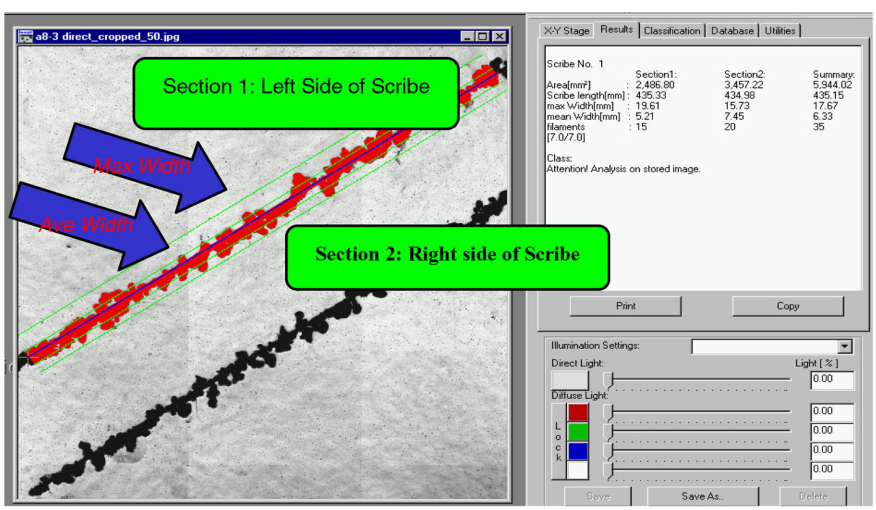

Figure 1. Typical output from the Vieew system.

shows typical output from the Vieew system. The Atlas terminology of width means the length of the creepback used in this paper.

One question posed by the team was whether the Vieew method correlates with the industry-accepted method of visual evaluation. A subset of the team visually evaluated multiple panels; those results were then compared with the output of the Vieew method. A sampling of the results is given in Figure 2.

These charts show the visual evaluations for maximum creepback of three different operators/evaluators compared with the maximum creepback identified using the Vieew image analyzer. Multiple panels were evaluated visually, and the Vieew output correlated well with all of the visual measurements.

The next question was to determine which outputs the team should use from the Vieew. The outputs from the Vieew include maximum creepback, average creepback from the scribe line, and area of corrosion about the scribe line. Figure 3 shows the correlation of the visual maximum creepback from the scribe to the Atlas average creepback for panels exposed to an accelerated corrosion test. The test was conducted at two laboratories and the results are compiled in Figure 3.

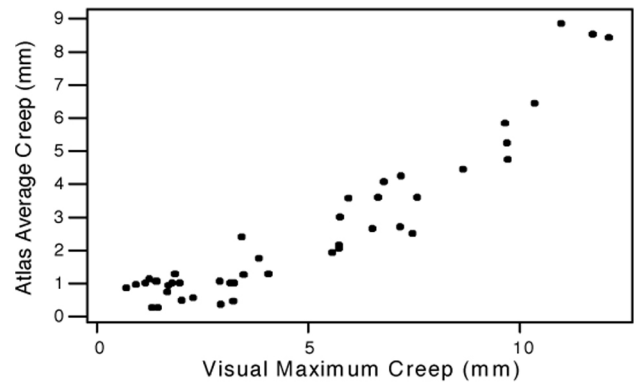

Figure 3. Results of lab tests.

The regression equation is

Atlas average creep = –0.556 + 0.639 visual max creep

R-Sq = 86.7% R-Sq(adj) = 86.4%

The results show good correlation between the Atlas average creepback and the visual maximum creepback, with an adjusted R-squared of 86%. The average creepback is difficult to measure in a visual evaluation, although it can be done. The average creepback provides clues on the extent of corrosion along the length of the scribe. Maximum creepback can be deceptive, because it may represent only a single filiform along the scribe, whereas average creepback

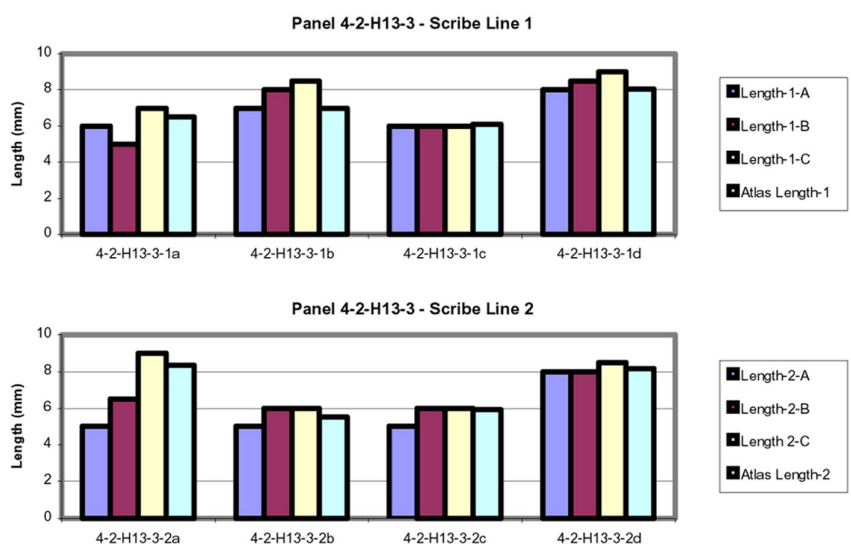

Figure 2. Visual evaluations for maximum creepback.

indicates the extent of corrosion along the entire length of the scribe.

A correlation was also established between Atlas maximum creepback and visual maximum creepback. The limitations of looking only at maximum creepback have been discussed, but once again there is good correlation between visual and Atlas data, as shown in Figure 4.

The regression equation is

Atlas max = 1.71 + 0.789 vis eval max

R-Sq = 79.8% R-Sq(adj) = 79.3%

Although the adjusted R-squared is not quite as good as when the visual maximum creepback was correlated to the Atlas average creepback, there is still a strong correlation between visual maximum creep and Atlas maximum creep.

A similar analysis was done to determine if Atlas area of corrosion correlates to visual maximum creepback. The results of the analysis are given in Figure 5.

The regression equation is

Atlas area = –83.8 + 106 visual max creepback

R-Sq = 83.9% R-Sq(adj) = 83.6%

The Atlas area of corrosion correlates to the visual maximum creepback in a very similar manner to the correlation of Atlas average creepback to visual maximum creepback.

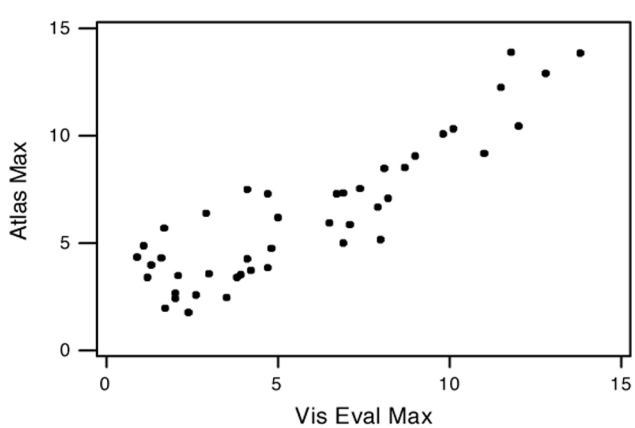

Figure 4. Correlation between visual and Atlas data.

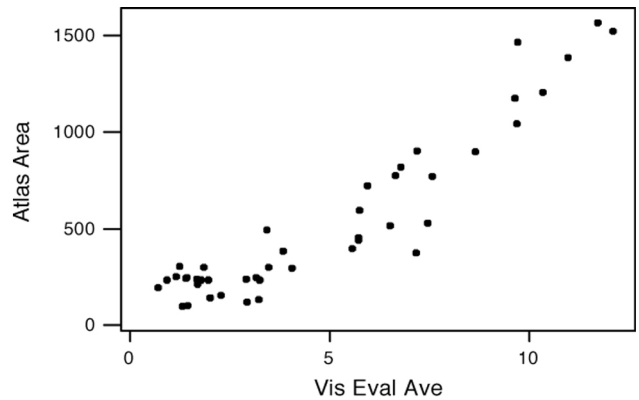

Figure 5. Results of the analysis.

Area of corrosion and average creepback are similar measures and could very likely be used interchangeably. For the data used to generate the above graphs, Atlas average creepback predicted Atlas area with an adjusted R-squared of 94%. It is expected that a similar correlation will be found for any data set of this type.

As a result of this study, the team gained confidence in using the Atlas Vieew method to evaluate corrosion performance. Additional work is still necessary to determine which output (area, maximum creep, average creep) or combination of outputs is necessary to fully understand corrosion performance. It is likely that a sampling of panels exhibiting varying levels of corrosion performance will need to be visually ranked and the Atlas data then correlated to that ranking. This has not yet been done, but it will be included in the next phase of evaluation.

To date the first round of accelerated testing has been completed. All of the panels that have undergone accelerated testing have been scanned using the Atlas Vieew and evaluated. The data are currently being analyzed by a statistician (Duncan McCune) to determine whether the panels show differences in corrosion performance. The statistician will also evaluate if the testing laboratory has an effect on corrosion performance when the same accelerated test is run.

The team also has test panels on the original equipment manufacturer (OEM) test tracks, in outdoor exposure, and on

in-service vehicles. Those panels will also be evaluated using the Atlas Vieew at the end of testing, as well as during regular intervals of testing whenever possible. A key evaluation criterion is to ensure that the mode of corrosion exhibited on in-service vehicles is the same as that exhibited during accelerated corrosion testing. We hope to also get data to understand the method of initiation of corrosion to determine which testing best predicts in-service performance.

E. Development of the Infrared Thermal Forming Process for Production of Aluminum Vehicle Components

Principal Investigator: G. Mackiewicz-Ludtka
Oak Ridge National Laboratory
P.O. Box 2008, Oak Ridge, TN 37831-6080
(865) 576-4652; fax: (865) 574-4357; e-mail: ludtkagm@ornl.gov

Technology Area Development Manager: Joseph A. Carpenter
(202) 586-1022; fax: (202) 586-1600; e-mail: joseph.carpenter@ee.doe.gov
Field Technical Manager: Philip S. Sklad
(865) 574-5069; fax: (865) 576-4963; e-mail: skladps@ornl.gov

---

Contractor: Oak Ridge National Laboratory
Prime Contract No.: DE-AC05-00OR22725

Objective

- Implement infrared (IR) thermal forming as a preform method for aluminum tubes prior to hydroforming to reduce vehicle weight and achieve greater fuel economy.
- Verify initial IR thermal forming estimates to determine concept feasibility for aluminum tubes.
- Develop IR thermal forming process to form basic preform aluminum tubes for subsequent hydroforming trials.
- Evaluate IR thermally formed tubes after hydroforming.

Approach

- Initiate a 1-year feasibility study, followed by longer-term activities (based on favorable results from this feasibility effort) to address the following four primary process concerns: (1) a process that produces bends in the tubes, (2) a process that can meet production rates required for automotive needs, (3) an estimated cost associated with the process and how it compares to present processes, and (4) the influence of the process on the applications, that is, effects on material properties.

Accomplishments

- Verified initial IR thermal forming estimates to determine concept feasibility for aluminum tubes. Verified order-of-magnitude for thermal forming time estimates using the IR process. Forming of a 45° bend is estimated to be achieved in 5–20 s. Results suggest that a minimum of ~5 s is required using optimized processing with cooling, and a range of 10–20 s without cooling.
- Completed initial basic experiments on thin plates, demonstrating the need for a more fundamental approach to bend the significantly more complex tube geometry.
- Identified preliminary IR heat flux issues to be addressed to form basic preform aluminum tubes for subsequent hydroforming trials.

- Developed initial modeling methodology and initiated preliminary model simulations that successfully predict IR thermal processing trends.
- Completed experimental and simulation modeling trials that indicate that further optics development and validation phases will be necessary to achieve the power distribution required to conform larger tubes to the shape needed for hydroforming preforms.

Future Direction

- Redesign and refine the IR thermal forming system as needed (reflector shape, focal length, power density, and cooling) for the more complex case of thermally forming tubes.
- Develop the appropriate reflector design (optics), based on initial experimental and simulation modeling results, that will enable the thermal flux contouring and the correct heat (power) distribution needed for preforming larger tubes to the shape needed for hydroforming preforms.
- Validate optics performance to achieve the power distribution required to form larger tubes to the shape needed for hydroforming preforms.
- Continue tube bending trials utilizing the newly designed IR thermal forming system to successfully bend a tube to be tested in hydroforming trials.

Introduction

During the last 9 years, N. A. Technologies (NAT) initiated thermal forming research utilizing the *laser* as the heat source. Using the laser, NAT has formed a wide variety of tubes in various sizes and materials. The laser thermal forming process has been found to work on both large and small aluminum tubes (see Figure 1). These experiments have demonstrated that the wall thickness of the outside bend of the tube is virtually unaffected and the inside bend actually thickened in all cases. However, the cycle times required for laser forming are too long to be considered for high-volume applications. Based on some work done on plate-stock, NAT has shown that if the thermal input power level is scaled-up from 4 kW (characteristic of laser technology) to 300 kW (characteristic of IR plasma lamp), IR thermal forming works similarly, but much faster. However, this process still has to be proven for tubes. Consequently, the Vortek lamp that is installed at Oak Ridge National Laboratory (ORNL), with its inherent power levels, offers the potential to move the thermal forming process to speeds that are high enough to reach production rate levels. In fact, the higher power levels available with the Vortek lamp are key to taking this process from the "prototyping" or low-volume production stage, to the actual high-volume production stage. NAT has estimated that utilizing the power capacity of the Vortek lamp, the

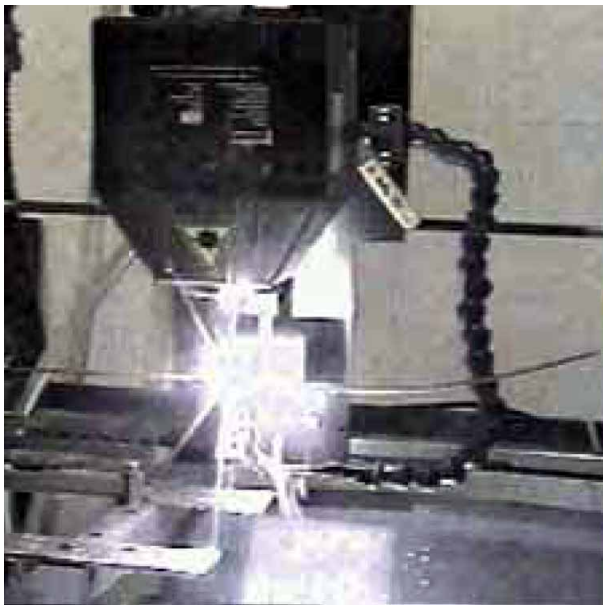

Figure 1. Laser thermal forming process has been demonstrated on small aluminum tubes.

thermal forming process can be put into *actual production (i.e., 60 units/h, as opposed to 2 units/h that can be achieved in the laser lab today)*. The key to tapping this higher power source to thermally form the tubes will be developing the correct heat distribution profile.

To date, a great deal of effort has been spent on finite-element modeling at Massachusetts Institute of Technology (MIT), Boeing, Rockwell, Penn-State, Ohio State, British Aerospace, and the best results (from MIT) provide predictions that are off by ±50%. These results emphasize the complexity of the IR thermal forming process. This complexity results directly from the extreme, transient nature of the process with continuously varying surface boundary conditions. Consequently, considerable work remains to be done to develop this process to distribute the heat properly around the tube. NAT has spent nearly a decade developing an understanding of the heat distribution needed to laser form a tube. Developing this process to distribute the heat from the Vortek heat source properly around the tube will be a significant effort. NAT is optimistic that, based on its success at scale-up of plate using the neural-network-based model,* developing the right thermal distribution with the Vortek lamp is possible. Success will be defined as demonstrating that the IR thermal forming process works and that it has the possibility of scale-up to real production.

Building on the NAT experience with laser forming and the results from the preliminary experiments involving the IR thermal forming process completed as part of the MPLUS program at ORNL, this project holds the promise of achieving DOE goals of reducing vehicle weight to realize greater fuel economy. The high thermal heat source of the IR lamp technology holds the key to unlock the potential in demonstrating that the IR thermal forming process is more than a laboratory demonstration so that the energy savings potential can be realized.

*Trained neural networks are attractive predictors for manufacturing processes because they can accurately capture material/process response without requiring actual physical data/models.

Status and Annual Summary—Feasibility Study

Introduction and Background

From the onset of this project, as noted above, it has been known that developing the thermal forming process to properly distribute the heat flux around the tube would be a significant effort. However, based on NAT successful results using laser forming on small-diameter tubes, and its subsequent success at trial scale-up efforts for translating these results to plate, with the neural-network-based model developing the right thermal distribution with the Vortek lamp seems very viable. Consequently, a preliminary ***feasibility study*** was initiated. Due to the limited project budget available in the first year, the most cost-effective approaches were attempted first to verify the viability of utilizing IR thermal forming to form tubes. Several experimental approaches were attempted to determine the concept feasibility of utilizing IR thermal forming as a fixtureless preforming operation for subsequently hydroformed aluminum vehicle components. These approaches were (1) adapting a long (4-cm) stand-off reflector that was available, (2) modifying the hardware below the reflector to obtain a smaller thermally controlled heat flux zone (thermal footprint), and (3) developing and testing a thermal processing model to run process simulations to determine the appropriate reflector design needed to produce the correct heat flux distribution around the tube. These cost-efficient methods/steps are described below.

Hardware Modifications

In the first attempt, the optics selected and utilized were those that enabled the largest (4-cm) stand-off from the work piece. To accomplish this, the already available

4-cm IR reflector optics were redesigned/reworked to attempt to provide the thermal flux and thermal footprint necessary to thermally bend tubes. Results from these experiments determined that a narrower beam and a higher heat flux are needed. To address this issue, a water-cooled, focusing plate was designed and fabricated to assist in controlling this heat input. The motive behind this inexpensive attempt was to constrain the heat flux at the surface of the tube by merely blocking and absorbing the heat outside of the targeted thermal footprint zone of the IR beam. Experimental trials, however, determined that not enough heat was available to form tubes because the thermal contour was not optimized yet for the tube geometry. However, these experiments did confirm the need to gain a more fundamental understanding of the heat flux required to design an IR thermal forming system in order to address the more complex case of thermally forming tubes. To accomplish this goal, an IR thermal forming system is needed to address several issues, including reflector shape, focal length, power density, and cooling.

Basic Experimental Trials

Initial IR thermal forming trials on 4-in.-diam tubes demonstrated the need for a more fundamental understanding of the thermal flux and approach needed to bend the significantly more complex tube geometry. To gain this fundamental understanding of the IR thermal forming process, basic experimental studies were initiated on thin plates instrumented with thermocouples (Figure 2). The purpose of these trials was first to obtain experimental temperature data to guide the selection of the heat flux needed to form aluminum plates and later extend this methodology to the more complex case of forming the tube geometry.

An example of the experimental setup used during the basic study trials is

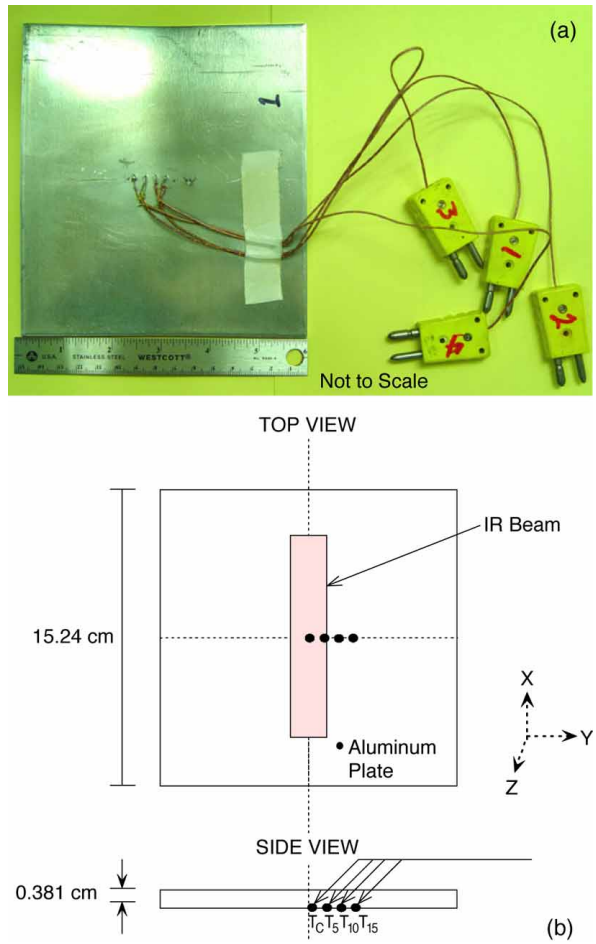

Figure 2. Experimental thermal forming specimens were instrumented during trials to gain a more fundamental understanding of the IR thermal forming process.

demonstrated in Figure 3(*a*). Figure 3(*b*) exhibits an example of the plate deflection obtained for a 0.125-in.-thick aluminum plate based on initial study.

To gain a more basic understanding of how the heat flux distribution needs to be tailored to obtain the amount of tube bending necessary to bend tubes, these initial experimental processing trials used a stationary IR pulse, and the resultant temperature was measured as a function of time at increasing distances from the heat source. The temperature was measured by thermocouples attached to the aluminum on the side opposite the IR source (Figure 2).

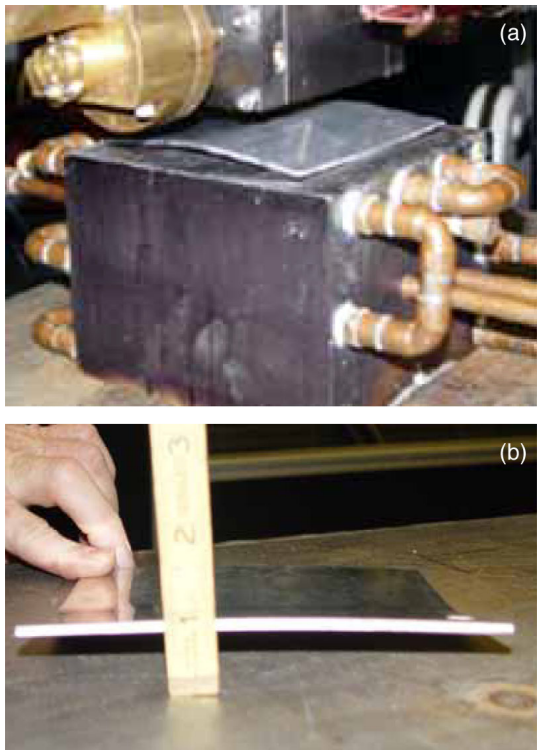

Figure 3. Examples of (*a*) the IR thermal forming setup and (*b*) the aluminum plate deflection observed during initial experimental IR thermal forming trials.

Thermal Forming Simulations

To gain a more fundamental insight into the heat flux power distribution required to conform larger tubes to the shape needed for hydroforming preforms and to guide us in the redesign of the IR forming system, a preliminary modeling methodology was developed first for the case of a flat plate. The modeling cases were set up to simulate the thermal processing conditions utilized during the basic experimental trials. Therefore, modeling simulations were run using the experimental parameters as a guide in setting up the modeling boundary conditions. Thermophysical parameters used for the simulations were obtained from the literature. The resulting model predictions were evaluated and compared with the experimental results. These preliminary model simulations successfully predicted the temperature trends observed during the experimental IR processing trials (Figure 4). To better understand and predict the influence of heat flux on the amount of deflection, a finite-element model also was set up and used to analyze the stresses resulting from the thermal processing parameters. The mechanical response of the aluminum plate to thermal forming process parameters was evaluated. Model assumptions for this analysis were as follows:

- Faces on x = 0 and y = 0 were constrained to be symmetry planes.

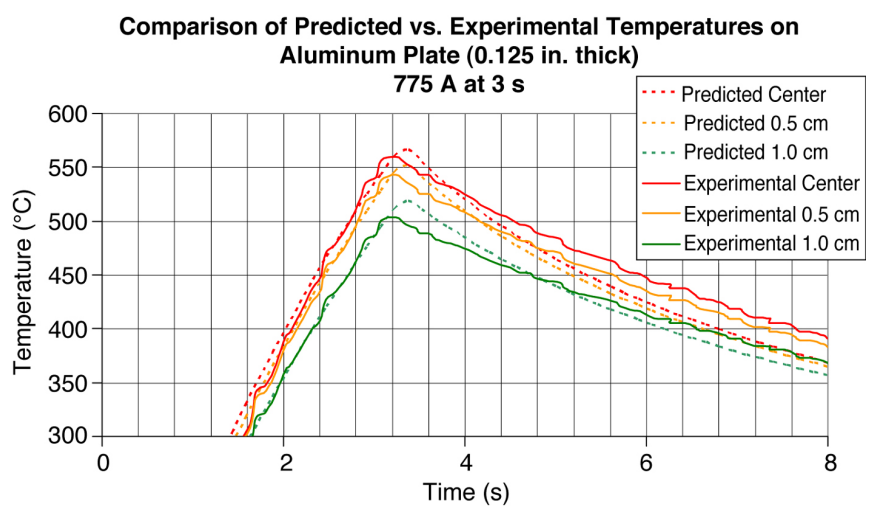

Figure 4. Comparisons between experimental results and modeling simulation predictions demonstrate excellent agreement.

- Bottom edge along x = x_max was constrained to have zero displacement along x-direction.
- Bottom edge along y = y_max was constrained to have zero displacement along y-direction.
- Bottom node at x = 0 and y = y_max was fixed to have no vertical displacement.

The modeling results successfully predict the same degree of plate deflection as those measured/obtained from the initial basic experimental study trials (see Figure 5).

A parametric study also was done (using these initial nonoptimized experimental results) as a method of estimating deflections anticipated based on plate thickness and the maximum heat flux input into the aluminum plates. These results (Table 1) indicate that as the maximum heat flux is increased, the deflection increases, and that as the plate thickness decreases, the plate deflects significantly more. Of course, the thicker plate also cools much more slowly, and additional localized cooling, applied immediately after heating likely would provide the necessary constraint to enhance bending. This would also be true for the thinner plate.

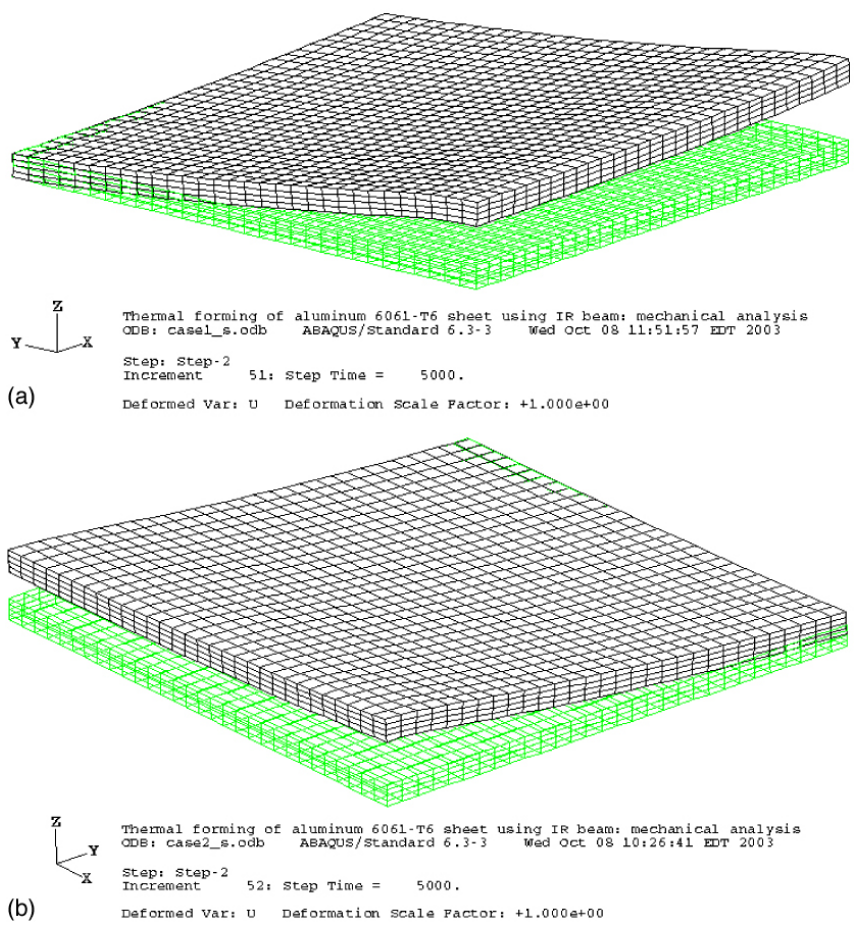

Figure 5. Modeling results demonstrating excellent agreement with finite-element stress analysis predictions for 0.125-in.-thick plate at the end of cooling step for two heat fluxes: (*a*) the deflection along the plate center relative to the edge, and (*b*) the small deflection of the corner opposite to the origin.

Table 1. Parametric modeling study results

Plate thickness (in.)	Maximum heat flux (W/mm^2)	Maximum temperature (°C)	Maximum deflection (mm)
0.125	2.25	641	10.92
0.125	2.0	574	9.58
1.0	2.25	203	0.016
1.0	2.0	184	0.014

Both experimental and simulation modeling results indicate that further optics development and validation phases will be necessary to achieve the power distribution required to conform larger tubes to the shape needed for hydroforming preforms.

Neural Net Modeling Results

To gain some insight into what the optimized thermal processing parameters need to be to thermally form an aluminum plate, a neural net model has been developed based on the initial experimental trials.

Results for the experimentally designed matrix determined that the maximum deflection can occur within the following processing parameter windows:

- Example 1
  - Lamp power: 755 A
  - Pulse duration: 3 s
  - Defocus: 16 mm
- Example 2
  - Lamp power: 815 A
  - Pulse duration: 3.3 s
  - Defocus: 20.8 mm

The model allows one to vary each of the three processing parameters independently, and/or as a group to assist in determining the most suitable set of processing parameters defined within the experimental data limits. Figure 6 depicts the graphical 3-D space within which one can determine the processing parameters to obtain the maximum deflection using the neural net modeling approach to graph a composite plot from which to estimate either the deflection per IR pulse, the number of pulses to obtain a 45° deflection angle, or the total time

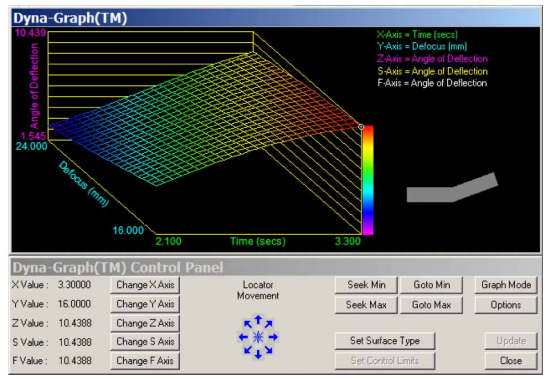

Figure 6. Graphical 3-D representation of neural net modeling results, indicating maximum deflection based on initial experimental trials.

necessary to obtain a 45° bend within the experimentally designed limits (see Figure 7). Our best results to date estimate excellent cycle times to thermally bend a tube to a 45° angle, even based on these nonoptimized, in-progress IR results. Model-predicted cycle time estimates are as follows:

1. a minimum of ~5 s using optimized processing with cooling;
2. a range of 10–20 s without cooling;
3. a maximum of 98 s for this nonoptimized data set.

Additional experiments are in progress to further optimize cycle times within broader processing limits. The next step will be to apply the knowledge gained from these plate

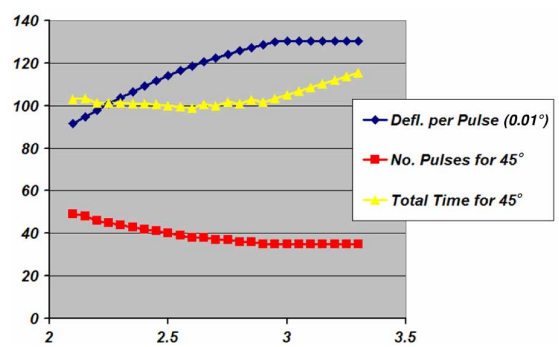

Figure 7. Neural network modeling results depicting the initial response diagram, indicating the sets of processing parameters that produce the maximum plate deflection, based on initial set of basic experimental trials.

results to develop the thermal forming processing parameters to form a tube.

Thermal Forming Current Status

Within the feasibility phase of this project, initial IR trials based on flat plates for thermal forming aluminum tubes have verified the relative order-of-magnitude of time estimates using the IR process. Forming of a 45° bend is estimated to be achieved in 5–20 s. Results suggest that a minimum of ~5 s is required, using optimized processing with cooling and a range of 10–20 s without cooling.

Currently, as part of the concept feasibility demonstration, work is under way to redesign and refine the IR thermal forming system as needed (reflector shape, focal length, power density, and cooling) for the more complex case of thermally forming tubes. This effort will include developing the appropriate reflector design (optics), based on initial experimental and simulation modeling results, that will enable the thermal flux contouring and the correct heat (power) distribution needed for preforming larger tubes to the shape needed for hydroforming preforms. Following this, optics performance to achieve the power distribution required for forming larger tubes to the shape needed for hydroforming preforms will be validated, and tube bending trials will continue utilizing the newly designed IR thermal forming system to successfully bend a tube to be tested in hydroforming trials.

Future Work

Current plans for Phase 3 tasks are as follows: (1) Bend full-size tubes. (2) Characterize and compare IR vs conventionally formed microstructures and properties for bent tubes. (3) Provide bent tubes to industry for hydroforming trials. (4) Evaluate material response, microstructure, and properties of posthydroformed IR processed tubes. (5) Optimize the IR thermal forming process to achieve bend required for subsequent hydroforming. (6) Utilize modeling to guide the thermal forming process development and optimization.

Conclusions

- Within the feasibility phase of this project, initial IR trials based on flat plates for thermal forming aluminum tubes have verified the relative order-of-magnitude of time estimates using the IR process. Forming of a 45° bend is estimated to be achieved in 5–20 s. Results suggest that a minimum of ~5 s is required using optimized processing with cooling, a range of 10–20 s without cooling.
- Both experimental and simulation modeling results indicate that further optics development and validation phases, in addition to cooling control, will be necessary to achieve the power distribution required to conform larger tubes to the shape needed for hydroforming preforms.
- We have completed initial experiments on thin plates to obtain the information; we need to redesign the system (reflector shape, focal length, power density, and cooling) for the more complex case of thermally forming tubes.
- The appropriate reflector design will be developed to provide the thermal flux contouring needed for forming tubes.

3. ADVANCED MATERIALS DEVELOPMENT

A. Low-Cost Powder Metallurgy for Particle-Reinforced Titanium Automotive Components

Russell A. Chernenkof
Ford Motor Company
SRL MD3135
2101 Village Road, Dearborn, MI 48124
(313) 594-4626; e-mail: rchernen@ford.com

Dr. William F. Jandeska
General Motors Corporation, GM Powertrain
895 Joslyn Ave. Pontiac, MI 48340
(248) 857-2184; e-mail: william.jandeska@gm.com

Dr. Jean C. Lynn
DaimlerChrysler
800 Chrysler Dr. East, CIM484-01-13, Auburn Hills, MI 48326
(248) 576-3192; e-mail: jcl6@daimlerchrysler.com

Technology Area Development Manager: Joseph A. Carpenter
(202) 586-1022; fax: (202) 586-1600; e-mail: joseph.carpenter@ee.doe.gov
Field Technical Manager: Philip S. Sklad
(865) 574-5069; fax: (865) 576-4963; e-mail: skladps@ornl.gov

---

Contractor: U.S. Automotive Materials Partnership
Contract No.: DE-FC05-02OR22910

Objective

- Demonstrate production-intent process scheme and fully densified titanium alloy powder metallurgy (PM) composite samples.
- Benchmark process capability using commercial-grade titanium powder feedstock, and follow with one of the proposed low-cost titanium powder materials. Blend additives to achieve final titanium alloy material with reinforcement.
- Perform microstructure characterization and interfacial studies.
- Confirm test specimens are crack-free by nondestructive evaluation method (Lawrence Livermore National Laboratory).
- Generate static mechanical properties and perform failure analysis.
- Perform a technical cost modeling study on the novel ADMA Products, Inc., process and establish sensitivity of each processing step for cost-effectiveness.

Approach

- Use titanium metal feedstock to produce blanks in simple shapes via the ADMA manufacturing process that will then be machined into coupons for mechanical property determination.
- Conduct microstructural and interfacial studies together with mechanical property testing by the team, including outside sources jointly selected.
- Preform a technical cost model on the ADMA manufacturing process.

Accomplishments

- Held project "kick-off" meeting at ADMA Products, Inc., on August 27, 2003.
- Purchased and received all raw materials required for the program.
- Produced and die pressed various powder blends in 0.500-in.-diam carbide tooling to 0.500-in. thickness for metallographic examination.
- Compacted powder blends into 3- by 5-in. samples for tensile testing.
- Continued metallographic examination.

Future Direction

- Complete microstructure characterization and interfacial studies.
- Complete mechanical testing and failure analysis.
- Complete a final report on the feasibility study by October 31, 2004.

Executive Summary

The goal of this concept feasibility study is to develop a low-cost PM manufacturing process to obtain fully dense parts based on current commercial-grade materials and a novel processing technology. The study will use particle-reinforced titanium metal feedstock in conjunction with PM press and sinter technology to manufacture simple parts for testing. A technical cost model will be performed to document the cost of the manufacturing process. The decision gate criteria are (1) a cost-competitive manufacturing process and (2) acceptable microstructure and mechanical properties that have been identified for connecting rods targeted for high-performance reciprocating engine applications.

B. Low-Cost Cast Aluminum Metal Matrix Composites

Principal Investigator: Darrell R. Herling
Pacific Northwest National Laboratory
P.O. Box 999, K2-03, Richland, WA 99352
(509) 376-3892; fax: (509) 376-6034; e-mail: darrell.herling@pnl.gov

Technology Area Development Manager: Joseph A. Carpenter
(202) 586-1022; fax: (202) 586-1600; e-mail: joseph.carpenter@ee.doe.gov
Field Technical Manager: Philip S. Sklad
(865) 574-5069; fax: (865) 576-4963; e-mail: skladps@ornl.gov

USCAR Project Steering Committee:
Bruce Cox—DaimlerChrysler
(248) 576-0235; fax: (248) 576-7288; e-mail: bmc8@daimlerchrysler.com
Rena Hetcsh—Ford Motor Company
(313) 322-9079; fax: (313) 390-0514; e-mail: rhecht@ford.com
James Quinn—General Motors
(586) 986-6712; fax: (586) 986-9204; e-mail: james.f.quinn@gm.com

---

Contractor: Pacific Northwest National Laboratory
Contract No.: DE-AC06-76RL01830

Objective

- Develop low-cost aluminum metal matrix composite (MMC) materials that are cost competitive with typical aluminum alloys used in the automotive industry.
- Provide lightweight, cost-effective aluminum MMC material options for powertrain and structural automotive applications for future vehicles.
- Develop a modular compositing (mixing and holding) system for the production of low-cost aluminum MMC materials. This portion of the effort was conducted under a cost-shared contract with MC-21, Inc., Carson City, Nevada, which has successfully been completed with the results exceeding expectations.
- Identify, evaluate, and develop, as necessary, economic innovative casting and finishing technologies to produce aluminum-MMC automotive brake system components.

Approach

- Develop rapid MMC mixing process and lower-cost, castable aluminum MMC material.
- Evaluate mechanical and physical properties, as well as castability of this material.
- Friction- and wear-test sample products produced from the low-cost MMC material.
- Explore innovative casting and finishing options.
- Design innovative brake system to utilize aluminum MMC materials.
- Prototype and full-scale test demonstration component (brake rotor).
- Optimize finishing technologies for cost-effective aluminum MMC components.

Accomplishments

- Completed the design and analysis of a brake rotor geometry designed specifically for aluminum MMC materials (Visteon-led activity).
- Transferred this innovative brake rotor design to THT Presses, Dayton, Ohio, for casting die design and fabrication in preparation for prototype brake rotor casting.
- Completed casting trials and process parameter development for full-scale component.
- Completed postprocessing (heat treating and machining) study of prototype brake rotors.
- Prototyped new brake rotors for evaluation.
- Validated the function of the close-die tooling and modified squeeze casting cycle process.
- Evaluated and approved prototype microstructure and mechanical properties.
- Completed initial phase of brake rotor dynamometer testing to determine performance and validate modeling results.

Future Direction

- Commence study on proper finishing methods and economics for automotive aluminum MMC components.
- Evaluate economy of centrifugal casting for large-volume production of aluminum components.
- Prototype selectively reinforced aluminum MMC brake rotors and conduct subsequent testing for comparison to the fully reinforced prototype pieces.
- Investigate the use of centrifugal casting to demonstrate the production of a selectively reinforced brake rotor caliper with the reinforcement located in the bridge region of the caliper (PNNL).

Introduction

The objectives of this project are (1) to provide lightweight, cost-competitive aluminum MMC options for future cars, sport utility vehicles (SUVs), and hybrid vehicles and (2) to demonstrate these developments on prototype brake system components such as a lightweight brake rotors. The approach is to develop advanced MMC material processing technologies and integrate these processes into an economical manufacturing cycle (i.e., low-cost material plus innovative shape casting plus low finishing cost), including consideration of product design that accounts for material-specific manufacturing characteristics and component performance.

In the first phase of the project, a novel mixing process was developed for the economical production of aluminum MMC materials under a cost-shared industrial contract with MC-21, Inc. This proprietary process rapidly mixes reinforcement particulate into the matrix alloy, by utilizing a specially designed mixing head that is rotated at high speeds. The process can produce aluminum MMC material for $1/lb, which is a significant cost savings of greater than 50% over other similar commercial products. This is a significant enabler for the automotive industry to utilize wear-resistant, high specific strength and stiffness MMC components.

In addition to reducing the production costs associated with MMC materials, innovative shape casting processes were evaluated for manufacturing aluminum MMCs. The general approaches investigated (depicted in

Figure 1) represent conventional casting methods as well as methods designed to produce selectively reinforced structures.

The objective of the final phase of this project is to demonstrate the benefits of lightweight aluminum MMC components by applying the low-cost MMC material to a brake rotor in an appropriate manner. The approach is to develop a novel brake rotor design that will properly utilize and exploit the properties of aluminum MMCs for high-friction and wear applications. Prototype castings of full-scale brake rotors are to be produced in order to be tested for performance and durability of the rotor design and MMC material under simulated vehicle operating conditions.

Innovative Brake Rotor Design, Prototyping, and Testing

A collaboration with Visteon Chassis Systems, Dearborn, Michigan, was initiated to design a brake rotor geometry utilizing aluminum MMC materials for construction. Instead of taking a direct materials substitution approach using a conventional cast iron brake rotor design, which has been tried in the past with poor results, the goal was to create a new design geometry that can exploit the properties of an aluminum MMC material with good thermal performance. With this approach, Visteon has developed a functional aluminum MMC brake rotor that can be used for both front and rear brake rotors of a typical midsize passenger vehicle. Visteon used computational fluid dynamic (CFD) simulations to help create the novel brake rotor design, using the materials properties provided by PNNL for the low-cost aluminum-MMC material. In addition, finite-element analysis (FEA) of the rotor was performed for this design to ensure that the stress levels in the rotor due to thermal gradients and braking loads were acceptable. Based on the modeling results, it was determined that the design should work well for a midsize sedan, even under severe and repeated stopping conditions without overheating. A solid-model representation of the innovative brake rotor design is shown in Figure 2.

THT Presses, Dayton, Ohio, was contracted under a 50/50 cost share agreement to design and fabricate closed-die casting tooling to produce full-scale prototypical

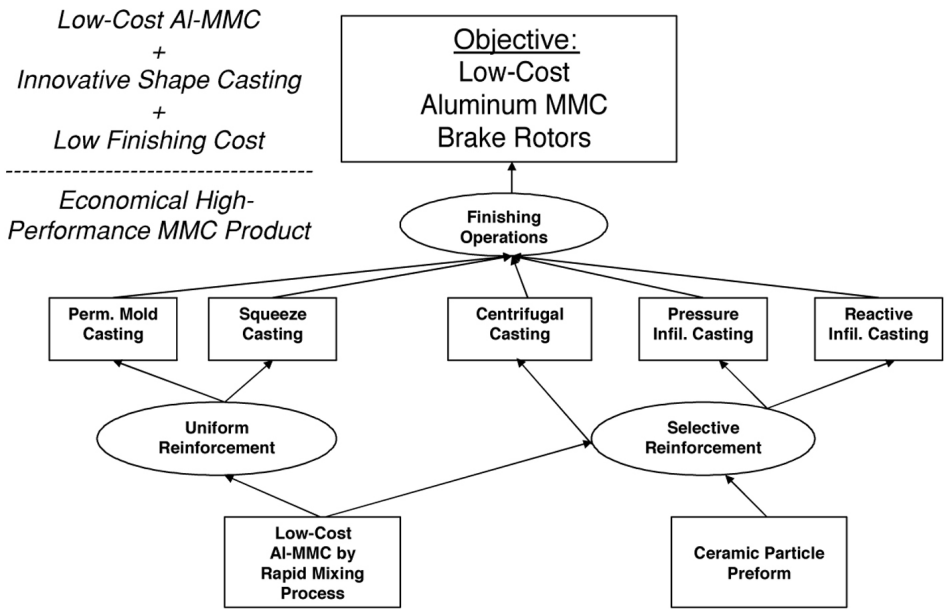

Figure 1. Processing routes investigated for the production of an aluminum MMC brake rotor.

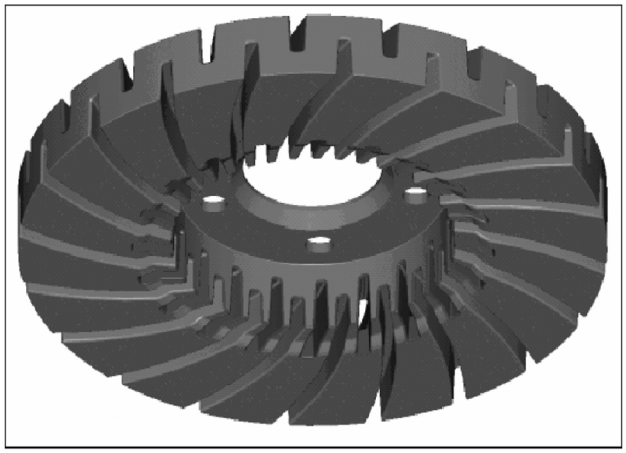

Figure 2. Solid model designed by Visteon specifically for aluminum MMC brake rotors; U.S. Patent No. 6,536,564.

rotors using the rotor design provided by Visteon. The new brake rotor design was transferred from Visteon to THT where casting molds were produced. Subsequent casting trials and die calibrations were performed to achieve the desired rotor casting tolerances. The material selected for these prototypes was produced by MC-21, Inc., using the low-cost 359/SiC/20p material made with the Rapid Mixing Technology developed earlier in the project.

The first round of prototype casting trials produced castings of poor quality, as shown in Figure 3(*a*). During a review by PNNL of the casting quality and process, it was revealed that mold filling and liquid-metal handling issues led to the casting defects and particle segregation. David Weiss, Eck Industries, and PNNL provided a technical review and suggestions on better melting and casting practices for MMC materials. In addition, modifications to the mold gating area were employed, which significantly enhanced the liquid-metal fill rate in the model. These enhancements to the casting process ultimately led to high-quality castings, as shown in Figure 3(*b*). The micrograph in Figure 4 is representative of the casting quality and good particle distribution produced using this modified squeeze casting method. This iteration of the casting parameters demonstrates the importance of using an optimized casting practice for aluminum MMC materials that is specifically developed with considerations for material properties and casting mold design.

A total of 48 prototype rotor castings were produced and then heat treated to T71 condition. Figure 4 shows one of the prototype brake rotors in cast form, as well as the representative microstructure and particle distribution of these parts. These rotors were machined at the direction of Visteon and then tested by Link Engineering on a brake dynamometer, utilizing industry standard test protocols for evaluation of disc brake rotor performance. The specified test

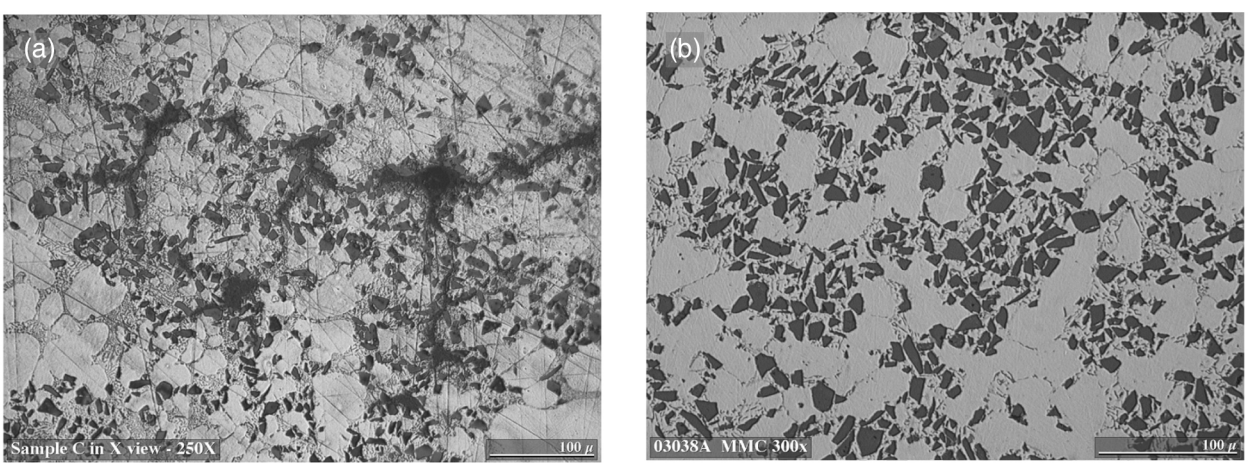

Figure 3. (*a*) Particle segregation and porosity that developed during poor MMC casting practices. (*b*) Appropriate melting and metal handling practices for MMCs, producing high-quality castings with the expected microstructure.

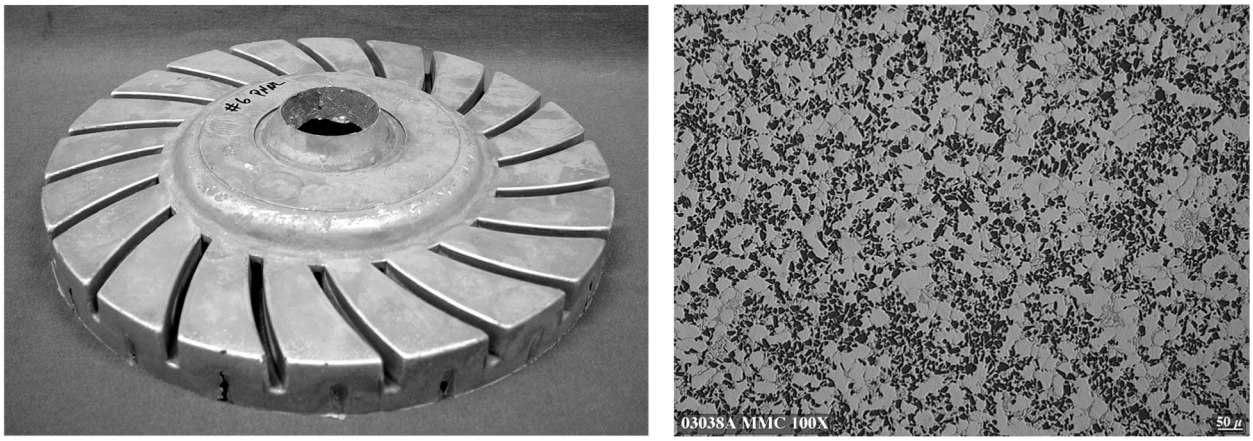

Figure 4. Prototype brake rotor cast from low-cost aluminum MMC material and utilizing a new rotor geometry. The micrograph is representative of the casting microstructure and particle distribution.

schedule called for a variety of different drive and braking conditions and cycles, including tests for: (1) brake thermal performance; (2) simulation of Laurel Mountain hot roughness brake; (3) lining wear vs temperature; (4) environmental brake noise tests (with steady drag); (5) disc wear with low-pressure drag; and (6) brake effectiveness. The results of the dynamometer testing are given in Table 1.

Centrifugal Casting Evaluation

There are many known technical benefits to centrifugal casting MMCs for the production of selectively reinforced axisymmetric components, such as high material yield, less casting cleaning requirements, locating high-performance particles where they have the most benefit, higher toughness of unreinforced areas, and easier machining requirements. However, there is very little known about the economics of this process for medium- or large-scale manufacturing, especially for aluminum-based materials. Although the technology of centrifugal casting MMCs has been demonstrated successfully in low-volume applications, there are no data of casting equipment for automotive component production. Some of the expected issues that need to be addressed include potentially long cycle times and adequate control of mold temperature and fill rates.

PNNL, in conjunction with Eck Industries, has initiated a study to investigate the economics of centrifugal casting for MMC brake rotors. The scope of this study includes designing and building tooling to demonstrate viability of "production" type

Table 1. Results of prototype brake dynamometer testing

Test description	Pass/fail
Dyno simulation of AMS and fade test	Pass
Dyno simulation of Laurel Mountain hot roughness brake test	Pass
Brake lining wear vs temperature test	Pass
Brake noise test (with steady drag)	Pass
Disc wear test (with low-pressure drag)	Pass
Brake effective test	Pass

centrifugal casting machines to cast MMCs as well as developing production parameters for the production of MMC rotor castings. This information will provide the necessary data to qualify rotors produced using centrifugal casting and will indicate whether it will be a valid commercial process for MMC automotive components.

Future Work

Additional dynamometer evaluations of full-scale rotors will be conducted at Link Engineering in the first quarter of FY 2004, and they will be performed with alternative brake pad chemistries. A progress report documenting the outcome of the evaluation and performance of fully reinforced rotors will be drafted and disseminated to the project team and the steering committee. The technical cost model originally developed will be revised based on new cost information from the prototyping phase of the project. Likewise, cost data will be revised as a result of the study to evaluate the commercial validity of centrifugal casting rotor production. This study will also include an evaluation of the need for higher reinforced rotors, or the potential to lower costs by starting with a lower volume fraction feedstock material and using centrifugal casting to achieve a nominal 20 vol % reinforced area.

The remainder of the work scope will focus on prototyping and demonstrating the performance of selectively reinforced aluminum MMC disk brake rotors, instead of the fully reinforced rotors. In addition, PNNL will investigate the use of centrifuge casting to demonstrate the production of a selectively reinforced brake rotor caliper with the reinforcement located in the bridge region of the caliper.

C. Structural Cast Magnesium Development

Project Chairman: Richard J. Osborne
General Motors Corporation
Mail Code 480-205-314
30007 Van Dyke Road
Warren, MI 81033-57039
(586) 575-7039; fax: (586) 492-5115; e-mail: Richard.osborne@gm.com

Project Administrator: D.E. Penrod P.E.
Manufacturing Services and Development, Inc.
4665 Arlington Drive
Cape Haze, Florida 33946
(941) 697-5764; fax: (941) 697-5764; e-mail: dep@gls3c.com

Technology Area Development Manager: Joseph A. Carpenter
(202) 586-1022; fax: (202) 586-1600; e-mail: joseph.carpenter@ee.doe.gov
Field Technical Manager: Philip S. Sklad
(865) 574-5069; fax: (865) 576-4963; e-mail: skladps@ornl.gov

---

Contractor: U.S. Automotive Materials Partnership
Contract No.: DE-FC05-020R22910

Objective

- Develop the science and technology necessary to implement a front structural cradle (from two different magnesium casting processes) that will interface with other concurrent magnesium programs proposed for the U.S. automotive industry.

Approach

- Improve our scientific understanding of magnesium alloys.
- Develop a cost model that compares cast magnesium chassis component costs to other materials and processing techniques.
- Provide comprehensive database and design guidelines.
- Develop improved casting processes.
- Identify and/or develop methods to improve corrosion resistance.
- Improve joining technologies.
- Transfer knowledge and lessons learned to industry.
- Obtain all of the scientific parts of the project that are required [microstructure; effects of modeling; corrosion and fastening properties, nondestructive evaluation (NDE) methods etc.].
- Convert an existing aluminum cradle to magnesium and to have parts ready for testing, and approved for Corvette's Job 1 for 2006. Therefore, the industry part of this project cannot wait for all of the intricate scientific parts of the project to be understood—before a process is chosen; tooling built; parts cast and the validation tests to be run. However, both aspects of the project must be constantly aware of the each other's needs and progress, as shown in Figure 1.

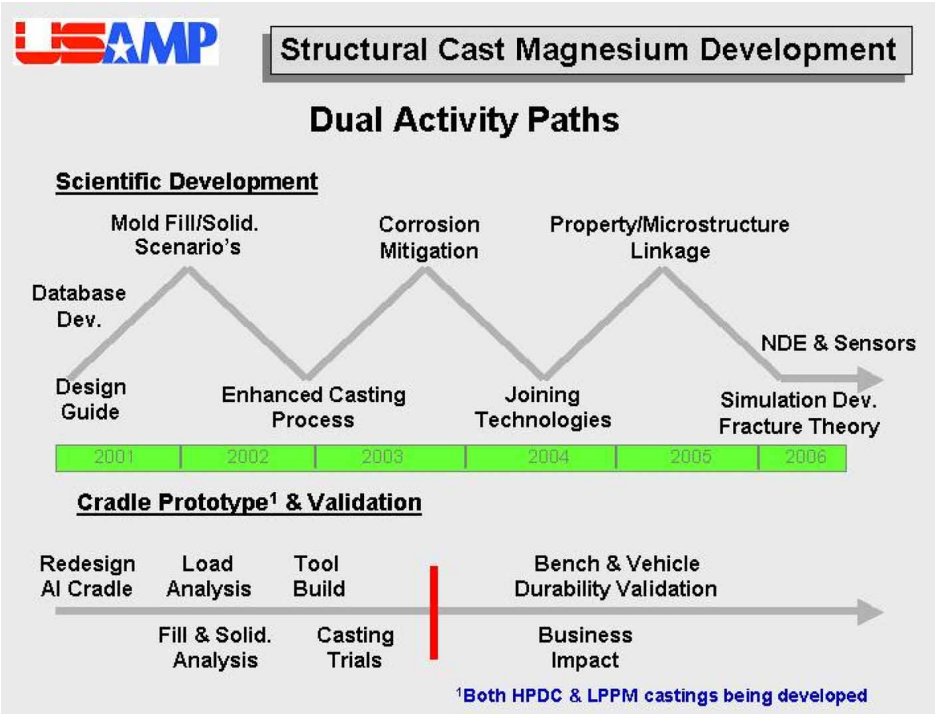

Figure 1. Dual-project path for science and magnesium prototype casting validation activities.

Accomplishments

- Expanded the development of the magnesium alloy database.
- Expanded the collection of magnesium alloy castings for the development of the database.
- Developed magnesium cradle casting parameters for both magnesium casting processes.
- Started durability testing procedures for one of the castings selected from one of the casting processes.
- Expanded the corrosion and casting protection evaluation for specific cradle connectors.
- Started the investigation of in-mold sensor applications.
- Continued the characterization of AM50 High-Pressure Die Cast Alloy by Georgia Institute of Technology

Future Direction

- Start the rigorous bench tests of both Corvette cradle designs. If acceptable, one design will be installed on a vehicle for actual road tests. There is a potential market for 35,000 vehicles for Job 1 for 2006.
- Follow the Structural Cast Magnesium Development (SCMD) Project's Statement of Work Tasks to complete the project on time, including both the scientific and manufacturing aspects of the project.
- Continue to work with the industrial participants with the development of sensors and practical applications developed by the SCMD project.

Introduction

The SCMD project has focused on resolving critical issues that limit the large-scale application of magnesium castings in automotive components. The project activities combine the science and manufacturing technology necessary to implement front and rear structural cradles. Such components offer all of the difficult manufacturing issues, including casting process (high-pressure die, semisolid, low pressure, squeeze, etc) and joining, along with harsh service environment challenges, such as corrosion, fatigue, and stress relaxation associated with fasteners.

The project team includes personnel from

- the "Big Three" automotive companies,
- 34 companies from the casting supply base,
- academic personnel,
- independent testing and research labs,
- American Foundry Society (AFS),
- technical associations,
- Oak Ridge National Laboratory (ORNL),
- Sandia National Laboratory (SNL),
- Lawrence Livermore National Laboratory (LLNL), and
- Natural Resources Canada (CANMET).

Industry Participants

An existing aluminum engine cradle (that is currently in production use) has been redesigned for two different magnesium casting processes: High-Pressure Die Casting (HPDC) and Low-Pressure Permanent Mold (LPPM). Utilization of computer simulations (prior to tooling design) indicated good correlation of casting fill operation (and their effects) to actual production experiences (see Figure 2).

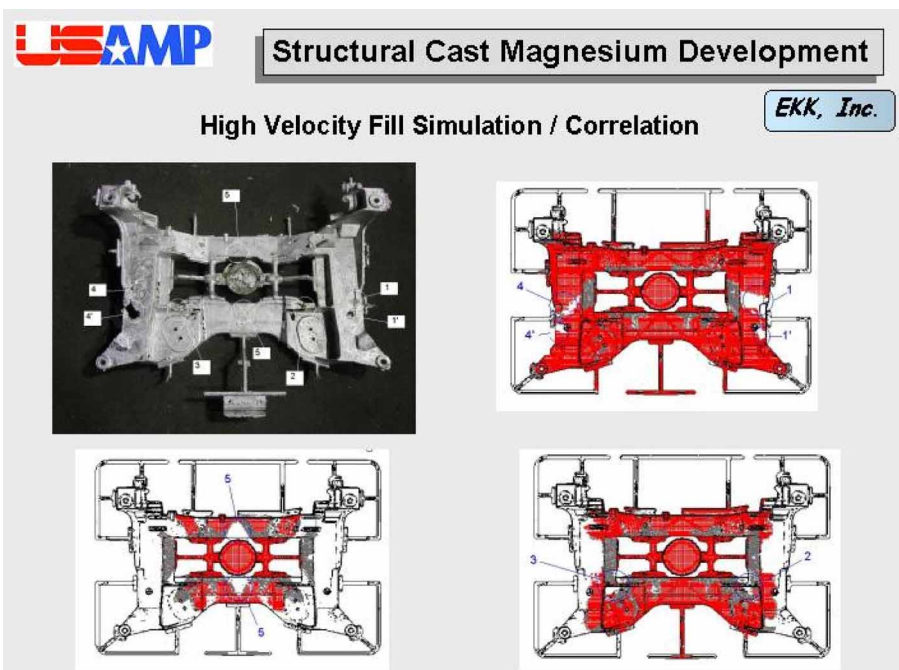

Figure 2. EKK, Inc. cavity fill simulations show excellent correlation with short fill castings.

Tools have been built for both processes, and preliminary prototype castings have been submitted for review (see Figure 3). Durability and other related tests are scheduled for the testing of both cradle designs. A selection will then be made to meet the timing date of Job 1 for the 2006 production year.

- **Importance/Significance:** Utilization of up-front computer modeling resulted in significant savings (time and costs) and eliminating casting defects in the initial castings.

  There is an estimated 35% weight saving in the magnesium cradle vs the current aluminum production part. This weight reduction (vehicle mass savings) will result in a reduction in fuel consumption, emissions and less dependence on foreign oil. Cast magnesium structures have the potential to reduce 100 kg of vehicle mass, which could reduce emissions by 5% and reduce fuel consumption by approximately 1.0 mpg (ignoring secondary mass savings).

  The investigation of producing the same casting by the two different processes (HPDC and LPDC) has a great potential for the utilization of existing aluminum casting companies to expand their operations into magnesium, without huge capital and facility expenditures.

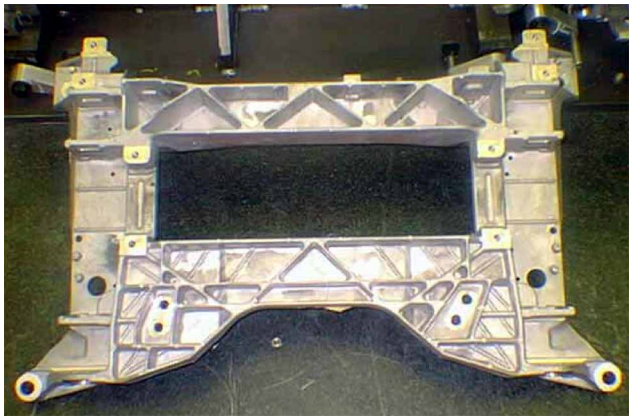

Figure 3. Initial machined HPDC magnesium cradle, August 20, 2003.

National Laboratory Participants

- **ORNL** is investigating the effects of using die lube for HPDC and LPDC operations.

  Importance/Significance: The investigation has already indicated that gas can be generated from the lube when molten metal (higher temperature) is introduced into the mold cavity. The gas then disperses throughout the casting, causing various types of porosity defects.

- **LLNL** is investigating the utilization of sensors in casting molds and the effects of impurities in material supplied by manufacturing plants (see Figure 4).

  Importance/Significance: Utilization of sensors will provide a more accurate report and understanding of the actual process parameters within the casting mold. Investigation and possible elimination of impurities in the metal charged into the furnace will reduce defects.

- **SNL** is expanding a "failure model" that was designed for the previously completed Cast Light Metals (CLM) project. SNL is coordinating all of information obtained from the project, and a mathematical model will be developed (see Figure 5).

  Importance/Significance: Designers can use the model to develop castings, with the accurate knowledge of providing know failure points.

- **Academia participants:** Academia participation is involved with
  - the investigation of and characterization of crack nucleation and growth; and
  - the investigation into the cause of casting defects and the ability to separate gas and shrinkage effects that are generated in the casting by the various processes and the resulting defects that can be generated (see Figure 6).

  Importance/Significance: The importance of understanding the crack

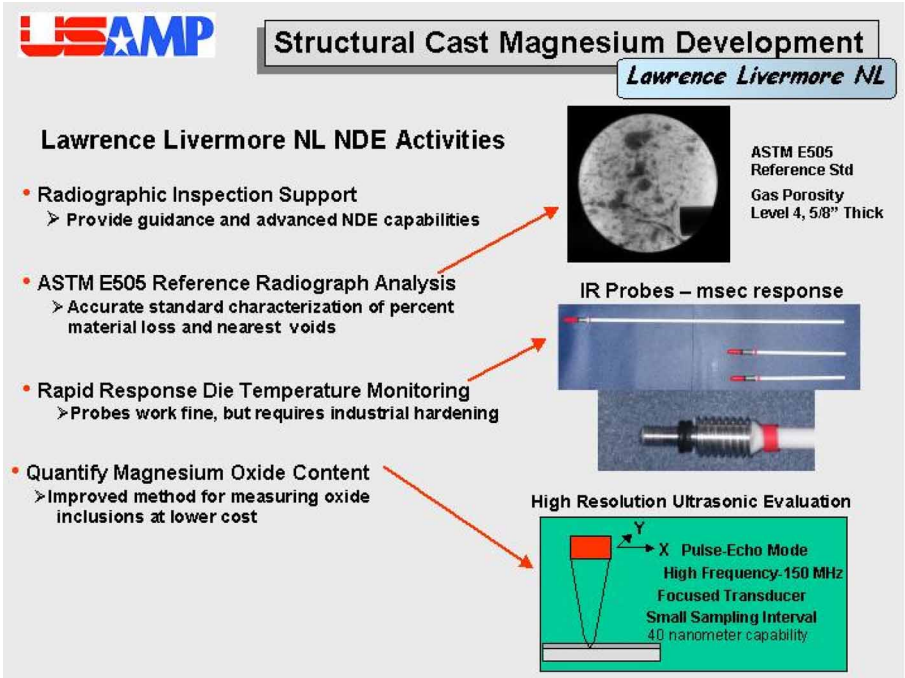

Figure 4. LLNL development activities.

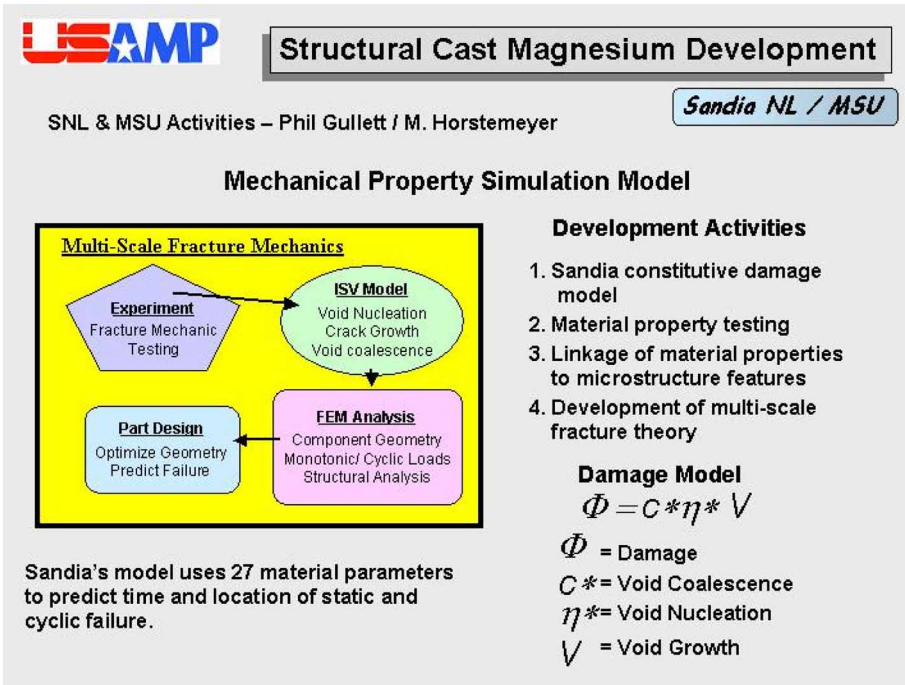

Figure 5. SNL damage model for simulating component material properties.

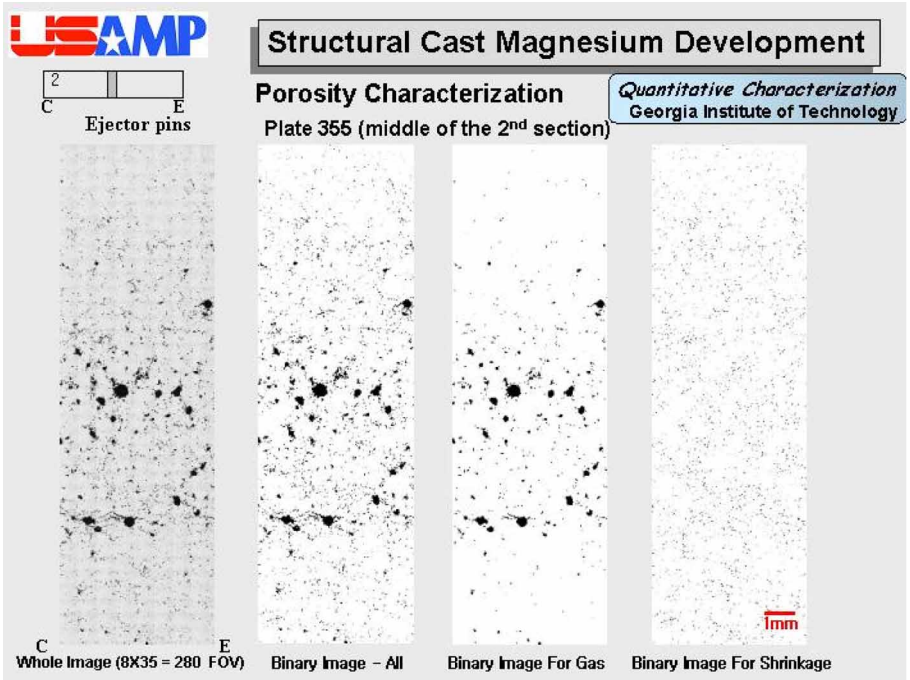

Figure 6. Georgia Institute of Technology characterization of AM50 HPDC alloy.

nucleation and the results of gas generated in magnesium castings will help to provide tools to manufacturing (or change process parameters) that will help to eliminate casting defects. Both of these investigations by academia are working with the information supplied by ORNL and sample parts provided by the manufacturing team. The understanding of the gas effects in castings, generated by die lube could be a major breakthrough in understanding defects in magnesium castings.

Project progress/status vs targets

Prototype magnesium alloy castings will be provided to the Corvette C6 team before year end (2003) to coincide with the cradle validation schedule.

Remaining Technical Challenges and Plans

1. Corvette will start the rigorous bench tests of both cradle designs. If acceptable, one design will be installed on a vehicle for actual road tests. There is a potential market for 35,000 vehicles for Job 1 for 2006.
2. An investigation is ongoing into the effects of corrosion, coatings, and protection; long-range effects of bolt load retention are all being studied by CANMET (see Figure 7). Similar magnesium production parts have been prepared and sent to Newfoundland, an area that is recognized for excessive corrosion. These parts are installed on vehicles and currently being studied, and the results will be incorporated into the final design of the magnesium cradle.

Milestones

Cooperative Agreement

- Magnesium front cradles have been cast by both of the chosen magnesium die cast processes.
- Detailed quantitative microstructural characterization continues for production components cast with AM 50, AM 60, and AZ 91 magnesium alloys.

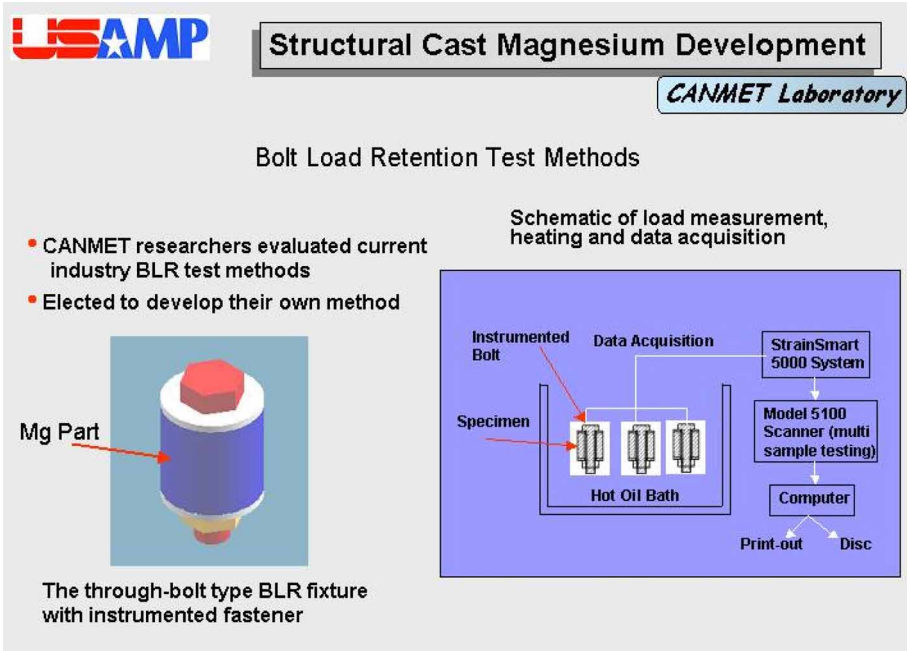

Figure 7. CANMET bolt load retention test method, which could become an industry standard.

- Actual casting results have coincided with predicted modeling techniques.
- Project Steering Committees are actively working with the project team and all industrial participants on major task issues.

Cooperative Research and Development Agreement (CRADA)

- **ORNL**—ORNL continues the investigation of modeling software from four of the supply teams. The results of the investigation will be applied to the ORNL models in current commercial software.
- **SNL**—SNL is coordinating and collecting all of the project data from all the testing sites and using the data to expand the mathematical "failure model" that was designed for the cast light metals (CLM) project. This information will be used for our multiscale fatigue model.
- **LLNL**—Radiographic analysis of production parts and test samples will determine discontinuity types and grades at predicted high-stress locations. Investigation of the possibility of using fiber optics in-mold thermal monitoring system for HPDC continues in a high-volume production facility. Investigation and possible elimination of impurities in the metal charged into the furnace will reduce defects.

Project Benefit

Expected DOE and U.S. industry benefits derived from successful completion of this CRADA would include the following:

- Vehicle mass savings for ground and air transportation, leading to reduction in fuel consumption, emissions, and less dependence on foreign oil.
- Automakers are under increasing pressure to reduce CO_2 emissions and increase corporate average fuel economy (CAFE). The North American auto industry currently uses approximately 70,000 MT/year of magnesium, which is equivalent to some 3.5 kg per vehicle.
- The ability to significantly increase magnesium usage will help the auto industry meet future Federal CAFE targets and reduce exposure to CAFE penalties.

Cast magnesium structures have the potential to reduce 100 Kg of vehicle mass, which could reduce emissions by 5% and reduce fuel consumption by approximately 1.0 mpg (ignoring secondary mass savings).

- Light metal alloys have greater recycling value with reduced energy consumption vs plastics (including melting, machining, handling, and transportation energy requirements).
- The Big Three competitive global postures will increase as a result of designing and manufacturing vehicles that offer greater consumer value. This can improve the U.S. trade balance with countries that market higher fuel efficiency vehicles than those produced in North America.
- Health and environmental issues for workers are reduced during light-metal casting operations when compared to ferrous foundries and polymer molding operations.
- Provide national laboratories with valuable manufacturing development and product application experience.
- Dual-purpose role of providing the national laboratories an opportunity to develop math-based simulation models and NDE technologies that benefit both the auto industry and federal ongoing technology programs.
- The successful casting of a magnesium cradle (by low-pressure diecasting) will indicate to the existing aluminum casting industry that the transfer of casting technology (aluminum to magnesium casting) can be achieved at a low facility cost.

D. Magnesium Powertrain Cast Components

Project Manager: Bob R. Powell
GM Research & Development Center
MC 480-106-212, 30500 Mound Road, Warren, MI 48090-9055
(586) 986-1293; fax: (586) 986-9204; e-mail: bob.r.powell@gm.com

Project Administrator: Peter Ried
Ried & Associates, LLC
6381 Village Green Circle, Suite 10, Portage, MI 49024
(269) 327-3097; fax: (269) 321-0904; e-mail: pried_imagineer@netzero.net

Technology Area Development Manager: Joseph A. Carpenter
(202) 586-1022; fax: (202) 586-1600; e-mail: joseph.carpenter@ee.doe.gov
Field Technical Manager: Philip S. Sklad
(865) 574-5069; fax: (865) 576-4963; e-mail: skladps@ornl.gov

---

Contractor: U.S. Automotive Materials Partnership
Contract No.: DE-FC-05-95OR22910

Objective

- Demonstrate and enhance the feasibility and benefits of using magnesium alloys in place of aluminum in structural powertrain components, thereby achieving at least 15% weight reduction of the cast components.

Approach

- The Magnesium Powertrain Cast Components Project (MPCC) contains two phases separated by a decision gate.

Phase I

- Task 1—Identify, benchmark, and develop a design database of the potential cost-effective, high-temperature magnesium alloys and, using this cast-specimen database, select the alloys that are most suitable for the magnesium components.
- Task 2—Finite-element analysis (FEA) design an ultra-low-weight, cost-effective-performance engine containing four magnesium components (block, bedplate, structural oil pan, and front cover) using the best low-cost, recyclable, creep- and corrosion-resistant magnesium alloys and create a cost model to predict the cost-effective performance of the engine.
- Task 3—During the execution of Tasks 1 and 2, identify and prioritize the critical gaps in the fundamental science of magnesium alloys and processing that are barriers to either the progress of the project or to the use of magnesium in future powertrain applications.

Decision Gate

- Conduct an in-depth review of the engine design, including performance and durability predictions, alloy requirements and measured alloy properties, cost model, and predicted weight reduction.

- Pass this necessary review for entry into Phase II of the Project, which has the goal of demonstrating/validating the Phase I engine design with respect to castability, manufacturability, performance, durability, and cost.

Phase II

- Task 4—Refine the engine component designs as necessary, design and build molds and patterns, and cast the engine components.
- Task 5—Assemble complete powertrains, dynamometer-test the components, and conduct end-of-test teardowns. Further develop the cost model to support determining the cost-effective performance of the engine.
- Task 6—Excise specimens from the cast components and develop a full mechanical and corrosion design database for the alloys. From this create an original equipment manufacturer (OEM)—common material specification for magnesium powertrain alloys.
- Task 3 (from Phase I)—Begin seed-funding critical research and promote additional identified needs to support further development of the magnesium scientific infrastructure in North America to enable more advanced powertrain applications of magnesium. This will be one aspect of the technology transfer deliverable of the MPCC Project.

Accomplishments

- Passed the October 2003 Decision Gate Review of the MPCC Project successfully. The project team is entering Phase II.
- Completed the static mechanical property testing of six high-pressure die casting (HPDC) alloys and three sand casting (SC) alloys, and cyclic tests (fatigue) are nearly complete.
- Completed thermo-physical property measurements of the three SC alloys.
- Completed hot surface and galvanic corrosion tests of the alloys with each of four, advanced engine coolants.
- Completed and documented the castability trials of both the HPDC and the SC alloys.
- Rebuilt the architecture of the computer database containing the above results. It is undergoing beta testing by the Project Team.
- Completed the FEA design of the magnesium version of the Duratec V6 engine. This included solving a significant problem associated with the high coefficient of thermal expansion of the magnesium alloys. The design underwent structural analysis, bending analysis, durability, and acoustic analysis.
- Completed and distributed the cost model to the OEM members of the project team for use in determining the cost-effective performance of the engine.
- Identified scientific gaps for presentation to the North American scientific community early in FY 2004.
- Created and implemented the MPCC Project Web site in VRoom, the USCAR Website.

Future Direction

- Finalize the Phase II Project plan and begin its execution.
- Complete populating the Task 1 cast-specimen database, and select the alloys for Phase II.

- Publish reviews of scientific research needs to support future advances in magnesium alloys, casting processes, and powertrain applications, and solicit research proposals to be considered for funding in Phase II.

Introduction

The MPCC Project will provide comprehensive answers to the questions of the technical feasibility and cost-benefit of using magnesium in powertrain components. The weight reduction target for the magnesium-intensive powertrain is 15% for each magnesium cast component. Since the launch of the MPCC Project in 2001, further worldwide advances have taken place with regard to powertrain applications of magnesium, the BMW composite engine being the most recent. The BMW engine comprises an aluminum core, around which is cast a magnesium shell. This rather expensive approach is based on an inline engine, which has the structural advantage of enabling through bolting to further minimize engine distortion. Other reported engine programs also rely on inline designs, whereas the MPCC engine is built around a V block, see Figure 1. Though bolting was not feasible for this engine, developing a practical design for the V block broadens the range of applications for magnesium—in particular the larger engines, for which the weight reduction potential of magnesium may achieve a greater benefit.

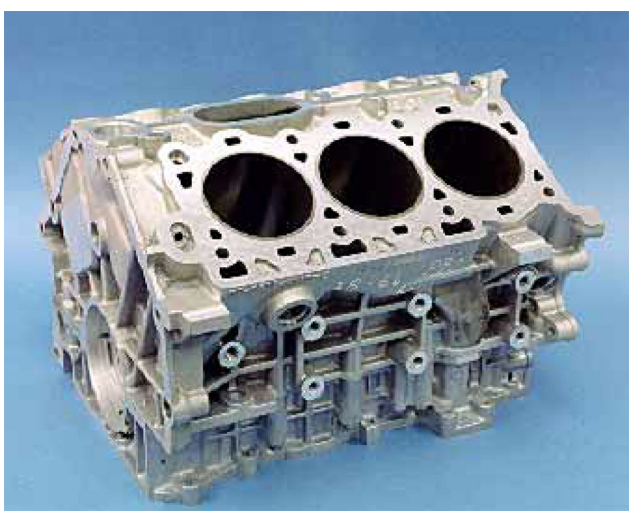

Figure 1. The Ford 2.5-L Duratec engine block.

Details of Phase I Progress

The Phase I goals of the project comprise three tasks: (1) evaluation of the alloys, (2) FEA design of the magnesium engine components, and (3) identification of the critical scientific knowledge necessary for future magnesium powertrain materials.

Task 1—Creep-Resistant Alloy Evaluation

The Task 1 goal was the evaluation of the new creep-resistant alloys based on cast specimens using common dies and patterns, and standardized mechanical property and corrosion tests. Evaluation was based on tensile and fatigue properties, creep and corrosion resistance, castability, recyclability, and estimated alloy costs. The alloys selected from the literature and cast into test specimens for this evaluation are shown in Table 1.

Table 1. Alloys cast and tested in the MPCC Project

Alloy name	Company	Casting process
AJ52X	Noranda	HPDC
AS21X	Norsk Hydro	HPDC
AS31	Avisma	HPDC
AXJ530	General Motors	HPDC
MRI153M	Dead Sea Magnesium	HPDC
MRI230D	Dead Sea Magnesium	HPDC
ML10	Solikamsk	Sand (SC)
MRI202S	Dead Sea Magnesium	Sand (SC)
SC1	Australian Magnesium Corp.	Sand (SC)

The HPDC specimens were cast at Lunt Industries using a die shot shown in Figure 2. The SC specimens were cast at Eck Industries. All castings were shipped to Westmoreland

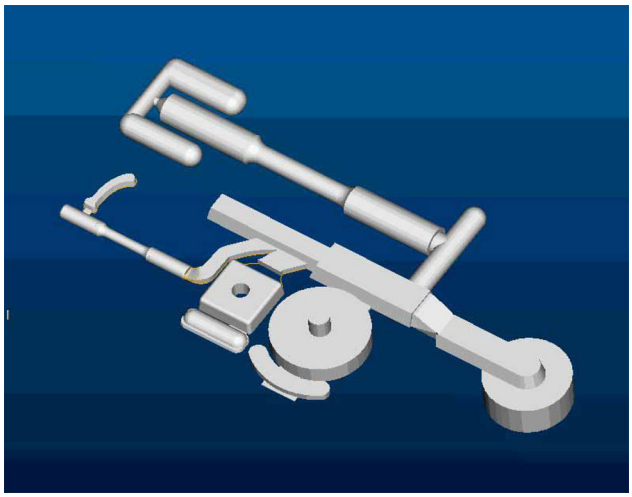

Figure 2. The specimen die shot from the four-cavity GM die used at Lunt Manufacturing.

Mechanical Testing & Research for machining and testing, either at Westmoreland, or at Amalgatech (coolant corrosion), or Auburn University (thermo-physical properties). Specimens for chemical analysis were shipped to Climax Research Laboratories.

All of the test data were put into a database that was developed at Westmoreland. Originally developed in support of the USAMP project Design for Product Optimization of Cast Light Metals (DPOCLM), the MPCC database was built using a substantially new architecture, which took advantage of database capabilities not available when the DPOCLM architecture was created. The title page for the MPCC database is shown in Figure 3. This new architecture has also been applied to the database of "room temperature" magnesium alloys being studied in the USAMP project Structural Cast Magnesium Development (SCMD) (described elsewhere in FY 2003 Progress Report). Together, the results of the MPCC and SCMD projects yield a database covering essentially the entire spectrum of cast magnesium alloys for automotive applications.

A typical working page of the database is shown in Figure 4. At the bottom of the page is shown the range of properties and data that are contained. The tree architecture on the left is used to select individual data sets or comparisons of multiple data sets. In this example of the tensile properties of SC1, tested at 125°C, each specimen test result is shown, specimen by specimen, as well as the statistical summary of the entire test set. Each tensile test graph is available to be

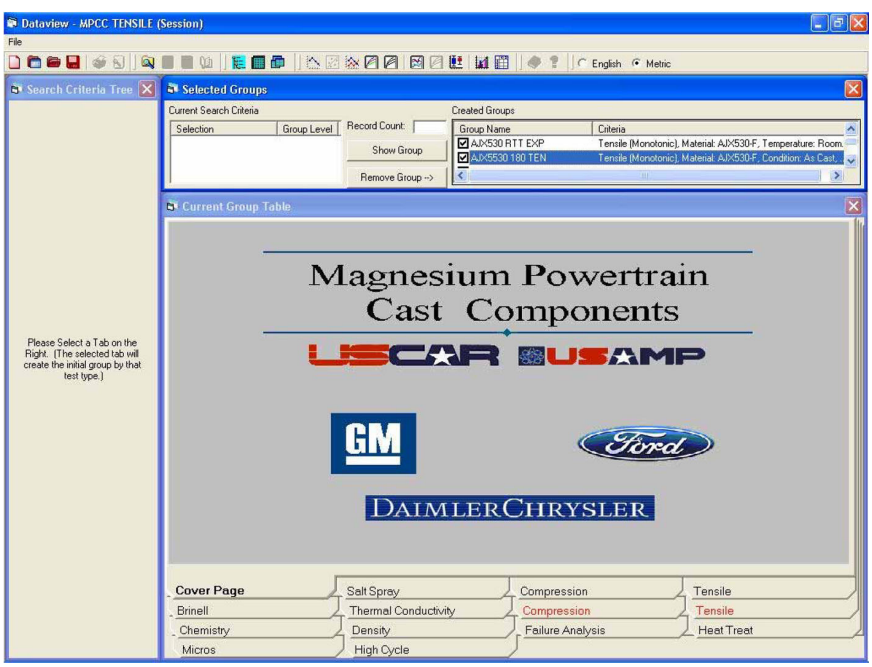

Figure 3. The title page of the MPCC cast specimen database.

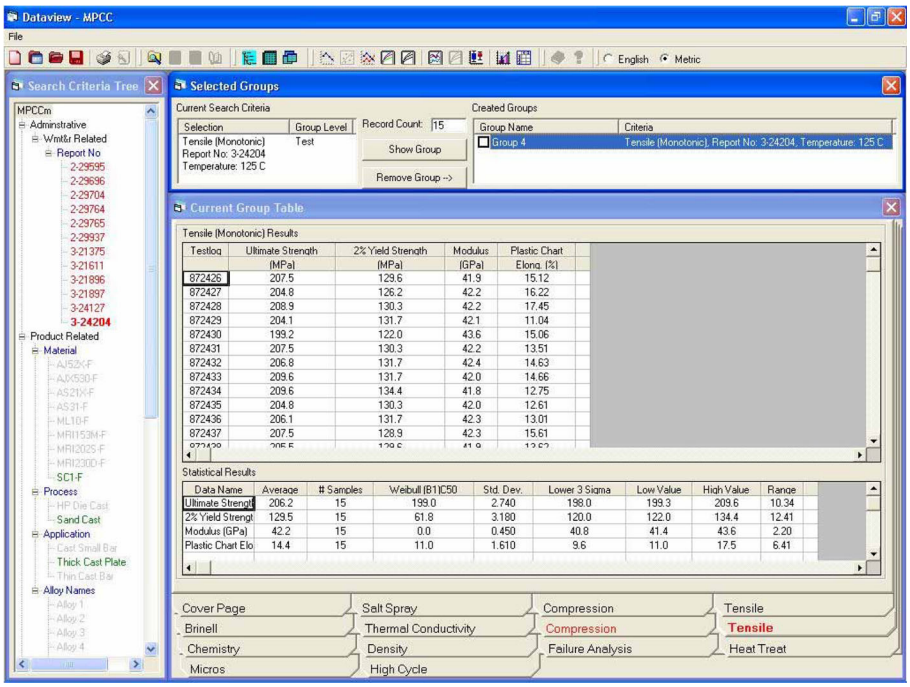

Figure 4. A working page from the MPCC database.

viewed or explored to facilitate use by either the design engineer or the research scientist. Additional information contained in the database includes test procedures, specimen geometries, and sample histories. Among the additional property information to be found in the database are the thermo-physical properties of the alloys, fractography, representative microstructures, and the chemical compositions. Three sets of corrosion test results will be included: salt spray and coolant tests, all of which were completed in the current year. The full database is so extensive that it exceeds the storage capability of a single CD and will ultimately use DVD disks as the storage medium.

The castability trials of both the HPDC and the SC alloys were completed. The HPDC alloys (cast using the die for the Ford transfer case) showed a range of castabilities, based on such factors as casting quality, process requirements, and anticipated die and furnace life, etc. The relative ranking of the HPDC alloys is shown in Figure 5.

The production alloy, AZ91D, showed the best castability rating, and three of the alloys (A–C) showed nearly as good ratings. Interestingly, these alloys showed moderate creep resistance. Alloys D–G, which showed very high creep resistance were more difficult to cast. Observations like this show the difficulty in arriving at overall rankings of the alloys for the powertrain components that will be cast in Phase II of the Project.

Task 2—Engine Design and Cost Model

The Task 2 goals, which were accomplished, are the FEA design of the engine with the magnesium components and the cost model for the engine. The initial designs were based on the property data for the alloys that came from the literature evaluation in Task 1. As casting and test results were acquired, the model was refined.

The FEA design and many of the design decisions are proprietary to USAMP and the MPCC Project team, so only an overview of the accomplishments of the design team is presented. Magna Automotive Testing (Magna Steyr) was chosen to do the FEA design. Ford, General Motors, and DaimlerChrysler team members agreed on the design approach, the underlying materials

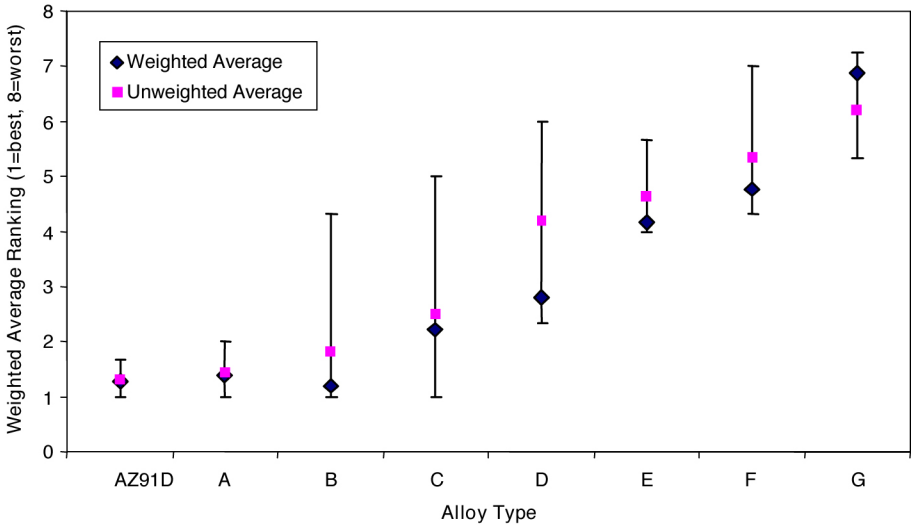

Figure 5. The castabilities of the HPDC alloys, AZ91D, and one other alloy, which was not included in the property database.

assumptions, and the various technology options for the engine. Several non-OEM members of the project team also made valuable technical contributions. Ford provided the initial computer-aided design (CAD) files for the engine and a considerable amount of technical background as the design effort progressed. The engine design had to ensure stiffness and clearances as well as overcome other technical challenges such as engine stability and durability at temperature, cooling the engine with a noncorrosive coolant, fastening and gasketing, and the bore/piston/ring strategy. The complete design is shown in Figure 6.

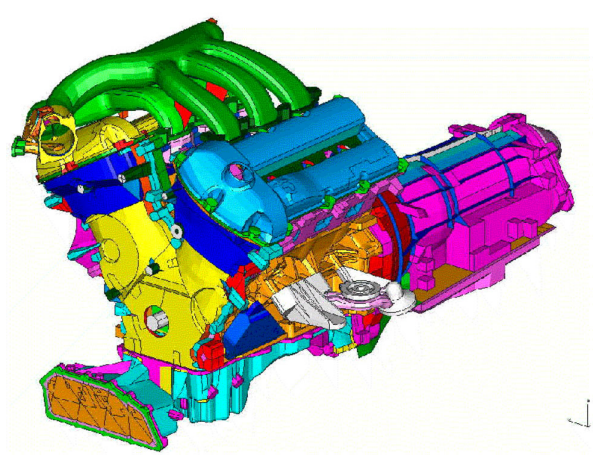

Figure 6. The magnesium-intensive Duratec powertrain.

The additional accomplishments of the design team were the complete structural analysis of the engine, including assembly bolt loads, primary and secondary creep behavior of the magnesium, and the cylinder gas forces as well as the inertial mass forces; fatigue analysis of the block to determine safety factors; and powertrain bending analysis and acoustic analysis of the assemblies. The baseline for comparison in bending and acoustic analysis was the engine design, but with aluminum components.

Four major coolant manufacturers are participants the MPCC Project. Each of them had, independent of the project, developed an anti-corrosion coolant/additive formulation for use with magnesium alloys. The Coolants and Corrosion team worked with them and the alloy suppliers to define a coolant evaluation protocol and to establish a common platform for testing the alloys and the coolant/additive packages. Three resulting American Society for Testing and Materials (ASTM) tests were completed:

- ASTM B117-97—Standard Practice for Operating Salt Spray (Fog) Apparatus
- ASTM D1384-01—Standard Test Method for Corrosion Test of Engine Coolants in Glassware

- ASTM D4340-96—Standard Test Method for Corrosion of Test Aluminum Alloys in Engine Coolants Under Heat-Rejecting Conditions

Amalgatech evaluated each of the candidate alloys using a "double-blind" approach to respect the intellectual property of each individual coolant supplier during testing. The results showed that some alloy coolant combinations were quite good, whereas others were poor. As of this time, the overall corrosion behavior of the magnesium alloys remains an issue for production-implementation of magnesium powertrains, but the test results show that considerable progress has been made. An example of the D4340 test results is shown in Figure 7, in which both the alloys and coolants are coded.

In Phase II of the project, the opportunity for the coolant suppliers to introduce better coolants based on their experiences with the Phase I testing should contribute significantly to the reliability of the engine.

The Cost Modeling team contracted IBIS Associates to develop a cost model of the engine. This sophisticated model enabled the project team to assess the

- cost impact of the alloy based on both intrinsic alloy costs and manufacturing process costs, furnace and die life predictions, and environmental and recycling considerations;
- cost of engine technologies required for successful operation with magnesium components; for example, coolant costs and unique fastening and gasketing requirements; and
- benefits of reduced weight and design advantages that are enabled by the use of magnesium.

IBIS Associates produced two independent models, one for the die cast components and one for the sand cast components. The model takes the form of an interactive spreadsheet, which is fully accessible with respect to the algorithms and constants used. It is "portable" and will be used by each of the OEM organizations to estimate engine costs. The models will be further developed in Phase II, as more is learned about all

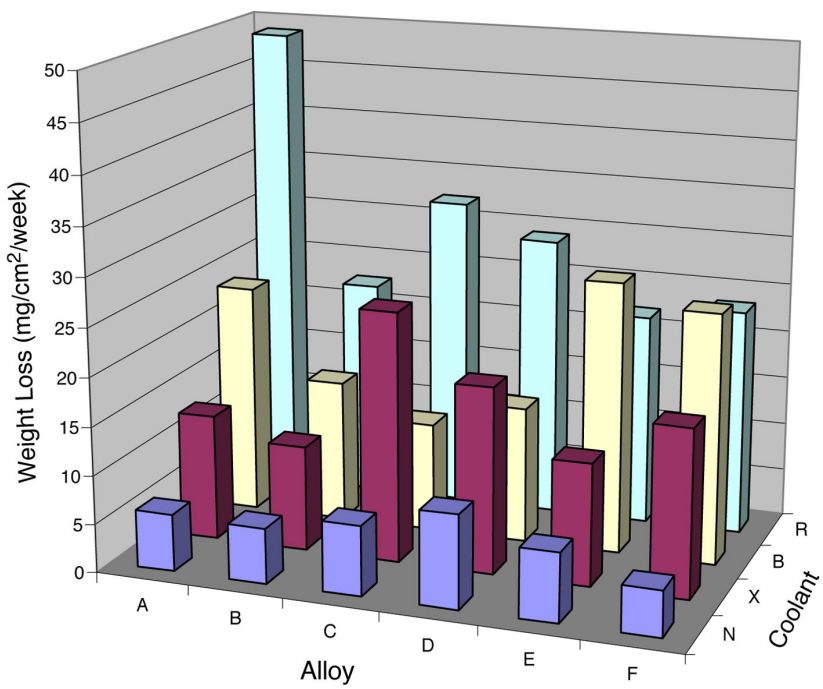

Figure 7. The results of the D4340 coolant tests for the six HPDC alloys and the four coolants.

aspects of producing the magnesium-intensive engine.

Task 3—Critical Scientific Gaps

The Task 3 objective of the MPCC Project is the legacy of the project. It seeks to promote the establishment of a scientific basis for future magnesium alloy and component developments by identifying the critical gaps in our understanding of magnesium alloys and casting processes, with respect to powertrain applications and other applications that require high-temperature alloys. The implementation of Task 3 was initiated in Phase I and will proceed through Phase II. In Phase I, the Project Team documented the scientific needs as they were recognized. In October 2003 a workshop was held at USCAR in Michigan to which North American universities and national laboratories were invited. At this workshop, the project team described the critical research areas and the specific needs within those areas.

Subsequent to the workshop, the information presented there will be made public at technical meetings and through other means to call attention to the research needs. Workshop participants and others will be invited to submit brief proposals to the project team for consideration for funding in Phase II. Ultimately, more formal requests for proposals (RFPs) to address those needs will be distributed to national laboratories and North American universities. The selected research proposals will be implemented in Phase II. The research that can be supported with MPCC Project funds will be small. However, it is anticipated that the promotion of these scientific needs will facilitate the funding of magnesium research by other organizations in North America.

Decision Gate Review

The MPCC Project passed the review in October 2003 and proceeded into Phase II. The success of the review was based on the predicted weight reduction benefit of the engine, its estimated cost/performance ratio and durability, and the existence of alloys with the properties required for the design. The review board made several suggestions, which will be incorporated in the Phase II program

Future Direction—Details of Phase II

Phase II is divided into three tasks: (4) die/pattern design, die build, and casting of the components; (5) assembly and testing of complete powertrains containing the magnesium components; and (6) completion of the alloy property database using specimens excised from the cast components. Additionally, the Task 3 scientific research will be started.

Task 4—Casting the Magnesium Powertrain Components

In Task 4, dies and patterns for the magnesium engine components will be built using designs based on fill and solidification models. The magnesium components may require some design alterations to incorporate new knowledge about the engine, the alloys, or the fill and solidification modeling results. Thus, all aspects of this task will be carefully reevaluated before proceeding with die and mold construction. The cast parts will be subjected to dimensional validation, X-ray inspection, and leak testing (following machining). As in Task 1, casting results will be thoroughly documented to extract and preserve as much information as possible about the behavior of the alloys. The machining experiences will also be documented.

Task 5—Validation Testing of the Assembled Powertrains

The castings from Task 4 will be assembled into complete powertrains and dynamometer tested to validate the design, performance, and durability of the components. All tested parts will be torn down for inspection. OEM consensus on all aspects of

testing and posttest analysis will be achieved. A final report containing these results will be produced.

Task 6—Completion of the Magnesium Alloy Property Database—Excised Specimens

The property database developed in Task 1 was based on cast specimens. Task 6 will yield a thermo-mechanical property and corrosion database for the magnesium alloys chosen for casting the engine components. In addition, the specimens will be excised from the cast components and tested. This will yield "actual" properties of the alloys and is expected to be very helpful in the long run to the design community. It is possible that the test matrix comprising the database will be changed or expanded to comprehend additional information that is found to be necessary. The results of Task 6 are likely to identify more areas of technical gaps and specific needs for scientific research, thereby furthering the objectives of Task 3.

Summary

The MPCC project is an aggressive attempt to address key concerns regarding the future prospects for a magnesium-intensive powertrain. Upon completion of the project, in addition to addressing these concerns, additional scientific and economic implementation barriers, if any, will have been identified, and programs to overcome the scientific barriers will have been undertaken by qualified U.S. universities and laboratories.

Acknowledgements

The author thanks his colleagues at Ford, DaimlerChrysler, and General Motors for their support in the development and implementation of this project. The active participation of all of the non-OEM companies, Tables 2–5, who are part of this project both enables the project and makes accomplishing the project goals a stimulating and enjoyable activity. Their commitment and support and the support of DOE is gratefully acknowledged.

Table 2. Alloys, casting houses, and recycler participants in the Magnesium Powetrain Cast Components Project

Magnesium alloys	Casting	Recycling
Australian Magnesium Corp.	Eck Industries	Amacor
Dead Sea Magnesium	Gibbs Die Casting	
General Motors	Hayes-Lemmerz International	
Hydro Magnesium	Intermet	
Noranda Magnesium	Lunt Manufacturing	
Solikamsk Magnesium Works	Meridian Technologies	
VSMPO-Avisma	Nemak, S. A.	
	Spartan Light Metals Products	
	Thixomat	

Table 3. Tooling, testing, and modeling participants

Tooling	Testing	Modeling
Becker CAD CAM CAST	Amalgatech	EKK
Delaware Machinery and Tool	CANMET Materials Technology Lab	Flow Science
EXCO Engineering	Climax Research Services	Magma Foundry Technologies
H. E. Vannatter	Quasar International	Technalysis
	Westmoreland Mechancial Testing and Research	ESI—Group

Table 4. Design, fasteners, and gasket participants

Engine design	Fasteners	Gaskets
Magna Automotive TESTING	Ribe	Victor Reinz

Table 5. Coolants, coatings, and association participants

Coolants	Coatings	Associations
Ashland/Valvoline	Henkel Surface Technologies	IMA
Chevron/Texaco	Keronite	NADCA
Honeywell International		
Intac Automotive Products		

E. Low-Cost Titanium Evaluation

Principal Investigator: Curt A. Lavender
Pacific Northwest National Laboratory
Richland, WA 99352
(509) 372-6770; Fax: (509) 375-4448; e-mail: curt.lavender@pnl.gov

Technology Area Development Manager: Joseph A. Carpenter
(202) 586-1022; fax: (202) 586-1600; e-mail: joseph.carpenter@ee.doe.gov
Field Technical Manager: Philip S. Sklad
(865) 574-5069; fax: (865) 576-4963; e-mail: skladps@ornl.gov

Participants:
Stanley Abkowitz, Dynamet Technology, Inc., Eight A Street, Burlington, MA 01803
Lance Jacobsen, International Titanium Powder, Inc., 20634 W. Gasken Drive, Lockport, IL 60441
Russell H. Jones and David S. Gelles, Pacific Northwest National Laboratory, Richland, WA 99352

Contractor: Pacific Northwest National Laboratory
Contract No.: DE-AC06-76RLO1830

Objectives

- Use Dynamet Technology's standard commercial powder methallurgy (PM) practice to evaluate the properties of compacts made from a low-cost titanium powder from International Titanium Powder, Inc. (ITP). Determine the tensile properties of compacted material and sintering behavior of both commercially pure titanium and Ti-6Al-4V alloy produced by addition of a master alloy.
- Investigate alternate powder and melt processing methods for low-cost titanium materials.

Approach

- Receive and evaluate eight lots of powder (about 5 lb each) from ITP.
- Process samples using Dynamet Technology's CHIP PM technology, consisting of cold isostatic pressing (CIP) of the powder into green bars and then vacuum sintering and hot isostatic pressing (HIP). The first samples were produced using Dynamet Technology's typical commercial practice.
- Examine the fracture surfaces of test specimens under a low-magnification microscope. The fracture surfaces were then examined by scanning electron microscopy (SEM).
- Perform wet chemical analyses of the powders and test bars.
- Conduct auger electron spectroscopy (AES) on the ITP powder to identify the location of the sodium on the powders.
- Conduct transmission electron microscopy (TEM) on compacted material to identify the location of sodium in the material and to identify other possible sources of embrittlement.
- Conduct in situ AES analysis of a fracture surface to determine the location of sodium or embrittlement elements on the fracture surface.

Accomplishments

- Successfully produced at Dynamet Technology near-net-shape components from ITP powder, showing that ITP powder is amenable to PM processing. For optimum properties in the sintered compact, the PM process parameters used for the ITP powder may be different from those used for conventional powders because of the characteristics of the powder.
- Concluded that the results strongly suggest that residual sodium may be responsible for, or at least contributes to, the swelling and embrittlement of the PM product. Analyses of fracture surfaces indicate the presence of complex oxides consisting of titanium dioxide and sodium oxide in combination with other constituents.
- Reviewed the results of this evaluation with ITP and provided feedback needed for process modifications to produce powder more suitable for PM products.

Future Direction

- Evaluate sinterability of powders produced in the pilot plant at ITP.
- Evaluate methods for reducing the sodium content of the ITP powders by chemical washing or thermal treatments prior to or during the sintering cycle.
- Continue evaluations to determine the cause of the low ductility of compacted material produced with ITP powder.
- Evaluate alternate low-cost titanium feedstocks for powder or melt processing to wrought products.

Introduction

An automobile design trend that has received much attention has been the reduction of vehicle mass. Reducing mass can improve both performance and fuel economy. While design changes can play a large role in reducing mass, large reductions ultimately will require the substitution of higher specific strength/stiffness materials in place of carbon steel. Primary contenders in this race are high-strength steels, aluminum, and fiber-reinforced polymer composites. One material, not on this short list, but which could provide further reductions, is titanium. Although titanium is light and strong, its role in the automobile has been almost nonexistent because of its exorbitant price. This high price is a direct result of the current production route, the Kroll process, which is time-consuming, energy-, capital-, and labor-intensive, and batch-based.

However, new technologies are emerging that may change the characteristics of the titanium market. In particular, these technologies may reduce the titanium price sufficiently to allow it to compete in high-volume markets, possibly even automotive. This project examines the PM behavior of titanium powder produced by a new process being developed by ITP.

Project Deliverables

- Evaluate the PM characteristics of ITP powder using Dynamet Technology's standard CIP/sinter/HIP processes (CHIP).
- Prepare compacted samples for physical and mechanical property evaluations using Dynamet Technoloy's standard CHIP processes.
- Provide feedback to ITP on modifications to powder properties for improved sinterability.

Approach

Eight lots of powder were received from ITP during a 12-month period. The samples

were processed using the CHIP process technology consisting of CIP of powder into green bars, then vacuum sintering and HIP. The first samples were produced using Dynamet Technology's typical commercial practice, as follows:

- CIP the powder in a cylindrical elastomeric mold at 55,000 psi to form a cylindrical bar in the green condition;
- vacuum-sinter the green bars at 2250°F for 2.5 h at 10^{-5} torr; and
- HIP the sintered bar at 1650°F for 2 h at 15,000 psi in argon.

Dynamet Technology's standard manufacturing procedure routinely produces full-density CP titanium and Ti-6Al-4V components with mechanical properties equivalent to conventional wrought products. The density of the bars was measured in the green condition dimensionally and by the Archimedes method after each subsequent processing step.

The ITP powder exhibited a different behavior with Dynamet Technology's standard process than conventional powders. In some instances, the green-pressed bars would swell during vacuum sintering. At other times, the bars would consolidate to full density while exhibiting low ductility during tensile testing; (i.e., the bars were brittle). Time and temperature for the sintering cycle was altered in an attempt to reduce the swelling observed in test bars. None of the processing modifications resulted in any significant improvement. The evaluation then focused on determining the causes of the swelling and embrittlement. The fracture surfaces of test specimens were examined under a low-magnification microscope. The microstructure consisted of isolated brittle zones and dispersed porosity. The fracture surfaces were then examined by SEM. In addition, wet chemical analyses of the powders and test bars were performed.

PM Powder Processing Results

Powder Characteristics

Eight lots of powder were received from ITP, varying in weights from a 0.5 lb to 5 lb. The powder samples had a dull gray appearance and contained agglomerated particles. Figure 1 shows the appearance of the as-received ITP powder at 20X and 250X as well as an SEM image at 2500X. These micrographs show the powder to be highly porous and spongy.

The as-received powder was milled and then sieved to –100 mesh. The tapped density of the powder was 16 to 18%. For CIP consolidation, a tap density of about 25% is desirable. The low tap density of ITP powder is attributed to its highly spongy morphology.

Chemical Analysis Results From Test Bars

The results of chemical analyses for samples of ITP powders and CP titanium products manufactured from ITP powder are presented in Table 1, along with specifications of various grades of wrought CP titanium and a comparative baseline of Dynamet Technology's typical powder metal. Table 2 shows results for Ti-6Al-4V with ITP along with the comparative specifications for Ti-6Al-4V alloy.

Oxygen levels in the specimens made using ITP powder were higher than those found in the as-received ITP powder and higher than allowed for CP titanium Grade 3. The Dynamet Technology sample, in contrast, showed oxygen levels at about the same level before and after processing. The increase in oxygen levels in the ITP material probably resulted from oxygen pickup during the milling of the ITP powder. Milling fractures the powder, exposing fresh surfaces that oxidize when exposed to the air. In addition, a –100 mesh fraction of the ITP powder was used for PM processing. The

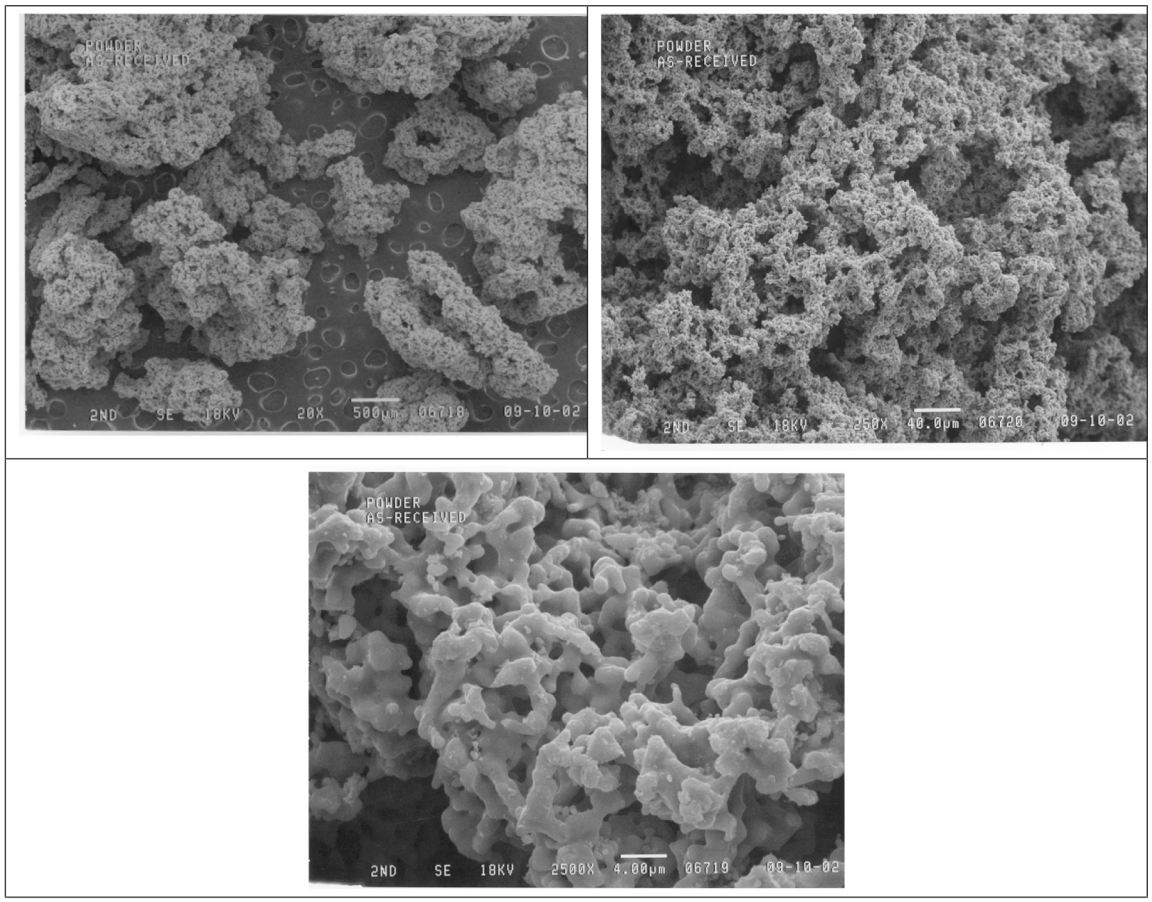

Figure 1. SEM micrographs of as-received powder at 20X (left), at 250X (right) and at 2500X magnification (bottom). These powders are highly porous and spongy.

Table 1. CP titanium specifications and results of processed bars

Element	ASTM B348 bar, billet Gr2 Gr3 Gr4			Dynamet Technology type PM	Sintered bars R-3402 and R3432	Tensile samples R-3395, 3402, and 3407
Ti	rem	rem	rem	rem	rem	rem
O	0.25	0.35	0.40	0.30	0.44 and 0.41	0.363
N	0.03	0.05	0.05	0.05	0.067 and 0.032	0.015
C	0.08	0.08	0.08	0.10	0.066 and 0.045	0.007
H	0.02	0.02	0.015	0.02	0.0007 and 0.0007	0.001
Cl	n/a	n/a	n/a	0.04		
Fe	0.30	0.30	0.50	0.40		0.01
Na	n/a	n/a	n/a	n/a	.074	
Si/Ni/Sn/Al						0.02/0.01/0.02/0.02
Others each Others total	0.10 0.40	0.10 0.40	0.10 0.40	0.10 0.40		

Table 2. Ti-6Al-4V alloy specifications and results

Element	ASTM B-348Gr5	Dynamet Technology specifications		Ti-6Al-4V material using ITP powder			
		Current powder	Hunter fines	B-3403	B-3408	B-3418	B-3419
Ti	rem	rem	rem				
Al	5.5–6.75	5.5–6.75	5.5–6.75		3.41		
V	3.5–4.5	3.5–4.5	3.5–4.5		2.57		
O	0.25	0.30	0.20	0.294	0.337	0.37, 0.39	0.40, 0.35
N	0.03	0.05	0.05		0.015		
C	0.08	0.10	0.10				
H	0.0125	0.015	0.015		0.0007		
Cl	n/a	0.04	0.13		0.01		
Fe	0.30	0.40	0.40				
Si							
Na	n/a	n/a	0.10		0.08		
Others each	0.10	0.10	0.10				
Others total	0.40	0.40	0.40				

smaller particles in –100 mesh powder contain more surface area and, thus, have a higher oxygen content then would be found in the as-received lot. The amount of carbon in the samples varied considerably between lots of powder and between the test bars. The level of sodium in the samples is about the same before and after processing as shown for sample R-3432.

Tensile Test Results

Test bars 0.75-in. diameter by 6-in. long were produced from each of the five batches of ITP powder. In addition, master alloy powder with the composition 60% aluminum and 40% vanadium was added to three batches in the proper proportions to produce Ti-6Al-4V test bars.

The density of the bars after sintering and HIP varied considerably from bar to bar with many bars swelling during sintering. While the test bars that Dynamet Technology produces are usually 94–97% dense after sintering, the ITP bars ranged from open porosity to 94% dense. The Ti-6Al-4V bars had a greater tendency to swell. Roughly two-thirds of these bars had lower density after sintering than before.

Tensile testing was conducted on specimens machined from bars that measured 100% density after HIP. A test bar produced using Dynamet Technology's standard CP titanium (produced by the standard CHIP process) was included as a witness bar during processing and as a control sample for comparison purposes. Tensile tests were conducted in accordance with ASTM Standard E-8.

The test material produced with the ITP powder had tensile and yield strengths in the specified range for CP titanium and Ti-6Al-4V. However, both materials were brittle, failing at elongations of only 2.2 to 2.7%. In contrast, the control sample processed by Dynamet Technology's standard process exhibited an elongation of 22%. The Ti-6Al-4V made with ITP powder failed at 1% elongation, while the Ti6Al4V control sample processed by Dynamet Technology's standard process exhibited 15% elongation.

Analyses of the fracture surfaces using SEM were conducted on the failed CP titanium (R-3395, Table 2) and Ti-6Al-4V (B-3396, Table 2) tensile specimens. Under low magnification, both samples had shown an area of brittle failure toward the center surrounded by material that failed in a

ductile mode. SEM, shown here by the micrographs in Figure 2, showed that the ductile area had a dimpled structure with microvoids dispersed throughout the structure. This structure is typical of ductile fracture surfaces. There were no signs of any particulates or anomalous phases.

The areas of brittle failure showed transgranular cleaved surfaces (Figures 3 and 4). Again, there were no signs of any particulates or anomalous phases. SEM did show that carbon and oxygen were present at the fracture surface. Fine pores, about 0.25 µm in diameter, are present in both samples. The pores were present on the surfaces of the cleaved grains (Figures 5 and 6).

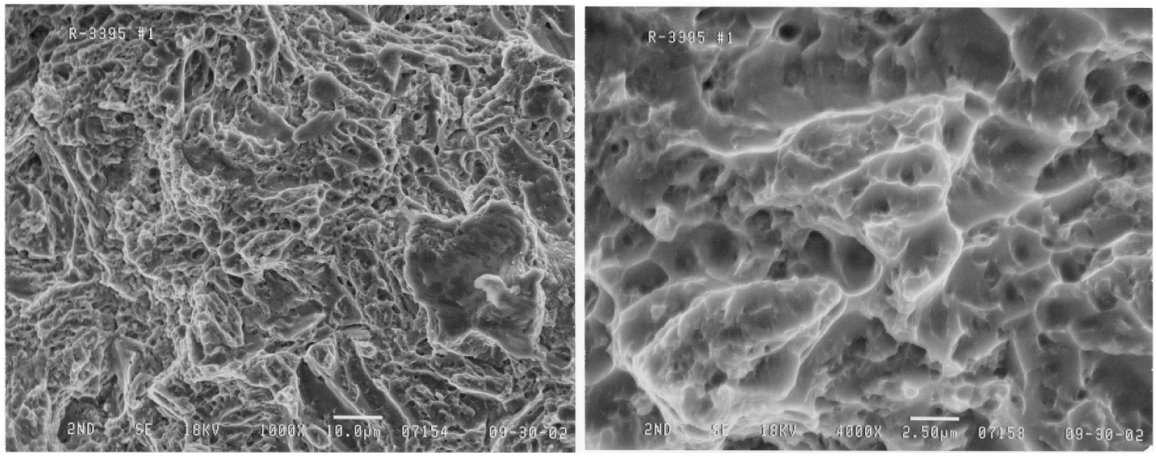

Figure 2. Ductile region of tensile failure in ITP CP titanium test bar R-3395 S/N 1 (1000X and 4000X).

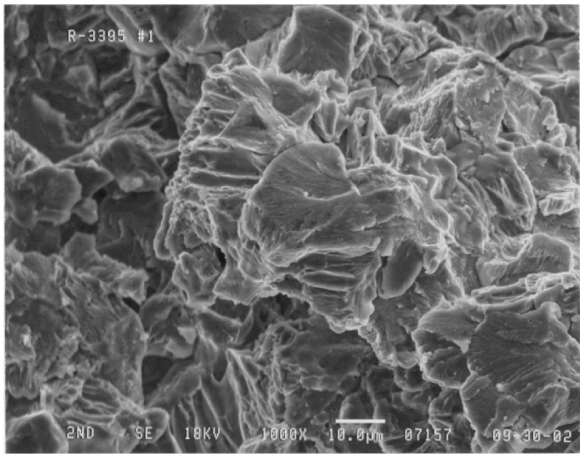

Figure 3. Brittle, transgranular failure in ITP CP titanium test bar R-3395 S/N 1 (1000X).

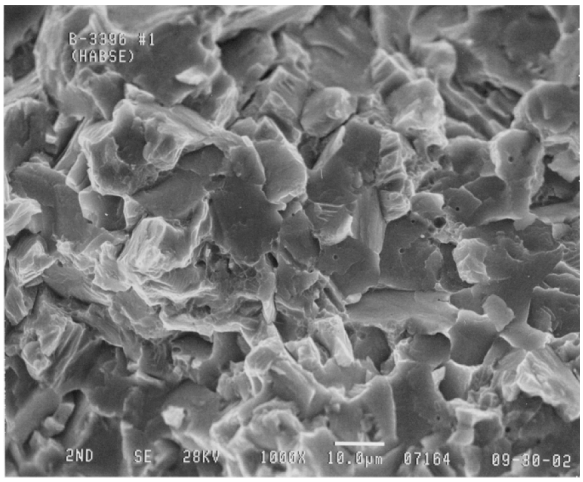

Figure 4. Brittle, transgranular failure in ITP Ti-6Al-4V test bar B-3396 S/N 1 (1000X).

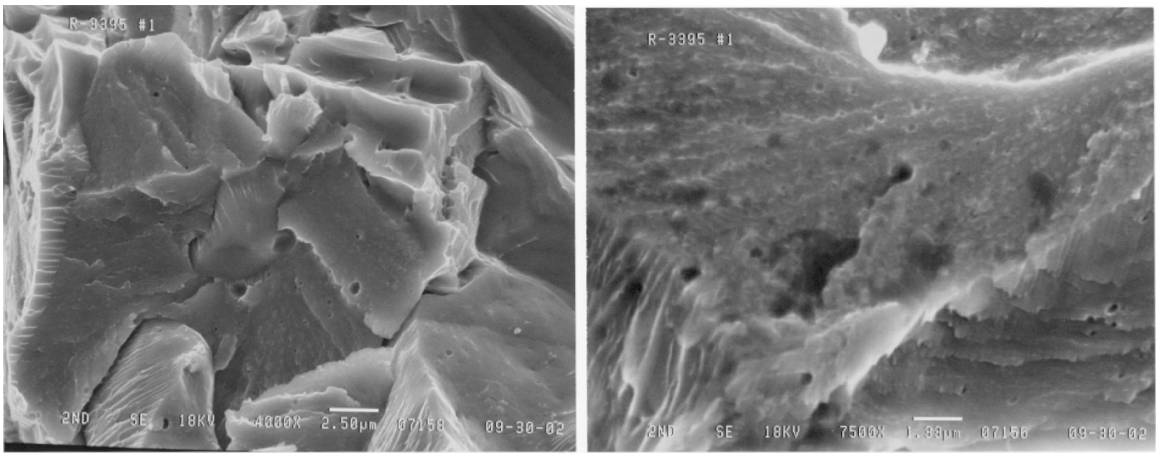

Figure 5. Cleaved grains in ITP CP titanium show very fine pores (4000X and 7500X).

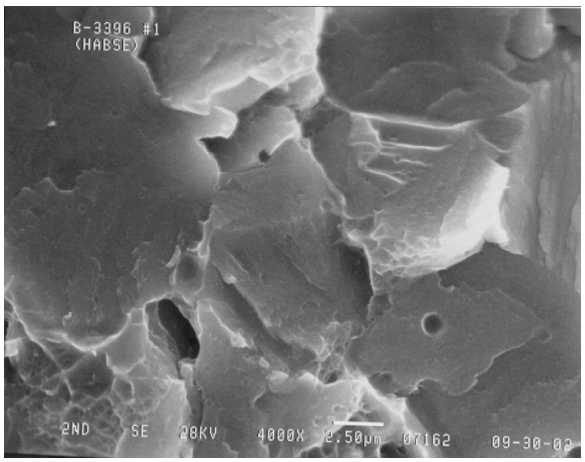

Figure 6. The fine pores were also found in cleaved grains in the ITP Ti-6Al-4V alloy (4000X).

Microchemical Analysis for Location of Sodium or Other Causes of Embrittlement

A tested tensile specimen made from ITP produced powder was evaluated using metallographic techniques, analytical electron microscopy, and surface spectroscopy techniques in order to provide an explanation for degraded tensile properties in comparison with powders from other sources. Electron microscopy demonstrated that the microstructure included a low dislocation density and a moderate density of nonuniformly distributed pores often containing sodium. AES analysis of a fracture surface produced *in situ* in the spectrometer vacuum system showed a uniform distribution of sodium on all surfaces, including microvoid coalescence and brittle surfaces. Electron beam microprobe analysis of ITP powders showed the presence of sodium as small particles on the surface of the titanium powders.

An optical micrograph of the as-electropolished TEM sample is shown in Figure 7. It reveals the presence of porosity on a fine scale. Pores as large as 1 to 2 µm can be identified.

SEM imaging gave clearer examples of the larger pores in the TEM sample. A series of images with increasing magnification is provided in Figure 8, showing (a) the TEM disk with a large perforation on the left; (b) at intermediate magnification showing the microstructure; and (c) examples of the pores. Note that some pores can be nonspherical and that an unusual halo of small pores was found. An estimate of the pore volume fraction was obtained later from Figure 12 at 0.46%.

The microstructure was also examined in TEM. Examination showed a moderate dislocation density, presumed to be a result of tensile testing, and a fine distribution of nonuniformly distributed pores. Examples at lower magnification are provided in Figure 8 and at higher magnification in Figure 9. Regions in Figure 9 show dislocation structure in the form of loose parallel lines in some grains. Several examples of subgrain structure can also be found that form nonequilibrium grain boundary junctions with

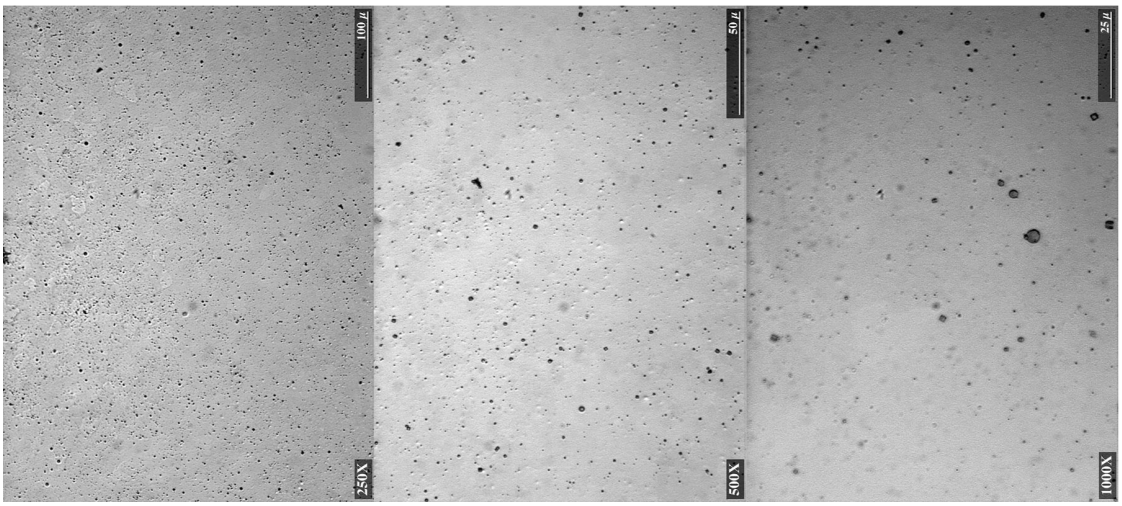

Figure 7. Optical metallography images of an electropolished surface of R-3395 at increasing magnification from left to right.

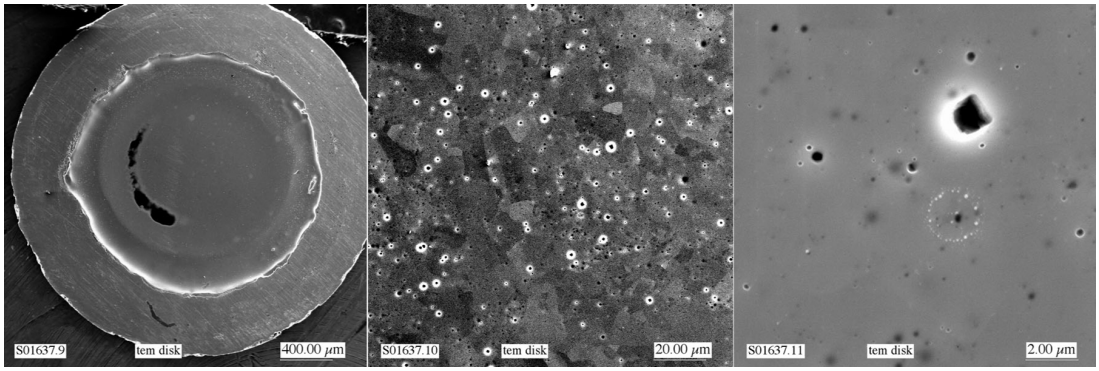

Figure 8. SEM images of the as-polished TEM disk at increasing magnification from left to right.

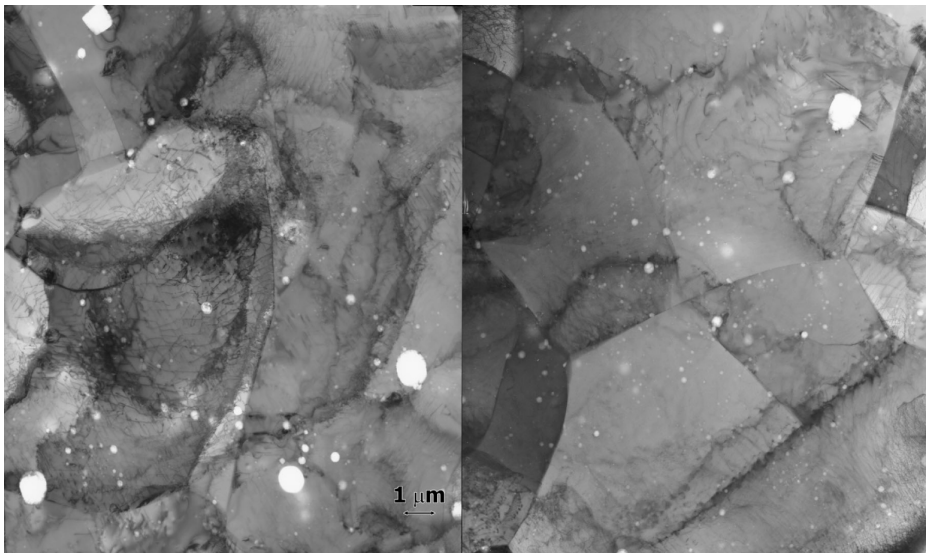

Figure 9. TEM showing microstructure and pores in compacted CP titanium made with ITP powder.

angles at 90º and 180º. Figure 10 indicates that pore distributions can be nonuniform, and pore sizes can be quite small. Figure 10(*b*) is imaged in an underfocused condition so that the pores appear dark, whereas the reverse applies to Figure 10(*a*). Smaller pores are on the order of 10 nm in diameter.

Analytical microscopy demonstrated that several of the pores contained sodium, but no composition segregation at grain boundaries could be found. An example of composition profiles is provided in Figure 11 with a

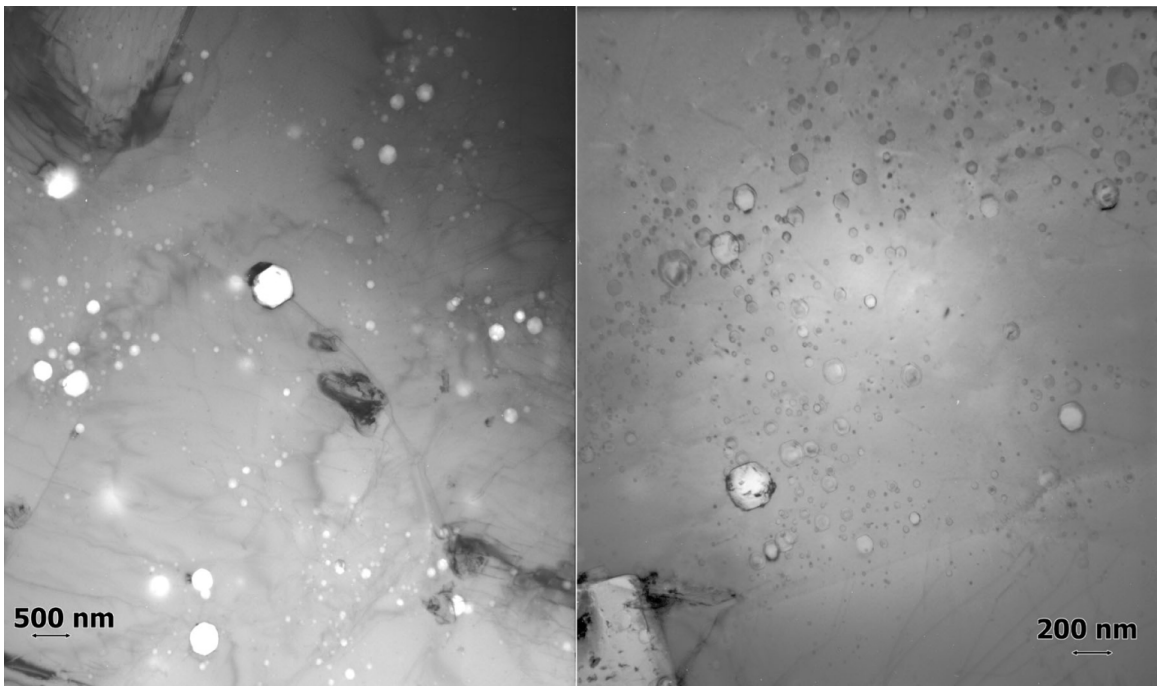

(*a*) (*b*)

Figure 10. Pore distributions at higher magnification using underfocus on the right (*b*) to illustrate the voids.

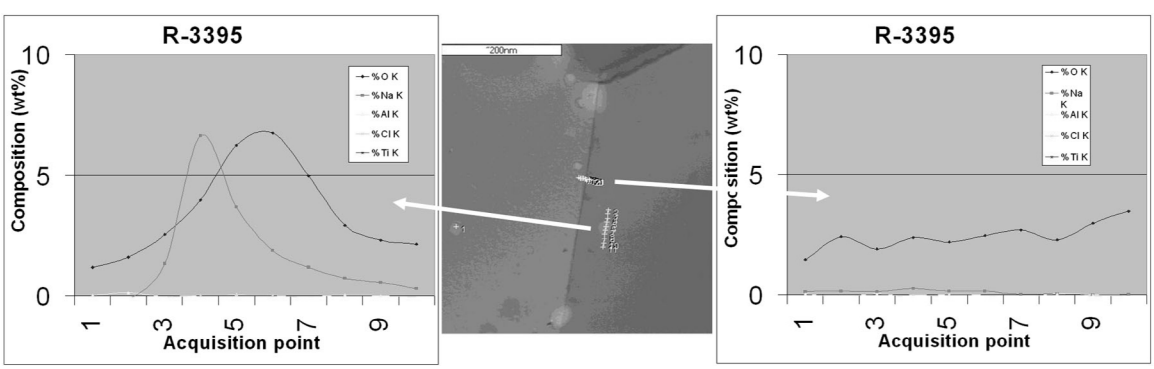

Figure 11. Composition profiles in the vicinity of a pore and a grain boundary.

pore containing sodium in Figure 11 (left) and a grain boundary traverse in Figure 11 (right). The image in the center defines the locations for the composition data points. The composition profile for the pore shows a shift in peak response for sodium and oxygen. This is expected to be due to the sensitivity of oxygen measurements with surface undulations. No significant compositional variation can be identified across the grain boundary. Many similar results were obtained for other boundaries, including several intended to sample grain boundary triple points. Boundary profiles showed only occasional enhancement of sodium, generally associated with a nearby pore. Therefore, the porosity contains sodium.

An *in situ* fracture of sample R3432 was produced using a notched cylindrical sample fractured at –197°C. The fracture was completed within the ultrahigh vacuum chamber of a PHI 680 AES with the goal of determining whether any microchemistry on the fracture surface could be traced back to the low-ductility fracture surfaces. Examples would be the presence of a mixed oxide of Na, Ti, and O, or Na segregation on interfaces. The results of sodium and oxygen were roughly equal on all fracture features, including brittle cleavage surfaces, microvoid coalescence, and other shear-type features. It was concluded that the fracture exposes the sodium-filled pores and that surface diffusion results in a uniform coverage before the first spectra could be taken, which is about 1 h. Examples of the fracture surfaces and AES analysis are given below in Figures 12 and 13.

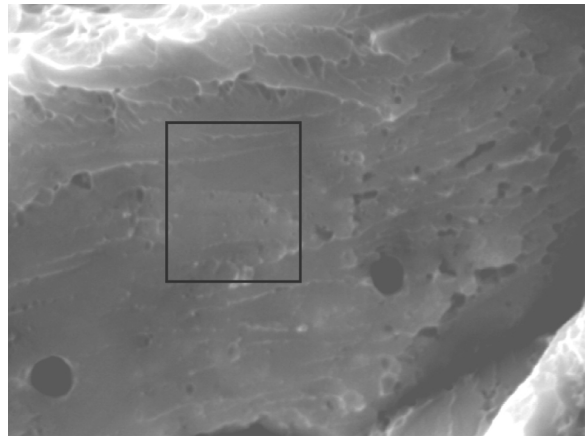

Figure 12. AES analysis of brittle, cleavage surface of CP titanium made with ITP powder: oxygen: 6.7% and sodium: 17.3% in marked area.

References

1. S. Abkowitz, S. M. Abkowitz, H. Fisher and P. Schwartz, Final Report of Contract No. 409117AU7, *Low-Cost Titanium Evaluation*, Dynamet Technology, Inc., November 29, 2002.

2. D. S. Gelles and R. H. Jones, *Report on Evaluation of Low Cost Titanium Powders; Microstructural Analysis*, February 6, 2003.

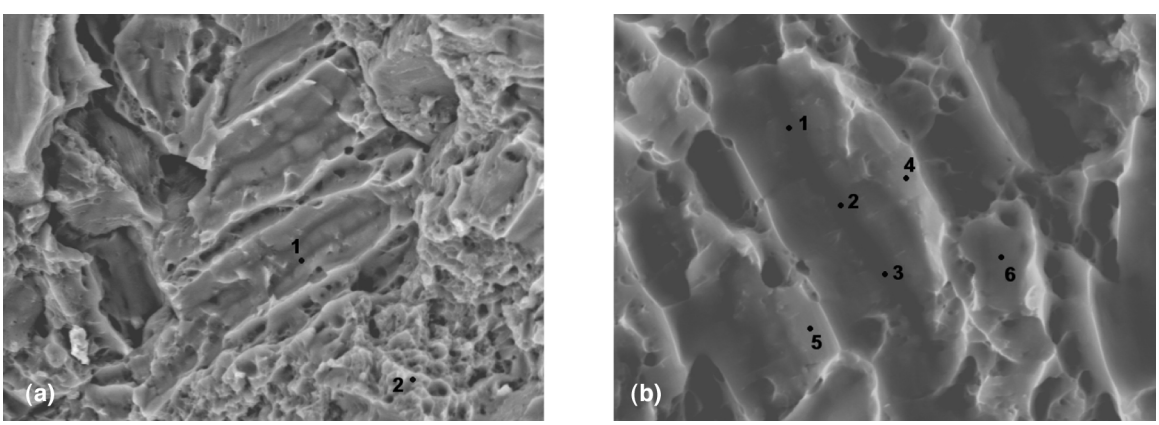

Figure 13. AES analysis of CP titanium sample made with ITP powder: oxygen concentration 7.6 to 9.1% at locations (*a*) 1, 2 in. and (*b*) 1–6 in. sodium concentration ranged from 21 to 27% at the same locations.

F. Structural Reliability of Lightweight Glazing Alternatives

Principal Investigator: Moe Khaleel
Pacific Northwest National Laboratory
P.O. Box 999/K9-95, Richland, WA 99352
(509) 375-2438; fax: (509) 375-6605; e-mail: moe.khaleel@pnl.gov

PPG Project Manager: Rick Rueter
PPG Industries, Inc., Glass Technology Center
P.O. Box 11472, Pittsburgh, PA 15238
(412) 820-8731; fax: (412) 820-8705; e-mail: rueter@ppg.com

Visteon Project Manager: Mike Brennan
Visteon Glass, 17333 Federal Drive, Suite 230, Allen Park, MI 48101
(313) 755-1879; fax: (313) 755-7485; e-mail: mbrenna1@visteon.com

Technology Area Development Manager: Joseph A. Carpenter
(202) 586-1022; fax: (202) 586-1600; e-mail: joseph.carpenter@ee.doe.gov
Field Technical Manager: Philip S. Sklad
(865) 574-5069; fax: (865) 576-4963; e-mail: skladps@ornl.gov

---

Contractor: Pacific Northwest National Laboratory
Contract No.: DE-AC06-76RL01830

Objectives

- Optimize glazing systems for cars of the future by decreasing sound transmission while maintaining structural rigidity.
  - Reduce sound transmitted through sidelights by 6 db by determining the effect of sidelight shape on sound transmittance, investigating sound-dampening materials for operating sidelight glazing, and quantifying the influence of alternate materials (e.g., laminated glass, bilayer glass) on sound attenuation.
  - Maintain the level of structural integrity while reducing glass thickness by validating the structural rigidity model for various types of urethane used in fixed glazing systems and by expanding/combining existing models to test various alternative constructions and glazing systems for side, rear, and roof windows.
- Reduce vehicle weight through alternate or thinner vision panels and/or by reducing the heat load transmitted through the glass. The goal is to improve the fuel economy of a car by requiring 30% less glass weight.
- Reduce side, rear, and potential roof window glass weight while maintaining acoustics and minimizing price increases.
  - Consider several material options, including laminated glass, cast-in-place pseudo-laminated glass, and bilayer materials.
  - Enhance fuel economy from reduced solar energy transmission.
  - Reduce solar energy transmission through glass by using absorbing substrates and reflective coatings.

— Quantify gas mileage improvement opportunities from improvement in solar energy transmission.

Accomplishments

- Fabricated new lightweight windshield and side-body glasses that are 30% lighter than conventional glazing systems.
- Fabricated new glass with polyvinyl butyral (PVB) thickness ranging from 0.5 to 0.76 mm.
- Developed experimental plan for modeling predictions, equipment, and experimental measurements of sound transmission losses in newly used interlayer materials.
- Determined the contributions of the newly used polymeric interlayer materials reduction in infrared (IR) transmittance.
- Designed and fabricated new tooling for ultraviolet (UV) curing of interlayer laminating resin.
- Designed tooling for laminating complex-shaped automotive side windows using newly developed injection technique.

Future Direction

- Develop lightweight side-door glass.
- Investigate the strength and thickness of new polymeric interlayer materials on overall windshield/side-door strength and performance.
- Investigate the overall thermal behavior based on the new interlayer materials, including the effect of the laminated side-door glass.
- Characterize the sound transmission loss of the new lightweight laminated glass.
- Verify and extend the predictive sound transmission loss models to investigate the effect of the new polymeric materials.
- Complete the modeling of the acoustical response of glass.
- Fabricate newly designed tooling for complex automotive side-window shapes and laminate with new interlayer materials.

Introduction

This project is a cooperative research and development agreement (CRADA) between the U.S. Department of Energy, Pacific Northwest National Laboratory (PNNL), Visteon Automotive Systems (Glass Division), and PPG, Inc., which was started in June 2002.

The project will evaluate designs for optimized glazing systems to be used in cars of the future and will work to achieve the goals of FreedomCAR. The primary objective of the project is to reduce vehicle weight, improve fuel economy, and reduce vehicle emissions. However, to achieve these goals, it is necessary to consider the needs for high levels of structural reliability, competitive manufacturing costs, and passenger comfort from the standpoints of minimal acoustical noise levels and controlled interior temperatures. Energy savings will come from reducing weight by using thinner glazing. Prior studies at PNNL have shown a potential for 30% reductions in weight from thinner glazing. Energy savings will also come from reducing interior heat loads that, in turn, will reduce the demand for air conditioning. The evaluation of alternative glazing concepts will also seek means to improve

acoustical characteristics that will minimize interior noise levels while maintaining glazing at minimal thickness and weight levels.

Lightweight Window Manufacturing

New lightweight window samples were fabricated using 1.6-mm and 2.3-mm glass plies (a conventional automotive glass ply has a thickness of between 2.4 and 2.6 mm; total windshield thickness is usually over 5.2 mm). The new lightweight samples were formed and laminated at PNNL using several different polymer interlayers for comparison.

New lightweight laminated side glass was fabricated using 1.6-mm and 2.3-mm plies. These new window glass samples were constructed:

- 1.6-mm glass, 1.8-mm polymer interlayer, and 1.6-mm glass
- 2.3-mm glass, 0.60-mm polymer interlayer, and 2.3-mm glass (see Figure 1).

During the fourth quarter of FY 2002, researchers completed the initial conceptual design for injection molding of cast-in-place pseudo-laminates. Initial feasibility studies conducted showed a wide range of flexibility with a variety of polymeric resin systems and viscosities that could be used for laminating the two glass plates. A database on PVB alternatives for the injection molding process was established by collecting information on clear polymer systems that could be used as potential interlayer materials. The database is based on commercially available materials.

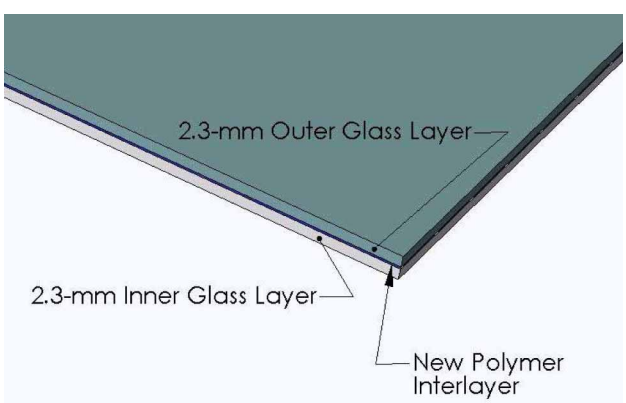

Figure 1. Typical window laminate construction.

The evaluations of properties and cost were also addressed. Three of the commercially available materials were altered for specific characteristics in curing and hardness. A table listing specific critical properties was created, and the properties were ranked by relative importance such as impact, tear resistance, and optical transmission. The database of materials was then compared with PVB as the baseline material. Because the optical requirements for the sidelights are not as stringent as those for the windshield, other materials may prove to be more attractive and cost-effective. Other properties are also less aggressive in the ANSI Standard for automotive sidelights, so the comparisons of PVB in properties are conservative. The weighted comparison approach will help determine the direction in which alternative PVB side lamination needs to focus relative to the critical properties.

Material Selection for PVB Alternatives

The material selection matrix evaluated six different classes of materials against the baseline PVB. The house of quality evaluation matrix compared 15 different criteria in 6 different categories. Table 1 shows how the matrix compares the materials against each other with each critical property and its ranking. The materials are then multiplied times the ranking and then compared against the total.

There were 13 materials evaluated, and 8 were selected to be placed into the House of Quality matrix. The materials selected were broken down into six polymeric systems, such as polyurethanes, acrylics, epoxies, silicones, polyesters, and phthalates.

Material Down-Selection

The material down-selection was based on the matrix totals and intuition. Sound transmission loss is an important criteria, but it is difficult to find data on commercially available materials. Stress relaxation data are currently being collected on the down-selected material for use in the acoustic

Table 1. Sample table of weighted material comparison matrix

Category	Measured criterion	Ranking (low 1–9 high)	Material 1	Material 2
Physical properties	Viscosity	8	5	9
	Color	9	5	8
	Tensile strength	8	5	7
Mechanical properties	Tensile modulus	5	5	9
	Flexural modulus	5	5	8
	Elongation at failure	7	5	7
	Hardness	5	5	7
	Tear resistance	8	5	6
Optical properties	Refractive index	9	5	9
	Transmittance	9	5	8
	Haze	9	5	6
Thermal Properties	Coefficient of thermal expansion	6	5	7
	Thermal conductivity, k	6	5	5
	Shrinkage	5	5	6
Other	Cycle time	8	5	9
	Total		535	798

modeling of the sound transmission loss equipment. However, the materials characteristics after lamination offer different sounds based on a qualitative tapping showing how much dampening is going through the laminate. Experiments are planned for two or three down-selected materials. The leading candidates for down selection are polyurethane, acrylic, polyester, and epoxy. Several tests have been conducted based on the SAE Z26.1 criteria for side-window laminations.

Injection Process Validation

A clear polycarbonate fixture was designed and built for observing flow behavior in 12-in. by 12-in. glass panels. Figure 2 shows the test fixture design and

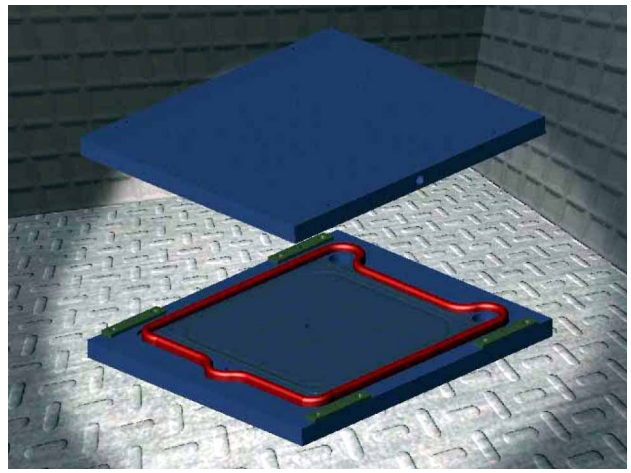

Figure 2. Test fixtures for injection process validation.

how the glass plates are held against the fixture surface using vacuum with a separation of 0.5-mm and 0.75-mm gaps for resin filling.

Initial flow studies used 8-in. head pressure to flow material the length of the plates and tooling. The viscosity changes the behavior of the flow front and the time to fill.

A viscosity of 123 cps had a fill rate of 14 in./min. A viscosity of 3000 cps had a fill rate of 1.4 in./min. Testing shows that a 200-cps viscous material injected at 10 psi fills the same areas and distance as the previously measured data in less than 5 s, and a 3000-cps viscous material fills in 15 s.

These fill rates equate to filling a side window on an SUV of roughly 650 in.^{2} in 25 to 70 s based on their viscosities.

With the validation of the injection process, the focus is currently on cure time of resins. The cure times are being evaluated on temperature and UV curing. Current cure times have been as low as 20–30 min, depending on the chemistry type. A new tool was designed to test cure times using UV curing for polyester and acrylic resins.

Transmittance Testing

Several transmittance tests were conducted on the laminates created in the injection validation process. The transmittance

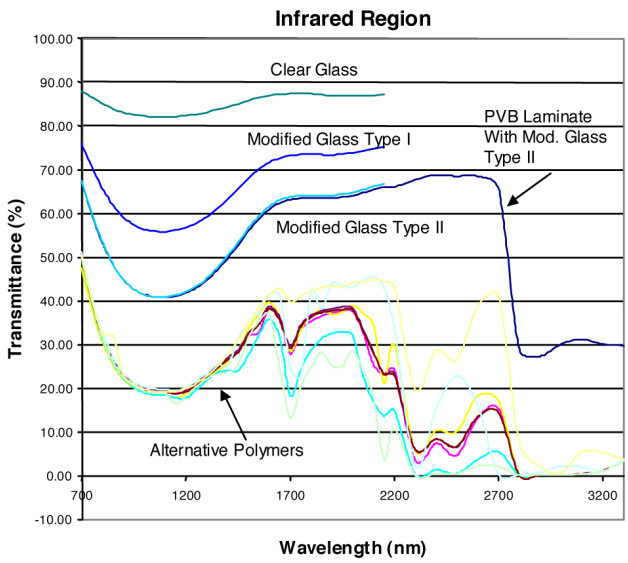

Figure 3. UV-Vis spectrum of various tested polymer systems.

test spectrum in Figure 3 shows all polymeric systems tested ranging from 77–79% with the exception of a material that was marginal at 67%. The UV spectrum shows a decrease of approximately 25% at 370 nm, and the IR spectrum shows a drop of approximately 45% compared to the current PVB interlayer.

Besides transmittance being satisfactory in the initial testing, it was also noted that a higher amount of IR absorption is shown well below the specially formulated glass. These samples were made using the special formulation of glass for UV and IR.

One material was tested using 0.1% Tinuvin P as a UV absorber in the polymer. The UV-Vis spectrum showed a decrease in UV transmittance. The decreased transmittance will also increase the protection of the polymer from UV degradation.

The material can accept higher loadings of the UV absorber up to a limit of yellowing the material. It was also noted that colorants can be added to the polymer system to hide any yellowing effects that may be caused by the UV inhibitor or aging. Other observable options are coated films to control UV, and IR could be embedded with the polymer interlayer.

Structural-Acoustic Study of Laminated Glass using Finite-Element Analyses

To study the structure vibration and acoustic behaviors of the injection-molded laminated glass, we have developed a coupled structural-acoustic modeling procedure using the commercial finite-element code ABAQUS. The typical laminated glass specimen consists of two glass layers and a thin resin layer to replace the traditional polyvinyl butyral layer. Our goal is to use the analytical modeling tool to examine the effects of resin properties on the acoustical performance of the laminated glass specimen.

In our first-phase results, we examined the sound transmission loss (STL) of different glass configurations and different resin properties on the STL of the glass panels. The predicted STL values for laminated glass specimens compare reasonably well with the experimental measurements. In the next phase, we plan to further calibrate the model and use the modeling procedure to determine the appropriate glass construction schemes and resin interlayer properties to meet regulatory or customer requirements on noise reduction of a vehicle structure while, at the same time, minimize the weight of the glass.

To analyze the acoustic chamber with an accurate yet efficient model, we assume that the air layer 1 in. above the top glass surface (top microphone location) experiences incident waves of the same amplitude and frequency. An axisymmetric model is used for simplicity, and the foam supporting the glass boundary is modeled with two-dimensional (2-D) connector elements (see Figure 4). In Figure 4, the air layers (green elements) are modeled with four-node linear acoustic elements ACAX4R, and the glass (blue elements) and the resin layer (red elements) are modeled with four-node bilinear solid elements CAX4R with different material properties. The interfaces between the air

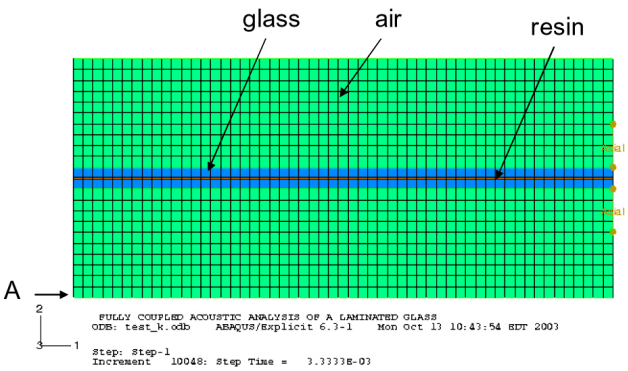

Figure 4. Coupled structural-acoustic finite-element model.

(acoustic elements) and glass (solid elements) are constrained at their abutting surfaces using the *TIE option. The thicknesses of both glass layers are set to be 2.3 mm, and the intermediate resin layer is 0.5 mm thick.

The incident wave comes from the top of the air layer with specified frequency and amplitude. The pressure response of the air at point A, 1-in. below the glass center, is monitored as output of the analyses. Both transient explicit dynamic analysis and steady state dynamics procedures are used, and the pressure results consist of both transient pressure responses and frequency sweep pressure response.

Figures 5(*a*) and (*b*) show the input pressure wave form at the top of the air layer and the output pressure wave form at point A for input frequency of 1000 Hz. As the transient response dies out, the dynamic pressure response at point A has the same frequency as the incident pressure wave frequency.

Steady state dynamic analyses are then performed to calculate the structure response for incident waves of 400 Hz to 8000 Hz. The structural response in terms of pressure amplitude vs incident frequency is then achieved. The values of sound transmission loss (STL) can then be determined using the following equation:

$$STL(dB) = 20\log\left(\frac{p_1}{p_{input}}\right) \quad , \qquad (1)$$

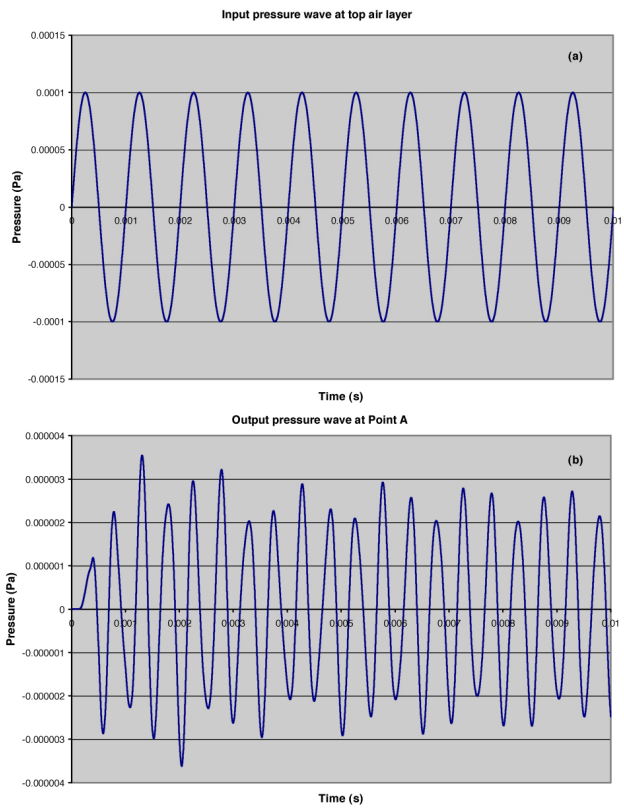

Figure 5. (*a*) Input acoustic wave form of 1000 Hz and (*b*) predicted acoustic wave form: transient behavior.

where p_1 is the response wave amplitude, and p_{input} is the input wave amplitude. Figure 6 shows the predicted STL values for the frequency sweep compared with discrete STL measurement from our experiments. Because

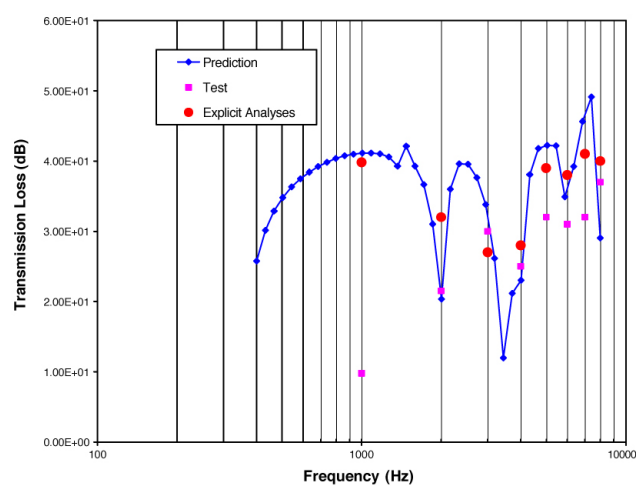

Figure 6. Predicted STL results compared with experimental results.

the system has a natural frequency around 3500 Hz, we observe a dip in STL around 3440 Hz. This is consistent with the experimental findings. The predicted STL values compare reasonably well with the acoustic chamber measurements at frequencies higher than 2000 Hz. For frequencies lower than 2000 Hz, the prediction is higher than measurement.

The next step of our work will be to establish the more realistic boundary conditions to model the acoustic chamber and to obtain better correlation for low-frequency responses between prediction and experiments.

Acoustic Chamber Test Setup

An acoustic chamber was designed and fabricated for testing 12-in. by 12-in. test panels. Figure 7 shows the newly built test chamber. The acoustic chamber is capable of covering the noise spectrum associated with automotive noises.

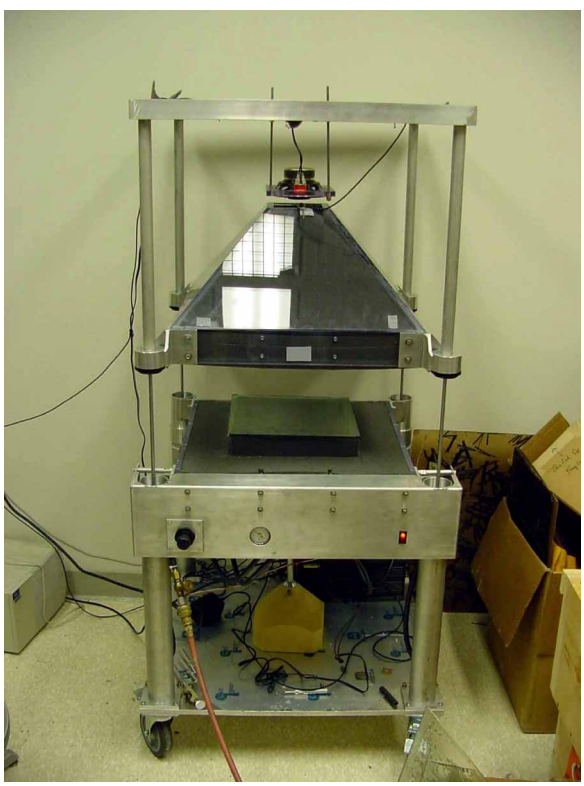

Figure 7. Acoustic test chamber for glass laminations.

The focus frequencies were from 1 kHz to 8 kHz. Comparative testing was initially done showing the difference between each one of the candidate interlayer materials. Figure 8 shows preliminary results of different candidate test materials. The STL was 3–7 db better than the PVB interlayer at different frequency ranges. A model of how modifying the interlayer material could further improve the acoustic properties of the side windows is ongoing.

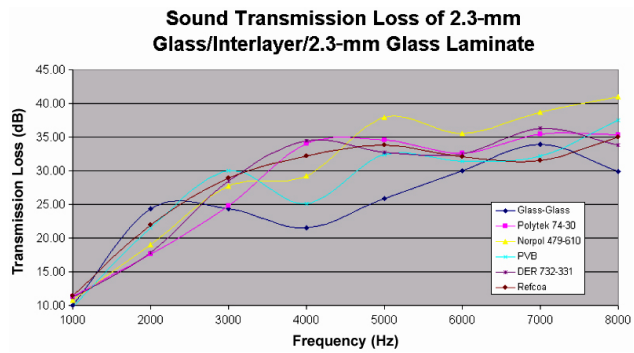

Figure 8. STL comparison of different polymer interlayers.

Ring-on-ring Testing

Comparative ring-on-ring testing was also performed on candidate interlayer materials. Figure 9 illustrates that all materials performed satisfactorily. Qualitatively, all materials bonded well to the glass. During glass fracture, none of the glass material was released from the interlayer. The sample size is too small for a statistical comparison of the PVB properties, but future work will look at different ball-and-dart impact testing.

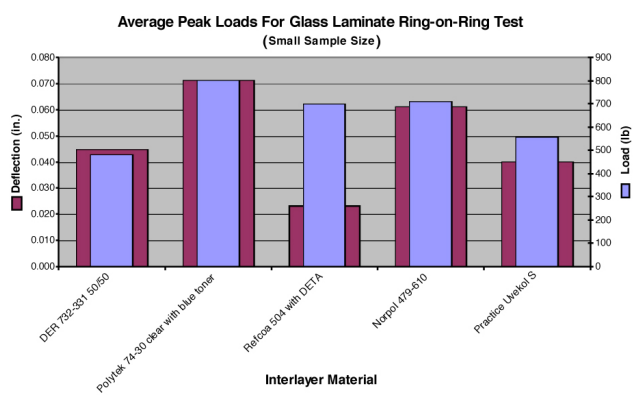

Figure 9. Ring-on-ring data.

Other Testing

PPG is currently testing one set of glass panels that will provide data on how well they hold up to rigorous testing by a leading window supplier. Preliminary testing done was boil testing for 6 h with good results on all candidate materials. Hot and cold testing was done with no delaminations, which PPG will also investigate further.

Future Work

Future work will focus on fabrication of larger automotive side windows and further testing by the glass manufacturer. New tooling for a 650-in.^{2} side window is designed, and materials are in the procurement process. Further, 12-in. by 12-in. testing plates will continue to be made with other interlayer materials and given to PPG for further testing. Other testing will focus on effects of the door slam on the larger windows. The overall mechanical, thermal, and acoustical behavior of the new lightweight glass will be evaluated using both experimental and analytical procedures. Modeling efforts will continue to focus on stone-impact studies and acoustics. Work will also be conducted to enhance and extend the numerical tool for design of lightweight glass to include stresses encountered during the glass fabrication process.

4. POLYMER COMPOSITES R&D

A. Development of Manufacturing Methods for Fiber Preforms

Program Manager: Jeff Dahl
Ford Motor Company, Scientific Research Laboratory
P.O. Box 2053, MD 3135 SRL, Dearborn, MI 48121-2053
(313) 845-1039; fax: (313) 390-0514; e-mail: jdahl@ford.com

Composite Materials Research Engineer: Thomas Hoseck
Oak Ridge National Laboratory, (On-site at the National Composite Center in support of ACC040)
National Composite Center
2000 Composite Drive, Kettering, OH 45420
(937) 297-9431; fax: (937) 297-9543; e-mail: hosecktm@ornl.gov

Project Manager: C. David Warren
Oak Ridge National Laboratory
P.O. Box 2008, Oak Ridge, TN 37831-8050
(865) 574-5069; fax: (865) 574-0740; e-mail: warrencd@ornl.gov

Technology Area Development Manager: Joseph A. Carpenter
(202) 586-1022; fax: (202) 586-1600; e-mail: joseph.carpenter@ee.doe.gov
Field Technical Manager: Philip S. Sklad
(865) 574-5069; fax: (865) 576-4963; e-mail: skladps@ornl.gov

---

Contractor: U.S. Automotive Materials Partnership
Contract No.: DE-FC05-95OR22910

Objective

- Develop and demonstrate new fiber preforming processes to decrease cost, increase manufacturing rates, and improve reproducibility of large preforms for composite molding.
- Provide process development support to the ACC Focal Project-3 (FP3).

Approach

- Identify carbon fiber properties required to permit rapid processing and achieve desired performance levels.
- Investigate materials, process equipment, and tooling technology to further reduce the cost and enhance the quality of chopped fiber preforms.
- Explore the extension of automated preforming technology to make preforms with thermoplastic matrix.
- Investigate methods to achieve rapid orientation of fibers.

Accomplishments

- Conducted preform optimization and carbon fiber preforming trials in support of ACC's FP3 B-pillar.
- Investigated 2Phase tooling material for random fiber performing.
- Developed program proposal and initiated program for carbon fiber roving bundle size reduction program with Hexcel Carbon Fibers.
- Developed program proposal and have contract in place for a carbon fiber roving development program with Fortafil.

Introduction

This project has focused on the development of the P4 process, a fully automated robotic preforming process. A prototype, two-station manufacturing cell was designed, fabricated, and installed at the National Composite Center in Kettering, Ohio.

To obtain higher mass savings with composites relative to steel (50–70%), carbon fiber must be utilized as the reinforcing fiber. The extension of this technology to manufacture carbon fiber preforms is now in progress to support the development of ultra-lightweight structures.

Carbon fiber requirements to permit rapid processing while achieving desired composite performance levels will be identified. This will provide guidance for fiber manufacturers to develop new products. Opportunities to extend automated preforming technology to make preforms containing a thermoplastic matrix, which can be consolidated to form the final part will be explored. Methods to achieve rapid orientation of reinforcing fibers will be investigated. Advances in preforming technology will be demonstrated in the structural automotive parts designed and prototyped as part of the ACC FP3 (see report 4.B).

B-Pillar Preforming Development

In support of the ACC FP3 program, researchers have been performing process development to facilitate manufacture of the FP3 B-pillar test section (Figure 1).

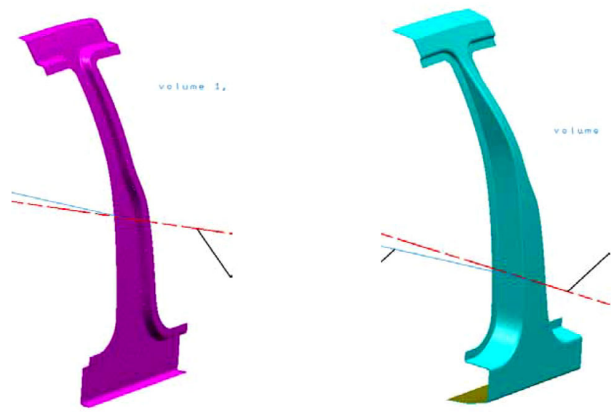

Figure 1. B pillar test section: inner and outer.

Preform optimization is an ongoing, iterative effort to enhance preform characteristics including areal density distribution. To enhance preform quality, substantial robotic programming has been required to achieve the appropriate fiber volume fraction in regions of the components that vary from 1.5 to 8.0 mm in thickness. As part of the carbon fiber preforming development, B-pillar inner and outer preforms have been manufactured using carbon fiber rovings (Figure 2).

Several preforming related issues have been identified when attempting to utilize carbon fiber rovings as the reinforcement material vs glass fiber rovings. The most significant obstacle at this time is the relatively poor fiber distribution on the part surface when compared with glass fiber. This issue is more prominent in the 1.5-mm sections of the components when attempting to

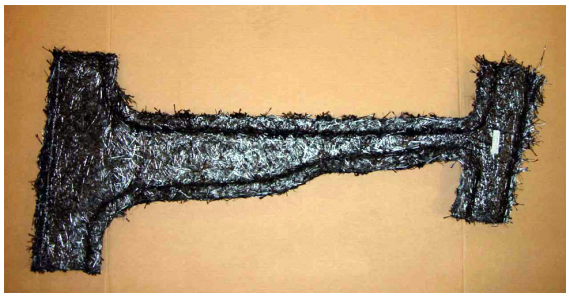

Figure 2. Carbon fiber B-pillar inner preform.

manufacture preforms at a fiber volume fraction of 40% (Figure 3).

The image in Figure 3 is a carbon fiber B-pillar outer preform that has been photographed on a light table. The white regions indicate regions of zero fiber content, an undesirable preform characteristic. Regions of zero fiber content will create regions in the molded component of reduced strength and stiffness and contribute to structural reaction injection molding (SRIM) issues, including fiber wash. In the same way, although not visible on a light table, are regions of excessive fiber content that lead to issues in the SRIM molding process, including dry spots.

Figure 3. Carbon fiber distribution issues.

To minimize the fiber distribution issues present on the surface of the component, a fundamental change to the material format is required. It has been demonstrated that carbon fiber rovings utilizing smaller individual bundle sizes (i.e., 3k vs 6k) will yield improved surface distribution of the fiber. These material format issues are being addressed in carbon fiber roving development programs with several carbon fiber manufacturers.

2Phase Tooling Technology

The ACC contracted with 2Phase Technology to investigate the use of their patent-pending reconfigurable tooling as a potential technology for P4 preform tooling. 2Phase's tooling technology is a method of forming prototype tooling rapidly and relatively inexpensively. This technology potentially could substantially reduce the cost of preform tooling.

Preliminary investigation indicated two areas of concern when attempting to incorporate 2Phase tooling in the P4 process; material strength and air flow through the tool. It was determined that the addition of reinforcement fibers and an increase in particle size as the reconfigurable tooling would be the best options to increase both strength and air flow, respectively. To address these issues, 2Phase fabricated flexural test samples and test preform tools from a variety of materials to investigate the effect.

Flexural test samples were initially made from the standard state-change reconfigurable tooling material. Additionally, two materials with larger particle sizes and two materials with reinforcing fibers in the largest particle size material were also fabricated for flexural testing. The flexural test results are shown in Table 1.

Table 1. 2Phase tooling flexural test results

Particle size (mm)	Fiber length (mm)	Flexural strength (MPa)
0.10–0.25	N/A	2.3
0.42–0.85	N/A	2.7
0.60–1.40	N/A	1.8
0.60–1.40	6	1.4
0.60–1.40	25	1.8

The maximum tensile and compressive stresses in an unsupported section of flat panel perform tooling (350 × 350 × 6 mm)

due to bending when subjected to a uniform load of 100 kPa would be approximately 100 MPa. This load of 100 kPa will be experienced within the process regularly and is approximately 50 times the measured strength of the tooling materials tested. Based upon this calculation, the flexural strength of the 2Phase tooling materials tested was deemed insufficient for P4 preform tooling.

Four plaque preform tools were submitted for testing in the P4 preforming process. The details of these four tooling materials are as follows:

- Material A: 0.42- to 0.85-mm particles
- Material B: 0.60- to 1.40-mm particles
- Material C: 0.60- to 1.40-mm particles plus 15% 25-mm fibers
- Material D: 0.60- to 1.40-mm particles plus 15% 25-mm fibers with a surface veil

The test tools were evaluated by measuring the airflow at six points behind the screen, with several damper openings to determine the air velocity through the screen relative to perforated materials. The preform tools were mounted vertically to investigate the most severe requirement for air flow during material deposition. The experimental setup is shown in Figure 4.

Based upon the experimental test results, the air velocity through the 2Phase tooling material is approximately an order of magnitude lower than standard perforated materials when compared with high internal backpressure (i.e., flow valve equal to 0%). However, when compared with lower internal backpressure (i.e., flow valve greater than 0%), the 2Phase tooling shows no increase in air velocity through the tool. This indicates that the tooling is creating a backpressure nearly equal to the flow control valve even with the flow control valve completely open. This is not the case with standard, perforated materials as indicated in Table 2. Reduced air velocity through the tool creates performing

Figure 4. Experimental testing of 2Phase tooling.

issues such as lack of material adhesion to the tool surface. In fact, this same issue was experienced during glass deposition trials using the four experimental tools. The experimental air velocity measurements for these materials are listed in Table 2.

Table 2. Air velocity measurement results

Flow valve (%)	Air velocity (m/s)						
	Point 1	Point 2	Point 3	Point 4	Point 5	Point 6	Mean
Material A							
0%	0.55	0.81	1.45	1.56	1.5	1.5	1.23
100%	2.17	1.36	1.6	N/A	1.66	1.73	1.70
Material B							
0%	0.94	3.41	4.21	1.21	1.2	0.98	1.99
100%	0.65	4.47	3.96	1.29	1.27	1.08	2.12
Material C							
0%	4.11	3.7	2.11	1.74	1.46	1.12	2.37
100%	4.59	4.53	2.65	1.84	1.56	1.21	2.73
Material D							
0%	1.58	2.71	0.72	0.53	0.5	0.42	1.08
100%	1.7	2.14	0.44	0.49	0.48	0.52	0.96
Perforated steel without 2Phase tooling							
0%	9.52	9.03	9.55	9.95	9.91	10.05	9.67
10%	22.23	21	22.06	23.33	22.72	23.64	22.50

Based upon the testing performed, 2Phase tooling was determined to be unsuitable for P4 preform tooling. For this technology to be suitable for chopped fiber preform tooling, airflow through the tool must be increased, and material strength/toughness must be dramatically increased.

Carbon Fiber Roving Development

To date, research and development of chopped carbon fiber preforming and molding has been limited due to material format and supply issues. To address these fundamental material format issues present with current carbon fiber rovings, development programs have been initiated with carbon fiber manufacturers to expedite material research. The focus of these programs is to investigate the technology required to achieve a reduction in bundle size and the effects of bundle size reduction in the preforming and molding processes.

Hexcel Carbon Fibers

A carbon fiber roving development program to investigate the effect of individual bundle size on preforming, molding, and composite material performance has been developed with Hexcel Carbon Fibers and is currently under way.

The development effort is focused on assessing the effect of individual bundle size on P4 preforming, SRIM molding, and the resultant composite material performance. It is theorized that a reduction in bundle size will improve material distribution in the preforming process and, therefore, positively impact the mechanical performance of the molded structures. To evaluate these materials, the program has been divided into four individual tasks (Table 3).

Table 3. Hexcel Bundle Size Reduction Program

Task 1	Carbon Fiber Roving Manufacture
Task 2	P4 Preforming Evaluation
Task 3	SRIM Molding Evaluation
Task 4	Material Characterization

Task 1. The work contained within Task 1 is to be performed by Hexcel Carbon Fibers under a subcontract with Oak Ridge National Laboratory (ORNL). To investigate the effect of individual carbon fiber bundle size, the research program calls for manufacture of seven different combinations of carbon fiber rovings. The remaining effort then includes precursor manufacture for all combinations to be investigated. Following precursor manufacture, all precursors will be carbonized on production equipment simultaneously. The carbon fibers will then be packaged according to the experimental matrix and shipped to the ACC for evaluation in the preforming process.

Task 2. Upon completion of Task 1, the entire matrix of carbon fiber rovings will be evaluated in the P4 preforming process using the ACC/DOE preforming equipment at NCC, Kettering, Ohio, by the ACC. The rovings will be tested and assessed within the preforming process, and flat panels preforms will be manufactured for in-plane permeability testing, light transmission testing, and flat panel molding trials. In-plane permeability measurements will be conducted on each carbon fiber roving evaluated utilizing ACC/ORNL equipment at NCC, Kettering, Ohio. These data will be analyzed to determine the effect of bundle size on in-plane permeability. Light transmission testing will be performed to determine the coverage characteristics of each carbon fiber roving evaluated. Winona State University will be contracted to perform this work based upon their past experience in developing an analysis technique under a previous purchased services contract with the ACC. Finally, flat panel preforms will be fabricated from all carbon rovings under investigation for SRIM molding trials.

Task 3. Upon completion of Task 2, flat panel preforms will be made available for SRIM molding trials. This effort will consist of molding approximately 10 panels of each carbon fiber roving under evaluation. Molding process data will be acquired and analyzed to determine the effect of individual

bundle size in the SRIM molding process. Subsequently, the molded carbon fiber panels will be used for characterization of the composite material.

Task 4. Upon completion of Task 3, molded flat panels will be available for composite material characterization. To determine the effect of individual carbon fiber bundle size on composite material performance, the current evaluation plan will consist of performing tensile and compressive mechanical testing in both the 0° and 90° directions throughout the range of carbon fibers evaluated. Additional characterization will be performed if determined necessary to fully ascertain the effect of carbon fiber bundle size. Additionally, fiber volume fraction via acid digestion will be performed on each tested panel to confirm the fiber content within each panel.

Summary. To date, the required precursor has been manufactured and is awaiting carbonization to complete Phase 1 of this program. Phases 2, 3, and 4 will commence using these experimental carbon fiber rovings in the second quarter of FY 2004.

Fortafil

A research program to develop carbon fiber rovings more amenable to the P4 preforming process has been developed and initiated during FY 2003. This program will focus on developing cost-effective methods to reduce the individual carbon fiber bundle sizes within a roving. A carbon fiber roving specification was developed jointly between the ACC and Fortafil as the target material for this program. The overall program is comprised of five phases to be completed over a 20-month time period.

This research program was officially started in August 2003. To date, administrative functions relative to the program have commenced as well as preliminary technical efforts related to Phase 1 of the program. Upon development of candidate carbon fiber rovings within this program, preforming and molding evaluations will be conducted by the ACC to determine the performance of these materials.

Conclusions

Process development on the B-pillar inner and outer is an ongoing and iterative effort in support of the ACC's FP3. Progress has been made in improving the material distribution and will continue to be an iterative effort between preforming and molding. The application of carbon fiber is currently proving to be challenging due to the current material format. However, development of carbon fiber rovings with various carbon fiber manufacturers will improve carbon fiber rovings and, subsequently, preform processing.

An alternative tooling technology was examined to ascertain the feasibility for application as P4 preforming tools. Prototype tools were manufactured and tested in the P4 process. Test results highlighted several issues with the technology as it relates to the P4 process, and it was determined that the technology was not applicable.

A carbon fiber roving bundle size reduction project proposal was developed within the ACC and Hexcel Carbon Fibers were selected as the carbon fiber supplier for this program. This program was initiated in FY 2003, and Task 1 is approximately 75% complete. Evaluation of experimental materials will begin following receipt of materials in the second quarter of FY 2004.

A carbon fiber roving development project was developed with Fortafil during FY 2003. A contract is now in place, and the program was officially kicked off on August 1, 2003. Preliminary administrative and technical work within Phase 1 has commenced.

Based upon the carbon fiber roving development projects with Hexcel and Fortafil, there is now an opportunity to advance the current carbon fiber roving technology and product form to make it more suitable for high-volume, chopped fiber preforming applications such as P4.

As materials from these programs are made available, the new and improved carbon fiber rovings will continue to be tested in the P4 preforming process to evaluate chopped fiber material processing and performance.

B. Composite-Intensive Body Structure Development for Focal Project 3

Nancy Johnson
GM Research & Development
MC 480-106-256
30500 Mound Road
Warren, MI 48090-9055
(586) 986-0468; fax: (586) 986-0446; e-mail: nancy.l.johnson@gm.com

Co-Principal Investigator: Raymond G. Boeman
Oak Ridge National Laboratory
P.O. Box 2008, MS 6053
(248) 452-0336; fax: (248) 452-8992; e-mail: boemanrg@ornl.gov

Project Manager, Composites: C. David Warren
Oak Ridge National Laboratory
P.O. Box 2008, Oak Ridge, TN 37831-8050
(865) 574-9693; fax: (865) 574-0740; e-mail: warrencd@ornl.gov

Technology Area Development Manager: Joseph A. Carpenter
(202) 586-1022; fax: (202) 586-1600; e-mail: joseph.carpenter@ee.doe.gov
Field Technical Manager: Philip S. Sklad
(865) 574-5069; fax: (865) 576-4963; e-mail: skladps@ornl.gov

---

Contractor: U.S. Automotive Materials Partnership
Contract No.: DE-FC05-02OR22910

Objective

- Design, analyze, and develop the technology to build a composite-intensive body-in-white (BIW), offering a minimum of 60% weight savings over steel at a cost close to that of steel, while meeting manufacturing, assembly, and performance targets.
- Provide a focus for bringing together technology developed by each of the Automotive Composites Consortium (ACC) working groups through emphasis on carbon-fiber-reinforced composites and the use of hybrid materials, faster manufacturing processes, design optimization including crashworthiness, and rapid joining methods.

Approach

- Optimize the design, and complete the finite-element analysis (FEA) (Phase 1—completed).
- Build one part of the BIW to demonstrate high-volume processing methods, including the component as well as the needed assembly fixtures (Phase 2). Test the component before continuing with the construction of the complete BIW.
- Build the complete BIW (Phase 3). To reduce cost, not all parts will be made from production tooling; however, care will be taken to ensure that the properties of each part are consistent with those that will be obtained from production tools.

Accomplishments

- Installed learning tool and preform screens at NCC in Dayton.
- Continued preforming and molding trials.
- Bonded B-pillar parts successfully.
- Completed cost estimates for body side.

Introduction

All of the materials, manufacturing processes, and fabrication and assembly methods to be considered in this project are to be consistent with the following overall objectives:

- High-volume production techniques (>100,000 units per year)
- Cost parity with equivalent steel structures
- Overall 60% mass reduction relative to steel BIW structure
- Structural performance equivalent to or better than that of a steel structure
- Dimensional tolerance equal to or better than that of steel

Much of FY 2003 was devoted to developing the manufacturing processes necessary to build the body side. Preforming and molding trials continue with the B-pillar learning tool. For more details on the preforming studies see the report on P4 preforming (4.A). For additional information on molding, see the report on High-Volume Composites Processing (4.D).

Learning Tool/B-Pillar Related Studies

A learning tool was designed to conduct the processing and materials research necessary to enable production of the body side. A section representative of the B-pillar portion of the design for the body side was selected for the learning tool, which had many of the features of the final part. The tool was made to be versatile for use in multiple processes such as structural reaction injection molding (SRIM), long-fiber injection (LFI), and sheet molding compound (SMC). It has a polished surface so that it can be used to develop class A surface techniques later if desired. The tool incorporates many challenging features not yet addressed by the composites industry, including liquid molding of variable-thickness sections at high-volume fractions.

Molding process development was initiated this year with the new B-pillar mold. The initial development work was with glass preforms, but at the 40% by volume targeted for the body side. The early molding showed that improvements were needed in the tool, especially seals to better contain the injected resin in the cavity. Seals were designed and installed in to B-pillar mold.

O-rings were installed in the vertical shear edges to provide a sliding seal against the resin while the mold was partially open at the injection gap (see Figure 1). Because the O-rings could not follow the sharp

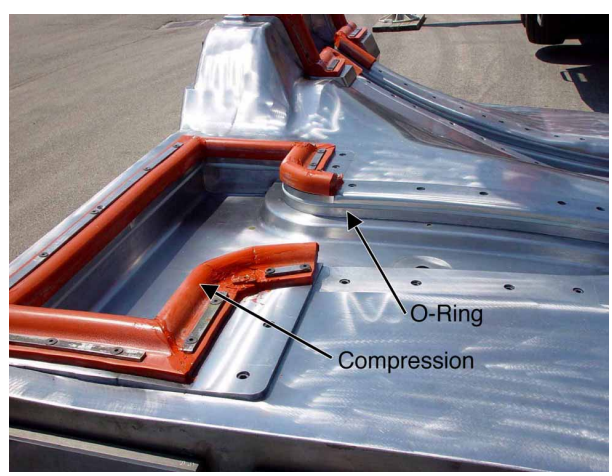

Figure 1. Modified tool with O-ring and resin seals highlighted.

curvature in the rail areas, a second compression seal was used in this area to seal the final stage of the compression stroke, when the resin would have reached the ends of the cavity. With the resin seals installed, it was now possible to hold pressure on the resin as the mold was closed during the compression stroke. As a result it was much easier to force the resin to the ends of the cavities and completely fill the preforms.

The effect of the resin seal is seen in Figure 2. Without the seal the pressure spikes and falls back to near zero. With the seal, the pressure holds at a high level after the initial spike. Flow modeling studies have been initiated with the University of Delaware to better understand the resin flow during molding.

Bonding

The Joining and FP3 Work Groups agreed, after considering four quotes, to contract with RP/C Alliance to design and build a hot-air impingement bonding fixture, as well as a CMM fixture (for dimensional checking), for bonding the two-piece B-pillar. RP/C Alliance also agreed to facilitate the bonding trials at EMC^2 and the CMM testing at Division Two. During the bonding fixture "buy-off" (the first bonding trial), six sets of B-pillar outers and inners were bonded. With some minor adjustments to the cure conditions and air orifices, the final two bonded parts were deemed acceptable. The latter two parts were then taken to Division Two for CMM testing. Based on the design data used to manufacture the molding tools for the inners and outers [where the computer-aided design (CAD) data was modified to be as if the parts were in vehicle position], the bonded assemblies exhibited good dimensional control. That is, the parts were, with a few exceptions, within approximately ±1.0 mm of the design.

Structural Testing

A subgroup of the Focal Project 3 team was formed to specify and conduct structural tests on the B-pillar. The objective of this effort is to assess the quality of the as-molded parts to provide feedback for process development and/or design modification. Notably, this effort is not intended to validate the BIW design or FEA analyses of the B-pillar performance.

The effort will eventually be extended to the demonstration part—the body-side assembly—but is initially focused on the B-pillar because it contains most of the generic geometric features that present the most significant processing challenges and consequently is being used for process

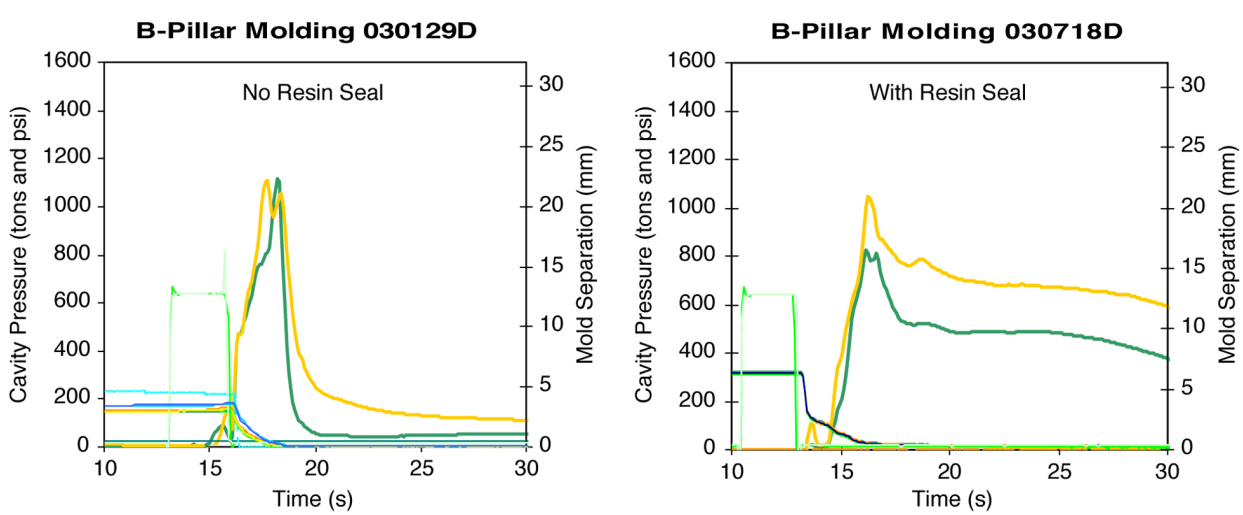

Figure 2. Effect of seals on cavity pressure.

"learning." The B-pillar inner and outer will be investigated individually and also as a bonded assembly.

The most straightforward approach to assess the quality would appear to be to completely characterize the structure, i.e., measure mechanical properties, at every point in the structure and compare these values to design properties. Clearly, this approach would be too costly and time-consuming and would present significant difficultly in measuring properties at potentially the most critical areas (e.g., corners, edges, etc.). Additionally, it is unclear how sensitive the global response would be to local variations. Because body structures are designed largely with respect to global stiffness, the approach adopted here is to conduct full (B-pillar) structural tests to compare with the response of a uniform, idealized good part, as predicted by FEA. Selective coupon testing will also be conducted as shown in Figure 3.

The criterion for selecting the physical tests is to ensure that they will highlight the effects of defects likely to occur in the part. Consequently, the specific approach taken is to first categorize the potential defects as to type, location, and magnitude. Then a FEA is carried out for a variety of loading conditions to assess each load condition's sensitivity to the defects. The loading conditions indicating the most sensitivity to specific defects will be selected for physical testing and correlation.

For this effort, it is assumed that the most significant defect will be variations in the fiber content: specifically, low fiber volume in critical areas. Fiber content measurements (e.g., resin burn-off) are conducted throughout the part to determine a reasonable range of fiber volume fraction variation (see Figure 4). Both the B-pillar inner and outer were segmented into zones, as shown in Figure 5, such that the material properties could be varied, corresponding to fiber content variations, in a systematic fashion.

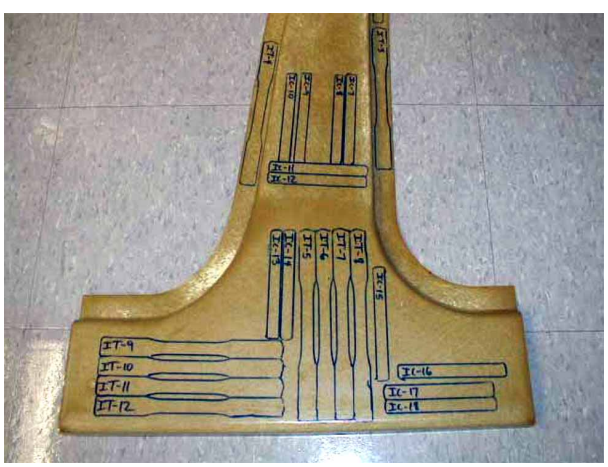

Figure 3. Selective coupon testing will be conducted where standard tensile and compressive coupons can be extracted.

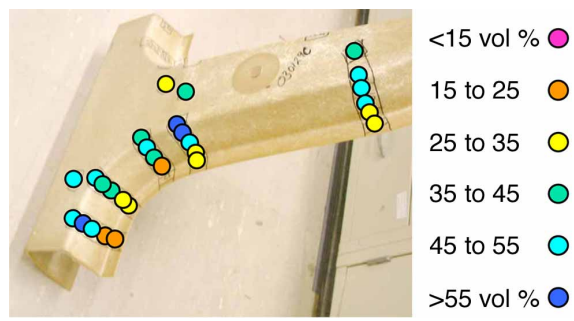

Figure 4. Fiber volume fraction variations are taken at discrete locations as shown for an early glass B-pillar outer molding.

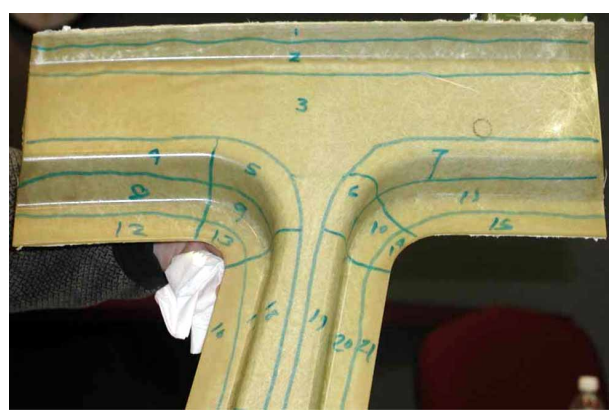

Figure 5. The B-pillar sections are segmented in discrete zones to permit an FEA sensitivity study on fiber volume fraction variation for a variety of load conditions.

Initially, six loading conditions are considered for the effect of defect sensitivity analysis—tension, lateral bending, rocker compression, torsion, lateral line at base of pillar, and distributed lateral rocker. These loading conditions are shown schematically in Figure 6 for a B-pillar outer. Note that the upper rail was omitted in this sketch but will be included in later detailed analyses.

The input properties will be varied systematically within the zones to determine which load conditions will highlight specific defect locations. These results will be used to down select to one to three physical tests to conduct.

The results of the physical tests will be compared to the predicted results for an idealized (e.g., uniform property) part to assess the overall quality of the part. Coupon data (Figure 3) will supplement the structural response data in this determination.

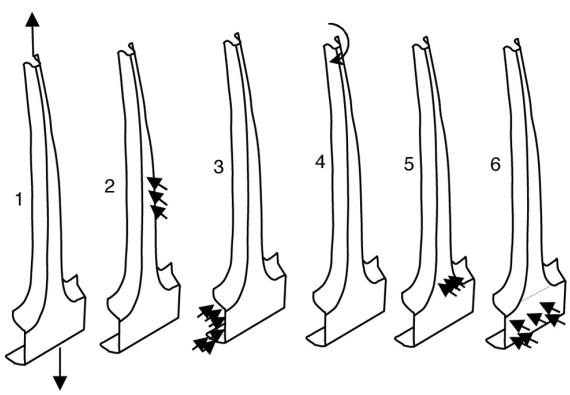

Figure 6. Six loading conditions are considered for effect of defect sensitivity analysis.

Status

Defect type, location, and magnitude have been defined and initial sensitivity analysis completed for the loading conditions shown in Figure 6. The FEA models are being refined to include the upper-rail section and recent minor modifications to the geometry, if determined to be significant. Discussions with a test lab have been held, and tests will be initiated when suitable parts are available and after the final sensitivity analysis results are obtained identifying the most relevant tests.

Bonded Joint Modeling

Phase I of the generic bonded joint modeling project continues at the University of Michigan (UM). This work is intended to validate the modeling approach taken previously at the University of Texas-Austin. The original work predicted that an all-composite bonded hat/flat section with an initial crack would fail (propagate the crack). In testing at ORNL, this did not occur. During the new work at the UM, it was determined that the issue with the initial prediction was that the large-scale bending of the composite flat section was not accounted for in the model. Therefore, a new model (UM) was developed to account for the actual behavior of the flat section. Calculations were performed which indicated that the most likely way to ensure crack propagation would be to fabricate the part using the same dimensions as the original part, but to make it out of steel. This new part has been prepared and bonded, and testing at ORNL should occur in the next quarter.

Meanwhile, the next phase of this project was initiated at UM. For this work it was decided to focus on a mixed material system. The hat section will be a commercial Quantum Composite material (essentially a carbon-fiber SMC) bonded to a flat steel plate. (Carbon composite)/steel strips were bonded to generate the "coupon-level" lab tests required for the initial modeling studies. The coupon-level tests have been completed, and the model has been verified at the lab scale. A publication, the first in what is planned to be a series of papers on this subject, is currently in editing. The Quantum Composite hat sections were molded earlier in the year, and the bonded parts will be prepared by next quarter.

C. High-Volume Processing of Composites

Co-Principal Investigator: Stanley A. Iobst
Motors R&D Center, MC 480-106-710
30500 Mound Rd., Warren, MI 48090-9055
(586) 986-1223; fax: (586) 986-1207; e-mail: stanley.a.iobst@gm.com

Co-Principal Investigator: Chao H. Mao
DaimlerChrysler Corporation, CIMS 482-00-13
800 Chrysler Drive, Auburn Hills, MI 48326-2757
(248) 576-7482; fax (248) 576-7490; e-mail: CHM@daimlerchrysler.com

Project Manager: C. David Warren
Oak Ridge National Laboratory
P.O. Box 2008, Oak Ridge, TN 37831-8050
(865) 574-9693; fax: (865) 574-0740; e-mail: warrencd@ornl.gov

Technology Area Development Manager: Joseph A. Carpenter
(202) 586-1022; fax: (202) 586-1600; e-mail: joseph.carpenter@ee.doe.gov
Field Technical Manager: Philip S. Sklad
(865) 574-5069; fax: (865) 576-4963; e-mail: skladps@ornl.gov

---

Contractor: U.S. Automotive Materials Partnership
Contract No.: DE-FC05-02OR22910

Objective

- To develop and demonstrate high-volume manufacturing technology to produce lightweight composite automotive body structures.
- To achieve higher fiber volumes in thinner sections than were successfully achieved in ACC Focal Project 2 (FP2).
- To support the goals of ACC Focal Project-3 (FP3).

Approach

- Investigate the structural reaction injection molding (SRIM) process at high fiber loadings using carbon fiber.
- Design and build a shape tool to investigate the complex preforming and molding processes required for the ACC FP3 program.
- Team with supplier partners to investigate alternative liquid molding processes.

Accomplishments

- Performed initial B-pillar molding trials with 40% glass fiber preforms.
- Modified the mold to incorporate the following improvements:

— resin seals added to each cavity,

— the transition regions between the thin and thick sections smoothed out, and

— an additional pressure transducer added to each cavity.

- Molded parts for bonder evaluation.

Introduction

The purpose of this project is to further develop the liquid composite molding technology previously demonstrated in the ACC FP2 with the large structural truck box. This project will extend the liquid molding process into more structurally demanding application of the ACC FP3 body-in-white. This will be accomplished by using carbon fiber reinforcement at 40% by volume, compared to the 30% glass fiber reinforcement used earlier. To maximize the weight savings, the minimum section thickness will be reduced to 1.5 mm.

Two basic approaches will run in parallel. The first is the extension of conventional SRIM technology to carbon fiber preforms of reduced section thickness in support of the ACC FP3. The plaque molding program demonstrated the ability to mold the 40% carbon fiber preforms at the required thin sections. The glass and carbon preforms at 40% required about the same molding pressure, which was substantially higher than required for 30% fiber reinforcement. The molding is now extended to the shaped panel, which represents the B-pillar section of the FP3 body side. This approach is under the direction and includes direct participation of ACC personnel.

The second approach will be to work with supplier-partners to adapt their liquid molding processes in the direction of being compatible with the material property and processing requirements of FP3.

The project team includes personnel from the Big Three automotive companies and Oak Ridge National Laboratory. The support team includes personnel from the National Composites Center (NCC). Bayer is a supplier-partner in the Long Fiber Injection (LFI) portion of the program.

B-Pillar Molding Program

The B-pillar molding is a joint program between this project and FP3. It is the process development step between the plaque molding and the FP3 body side molding programs. This mold is a simplified version of the B-pillar section of the full body side. The mold contains the minimum (1.5-mm) and maximum (8-mm) thicknesses of the full part and the bonding flanges. It will be used to generate data on the molding characteristics of the high-volume fraction carbon fiber preforms of complex shape and assist in the final design of the body side molds. The mold contains both the inner and outer cavities in the same base and will produce parts for bonding and structural analysis studies.

The molding during this time period was done with 40% glass preforms. There was only a limited supply of the Zoltek carbon fiber available, and it was decided to conserve that supply until the preforming and molding of the high fiber volumes were characterized with an available fiber.

After a set-up period, the molding program was kicked off in the fall of 2002. Mold filling was characterized by a number of techniques, including a series of short shots (Figure 1), data traces (discussed below), and observation of any patterns of dry fiber areas. Where appropriate, this information was fed back to the preforming team.

The initial molding study looked at the effect of injection gap height, time between injection and compression, and press

Figure 1. Flow characterization by short shot experiments: 25%, 50%, and 75% fills.

tonnage on the preform filling behavior. The injection gap height was found to be an important parameter due, in part, to the significant curvature of the B-pillar. To accommodate the mold draw, this curvature caused a large vertical separation between the ends of the cavities. Also, the part is designed with a thin section between the two thicker ends; this prevents an excess of resin in one end from flowing back toward the other end of the part. It was found that if the injection gap was too large, then excess resin flowed toward the lower part of the cavity, and the opposite end of the part did not fill. If the injection gap was too small, then the flow resistance was too great, and the mix-head faulted out. However, by controlling the injection gap to between 3 and 7 mm, a good resin distribution was obtained.

A major tool in the molding program was the data acquisition system. This allowed the resin injection and press closing dynamics to be observed. An example is given in Figure 2. The mold is paused at a gap of 3.7 mm above stops for injection. The injection time is shown on the chart followed immediately by full mold closure. This action forces the resin through the preform and pressurizes the resin in the cavity.

During this first phase of B-pillar molding trials, it was observed that resin leaked outside the mold cavities and that compression pressure could not be held on the parts (Figure 3). This also limited the capability to force the resin to the ends of the preforms. A temporary fix was devised by placing a veil over the perform, which partially sealed the cavity edge. This allowed

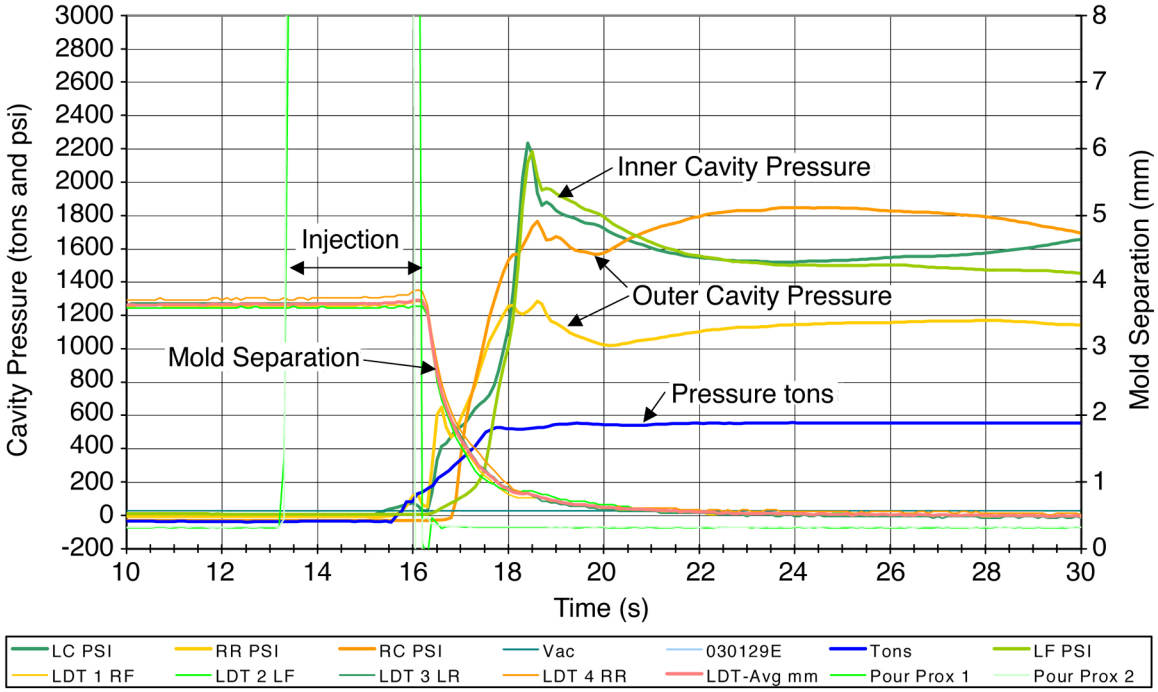

Figure 2. B-pillar mold dynamics showing mold half separation, resin injection, and cavity pressure as a function of time.

Figure 3. Photograph showing resin leaking outside the B-pillar mold cavities, and resulting dry preforms in rail areas.

the initial molding phase to be completed, to establish molding parameters, and to supply feedback to preforming.

It was decided to pull the mold and have seals installed around the cavities. At the same time, an additional pressure transducer was added to each cavity, and the transition zones between the thin and thick cross sections were reworked. The seals did contain the resin within the cavities and provided better compression within the cavities (Figure 4).

Some additional refinements will be made in the preforming program using glass before starting the carbon fiber work.

Figure 4. Nested B-pillar inner and outer set.

Supplier-Partner Liquid Molding Program-LFI

ACC Project 115 has previously included a segment focused on developing alternative liquid molding processes. This has continued in 2003 but has been expanded to assess the potential for achieving a Class A surface finish with these materials/processes. In this capacity the ACC Team has partnered with Bayer to investigate Long Fiber Injection PUR (LFI) processing and material properties.

The LFI process involves cospraying the urethane resin along with chopped fiber reinforcement into an open mold, then closing the mold and curing. One primary goal will be to characterize this process/material for its ability to meet the more demanding structural applications of FP3. Concurrently, another challenge has been added: to assess LFI's potential for Class A surface optimization.

The first step for the ACC Team has been to establish a surface acceptance standard that could be used to gage the progress through stages of LFI development. Various materials used for automotive Class A exteriors were benchmarked, using a variety of known quantitative techniques as well as a subjective jury evaluation. Plaques were prepared and finished at a common source in various stages of the painting process (initial, E-coat, primer/sealer, topcoat). This work is in progress with a scheduled completion of mid-December 2003.

Having established the standard, the project was organized into distinct phases, covering the next 6 months. The initial step was to construct an LFI plaque tool with suitable surface finish and ability to vary thickness. It is to be used for molding trials at Bayer in their Pittsburgh labs. This tool modification is targeted for completion by the end of November 2003. Follow-up phases include two separate designs of experiment (DOE). The first will screen for such elemental parameters as glass type, fiber length, and percent by weight. A second DOE will build on these results to assess the effects of thickness, mold time, postcure, and surface veil. In both phases, the plan is to finish coat the plaques and evaluate them against the agreed-upon "standard." The DOE plans have been finalized, and the testing is anticipated to begin in early 2004.

Based on the results, the ACC Team will decide on the next most appropriate course

of action. Use of in-mold coatings and other surface enhancement techniques are the most logical direction. Given a successful outcome of this plan, subsequent work could include evaluating critical design and process conditions (i.e., larger areas, irregular sections, molded-in features…). Continued progress could also drive the investigation of carbon fibers for additional weight savings.

D. Thermoplastic Composite Sheet Manufacturing: Study of Thermoplastic Powder-Impregnated Composite Manufacturing Technology

Project Manager: Mark T. Smith
Pacific Northwest National Laboratory
P.O. Box 999, Richland, WA 99352
(509) 376-2847; fax: (509) 376-6034; e-mail: Mark.Smith@pnl.gov

James Grutta and Larry Stanley
Delphi Automotive Systems
8385 South Allen Street, #140, Sandy, UT 84070-6434
(801) 568-0170; e-mail: itgrutta@hotmail.com

Technology Area Development Manager: Joseph A. Carpenter
(202) 586-1022; fax: (202) 586-1600; e-mail: joseph.carpenter@ee.doe.gov
Field Technical Manager: Philip S. Sklad
(865) 574-5069; fax: (865) 576-4963; e-mail: skladps@ornl.gov

---

Contractor: Pacific Northwest National Laboratory
Prime Contract No.: DE-AC06-76RL01830

Objectives

- Demonstrate and develop glass and carbon-fiber-reinforced thermoplastic matrix composites at production rates consistent with high-volume automotive structural applications.
- Investigate and develop methods for shortening the process cycle times and improving materials performance.
- Develop methods for achieving a Class A surface finish requirement, consistent with outer body panels for automotive use.
- Investigate the potential for cored (sandwich) structure composites with thin-walled thermoplastic matrix composite skins.
- Determine the cost-effectiveness of thermoplastic matrix composites in production volumes consistent with automotive applications and the potential to achieve cost targets in the future.

Approach

- Use data from previously completed parametric studies of time, temperature, and pressure profiles required to achieve properties for structural automotive composites; and determine combinations of processing factors that will accelerate process cycle to under 1 min.
- Develop methods of heating and cooling, and process operations to achieve consistent cycle times.
- Analyze alternative methods of melt processing for the various operations required for consolidation, including experimental evaluation of cored structures.
- Apply a multiscale materials modeling approach to develop predictive numerical models for thermal and structural responses for constituent materials and architectures; and apply to

processing conditions for cycle optimization, material property predictions, and end-use performance predictions.

- Use data to influence materials suppliers in modification of base material feeds in ways that support increased cycle times.
- Use complex-shaped components to determine process limitations and factors for economic evaluation.
- Evaluate methods to achieve Class A surface finish with reinforced thermoplastic matrices and analyze them in production cycles on complex tooling.

Accomplishments

- Completed a two-press system installation and demonstrated the operation using a single, modified cone mold. The operation demonstrated the need for emphasis on tool design, specifically in optimization of tool mass and heating and cooling times.
- Concluded from results of the two-press system that current material forms cannot be processed in cycle times that are compatible with the higher volume automotive production cycle time goals, but they may still show potential for some of the lower volume ranges. The project is now investigating alternate thermoplastic composite materials that either require shorter consolidation times or are preconsolidated.
- Investigated preconsolidating of the powder-impregnated materials by melt and pressure and then reheating and stamping into final part shape, which offers the ability to reduce dwell time and meet cycle time goals. However, mechanical testing of materials processed in this manner showed property losses (compression strength) in the range of 30%. The reason for these property losses is being investigated.
- Developed a new processing method for continuous processing with multiple tooling sets, with optimized heat/cooling methods. Delphi has filed a record of invention for this process. This approach is being demonstrated as part of the two-press system development.
- Automated the two-press system partially to simplify and ensure proper operation of the system. All safety critical operations, such as closing the press, are still controlled manually to ensure that the operator is at an adequately safe distance.
- Investigated infrared (IR) heating as a means for preheating the tool surface.
- Created a finite-difference model of the effects of IR heating to explore and determine the feasibility of using IR energy as a means of rapid preheating and a reduction of thermal momentum.
- Completed a new seven-sided forming tool with flat sections at 0°, 30°, 60°, and 87° from perpendicular to the loading direction. This tool should allow structural testing and show the effects of slope angle on structural integrity.
- Initiated action to purchase alternate thermoplastic composite materials. Evaluation will include DRIFT woven into fabric form. To date the suppliers of DRIFT material have not been able to successfully deliver the required material, so this task will be dropped.
- Completed micro-scale models for simulating the behavior of unidirectional reinforced-fiber composites. The primary model is based on assumed hexagonal packing of fibers and is parameterized to allow any possible volume fraction of fibers and any desired finite-element mesh refinements to be applied.
- Developed a numerical model of a consolidated 4-harness satin fabric-reinforced composite.

- Developed a numerical model that predicts 2 × 2 twill unconsolidated fabric shear behavior for simulating properties useful for macro-models of stamp-forming process modeling.
- Developed relations between fabric openness, in-plane shear locking angle, and effective normal strains for better understanding of fabric formability characteristics.
- Constructed four different fabric (mesoscale) models. The model for simulating a consolidated plain weave lamina has been completed for mechanical property prediction. A model for a consolidated 2 × 2 twill weave has been completed for simulating thermal properties. The more complex weaves (2 × 2 twill and 4-harness satin) continue to provide difficulties for establishing mechanical periodic boundary conditions. However, many of the issues have been resolved, and rapid progress on three models is expected.
- Began development of a fabric shear model for the 2 × 2 twill material. A complex set of boundary conditions has been developed, and the final issue of contact conditions during shear locking is being resolved.
- Developed a number of variations on macro-modeling of the forming process. Results show a strong relationship between in-plane shear properties and propensity for wrinkle formation, die surface interaction, and the ability to suppress developing wrinkles, material and die surface characteristics. and forming pressure distribution in the die.

Future Direction

- Complete the final report with updated fabric modeling results.

Introduction

Polymer matrix composites are a class of materials identified as having a combination of properties required to achieve very significant reductions in vehicle mass as compared to conventional materials. Although widely regarded as having the most potential for future weight savings, their applications are severely restricted by fundamental issues in achieving required production volumes and cost of basic materials. These issues have been primarily studied and analyzed based on liquid thermosetting matrix composites, such as structural reaction injection molding (SRIM) as used in the ACC focal projects. Fiber materials cost and availability, especially for carbon fiber, are being addressed by the DOE program under the low-cost carbon fiber projects.

This project has identified the carbon fiber thermoplastic matrix composites as having significant potential to meet structural property requirements as well as to achieve rapid processing cycles similar to stamping of metal components. Automotive applications will be most widespread if two other fundamental issues can be addressed; namely, cored, thin-walled structures (for optimum structural performance and minimum weight) and Class A surface in a semi-structural component. Development of the thermoplastic composites to meet these requirements will require a combination of experimental approaches, materials and process modeling, and modification of materials forms and processing methods to achieve an optimum manufacturing process.

Project Deliverables

This multiyear program will develop and demonstrate knowledge concerning four areas of thermoplastic composite forming process technology, including (1) results of process cycle time and materials property achievements at high forming rates; (2) results of Class A surface finish trials; (3) methods for manufacture of thin face-sheet cored structures; and (4) modeling

tools for predicting and optimizing the thermal and structural materials behavior for fiber-reinforced thermoplastics.

Planned Approach

Experimental and analytical methods are being used and developed for high-rate forming of thermoplastic composite sheet and cored structures. The research team is focusing on achieving automotive stamping production rates and materials modifications to achieve rapid flow and consolidation. By integrating these two approaches, we are able to determine where difficulties in the process and materials form occur and can suggest methods to overcome these barriers. Several significant invention disclosures have resulted. Further focus on the process and materials kinetics will allow the bench-scale demonstration of high-rate stamping. Recent experiments using complex three-dimensional (3-D) molds indicate that longer dwell times are required to consolidate materials in draw and draft angle portions of the dies. This points to the need to explore alternate material forms in future work, including preconsolidated thermoplastic sheet materials.

Experimental Methods—Manufacturing Tasks

The initial experimentation used flat plate molds and developed a process diagram based on achieving a predefined "acceptable" quality of consolidation, as measured by compressive strength of the coupons. These process conditions were used as a basis for processing a conical mold that had varying angles of fabric shear (deformation) and varying forming radii (both convex and concave) to provide an understanding of the forming limits under different process conditions. Coupons have been taken from the conical mold and tested in compression to match the consolidation results to the results from the basis flat plate mold.

Methods for achieving rapid process cycles were developed as an ongoing part of the conical mold trials. A two-press system (Figure 1) was developed during the past year to simulate a newly developed continuous cycle process. However, with the use of more complex, 3-D molds, experimental results indicate the need for increased dwell time to achieve consistent, full consolidation of the powder-impregnated materials. As a result, additional investigation will focus on the application of pre-consolidated thermoplastic composite materials, and the use of a new mold design that incorporates multiple entrance angles so that the influence of die geometry on cycle dwell times can be quantified.

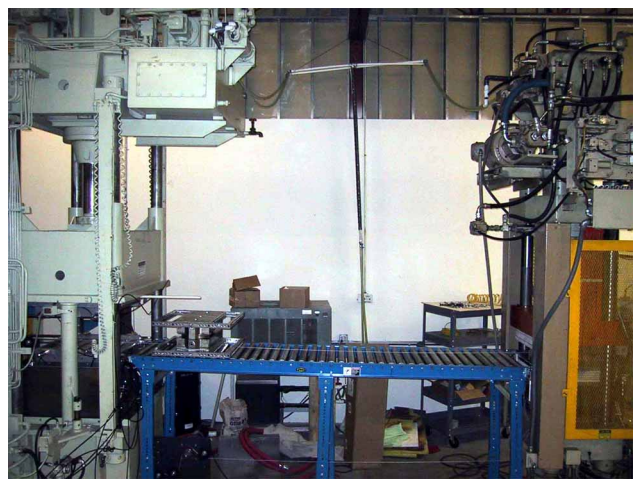

Figure 1. Two-press system with tool shuttle.

Approaches using combined hot stamping and consolidation as a single step have indicated a long dwell time necessary for fiber wetting and optimum resin distribution to occur when fabricating trial parts under realistic processing conditions. Although the materials properties can be developed for simple sections—here conditions of combined temperature, pressure, and time meet our original process map—we find that when working on areas with other high draft angles and lack of directly applied pressures, a longer dwell time is required. Although this is still consistent with the process map, it is operating further out on the boundaries of allowed conditions, which leads to a longer process cycle.

In an effort to reduce cycle time, preconsolidation of the powder-impregnated material was evaluated. With this approach, Delphi heated and pressed sheet layers into fully consolidated flat sheet, which could be done outside of the main forming press step and, thus, eliminate most of the dwell portion of the forming cycle. Experimentally, the pre-consolidated sheet was then reheated to forming temperature and formed into the die and final component shape. However, measurement of mechanical properties from the preconsolidated material stampings showed up to a 30% drop in compression strength. Although the reason for this property knock-down is not known, further investigation is planned.

Modeling Task—Analytical Methods

Approach

Apply a multiscale material modeling approach to develop predictive numerical models for thermal and structural response for constituent materials and architectures, and apply to processing conditions for cycle optimization, material property predictions, and end-use performance predictions.

Accomplishments

- Extended the numerical model of a consolidated four-harness satin fabric-reinforced composite to model inelastic behavior for in-plane shear loading.
- Obtained properties from previous work to predict 2×2 twill unconsolidated fabric shear behaviors that have been applied in macro-models of stamp-forming process modeling. Some qualitative comparisons with experiments have shown some key correlations that suggest the modeling approach is very good at predicting fabric wrinkling during forming.
- Started efforts to consolidate the documentation of modeling work performed during the course of this project.

Future Direction

Complete the documentation of the project modeling work.

Analytical Methods

A multiscale modeling approach has been developed and applied to demonstrate modeling tools with long-term value to the technology of fabric-reinforced thermoplastic composites. As illustrated in Figure 2, three important materials scales have been addressed. A description of and motivation for the multiscale approach is available in the FY 2001 annual report for this project. Here we will review some past results

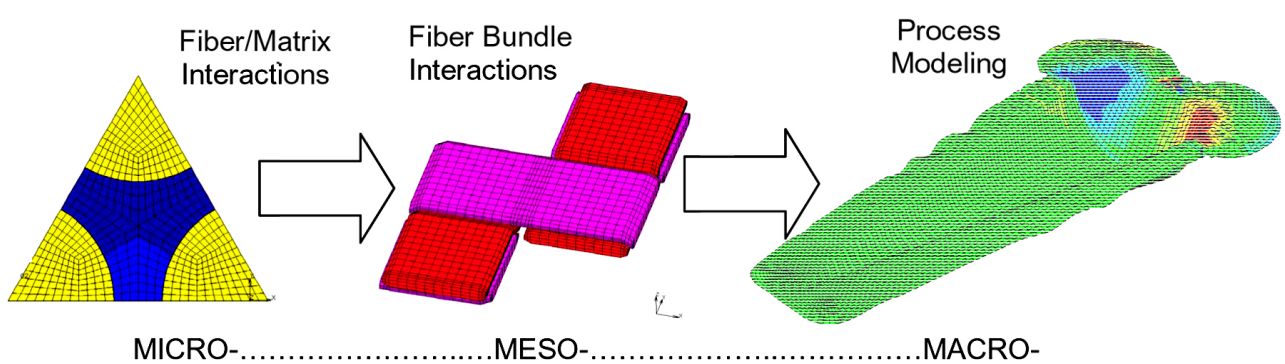

Figure 2. Multiscale modeling of fabric-reinforced composites. Shown are a hexagonal fiber pack unit cell for microscale modeling, a 2×2 twill fabric unit cell for mesoscale modeling, and cone forming process model results at the macro-scale.

and describe progress made concerning modeling activities during the past year.

The microscale models were developed in previous years. In addition, some mesoscale models were developed previously to predict thermal and structural behavior for the 2 × 2 twill woven fabric material in a consolidated form. Process (macro) models have been developed to study initially the effect of in-plane shear stiffness on formability and drape characteristics for the cone-shaped mold. Also, macro-models were applied to predict in-mold pressure distributions during forming.

Efforts since the last report (October, 2002) have been primarily to integrate results from the consolidated fabric shear model with the macro-forming model for the cone-shaped mold. Also, some new results have been generated for a four-harness satin weave model.

An image of the four-harness satin weave unit cell model is shown in Figure 3. A nonlinear material model was applied to study inelastic materials behavior for in-plane shear loading. The stress plot on the right in Figure 3 indicates where damage occurs due to microcracking in the matrix during in-plane shear loading. The constitutive law is base on micromechanics at the fiber matrix level (microscale model in Figure 2) with the kinetic theory of fracture applied to the polymer matrix.

The fabric shear model for the unconsolidated 2 × 2 twill weave and three deformed configurations of the same are shown in Figure 4. In the second image, the model has been loaded to simulate the geometry and

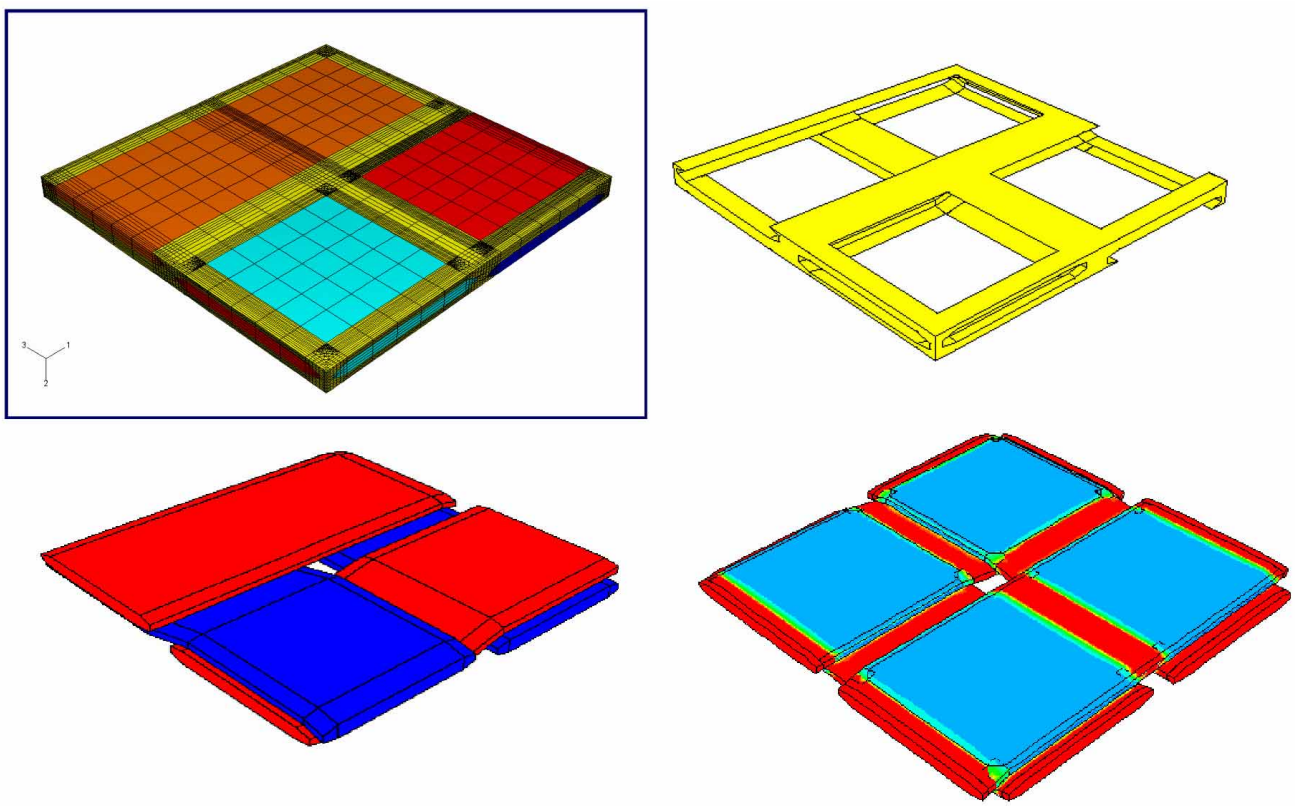

Figure 3. One-quarter periodic unit cell finite-element model for a consolidated four-harness satin weave reinforced composite with colors indicating separate tows in the weave (upper left). Pure matrix regions are shown in the upper right. The tow architecture is shown in the lower left. Contour plot on the lower right indicates regions where matrix damage has occurred (red) as well as low-damage regions (blue) for the case of in-plane shear loading.

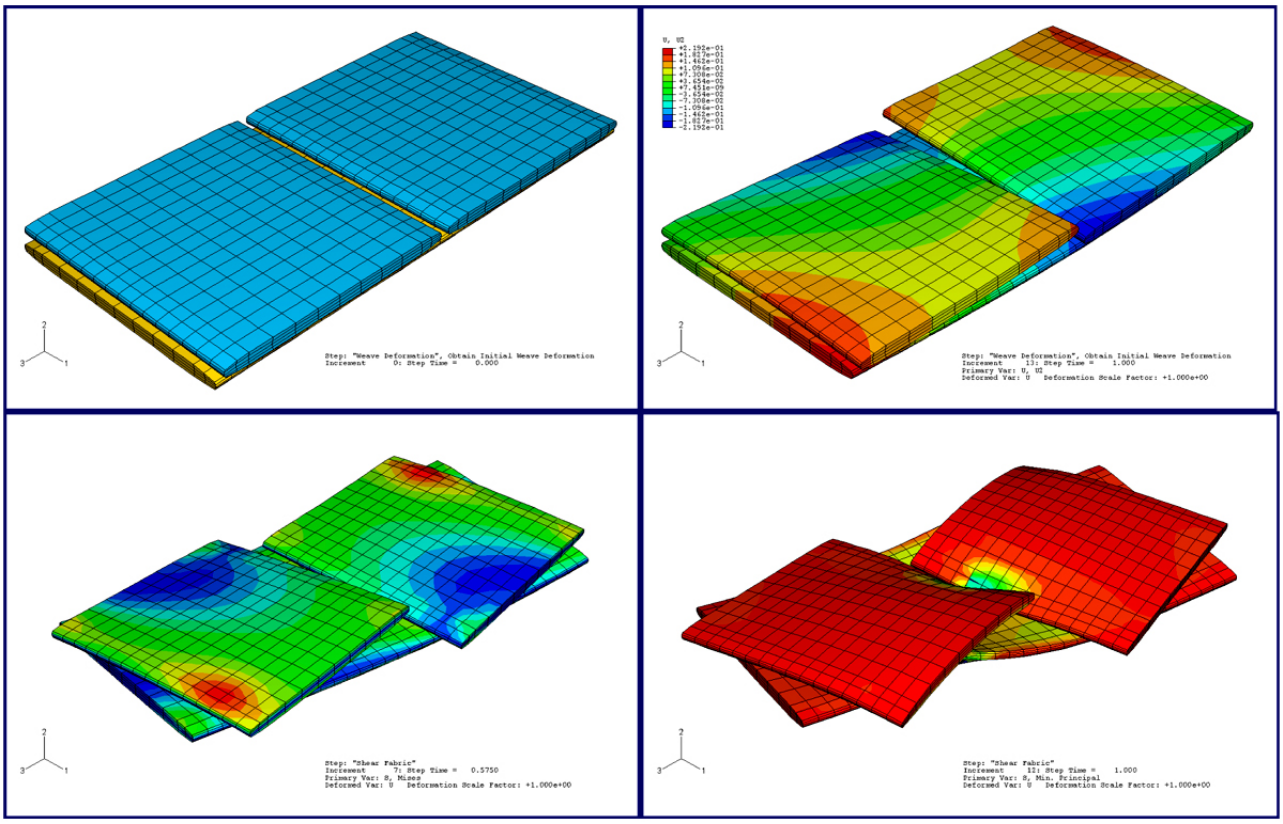

Figure 4. Fabric shear model for 2 × 2 twill weave. Initial model geometry and mesh (upper left); model deformed into weave pattern (upper right); shear deformation before tow edge contact (lower left); shear deformations after tow edge contact (lower right).

stresses due to weaving. In the third image, fabric shear is simulated where the shear angle is less than the initial locking angle so that contact between adjacent tows has not yet occurred. In contrast, the last image shows the deformation resulting from such contact. It is this contact between parallel tows that causes a dramatic rise in in-plane shear resistance as indicated in Figure 5. This resistance limits the formability because increased shear resistance causes in-plane stress and eventually causes buckling (wrinkling) of the sheet.

The importance of the in-plane shear deformation mode for fabric formability was described in a previous report. The in-plane shear stiffness is of particular importance. As seen in Figure 5, the stiffness can be well characterized by a bilinear stress strain curve. The initial, very low, shear resistance is due to friction between tows as they slide against

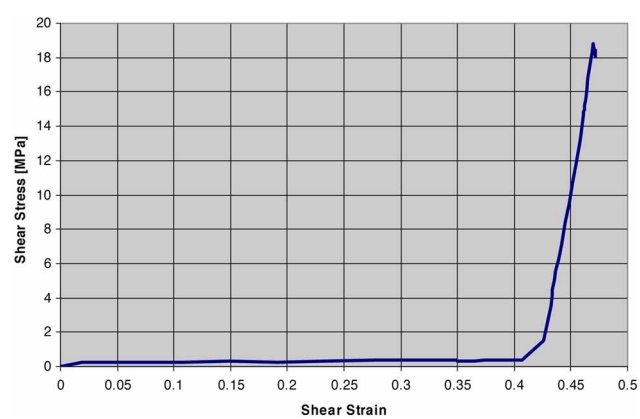

Figure 5. Shear force history showing sharp rise in shear resistance after two-edge contact.

one another during shear deformation. The sudden change in resistance occurs when the gap between parallel tows closes, and additional shear deformation is accompanied by a buildup in compression between tows. So, as was also described in the previous report,

the initial gap between parallel tows is a controlling factor in the overall in-plane shear resistance during forming. Large in-plane shear resistance causes in-plane compressive normal stresses that eventually buckle the fabric, thus creating wrinkles.

Recently, the results from modeling the in-plane shear behavior have been used to construct a nonlinear elastic constitutive law for application in forming process modeling. Prior process modeling efforts have used a range of hypothetical properties to study the sensitivity of model-predicted forming behaviors to material parameter variations. This recent effort was the first attempt to approximate actual material behavior with an appropriate set of nonlinear orthotropic material constants based on the in-plane shear behavior predicted by the mesoscale modeling. Previously, we had shown that high in-plane shear resistance could result in a large wrinkle or fold in the material at the large end of the cone-shaped mold.

A similar fold had been observed experimentally for a plain weave material known to have higher in-plane shear resistance than the 2×2 twill. Here, with the predicted properties we again predict a fold, although a small fold. A visual comparison of the model-predicted and experimentally generated folds is shown in Figure 6. The comparison would be remarkable except that they involve two different materials. The plane weave material would have a smaller locking angle and would be expected to have overall higher in-plane shear resistance and, therefore, less resistance to wrinkling than the 2×2 twill weave. The experimental fold/wrinkle for the plane weave is more severe than that predicted for the 2×2 twill weave. However, the experiments with the 2×2 twill material did not produce such a wrinkle.

Future work will be directed at consolidating and documenting the various models for future reference.

Figure 6. Comparison of model-predicted wrinkle defect and defect produced in a formed part.

5. LOW-COST CARBON FIBER

A. Low-Cost Carbon Fibers from Renewable Resources

Project Contact: C. F. Leitten, Jr., W. L. Griffith, A. L. Compere, J. T. Shaffer
Oak Ridge National Laboratory
P.O. Box 2008
Oak Ridge, TN 37831-8063
(865) 576-3785; fax: (865) 574-8257; e-mail: LeittenCFJ1r@ornl.gov

Project Manager, Composites: C. David Warren
Oak Ridge National Laboratory
P.O. Box 2008, Oak Ridge, TN 37831-8050
(865) 574-9693; fax: (865) 574-0740; e-mail: warrencd@ornl.gov

Technology Area Development Manager: Joseph A. Carpenter
(202) 586-1022; fax: (202) 586-1600; e-mail: joseph.carpenter@ee.doe.gov
Field Technical Manager: Philip S. Sklad
(865) 574-5069; fax: (865) 576-4963; e-mail: skladps@ornl.gov

---

Contractor: Oak Ridge National Laboratory
Contract No.: DE-AC05-00OR22725

Objective

- Demonstrate the use of new precursor materials that decrease the cost and increase the availability of carbon fiber, which meets the performance and price needs of the automotive market.
- Demonstrate that one or more renewable/recycled precursor formulations can be expected to produce industrial-grade carbon fibers at a cost of $3.00–$4.00/lb.

Approach

- Develop systematically the technical base needed to produce lignin-blend carbon fiber feedstocks at industrial scale:
  1. Produce lignin to obtain best molecular weight, low-volatile, low-salt material.
  2. Use spinning, oiling, and sizing technology.
  3. Use spinning technology, including production die structure, plasticizers, and nucleating agents.
  4. Use plasma treatment and sizing technology to make the fiber compatible with selected resin systems.
  5. Select appropriate polyesters.
  6. Evaluate properties and economics of fiber and composite systems.
- Work with industrial partners to scale and transfer the technology for the production of carbon fiber precursors from lignin blend feedstock.

1. Evaluate melt-extrusion properties of lignin-based feedstock at increasing scale, using near-industrial equipment that can be readily obtained by fiber manufacturers.
2. Evaluate production of carbon fiber using a research production line at an industrial facility.
3. Evaluate mechanical and composite compatibility properties of graphitized melt-spun lignin-blend fibers.
4. Work with partners to better define process economics.

- Transfer technology, including intellectual property, for the production of carbon fibers from lignin to industrial partners.

Accomplishments

- Conducted proof-of-concept demonstration of the melt extrusion of 28-filament tow of lignin-based fibers:

  1. compositions
  2. processing methods
  3. evaluations
  4. fiber quality.

- Indicated by preliminary data that yields of 50%, consistent with those obtained commercially for lignin-based activated carbon, are feasible.
- Successfully spun significant amounts of 28-filament tow at the University of Tennessee (UT) using a two-step process. No sticking problems were apparent, and fiber diameter was reduced from ~45 µm to ~15 µm, with an apparent increase in mechanical properties.
- Conducted preliminary evaluations of a plasma surface treatment plus silanation for lignin-based fibers, which indicated a significant improvement in fiber-resin bonding over conventional carbon fibers.
- Made small epoxy resin composites using carbon fibers produced from UT 28-filament tow, which showed composite mechanical properties.

Future Direction

- Develop methods for production of industrial-quality carbon fibers from lignin blend feedstocks. Studies will include the following:

  1. Optimize lignin preprocessing to minimize contaminants (salts and particulates) and provide the best molecular weight.
  2. Develop conditioning and spinning processes that remove water and volatiles prior to fiber production.
  3. Select and design spinning dies that provide the best internal structure.
  4. Select plasticizers and nucleating agents for lignin-polyester fiber blends.
  5. Select and develop techniques for spooling and oiling lignin blend fiber at each step.
  6. Develop methods for surface treating and sizing the surface of carbon fibers to improve compatibility with proposed resin systems. This is particularly critical for chopped fiber–resin composites.

- Work with project partners to

  1. address raw fiber production issues (lignin, preconsumer recycled polyesters, spinning and winding technologies), and
  2. evaluate carbon fiber production from lignin-based multifilament tow using an industrial research process line.

- Transfer technology, including any intellectual property, to industry.

Introduction

This project focuses on development of carbon fibers from high-volume, low-cost, renewable or recycled fiber sources to reduce precursor and processing costs. Use of these materials also decreases sensitivity of carbon fiber cost to changes in petroleum production and in energy cost.

The early stages of this project focused on proof-of-concept demonstration of the production of single fibers from a variety of high-volume natural, renewable, and recycled materials. These studies showed that carbon fiber, which was primarily composed of Kraft lignin, an inexpensive, high-volume wood pulping byproduct, could be blended with small amounts of a variety of polyolefins and polyesters and melt spun to produce single fibers that could be processed using conventional furnacing sequences to yield carbon fibers.

Single fiber experiments showed that lignin-blend fibers were, in many respects, similar to conventional carbon fiber feedstocks. The fibers, spun at North Carolina State University, required a stabilization (oxidation) cycle, followed by carbonization and graphitization (furnacing in an inert atmosphere). Graphite content, measured with X-ray diffraction, increased with increasing graphitization temperature. The yield from this lignin-blend feedstocks was ~50%, and the fibers were dense, smooth, and round. Fiber properties improved if the fibers were stretched during furnacing.

Based on these studies, it was decided to produce larger amounts of lignin-blend feedstock melt extruded as a multifilament tow. Fiber spinning was moved to UT where a twin-screw Leistritz extruder was available. Using this unit, initial production of multifilament tow was achieved. The major problems encountered were due to contaminants in the desalted commercial lignin used and were resolved by (1) separation of particulate and fibrous contaminants from the lignin, (2) development of a two-step blending and extrusion process, and (3) installation of a filter on the extruder.

This year, larger amounts of multifilament tow were produced using lignin-based feedstocks. In December 2002, 28-filament tow was produced using the Leistritz extruder. As earlier, no interfiber sticking was observed, and small diameter fibers could be produced and spooled. A shear die similar to those used for production of pitch fibers was used to modify the internal structure of the lignin blend fibers. A pre-consumer recycled polyester was used in the lignin fiber blends. Methods for modifying the fiber surface to increase adherence of resin to the fibers were evaluated and used in the successful production of small epoxy resin–carbon fiber composites.

Project Deliverables

By the end of this multiyear program, production of one or more environmentally friendly, economically feasible carbon fiber precursors will be demonstrated, and transfer of production technologies and related intellectual property to industry will be initiated.

In fiscal 2003, two major milestones, the extrusion of 28-filament lignin-blend fiber tow (11/2002) and the production of small resin-fiber composites (9/2003) were completed on time.

Planned Approach

Production of industrial-grade carbon fibers from a radically new type of feedstock requires the simultaneous development of methods for feedstock recovery, preparation, blending, spinning, handling, and spooling in addition to the furnacing, stretching/orientation, oiling, and sizing technologies required for conventional fibers.

Because of high levels of emissions and costs typically associated with spinning of fiber from liquids, first priority was placed on development of melt-spinning techniques for fiber. Use of lignin and other

nonnitrogenous feedstocks was preferred because it would eliminate cyanide emissions during furnacing. Use of modern furnacing techniques, such as hot-stretching and controlled atmosphere processing, are being evaluated to improve properties and yield of carbon fiber precursors from feedstock.

After lignin is dried, desalted, and, if necessary, further purified, lignin blend feedstocks will be extruded in a two-step process. First, lignin and a small amount of polyester are blended and extruded as pellets. The pellets are later extruded as small tow (25 to 50 fibers) and will be stabilized and carbonized to permit evaluation of finished fiber structure and mechanical properties. Because the fiber is intended to be used in chopped fiber composites, the fiber will be also be surface treated and sized to increase compatibility of the resin with the fiber surface.

Industrial partners are increasingly involved in the development of process technologies. They have been working with project staff on the selection of blending polymers for lignin, purification of lignin, strategies for production of cleaner lignin, and spinning of fiber. In the later stages of the project, industrial partners will also assist in production of lignin-based carbon fiber, using a research industrial production line.

Transfer of project technology, including any intellectual property, is planned.

Precursor Evaluation

Lignin is an inexpensive, high-volume byproduct of Kraft pulping to produce paper. For lignin to be used as a fiber feedstock, it needs to be purified to remove materials such as particulate, cellulosics, volatile, and pulping chemicals that would interfere with the formation of satisfactory carbon fibers. Byproduct lignin derived from the Kraft pulping process is currently produced as a free-flowing spray-dried powder and is used in a variety of different industrial applications.

Project staff has been working with MeadWestvaco, a project partner which is the major domestic producer of Kraft lignin, to evaluate methods for lignin purification. As commercial lignins contain significant quantities of salt, desalting was the first type of purification investigated. At present, lignin for experimental use is desalted by washing with distilled water and is then dried for experimental use.

During FY 2002 experiments with the UT twin-screw extruder, it was noticed that dies became clogged during extrusion. The 28-filament dies used in extrusion had an average hole size of 225 μm, and future multifilament dies are expected to be smaller. Raw desalted lignin was screened, and contaminants ranging from sand grains and diatoms to nonmelting cellulosic fibers were identified. It was determined that these materials could be decreased significantly by: (1) using a two-dimensional (2-D) sieving technique to remove the bulk of the material from lignin and (2) adding a sandpack filter to the extrusion train.

The hardwood lignin used in current experiments is a finely divided powder. It will naturally contain small amounts of wood-derived volatiles that partition into lignin from pulping liquors. Lignin also sorbs water. Because the extrusion temperature is above the boiling point of water and many volatile organics, single-step extrusion of lignin blends results in the formation of bubbles within the fibers. To decrease bubble formation, a two-step extrusion process has been developed. In this process, lignin and polyester powders are mixed, melted, and extruded to form pellets. Water vapor and volatiles are substantially removed during the pellet extrusion, and the pellets are re-extruded to form fibers. This method was used in spinning the fibers used for composite tests and was effective in preventing the development of most large bubbles. Small angle X-ray examination of fiber bundles does, however, indicate the presence of submicron bubbles in fibers.

If the lignin polyester blend is held in the extruder at high temperatures (>225°C) for extended periods, char formation has been noticed. Examination of lignin powders by nuclear magnetic resonance (NMR) indicates that the charring may be due to short chains of beta-linked sugars attached to the lignin. As the sugars have only small amounts of carboxyl groups, they appear to be derived from a lignin-carbohydrate complex in the wood, rather than from repolymerization of carbohydrates in pulping liquors.

The project staff is currently evaluating the simple industrially feasible methods for carbohydrate removal from lignin.

Working with Eastman Chemical Company staff members, the project staff has been able to use high-volume preconsumer recycled polyesters in feedstock. This is providing a completely renewable and recycle-derived carbon fiber feedstock.

Fiber Spinning

Fiber spinning technology was improved in several different ways during this fiscal year. As described above, the feedstock for fiber was improved by removal of contaminants from lignin and by addition of preconsumer recycled polyesters. The spinning process was modified as a two-step process; pellet extrusion followed by fiber extrusion significantly decreased voids in the fiber.

As described above, a sandpack filter was added to the Leistritz extruder at UT. This is a conventional industrial technology that decreases plugging of the extrusion die.

However, the most significant modification to the fiber spinning process was a change in the spinning die design. In single-fiber extrusion, an untapered cylindrical die was used. This provided dense, smooth-surfaced fibers but did not provide either improved polymer mixing or orientation. In early experiments using the UT Leistritz extruder, the internal fiber structure was dense and without "onion-skin" layers. However, the dies used in fiber extrusion were tapered textile dies that provided minimal mixing and did not alter the structure of polymers within the fiber.

Microscopic examination of surface fracture patterns on ends of fibers broken during mechanical property testing showed that lignin-based carbon fibers did not have an internal structure comparable to that of pitch fibers.

To create a "pitchlike" structure in lignin-blend fibers, a shear die like that used for extrusion of pitch fibers was designed and fabricated. This type of die provides high-shear at the point of fiber extrusion. In addition to ensuring good mixing of fiber components, high-shear mixing increases fiber stiffness. This is shown in Figure 1 and Table 1.

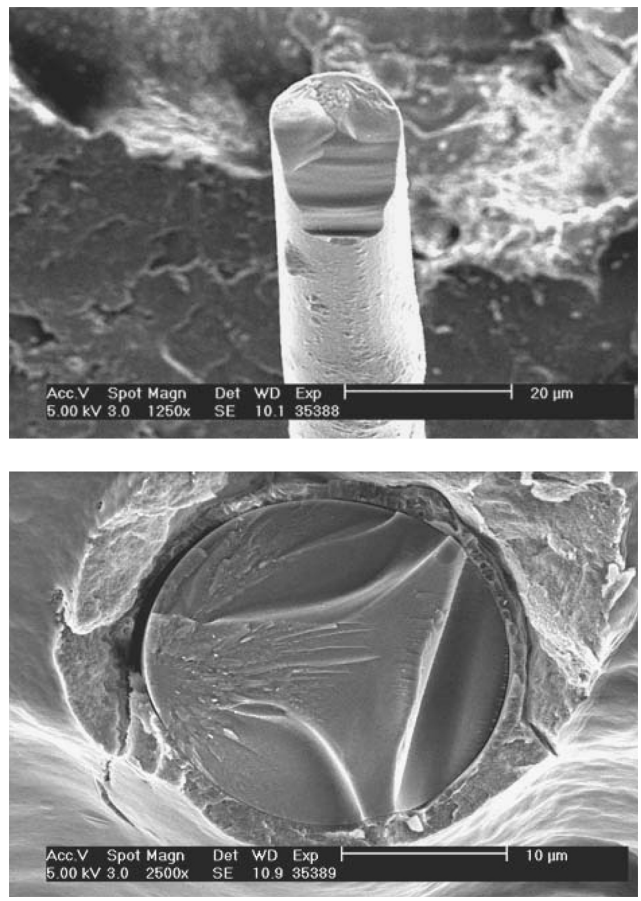

Figure 1. Ends of carbon fiber fracture test specimens showing improved fracture patterns.

Table 1. 1200°C carbonized lignin-blend single-fiber tensile data

Specimen	Diameter (μm)	Peak stress (ksi)	Modulus (Msi)	Strain at peak stress (%)
Spun 11-12/2002 using textile die				
SP2-S4	13.0	125.2	7.9	1.63
Sp2-S5	12.3	110.4	10.3	1.14
Sp2-S7	13.4	149.5	9.2	1.69
Sp2-S9	10.8	141.8	10.1	1.49
Spun 7/2003 using shear die				
Sp5-S2	11.8	149.5	15.8	1.07

Future studies will focus on a combination of die design, spinning conditions, and development of the winding, coating, and spooling technologies required to support technology implementation.

The lignin manufacturer, MeadWestvaco, expects to prepare and store a large batch of hardwood lignin for use by this project.

Fiber Surface Treatment

Lignin fibers are smooth-surfaced and dense. For these fibers to be used in chopped fiber composites, as planned, the surface of the fibers must be modified to increase resin compatibility. In production of conventional pitch and polyacrylonitrile fibers, this is achieved using surface treatments that oxidize the fiber surface and application of a surface coating, or sizing, which improves fiber-resin compatibility. Surface oxidation generally employs wet chemical treatment with strong acids, electrolysis, or a combination of these methods.

Based on earlier experience, it was decided that a combination of plasma treatment of the fiber surface and silanation could provide similar surface treatment with decreased environmental impact. Proof-of-principle tests on small amounts of fiber were completed.

As shown in Figure 2, measurements of fiber surface compositions using an energy dispersive X-ray (EDX) showed significant silanation. This was followed by examination of the retention of fibers in small composite specimens.

The method was scaled up and used for the preparation of small test composites to meet the September milestone.

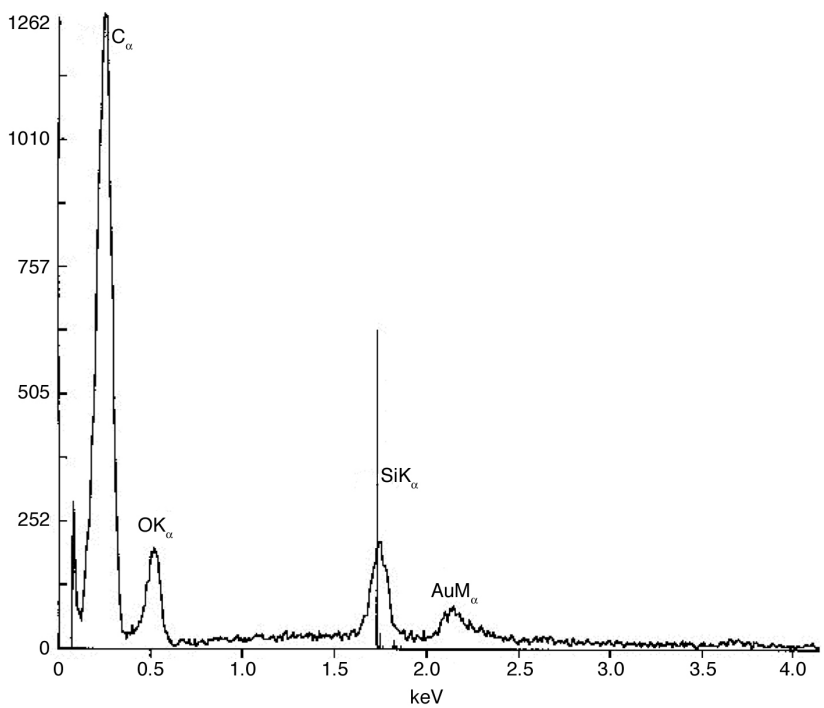

Figure 2. Measurements of fiber surface compositions using EDX showing significant silanation.

As shown in Figure 3, commercial fibers prepared by conventional surface treatment and sizing showed poor adhesion to the resin in small composite fracture tests. However, the plasma treated and silanated lignin-based carbon fibers shown in Figure 4 had excellent retention in the test composite.

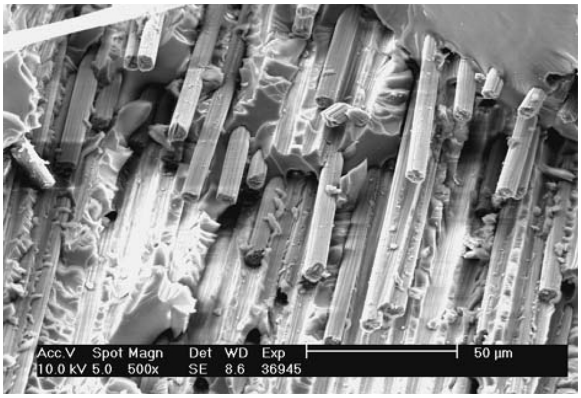

Figure 3. Commercial fibers prepared by conventional surface treatment and sizing showing poor adhesion to epoxy resin and slip out of the resin matrix in small composite fracture tests.

Composite Production

A significant amount of raw lignin-recycled polyester fiber was melt extruded at UT as 28-filament tow and furnaced at ORNL. Some difficulties were encountered due to the fiber being wound as an uncoated textile fiber, rather than as a 30° coated small tow. The need to hand-stretch, fire, and plasma treat individual strands of fiber, rather than a tow, limited the size of samples. The sample is shown in Figure 5. A small composite using an industrial carbon fiber with conventional sizing was also prepared.

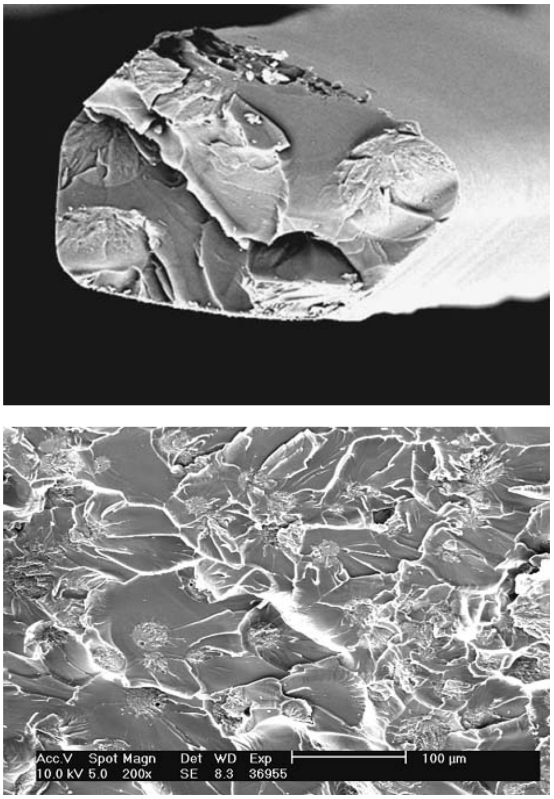

Figure 4. Plasma treated and silanated lignin-based carbon fibers with excellent adhesion to epoxy resin. (*a*) Small test specimen and (*b*) edge of larger composite test specimen.

Figure 5. Small composite prepared from lignin-based carbon fiber.

Evaluation of the composite, a September 2003 milestone, provided an early test to ensure that, further downstream, lignin-blend feedstocks will be useable in resin-fiber composites. To do that, proof-of-concept had to demonstrate these successes: (1) lignin-blend fiber can be melt-extruded as a small tow using near-commercial spinning equipment; (2) composites made from graphitized lignin-blend fibers can be used in resin-fiber composites that have normal fracture patterns, and (3) although very smooth, lignin-blend fibers can be plasma treated and silanated to provide good fiber/resin adhesion.

Future Directions

Significant production of lignin-based multifilament (28-strand) tow and successful use of this material in small resin-fiber composites were demonstrated this year. The project was reproposed and extended to permit evaluation of methods for producing high-quality lignin-based feedstocks for low-cost production of automotive carbon-fiber resin composites.

Having established proof-of-concept, the project staff will systematically address the technical issues required to produce industrial-grade lignin-based carbon fiber at prices and properties meeting automotive need. As the bulk feedstock used in this process is derived from Kraft pulping, a major concern is developing methods for consistently recovering clean, high-quality lignin low in volatiles, water, particulates, and salts. Additionally, the molecular weight of lignin varies considerably with pulping conditions, so delineation of the pulping conditions required to consistently produce industrial-grade carbon fiber will be evaluated.

Spinning die designs for production of lignin-based fibers will be evaluated. Initial tests indicated that dies, similar to those used for spinning pitch-based feedstocks, which provide high shear, create a more uniform internal structure in the raw fiber. Spinning parameters, including rheology, of the blend will be optimized for multifilament production.

Production techniques that provide high-quality, handleable, spoolable raw lignin-based fiber will be required. This will include selection and evaluation of plasticizers and nucleating agents, as well as raw fiber coatings and oils. Spooling techniques will also be evaluated.

After lignin-based fiber is carbonized, it must be surface treated and sized to increase compatibility with the resin system. Fiber-resin compatibility is particularly critical in automotive applications because the current program plan calls for use of chopped, rather than woven or wound, fiber.

Throughout the period, a variety of analytical techniques, including physical property evaluations of fiber and resin, as well as x-ray diffraction and electron microscopic examination, will be used to assess fiber quality.

As studies proceed, project partners expect to become increasingly involved in research activities. These will include tests of the fiber on a research furnacing line of an industrial partner. In 2006, formal transfer of technology for production of carbon fiber from Kraft lignin blend feedstocks, and associated intellectual property, will be initiated.

Partnerships

A number of different entities have been instrumental in development of this technology. North Carolina State University earlier spun a variety of lignin-blend polymers as single fibers. These were used in earlier feasibility evaluations. At present, UT

is working to prepare significant quantities of multifilament tow for project use.

The project also benefits from the participation of Eastman Chemical Company, which provides both technical assistance in spinning protocols and significant quantities of polyesters for spinning. Eastman Chemical Company of Kingsport, Tennessee, has also provided preconsumer recycled polymers. Mead-Westvaco at Charleston, South Carolina, has provided hundreds of pounds of lignins, including a wide variety of research lignins, and it has worked closely with the ORNL staff in lignin purification.

Conclusions

During this period, the project staff met all major goals and milestones. Spinning of significant quantities of 28-filament tow from a feedstock composed of Kraft Lignin and preconsumer recycled polyester, was successfully demonstrated. This material was successfully stabilized and carbonized, plasma treated and silanated, and used to prepare small epoxy resin composites.

As a part of this effort, a number of improvements were made to the feedstock production process. These included: (1) characterization of impurities and Kraft lignin feedstocks and development of methods for their removal, (2) development and implementation of a two-step extrusion process that greatly decreased flaws in raw lignin-blend fiber, (3) demonstration of use of preconsumer recycle polyester as the alloying polymer in the raw feedstock, (4) proof-of-principle demonstration of the use of high-shear dies in improvement of lignin-based carbon fiber properties, (5) proof-of-principle demonstration of a plasma surface treatment process that greatly improved adhesion of lignin-based carbon fiber to epoxy resin, (6) preparation of significant quantities of multifilament lignin-based fiber for use in manufacture of small test composites, and (7) preparation and evaluation of the small composites.

The project was retasked, partnerships with Eastman Chemical Company and Mead-Westvaco formalized, and the staff is developing the technical base required to support larger scale production of carbon fibers from high-lignin feedstocks.

B. Low-Cost Carbon Fiber Development Program

Program Manager: Mohamed G. Abdallah
Hexcel Corporation
P.O. Box 18748, Salt Lake City, UT 84118
(801) 508-8083; fax: (801) 508-8103; e-mail: mohamed.abdallah@hexcel.com

Project Manager, Composites: C. David Warren
Oak Ridge National Laboratory
P.O. Box 2008, Oak Ridge, TN 37831-8050
(865) 574-9693; fax: (865) 574-0740; e-mail: warrencd@ornl.gov

Technology Area Development Manager: Joseph Carpenter
(202) 586-1022; fax: (202) 586-1600; e-mail: joseph.carpenter@ee.doe.gov
Field Technical Manager: Philip S. Sklad
(865) 574-5069; fax: (865) 576-4963; e-mail: skladps@ornl.gov

Principal Investigators:
Harini Dasarathy, Carlos Leon y Leon, Stephen Smith, and Brent Hansen

---

Contractor: Hexcel Corporation
Contract No.: 450001675

Objective

- Define technologies needed to produce a low-cost carbon fiber (LCCF) for automotive applications at a cost of $3.00 to $5.00/lb in quantities greater than 1M lb/year. The required carbon fiber properties are tensile strength greater than 400 ksi, modulus greater than 25 Msi, and strain to failure greater than 1%.

Approach

- Develop new precursors that can be converted into carbon fiber at costs below the costs of current processes.
- Explore processing by methods other than thermal pyrolysis.
- Develop technologies leading to significant improvements in current production methods and equipment.
- Develop alternative methods for producing carbon fiber from pitch, polyacrylnitrile (PAN), or other precursors.
- Reduce precursor cost by the use of commercially available energy-efficient precursors and high conversion yields.
- Improve precursor production economics of scale and throughput.
- Introduce novel LCCF production methods.

Accomplishments

- Evaluated proposed research areas through laboratory trials and refinement of manufacturing cost analyses:
  - PAN-based precursors: large-tow benchmark, commodity textile acrylic tow, chemical modifications, acrylic fibers spun without solvents, and radiation and nitrogen pretreatment of PAN-based materials.
  - Precursors other than PAN: polyolefins—polypropylene (PP), linear low-density polyethylene (LLDPE) and high-density polyethylene (HDPE); polystyrene; and polyvinyl chloride (PVC) pitch.
- Scaled-up promising technologies to pilot line trials.
- Assessed the technical and economic feasibility of the proposed research areas.
- Down-selected the most promising technologies to meet the program objectives:
  - Commodity textile acrylic tow with chemical modification or radiation pretreatment.
- Developed detailed manufacturing cost models for the downselected technologies.
- Completed the engineering feasibility studies for large-scale production line.
- Completed the economical analysis to predict product production costs.
- Awarded a short-term (1-year) program to develop carbon fiber roving for the P4 process to meet the immediate needs of the ACC development programs.
- Proposed a Phase II long-term (3-year) program to build on the results of the LCCF program to produce production quantities of commodity textile-acrylic-based carbon fiber for the ACC programs (under review by ORNL).

Future Direction

- Complete the program final report.
- Complete the short-term program for the manufacturing and delivering carbon fiber roving to meet the immediate needs of the ACC development programs.
- Start working on the proposed long-term program (if the program is awarded).
  - Long-term (3-year) program to build on the results of the LCCF program to produce production quantities of commodity textile-acrylic-based carbon fiber for the ACC programs.

Introduction

The goal of this program is to define and demonstrate technologies needed for the commercialization of LCCFs to be used in automotive applications. Lighter-weight automotive composites made with carbon fibers can improve the fuel efficiency of vehicles and reduce pollution. For carbon fibers to compete more effectively with other materials in future vehicles, their cost must be reduced. Specifically, this program targets the production of carbon fibers with adequate mechanical properties, in sufficiently large quantities, at a sustainable and competitive cost of $3 to $5/lb.

Project Deliverables

At the end of this multiyear program, technologies for LCCF production will be defined. This definition will include the

required materials and facilities and will be supported by detailed manufacturing cost analyses and processing cost models. Laboratory trials and pilot-scale demonstrations will be performed to support the defined technologies.

Planned Approach

This program was divided into two phases:

Phase I: Critical review of existing and emerging technologies, divided into two tasks:

Task I.1. Literature review and market analysis.

Task I.2. Laboratory-scale trials and preliminary LCCF manufacturing cost assessments of the proposed technologies. Phase I led to further refinement and down-selection of the most promising technologies for Phase II.

Phase II: Evaluation of selected technologies using pilot-scale equipment and cost models. Phase II was divided into three tasks:

Task II.1. Pilot-scale design for the evaluation of selected LCCF technologies. This included modifications of a PAN spinning pilot line and two different carbon fiber conversion lines (a single-tow research line and a multitow pilot line) and the construction of continuous sulfonation processing equipment

Task II.2. Experimental evaluation of down-selected LCCF technologies, including commodity textile-tow PAN (with chemical modification and radiation and/or nitrogen pretreatment) and polyolefins (LLDPE and PP).

Task II.3. Large-scale feasibility study of selected LCCF technologies.

Conclusions of FY 2001 Results

(October 1, 2000 to September 30, 2001)

The results of the laboratory trials of proposed technologies were as follows.

1. Further work on acrylic fibers spun without solvents, plasticized PAN, PVC, and polystyrene were halted because of technical, environmental, and cost issues.
2. The following most promising LCCF technologies for Phase II were evaluated and selected: commodity textile PAN-based precursors (as-received and with pretreatment using chemical modification, radiation, and nitrogen prestabilization technologies) and polyolefin precursors (LLDPE and PP).
3. A large-tow PAN precursor technology benchmark was used as a metric to evaluate the proposed technologies in terms of their potential to meet the LCCF program's cost targets. The difference between commodity textile PAN and large-tow precursor, based on carbon fiber cost, is approximately $1.80 vs $3.10/lb.

Conclusions of FY 2002 Activities

(October 1, 2001 to September 30, 2002)

These are the highlights of the progress made during FY 2002:

1. Demonstrated the technologies of using chemical modification and radiation pretreatments of commercial commodity textile (28K) tow to produce LCCF that meets the program targeted properties and estimated cost predictions.
2. Developed manufacturing recipes for the conversion of commodity textile acrylic fibers into LCCF using the technologies of chemical modifications and radiation treatments.
3. Developed estimated carbon fiber cost using chemical modification and radiation pretreatments of commercial commodity textile acrylic fibers.
4. Demonstrated the conversion of LLDPE to LCCF that meet the targeted properties of the program and estimated cost

predictions. Due to the issues of sulfuric acids recycling and the available precursor, we concluded that the LLDPE-based technology would need more development efforts to compete with modified textile PAN-based technologies.

5. Commenced the engineering feasibility study of the production lines to produce LCCF based on commodity textile acrylic PAN using chemical modification and radiation pretreatment technologies.
6. Started the plans and statements of work for the long-term and short-term follow-up programs.
7. Updated and refined cost models to reflect the accomplishments in FY 2002.
8. Produced four papers (three published during SAMPE 2002, in Baltimore, Maryland, and one for the Global Outlook for Carbon Fiber 2002, in Raleigh, North Carolina, and a presentation during the SAMPE 2002, in Long Beach, California).

Summary and the Results of FY 2003

Task II.3. Large-scale feasibility study of selected LCCF technologies

During FY 2003 activity was concentrated on task II.3 the large-scale feasibility study for the selected technologies and the economical analysis for predicting product costs. The baseline for this task was a carbon fiber conversion process based on subscale work done during this program using textile acrylic fiber, chemically modified in acrylic fiber manufacturing process, and radiation pretreatment in-line carbon fiber manufacture. The production facility was based on two manufacturing lines in a common building of 2.0 MM lb/year per line. The feed material is 505K, 1.5 dpf textile acrylic fiber. The engineering feasibility study included the following:

1. manufacturing equipment needed for product "recipe,"
2. facility layout and design,
3. material flow and handling,
4. equipment and facility capital costs,
5. manufacturing utility costs,
6. supply of raw materials, and
7. economical analysis of predicted product costs for the selected technologies.

The following is a summary of the design guidelines and processing parameters that we used in this study:

1. production facility based on nominal 2.0M lb/year per line,
2. two manufacturing lines in a common building (baseline case),
3. feed material is 8 tows of 505K at 1.5 dpf, in boxes containing 1500 lb of PAN,
4. final line speed is 420 m/h =1378 ft/h (baseline case),
5. three oxidation ovens (11 passes of 43 ft each, total heated length = 1419 ft, and residence time = 64 min),
6. carbonization (LTF = 30 ft–1.2 min, and HTF = 36 ft–1.5 min),
7. surface treatment using electrochemical (anodic) oxidation,
8. sizing bath (double-roll dip),
9. sizing drying (heated drums), and
10. product take-up (piddle-pack in boxes).

Figure 1 shows the building and equipment layout. Each creel has 2 times 8 positions for continuous feeding, and the facility layout allows a "mirrored" second building to add another 4.0M lb/year.Table 1 gives the estimated facility costs, and Table 2 gives the estimated utility costs. Table 3 gives the estimated product cost for baseline for 2 lines (4.0M lb/year).

Economic Analysis and Cost Model—Baseline Assumptions

1. **Raw material**
   - Textile acrylic fiber $0.80/lb
   - Same, chemically modified $0.91/lb
   - Box weight 1,500 lb
   - PAN length per box 8,089 m (26,540 ft)

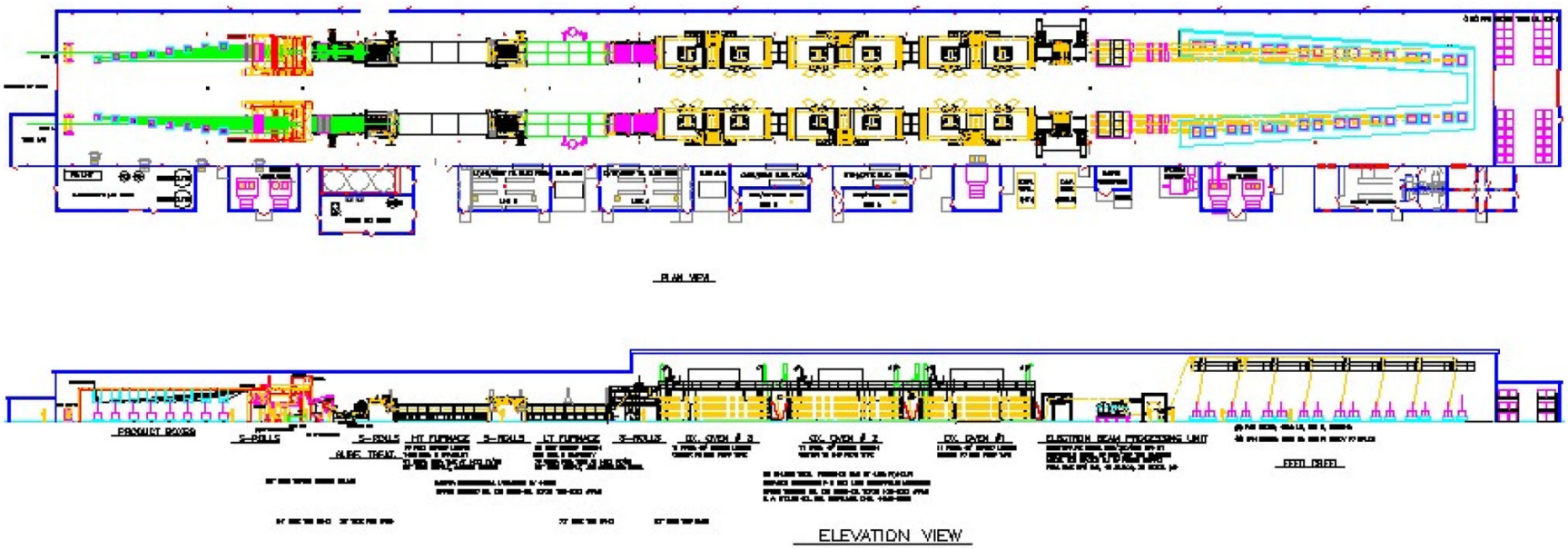

Figure 1. Building and equipment layout.

Table 1. Estimated facility costs

Facility configuration nominal capacity	1 Line (2.0M lb/year)	2 Lines (4.0M lb/year)	4 Lines (8.0M lb/year)
Building	$2,938K	$2,938K	$5,876K
Feed creel and oxidation	$5,601K	$11,055K	$22,111K
Carbonization	$6,162K	$12,199K	$24,397K
Aftertreatment	$2,449K	$3,982K	$7,963K
Engineering costs	$1,630K	$2,119K	$2,771K
Total facility costs	$18,780K	$32,293K	$63,119K
Capital cost (per lb/year CF)	$9.39	$8.07	$7.89
Optional equipment			
Radiation pretreatment	$2,379K	$4,671K	$9,343K
Distributed control system	$1,010K	$2,021K	$4,041K

Table 2. Estimated utility costs

Facility configuration nominal capacity	1 Line (2.0M lb/year)	2 Lines (4.0M lb/year)	4 Lines (8.0M lb/year)
Electricity	$429K	$805K	$1,610K
Natural gas	$446K	$867K	$1,734K
Water	$2K	$3K	$6K
Nitrogen	$106K	$213K	$425K
Steam	$19K	$39K	$77K
Compressed air	$1K	$1K	$2K
Sewer	$1K	$2K	$4K
Total utility costs	$1,004K	$1,930K	$3,859K
Utility cost (per lb/year CF)	$0.50	$0.48	$0.48
Optional equipment			
Radiation pretreatment	$63K	$126K	$252K

Table 3. Estimated product costs (baseline: 2 lines = 4.0M lb/year

Hexcel proposed processes	Large tow precursor		Textile acrylic tow with			
			Chemical modification		Radiation treatment	
Process steps	Mill cost	With 20% ROI	Mill cost	With 20% ROI	Mill cost	With 20% ROI
Precursor ($/lb)	1.59		0.91		0.80	
Precursor ($/lb of CF)	3.53	3.53	2.02	2.02	1.78	1.78
Pretreatment					0.15	0.49
Stablization/oxidation	0.79	1.47	0.79	1.47	0.79	1.47
Carbonization	0.67	1.35	0.67	1.35	0.67	1.35
Sizing, S.T., packaging, Q.C.	0.56	0.81	0.56	0.81	0.56	0.81
SG&A/IR&D	0.40		0.40		0.40	
Total per pound of CF	$5.95	$7.56	$4.43	$6.05	$4.34	$6.30
Changes from baseline	None					

2. **Processing**
   - Product speed 420 m/h (1378 ft/h)
   - Maintenance downtime 15 d/year
   - Production cycle 18 creel loads (~15 d)
   - Downtime per cycle 1.87 d
   - Uptime per year 85.4%
   - Conversion yield 50%
   - Production yield 90%
3. **Labor costs**
   - Average compensation $16.50/h
   - Taxes and benefits 40% of compensation
4. **Staffing** (paid 365/24)
   - Operators (direct labor) 8 (1 line = 6; 4 lines = 14)
   - Technicians (direct labor) 2 (1 line = 2; 4 lines = 3)
   - Indirect labor 40% of direct labor
5. **Labor allocation**
   - Creel—oxidation 35%
   - Carbonization 15%
   - After treatment 50% (includes surface treatment, sizing, packaging, QC)
6. **Other expenses (per year) of invested capital**
   - Capital charge (depreciation) 5%
   - Taxes and insurance 2%
   - Maintenance 3%
   - Return on investment (ROI) 20%
7. **SG&A/IR&D (per year)**
   - 4.0M lb/year on 2 lines (baseline) $1.6M = 10% of mill cost
   - 2.0M lb/year on 1 line $1.2M = 75% of baseline
   - 8.0M lb/year on 4 lines $2.4M = 150% of baseline
8. **Utilities & materials**
   - Utilities rates (based on SLC, UT)
   - Materials (electrolyte, sizing) $0.054/lb of CF
   - Packaging Use PAN boxes

The conclusions of the baseline product costs/price follow:

1. LCCF technologies can reduce product price compared to large tow precursor:
   - Chemical modification by $1.50/lb of CF
   - Radiation treatment by $1.25/lb of CF
2. To achieve a sustainable price of <$5.00/lb, additional measures are needed by implementing the following. Improvements in cost/price are feasible by
   - reduction of invested capital cost,
   - higher line speed,
   - shorter downtime per cycle,
   - longer production cycles,
   - increased throughput over time (learning curve), and
   - higher conversion yield (optimized chemical modification).

Figure 2 shows the impact of implementing these improvement measures on the baseline estimated product cost.

Summary of Task II.3. Large-scale feasibility study of selected LCCF technologies

1. Defined manufacturing facility and processing conditions.
2. Sustainable price of just below $5/lb of LCCF appears achievable.
3. Cost drivers are
   - precursor (commodity acrylic fiber) $1.94
   - invested capital (ROI) $1.06
   - labor and SG&A/IR&D $0.81
   - utilities and materials $0.48
   - depreciation $0.26
   - maintenance $0.14
   - taxes and insurance $0.10
4. Further reductions in product cost should focus on
   - precursor and capital cost
   - fine tuning other cost contributors

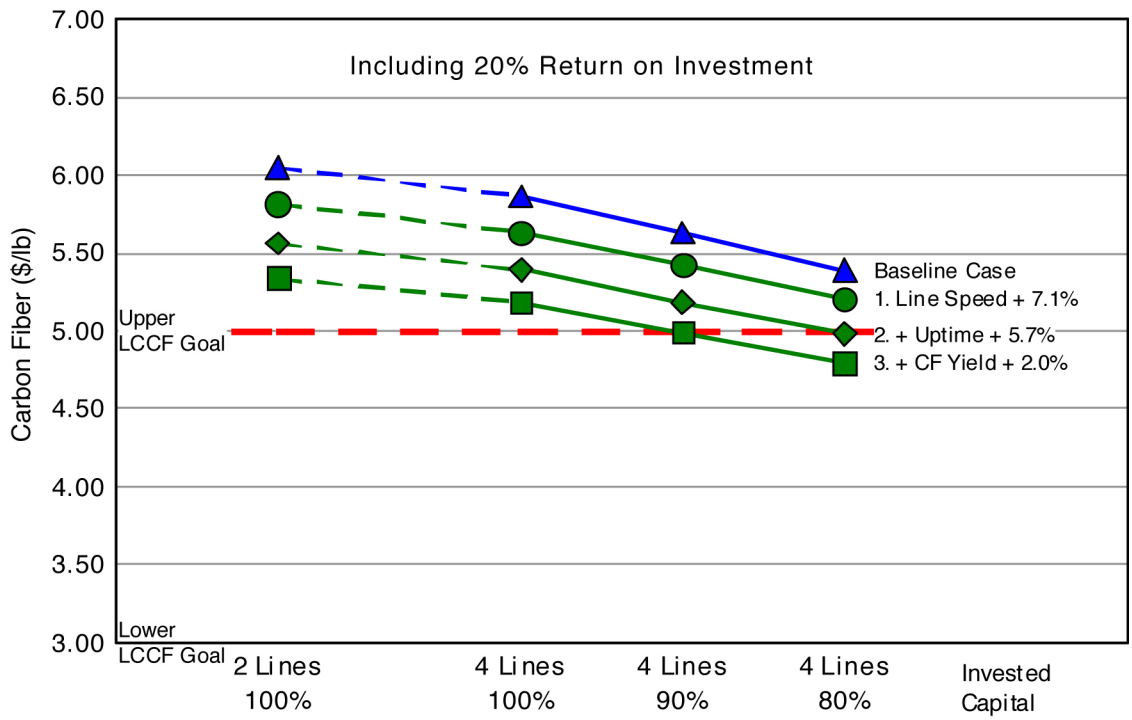

Figure 2. Estimated product cost—improved conversion yield.

Future Work

A Phase II program that is built on the results of Hexcel's LCCF Phase I program was proposed with the following objectives: (1) scale-up and verify the defined technologies and (2) integrate in ongoing automotive research activities by DOE/ORNL and USCAR/ACC. The goals of this future work follow.

1. Develop production technologies utilizing commodity textile acrylic precursor with chemical modification.
2. Identify product forms for automotive applications.
3. Develop and apply suitable technologies to make the identified product forms.
4. Provide needed quantities to support DOE/ORNL programs.

A program plan that addresses the above goals into three major tasks was developed. The following is a summary of these tasks.

Task 1. Develop plans for the integration of defined technologies for use in on-going research activities by DOE/ORNL and USCAR/ACC

The major milestones for this task follow:

1. Develop integration plan for review and approval by all parties involved.
2. Define the requirements for precursors and carbon fiber to meet the needs of the on-going research activities, that includes the following:
   - precursors for oxidation studies and oxidized/stabilized precursors for microwave processing, and
   - carbon fiber product forms for the automotive industry that include surface treatment, sizing systems, make-up and packaging.
3. Finalize the integration plans and material requirements.
4. Plan a design review meeting to approve the integration plan.
5. Commence implementation of production technologies.

Task 2. Implement technologies for chemical modification of textile acrylic and its conversion to carbon fiber

The major milestones for this task follow:

1. Implement chemical modification equipment into textile acrylic production line.
2. Modify carbon fiber (pilot) line to handle textile acrylic tow (unsplittable and splittable tows).
3. Develop production procedures for precursor and carbon fiber line operations.
4. Conduct trials to verify Phase I results for precursor and carbon fiber.

Task 3. Develop and implement techniques to manufacture Product Forms (as defined in Task 1)

The major milestones for this task follow:

1. Support of ongoing research at DOE/ORNL for integration into oxidation studies and oxidized/stabilized precursors for microwave processing.
2. Carbon fiber of various forms to support ongoing research and development by DOE/ORNL and USCAR/ACC, such as continuous tow for prepreg, woven fabrics, and chopped fiber (HexMC).
3. Carbon fiber roving for the P4 process using splittable precursor or carbon fiber tow dividing.

The proposal for this Phase II program for consideration and evaluation was completed and submitted to ORNL. The proposed Phase II program is for 3 years. Hexcel planned this Phase II scope based on input and results of the joint working relationship with Sterling Fiber of Pace, Florida, during Phase I of the LCCF program.

Summary and Conclusions of FY 2003 Activities

These are the highlights of the progress made during FY 2003.

1. We completed Task II.3, the large-scale feasibility study, for the selected technologies and the economical analysis for predicting product costs, based on subscale work done during this program using textile acrylic fiber, chemically modified in an acrylic fiber manufacturing process, and radiation pretreatment in-line carbon fiber manufacture.
2. We proposed a Phase II program that is built on Phase I results with the following goals
   - Scale-up and verify the defined technologies.
   - Define product forms.
   - Develop and implement techniques to manufacture product forms.
   - Integrate results in ongoing automotive research with other activities by DOE/ORNL and USCAR/ACC.

C. Microwave-Assisted Manufacturing of Carbon Fibers

Principal Investigator: Felix L. Paulauskas
Oak Ridge National Laboratory
P.O. Box 2008, MS 6053
Oak Ridge, TN 37831-8048
(865) 576-3785; fax: (865) 574-8257; e-mail: paulauskasfl@ornl.gov

Project Manager, Composites: C. David Warren
Oak Ridge National Laboratory
P.O. Box 2008, Oak Ridge, TN 37831-6065
(865) 574-9693; fax: (865) 576-4963; e-mail: warrencd@ornl.gov

Technology Area Development Manager: Joseph A. Carpenter
(202) 586-1022; fax: (202) 586-1600; e-mail: joseph.carpenter@ee.doe.gov
Field Technical Manager: Philip S. Sklad
(865) 574-5069; fax: (865) 576-4963; e-mail: skladps@ornl.gov

Participants
Terry L. White, Oak Ridge National Laboratory
Kenneth D. Yarborough, Oak Ridge National Laboratory
Professor Roberto Benson, University of Tennessee

Contractor: Oak Ridge National Laboratory
Contract No.: DE-AC05-00OR22725

Objective

- Investigate and develop a microwave-assisted technical alternative to carbonize and graphitize polyacrylonitrile (PAN) based precursor.
- Prove that carbon fiber with properties suitable for use by the automotive industry can be produced inexpensively using microwave-assisted plasma (MAP) processing.
- Demonstrate that MAP processing can produce acceptably uniform properties over the length of the fiber tow.
- Show that for specified microwave input parameters, fibers with specific properties may be controllably and predictably manufactured using microwave furnaces.
- Most important, demonstrate the economic feasibility for producing approximately 30-Msi modulus fibers at a significant cost reduction relative to those produced conventionally.

Approach

- Demonstrate the ability to deliver high fiber throughput by increasing line speed and tow count.
- Conduct parametric studies on the continuous carbon-fiber processing pilot unit to continually improve the system design, process parameters, and fiber properties.
- Characterize MAP processed carbon fibers to confirm that they satisfy program requirements.

- Continually evaluate, develop, and characterize "spin-off" technology, hardware, and ideas that improve upstream or downstream processing, or facilitate more efficient utilization of fiber.

Accomplishments

- Carbonized 50-K PAN fiber tows were successfully processed at single-tow line speeds up to 200 in./min. This is approximately twice the typical line speed employed in conventional processing. Based on the knowledge and experience gained in this project, the research team believes that processing speeds considerably exceeding 200 in./min are achievable after appropriate system modifications.
- Upgraded the pilot line to simultaneously process three 50-K tows.
- Carbonized 50-K PAN fiber tows successfully at three-tow line speeds up to 12 in./min.
- Discovered a stable three-tow operating mode that requires very little feed gas and yields excellent mechanical properties at 12-in./min line speed.
- Evaluated physical, mechanical, and morphological properties for fiber samples manufactured at single-tow line speeds up to 200 in./min and three-tow line speed of 12 in./min.
- Completed initial software development for an improved dielectric measurement system that can operate from 250°C to >1,000°C with kilohertz sampling rates.
- Issued a patent, entitled "Microwave and Plasma-Assisted Modification of Composite Fiber Surface Topography."
- Performed physical and morphological evaluations to support Argonne National Laboratory's (ANL's) carbon-fiber recycling program, and delivered results to ANL researchers.

Future Direction

- Increase 3-tow line speed to 40 in./min.
- Continue parametric studies and fiber characterization to better understand process effects and processing window, and to quantify fiber properties.
- Achieve integration with other carbon-fiber technology developments, for example, new precursors, rapid oxidation/stabilization processes, advanced surface treatment, advanced downstream formatting, and/or component manufacturing processes (future project).
- Develop and demonstrate related technologies in the area of carbon-fiber manufacturing (e.g., advanced characterization, surface treatment, sensing and control technology, recovery and reuse) as resources and time permit.
- Develop partnership(s) to commercialize the technology.

Introduction

The purpose of this project is to investigate and develop a microwave-assisted technical alternative to carbonize and partially graphitize the PAN precursor. The project is to prove that carbon fiber with properties suitable for use by the automotive industry can be produced inexpensively using MAP processing. It is to be demonstrated that MAP processing can produce acceptably uniform properties over the length of the fiber tow. The project is also to show that for specified microwave input parameters, fibers with specific properties may be controllably and predictably manufactured using microwave furnaces. Finally, but most important, this

project is to demonstrate the economic feasibility for producing approximately 30-Msi modulus fibers at a significant cost reduction below those produced conventionally.

Project Deliverables

At the end of this multiyear program, a continuous, multiple-tow, scalable, high-production line speed MAP carbon fiber prototype unit will have been developed, constructed, and tested. A final report will be issued with the test results of the carbon fibers processed with this unit. Appropriate industry briefings will be conducted to facilitate commercialization of this economically enabling technology.

Fiber Properties

A key goal of this project is to demonstrate that carbon fibers with satisfactory material properties can be produced by the MAP process. Program goals established for fiber properties are 25-Mpsi tensile modulus, 250-ksi ultimate tensile strength, and 1.0% ultimate strain. During this reporting period, the project team evaluated the physical, mechanical, and morphological properties of carbon samples that were carbonized and partially graphitized at single-tow line speeds of 130 to 200 in./min, and at three-tow line speed of 12 in./min. Results are compared to commercial fibers that were tested by the same method, as well as to program requirements. Mechanical properties are shown in Figure 1, where 97.7% basis means that 97.7% of property data should exceed the indicated value, and MAP3@12 indicates three tows MAP processed at 12 in./min. Mechanical property results generally satisfied the specified requirements, except that the ultimate tensile strength was slightly deficient at the highest single-tow line speeds. This is attributed to the fiber transport and tensioning system that was not designed for high line speeds. To resolve this problem, a commercial, high-speed, fiber transport and tensioning system was installed during the upgrade to three-tow

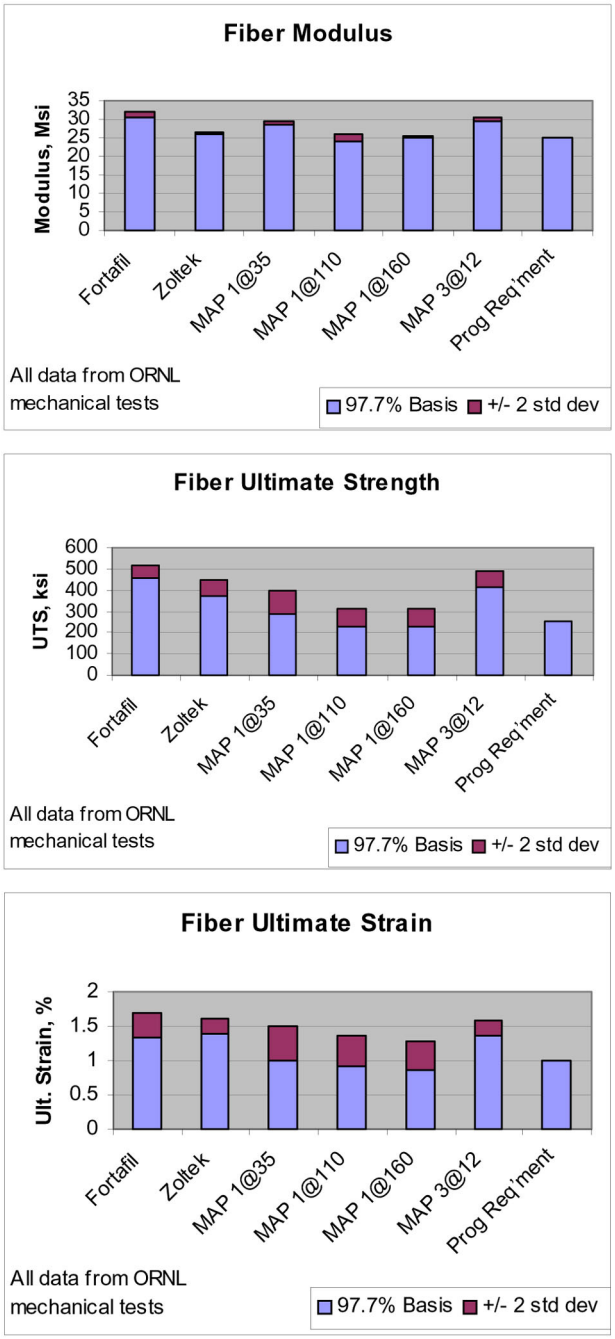

Figure 1. Measured carbon-fiber properties.

capacity. Physical and morphological fiber test results are tabulated in Table 1. Physical properties generally compared favorably with those of commercially available, large-tow commercial-grade fibers.

Fiber morphology was measured by X-ray diffraction. Figure 2 shows plots of intensity vs 2θ for four of the MAP fibers prepared at

Table 1. Physical test data

Fiber type	Production line speed (in./min)	Tow linear electrical resistance (Ω/m)	Electrical resistivity 10^{-3} (Ω-cm)	Calculated filament diameter (μm)	Calculated tow area 10^{-2} (cm^2)	Density (pycnometer) (g/cm^3)
	35	8.9	1.82	7.20	2.04	1.77
MAP 1-tow	45	11.8	2.30	7.18	2.03	1.84
moderate line	60	14.6	4.30	7.36	2.13	1.77
speed	80	14.9	4.35	7.44	2.17	1.83
	110	20.3	4.39	7.43	2.17	1.80
	130	13.48	3.12	7.57	2.32	1.80
MAP 1-tow high	160	13.75	3.23	7.62	2.35	1.79–1.86
line speed	180	21.44	5.10	7.68	2.38	1.79
	200	23.81	5.22	7.73	2.39	1.79
Zoltek PANEX 33	—	8.23	1.62	7.37	1.96	1.81
Fortafil 3(C)	—	7.80	1.67	7.43	2.17	1.77

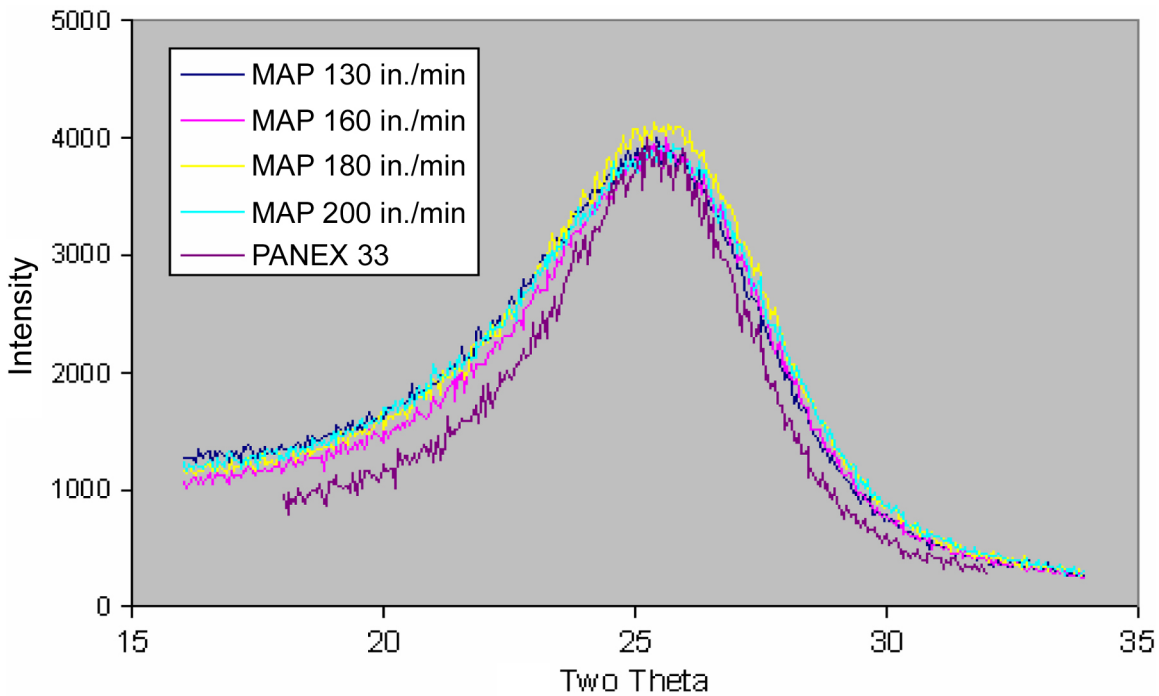

Figure 2. Intensity vs 2θ for the 002 reflection for selected carbon fibers.

the highest single-tow production speeds and compares them to data for the commercial Zoltek Panex 33 fiber. The position of the peak determines the (002) d-spacing, while the breadth of the peak is inversely related to the 'stack height', L_c, of the graphene planes. The plot illustrates that the d-spacings and L_c values are virtually the same, within our ability to measure them, for the four MAP fibers. The values of the d-spacings for these fibers are quite similar to that of the PANEX 33 fiber, but the values of L_c are lower than that of the PANEX 33 fiber. These values are given in Table 2 for these fibers as well as other MAP and commercial fibers. Although there is some scatter in the data, it appears that there is a small, but detectable, tendency for L_c to decrease with increasing production

Table 2. Comparison of MAP and commercial fiber morphologies

Sample description	Misorientation angle[a] (deg)	(002) d-spacing (Å)	Stack height,[b] L_c (Å)	In-plane crystal size,[c] L_a (Å)
MAP 7.5 in./min	19.3	3.465	16.4	39
MAP, 20 in./min	17.4	3.492	16.7	43
MAP 35 in./min	18.5	3.465	17.6	47
MAP, 45 in./min	18.0	3.485	15.2	39
MAP, 60 in./min	18.8	3.453	14.5	35
MAP, 80 in./min	18.9	3.455	14.2	36
MAP, 110 in./min	19.0	3.460	14.2	35
MAP 130 in./min	18.2	3.470	14.7	36
MAP 160 in./min	19.6	3.449	14.4	34
MAP 180 in./min	19.9	3.454	14.4	34
MAP 200 in./min	21.2	3.453	13.9	34
Fortafil 3(C)	19.9	3.503	17.1	45
Zoltek Panex 33	19.1	3.483	17.5	50
Hexcel IM7[d]	15.3	3.495	15.8	44
Thornel P120[e]	3.3	3.378	283	435

[a]Average angle of the graphene planes relative to the fiber axis, as measured by the half-width of the 002 planes in the azimuthal direction.
[b]Average stack height of the graphene planes.
[c]Average crystal size in the direction parallel to the graphene planes.
[d]Aerospace-grade, intermediate-modulus, PAN-based fibers.
[e]Aerospace-grade, high-modulus, pitch-based fibers.

speed of the MAP fibers. This seems reasonable, since increased production speed corresponds to less time at temperature and less time for improvement in the graphene plane stacking. A similar behavior is also observed for the crystal size parallel to the graphene planes, L_a, measured from the breadth of the 100 reflection. The data in Table 3 also shows that the misorientation angle of the graphene planes tends to increase slightly with single-tow production speed of the MAP fibers, but they remain about the same as that of the Panex 33 and Fortafil 3(C) fibers at the highest production speeds.

The tilt angle of the graphene planes with respect to fiber axis is shown in Figure 3,

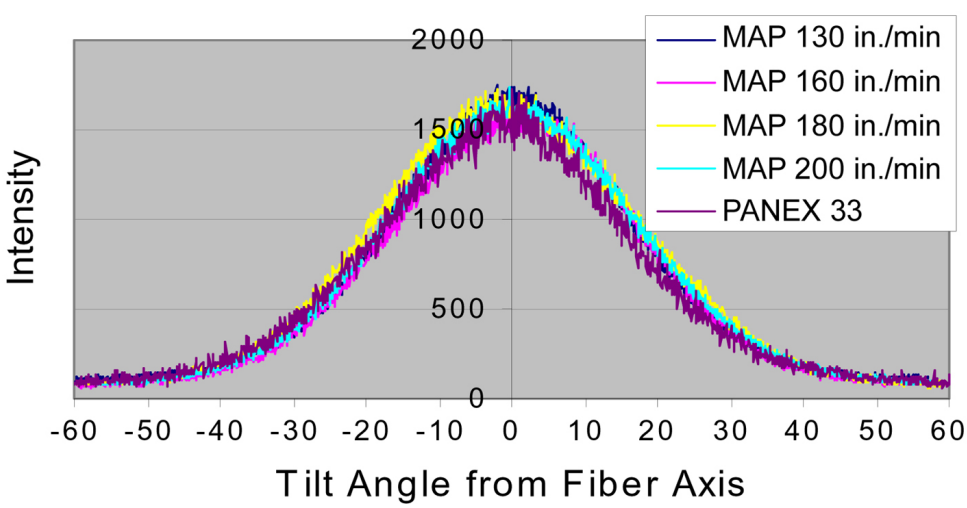

Figure 3. Graphene plane orientation data for selected carbon fibers.

where the distribution of tilt angles is the same for all samples. Slight differences in the average tilt angle can be detected upon careful examination of the data for the individual samples. These differences are reflected in the values recorded for each sample in Table 2. It appears that the primary factor determining the final orientation of the graphene planes is the degree of orientation in the PAN precursor, though there is a very slight tendency for decrease in orientation (greater tilt angles) with increase in processing speed.

Throughput

The economics "figure of merit" is cost per unit throughput. Increasing throughput usually reduces unit cost. Hence the MAP process must be operable at production line speeds and "bandwidth" (number of tows) comparable to or exceeding those of conventional fiber manufacturing lines if it is to realize the desired cost effect. Conventional large-tow carbon fiber manufacturing lines normally run at line speeds in the 90 to 120-in./min range, with about 100 tows per line (a typical line is rated at nominally 1M lb/year when processing 50-K tows).

At the beginning of FY 2003, the researchers had demonstrated a MAP production line speed of 110–120 in./min. In November 2003, the researchers conducted the final experiments on the single-tow line, achieving speeds up to 200 in./min. The researchers speculate, based on their discoveries, that they can substantially exceed 200 in./min on a single-tow line with proper equipment upgrades. However, the decision was made at this point that the project should shift its focus from increasing line speed to increasing the line tow count. Hence the single-tow line was dismantled, and the equipment was reused to construct a three-tow line.

Scale-Up to Multiple Tows

For scaling to multiple-tow processing, a "mitered" MAP applicator design was selected. The "mitered" MAP applicator is similar to the single-tow MAP system except for dimensional scaling and waveguide applicator. The waveguide applicator was redesigned to improve the power distribution profile. An improved waveguide tuner was also built to reduce the anticipated reflected power from the new applicator. The new three-tow feedthrough system is conceptually identical to that used in the single-tow MAP system, but details were revised to improve sealing.

In May, the three-tow mitered MAP system was operated for the first time. Initial operations utilized finished tows to test and adjust mechanical parameters such as tow transport, tensioning, and sealing, at 13-in./min line speed. Plasma conditions were also monitored; however, significant differences in the properties of oxidized and finished fibers limited the value of observations about the plasma behavior. Observed parameters were consistent with expectations during operation of the three-tow mitered MAP system using standard fully oxidized tows, also at 13 in./min line speed. Background pressure was satisfactory, and the plasma power distribution was improved. Measured tow linear resistance was satisfactory. In August the researchers conducted a three-tow run at 12 in./min. to produce a quantity of carbon fiber sufficient for mechanical testing. Excellent mechanical properties resulted, as shown in Figure 1. A stable operating mode that requires very little feed gas was unexpectedly discovered during this experiment. During attempts to run the three-tow line at a higher speed, the reflected power rapidly rose too high, limiting the maximum line speed to 13 in./min. Improved component matching is needed to push the system to higher line speeds, and the necessary design modifications are under way.

Parametric Studies

During the final single-tow MAP high-speed run, a series of microwave electric field

measurements were made along the waveguide applicator to understand how the microwave power, and therefore the plasma power, is distributed along the tow. The results indicate that the plasma power drops off rapidly from the microwave feed point (tow output) and then levels out midway along the length of the waveguide applicator to the other end where the tow is introduced. Superimposed on this variation is a standing wave pattern. Therefore, a point on the moving tow is subjected to an alternating series of high- and low-power processing steps that rapidly increase until that point on the tow leaves the chamber at the microwave feed point.

Instrumentation and Control

Further evaluations were undertaken to calibrate the high-temperature resonance cavity for in-line, real-time dielectric measurement of carbon-fiber tows, with the goal of elevating the cavity's maximum service temperature from ~500°C to ~1,000°C. Because the carbon fibers become very electrically conductive at high temperatures, the resonance cavity must necessarily be very sensitive at high temperatures. The high-temperature resonance cavity was electroplated. The conventional oven and required temperature controls were evaluated. Control software was acquired and customized to closely mimic the real production temperature profile during any stage of processing. The data acquisition software was installed and tested. The medium-temperature system for dielectric measurements of the carbon-fiber tows, from oxidized state to 500°C, is ready for functional testing.

New tow winding and tensioning equipment was installed on the multiple-tow processing line as follows:

- Designed for 200 in./min and readily upgradeable to 400-in./min line speed.
- Designed for 50-K nominal tow size, but can handle tow sizes ranging from 3 K to 64 K with minor modifications to the processing line. Up to three different tow sizes can be processed simultaneously.
- Triple tension-controlled creel for independently controlling tension in three tows.
- Triple take-up winder with feed roller and independent speed control. It provides very well-controlled constant speed, independently controllable for each tow, during processing. This permits simultaneous evaluation of different processing conditions for each tow, e.g., different tension levels, line speeds, and tow size during a single experiment.

Patents

Patent No. 6,514,449 B1, entitled "Microwave and Plasma-Assisted Modification of Composite Fiber Surface Topography," issued February 4, 2003.

Spin-Offs

A number of "spin-off" developments have resulted from this project. Work in the following areas was conducted at a low level of effort as part of this project during this reporting period.

- **Carbon-fiber recycling**—Performed X-ray photoelectron spectroscopy (XPS) and scanning electron microscope (SEM) evaluation and characterization of fibers that were recovered in ANL recovery process.
- **Surface treatment**—Evaluated and compared surface chemistry and surface roughness of ORNL's MAP fibers and commercial fibers.
- **Storage**—Discovered a way to repeatably produce fibers with a layered morphology that may be useful in gas storage applications.

Education

The materials characterization, notably utilizing SEM and spectroscopy methods such as XPS and secondary ion mass

spectrometry (SIMS), has been conducted in partnership with the University of Tennessee's Materials Science Department. Three UT graduate students, one a Ph. D. candidate and two M.S. candidates, were provided characterization support to the project. One M.S. candidate was awarded his degree during this reporting period, based in part upon his contributions to this project.

Conclusions

The development of MAP carbonization and graphitization technology has progressed according to plan. All FY 2003 milestones were satisfied on schedule. Construction and initial operation of a three-tow research line has been successfully completed, with the fibers initially produced therein exhibiting excellent mechanical properties. MAP processing is generally considered to be an evolving "success story" with great potential for making an impact on carbon-fiber technology and cost.

Summary

These are highlights of the progress during FY 2003.

- The continuous single-tow MAP carbon-fiber pilot facility was successfully operated, and 50-K PAN fiber tows were carbonized/graphitized at processing line speeds up to 200 in./min.
- The continuous three-tow MAP carbon-fiber pilot facility was constructed and successfully operated. Three 50-K PAN fiber tows were simultaneously carbonized/graphitized at processing line speeds up to 12 in./min.
- Physical, mechanical, and morphological properties were evaluated for fiber samples manufactured at single-tow line speeds up to 200 in./min. Physical and mechanical properties were measured for fiber samples manufactured at three-tow line speeds up to 12 in./min. In most cases, properties exceeded program requirements.
- We calibrated the improved resonance cavity for a dielectric measurement system that can operate at >1,000°C with kilohertz sampling rates.
- We installed a new three-tow winding and tensioning system designed for line speeds up to 200 in./min, readily upgradeable to 400 in./min, with independent control for each tow.
- One patent was formally issued.

6. RECYCLING

A. Recycling of Polymer Matrix Composites

Principal Investigator: Bassam J. Jody
Argonne National Laboratory
9700 South Cass Avenue, Argonne, IL 60439
(630) 252-4206; fax: (630) 252-1342; e-mail: bjody@anl.gov

Project Manager: Edward Daniels
Argonne National Laboratory
9700 South Cass Avenue, Argonne, IL 60439
(630) 252-4206; fax: (630) 252-1342; e-mail: edaniels@anl.gov

Technology Area Development Manager: Joseph A. Carpenter
(202) 586-1022; fax: (202) 586-1600; e-mail: joseph.carpenter@ee.doe.gov
Field Technical Manager: Philip S. Sklad
(865) 574-5069; fax: (865) 576-4963; e-mail: skladps@ornl.gov

---

Contractor: Argonne National Laboratory
Contract No.: W-31-109-Eng-38

Objective

- Develop efficient and cost-effective processes for recovering carbon fibers from polymer matrix composites (PMCs).

Approach

- Continue the development and testing of processes to separate and recover carbon fibers from PMC scrap made with different thermoset and thermoplastic polymer substrates.
- Conduct an economic analysis of the process to determine its economic competitiveness.
- Work with a carbon fiber manufacturer to produce and test PMC panels made with recovered fibers and compare their properties with those of similar virgin-fiber panels.
- Recover carbon fibers for reuse in an automotive application.

Accomplishments

- Completed the development, evaluation, and testing of the thermal process to separate and recover carbon fibers from PMC scrap. The thermal method, a single-step process, recovered carbon fibers from PMCs made with different polymeric substrates with minimal changes in the properties of the original fibers. For most PMCs and mixtures of PMCs, the process is energy self-sufficient using the polymer substrate as an energy source.
- Conducted an economic analysis of the process, and it predicted a potential payback of less than 2 years, assuming a value of only $1.5/lb of recovered carbon fibers.

- Recovered carbon fibers from "control" panels that were made by Hexcel Corporation,[1] with well-characterized carbon fibers, and the recovered fibers were sent back to Hexcel to re-make similar panels and to determine the suitability of the recovered fibers for making quality products. Hexcel found the fibers suitable for short fibers applications and reported that "Suggested applications of recycled carbon fiber are SMC (sheet molding compound), PEM (Proton Exchange Membrane for Fuel Cells), Batteries, and Concrete Reinforcement."[1]
- Oak Ridge National Laboratory (ORNL) also analyzed the fibers and found "the recovered carbon fibers from the ANL-pyrolytic based process—exhibit higher O/C chemical ratios than the corresponding virgin, treated but unsized—(finished product) carbon fibers. At the first moment, this result could indicate that these recovered fibers very likely will not require additional surface retreatment."[2] Avoiding the need for retreatment of the fibers saves about $0.40/lb of fibers.
- Produced more than 20 lb of recovered carbon fibers from two types of PMC scrap and shipped them to ORNL to be used in making an actual automotive application [skid plates for a sport utility vehicle (SUV)] using the Budd process.
- Published two articles[3,4] describing the process. One of these publications[4] received the Arch T. Colwell Merit Award. The award will be presented at the Honors Convocation during the SAE 2004 World Congress. A third publication[5] is under preparation.
- Completed the project and accomplished its objective. The process developed and the characteristics of the carbon fibers that were recovered confirmed the technical feasibility and cost-effectiveness of recycling carbon fibers from PMCs into value-added products. The ANL process could use commercially available heat-treating equipment with minor modifications, and it is ready for testing on a larger scale once enough PMC scrap is available.

Future Direction

- Recommend that the process be demonstrated on a larger scale once large quantities of PMC scrap become available. Large-scale testing, field demonstration of the process, and production of large enough quantities of recovered fibers to make a variety of quality products is necessary to determine the application limitations of the recovered fibers and their fair market value.

Testing of the Process Using PMC Panels Made with Well-Characterized Fibers

Hexcel corporation supplied PMC panels with known properties for carbon fiber recovery tests. We processed some of these panels under different operating conditions and sent the recovered fibers back to Hexcel for evaluation and comparison of their properties before and after recovery. Hexcel[1] found that "The surprising results were the high shear strength of the recycled materials. These shear strength results indicated that the recycling process had small effects on the surface treatment conditions of the fibers. This reveals that the recycled fibers may not require to be surface treated again. The recycling process may activate the fiber surfaces."[1] Based on the results of these tests, appropriate recovery conditions that resulted in minimal changes in fiber properties were established. These conditions were then used to recover fibers from similar panels (Figure 1). Hexcel then used the recovered fibers as-is to fabricate new panels of equivalent geometry as the virgin panels and compared their properties with those of the panels from which the fibers were recovered. The data showed a reduction of only 10% in panel stiffness and ~12% in short beam strength. The panels also showed about 50%

Figure 1. Carbon fibers recovered from PMC scrap.

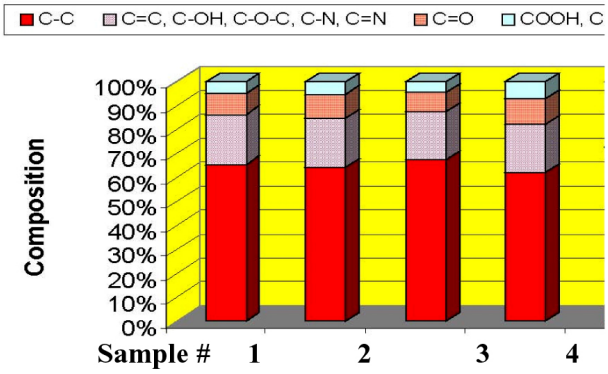

Figure 2. Comparison of functional groups chemistry on the surfaces of ANL recovered fibers (1,2) and virgin untreated (3) and virgin treated (4) fibers (Ref. 2).

reduction in strength and elongation. Obviously, during the treatment process and handling of the recovered fibers afterward in the hood, some of the fibers were lost; and some lost their original direction and place.

Therefore, the recovered fibers could be used in many applications that require chopped fibers, such as sheet molding compounds or preform products like those made in the slurry process to manufacture automobile parts.

ORNL[6] also conducted extensive analysis of the recovered fibers and found that the recovered fibers had characteristics similar to those of the original virgin fibers. For example, the density and diameter of the recovered fibers were essentially the same as those of the virgin fibers, and the morphology of the recovered fibers was nearly identical to that of the virgin fibers.

These data prove that at the appropriate processing conditions, the thermal treatment process does not degrade the morphology in the interior constituent material. The recovered fibers also exhibited high shear strength and high oxygen concentration on the fiber surface,[1,2,6] indicating that the recovered fiber should adhere well to matrix resins without the need for additional surface treatment. The surface chemistry of the recovered fibers was similar to that of the treated virgin fibers (Figure 2). Surprisingly, some of the recovered fibers exhibited higher concentrations of elemental oxygen at and just beneath the fiber surface than the corresponding virgin control fibers. ORNL concluded that "the recovered carbon fibers from the ANL-pyrolytic based process—exhibit higher O/C chemical ratios than the corresponding virgin, treated but unsized—(finished product) carbon fibers. At the first moment, this result could indicate that these recovered fibers very likely will not require additional surface retreatment."[2] Avoiding the need for retreatment of the fibers saves about $0.40/lb of fibers. "The most significant observation is that the ANL-recovering process yields fibers where all the four peaks are present."[2]

During FY 2003 we treated additional panels as well as other PMC scrap made with different carbon fibers and different substrates, including nylons, to identify conditions that would result in degradation of the fibers as evidenced by their oxidation. The results indicated that at temperatures above 1200°F in the presence of "enough" air, oxidation of the fibers did occur after the substrate was essentially removed. The degree of oxidation increased as the amount of air (oxygen) in the thermal reactor was increased. This was the case with all PMC samples tested. Therefore, the process design should take in consideration the need for oxygen in the reactor to oxidize the substrate

and its decomposition products, but the air supply rate should be kept at a minimum during the treatment of the residual substrate after the bulk of it is removed in order to prevent the oxidation of the fibers. In addition, when a mixture of different PMC scrap was treated, the energy released by the decomposing and oxidizing substrate was more than enough to drive the process. As a matter of fact, the temperature in the reactor was exceeding the set point by as much as 100°F. Therefore, the process design should take in consideration the need to manage the changing amounts of thermal energy released during the process as different PMC scrap materials are treated.

Recovery of Carbon Fibers for Reuse in an Automotive Application

During the previous reporting period, arrangements were made with Hexcel to provide ORNL with carbon fibers having known properties to make PMC samples for us to recover their carbon fibers for reuse in making "skid plates" for SUV application. During this reporting period, ORNL made the PMC scrap panels, and we processed about 80 lb of these panels and recovered carbon fibers from them. More than 20 lb of recovered fibers were sent to ORNL to use in manufacturing skid plates for SUVs using the Budd slurry process.

Disposal and Treatment of the Effluent Gas Stream

Work done on this topic during prior reporting periods showed that, as expected, different substrates generate different pyrolysis and oxidation products, including volatile and semivolatile organic compounds. Previously, we analyzed the gases and vapors generated during the thermal treatment of PMC scrap. The analysis showed that carbon monoxide and volatile and semivolatile compounds were present. The number, type, and amount of these species depends on the treatment temperature, oxygen availability, and composition of the PMC feed material. Therefore, an after-burner is required to destroy these species. In FY 2003 we examined an opportunity to recover some of the organic products by condensation followed by distillation, or by other means, especially when they are not required to provide the energy to drive the process. This option is technically feasible. However, its cost-effectiveness depends on the composition of the generated gas, and this depends on the composition of the scrap stream. For example, epoxy resins can generate substantial amounts of acetone that is widely used as a solvent and as a raw material in the synthesis of other chemicals. Acetone can be condensed and/or scrubbed from the gaseous stream using water because it is highly soluble in water.

Updating of the Conceptual Design and Economic Analysis

The thermal treatment process conceptual design developed during previous periods was also updated especially as to controlling the air supply to the reactor. We also reevaluated the economic analysis for a full-scale plant processing 1,000,000 lb/year of PMC scrap (500 lb/h or 10 tons/week). The estimated payback of about 2 years is still valid based on a value for the recovered fibers of $1.5/lb. This value is used in the analysis assuming that a value of $3–$5/lb of virgin fibers is required before carbon fibers are widely used in the automotive industry.

Conclusions

Work conducted on this project demonstrated that the recovery of carbon fibers from PMC scrap is technically feasible and potentially economical. The recovered fibers have properties that make them usable in chopped-fiber applications for making value-added products such as various automobile parts. The process that was developed in this project is now ready for testing at a larger scale. Therefore, the objective of the project was accomplished.

References

1. M. G. Abdallah, Hexcel Corporation, private communication, 2002.

2. F. L. Paulauskas, Oak Ridge National Laboratory, private communication from M. J. Williams, 2003.

3. B. J. Jody, J. A. Pomykala, Jr., and E. J. Daniels, "A Process to Recover Carbon Fibers From Polymer Matrix Composites," presented at the 2003 IdentiPlas Conference, April 28–29, 2003, in Brussels, Belgium.

4. B. J. Jody, J. A. Pomykala, Jr., and E. J. Daniels, "A Process to Recover Carbon Fibers From Polymer Matrix Composites," *SAE 2002 Transactions—Journal of Materials & Manufacturing,* SAE paper 2002-01-1967, ISBN Number 0-7680-1289-9, September 2003.

5. B. J. Jody, J. A. Pomykala, Jr., E. J. Daniels, F. Paulauskas, and M. G. Abdallah, "A Process to Recover Carbon Fibers From Polymer Matrix Composites." Prepared for *SAMPE 2004 Conference*, "Materials and Processing Technology—60 Years of SAMPE Progress," Long Beach Convention Center, Long Beach, California, May 16–20, 2004.

6. F. L. Paulauskas, Oak Ridge National Laboratory, private communication from M. J. Williams, 2002.

B. Recycling Assessments and Planning

Principal Investigator and Project Manager: Edward J. Daniels
Argonne National Laboratory
970 S. Cass Avenue
Argonne, IL 60439
(630) 252-5279; fax: (630) 252-1342; e-mail: edaniels@anl.gov

Technology Area Development Manager: Joseph A. Carpenter
(202) 586-1022; fax: (202) 586-1600; e-mail: joseph.carpenter@ee.doe.gov
Field Technical Manager: Philip S. Sklad
(865) 574-5069; fax: (865) 576-4963; e-mail: skladps@ornl.gov

---

Contractor: Argonne National Laboratory
Contract No.: W-31-109-Eng-38

Objectives

- Establish priorities for cost-effective recycling of advanced automotive technology materials and components.
- Focus long-term efforts on enhanced recovery/sorting procedures and advanced recycling technologies that are the enabling factors in a vision for 100% recyclability.

Approach

- Consult with automotive manufacturers and recycling industries, the U.S. Council on Automotive Research (USCAR) and its affiliates, national laboratories, universities, and other relevant organizations to assess critical recycling needs/barriers.
- Develop a recycling R&D program plan that will serve as a "working document" to guide DOE/FCVT in establishing priority goals, with an initial emphasis on lightweight body and chassis materials.
- Assist DOE in establishing advanced recycling R&D initiatives and provide technical oversight to ensure that priority objectives/goals are accomplished.

Accomplishments

- Prepared a draft 5-year program plan based on the recommendations and priorities identified in the Roadmap and based on an initial planning meeting with the management council of the Vehicle Recycling Partnership (VRP) of USCAR.
- Negotiated a cooperative research and development agreement (CRADA) with the VRP, the American Plastics Council (APC), and Argonne National Laboratory (ANL), as partners, and initiated effort under the CRADA in August 2003.
- Initiated construction on a large-scale pilot separation facility at ANL. This facility will serve as a focal point for the recycle research to be conducted as part of the CRADA with the VRP and APC.
- Developed an Excel-based process cost model that incorporates two primary modules for recovery automotive plastics: the first module includes the unit operations required for

recovering a plastics concentrate from shredder residues, and the second module includes the unit operations required to recover selected plastics from the mixed-plastics concentrates. The second module allows the user to specify the type of plastics that are to be recovered and the number of recovery stages required.

- Initiated an assessment of a new plastics separation technology under development by Salyp NV of Belgium with support from the VRP, APC, and Association of Plastics Manufacturer's of Europe. Controlled tests of this new "thermoplastics sorting" technology are being done using shredder residues from two European and one U.S. location as feed material.

Future Direction

- Continue development of the Recycling R&D Plan through collaboration with the USCAR VRP and associated USCAR affiliates, the APC, the Automotive Parts Rebuilders Association, remanufacturing industries, materials trade organizations, and other appropriate industries involved in automotive recycling.
- Continue ongoing efforts toward the milestones and objectives of the CRADA statement-of-work.
- Continue evaluations of recycling technology progress in Europe and Japan, along with assessments of critical recycling technologies as new needs are identified.
- Continue ongoing project efforts to assist DOE in preparation of planning documents, priority recycling R&D needs, proposal reviews, and related tasks.

Summary

The objective is to establish priorities and develop cost-effective recycling technologies and strategies in support of the DOE FCVT long-term objectives and goals. Automobile recycling is the final productive use of end-of-life vehicles (ELVs). The obsolete car has been a valuable source of recycled raw materials and useable parts for repair because cars have been mass-produced. Today, cars that reach the end of their useful service life in the United States are profitably processed for materials and parts recovery by an existing recycling infrastructure. That infrastructure includes automotive dismantlers who recover useable parts for repair and reuse; automotive remanufacturers who remanufacture a full range of components, including starters, alternators, and engines to replace defective parts; and ultimately, the scrap processor who recovers raw materials such as iron, steel, aluminum, and copper from the remaining auto "hulk" after components have been recovered for recycling. Each of these activities contributes to the recycling of obsolete vehicles.

Today, less than 25 wt % of obsolete cars is not profitably recoverable for recycling and is therefore landfilled. For the past 10 years, the original equipment manufacturers—Ford, General Motors (GM), and DaimlerChrysler—through the VRP and other organizations including the Aluminum Association, APC, the Institute of Scrap Recycling Industries, Automotive Recyclers Association, Automotive Parts Rebuilders Association, and the federal government have been working both collaboratively and independently to address technical, institutional, and economic issues that currently limit the recycling of ELVs. Progress has been made in understanding some of these issues, and technology has been developed that can impact the level of ELV recycling.

The recyclability of ELVs is presently limited by the lack of commercially proven technical capabilities to cost-effectively separate, identify, and sort materials and components and by the lack of profitable postuse

markets. While nearly 75 wt % of ELVs is currently recycled in some form, the remaining 25% is sent to landfills each year. During the next 20 years, both the number and complexity of ELVs are expected to increase, posing significant challenges to the existing recycling infrastructure. The automobile of the future will use significantly greater amounts of lightweight materials (e.g., ultra-light steels, aluminum, plastics, and composites) and more sophisticated/complex components.

New technology is and will continue to be needed to improve vehicle recyclability. Using the Roadmap as a framework, we will work with the key stakeholders over the next year to structure a suite of projects to be undertaken in this program area.

The Recycling Strategy

The following strategy outline was developed as part of the Roadmap to maximize the value recovered from ELVs.

- Come together as a unified recycling community to cost-share the development of required new technology.
- Incorporate reuse, remanufacturing, and recycling into the design phase for cars whenever possible.
- Recycle as early in the recycling stream as possible, while relying on the market to optimize the value and amount recycled at each step.
- Maintain a flexible recycling process that can adapt to diverse model lines fabricated with different techniques and materials from various suppliers.
- Develop automated ways to recover bulk materials.
- Emphasize R&D on postshred material identification, sorting, and product recovery.
- Focus R&D efforts on materials not recycled today by sorters (e.g., postshred glass, rubber, fluids, textiles, plastics).
- Develop uses for recovered materials (whether in the same or different applications) and testing specifications.
- Encourage investment in the infrastructure needed to achieve the recyclability goal. Build on the existing infrastructure.
- Develop a means to prevent the entry of polychlorinated biphenyls and other hazardous materials into the recycling stream, and promote acceptable limits in shredder residues.
- Consider the recycling requirements of new technologies entering fleets as early as possible.

The 5-Year R&D Plan

Based on the Roadmap and continuing discussions with key stakeholders, a 5-year R&D plan has been prepared. The plan includes the following three focus areas:

Area 1. Baseline Technology Assessment and Infrastructure Analysis

Understanding the state of the art is critical to moving forward. As stated in the Roadmap

> … the status of technologies used, existing process capabilities, and the mass balance flow of automobiles at end-of-life is not known with the level of confidence needed to assure that the industry is making the best choices to optimize recyclability. A better understanding of the interrelationships of all steps in the recycling process from a financial perspective will promote development of [the] infrastructure … analysis of data is needed to better understand the environmental and economic trade-offs.

The focus of the work under this activity will be to develop the tools and document the information necessary to make effective decisions relative to technology needs to facilitate sustainable future vehicle recycling, and to make effective decisions regarding allocation of R&D resources. Research conducted under this area generally addresses the broader priorities of "proactive industry wide-action" and "industry-wide analysis"

for which a number of specific needs are identified in the Roadmap.

In FY 2004, the focus of this area will be on developing a catalogue of available and emerging automotive recycling technologies and preparing an updated assessment of the state of the art of the recycling industry.

Area 2. Materials Recovery Technology Development and Demonstration

Development of technology that can lower the cost of recycling and meet the financial and institutional requirements of the market is critical to improving the recycling rate of automotive materials. Technology development and demonstration is the cornerstone of this program and will serve as the program's focal point. Although research to be conducted in this area will initially focus on addressing technology needs for postshred materials recovery, projects that enhance preshred recovery, including disassembly for materials recovery and direct reuse and remanufacturing of components, will also be included. In the long term, components such as fuel cells, advanced batteries, and hydrogen reformers are more likely to enter the recycle stream through preshred recovery for remanufacturing, repair, and materials recovery. Research will be undertaken to determine the technology needs to ensure the recyclability of these very advanced automotive components. This area of research generally supports the needs of the broad priorities of "lowering the risk of technology development and purchase," "preshred recovery," and "postshred material identification and sorting" that are outlined in the Roadmap.

In FY 2004, the focus of this area will be to support development and demonstration of postshred separation technology, building upon the technology development efforts previously undertaken by ANL, the VRP, the APC, and others. Development of technology to cost-effectively sort postshred material is a top-priority need.

Area 3. Recovered Materials Performance and Market Evaluation

Understanding and enhancing recovered materials performance is an essential ingredient to a successful recycling program. This is especially true in automotive systems when the materials and components that are recovered have been in use for an average of 10 to 15 years. This area will include projects to quantify the relative performance of recovered materials vis-à-vis new or virgin materials; research on compatibilization of recovered polymers to improve performance properties; development of technologies to upgrade the recovered materials, such as separation of fibers from polymeric substrates; and development of applications for other recovered materials, such as rubber and glass.

In FY 2004, materials and plastics that are recovered as part of the technology demonstration area of research will be evaluated to define the performance properties of those material vis-à-vis "virgin" materials.

7. ENABLING TECHNOLOGIES

A. Durability of Carbon-Fiber Composites

Principal Investigator: Dan J. Naus; J. M. Corum, R. L. Battiste, M. B. Ruggles-Wrenn, Y. J. Weitsman, A. Ionita
Oak Ridge National Laboratory
P.O. Box 2009
Oak Ridge, TN 37831-8056
(865) 574-0657; fax: (865) 574-8257; e-mail: nausdj@ornl.gov

Field Project Manager, Composites: C. David Warren
Oak Ridge National Laboratory
P.O. Box 2008, Oak Ridge, TN 37831-6065
(865) 574-9693; fax: (865) 574-4963; e-mail: warrencd@ornl.gov

Technology Area Development Manager: Joseph A. Carpenter
(202) 586-1022; fax: (202) 586-1600; e-mail: joseph.carpenter@ee.doe.gov
Field Technical Manager: Philip S. Sklad
(865) 574-5069; fax: (865) 576-4963; e-mail: skladps@ornl.gov

---

Contractor: Oak Ridge National Laboratory
Contract No.: DE-AC05-00OR22725

Objective

- Develop experimentally based, durability-driven design guidelines to ensure the long-term (15-year) integrity of representative carbon-fiber-based composite systems that can be used to produce large structural automotive components. Durability issues being considered include the potentially degrading effects of cyclic and sustained loadings, exposure to automotive fluids, temperature extremes, and low-energy impacts from such events as tool drops and kickups of roadway debris on structural strength, stiffness, and dimensional stability.

Approach

- Characterize and model the durability behavior of a progression of three representative carbon-fiber composites, each with the same thermoset urethane matrix but having a different reinforcement preform: (1) continuous fiber, ±45° crossply; (2) continuous fiber, quasi-isotropic; and (3) random chopped fiber.
- Replicate on-road conditions in laboratory tests of each composite to generate durability data and models.
- Develop and publish durability-based design criteria for each composite.
- Shift focus to suitable thermoplastic composites, for which durability issues are generally more significant.

Accomplishments

- Published report providing aspects of mechanical behavior of stitched T300 mat/urethane 420 IMR composite (ORNL/TM-2002-86).
- Completed planned durability tests of 3-mm-thick and 1.5-mm-thick chopped-carbon-fiber thermoset composite plaques.
- Published report on durability-based design criteria for a chopped-carbon-fiber automotive composite (ORNL/TM-2003-86).
- Published two reports on effects of temperature and environment on chopped-fiber automotive structural composites (ORNL/TM-2003/114 and ORNL/TM-2003/117).
- Published three technical papers.
- Completed initial baseline testing for the quasi-isotropic carbon-fiber poly (phenylene sulfide) (PPS) material.
- Fed data on chopped-carbon-fiber composite directly into the planning and analysis for the Focal Project III carbon-fiber body-in-white.

Future Direction

- Investigate relationship between processing of PPS materials and crystallinity as well as relationship between crystallinity and material properties.
- Complete baseline characterization of carbon-fiber-reinforced PPS material.
- Complete durability assessment of carbon-fiber-reinforced PPS material.
- Publish durability-driven design criteria documents for representative thermoplastic composites suitable for automotive structural applications.

Introduction

Before composite structures will be widely used in automotive applications, their long-term durability must be assured. The Durability of Carbon-Fiber Composites Project at the Oak Ridge National Laboratory was established to develop the means for providing that assurance. Specifically, the project is developing and documenting experimentally based, durability-driven design criteria and damage-tolerance assessment procedures for representative carbon-fiber composite systems to assure the long-term (15-year) integrity of composite automotive structures. Durability issues being considered include the potentially degrading effects of cyclic and sustained loads, exposures to automotive fluids, temperature extremes, and incidental impacts from such things as tool drops and kick-ups of roadway debris. Research to determine the effect that these environmental stressors and loadings have on structural strength, stiffness, and dimensional stability is being conducted. The project is carried out in close coordination with the Automotive Composites Consortium (ACC).

It is envisioned that about 15% of the Focal Project III carbon-fiber-composite body-in-white will utilize directed continuous-fiber reinforcement architectures, while the remainder will employ random chopped-fiber reinforcement. The approach to investigating durability has thus been to address a progression of thermoset composites, each of which has the same urethane matrix:

- reference [±45]3S crossply composite,
- [0/90/±45]S quasi-isotropic composite, and
- randomly oriented chopped-carbon-fiber composite.

Characterization of the first two, continuous-fiber composites has been completed, and design criteria documents were published. In mid-FY 2002 the focus turned to chopped-carbon-fiber composites. Characterization of the randomly oriented chopped-carbon fiber composite was completed in FY 2003. Also in FY 2003 investigation of carbon-fiber-reinforced thermoplastic materials for structural automotive applications was initiated.

Chopped-Carbon-Fiber Material

The ultimate goal for the Focal Project III carbon-fiber composite body-in-white is to achieve a fiber-volume fraction of 40% and a minimum thickness of 1.5 mm over 70% of the structure.

The ACC successfully molded chopped-carbon-fiber plaques meeting these Focal Project III requirements. The carbon fiber, chopped by the P4 machine in 50-mm lengths, was Zoletek Panex 33, seven-split 46K. The urethane matrix was Bayer 420 IMR, the same as in previous composites addressed by the Durability Project. Unfortunately, while the average properties of the 1.5–mm-thick plaques satisfied Focal Project III design requirements, the variability was excessive. It was originally planned to use 1.5-mm-thick plaques for durability studies. However, because of the larger than expected variability in the 1.5-mm material, the ACC instead fabricated and supplied 3-mm-thick plaques in March of 2002. These 3-mm-thick plaques, which exhibit reduced variability, have been adopted as the reference chopped-fiber material. The general project approach has been to first replicate on-road conditions in laboratory specimens to generate data to form the basis for developing correlations and models. These correlations and models were then used to formulate design criteria. Tests included the following:

- basic short-time tension, compression, and shear;
- uniaxial and biaxial flexure;
- cyclic fatigue, including mean stress effects;
- tensile and compressive creep and creep rupture;
- hole and crack effects;
- low-energy impact; and
- tension- and compression-after-impact.

In most cases, characterization of effects of temperature and fluid exposure were included in the test effort that involved almost 2,200 individual tests. Provided below are examples of results that were obtained under the test program. Although all tests noted above are not discussed below, additional information to that provided as well as results for tests not discussed can be obtained from report 2 in the "Publications" section of this report.

Table 1 presents average in-air room-temperature (RT) baseline properties for the chopped-carbon-fiber composite.

Table 1. Tensile, compressive and shear properties

Property	Tension	Compression	Shear
Modulus, GPa	27.7	28.9	9.37
Poisson's ratio	0.34	—	—
Strength, MPa	203	173	153
Failure strain, %	0.90	0.77	2.34[a]

[a]Engineering shear strain.

From a durability standpoint, it is assumed that an automobile with a composite structure must last for 15 years and 150,000 miles. It is further assumed that during the 15 years the vehicle will actually be operated between 3,000 and 5,000 h. The design temperature range is taken to vary from a minimum of –40°C to a maximum of

120°C, with the possibility of the highest temperature occurring only during operation. The effect of thermal cycling is also a concern. The structures must support and resist a variety of dead and live loads. Also, the structures will be subject to common vehicle fluids and operating atmospheres, and design limits must take the resulting property degradation into account.

Temperature multiplication factors for relating at-temperature stiffness and strength to reference baseline RT values are provided in Figures 1 and 2, respectively. The basic time-dependent allowable stress, S_o, defined as two-thirds the minimum ultimate tensile strength (UTS) at RT, is about 52% the average UTS. Values of S_o at other temperatures are obtained by multiplying the above RT S_o value by the UTS factors provided in Figure 2. Prior thermal cycling (25 cycles from RT to 120°C to –40°C to RT) had a small effect on tensile strength and stiffness (≤3%), whereas compressive and shear stiffness dropped 5% and 11%, respectively.

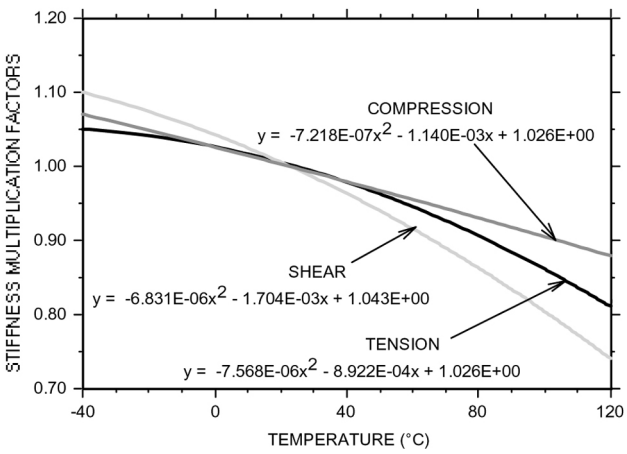

Figure 1. Temperature multiplication factors: stiffness.

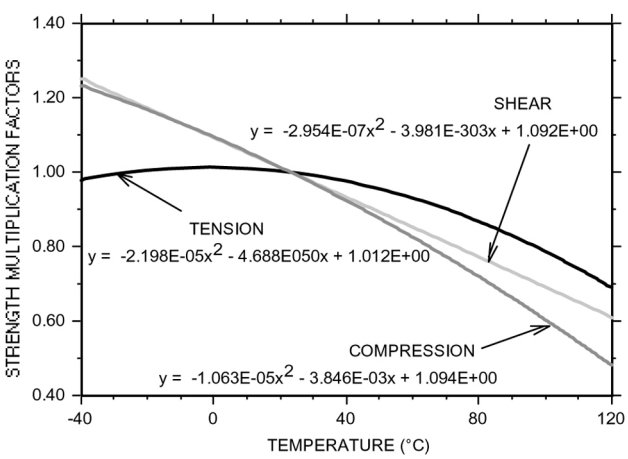

Figure 2. Temperature multiplication factors: strength.

In the durability assessment, it is assumed that structures will be subjected to common vehicle fluids and operating atmospheres, therefore design limits must take the resulting property degradation into account. Figure 3 presents effects of exposure to eight automobile fluids on apparent shear strength. Based on these results, plus results from weight gain and tensile properties vs exposure time, the fluids most extensively examined were distilled water and windshield washer fluid for exposure times of 1000 h and 100 h, respectively. To bound fluid effects on stiffness, a 4% reduction value is recommended.

Biaxial stress states exist in real structures, and bending is unavoidable at some locations. Both uniaxial and biaxial tests were performed at various temperatures and in both air and representative fluids, Figures 4 and 5, respectively.

In the simple beam tests, the modulus of rupture (maximum elastically calculated stress determined from simple bending theory) varied from 2.1 times the UTS at –40°C down to 1.3 at 120°C. Biaxial flexural

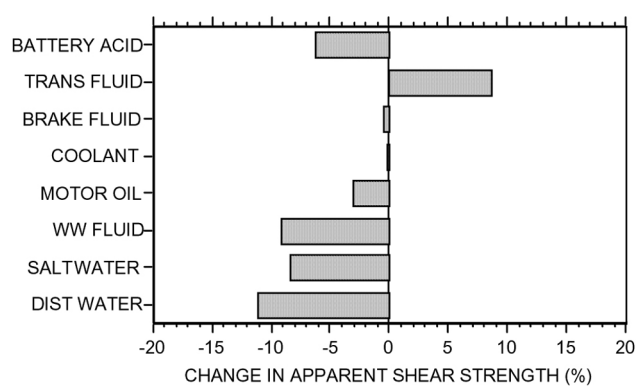

Figure 3. Effects of exposure on apparent shear strength.

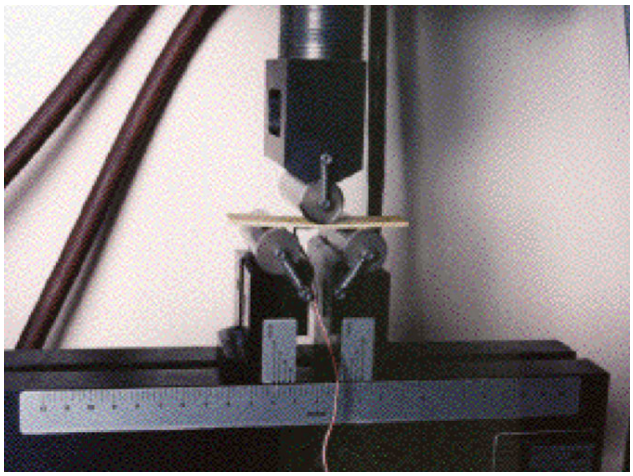

Figure 4. Uniaxial flexural test setup.

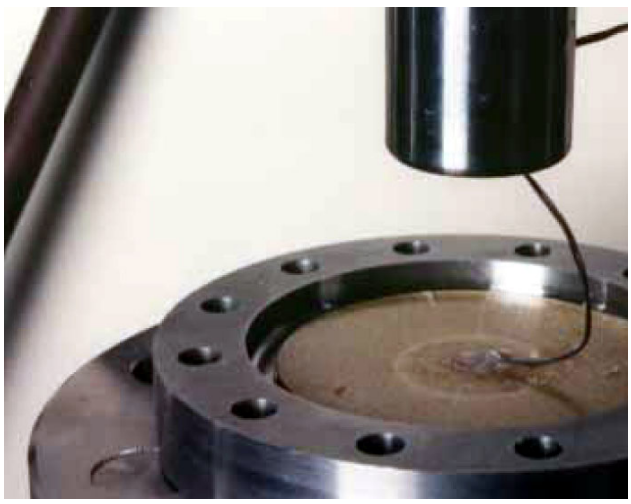

Figure 5. Biaxial flexural test setup.

strength results in which the average failure loads under different environments were compared to as-received RT results varied from 1.03 for 100-h presoak in windshield washer fluid down to 0.60 for 120°C exposure. Resulting failure data have been used in formulating a biaxial strength theory for the final design criteria. Table 2 provides a summary of strength multiplication factors relative to in-air RT values for short-time static loadings.

Fatigue S-N curves (stress vs number of cycles) for a number of loading conditions (e.g., tensile cycling, compressive cycling, and completely reversed stress cycling) were developed over the –40°C to 120°C temperature range and for specimens soaked for

Table 2. Summary of strength multiplication factors for short-time static conditions

Stress state	1000 h in distilled water	100 h in windshield washer fluid	120°C
Tension	0.94	0.98	0.69
Compression	0.86	0.95	0.48
Shear	0.95	0.99	0.61
Uniaxial flexure	0.92	1.06	0.54
Biaxial flexure	0.90	1.03	0.60

100 h in windshield washer fluid or 1000 h in distilled water prior to testing. Figure 6 presents the single RT, ambient air design curve that has been developed. A special stress parameter, S, that combines the maximum stress, S_{max}, or in the case of a compressive cycle the absolute value of the minimum stress, $|S_{min}|$, with the alternating component of the stress, S_a, is used for all fatigue evaluations. The curve in Figure 6 is applicable to all cycles with mean stress of zero or greater. Fatigue strength multiplication factors have been developed to address situations where cycling into compression and a compressive mean stress is developed and to address temperatures other than RT and fluid exposures.

In the case of long-term sustained loadings—either those associated with the 3000-h or 5000-h operating life of a vehicle—time-dependent creep deformations may become an important consideration and

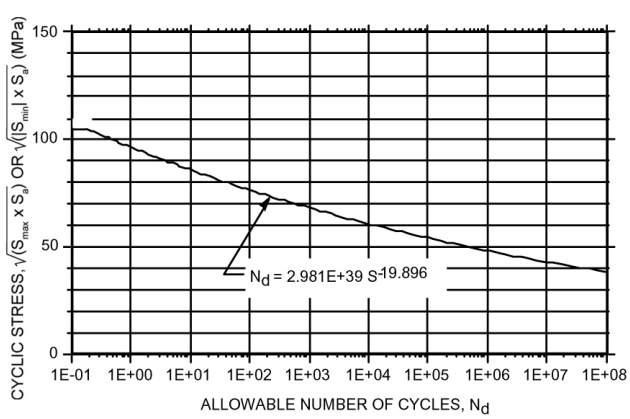

Figure 6. RT design fatigue curve.

need to be accounted for in the design analysis. Constant-load tensile creep deformation tests were performed in RT air, at elevated temperatures (70°C and 120°C), and in fluids (distilled water with a nominal presoak of 1000 h and windshield-washer fluid with a 100-h presoak). A limited number of compressive creep tests were also performed in RT air and elevated temperature. The approach was to develop an RT, in-air, tensile creep equation and to then develop creep multiplication factors to approximately characterize the effects of temperature, fluids, and compressive loadings in terms of RT, in-air, tensile response. Figure 7 presents tensile creep-rupture data and the design curve at 120°C compared to the RT curve. The design curve is 77% of the average curve as has been used with previous composites.

Damage tolerance is the ability of a material or structure to continue to perform its function in the presence of damage, which might occur in the form of initial flaws or as service-induced damage, such as that due to incidental low-energy impacts. Impact tests using a pendulum to represent tool drops and an air gun projectile to represent roadway kickups have been performed on plates of the chopped-carbon fiber material. Also, brick-drop tests were performed to determine the ability of the baseline tests to cover that event, which is of

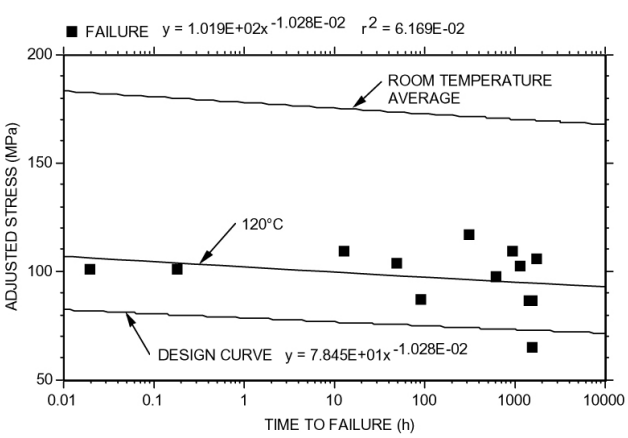

Figure 7. Tensile creep-rupture data and design curve at 120°C.

interest in the design of pickup truck boxes. In addition to baseline tests performed in ambient air, tests were performed at –40°C. Figure 8 presents the design curve that was developed for conservatively estimating damage from impactor mass and velocity.

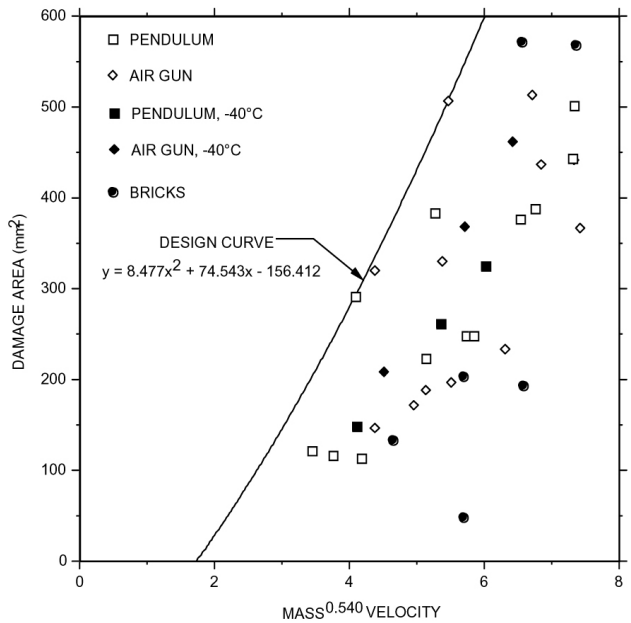

Figure 8. Design curve for estimating damage.

Carbon-Fiber-Reinforced Thermoplastic Material Investigation

A quasi-isotropic carbon-fiber-reinforced PPS material has been selected as the next material to be investigated. The ACC has supplied 43 plaques, 510-mm by 610-mm by about 3-mm thick, for use in durability studies. Plaque reinforcement is symmetrical and consists of 16 plies of carbon-fiber unidirectional tape, [0/90/±45]2S. This is the first thermoplastic composite matrix material to be investigated under the durability program.

Processing conditions are very important because they affect the crystallinity of a semicrystalline polymer such as PPS. Crystallinity changes of thermoplastic materials can result in significant changes in the mechanical behavior of composites containing them, particularly with respect to matrix-dominated properties such as

compressive strength and creep. For this reason the ability to precisely characterize the polymer crystallinity in a thermoplastic material becomes an important requirement. Unfortunately the precise processing procedure followed for preparing the PPS plaques is not available because the process is considered proprietary. Efforts are under way to obtain background information and data on the effects of processing on PPS crystallinity and the relationship between crystallinity and properties. Also, techniques are being identified for determining the crystallinity of the material supplied and determining the effect that specific durability issues addressed may have on the material crystallinity (e.g., 120°C thermal exposure, depending on the processing temperature, may increase material crystallinity).

Tests to evaluate specimen orientation effects and to establish baseline RT tensile and compressive properties of the PPS composite material have initiated. Figures 9 and 10 present the effect of specimen orientation on tensile strength and tensile modulus of elasticity (0° orientation is in long direction of plaque), respectively.

Additional baseline tensile and compressive properties have been obtained from specimens obtained from three of the plaques. Six specimens each in the 0° and 90° orientations were tested from each

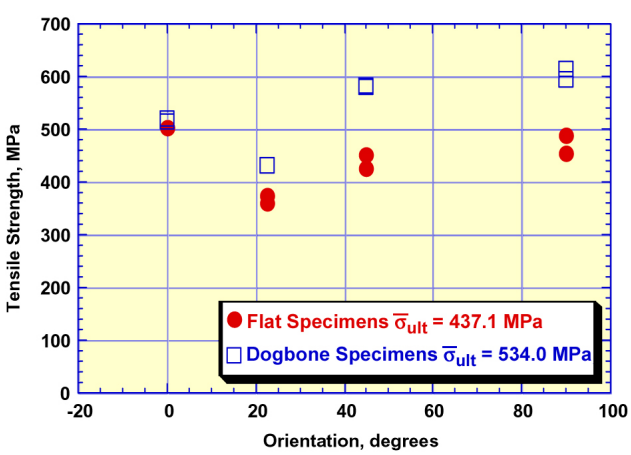

Figure 9. Specimen orientation and tensile strength.

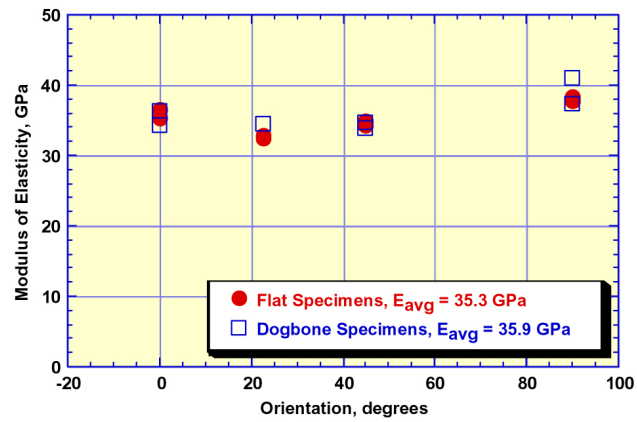

Figure 10. Specimen orientation and tensile modulus.

plaque. Table 3 presents preliminary average tensile and compressive properties obtained (tensile results also include those investigating specimen orientation effects).

Once the baseline shear properties are determined, testing to develop durability-based design criteria for the quasi-isotropic carbon-fiber reinforced PPS material will be initiated.

Table 3. Baseline tensile and compressive properties

Tensile		
Orientation	Strength (MPa)	Modulus (GPa)
0°	523 (16.6)	36.9 (1.0)
90°	570 (24.8)	40.1 (0.9)
Compressive		
Orientation	Strength (MPa)	Modulus (GPa)
0°	314 (19.6)	35.3 (1.3)
90°	353 (22.8)	37.4 (1.1)

Summary

Recommended durability-based design properties and criteria have been developed for a quasi-isotropic carbon-fiber composite for possible automotive structural applications. The durability issues addressed included the effects on deformation, strength, and stiffness of cyclic and sustained

loads, operating temperature, automotive fluid environments, and low-energy impacts. Guidance has been developed for design analysis, time-dependent allowable stresses, rules for cyclic loadings, and damage tolerance design guidance.

A quasi-isotropic carbon-fiber reinforced PPS material has been selected as the next material to be investigated. This is the first thermoplastic material to be investigated under the durability program. The ACC has supplied 43 plaques, 510-mm by 610-mm by about 3-mm thick, for use in durability studies. Plaque reinforcement is symmetrical and consists of 16 plies of carbon-fiber unidirectional tape, [0/90/±45]2S. Processing conditions for these plaques are very important because they affect the crystallinity of a semicrystalline polymer such as PPS, which can result in significant changes in the mechanical behavior of composites containing them. Because precise processing information on the plaques is not available due to the proprietary nature of the processing, the crystallinity of the material is being investigated. Initial tests to evaluate specimen orientation effects and to establish baseline RT tensile and compressive properties of the PPS composite material have been completed.

Publications

1. S. Deng, X. Li, and Y. J. Weitsman, *Aspects of the Mechanical Behavior of Stitched T300 Mat/Urethane 420 IMR Composite*, ORNL/TM-2002/86, Oak Ridge National Laboratory, Oak Ridge, Tenn., October 2002.

2. J. M. Corum, R. L. Battiste, A. Ionita, M. B. Ruggles-Wrenn, and Y. J. Weitsman, *Durability-Based Design Criteria for a Chopped-Carbon-Fiber Automotive Composite*, ORNL/TM-2003/86, Oak Ridge National Laboratory, Oak Ridge, Tenn., May 2003.

3. J. M. Corum, R. L. Battiste, and M. B. Ruggles-Wrenn, "Low-Energy Impact Effects on Candidate Automotive Structural Composites," *Composites Science and Technology* **63**(6), 755–769, 2003.

4. S. Deng, X. Li, and Y. J. Weitsman, "Time-Dependent Deformation of Stitched T300/Mat/Urethane 420 IMR Cross-ply Composite Laminates," *Mechanics of Time-Dependent Materials* **7**(1), 41–69, 2003.

5. M. B. Ruggles-Wrenn, J. M. Corum, and R. L. Battiste, "Short-Term Static and Cyclic Behavior of Two Automotive Carbon-Fiber Composites," *Composites* Part A **34**, 731–741, Elsevier Ltd., 2003.

6. M. B. Ruggles-Wrenn, *Effects of Temperature and Environment on Mechanical Properties of Two Chopped-Fiber Automotive Structural Composites*, ORNL/TM-2003/114, Oak Ridge National Laboratory, Oak Ridge, Tenn., July 2003.

7. M. B. Ruggles-Wrenn, *Effects of Temperature and Environment on Mechanical Properties of Two Continuous Carbon-Fiber Automotive Structural Composites*, ORNL/TM-2003/117, Oak Ridge National Laboratory, Oak Ridge, Tenn., July 2003.

B. Low-Cost Test Methods for Advanced Automotive Composite Materials; Creep Compression Fixture

John M. Henshaw
The University of Tulsa
600 South College
Tulsa, OK 74104
(918) 631-3002; fax: (918) 631-2397; e-mail: john-henshaw@utulsa.edu

Ben Pierson
The University of Tulsa
e-mail: ben-pierson@utulsa.edu

ACC Project Contact: Dan Houston
Ford Motor Company
20000 Rotunda Dr., MD 3182 SRL, P.O. Box 2053
Dearborn, MI 48121-2053
(313) 323-2879; fax: (313) 323-0514; e-mail: dhousto2@ford.com

Field Project Manager, Composites: C. David Warren
Oak Ridge National Laboratory
P.O. Box 2008, Oak Ridge, TN 37831-8050
(865) 574-9693; fax: (865) 574-0740; e-mail: warrencd@ornl.gov

Technology Area Development Manager: Joseph Carpenter
(202) 586-1022; fax: (202) 586-1600; e-mail: joseph.carpenter@ee.doe.gov
Field Technical Manager: Philip S. Sklad
(865) 574-5069; fax: (865) 576-4963; e-mail: skladps@ornl.gov

---

Contractor: U.S. Automotive Materials Partnership
Contract No.: DE-FC05-02OR22910

Objective

- Design and develop low-cost, reliable fixtures and methods for the characterization of compression creep behavior of automotive composites with and without environmental exposure. Confirm results generated by the new fixture with those from conventional testing systems.
- Incorporate the fixtures and methods in the above objective into industry-standard test methods for automotive composites.
- Using results of short-term tests, develop predictive models for lifetime property degradation.
- Investigate the fundamental damage mechanisms in polymer-matrix, carbon-fiber, and E-glass composites as a function of specific, varied mechanical loading with concurrent environmental exposure.

Approach

- Design and develop a compact compression creep test fixture system and confirm its performance.
- Use the new fixture system to develop a compression creep database.
- Develop a standard procedure for compression creep testing using the new system.
- Develop and verify damage and creep models for structural automotive composites.

Accomplishments

- Developed, fabricated, and tested initial fixture prototype and isolated problem areas.
- Designed, developed, and fabricated two new fixtures to enhance capability of first-generation prototype.
- Fabricated second prototypes and performed initial prove-out testing.
- Implemented new data acquisition system.

Future Directions

- Continue prove-out of fixture system.
- Evaluate varying environments on the fixture system and the test materials.
- Design and develop additional fixtures if required.
- End project on 12-31-2005.

Introduction

Because of insufficient information on the long-term durability of lightweight composite materials, reliable methods and models requiring relatively short-term tests are essential to composites achieving their full potential in the automotive industry. The purpose of this project is to develop simple low-cost fixtures and methods for the creep and creep rupture characterization of automotive composites and confirm the in-situ creep test fixture results with those obtained using conventional testing methods.

Initial Design Concept For The Compression Creep Fixture

Several design specifications were targeted when developing the initial prototype fixture. It must simulate in-service loading conditions by exposing the specimen to various environments. The fixture should also be lightweight, compact, relatively inexpensive, and portable compared to industry standard deadweight creep testing fixtures. Lastly, the data generated by the fixture should be of design quality while comparing favorably to Oak Ridge National Laboratory (ORNL) and literature data. A successful fixture would also be corrosion-resistant, capable of testing American Society of Testing and Materials (ASTM) standard compression coupons, and exhibit no signs of specimen buckling.

Prototype 1 Design Details

The initial prototype utilizes a four-pin design where the specimen fits inside two compression blocks that are pressed toward each other by load reversing pins. The ends of the pins are threaded into a connecting bracket that, in turn, mounts to a clevis joint on a spring-loaded moment arm (see

Figures 1, 2, and 3). This prototype is capable of testing compression specimens up to 2.5 in. in length. This is exactly one-half of the ASTM standard length. The second set of prototypes is designed to use the full-sized specimen.

Figure 1. Compression Blocks with 2.5 in. specimen.

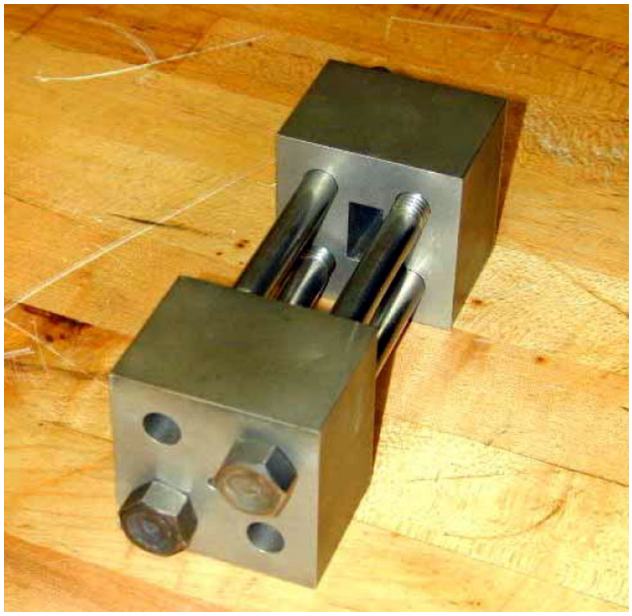

Figure 2. Compression blocks assembled with load reversing bolts.

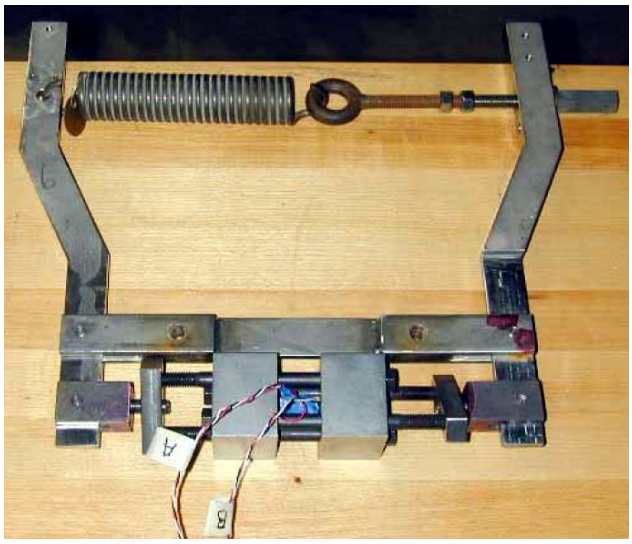

Figure 3. Assembled prototype #1 compression creep fixture.

Prototype 1 Test Results

Initial testing of P4 glass material with prototype 1 showed compression creep behavior very similar to the compression creep curves generated by ORNL (see Figure 4). When a strain gage was mounted on each side of the compression specimen a difference in strain levels was shown (see Figure 5). This indicates a bending load being placed on the specimen. ASTM requires compression tests to exhibit less than 5% bending to be considered valid. The bending is attributed to end loads placed on the specimen by the compression blocks and misalignment of the specimen in the pockets. Because of these bending loads, a new design is required.

Prototype 2a Design Details

After determining that a second prototype was necessary, two alternatives were designed and fabricated. Prototype 2a uses compression blocks and load reversing pins very similar to those used in prototype 1; 2a has an added feature of two bolts though the side of the compression blocks that fit to a gripping pad. When the 5-in. compression specimen is loaded into the compression blocks the two bolts can be tightened to

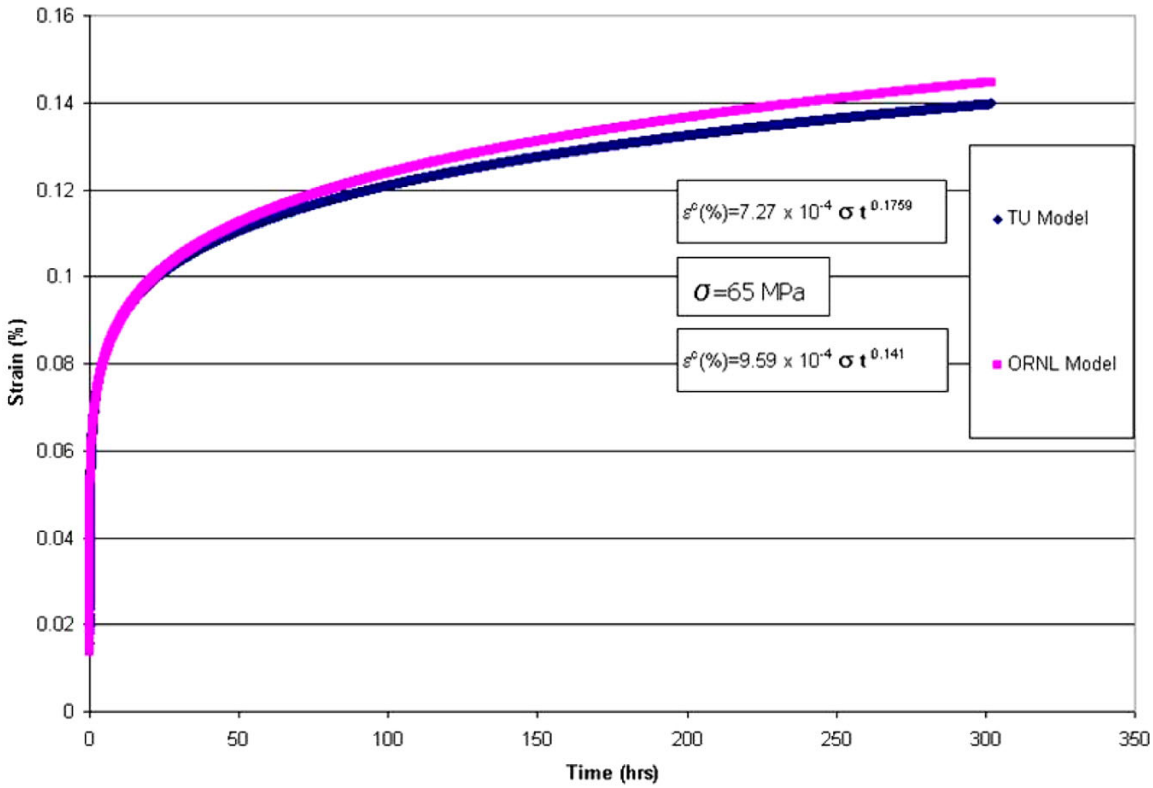

Figure 4. Preliminary creep data from prototype 1 and ORNL experiments.

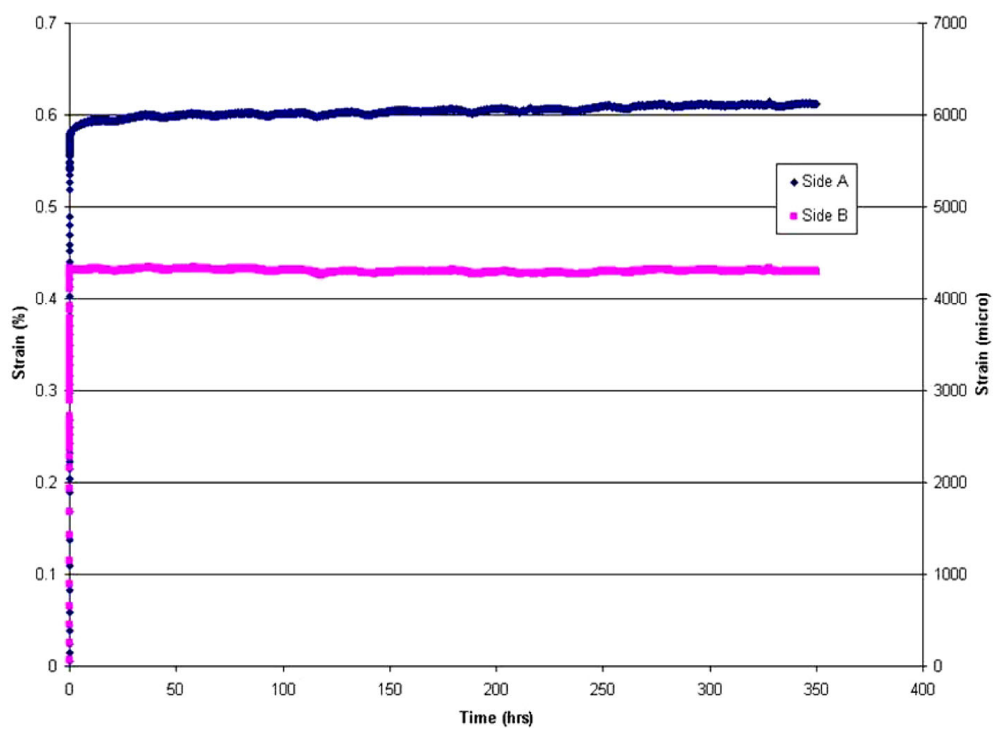

Figure 5. Differences in strain levels on each side of the specimen indicating bending.

align and hold the specimen in the compression blocks (see Figures 6 and 7).

Figure 6. Fixture 2a components.

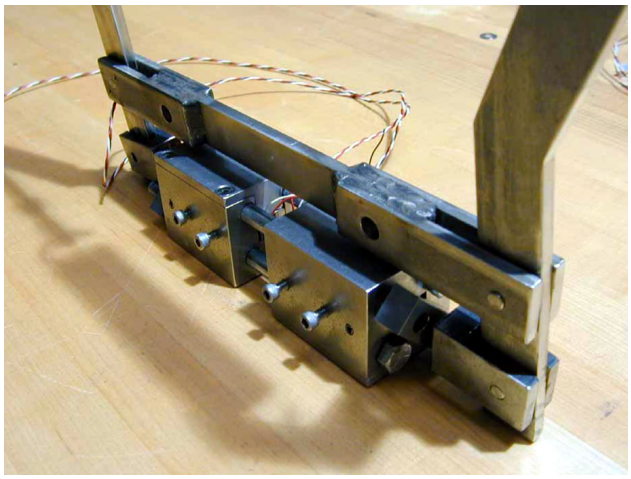

Figure 7. Fixture 2a with loaded specimen.

Prototype 2b Design Details

Prototype 2b utilizes four wedge-shaped grip faces. As the compression blocks are pressed toward each other with load reversing pins, the wedge grips squeeze the 5-in. compression specimen with increasing pressure. This fixture design utilizes symmetry and the compression force being placed on the specimen to eliminate bending and end loading of the specimen (see Figures 8 and 9).

Figure 8. Fixture 2b components.

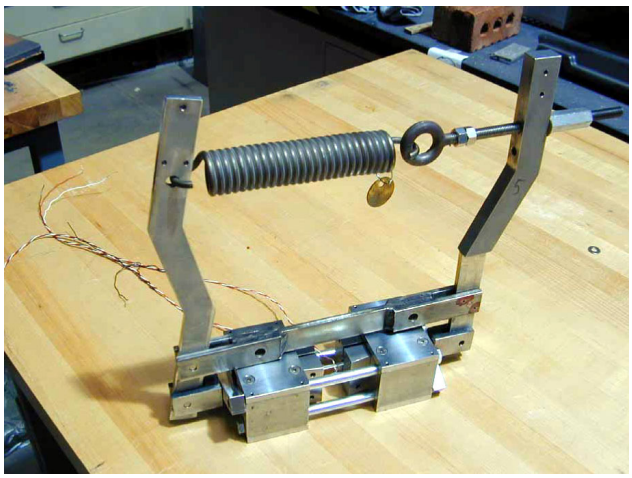

Figure 9. Fixture 2b with spring-loaded moment arms.

Ongoing/Future Work

- Continued evaluation of prototype 2a and 2b performance through short-term tests, using composite and aluminum specimens.
- Determination of a final prototype able to meet all design requirements and criteria.
- Refining of final prototype.
- Fabrication of a series of compression fixtures for evaluation of polymer composite material systems.
- Creep, stressed environmental durability, and in-service testing using the creep compression fixture.

C. Intermediate-Rate Crush Response of Crash Energy Management Structures

Co-Principal Investigator: Raymond G. Boeman
Oak Ridge National Laboratory
53-1/2 W. Huron St., Suite 213
Pontiac, MI 48342
(248) 452-0336; fax: (248) 452-8992; e-mail: boemanrg@ornl.gov

Co-Principal Investigator: J. Michael Starbuck
Oak Ridge National Laboratory
P.O. Box 2008, Oak Ridge, TN 37831-8048
(865) 576-3633; fax: (865)-574-8257; e-mail: starbuckjm@ornl.gov

Project Manager, Composites: C. David Warren
Oak Ridge National Laboratory
P.O. Box 2008, Oak Ridge, TN 37831-6065
(865) 574-9693; fax: (865) 576-4963; e-mail: warrencd@ornl.gov

Technology Area Development Manager: Joseph A. Carpenter
(202) 586-1022; fax: (202) 586-1600; e-mail: joseph.carpenter@ee.doe.gov
Field Technical Manager: Philip S. Sklad
(865) 574-5069; fax: (865) 576-4963; e-mail: skladps@ornl.gov

---

Contractor: Oak Ridge National Laboratory
Contract No.: DE-AC05-00OR22725

Objective

- Develop unique characterization facility for controlled progressive crush experiments, at intermediate rates, of automotive materials (polymer composites, high-strength steels, aluminum) and structures.
- Study the deformation and failure mechanisms of automotive materials subjected to crush forces as a function of impact velocity.
- Obtain specific energy absorption and strain data, and correlate with deformation and failure mechanisms to describe the unknown transitional effects from quasi-static to high loading rates for polymer composites.
- Characterize the strain rate effects for metallic materials and components.
- Provide access to unique test capability to university, industry, and government users for collaborative research.

Approach

- Develop a unique high-force (270-kN), high-velocity (8 m/s) servo-hydraulic machine to conduct progressive crush experiments on structural components at intermediate rates.
- Use high-speed imaging to observe and document deformation and damage mechanism during the crush event.

- Conduct strain measurements at discrete locations and explore full-field measurements of strains and curvatures.
- Coordinate polymer composites investigations with the Automotive Composites Consortium (ACC) Energy Management Group.
- Coordinate steel investigations with the Auto/Steel Partnership.

Accomplishments

- Completed design modification and fabrication to achieve increased performance (125%) up to 8 m/s.
- Completed installation and initial operator training at the National Transportation Research Center (NTRC).
- Completed new acceptance tests on-site to demonstrate enhanced performance.
- Completed design and fabrication of test fixtures for testing five different tube geometries.
- Completed integration of high-speed data acquisition with test operation.
- Completed vendor demonstrations on four high-speed video systems.
- Completed a total of 38 shakedown tests as part of high-speed video assessments, capability demonstrations, and machine commissioning.
- Held official dedication ceremony in August 2003.

Future Direction

- Procure high-speed video.
- Explore techniques for full-field measurements of strains and curvatures.
- Develop User Interaction Plan.
- Support user collaboration as required.

Introduction

Progressive crush is an important mechanism by which the kinetic energy of a traveling automobile is dissipated in a collision to protect the safety of occupants. Unfortunately, the mechanisms governing the progressive crush response of some emerging automotive materials are not well understood. Additionally, many of these materials are known to exhibit responses that are sensitive to rate of loading.

Understanding the influence of impact velocity on the crush response of materials and structures is critically important for crashworthiness modeling inasmuch as collisions occur at a range of velocities. Additionally, from a structural standpoint, the deformation (or strain) rate is generally not unique from either a spatial or temporal standpoint. Consequently, it is important to quantify the behavior of materials at various strain rates.

Test Machine for Automotive Crashworthiness (TMAC)

Typically standard test machines are employed for experiments at quasi-static rates whereas drop towers or impact sleds are the convention for dynamic rates. These two approaches bound a regime within which data, for experiments at constant impact velocity, are not available by conventional

experimental practice. This regime is termed herein the intermediate-rate regime and is defined by impact velocities ranging from 1 m/s to 5 m/s. Investigation of rate effects within this regime requires experimental equipment that can supply a large force with constant velocity within these rates. Using a drop tower or sled at intermediate rates, although technically possible, is problematic due to the prohibitively large mass required to maintain constant velocity during the crush. Consequently, the Oak Ridge National Laboratory (ORNL) and the Automotive Composites Consortium (ACC) collaborated to define specifications for a unique experimental apparatus that mitigates the shortcomings of existing equipment. MTS Systems Corporation designed and built the servo-hydraulic test machine, referred to as the TMAC. As shown in Figure 1, TMAC is uniquely capable of conducting controlled progressive crush tests at constant velocity in the intermediate velocity range (i.e., less than 5m/s) owing to the large energy available at those rates and to the sophisticated simulation and control software that permits velocity uniformity to within 10%.

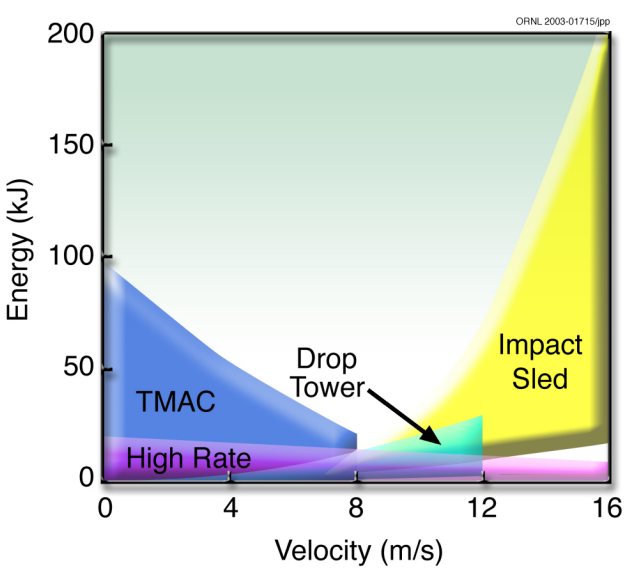

Figure 1. Energy plot indicating TMAC's unique capability of supplying enough energy at the intermediate rates for controlled, constant-velocity crush tests.

The new experimental facility will be used to understand the crush behavior between the static and dynamic (8-m/s) conditions.

Status

Since the last reporting period, the machine was disassembled at the vendor's location (MTS Systems Corp., Eden Prairie, MN) for shipment to the NTRC. A delay of approximately 1 month was encountered due to the replacement of a leaking actuator seal. The machine arrived for installation at NTRC in late October 2002. MTS personnel were on site for approximately 2 weeks for the installation, which was completed on November 1 (see Figure 2). The acceptance tests were executed again at NTRC to verify that the performance was not altered during the shipment process (see Figure 3). The machine met or surpassed the enhanced specifications including:

- No-load velocity of 8 m/s constant to within 10% over 115 mm.
- Sustained crush force of 133 kN at 6 m/s constant to within 10% over 115 mm.
- Sustained crush force of 267 kN at 4 m/s constant to within 10% over 115 mm.

Limited training was provided by MTS, but training videos and brief documentation in the form of PowerPoint presentations were provided. The vendor training videos that describe the detail procedures for simulation and iteration—for obtaining constant velocity—were not received until the end of February which delayed extensive use of the machine.

Meanwhile, mounting fixtures for 3-in. circular steel tubes, 4-in square composite tubes, 2- by 4-in rectangular tubes and 2-in square tubes were designed and fabricated. The designs incorporate a quick change out feature to expedite testing as opposed to the potting (bonding) approach that is common to drop tower and impact sled testing. The 4-in. square fixture was manufactured first to validate the concept to permit modification

Figure 2. TMAC installation at NTRC.

Figure 3. Aluminum honeycomb specimen before and after crush during acceptance test demonstrating sustained crush force of 133 kN at a velocity of 6 m/s constant to within 10% over 115 mm.

as necessary (see Figures 4 and 5). A series of tests were run using the 4-in. square composite tubes provided by the ACC that demonstrated external clamping of the specimens was a valid concept. A typical failed

Figure 4. Square composite tube specimen in prototype fixture.

Figure 5. Square tube test fixture.

specimen is shown next to an untested specimen in Figure 6. An internal plug fixture was also designed and fabricated for testing the 4-in. square tubes, but this

Figure 6. Uncrushed and crushed polymer composite tubes (4-in. square cross-section).

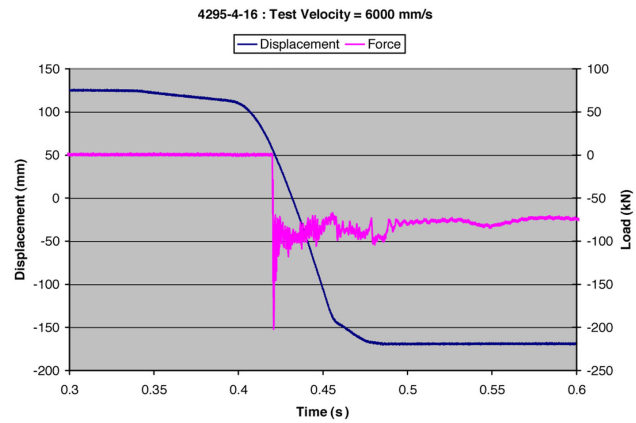

Figure 7. Typical load and displacement data for a 4-in. square carbon fiber composite tube tested at 6 m/s.

concept has not yet been evaluated. Fabrication has now been completed on various fixtures and supporting hardware that will enable testing of five different tube geometries. The fifth geometry that is not described above is a 4-in. circular tube.

A LabView program was developed to obtain the test data from two high-speed data acquisition (DAQ) modules—a 12-bit synchronous card with four channels, and a 16-bit asynchronous card with eight channels. The program synchronizes the data and is triggered from the TMAC control software that initiates the impact. One card has higher signal resolution at the expense of temporal resolution and synchronicity, while the other card sacrifices signal resolution for fast, synchronous measurements. The merits of the two cards are being assessed.

The functionality of the data system was demonstrated and will be refined and updated as future test requirements are defined, including the capability for recording strain gage signals. The current DAQ configuration reads one LVDT for displacement, a load cell and load washer for force, and two accelerometers. The accelerometers were chosen to provide 1-g/V sensitivity and 10-g/V sensitivity. Figure 7 shows a typical response of a 4-in. square composite tube tested at 6 m/s. The measured displacement from the LVDT is plotted on the left ordinate, and the measured force from the load washer is plotted on the right ordinate. The force trace is typical of a progressively crushed specimen with a distinct initial peak, followed by drop off in load to a relatively constant level for the remaining crush distance. A similar plot of a 3-in.-diam steel tube is shown in Figure 8. The steel tube, which progressively crushes by plastic hinge formation (see Figure 9), shows much fewer oscillations in the force data than the composite tube.

The accelerometer data are integrated to calculate the velocity, and this is being compared with the differentiated displacement data. Preliminary tests have shown that essentially the same velocity is calculated using the two different measurements, but issues related to signal noise and filtering need to be resolved. To illustrate this point, results from a 6-m/s test without a specimen are shown in Figure 10. There are three plots in this figure, the LVDT displacement data, the velocity calculated from the 10-g/V accelerometer, and the velocity calculated from the displacement using a 25-point moving average. Ultimately, data for force, displacement, time, acceleration, and strain will be acquired and synchronized with high-speed video for complete characterization of the event.

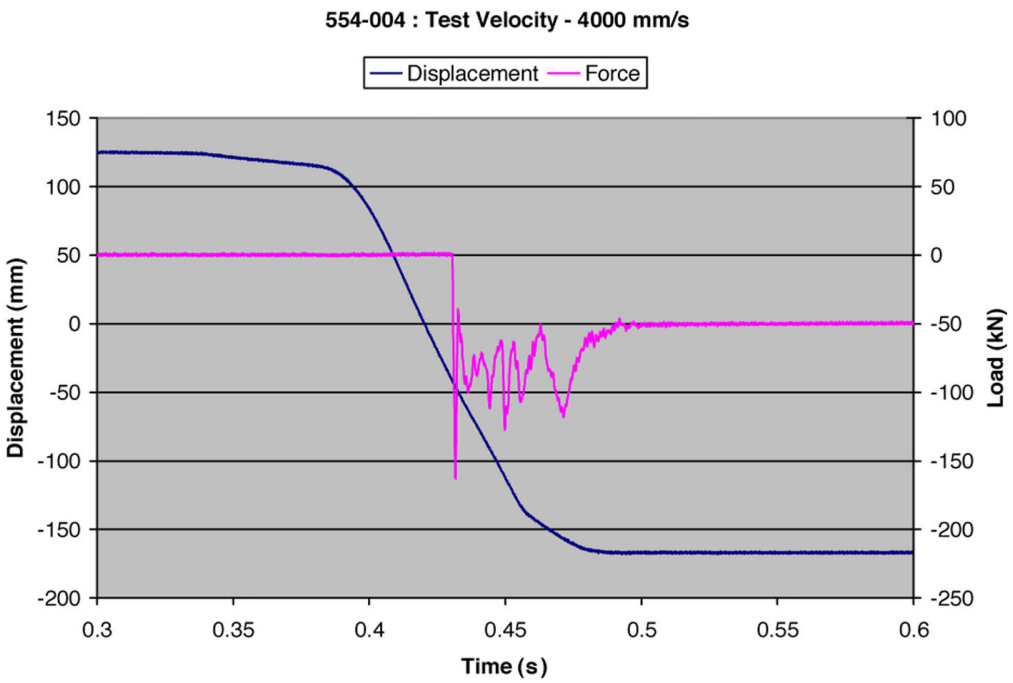

Figure 8. Typical load and displacement data for a 3-in. diam steel tube tested at 4 m/s.

Figure 9. Metallic tubes tested in TMAC demonstrate the conventional folding pattern associated with plastic hinge formation.

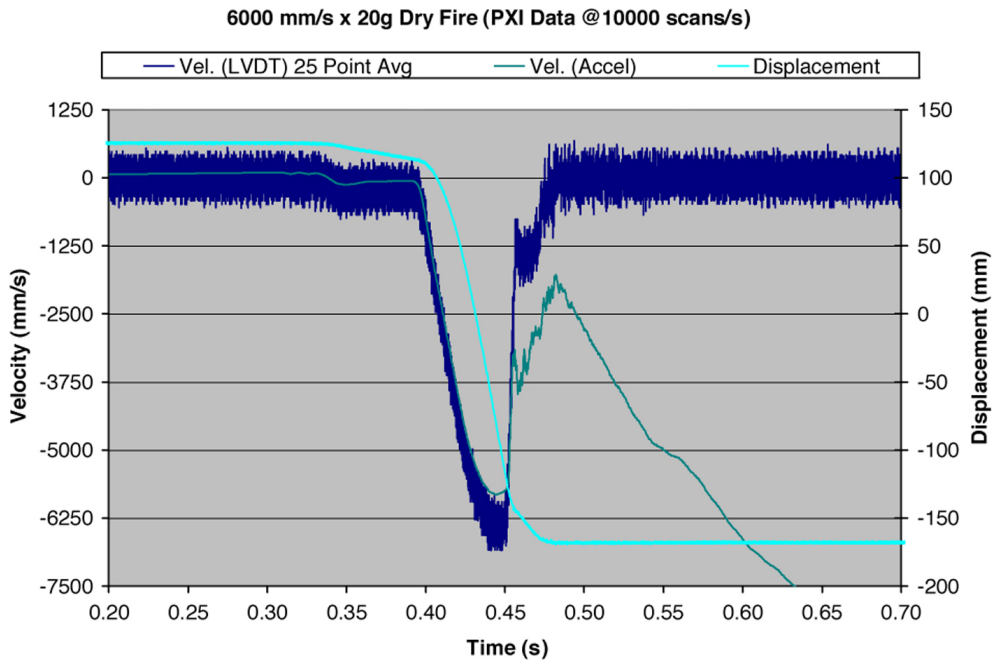

Figure 10. Calculated velocities from a 6-m/s test without a specimen.

The pressure accumulators were replaced with American Society of Mechanical Engineers (ASME) code-stamped versions per regulation, and an air abatement system to collect the carbon fiber dust cloud was implemented. The latter was required for health concerns as well as for improved imaging.

Five high-speed video vendors were contacted to identify suitable candidates for the imaging needs. Demonstrations of the three most promising systems were held at NTRC during the third week. Final selection of the video system was delayed to review the next-generation systems, which are expected to be released in the first quarter of FY 2004. The new systems offer a combination of increased resolution, decreased shutter speed, and greater light sensitivity at essentially the same cost.

A dedication ceremony was held in August, which marked the official commissioning of the capability. A total of 38 experiments have been conducted as part of shakedown experiments, high-speed video assessments, capability demonstrations, and machine commissioning.

Conclusions

TMAC has passed and exceeded the performance specifications as demonstrated by acceptance tests conducted at both the vendor site and after installation at NTRC. It provides a unique capability to measure the specific energy absorption on crush tubes as a function of (constant) impact velocity within a range from quasi-static to 8 m/s.

Progress in conducting experiments has been delayed due to replacement of pressure accumulators and the learning curve associated with the software operation to optimize machine parameters for constant velocity tests. Conducting the physical test is more complex than typical test operations, but sufficient expertise has been developed to render it rather routine. However, conducting the virtual test to determine the precise machine parameters to provide constant velocity is quite complex. The full documentation describing the multiple steps in the software was not received from the vendor until February 2003, which resulted in delays in developing the requisite expertise. Sufficient experience to conduct constant

velocity tests for a general specimen behavior is expected by the end of the first quarter FY 2004.

Additional work is required to refine the data acquisition, particularly with regard to comparisons of the two data acquisition cards, filtering of data, and determination of velocity from accelerometer signals.

D. Composite Crash Energy Management

Principal Investigator: Richard Jeryan
Ford Research Laboratories
2101 Village Road
MD2115 SRL, Rm. 2621D
Dearborn, MI 48124-2053
(313) 594-4903; fax: (313) 845-4724; e-mail: rjeryan@ford.com

Field Project Manager: C. David Warren
Oak Ridge National Laboratory
P.O. Box 2008, Oak Ridge, TN 37831-8050
(865) 574-9693; fax: (865) 574-4963; e-mail: warrencd@ornl.gov

Technology Area Development Manager: Joseph Carpenter
(202) 586-1022; fax: (202) 586-1600; e-mail: joseph.carpenter@ee.doe.gov
Field Technical Manager: Philip S. Sklad
(865) 574-5069; fax: (865) 576-4963; e-mail: skladps@ornl.gov

---

Contractor: U.S. Automotive Materials Partnership (cooperative agreement) Automotive Composites Consortium Energy Management Working Group
Contract No.: DE-FC05-02OR22910

Objective

- Determine experimentally the effects of material, design, environment, and loading on macroscopic crash performance to guide the design and the development of predictive tools.
- Determine the key mechanisms responsible for crash energy absorption, and examine microstructural behavior during crash to direct the development of material models.
- Develop analytical methods for predicting energy absorption and crash behavior of components and structures.
- Conduct experiments to validate analytical tools and design practices.
- Develop and demonstrate crash design guidelines and practices.
- Develop and support design concepts for application in demonstration projects.

Approach

- Conduct experimental projects to increase understanding of the global and macro influences of major variables on crash performance.
- Use the data from these experiments to create crash intuition, guidelines, rules of thumb, and data for the validation of analysis developments.
- Conduct microscopic experimental characterization to define the mechanisms that occur during and as a result of the crash process.

Accomplishments

- Completed crash testing of square and rectangular braided carbon tubes to determine the effects of fiber type and architecture, tube shape, and temperature on energy absorption performance.
- Completed crash testing of circular and square tubes made of noncrimped fabrics (NCFs) to determine the effects of preexisting damage, laminate inserts and shape on static and dynamic energy absorption.
- Designed and used laboratory test fixture to determine effects of friction during sliding and bending.
- Conducted LS-DYNA analyses of adhesive material test specimens and modeled simple joints with nonlinear adhesive properties.
- Completed initial screening of 13 configurations of composite sandwich face/core.
- Modified a user subroutine originally developed for quasi-static analysis for dynamic analysis with the ABAQUS explicit finite-element (FE) code.

Carbon-Reinforced-Tube Performance

The objective of this project is to experimentally determine the effects of material, design, environment, and loading on carbon-fiber-reinforced tubes to guide automotive design and analysis development, including the development of analytical material models.

The carbon tube test program was completed in 2003. Braided tubes of square and rectangular cross sections were tested dynamically to evaluate their crush performance. A series of hot (82°C) and cold (–40°C) temperature tests were conducted on the drop tower, and these results were compared to the room temperature tests conducted previously. The tubes tested at hot temperature were also exposed to moisture. Mean crush force and specific energy absorption were compared for each class of materials. Table 1 shows the average mean crush force values at each of the temperatures tested. There was no significant difference in force levels between temperatures. Progressive crush was obtained for each architecture. An example of a 12k carbon tube is shown in Figure 1. This tube was tested at elevated temperature.

Table 1. Average mean crush as a function of temperature

Average Mean Crush Force (kN)						
Tube Dimensions	Tube ID	Fiber Type	Lay-up	Cold Temp. (-40 C)	Room Temp.	Hot Temp. (82.2 C)
50 x 100	4280-2	Grafil 12k Carbon	$(0/\pm30°)_2$	12.0	12.3	14.0
100 x 100	4290-2			18.8	22.8	24.9
50 x 100	4281-2	Fortafil 80k axial Grafil 12k off-axis	$(0/\pm45°)_2$	31.9	31.3	34.4
50 x 100	4283-2	Fortafil 80k axial 250 Yld. E-glass	$(0/\pm30°)_2$	44.0	40.4	49.1
100 x 100	4293-2			61.1	61.4	64.1
50 x 100	4284-2	Fortafil 40k axial Grafil 12k off-axis	$(0/\pm30°)_2$	20.1	22.9	20.5
100 x 100	4294-2			31.0	31.4	31.7

Figure 1. Elevated temperature crush sample.

Results from the room temperature tests continue to be utilized by the groups developing analysis methods for these braided carbon materials.

Static vs Dynamic Performance

This project's objectives are to experimentally determine the microstructural factors and behaviors that lead to decreased energy absorption when crushing tubes dynamically. This study focuses mainly on braided carbon fiber materials where the tube tests showed a decrease in energy absorption of 50% when crushing dynamically. Strain rate effects in braided carbon fiber samples with notches have shown that under static three-point bend loading fiber bridging of cracks occurs. Fiber bridging is a well-known phenomenon in composites that leads to increased fracture toughness. In dynamic rates, there was almost no observable fiber bridging in the samples. Furthermore, the crack faces were smoother than those tested statically. The load and energy absorption capacity at dynamic rates were found to be much lower than those measured on the static tests. The intermediate strain rate testing machine designed to evaluate the crush performance of structures at constant elevated impact rates is fully operational at the National Transportation Research Laboratory at Oak Ridge National Laboratory (ORNL). The official dedication of the machine was in August 2003 (see 7C).

Effects of Preexisting Damage on Crash Behavior

The objective of this project is to provide an understanding of the effects of a range of material variability on the mode of crush and consequent energy absorption characteristics of generic and practical vehicle structure geometries. Specifically, the work focuses on the effect on energy absorption associated with delamination, through-thickness, and local point loading on generic circular and square tubular components. At the conclusion of the project, a generic guideline will be created that will help in designing more robust crash structures that are less sensitive to manufacturing and variability. In previous phases of this study, only circular cross sections using random chopped fibers were examined. In the present phase of the work, the effects of various damage modes were studied on tubes of NCF, circular and square cross sections, and interleaved inserts. Overall, NCF structures showed lower specific energy absorption (SEA) than random chopped structures. However, overall trends of sensitivity to damage were similar to those of random chopped materials. Specifically, the effect of damage was more pronounced at static rates. The study also showed the square geometries to be more sensitive to damage imparted at the corners, because these areas of the tube have higher crush stresses. Finally, the effect of adding thermoplastic interleaves was an increased resistance to damage; however, the overall SEA was reduced for undamaged structures when compared to noninterleaved structures.

Friction Effects on Crash Performance

The objectives of this work are to (1) experimentally determine the relative energy absorption due to each mode of a progressively crushed composite tube and isolate that portion of energy absorption due to friction and (2) evaluate differences in friction energy absorption between quasi-static and dynamic crush.

A test fixture, Figure 2, was designed and fabricated that allows the measurement of energy absorption due to matrix damage during bending and sliding friction and can isolate the sliding friction component of crush energy absorption. The fixture uses strip specimens that are commonly tested in a standard materials testing device such as an MTS machine. The test fixture can accommodate strips of varying width up to 1-3/4 in. and up to 3/16 in. thick. Preliminary testing results show that more that half of the energy absorbed during a strip test is attributable to friction. These results are presented in the Figure 3. Energy absorbed is the integrated area under the curve for each test specimen.

The top two curves in Figure 3 show the total energy due to sliding friction and matrix damage due to bending. The lower two curves show energy absorption attributable only to matrix damage due to bending and excludes energy absorption due to sliding friction.

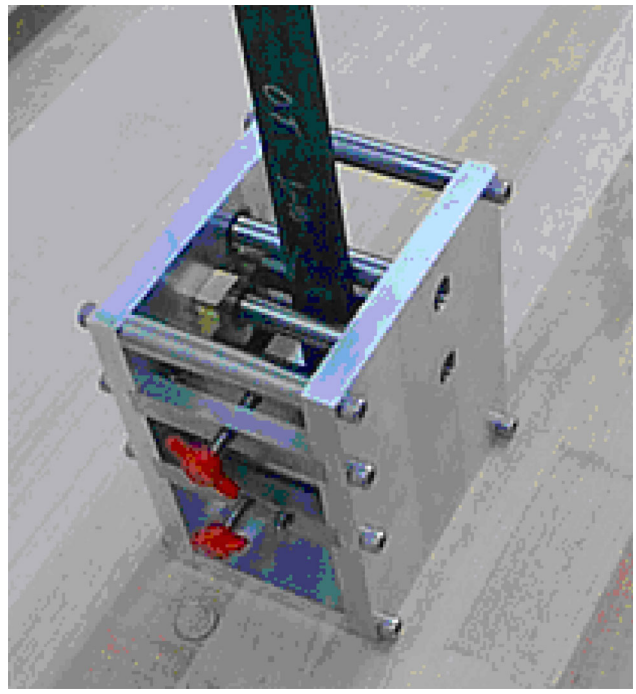

Figure 2. Friction test fixture.

Material characterization testing has been completed for 0/±45 braided graphite/

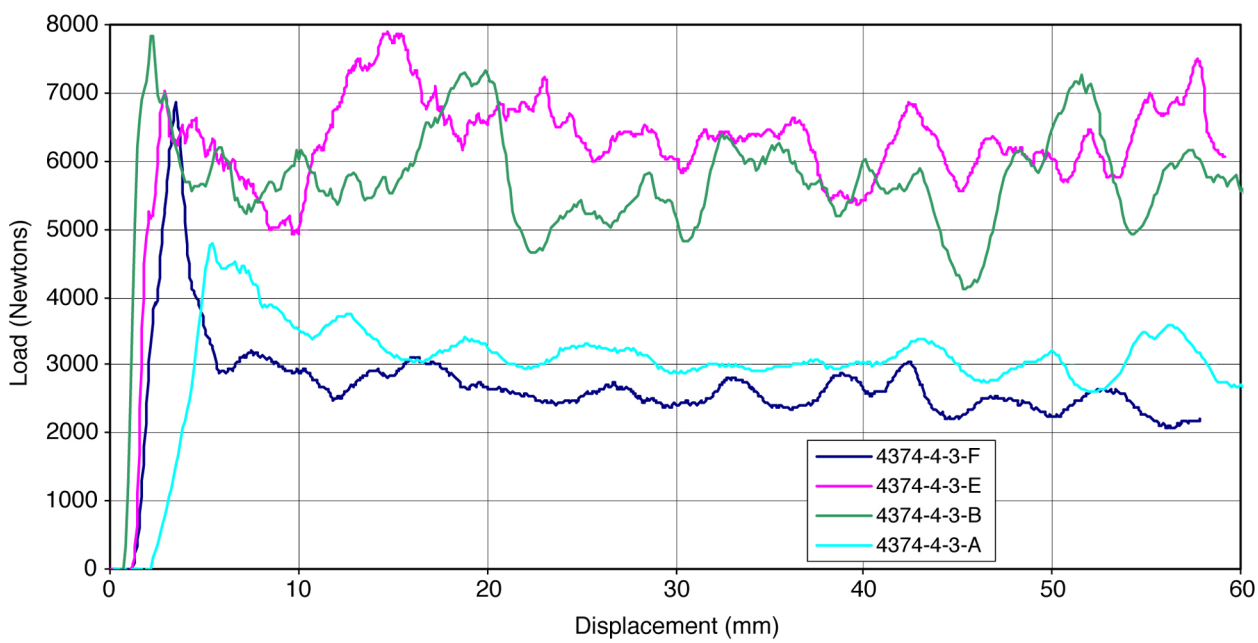

Figure 3. Strip test load deflection results as a function of loading mode.

vinyl ester composite. Standard 2-in. square graphite/vinyl ester test tubes have been quasi-statically tested using the standard crush trigger and the tapered 5° trigger described previously. Energy absorption modes observed were corner splitting, delamination, sliding friction, and matrix fracture due to bending.

Impact Performance of Bonded Structures

The objectives of this effort are to (1) evaluate the performance of bonded structures under crash loads; (2) examine the influence of bond design concepts, impact velocity, environmental conditions, and other material issues; and (3) fabricate new molding tools to produce simulated automotive structures. This is a joint program with the ACC Joining Work Group and part of Focal Project 3 (FP3) design studies.

Visteon Corporation, a Tier I automotive supplier, is leading this effort jointly with FP3 and ACC Energy Management and Joining Work Groups. A comprehensive work plan was established to develop experimental and analytical methodologies to analyze and design adhesively bonded automotive composite structures that can sustain axial, off-axis, and lateral crash/impact loads. The key tasks of the work plan are

- selection of representative subcomponent geometry and substrate and adhesive material systems,
- generation of coupon level material data for substrate and adhesive materials for static and dynamic loading at various strain rates,
- fabrication and testing of the subcomponent geometry under quasi-static and dynamic impact loads at various strain rates,
- development of FE-based computational tools with adhesive material models and progressive damage/debonding algorithms,
- development of standard tests and procedures to characterize Modes I, II, and III and mixed-mode dynamic fracture in adhesively bonded joints,
- incorporation of the complete design methodology into a commercial FEA code such as ABAQUS or LS-DYNA, and
- validation computational tools with test results.

The current status of the key tasks follows.

Task 1: Select a Representative Subcomponent Geometry, Substrate, and Adhesive Material

Hexcel's HexMC® was selected as the initial substrate material for the project. HexMC®, a random chopped prepreg with carbon fibers in epoxy matrix, can be compression molded at about 1000 psi and 100ºC to 150ºC and has a 4- to 15-min cycle time. The molding, however, posed considerable challenges including,

- difficulty of molding plaques,
- variation in thickness and curvature,
- 20–30% coefficient of variation (COV) in preliminary testing results,
- difficulty molding hat sections, and
- concerns about compression molding closed-section, noncircular tubes.

The selection of the substrate material system was revisited, and a 3K high-tensile plain-weave fabric (aerial weight: 193 gsm) carbon/epoxy prepreg system from Advanced Composites Group was selected. The plain-weave system is designated ACG MTM 49/CF0501-42% Resin Weight. The carbon fiber is T300B 40B from Toray. Plaques of ACG MTM 49 carbon/epoxy material system have been manufactured and scheduled for static and dynamic material characterization by ORNL in FY 2004.

SIA 731SI, two-part toughened epoxy, was chosen as the adhesive. Standard surface preparation, for example, sanding with Scotch Brite and subsequently, using solvent

wash, were used to prepare both bonded joint specimens and subcomponents.

Task 2: Generate Coupon-Level Material Data for Substrate, Adhesive Materials, and Single-Lap Joint Configurations for Static and Dynamic Loading

Characterization of bulk properties of SIA 731SI adhesive system at ORNL is in progress. Typical tension and compression stress/strain curves are shown in Figures 4 and 5.

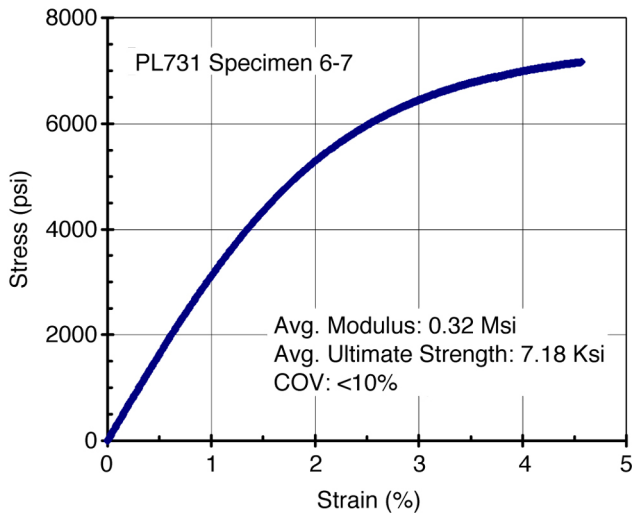

Figure 4. Adhesive tension test data.

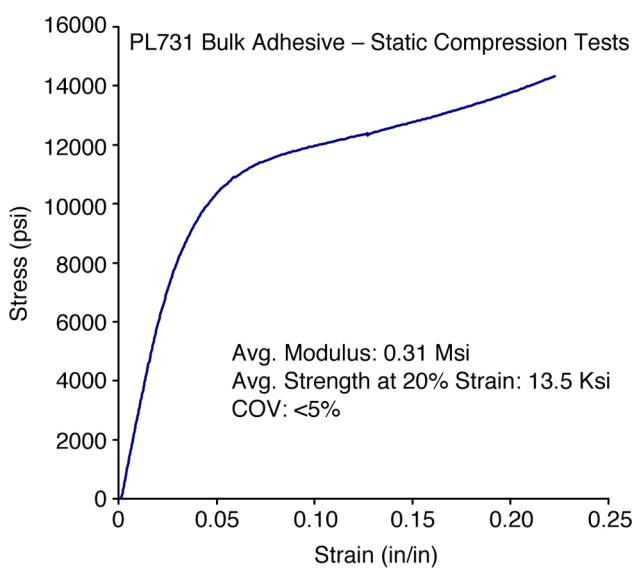

Figure 5. Adhesive compression test data.

Task 3: Build Unbonded and Bonded Subcomponents and Test Them Under Quasi-Static and Dynamic Loads

The tool for building square section tubes using the new plain-weave ACG MTM 49 carbon/epoxy material substrate system was fabricated. Both unbonded and bonded square tubes will be fabricated. The process of building the bonded tubes with two different overlap thicknesses and two types of bond lengths is currently being investigated.

Task 4: Develop Analytical Tools Incorporating Adhesive Elements, Material Models, and Progressive Damage Algorithms and Correlate Them With Coupon and Subcomponent Test Results

As part of the efforts on this task, the team

- initiated analysis of adhesive material test specimen using MAT 24 model in LS-DYNA,
- modeled a single-lap joint with nonlinear adhesive properties using true stress-strain curve derived from the uniaxial tension test data measured at ORNL, and
- partnered with Virginia Tech to develop material models and advanced computational techniques for predicting crash energy absorption of adhesively bonded automotive structures.

Performance of Novel Sandwich Composites

The objective of this project is to investigate the viability and crashworthiness of novel sandwich composite concepts for automotive applications

Topics such as wrinkling, face-sheet debonding, Poisson's effects and core-skin property mismatch, load rate effects, impact damage modes, and energy absorption were identified as part of the research effort. The research work being performed at the University of Utah is split into three phase-specific objectives:

Phase I: To evaluate candidate materials, concepts, and manufacturing methods for automotive sandwich composites. This two-round experimental evaluation of energy absorption, damage mechanisms, and mechanical properties will be used to identify the best-suited sandwich composite concepts for further investigation in the second phase.

Phase II: To develop an understanding of the structural response of selected sandwich composite concepts identified in Phase I. This investigation will focus on damage modes and energy absorption mechanisms during impact loading as well as static loading.

Phase III: To develop and validate FE based methodologies for predicting damage formation and energy absorption in candidate sandwich composite concepts identified in the first two phases of the program.

Phase I resulted in the mechanical evaluation of 13 sandwich facesheet/core combinations. These were subjected to three types of testing, for example, flat-wise tensile, three-point bending, and edgewise compression. The configurations tested include both thermoset and thermoplastic facesheets. Five candidate configurations will be chosen from these combinations, based on the criteria of mechanical performance, manufacturing ease, and cost. These configurations will be subjected to an additional round of testing that will include edgewise impact, flexural impact, interlaminar shear, and flexure creep tests.

Energy Absorption of Triaxial Braided Composite Tubes

The objective of the project is to develop a predictive tool for crush analysis of triaxial braided composite structures based on a smeared micromechanics model. A smeared micromechanics model developed under an earlier contract is being further explored to extend it to dynamic analysis. The project will answer questions pertaining to the basis of the mathematical representation of the energy absorbing mechanisms, unit cell size relative to FE size, stress concentration effects on load sustaining ability, objectiveness of damage evolution assumptions, and micromechanics application to shell FEs.

The smeared micromechanics unit cell model code has been rewritten to improve its computational efficiency. The smeared micromechanics model can currently be run in a fraction of the time that was necessary in the previous project.

The effect of stress-concentration on damage evolution has been studied using X-rays and die penetration in tension specimens with holes and in square tubes. The effect of stress concentration has been modeled through the fiber bundle theory to capture the delay in bulk damage progression exhibited by square tubes.

The scissoring behavior of composite fiber tows has been experimentally observed, and the extent of rotations in tows due to missing matrix has been modeled using the micromechanics based code. Work related to calculating the load-carrying ability of jammed tows is ongoing.

The micromechanics model has been used with shell elements in an attempt to investigate if large-scale application to automotive structures would be feasible at low computational costs. Initial attempts did not lead to encouraging results. The demands of micromechanics approaches on accurate 3-D stress calculations are high, making shell elements inefficient for the purpose.

The user subroutine developed for quasi-static analysis has been modified for dynamic analysis with the ABAQUS explicit FE code. This subroutine will be evaluated against dynamic tube crush test results during the final year of the contract.

Lateral Impact Study

The objective of the project is to achieve a fundamental understanding of the energy-absorbing mechanisms in triaxial braided composites subjected to lateral bending. A combined experimental and analytical

approach is planned for this purpose. The analytical study would use the smeared micro-mechanics material model developed in a previous ACC100 funded project, available as a user subroutine with ABAQUS. Based on the study of a simple test specimen, a specimen representative of an automotive component will be proposed. Because this is an initial investigation into energy absorption lateral bending of triaxial braided composites, the current project will be restricted to quasi-static loads.

The user subroutine for the smeared micromechanics model had been first checked for bugs by running circular tube problems on the user machine before it was implemented to composite strip lateral bending applications. Many issues relevant to the model usage and implementation, including scissoring effect, have been studied. Initial runs have been completed on a $[0_{80k}/\pm45_{12k}]$ triaxial carbon fiber braided composite strip subjected to off-axis compressive loading. Damage initiation and accumulation at the midlength of the strip have been observed with identification of many energy absorption modes including tow splitting—in-plane and out-of-plane, axial tow compression, matrix cracking, and interply delamination, which all contribute to some degree to material degradation/softening in the strip subject to lateral bending. The axially braided composite exhibits, as observed in the micromechanics model, a phenomenon that the material within the representative unit cell (RUC) can regain a prominent stiffness even after a peak load point. This would be caused by a dramatic change of stiffness distribution in the RUC as a certain scale of accumulated micromechanics damage zone has been reached. Experimental investigation into the composite strips for validating the model effectiveness is being carried out.

E. Energy Absorption in Adhesively Bonded Composites

Co-Principal Investigator; J. Michael Starbuck
Oak Ridge National Laboratory
P.O. Box 2008
Oak Ridge, TN 37831-8048
(865) 576-3633; fax: (865)-574-8257; e-mail: starbuckjm@ornl.gov

Co-Principal Investigator: Raymond G. Boeman
Oak Ridge National Laboratory
53-1/2 W. Huron St., Suite 213, Pontiac, MI 48342
(248) 452-0336; fax: (248) 452-8992; e-mail: boemanrg@ornl.gov

ACC Collaboration Contact: Naveen Rastogi
Visteon Corporation
6100 Mercury Drive, #SW61-025, Dearborn, MI 48126
(313) 755-6264; fax: (313) 755-4229; e-mail: nrastogi@visteon.com

Project Manager, Composites: C. David Warren
Oak Ridge National Laboratory
P.O. Box 2008, Oak Ridge, TN 37831-6065
(865) 574-9693; fax: (865) 576-4963; e-mail: warrencd@ornl.gov

Technology Area Development Manager: Joseph A. Carpenter
(202) 586-1022; fax: (202) 586-1600; e-mail: joseph.carpenter@ee.doe.gov
Field Technical Manager: Philip S. Sklad
(865) 574-5069; fax: (865) 576-4963; e-mail: skladps@ornl.gov

---

Contractor: Oak Ridge National Laboratory
Contract No.: DE-AC05-00OR22725

Objectives

- Develop a comprehensive experimental and analytical methodology to analyze and design adhesively bonded automotive composite structures to sustain axial, off-axis, and lateral crash/impact loads.
- Determine the rate sensitivity of bonded tubes to crush through experiments on the ORNL Test Machine for Automotive Crashworthiness (TMAC).
- Determine influence of critical joint design parameters, for example, bond length, bond thickness, and fillet, on specific energy absorption.
- Experimentally determine the full-field deformations at joint discontinuities for validation of analytical/numerical results.

Approach

- Coordinate with the bonded joint experimental and analytical efforts undertaken in ACC project Composite Crash Energy Management.
- Select a substrate, adhesive, and representative subcomponent joint geometry for evaluation.

- Characterize substrate material, adhesive material, and coupon level joints under static and dynamic loads.
- Build and test unbonded and bonded rail components under static and dynamic crush loads.
- Correlate experimental results with analytical results by developing finite-element-based tools with appropriate material models and progressive damage algorithms.
- Enhance the understanding of joint performance by conducting full-field deformation measurements using moiré interferometry.

Accomplishments

- Fabricated near void-free bulk adhesive panels and cylindrical rods for adhesive characterization studies.
- Fabricated tensile, compression, compact tension (fracture toughness), and shear specimens.
- Characterized tensile and compressive response and fracture toughness of bulk adhesive at quasi-static load rates.

Future Direction

- Design and fabricate required test fixtures for conducting dynamic tests on TMAC.
- Complete static and dynamic testing of substrate, bulk adhesive, and coupon level joints.
- Install and set-up moiré interferometric test equipment for characterizing full-field deformation patterns in adhesive joints.

Introduction

The objective of this project is to develop a comprehensive experimental and analytical methodology to analyze and design adhesively bonded automotive composite structures to sustain axial, off-axis, and lateral crash loads. This direct-funded project will be closely aligned with the experimental and analytical efforts undertaken in ACC 100 (7D) for composite substrates. The focus of this work, however, will be restricted to the adhesive joint related issues. The key to the methodology development is the understanding of how critical joint design parameters, for example, bond length, bond thickness, and fillet, affect the energy absorption. Recent investigations at ORNL have provided valuable insight toward the understanding of composite joint performance and composite crashworthiness. The next logical step is determining the correlation between measurable adhesive joint parameters and their influence on the structure to dissipate energy and ultimately predict crashworthiness for a particular composite design.

Experimental tasks include material testing under quasi-static and dynamic loads for substrates, adhesives, and joints; full-field deformation mapping of joints with moiré interferometry for correlation with computational results; strain-rate sensitivity studies; fracture toughness testing; and test method development as required. These experimental results will provide the building blocks for model developments—first at the coupon level, then progressing in complexity to component level. Correlation with experimental results will provide the basis for which the analytical developments including development of constitutive laws, materials models, damage algorithms, and new finite elements will be made. Structural tests will be conducted on the new intermediate-rate test machine (TMAC) at ORNL (7.C).

Project Deliverables

At the end of this multiyear program, joint parameters that have significant influence on energy dissipation will be identified, and their influence quantified, using appropriate analytical models and experimentation. In collaboration with the ACC Composite Crash Energy Management project, a predictive capability for joint performance will be demonstrated, and the validity of the prediction will be assessed through structural crash testing.

Approach and Results

The technical approach involves both experimental and analytical tasks. There are four main tasks:

- Task 1—Materials Selection and Screening,
- Task 2—Material Characterization,
- Task 3—Component Testing, and
- Task 4—Computational Tools Development.

Task 1 was completed and reported on in the FY 2002 annual report. The selected chopped carbon fiber prepreg material system was characterized from flat plaques provided by the vendor. Discussions with the vendor lead to an overly optimistic view of the suitability of the material for this project. Additionally, delays in receipt of the material from the supplier resulted in consideration of a carbon fiber sheet molding component (SMC). Both materials are unsatisfactory due to processing difficultly and material variability. As a result of the variability in the initial material screening tests and difficulty in fabricating tubes with this material, the substrate material was changed to a carbon fiber braided system. The woven fabric prepreg is comprised of T300B carbon fiber with a tow size of 3K and 42% (by weight) epoxy resin.

Task 2 was initiated during FY 2002 and was originally scheduled to be completed in the third quarter of FY 2003. The schedule has been adversely impacted by several factors, including delays in substrate material acquisition due to supplier manufacturing constraints and then actually changing the substrate (discussed above), laboratory-initiated relocation of test facilities from Y-12 National Nuclear Security Complex to ORNL, operation constraints on TMAC pending pressure vessel certification, and budget constraints. A new schedule is being prepared that takes into account the impact of all these factors.

The substrate will be fully characterized by conducting tension, compression, and in-plane shear tests. The degree of anisotropy in the material will be qualified by testing specimens that are machined from two different orthogonal directions in the panels. This work will be contracted out to an independent testing laboratory by the ACC.

The adhesive used in this study is an epoxy paste designated as Sovriegn PL731 and is used in many of the research projects within the ACC. The bulk adhesive testing consists of tension, compression, shear, and fracture toughness. In addition, DSC/DMA tests will be conducted to verify the degree of cure. The key to this task is the successful fabrication of high-quality specimens (e.g., low void content) to accurately quantify the bulk adhesive mechanical properties. The compression and shear testing will be accomplished using cylindrical rod specimen geometries. Cylindrical rod specimens were fabricated using centrifugation and glass test tubes as molds. Initial difficulties in producing flat plaques were alleviated by developing a mold-filling process that uses an adequate supply of excess adhesive under pressure to back fill the mold cavity. High-quality specimens for all bulk adhesive tests were fabricated with these two approaches.

Characterization of the tensile and compressive responses is complete and indicates excellent consistency from specimen to specimen and from plaque to plaque. Tensile results for 18 samples from two different plaques indicate average ultimate strength and modulus for the adhesive is 7.3 ksi and 0.31 Msi, respectively. Coefficients of

variability (COVs) for the strength and modulus results are 4.8% and 1.6%, respectively, which is excellent. A typical tensile stress strain curve for this adhesive is shown in Figure 1.

Eight cylindrical samples—1 in. long, 0.5-in. diameter—were subjected to compressive loads (ASTM D695) up to strains of 22% without global failure. Compressive modulus for the adhesive, taken from a range of 1% to 2% strain, is 0.31 Msi, identical to the tensile value. The COV is 1.6%, consistent with the tensile results. Figure 2 depicts representative

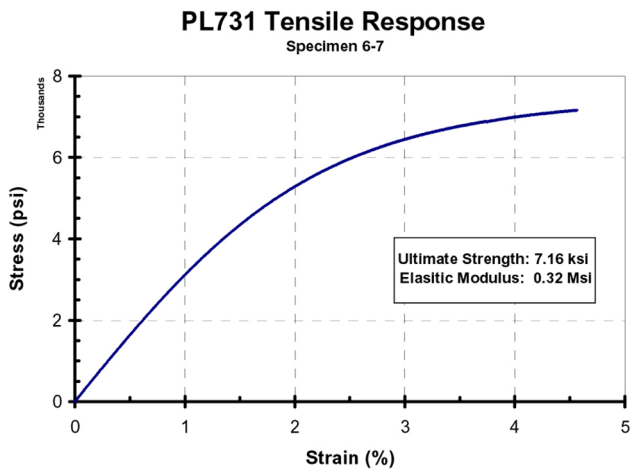

Figure 1. Typical tensile stress-strain curve for the bulk adhesive.

Figure 2. Typical posttest condition of compression samples, indicating plastic deformation and local cracking associated with large strains.

"failed" test samples that indicated plastic deformation with small local cracks being present in some samples. Figure 3 illustrates the consistency of the compressive response out to more than 20% strain.

Preliminary quasi-static and low-speed dynamic fracture toughness tests were completed using the compact tension specimen geometry. The specimens were machined from an 8-mm-thick bulk adhesive plaque per the geometry specified in ASTM D5045. The technique developed for making near void-free 3-mm-thick plaques was also used for making these plaques. The tests were conducted on a conventional closed-loop servo-hydraulic machine at rates of 0.02, 2.5, 25, and 1000 mm/s with three specimens tested at each rate. An untested and a tested specimen are shown in Figure 4, and a typical load-displacement curve for the quasi-static tests is shown in Figure 5. The apparent fracture toughness of the bulk adhesive was estimated using the maximum load, and the average results at each load rate are plotted in Figure 6. There appears to be an initial drop in the fracture toughness as a function of load rate but the initial quasi-static value appears to be much greater than typical values for epoxy systems. Consequently, the experimental data and test methodology are being evaluated for their validity.

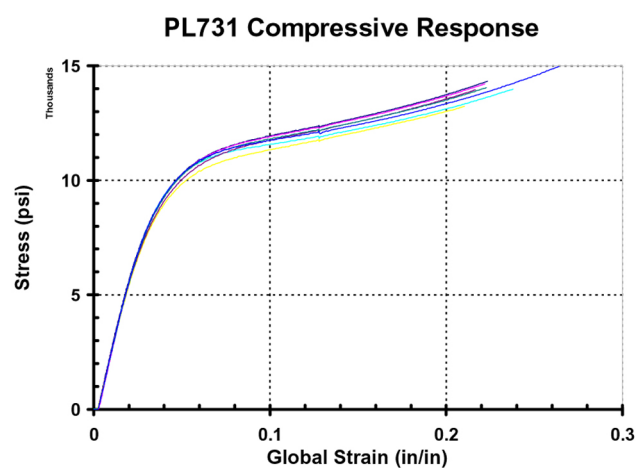

Figure 3. Combined compressive stress-strain curves for the bulk adhesive (eight samples).

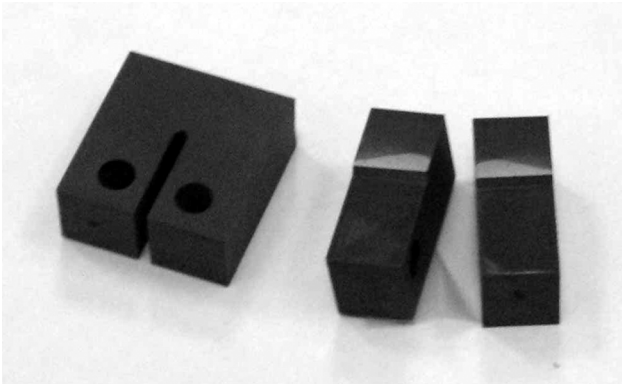

Figure 4. An untested and a tested bulk adhesive compact tension specimen.

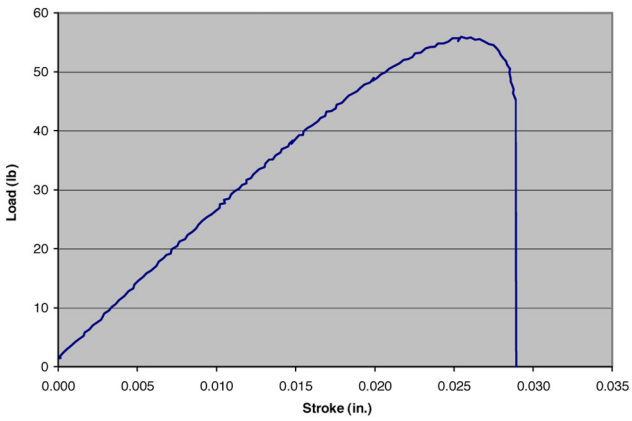

Figure 5. Load-displacement data from quasi-static compact tension test on bulk adhesive.

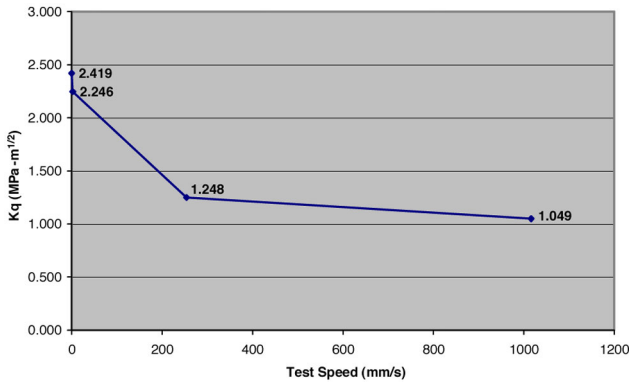

Figure 6. Apparent bulk adhesive fracture toughness as a function of testing rate.

Coupon-level joint configurations will consist of double-notch shear (DNS) and single-lap shear (SLS) test specimen geometries. Joint parameters that will be investigated are the adhesive thickness, overlap length, and fillet geometry. Moire interferometry will be used to study the full-field deformation pattern in the bond-line during static testing of the SLS joint specimens. The crack growth characteristics of an adhesive joint will be quantified by conducting Mode I, Mode II, and Mixed Mode fracture tests using double cantilever beam (DCB), end-notch flexure (ENF), and mixed-mode bending (MMB) specimen geometries, respectively.

Component testing in Task 3 was scheduled to commence in the last half of FY 2003 but will likely be delayed due to the issues stated above. Component testing will consist of unbonded and adhesively bonded upper rail sections. The testing will include static and dynamic crush loads, and axial and lateral impact loads. The TMAC at ORNL and test sleds will be used for the dynamic testing. The unbonded tests are to establish a baseline, and then the results from Task 2 will guide the joint design such that bonded sections will be built to either fail or not fail in the joint. Some of these tests will be repeated using scaled geometries to get an initial look at scale effects.

In Task 4, the computational tools development will consist of analyzing the test geometries at both the coupon level and component level, developing new material models, and developing new test methods to support the model development. This task is conducted in parallel with Tasks 2 and 3. The coupon and component level analyses will be completed using existing material models that are available in FEA tools such as ABAQUS and LS-DYNA. The bond-line deformations predicted by the analyses will be compared with the Moire experimental results. Also, the effects of bond-line thickness and length, fillet, and loading rate on the stress distribution in the joint will be correlated with the experimental results. The model development effort will consider new constitutive laws, progressive damage algorithms, new finite elements for modeling the adhesive layer, and new computationally

efficient techniques. In support of this effort, new test methods will be developed for characterizing strain-rate effects and dynamic fracture

Summary

Highlights of the progress during this reporting period follow:

1. Manufactured all bulk adhesive samples for tension, compression, shear, and fracture tests.
2. Completed bulk adhesive tensile and compression tests. Results indicate excellent consistency. Data have been supplied to the ACC partners for implementation in the FEA.
3. Completed preliminary fracture toughness tests on bulk adhesive, and the results are being reviewed by the project team for their validity.
4. The chopped carbon fiber substrate material was replaced with a carbon fiber braided material as a result of excessive variability in the chopped fiber material data and inability to fabricate high-quality tubular specimens.

F. Long-Life Electrodes for Resistance Spot Welding of Aluminum Sheet Alloys and Coated High-Strength Steel Sheet

Project Manager: Eric Pakalnins
DaimlerChrysler Corporation
Body Materials Engineering
800 Chrysler Dr.
CIMS 482-00-11
Auburn Hills, MI 48326-2757
(248) 576-7454; fax: (248) 576-7490; e-mail: ep18@daimlerchrysler.com

Project Administrator: Warren Peterson
Edison Welding Institute
1250 Arthur E. Adams Drive
Columbus, OH 43221-3585
(614) 688-5261; fax: (614) 688-5001; e-mail: warren_peterson@ewi.org

Technology Area Development Manager: Joseph Carpenter
(202) 586-1022; fax: (202) 586-1600; e-mail: joseph.carpenter@ee.doe.gov
Field Technical Manager: Philip S. Sklad
(865) 574-5069; fax: (865) 576-4963; e-mail: skladps@ornl.gov

---

Contractor: U.S. Automotive Materials Partnership
Contract No.: DE-FC05-02OR22910

Objectives

- Survey the currently available technology for achieving long electrode life.
- Comparatively test a broad selection of existing and developmental electrode technologies that have technical merit.
- Investigate the electrode wear process through a combination of testing, metallography, and computer modeling.
- Evaluate a "best practice" electrode(s) through beta-site automotive production testing.

Approach

- Conduct benchmarking (Phase 1). The open literature and available corporate literature will be reviewed along with interviews of industry experts in an effort to produce a state-of-the-art report on electrode wear. This phase has been completed.
- Conduct testing (Phase 2). This involves screening of candidate electrode technologies, in-depth testing of electrodes, and beta testing of selected electrode technologies in a production environment.
- Conduct computer modeling (Phase 3) of the electrode metallurgical and mechanical changes that occur as a result of electrode wear. The models will be used to define the mechanism(s) of electrode wear.

Accomplishments

- Completed screening of standard electrode compositions and designs. The influence of electrode geometry was determined from this work.
- Examined the metallographic changes that occur after completion of electrode life.
- Evaluated five developmental electrode material compositions (using a standard electrode design). Two materials were selected for a detailed sequential electrode wear examination.
- Continued metallographic investigation of the wear process through a sequential examination of electrode wear for three electrodes using two standard electrode geometries.
- Continued to develop and improve computer models to predict electrode life. This includes wear due to both electrode deformation and chemical attack.
- Continued initial beta site test planning.

Future Direction

- Complete sequential life testing.
- Integrate results with computer modeling to produce an electrode for beta site testing.
- Complete planning and execution of beta site test(s).
- Complete final report on project.

Introduction

Resistance spot welding (RSW) has been heavily adopted by the automotive industry due to its relatively low capital and operating costs and its potential for high production rates. However, electrode wear of coated steels and aluminum has been a continuing and significant problem. Electrode wear adversely affects the cost and productivity of automotive assembly welding because it reduces weld quality reliability and robustness. This requires additional inspection and mandates more strict control of the welding parameters. Electrode life potentially becomes especially problematic for high-strength steels. Ultimately, worn electrodes result in deteriorated weld performance. Consequently, large potential cost savings and quality improvements are expected from substantial improvements in electrode life.

As technology has developed during years of use, few engineering solutions have been successfully introduced into the manufacturing process to manage the issues caused by electrode wear. Weld current steppers and electrode cap dressers have been used for many years to address electrode wear, but these techniques do not resolve the underlying causes of electrode degradation. More recent efforts to remedy electrode wear have resulted in innovative electrode technologies, such as new material compositions, material inserts at the electrode face, surface-coated electrodes, and nontraditional electrode geometries (P-, G-, and S-nose). The objective evaluation of existing and developmental electrode material and geometry technologies is one of the aims of AMD project 302.

The AMD 302 project team is composed of representatives of General Motors, Ford, and DaimlerChrysler, as well as electrode manufacturers, an automotive supplier, a steel company, and researchers from Oak Ridge National Laboratory (ORNL), University of Windsor, and Edison Welding Institute (EWI).

A flowchart of activities included in AMD 302 is given in Appendix A. The activities in

Phase I and the electrode screening in Phase II have been completed. Sequential life testing and beta site testing of Phase II are under way. The computer models in Phase III are nearly ready to accept data from the sequential life testing and screening results. Each activity will be reviewed as follows.

Initial Electrode Screening Tests on HDG Steel

The initial screening tests for seven 6.4-mm face diameter, RWMA 5 electrodes using 1.1-mm, 350-MPa hot dip galvanized (HDG) steel have been completed. These tests include AWS D8.9-97, a single-current electrode life test, and GM WS5A, Part 3, a stepper electrode life test. The electrodes were largely composed of standard or commercially available electrode materials, namely:

- CuZr, 45° E-cap
- Al_2O_3 (Al60) dispersion strengthened copper (DSC), 45° E-cap and P-nose
- TiC coated CuCrZr, 30° E-cap
- DSC core, CuZr body composite electrode, 45° E-cap
- CuCd (with internal cooling fins), 45° E-nose electrode
- W insert brazed to CuZr, 45° E-nose electrode

These electrodes were tested in E-nose geometry with the DSC material also tested in P-nose geometry as shown in Appendix B. The CuCd was a full-length electrode. All of the E-cap electrodes had a 45° taper except for the 30° TiC coated electrode. Screening of developmental electrode materials was accomplished using a standard E-nose and B-nose geometry.

The initial screening tests were performed using both test procedures; however, the screening of the developmental electrodes was done using AWS D8.9-97. Depending on performance, the developmental electrodes were further tested using a B-nose design; and, both E-cap and B-cap electrodes were sequential life tested, followed by testing using the GM stepper test.

Single-Current Electrode Life Tests on HDG Steel

As provided in the last annual report, the results from the initial electrode life tests using AWS D8.9-97 are shown in Figure 1. The electrode life for DSC material in a P-nose electrode produced 5800 welds before

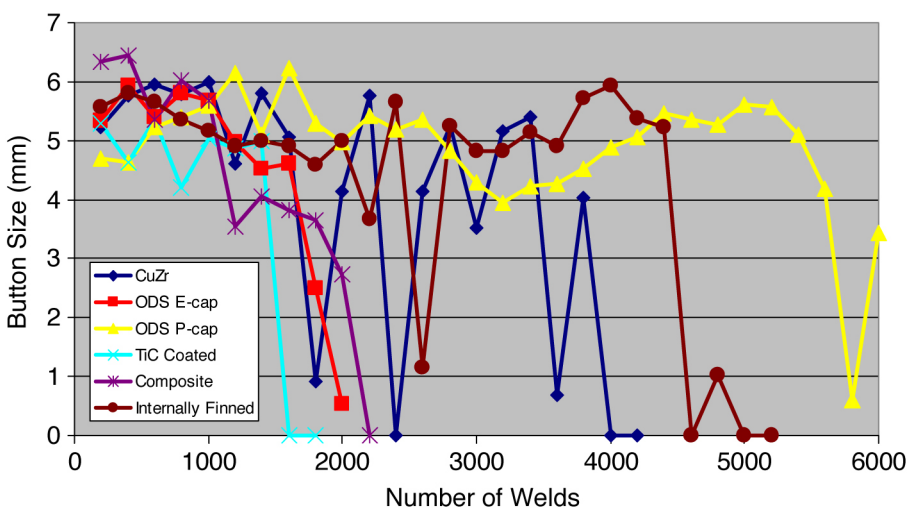

Figure 1. Summary of single-current electrode life (AWS D8.9-97) data for several electrodes on 1.1-mm 70/70 HDG 350-MPa high-strength steel. All of the electrodes were 45° E-cap designs, except the P-cap and the 30° TiC-coated electrode.

failing the test specification requirements, while the E-nose electrode produced only 1800 welds. Electrode geometry appears to play an important role in improving electrode life for the DSC electrode material.

Internal electrode cooling was also effective in extending electrode life, producing 4600 welds before test termination.

The performance of the other electrode materials, with exception of the W faced electrodes, was comparable and provided between 1800–2200 welds of electrode life. The two DSC E-nose electrodes had very similar performance. The W faced electrode had excessive sticking to the galvanized coating that caused it to catastrophically fail during electrode conditioning. These results are not shown on the graph.

Stepper-Current Electrode Life Tests

The GM WS-5A test results are shown in Figure 2. Most of these electrodes were studied in the AWS D8.9-97 test series. Not all of these tests had been completed at the last reporting period. In this test, ideal stepper electrode life test performance was noted by both low-current stepper slope and predictable current step frequency. The test represents the current required to maintain an above minimum sized weld button.

Nearly all of the electrodes had similar performance in this test; however, the P-nose electrode and the 30° E-cap TiC-coated electrodes produced notable responses. The P-cap electrode had half of the stepper slope compared to the best of the other electrode materials. The TiC-coated electrode also performed well due to its lower slope and regular stepping current frequency. The other materials performed similarly in overall stepper slope, except for the W-faced electrodes, which encountered sticking problems similar to that experienced in single-current electrode life tests. The DSC composite electrode did not have a current step until 4000 welds.

Role of Current Density in Electrode Life Testing

Both the single-current and stepper-current electrode life test results had similar current density characteristics during life testing for welds that produced subminimum sized welds. The current densities from the single-current and stepper tests are shown in Figures 3 and 4, respectively.

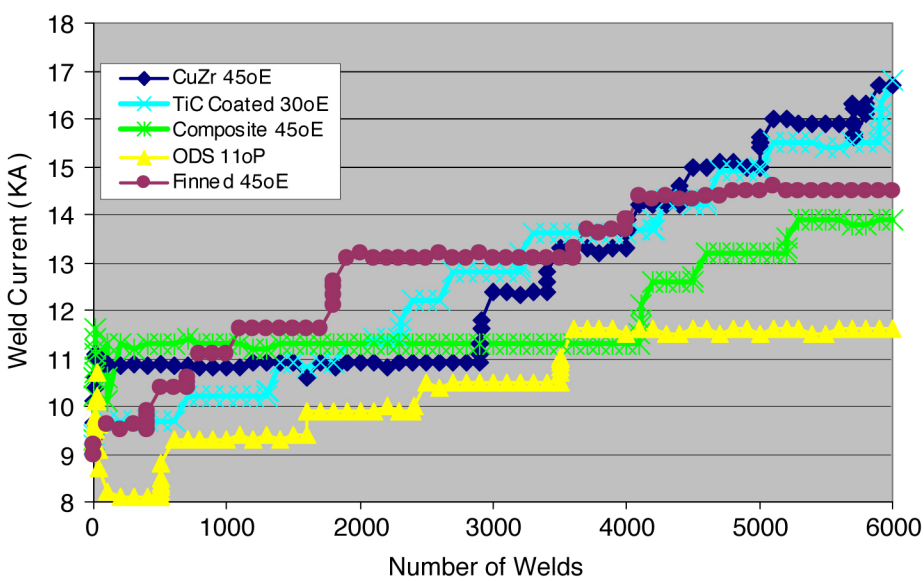

Figure 2. Summary of stepper-current electrode life (GM WS-5A Part 3) data for several electrodes on 1.1-mm 70/70 HDG 350-MPa high-strength steel.

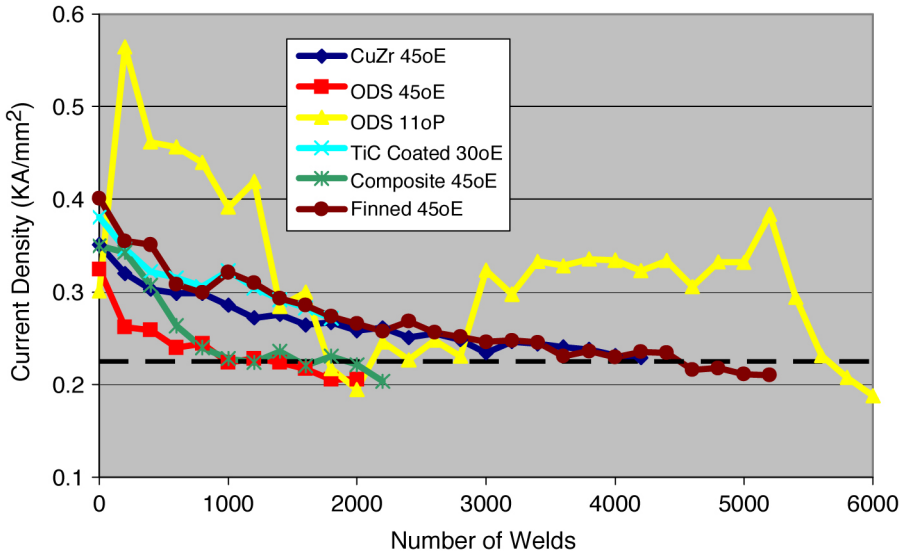

Figure 3. Summary of current density for single-current electrode life (AWS D8.9-97) data for several electrodes on 1.1-mm 70/70 HDG 350-MPa high-strength steel.

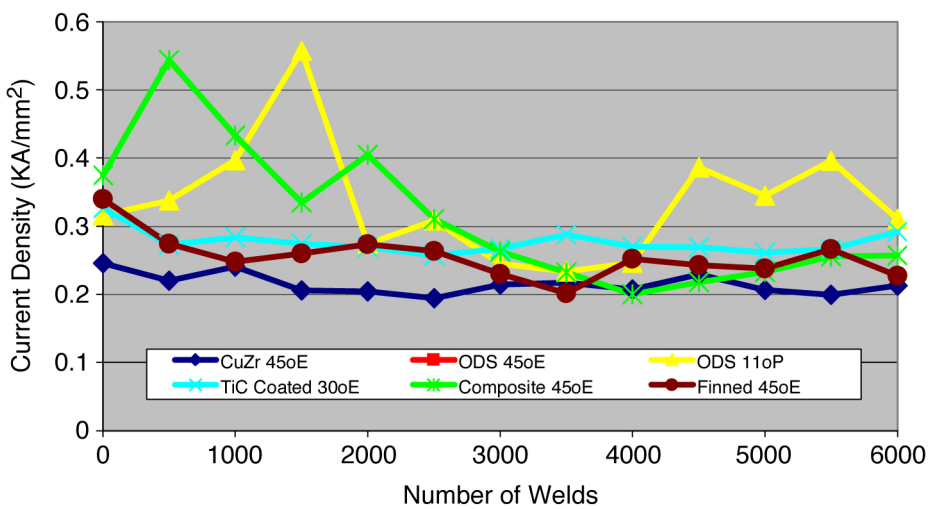

Figure 4. Summary of current density for stepper-current electrode life (GM WS 5A) data for several electrodes on 1.1-mm 70/70 HDG 350-MPa high-strength steel.

Both of these figures demonstrate that the minimum weld size occurred at a current density of approximately 0.225 KA/mm^2 for the HDG steel tested. Current density below this value tended to produce button failure in these two tests. This is a result of electrode face enlargement during testing.

Generally, the bottom electrode did not wear as fast as the top electrode and tended to control the current density needed to establish an above minimum sized weld nugget. The button size is of interest in the stepper test in conjunction with the current densities shown in Figure 4. These welds often exhibited very large button sizes while still producing minimum sized weld buttons. These large welds were shown to suddenly produce near no-weld conditions once the current density fell below the critical value.

Spot Weld Metallographic Evaluation

To better understand the rapid loss in weld button diameter in the GM stepper test, metallographic sections of spot welds made in HDG steel were made before and after the current step increases for the internally finned electrodes. This electrode provided the best demonstration of this effect. These cross sections are shown in Figure 5.

The nugget penetration is relatively stable prior to the production of a weld with subcritical current density. As the current density neared the critical level, the nugget penetration became shallower, changing from about 80% to 70% penetration. Additional wear failed to produce melting, causing the nugget to disappear in some conditions. Weld nugget penetration was reestablished after subsequently stepping the current level to a weld current set at 500 A above that required to produce a minimum weld size.

Metallographic Evaluation of Electrodes Tested on HDG Steel

Each of the electrodes tested were metallographically examined after completion of the AWS and GM tests. A summary of the electrode hardness profile through the centerline of the electrode for the AWS test is given in Figure 6. This plot show that the oxygen-dispersion-strengthened (ODS) materials retained their hardness up to electrode face while the non-ODS materials were substantially softened by the repeated welding operations.

Three optically distinct alloy phases were present at the electrode face. These were noted as a soft inner yellow layer composed of beta brass, a hard intermediate white layer composed of delta brass, and a dark outer layer with a variable composition and hardness. The relative thickness of these layers are shown in Figures 7 and 8 for the AWS and GM stepper tests, respectively. These figures show that the higher heat input from

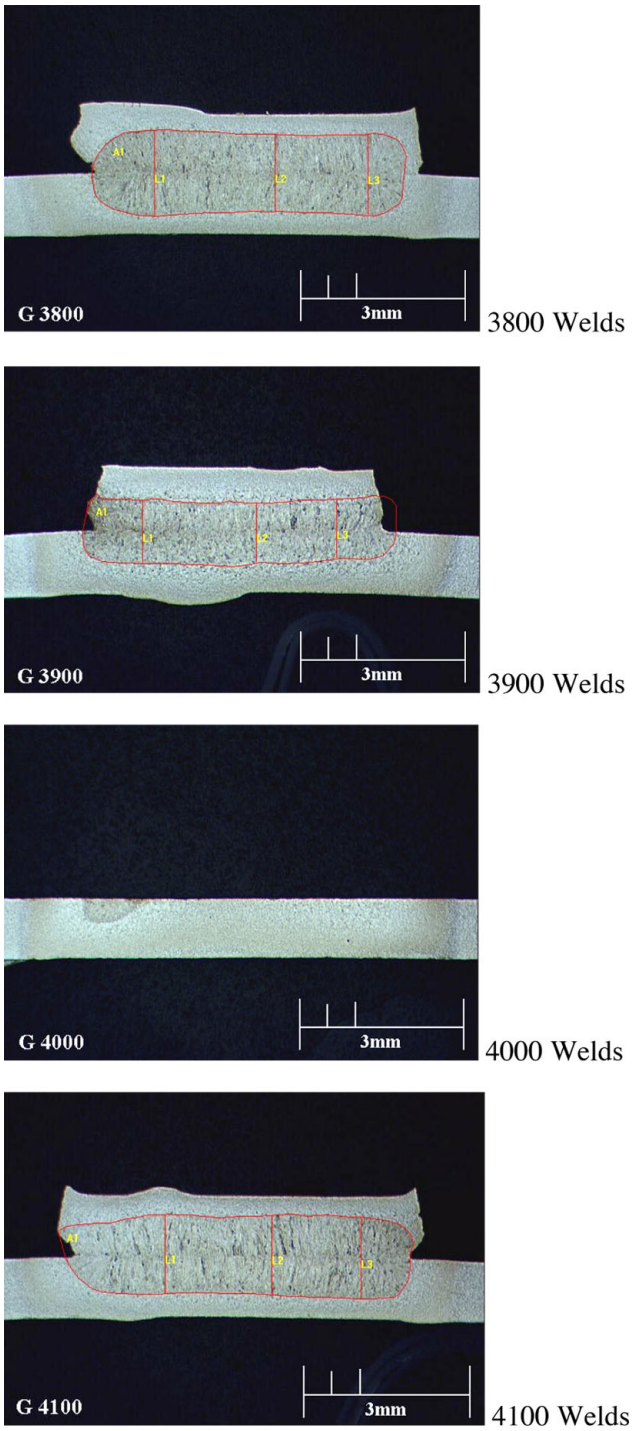

Figure 5. Weld button cross sections from welds 3800, 3900, 4000, and 4100 from stepper test (GM WS 5A) with internally finned electrodes on 1.1-mm 70/70 HDG 350-MPa high-strength steel. Nugget penetration decreases before button failure.

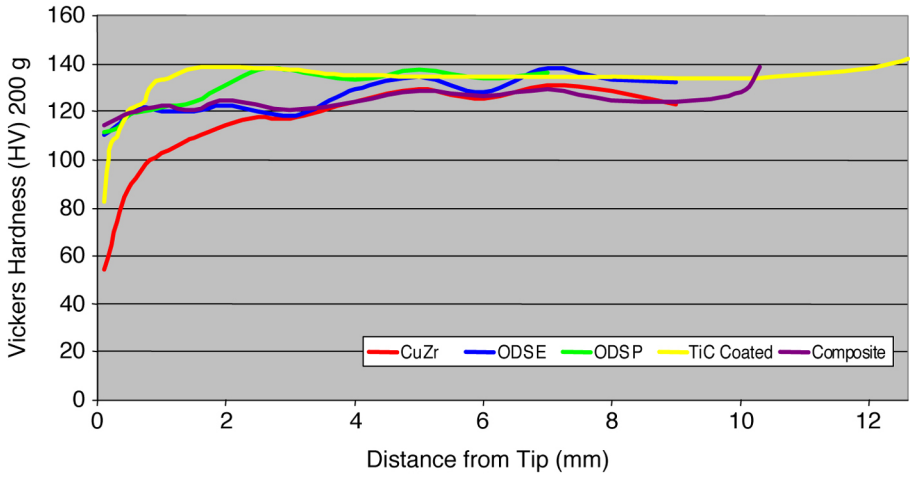

Figure 6. Summary of hardness profile at the centerline of the electrode for several electrodes after the AWS D8.9-97 test on 1.1-mm 70/70 HDG 350-MPa high-strength steel.

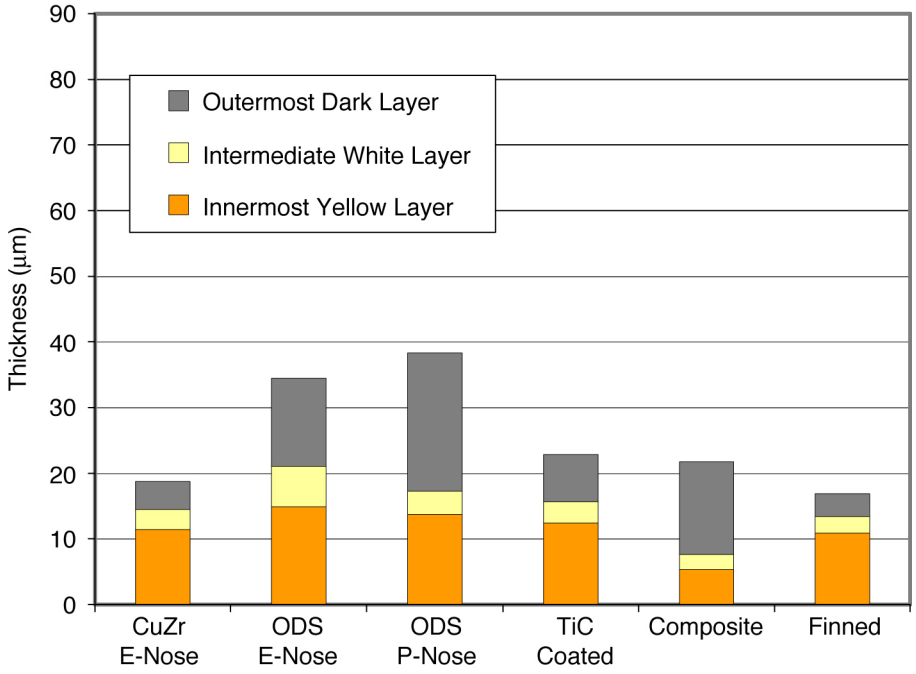

Figure 7. Alloy layer thickness at the electrode surface after AWS D8.9-97 testing 1.1-mm 70/70 HDG 350-MPa high-strength steel.

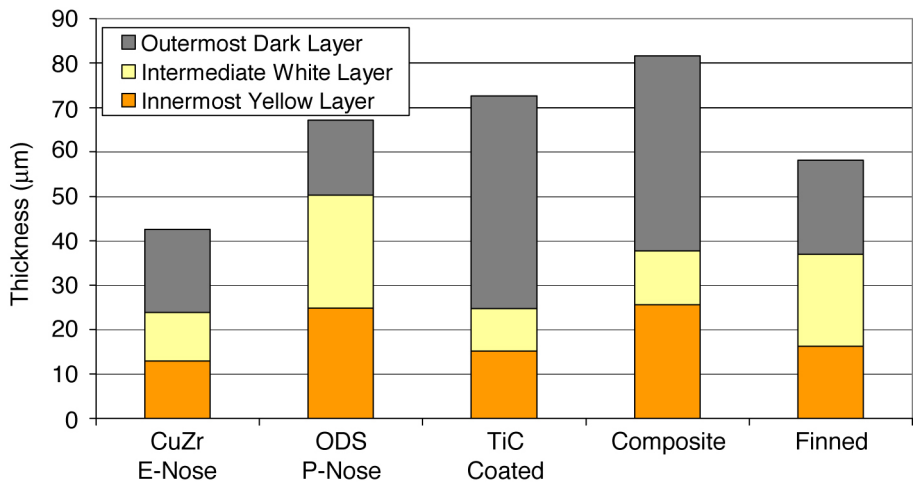

Figure 8. Alloy layer thickness at the electrode surface after GM WS 5A testing 1.1-mm 70/70 HDG 350-MPa high-strength steel.

the GM test increased the total alloy thickness and increased the thickness of the two layers near the electrode surface. The outer layer was found to fill pits and probably acted as a parting layer to the electrode surface.

Electrode Life Testing of Aluminum

The electrode life test performed on uncoated 1-mm Al5754 sheet used a modification of the Ford BA113 specification for assessing electrode wear in aluminum. The frequency of button size assessments were modified to peel test nearly every weld made in this program. Weld button size and quality were recorded. The electrodes for testing aluminum used a similar E-nose geometry as used in the HDG wear study. The electrode materials tested were

- CuZr
- CuCd (internally finned)
- C107 oxygen-free copper (OFC)

These electrodes were tested with a large pedestal welder. The mass of the ram in this machine is characterized by a slow electrode followup characteristic. A spring pack was alternately employed to isolate the mass and accelerate the electrode followup. This is needed to avoid excessive weld metal expulsion. Graphs of typical electrode life observed in this study are illustrated for the C107 electrode tested using both fast and slow electrode followup characteristics, as shown in Figures 9 and 10.

Electrodes on a slow followup welding machine generate more heat at the electrode-sheet interface resulting in excessive sticking. Ultimately, sticking was manifested by adherence of large chunks of aluminum from the sheet onto the electrode during electrode retraction. Additional welds with this adhered material would have produced massive expulsion, severely damaging the electrodes and putting a hole in the sheet. This event signals the end of electrode life without a fast followup head.

Besides the catastrophic sticking event observed for the welding machine configured with a slow followup characteristic, electrode life was largely governed by weld button quality and scatter in the button size results. The average weld button size did not decrease during electrode life as observed during testing HDG steel. Rather, the consistency of weld size from weld to weld became an issue, together with other weld quality indications.

The welds produced using slow electrode followup had less button size variability compared to welds produced with a fast followup head assembly. Conversely, the welds made using a fast followup head assembly

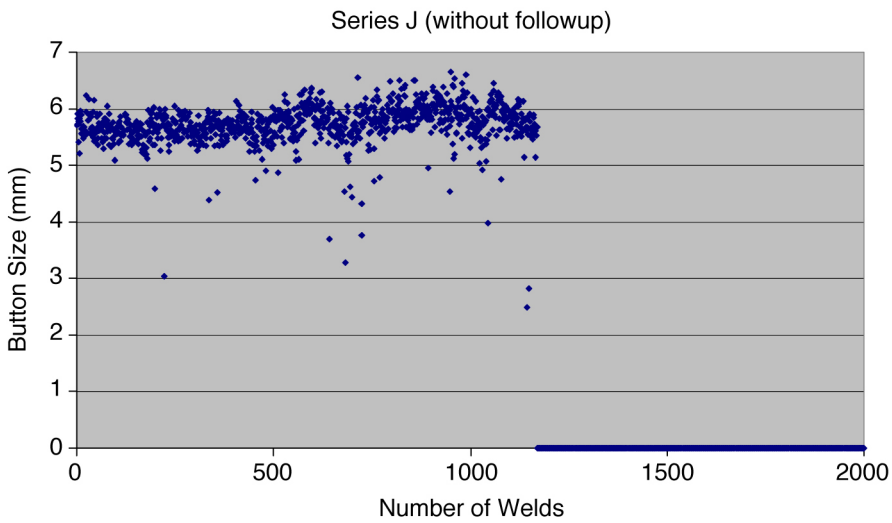

Figure 9. Summary of single-current electrode life (Ford BA 113) data without fast followup head on E-nose C107 electrodes on 1.0-mm Al 5754.

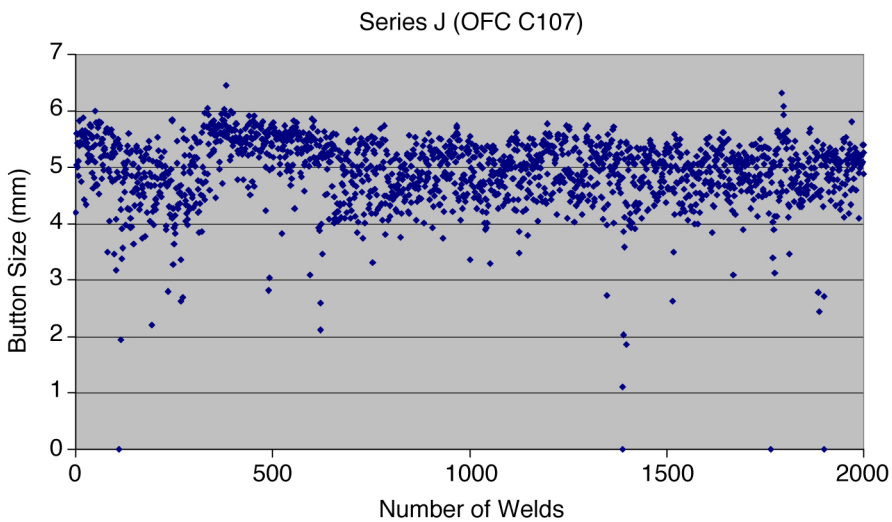

Figure 10. Summary of single-current electrode life (Ford BA 113) data with fast followup head on E-nose C107 electrodes on 1.0-mm Al 5754.

were much more likely to produce sudden losses in peel button size early in electrode life compared to welds made without a fast followup head. Overall, welds made with a fast followup head had greater variability in average weld size but were less likely to produce weld button failures and other button quality problems later in electrode life compared to welds made without a fast followup head.

A summary of weld quality indication rates for the electrode life tests in the aluminum is given in Figure 11. This plot shows the frequency of occurrences for undersized welds, partial interfacial and full interfacial fractures, cracks, holes on top surface of button, and porosity visible on button fracture face. As can be seen, all of the electrodes had different weld quality issues. However, the more conductive electrode materials

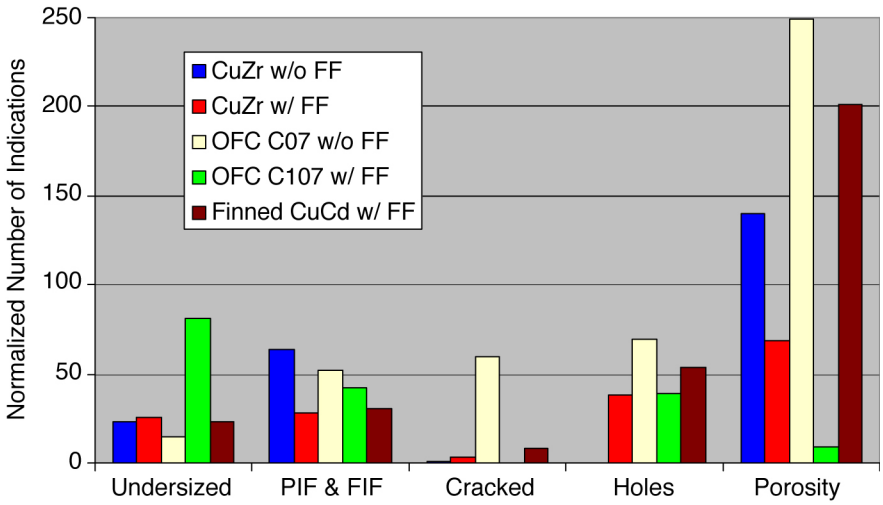

Figure 11. Summary of button quality problems for various electrodes during electrode life testing (Ford BA 113) on 1.0-mm Al 5754.

generally produced the least number of significant weld button quality problems.

The reason for this relates to the manner of electrode wear in aluminum. Much of the heat used to initiate and grow the weld nugget comes from the breakdown of the oxides at the electrode-sheet and sheet-sheet interfaces. Because of the high thermal conductivity of aluminum, heat generated at the electrode-sheet interface can be quickly diffused to the weld nugget. Welds made without a fast followup electrode system increase resistive heating at the electrode-sheet interface. This heat is diffused to increase and maintain a more consistent weld size. However, the large weld size also exaggerates the severity of expulsion of weld metal, which causes porosity. The location of nugget porosity is important to random nature of the sudden loss in weld button size, which is the result of fracture propagation across a weld nugget through adversely positioned porosity distributions.

Excessive heating of the weld nugget generally promotes the poor weld quality indications, as noted in Figure 11. Thus, the more conductive electrode materials appeared to produce better overall weld button quality results as a result of electrode wear. This is because greater conduction of heat from the electrode face results in less overheating the weld nugget and fewer severe weld metal expulsions.

No clear direction in electrode material composition was established for welding aluminum as a result of this testing because those factors that improved weld button stability also contributed to poorer weld quality. Additionally, the test results in aluminum appear to be machine specific.

Changes to the Program

As a result of the testing on aluminum, the AMD board chose to focus the remainder of the program on improving the performance of electrode materials for welding HDG steel. This effort will concentrate on E-nose and B-nose electrode geometries for testing developmental electrode materials. While the P-nose electrode geometry produced good results, the performance of electrode materials needed to be addressed separately. In addition, there was concern with implementation of P-caps in production. Normally, the P-nose electrodes have been used in conjunction with a B-nose electrode. It is thought that the B-nose electrode performance could govern the performance of the electrode pair.

Electrode Wear Computer Modeling

Computer models describing both electrode deformation and surface chemical attack are being developed at ORNL and are nearly complete. The deformation model is based on deformation of disks of material at the electrode face. These should be ready in time to accept the sequential life test results. Additionally, high-temperature electrode material properties are being developed at ORNL to support the modeling effort.

An analytical model is also being formulated at EWI. This will be based on previous work and will also describe the thermo-mechanical deformation aspect of electrode wear. Both models will support each other and strengthen the overall data interpretation effort.

Sequential Life Testing

A sequential study of the stages of the progression in electrode wear is under way for CuZr and two developmental electrodes selected from screening tests performed on developmental electrodes. Five developmental electrode materials using the E-cap design were screened using AWS D8.9-97. The results of these screening tests are shown in Figure 12. The M and R electrode materials were selected for further evaluation in the sequential life testing program. Additionally, these electrode materials were AWS D8.9-97 tested in a B-cap design. Furthermore, both E-cap and B-cap designs for these materials were GM stepper tested for comparison with previous screening results. A summary of the GM stepper test results are presented in Figure 13.

The sequential life testing phase involves the production and metallurgical evaluation of progressively longer electrode lives. The electrodes were removed at set intervals using standard life testing procedures. These electrodes are currently being metallurgically sectioned and examined to show the progression and stages of electrode wear. Chemical evolution of electrode surface will be tracked. Additionally, microstructural and phase changes will be tracked as a function of depth from the electrode face.

Electrode samples for the CuZr, M, and R electrode materials with both E-nose and B-nose electrode geometries have been produced. A plot of button size vs number of welds for the E-nose electrode is shown in Figure 14. The electrodes were removed after 25, 50, 100, 250, 500, 1000, and 2000 welds. The electrodes from the standard AWS D8.9-97 test were used as the end-of-life condition.

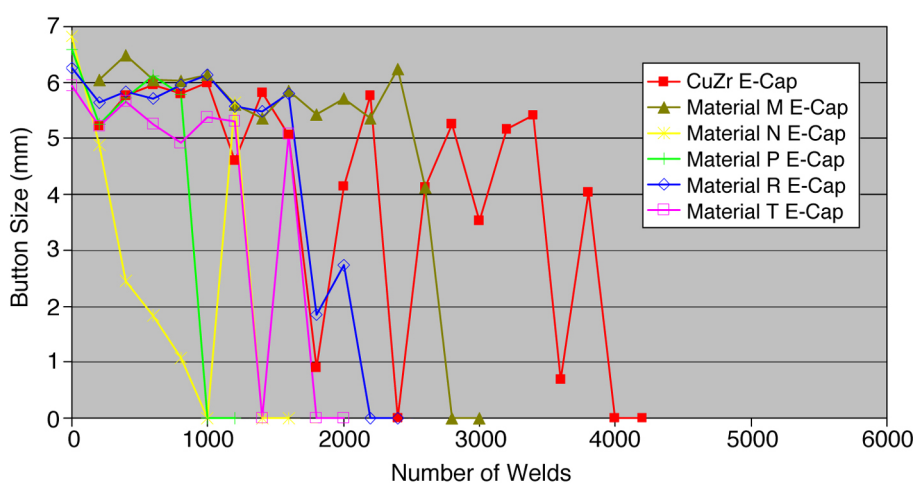

Figure 12. Summary of screening tests for CuZr and five developmental electrode compositions tested in 45° E-cap design using AWS D8.9-97 on 1.1-mm 350-MPa HDG steel.

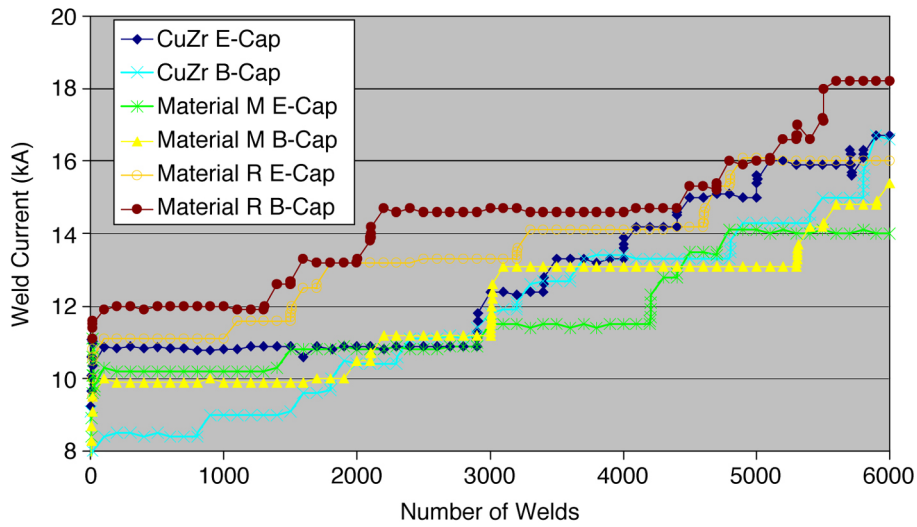

Figure 13. Summary of GM WS 5A Stepper Test results for CuZr, M, and R electrode materials in 45° E-cap and B-cap designs on 1.1-mm, 350-MPa HDG steel.

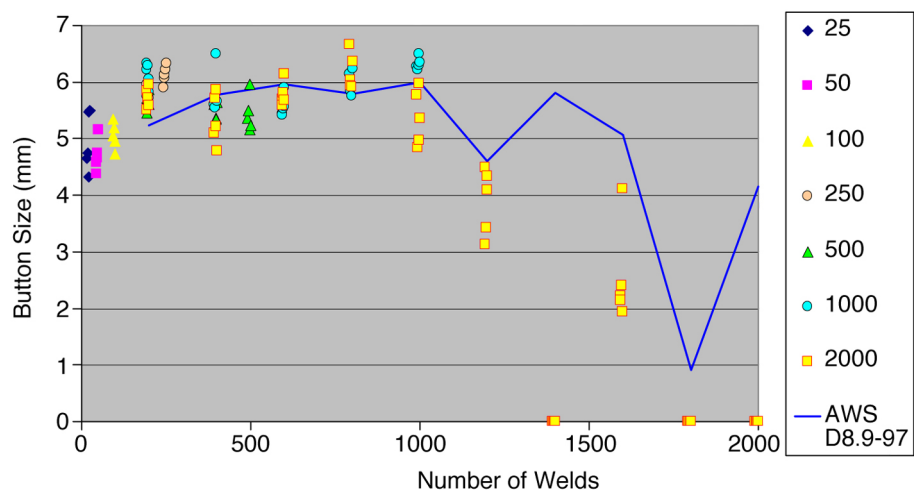

Figure 14. Button size measured during interrupted electrode life tests with CuZr electrodes on 1.1-mm, 350-MPa HDG steel (solid line indicates standard AWS D8.9-97 results).

The button size, welding parameters, electrode face diameter, and electrode C-imprint data from the screening and sequential life test data will be combined with the computer models to interpret and evaluate the surface and microstructural changes that describe electrode wear in electrode life for HDG steel. This information will be used to predict the "best practice" electrode material and electrode design to be evaluated during the beta site test(s).

Planning Beta Site Testing Activities

Possible beta site test locations have been identified at DaimlerChrysler and other automotive companies. These locations need to be further evaluated. Additionally, initial experimental plans have been sketched for the trials. These plans include standardized "optimization" procedures, the list of requested and required measurements and observations needed to analyze the results,

etc. These plans will be developed quickly in preparation as the beta site test phase of the program initiates.

The beta tests will occur after the sequential life testing has been completed and "optimized" electrodes have been produced for testing. Two sessions are expected. The first session will indicate deficiencies between laboratory and production conditions, and the second iteration is expected to demonstrate the electrode life improvements under production constraints. The data gathered during the first beta site evaluation will be coupled with the computer and analytical modeling to produce an updated electrode for evaluation during the second beta site test. The specification of the electrode geometry for these electrodes will need to be worked out in conjunction with the beta test site.

Future Work

Future work on this project should lead to a more effective, accurate, and efficient electrode development effort. New copper alloys, with targeted material properties, can be produced and evaluated using the predictive capabilities provided by the models developed during this program. The alloys thus developed should show deliberate improvement in electrode life.

Additionally, the computer models can be adapted to improve schedule development for stepper and electrode dressing techniques. This will further improve electrode performance, improve weld quality and productivity, as well as reduce setup costs in automotive production.

Appendix A

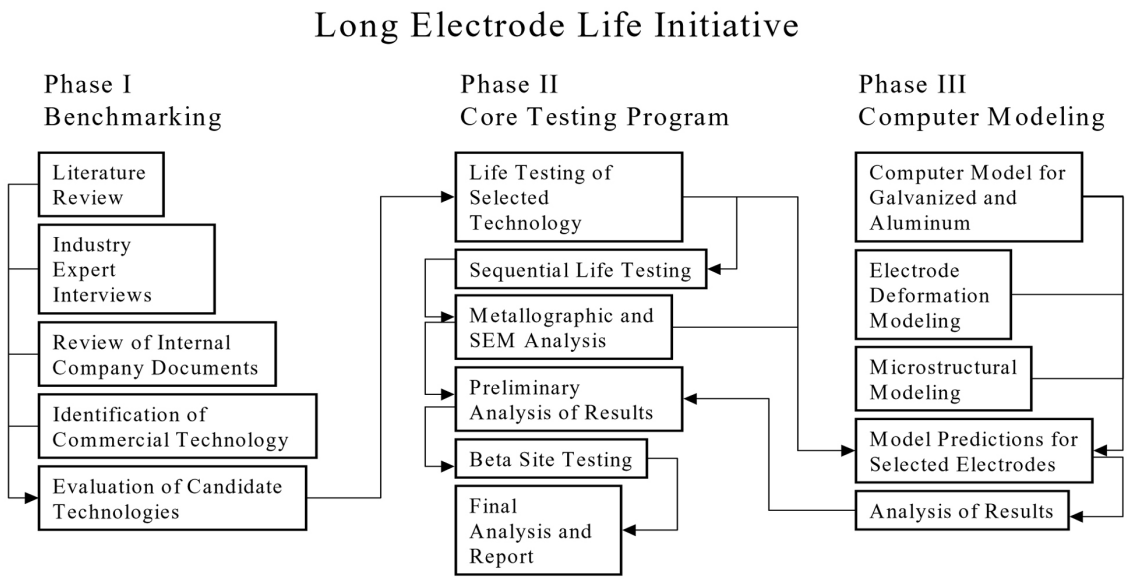

Appendix B

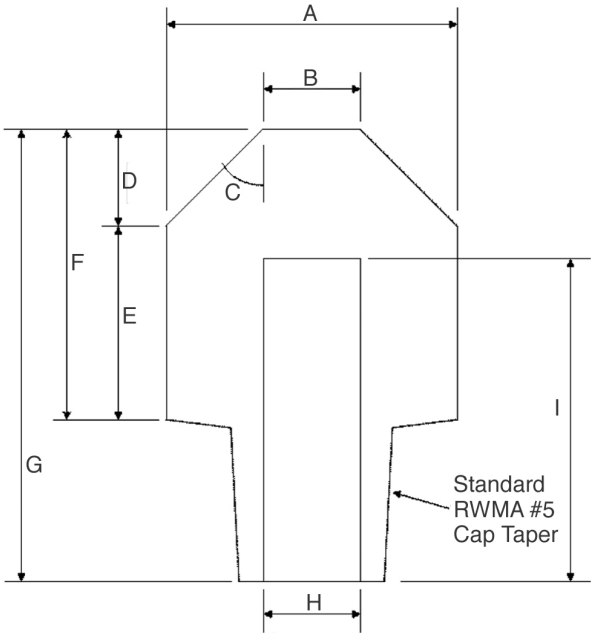

G. Plasma Arc Welding of Lightweight Materials

Project Manager: William Marttila
DaimlerChrysler Corporation
800 Chrysler Dr.
CIMS 482-00-11
Auburn Hills, MI 48326
(248) 576-7446; fax: (248) 576-7490; e-mail: wam8@daimlerchrysler.com

Technology Area Development Manager: Joseph Carpenter
(202) 586-1022; fax: (202) 586-1600; e-mail: joseph.carpenter@ee.doe.gov
Field Technical Manager: Phillip S. Sklad
(865) 574-5069; fax: (865) 576-4963; e-mail: skladps@ornl.gov

Contractor: U.S. Automotive Materials Partnership
Contract No.: DE-FC05-02OR22910

Objective

- Develop and verify the welding technology required for the joining of lightweight materials (aluminum and magnesium) using plasma arc spot welding technology.
- Develop the necessary weld parameters and techniques required for a robust joining process.
- Develop guidelines for testing mechanical properties of the new technology that are appropriate for the various anticipated applications.

Approach

This project is divided into three phases: testing, analysis, and summary.

- Produce approximately 5000 material coupons to be used for tensile, shear, and metallurgical analysis and testing (Phase 1).
- Modify the material alloys based on Phase 1 results (Phase 2).
- Produce guidelines for welding parameters and quality control (Phase 3).

Future Direction

- Verify the capabilities of the process in joining lightweight material sheet stock to tubular structures.
- Investigate alternative designs and materials used for the process consumables with a view to increasing service intervals beyond presently known levels.
- Devise and implement a software-based process operation strategy that optimizes the weld through adaptive control.

Introduction

The overall deliverable for this project is a robust process to join lightweight materials economically. Current technology relies heavily on conventional resistance spot welding. High maintenance, tip wear, and accessibility continue to be major concerns. Rivets and/or mechanical clinching are costly alternatives that require high capital investment. The viability of plasma arc spot welds has been validated through the efforts of Arc Kinetics, Ltd., which developed a single-sided plasma arc spot welding process for Jaguar. It was used for joining the sheet metal floor pan assembly, which was not accessible with conventional resistance spot welding equipment. Arc Kinetics also developed a process called aluminum plasma arc welding (APAW). By combining the two processes (single-sided spot welding and APAW), Arc Kinetics developed a process that demonstrates excellent potential for joining lightweight materials.

Material Selection

The team decided by consensus that the most suitable alloy and thickness combinations for potential use in the automotive industry were those in the following table.

Alloy	Thickness	to	Alloy	Thickness
6022	1 mm		6022	1 mm
6022	1 mm		5754	3 mm
5754	2 mm		5754	2 mm
6022	1 mm		5754	1 mm
5754	2 mm		6022	2 mm

Tooling

Shield cup development. As developed for Jaguar Cars, the shield cup of the plasma spot welding gun was manufactured from a work-hardening grade of cupro-nickel, which was then plated with electroless nickel. The interior surface of the shield cup was plasma sprayed with a titania/alumina coating to a thickness of 0.15–0.2 mm to prevent adherence of any weld spatter and minimize radiated heat absorption into the cup. The production life of the part averaged 850,000 welds, and the cups cost around $200 each.

It was found that the bursts of reverse polarity arc current used for welding aluminum were destructive to both the ceramic coating and the copper alloy used in the manufacture of the shield cup. On the basis of durability and cost, we decided to investigate the potential of using a cup machined from 6××× grade aluminum bar stock that could be hard-anodized to completely prevent electrical conduction. Early trials focused on a free-floating cup design (Figure 1), which was only partially successful:

- During rapid cycling of the weld gun, excessive heat buildup was apparent.
- Coating adherence to the cup in the region of the contact annulus was poor when it was subjected to the impact of the welding gun on the workpiece.
- Once the coating was compromised, breakdown was rapid. The plasma arc then impinged on the inside of the cup, entirely destroying the anodic coating and even causing the cup to stick to the workpiece.

Enlarging the bore of the shield cup to increase the weld pool and arc-to-cup distance increased durability significantly; however, once the annular clamp face became damaged by impact, micro-arcing followed by breakdown of the anodizing still occurred on a less dramatic scale. Further revision of the cup profile to give a radiused inner and outer edge to the annulus, together with a thickening of the anodic coating from 50 to 80 μm, produced a robust part (Figure 1). Alternative anodic coatings such as "keronite" were tested but were found to be less durable than sulfuric acid hard anodizing.

Tip design. The original Jaguar gun used a Thermal Dynamics PWM6A machine torch. Consumable changes involved replacing two O-rings during servicing of the water-cooled tip. Experience indicated a skills issue for this operation. To preclude recurrence of this

Figure 1. (Left to right): Small-diameter free-floating shield cup showing breakdown of anodic coating. Large-diameter fixed shield cup with impact damage on annulus and subsequent breakdown of coating. Final design showing radiused contact annulus that provides increased durability under impact.

issue, a dry change tip design was adopted; the plasma gun in this case was manufactured by PWP Industrial in the United Kingdom. The tips used with this gun had a flat front face of approximately 10-mm diameter into which the arc orifice was drilled. During the reverse polarity current cycles of the alternating current (ac) power source, a phenomenon known as "double-arcing" regularly occurred. A thin ceramic coating was applied to the front face of the tip to eliminate this condition; however, the coating rapidly cracked as a result of thermal expansion, and small pieces detached themselves from the tip. Experiments showed that radiusing the front face was the best method of preventing double arcing. The current-carrying capacity was somewhat reduced, but the reduction was insufficient to be problematic within the current range available from the power source (300-A rms).

Because it is not feasible to change the tip orifice diameter from weld to weld in a production environment, work focused on coping with all the sheet thickness combinations previously outlined with one size of tip. After considerable experimentation, good welds could be made throughout the range with a 4-mm-diam tip orifice.

Downsizing of weld gun assembly. The original spot weld gun, designed to effect good fit-up between steel panels, had a clamp force capacity of 200 kg (450 lb). The coaxially configured pneumatic ram assembly produced a relatively bulky package that was about 5 in. in diameter and 18 long. With a wire feeder incorporated, the assembly weighed approximately 22 kg (47 lb). Selection of the PWP torch with an offset pneumatic actuator reduced the bulk of the gun assembly considerably—the gun width was reduced to under 3 in. Trials conducted during this work indicated that much lower clamp forces were required for welding lightweight materials than for welding steel. The maximum clamping force found necessary was 30 kg (65 lb); therefore, the pneumatic cylinder required could be of 1-in. diameter or smaller. Thus, much potential exists for further downsizing the gun assembly, which presently weighs about 12 kg (25 lb).

Development of weld backups. During the early development of the AC-Thermospot process with Alcan, Arc Kinetics made important discoveries relating to the design of weld backups. At Jaguar, attention had focused on the single-sided access capabilities of the plasma arc spot welding process, provided the rigidity of the parts being welded could support the gun clamping forces. In the case of the XJ40 transmission tunnel, special supports had to be built into the tooling where such rigidity did not exist. It was noted at that time that additional scope for the process existed in the building of monocoque vehicles if a C-frame gun configuration were used. To produce weld coupons as in this program, some form of backup was obviously required. Much work was

undertaken to find a single configuration that can encompass all the thickness combinations investigated during the program. Concave designs in a variety of radii and diameters were tested, as described in the original patent; however, no one configuration suited all the thickness combinations. A perfectly flat-faced backup was tried, with encouraging results. Additional tests showed that configuring the backup with a gap between the lower sheet and the flat face of the backup of about 30–40 thousandths of an inch (0.75–1.0 mm) gives satisfactory results.

Torque tester for destructive evaluation of weld specimens. Weld porosity is one of the most significant issues common to welding lightweight materials using arc and laser welding techniques. Minimizing porosity is important in optimizing weld strength and dynamic performance. Although gross porosity can often be seen with the naked eye and is usually clearly evident in a weld subjected to tensile testing, reduced levels of macro- and micro-porosity are not easily identified through mechanical testing. Work with Alcan showed that subjecting the weld to pure torsional failure reveals porosity defects in a spot weld simply and cost-effectively. Subjecting a coupon to torsion testing immediately after welding provides useful data that speed the process of weld parameter optimization.

A simple torsional testing rig was designed and manufactured by which all the thickness combinations considered could be tested in a reasonably consistent manner; the use of an indicating torque wrench to apply torsional loading to failure allowed a strength value to be assigned to any given coupon, another useful indicator to assist with parameter optimization. This simple piece of equipment has been effective in revealing macro-porosity, outgassing, nugget size and shape, base material thinning, and the efficacy of various surface oxide removal/stabilization treatments.

Process

Software development. The software package and weld parameters enumerated in the standard Arc Kinetics aluminum weld process controller had been highly refined before this project began, partly as a result of collaboration with European auto manufacturers and suppliers. A puddle welding procedure for aluminum had been developed and implemented for a DaimlerChrysler product at Denso manufacturing in Battle Creek, Michigan. One important parameter added to the software package was preheat time—a short period immediately after the welding arc was established at its start-current level that aided initial removal of the surface oxide film, stabilizing the surface area of the weld before the rapid increase in arc current and heat input. Consistency of weld pool formation, particularly as filler wire was introduced into the weld puddle, was improved considerably. Preheat times in the region of 200 ms were found to be effective, adding little to the cycle time required per weld.

Filler metal selection. The logical first choice for filler wire composition when joining 6xxx, 5xxx, and combinations thereof was 4043 grade (5% silicon alloy). In cases where the formation of magnesium silicide would be a concern (possibly when welding 5754 to itself), an alternative composition of 5554 grade (5% magnesium alloy) may offer an advantage. For ease for feedability, a 1.2-mm diameter was selected for the two wires. X-ray and photomicrographical analyses indicated that certain combinations evaluated might suffer from slight but persistent solidification cracking toward the center of each spot weld. Consultation with program partner AlcoTec suggested a filler wire with a broader freezing temperature range might help eliminate the problem. AlcoTec supplied 4047 (12 % silicon alloy), which did help control solidification cracking.

Cleaning. We anticipated that joining lightweight materials to form a vehicle structure would always involve a variety of joining processes [e.g., riveting and bonding, metal inert gas (MIG) welding, laser-MIG hybrid welding, toggle-locking, bolting]. An enabler for some of these processes is surface conditioning via chemical cleaning to ensure stability of the surface film. Initial studies with Alcan had shown that welding of material coated with ALO70 wax-based press lube (generally applied to 5754 material for pressing purposes) or Hannifin MP404 oil-based press lube (applied to 6111/6022 material during pressing) could be hazardous because those compounds produce toxic vapors. In this project, all weld coupons were degreased/cleaned with acetone before welding. Additional mechanical and chemical conditioning processes undertaken are discussed in the test results.

Results

Background

Collaboration between Arc Kinetics and Alcan prior to this project had yielded encouraging results for the potential of plasma arc spot welding of lightweight materials. Tensile testing done at an Alcan laboratory in England for a variety of material combinations indicated average tensile strengths to be 20 to 50% higher than the strengths specified in military standard specifications. Microsectional analysis indicated that porosity levels within the spot welds were in the range of 1–5%. Gross porosity was not evident in any sample sections. International standards for allowable porosity levels vary; they generally are stated in terms of pores per linear inch of weld rather than for individual spot weldments. Alcan's technical advisors thought, however, that if porosity consists of randomly distributed spherical voids, levels of up to 20% porosity would have little effect on overall structural behavior.

Fatigue testing was limited because of limited test equipment availability; however, performance results were encouraging compared with those for resistance spot welds in identical material and thickness combinations. The good performance was attributed to the relatively large diameter of weld nuggets attainable compared with resistance spot welding.

Test Results

Using the example of the Jaguar XJ8 aluminum monocoque as a structure that could potentially use plasma arc spot welding, weld trials initially focused heavily on joining 5754 material. The greatest number of welds would be made in this material, because it forms the entire underbody and main structure of the vehicle. This section briefly outlines some of the issues encountered during the production of test coupons in this material.

Solidification cracking

Early test results from the United Kingdom on welding 5754 base material with a 5554 filler wire did not identify solidification cracking as an issue, but work conducted in the United States demonstrated sometimes severe solidification cracking. Exploration of a wide range of weld parameter settings, inert gas combinations, and amount of filler wire addition failed to completely eliminate the problem. The composition of filler wires was explored as an issue in solidification cracking. The broader freezing range offered by silicon-based filler wire alloys such as 4043 (5% silicon) was expected to be helpful, but X-ray analysis and macrosectioning of sample welds revealed only partial success with the use of this wire. A higher-silicon-content filler wire, 4047 (12% silicon), was tried, and the cracking problem was reduced, though not completely eliminated. Adding larger amounts of this filler to the weld pool eventually eliminated (Figure 2) the appearance of microcracking.

Spot welds produced in 6022, 6111, and combinations of the two with 5754 sheet were all performed with 4047 filler wire.

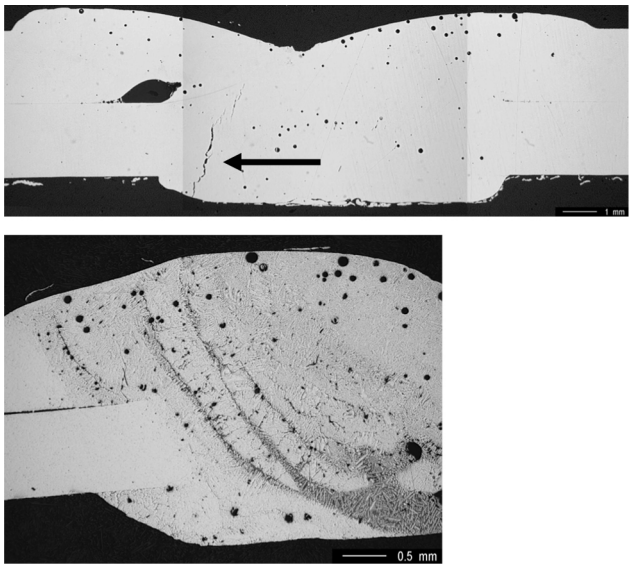

Figure 2. Macrosection showing solidification cracking within the weld on 5754 base material (top). Use of 4047 filler addition slightly increased microporosity but substantially reduced solidification cracking.

Samples of 1-mm 6022 to 3-mm 5754 were produced using 5554 filler wire as a comparison, and despite the expectation that cracking would be present in the latter, strength and fatigue results (discussed later in this section) indicated that microcracking had no effect on overall structural performance.

Porosity

Porosity within welds in aluminum alloys can result from various conditions: the presence of press lubricants and drawing oils, moisture within the parent material oxide film, moisture and drawing oils within the filler wire, and possibly inadequate flow or contamination of the plasma and shielding gases. Welds made with silicon-based filler wires by any arc process usually exhibit more microporosity than those made with magnesium-based filler wires because the former tend to absorb more moisture. Generally speaking, although some microporosity was always evident in the welds made during this project, the levels were sufficiently low not to be considered detrimental to structural performance. Certainly excessively large pores could be produced, particularly in the underside of the spot welds, but optimization of the backup design to a flat, rather than concave, surface appears to have effectively discouraged such formations (Figure 3). Investigation into the most significant of the potential sources for microporosity focused on the condition of the parent material. The use of filler wires generally regarded as being of the highest quality available (supplied by AlcoTec), and shielding gases of certified composition, relegated the impact of these potential sources of microporosity to a minimal level.

The parent sheet was cleaned by various means, because differences were apparent in the effectiveness of the processes used during the manufacture of sheet material in Europe and those used in the United States; more microporosity was evident in welds made in

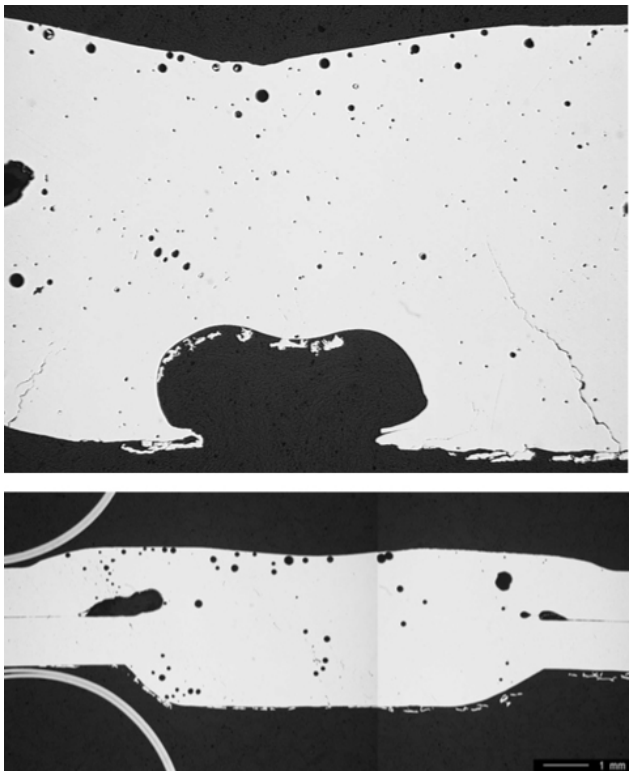

Figure 3. Macrosection illustrating the formation of a cavity on the weld underside due to entrapment of gases in the concave designs of the backup (top). The use of a flat backup eliminated the voids (bottom).

the United States on domestically sourced material.

All sample material was washed with acetone before welding to remove wax or oil lubricant from test coupon material, thus minimizing weld contamination and providing a hazard-free environment for the operatives. Welding material in this condition produced the highest levels of microporosity.

Three different cleaning techniques were tried: mechanical abrasion of the sheet surfaces immediately before welding, immersion in a warm caustic solution of sodium hydroxide and potassium hydroxide followed by water rinsing and air drying (using a commercially available solution), and a cleaning process used by Alcoa based on a phosphoric acid treatment. All three processes reduced microporosity levels; the chemical treatments generally appeared to be the most effective. Probably because of closely controlled processing, the process used by Alcoa seemed to offer the greatest consistency.

Haloes

Haloes are tunnel-like pores or indentations on the underside of the top sheet of parent material surrounding the part, and sometimes the whole periphery of the weld, that create annular voids. Their appearance was the least anticipated, most significant difficulty encountered in this project. These voids often reduced the effective thickness of the upper sheet to 25% of its specified thickness in the area surrounding the weld. The most likely root cause was determined to be the outgassing of hydrogen entrapped within the surface oxide films at the sheet interface. Mechanically abrading both faying surfaces immediately before welding dramatically reduced the size and extent of halo formation; however, from a production standpoint, abrasion was considered unrealistic outside the aircraft industry (Figure 4). Several chemical cleaning methods were investigated for their potential to replace mechanical abrading as a way to remove entrapped hydrogen. A cleaning process suggested by Alcoa, involving treatment with a phosphoric acid-based solution, was found to be the most successful. Hundreds of coupons in all the material grades and combinations were treated by this process and torsion tested, and halo formation was never evident. The success resulting from this cleaning process is a key factor for the acceptability of the plasma spot welding technique in lightweight materials.

Strength

It can be anticipated that the tensile strength of a spot weld will be in direct proportion to the diameter (and thus shear area)

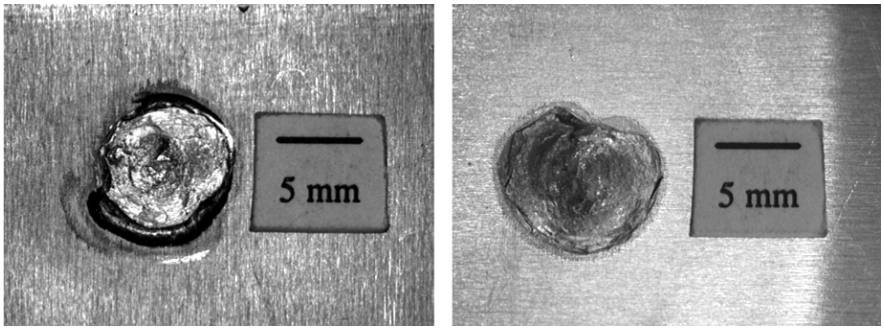

Figure 4. The underside of the a sheet showing the halo effect around 75% of the weldment periphery (left). The material in this case was cleaned using acetone washing only. At right, a phosphoric acid–based cleaning process has completely eliminated halo formation.

of the weld nugget. It is difficult to develop weld nuggets larger than 7 mm in diameter with resistance spot welding of lightweight materials because extremely large equipment is required to do so. In plasma arc spot welding, the lower rate of energy input and high thermal conductivity of the alloys used tends to engender the formation of a larger weld puddle and weld nugget. In this project, nugget diameters typically ranged between 6 and 11 mm, and 8-mm-diam welds were possible in all thickness combinations tried. As a consequence, the tensile strengths of plasma spot welds were significantly higher than those of resistance spot welds (Figure 5).

At Jaguar Cars, thickness combinations similar to those used in this program are all joined with a 5-mm rivet on the XJ8 monocoque. Thus, this was the only size of rivet used in this project.

Fatigue

Fatigue testing of all specimens was conducted on a single Instron machine calibrated to international standards to avoid differences in test equipment. All specimens were tested at a frequency of 10 Hz. In all cases, the fatigue curves generated for the plasma arc spot welds were classic representations of the concave, exponential curve associated with this test method. The same cannot be said in all cases for the riveted specimens; however, the endurance of these coupons to 2 million fatigue cycles was at a higher percentage of their tensile strength than that of plasma arc or resistance spot welds.

It is significant (particularly in light of the testing performed in the joining of 1-mm 6022 to 3-mm 5754 where a 5554 filler wire was used) that plasma arc spot welding specimens known to contain microcracks did not appear to suffer in strength or durability compared with uncracked welds (Figure 6). The suppliers of lightweight materials acknowledge this and consider microcracking within the weld to be of relatively low significance; the automotive manufacturers remain much more circumspect on this matter. However, the automakers have amassed few or no data to support this stance.

Process/consumable robustness

A 486 microprocessor was used to manage current regulation, waveform shape, timing, plasma gas flow, filler wire feed velocity, and retraction during the plasma arc spot welding event; consistency of the arcing event thus was highly accurate and repeatable. Weld power input variance caused by inconsistency in the distance from torch tip to workpiece was prevented because

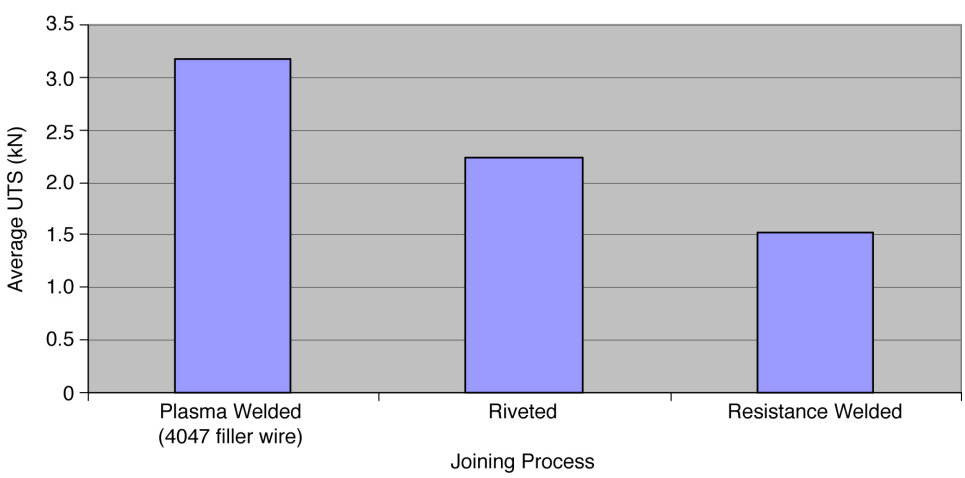

Figure 5. Comparison of tensile strengths attained by plasma arc welding, riveting, and resistance welding in joining 6022 steel.

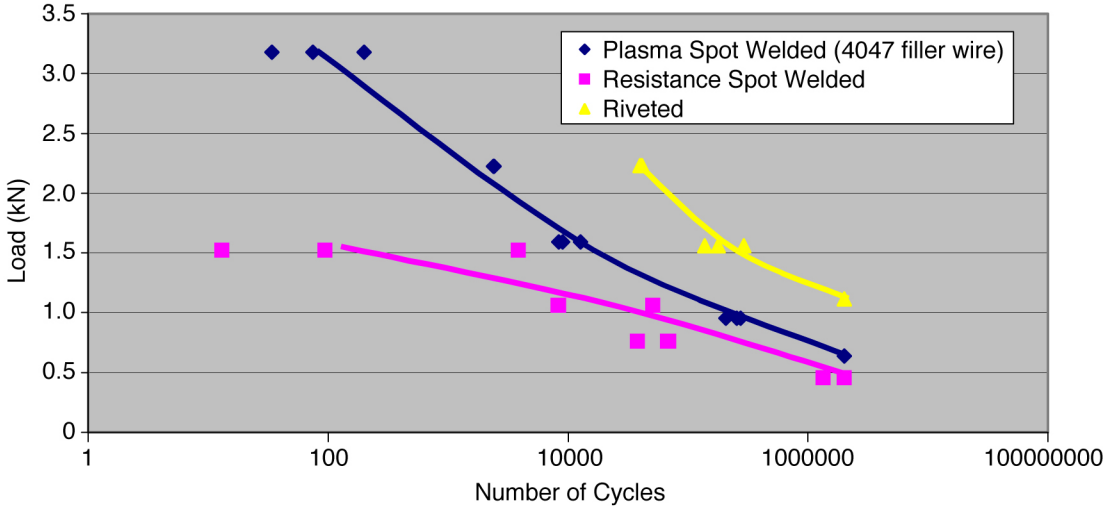

Figure 6. Comparison of fatigue tests for joining 6022 to 6022 by plasma arc spot welding, resistance spot welding, and riveting.

the shield cup contacting the workpiece controlled the distance in every case.

The main factors likely to cause variance in the weld thus became the parent material itself, the presence of contaminants, plasma torch electrode or nozzle erosion, or shield cup damage. The integrity of the shield cup was maintained though careful design and manufacture; likewise the nozzle geometry prevented double arcing. The only choice of electrode material for ac welding is tungsten, containing 2% thorium oxide, all other rare-earth elementally doped varieties of tungsten having failed in earlier trials by Arc Kinetics. The design and geometry of electrodes made from this material have been subject to intensive investigation prior to this project, so no work was considered necessary in this area.

In resistance spot welding of uncoated steels, the ability to perform 3000 spot welds has historically been the benchmark for electrode life. Resistance spot welding of lightweight materials has yet to achieve such long electrode life. It was perceived that if plasma arc spot welding could match the benchmark used for uncoated steels, acceptance of the process for production would be likely. Erosion of the electrode during 3000 or more welds has not been found to significantly affect the quality or size of spot welds produced in the trials to date.

The 4-mm-diam nozzle orifice selected as encompassing all the thickness combinations of parent material used in the program also performed well in achieving 3000 or more welds. Erosion of the copper backup in the design evolved in this program did not appear to significantly affect spot weld nugget size. Redressing this part, much as is done in resistance welding, rather than replacing it during weld torch servicing could offer an economic advantage.

Project Status

- Fatigue testing of two batches of resistance spot welded coupons remains to be completed. Completion is expected in late 2003.
- Additional testing to 2,000,000 cycles of some plasma spot welds is needed if the statistical data are to be fully satisfied. However, each test occupies 55 h of machine time at considerable expense.
- When the data available on the resistance weld fatigue tests are received, complete comparative analysis of the three processes will be possible.
- Plans were to produce some coupons incorporating Alcan 6111 material in

much the same way as alternative Alcoa 6022 material was used. There may now be little value in performing such a study because promotion of this material for use in the automotive industry is to discontinue in favor of 6022 and/or alloys of similar composition and performance.

Conclusions

- Absorbed hydrogen compounds (i.e., hydrated oxides) in the surface films of sheet aluminum at present require a phosphoric acid-based pretreatment prior to plasma arc spot welding to eliminate haloes.
- The addition of appropriate amounts of 4047 grade filler material appears to eliminate microcracking within spot welds.
- Destructive testing of spot welds by torsional shear is valuable for assessing the likely strength, degree of macroporosity, and material thinning through the outgassing effects of the welds.
- Plasma arc spot welds typically offer tensile shear strengths 40% higher than those of competitive technologies.
- Under ac welding conditions used in this project, use of a convex radiused tip geometry prevents damage to the plasma torch nozzle through double arcing.
- Service intervals in excess of 3000 welds can be achieved for the consumables associated with plasma arc spot welding. This greatly exceeds service intervals associated with resistance spot welding of lightweight materials.
- Hard anodizing of an aluminum shield cup of appropriate design can produce a cup that is lower in cost and more robust than the ceramically coated copper alloy shield cups previously associated with the process.
- A flat-surfaced backup positioned between 0.75 mm and 1.0 mm below the lower sheet surface gives better performance in terms of weld quality than do alternative geometries.

H. Performance Evaluation and Durability Prediction of Dissimilar Material Hybrid Joints

D. L. Erdman
Oak Ridge National Laboratory
P.O. Box 2009, Oak Ridge, TN 37831-8048
(865) 574-0743; fax: (865) 574-8257; e-mail: erdmandl@ornl.gov

Field Project Manager: C. David Warren
Oak Ridge National Laboratory
P.O. Box 2008, Oak Ridge, TN 37831-8050
(865) 574-9693; fax: (865) 574-0740; e-mail: warrencd@ornl.gov

Technology Area Development Manager: Joseph A. Carpenter
(202) 586-1022; fax: (202) 586-1600; e-mail: joseph.carpenter@ee.doe.gov
Field Technical Manager: Philip S. Sklad
(865) 574-5069; fax: (865) 576-4963; e-mail: skladps@ornl.gov

---

Contractor: Oak Ridge National Laboratory
Contract No.: DE-AC05-00OR22725

Objective

- Develop new experimental methods and analysis techniques to enable hybrid joining as a viable attachment technology in automotive structures. This will be accomplished by evaluating the mechanical behavior of composite/metal joints assembled using a variety of hybrid joining methods and quantifying the resulting damage mechanisms under environmental exposures, including temperature extremes and automotive fluids, for the ultimate development of practical modeling techniques that offer global predictions for joint durability.

Approach

- Characterize the structural hybrid joint to quasi-static load conditions.
- Characterize response to fatigue, creep, and environmental exposures.
- Conduct predictive analysis.

Accomplishments

- Developed new procedures for manufacturing adhesive coupon specimens to eliminate undesirable voids during processing; the voids resulted in inconsistent material properties.
- Completed static and time-dependent testing of the adhesive for modeling input parameters.
- Implemented new adhesive material properties in the structural rail models and assessed the sensitivity of the adhesive time-dependent behavior on overall structural response.
- Evaluated basic damage modeling techniques employing finite-element method (FEM) analysis to improve predictive modeling accuracy.

- Evaluated the fundamental mechanical properties of the newly acquired Quantum carbon composite material at the coupon level.
- Carried out quasi-static, fatigue, and creep testing of hybrid rail joints composed of Quantum carbon composite.
- Completed cold testing (–40°C) of the Quantum carbon composite hybrid rail specimens.

Future Direction

- Continue to explore the material nonhomogeneity of the Quantum carbon composite and evaluate the influence on structural behavior and ramifications related to predictive modeling.
- Develop damage modeling schemes to enhance hybrid joint durability predictions.
- Explore methods to develop fatigue life predictions in hybrid joints.

Introduction

Weight can be reduced and fuel efficiency increased in automobiles, without compromising structural integrity or utility, by incorporating innovative designs that strategically utilize modern lightweight materials—such as polymeric composites—in conjunction with traditional structural materials such as aluminum, magnesium, and steel. Despite the advantages associated with such dissimilar or hybrid material systems, there is reluctance to adopt them for primary structural applications. In part, this reluctance can be attributed to the limited knowledge of joining techniques with such disparate materials where traditional fastening methods such as welding, riveting, screw-type fasteners, and bolted joints may not be appropriate.

One solution to this problem is the use of hybrid joining techniques by which a combination of two or more fastening methods is employed to attach similar or dissimilar materials. One example is a mechanically fastened joint (i.e., bolted or riveted) that is also bonded with adhesive. These types of joints could provide a compromise between a familiar mechanical attachment that has proven reliability, and the reduction of problematic issues such as stress concentrations and crack nucleation sites introduced by using mechanical fasteners with polymeric composites.

The use of hybrid joining could also lead to other potential benefits such as increased joint rigidity, contributing to overall stiffness gains and a reduction of vehicle mass. Additionally, the use of adhesives in conjunction with mechanical fasteners could significantly reduce stress concentrations, which serve as locations for crack starters. Hybrid joining methods can also provide additional joint continuity to allow increased spacing between fasteners or welds.

Although numerous benefits are derived from using hybrid joining techniques, and the joining of dissimilar materials is becoming a reality, little or no practical information is available concerning the performance and durability of hybrid joints. Therefore, this project has taken on the task of developing new technologies to quantify joint toughness and predict long-term durability. This will necessitate identifying and developing an understanding of key issues associated with hybrid joint performance, such as creep, fatigue, and effects of environmental exposure.

To initiate this study, it was necessary to choose a candidate hybrid joint representative of those typically encountered in automobiles. Because of their wide applicability in automotive structures, several

combinations of hat-section geometries were considered. Hat-sections can be incorporated into a variety of generic automotive structural components, such as crush-tubes or frame rails, when they are bonded and mechanically fastened to other geometries. For the current study, the Joining Task Force selected a composite hat-section bonded and riveted to a steel base, as shown in Figure 1. This selection was made on the basis of general applicability to a variety of automobile structural components. Members of the Joining Task Force identified industry partners for sources for the steel, rivets, composite hat-section, and adhesive.

To determine the influences of the adhesive and the rivets on the structural performance of the rail, it was also decided to investigate bonded specimens without rivets and riveted specimens without adhesive.

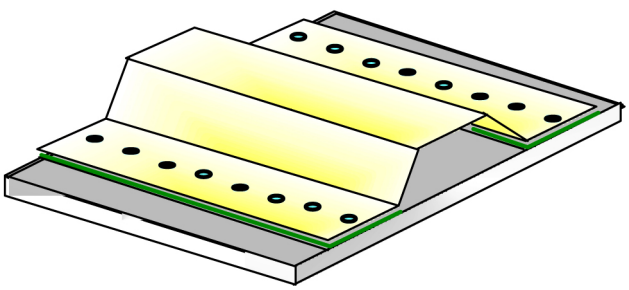

Figure 1. Hybrid joint schematic.

Adhesive Processing Refinement and Re-evaluation of Adhesive Material Properties

Although tensile testing of the 654ETG adhesive was carried out at the start of this project, comparisons of the results with recent tests of the same material in another lightweighting materials project [Energy Absorption in Adhesively Bonded Structures (7E)] revealed inconsistencies in the stiffness, strengths, and relative scatter between the two data sets. The fracture surfaces of suspect specimens that exhibited lower than average strength and/or stiffness often showed large voids created by trapped air introduced during the molding process. The voids are easily discernable with the naked eye (Figure 2). Effectively, the bubbles in the

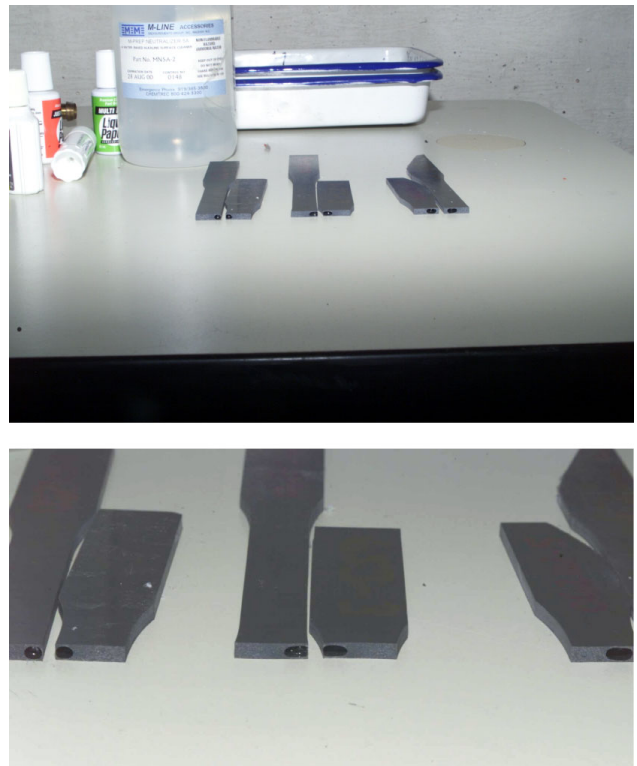

Figure 2. Internal bubbles/voids on tensile specimen fracture surfaces contributed to inconsistent scatter in material properties.

material provide crack starter sites and reduce the cross-sectional area of the specimen, resulting in the inconsistencies mentioned. To eliminate this problem, a new procedure was developed to deposit the highly viscous adhesive onto the molding platens after centrifuging it to remove any air introduced during mixing. Any manipulation of the adhesive that would result in shearing or creating tension was eliminated, and only compressive forces were used to distribute the adhesive to fill the mold. Machining of the specimens from plaques molded in this manner revealed much more homogeneous, void-free specimens. Posttest examination of the fracture surfaces indicated failure of the material that was not initiated from voids in the material, resulting in much more consistent stress-strain behavior (Figure 3 and Table 1). This processing technique was adopted for use in all tensile and creep test specimen preparation.

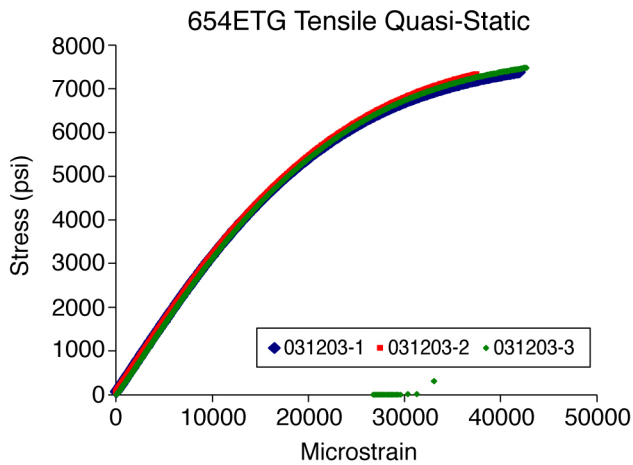

Figure 3. Typical stress-strain curves with the new specimen processing techniques reduced scatter.

Table 1. Static test results for tensile tests plotted in Figure 3

	Strength (ksi)	Modulus (Msi)
	7.378	0.3274
	7.332	0.3268
	7.476	0.3262
Average	7.395	0.3268
Standard deviation	0.073	0.0006

Adhesive Creep Testing

Because of the time-dependent response of adhesives under constant load, we needed to establish the sensitivity of the rail specimens to adhesive creep for the modeling effort. The first step was creep testing of tensile specimens to determine strain accumulation over time. Typical creep curves are plotted in Figure 4. Although there is noticeable scatter in the curves (variation in strain levels despite identical stress levels for all specimens) these data could be used within the FEM model to determine if the creep response of the adhesive contributed significantly to the overall response of the rail. The creep data in Figure 4 were curve-fit with a standard power-law representation suitable for the FEM program (ABAQUS) input:

$$\varepsilon_{creep} = C\sigma t^{n}$$

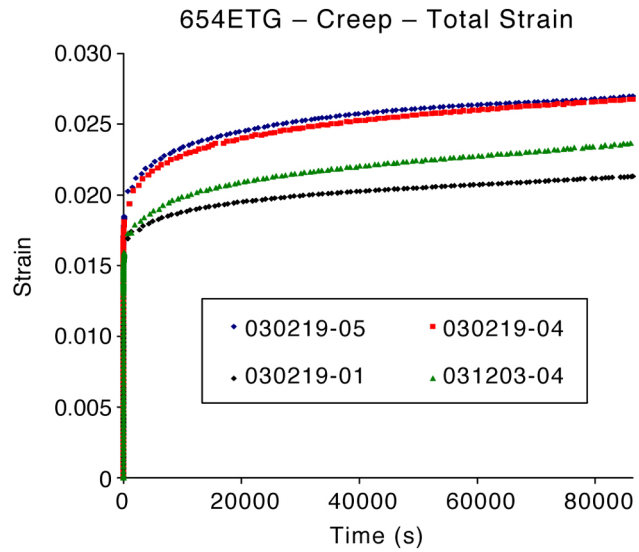

Figure 4. Creep test data for four specimens conducted at 60% of failure stress show noticeable scatter.

where

ε_{creep} = creep strain
σ = applied stress
t – time
C,n = power law coefficients

Because the applied stress and the time are known test parameters, simple curve-fitting techniques were used to determine the coefficients for the power law. The creep strain, which increases with time, was added to the instantaneous strain obtained at the start of the test to obtain the total strain. This information was then used as input in the rail model, with similar creep properties for the composite supplied by the Composite Durability Project. The complete rail was then analyzed in three runs, considering only creep of the adhesive, only creep of the glass composite, and creep behavior for both the composite and the adhesive. Although the adhesive alone exhibits significant creep response, the effect is negligible on the overall rail response. However, including the creep response of the glass composite results in substantial creep of the rail. This result indicates that the additional computation to

include the creep response of the adhesive is unnecessary and can be omitted in future model development. When the model results were compared with results of a creep test on a glass-composite rail specimen, large discrepancies were evident. This is not surprising, considering the level of damage observed during the test (tearing of the composite was obvious) that was not included in the current model. Therefore, damage needs to be introduced into the model. Note, however, that the test on the rail specimen was run at 85% of failure load, which resulted in the large damage accumulation indicated by the periodic jumps in strain level over time. Better agreement may exist at lower levels of creep loading. This issue will be studied with the new Quantum carbon material being procured for rest of this project.

Preliminary Damage Modeling

Three types of exploratory damage models were implemented in ABAQUS to explore the existing capabilities of the FEM program and initiate the introduction of damage into the existing modeling scheme. All three damage models are smeared in that individual cracks are not included; instead, reduction in material stiffness properties is simulated. Hence, the packaged damage capabilities simulate global degradation of material properties. The simplest analysis, which assumed the composite to be perfectly plastic, was performed primarily for comparison with the following two models. The other two models attempt to simulate experimentally observed brittle behavior. Both models predict material softening to occur after a certain stress level is attained. The softening is defined by either a stress-strain relationship or a stress-displacement relationship. In certain situations, the simpler strain softening may produce undesirable mesh sensitivity, yielding indistinct results for the same structure, or may not converge at all. The displacement-softening model avoids this difficulty; however, additional restrictions are placed on the mesh, limiting the analysis.

A typical mesh used for modeling is depicted in Figure 5. It is obvious that the global damage analysis routines packaged with ABAQUS are inadequate to model the extensive tearing of the composite material that was observed experimentally and will need to be addressed with some other user-defined subroutines slated for development in FY 2004.

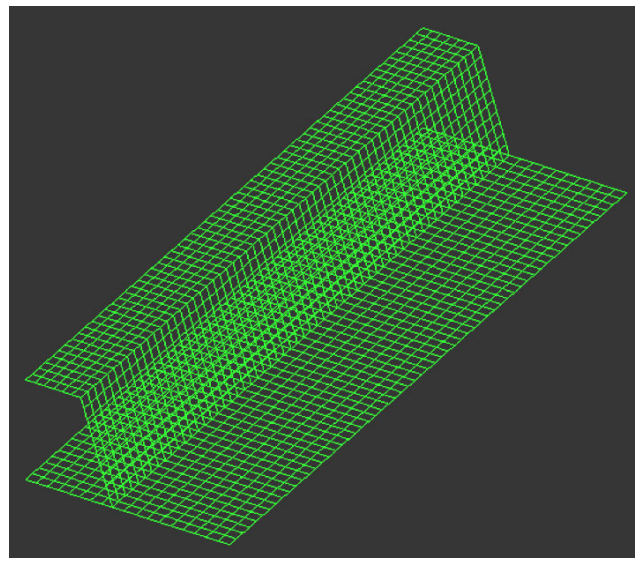

Figure 5. Typical mesh used to model the hybrid joint.

Mechanical Hybrid Rail Studies with Quantum Carbon Composite Material

In the second half of FY 2003, the selected composite material for the hybrid rail structure was introduced. Because the new material had not been characterized at Oak Ridge National Laboratory, coupon specimens were tested to evaluate basic material properties; this was in addition to testing of the structural hybrid rail specimens consisting of new composite hat sections bonded to steel base plates. Large scatter in the coupon tensile properties was observed for the Quantum material, which poses a new challenge in evaluating the failure mechanisms witnessed during the bending tests on hat sections. This scatter led

to a thorough investigation of the composite materials properties unanticipated at the onset of this work.

As previously, the composite hat sections were joined to metal sheet bases by riveting, adhesive bonding, or a combination of the two. All testing was conducted in the same manner as for the swirled glass hat specimens. Bending fixtures, data acquisition software, and experience acquired from the glass specimen tests helped accelerate the testing of Quantum specimens over the last 6 months of FY 2003. Replicate tests were conducted for each hybrid rail specimen in the three joining configurations in quasi-static mode at room temperature and low temperature (–40°C). In addition, fatigue and creep testing at room temperature provided additional information for predictive modeling efforts.

Static Coupon Properties of Quantum Composite Material

Coupon tensile testing was performed on the Quantum material, which was also used for the latest set of hat section specimens making up the hybrid joint rail under consideration. Exploratory tensile testing of flat coupon specimens showed substantial variations in stiffness and strength. Therefore, many tests were required to statistically quantify the material properties being observed to provide reasonable material properties for FEM predictions in the structural modeling of the rails.

Stiffness was measured on 0.5-in.-wide tensile specimens using an extensometer with 1-in. gage length. Stiffness varied among replicate specimens, as well as at various locations on a single specimen, because the extensometer location on a single specimen indicated a high level of nonhomogeneous material behavior. Incremental loading tests were carried out by subjecting the specimen to monotonically increasing load cycles to observe a global indication of damage progression through reduction of stiffness. Tensile coupons were loaded in 200-lb increments, and stiffness was measured by three checks after each loading cycle. A modest decrease in Young's modulus was observed through a general decrease in specimen stiffness with increased load level. This inconclusive reduction in stiffness may be attributed in part to the nonhomogeneous properties of the material.

Hybrid Rail Joint Testing

In conjunction with the tensile testing of the Quantum material at the coupon level, we conducted quasi-static, fatigue, and creep tests of the hybrid rail specimens to assess their mechanical performance and validate future modeling endeavors. Joining methods were consistent with earlier rail tests conducted primarily on swirled glass hat specimens. The specimens joined via adhesive bonding, riveting, and a combination of the two were revisited. The loading conditions were also adopted from previous studies with the hat section being loaded in both tension and comprehension.

Quasi-Static Tests at Room Temperature

Three replicate specimens were tested for each combination of loading (tension and compression) and the three joint configurations. Two of the three replicate tests were instrumented with linear variable differential transformers (LVDTs) for the case of the hat section in tension, and a single displacement gage for the case of the hat in compression. The results from these displacement measurements will be used to correlate with the predicted displacements from analytical models.

Damage and failure behavior observed during the quasi-static tests of the Quantum hat section specimens was somewhat similar to previous test specimens consisting of swirled-mat-glass hat sections; this indicates the damage characteristics are probably dictated more by the geometry of the specimen than the composite material.

The specimens tested in compression exhibited slight degradation in stiffness and almost no discernible damage until the composite flanges catastrophically separated from the metal base of the hat-section at the location of contact with the support rollers. At this point a discernable drop in load occurs as shown in Figure 6. This first step in the failure process was also accompanied by a saddlelike deformation of the steel base, which became more pronounced as the load increased up to failure, indicating large-scale plastic deformation of the steel. As the failure process progressed from the initial drop in load due to the rapid failure at the flanges, continuous longitudinal tearing of flanges occurred, extending from the initial flange to the steel separation point and continuing to grow until the final specimen failure.

For hat section specimens in tension, catastrophic failure occurred at the top of the hat section and remained solely in the composite material. The crack was often located away from the longitudinal center of the specimen, where the bending stresses are the greatest, and is most likely attributable to the variation of properties in the Quantum composite material. Hence, the specimen is failing at a location where the stresses are lower but where the material strength is also lower.

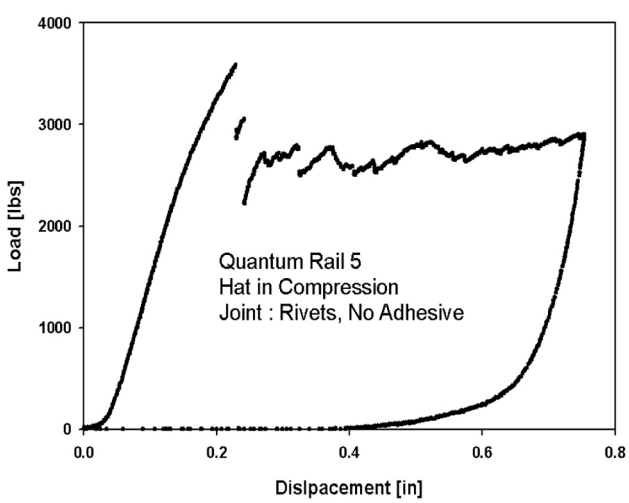

Figure 6. Typical load displacement curve indicating longitudinal tearing of flanges for hat loaded in compression during quasi-static test.

Only two specimens sustained significant push-through damage caused by contact stresses from the rollers that would influence the load-displacement behavior. In previous tests on glass composite specimens, there was a completely different failure process between the specimens that were adhesively bonded and those that were riveted. In the case of glass specimens with rivets only, cracking initiated from the location of the roller contact points, and failure occurred in the flange. Glass specimens bonded with adhesive failed in the composite at the top of the hat. In contrast, the Quantum specimens joined solely with rivets or adhesive specimens exhibited only catastrophic failure of the composite hat section with no preliminary damage in the flange region prior to failure.

Table 2 summarizes briefly the relative strengths measured in the tests of the Quantum rail specimens. Note that, for tests with the hat in tension or compression, the loads attained are consistently higher for joints that are both bonded and riveted. This suggests a single joining method may be inferior to hybrid joints using both mechanical attachment and adhesive bonding.

Table 2. Average maximum load (lb) obtained from three sets of quasi-static tests

Average maximum load (lb)	Tension	Compression
Rivets and adhesive	4044	4183
Rivets	3099	3501
Adhesive	3820	3497

Fatigue Testing

Fatigue tests were performed at 70% of ultimate load determined from the average of the quasi-static tests for each loading/joint attachment configuration. As with most S-N fatigue testing, an order of magnitude difference was observed in the number of cycles to failure for replicate fatigue tests. Specimens failing at fewer cycles generally sustained damage comparable to the specimens tested in quasi-static mode, indicating weak regions

in the hat sections. This result was not surprising considering the nonhomogeneity of the composite and variability of composite strength and stiffness among the various specimens. Specimens failing at higher cycle counts exhibited extensive progressive damage, including multiple rivet failures, widespread adhesive cracking, and cracks originating from rivet holes that developed and grew in the metal base of the specimen prior to failure.

This failure behavior is consistent with the large variation in properties in the Quantum material and can be described by the following scenario. When highly stressed areas of the specimen coincide with weak material areas in the composite hat, the hat failed in these regions as in the quasi-static tests. When the material in highly stressed areas of the hat was strong enough to sustain the fatigue loading without immediate failure, other components of the structure failed and redistributed the stresses, enabling the structure to sustain a much higher level of damage before collapsing. Examples of these types of extensive damage are shown in Figures 7 and 8, where numerous rivet pull-outs and extensive cracking of the metal base can be seen observed without difficulty.

Figure 7. Broken and missing rivets—riveted specimen failed after 30,000 cycles at 70% of static ultimate load with the hat in compression.

Creep Testing

A complete permutation of the three specimen types and the two loading conditions was included in the creep test matrix.

Figure 8. Cracking of metal during fatigue test—adhesively bonded specimen.

Specimens were tested for creep at 40% of ultimate load to avoid large-scale damage because the viscoelastic response of the material was needed for modeling efforts that currently do not contain damage analysis. There was no visible damage on the Quantum hats, although some imprints from the rollers were detectable in the metal part of the structure; also, minor matrix cracking could be heard on initial loading for some specimens, indicating minimal damage in the composite. Hence, the time-dependent increase in displacements recorded throughout the creep test was thought to be a result of material response and not an artifact of extensive damage, which would be indicated by large jumps in displacement at intermittent points in the test. The level and significance of any indiscernible damage could possibly be estimated by evaluating the residual deformation after unloading and comparing the test results with time-dependent FE simulations, which do not include damage. Comparisons of the creep results with FEM models are under way.

Cold Static Testing

A set of quasi-static tests was carried out at –40°F. A Styrofoam environmental chamber designed in-house was cooled with liquid nitrogen to the desired temperature and then allowed to reach equilibrium. The test was then carried out in a manner identical to the quasi-static test at room temperature. The major difference in the results for cold

testing was an increase in the load at failure at –40°F, which significantly exceeded the average load values obtained at room temperature. Bond failure was observed for some adhesively bonded specimens; however, it is unclear if the failure occurred during the test or after the composite failure, because the specimen could not be visually observed during the test because of the chamber design. The increase in strength in the cold condition may be attributable to an increase in the stiffness of the composite material, leading to smaller displacements possibly accompanied by a higher yield point in the steel. The cold environment did not appear to have a detrimental effect on the strength of the structure. Strength results for these tests are listed in Table 3 (see Table 2 for room-temperature results).

Table 3. Maximum load (lb) for quasi-static tests at –40°F

Maximum load (lb)	Tension	Compression
Rivets and adhesive	4662	4497
Rivets	3531	4000
Adhesive	3774	4805

Conclusions

New methods of manufacturing specimens were developed to enable the collection of test data on material properties of the adhesive in a hybrid rail structure. Because these properties are used as inputs to FEM modeling, consistent data are necessary to ensure accuracy in model predictions.

Our study of creep behavior in the hybrid rail revealed that the effects of creep in the adhesive have little or no effect on the global response of the structure and can be omitted from the analysis. However, the creep behavior of the composite drastically affects the behavior of the rail and should be included in the modeling scheme.

Exploratory testing with the damage routines included with the FEM package found them inadequate to model the complex cumulative damage observed experimentally in the hybrid rail specimen. This inadequacy will need to be addressed in the next phase of the modeling, possibly with the implementation of user-defined subroutines.

In general, significant differences between Quantum composite material and the glass composites studied earlier were observed in virtually all aspects of the test program. Tensile testing at the coupon level revealed large levels of scatter in material strength and stiffness. In addition to the scatter in properties among replicate specimens, we discovered that the material is highly nonhomogeneous in composition. There are regions of randomly occurring variation in properties, including strength and stiffness, throughout the material. This nonhomogeneity not only is observable at the coupon level but also has evident effects on the structural response of the hybrid rail specimens constructed from the composite hat sections. One of the greatest concerns associated with this material feature is its effect on fatigue life: two random samples of the material can exhibit completely different fatigue behaviors. The first is a number of short-lived cycles to failure with a simple nonprogressive damage pattern similar to that observed in quasi-static loading tests if the sample is from the lower strength and/or stiffness range of the scatter. If the sample chosen is on the higher end of the spectrum, with higher material properties, the fatigue life is longer, and the damage accumulation is extensive and progressive, involving a number of mechanisms in addition to simple catastrophic composite failure. This pattern is further exemplified by failures occurring in regions of the structure where the stress levels are below the maximum as a result of weak locations. Overall, this extensive scatter in material properties poses new challenges to evaluating the failure mechanisms exhibited during bending tests on hat sections and other structural components. The challenge will be even greater for the future modeling effort, which will strive to accurately and

efficiently represent the behavior of a structure made from this material.

In addition to the nonhomogeneous properties inherent in the chosen composite material system, it was observed that measurable displacements could be tracked over time at relatively low-load levels below the damage threshold. Future testing will reveal if the scatter and variation in specimen stiffness play a significant role in creep response, or if they are periodic within the hybrid-joint structure to the extent of being smeared out or producing an average response for the structure below the damage levels. Additional replicate tests are being conducted to determine the levels of scatter among creep specimens.

Quasi-static cold testing of the hybrid rail specimens revealed a marked increase in strength. It may be due to a shifting of yield points in both the steel and the composite and stiffness changes in the composite. Additional coupon tensile testing in the cold environment will provide further information concerning composite behavior under this condition.

I. Joining of Dissimilar Metals for Automotive Applications: From Process to Performance

Principal Investigator: Moe Khaleel
Pacific Northwest National Laboratory
P.O. Box 999/K9-95, Richland, WA 99352
(509) 375-2438; fax: (509) 375-6605; e-mail: moe.khaleel@pnl.gov

USCAR Joining Team Contact: Jim Quinn
GM R&D Planning
30500 Mound Rd., MC 480-106-212, Warren, MI 48090-9055
(248) 680-4732; fax: (248) 680-2874; e-mail: james.f.quinn@gm.com

Technology Area Development Manager: Joseph A. Carpenter
(202) 586-1022; fax: (202) 586-1600; e-mail: joseph.carpenter@ee.doe.gov
Field Technical Manager: Philip S. Sklad
(865) 574-5069; fax: (865) 576-4963; e-mail: skladps@ornl.gov

---

Contractor: Pacific Northwest National Laboratory
Contract No.: DE-AC06-76RL01830

Objective

- Develop and evaluate different technologies for joining dissimilar aluminum alloys and aluminum to steel.
- Characterize the performance of these joints.
- Develop a unified modeling procedure to represent these joints in vehicle structural simulation. The steel materials include mild, high-strength, low-alloy, and dual-phase steels.

Approach

- Further develop and/or enhance self-piercing rivets (SPRs) and resistance spot welding (RSW), with and without adhesives, for joining dissimilar metals.
- Develop a database for the static, dynamic, fatigue, and corrosion behavior of dissimilar material joints, consisting of different material selections and different joining techniques.
- Incorporate and represent the joint performance data into current computer-aided engineering (CAE) codes for evaluation of impact and fatigue performances of joint components.
- Develop design guidelines in the forms of tables and charts for use in joint structural and crash design.

Accomplishments

- Joined high-strength steel (HSLA 350 and DP 600) and 5000-series aluminum alloy specimens, using self-piercing rivets with adhesive (DOW Betamate 4601).
- Accomplished spot welding of dissimilar metals (mild steel and 5000-series aluminum alloy), using a transition material (aluminum-clad steel strip).

- Conducted salt spray corrosion tests (according to ASTM B117) on all current and past populations evaluated. All SPR and RSW joints were exposed for 500 h and examined using both scanning electron microscopy (SEM) and electron dispersive x-ray spectroscopy (EDS).
- Applied the analytical method developed for estimating rivet strength for similar and dissimilar materials to Joint ID 12. The rivet length was increased from 6 mm to 6.5 mm to determine the effect on the joint performance .
- Investigated experimentally the static, fatigue, and dynamic behavior of several combinations of joined dissimilar materials:

Joint ID 10A:	SPR 5182-O (2 mm) and HSLA 350 (1 mm) with Betamate adhesive
Joint ID 11:	SPR HSLA (1 mm) and 5182-O (2 mm)
Joint ID 11A:	SPR HSLA 350 (1 mm) and 5182-O (2 mm) with Betamate adhesive
Joint ID 12A:	SPR 5182-O (2 mm) and DP 600 (1.6 mm) with Betamate adhesive plus 6.5-mm rivet
Joint ID 12L:	SPR 5182-O (2 mm) and DP 600 (1.6 mm) with 6.5-mm rivet
Joint ID 13:	SPR DP 600 (1.6 mm) and 5182-O (2 mm)
Joint ID 16:	RSW 1008 (1.4 mm) and 5182-O (2 mm) with aluminum clad steel interlayer (1.5 mm)

- Conducted mechanical and microstructural evaluation of dissimilar metal joints subjected to static, dynamic, and fatigue loads. Also investigated the effects of structural adhesives, temperature, piercing direction, dissimilar materials combinations, and loading rates.
- Developed component-level joint fatigue analyses, using experimentally obtained master stress-intensity factor (SIF) life curves.
- Investigated the influence of weld ductility on component crash behaviors.
- Incorporated the joint overload failure criterion.

Future Direction

- Complete joint durability testing of DP600 and 5000-series aluminum alloy specimens in which a group is exposed to 500 h of salt spray/fog and then tested (static and fatigue).
- Transfer joint performance database to members of the joining team.
- Incorporate the proposed failure criterion with software developers.

Introduction

This project is a collaborative effort between DOE, Pacific Northwest National Laboratory, and the Metals Joining Team of the U.S. Council for Automotive Research (USCAR). The work started in April 2001.

The automotive industry envisions that an optimized vehicle, in terms of performance and cost, can be achieved only by using different materials at different vehicle locations to utilize the materials' functionalities to the fullest extent. Currently, aluminum and steel are the most important construction materials for the mass production of automotive structures. High-volume, nonsteel joining is a significant new problem to the industry. For joining dissimilar aluminum alloys, the leading candidate joining methods are spot welding and SPRs with or without adhesives. The major concerns with aluminum spot welding are its high-energy consumption, low electrode life (see report 7F), and structural performance concerns related to

weld porosity. For joining aluminum to steel, the industry is currently comfortable with SPRs (with and without adhesives). However, there are a number of barriers to the widespread exploitation and high-volume production of the riveting technology. One of these barriers is the limited performance data relative to automotive applications.

In contrast, to shorten the vehicle development cycle, more and more CAE analyses are performed before the actual prototype is built. The question that the CAE engineers ask most often is how to represent the structural joints in crash simulation and fatigue simulation. Currently, there is no unified approach to representing the structural joints that works for different material combinations under multiaxial loading. This is particularly true for dissimilar material joints, where even the basic performance information on the joint coupon level does not exist.

Joint Populations

We experimentally investigated the static, fatigue, and dynamic behavior of several dissimilar material joint populations:

Joint ID 10A:	SPR 5182-O (2 mm) and HSLA 350 (1 mm) with Betamate adhesive
Joint ID 11:	SPR HSLA 350 (1 mm) and 5182-O (2 mm)
Joint ID 11A:	SPR HSLA 350 (1 mm) and 5182-O (2 mm) with Betamate adhesive
Joint ID 12A:	SPR 5182-O (2 mm) and DP 600 (1.6 mm) with Betamate adhesive and 6.5-mm rivet
Joint ID 12L:	SPR 5182-O (2 mm) and DP 600 (1.6 mm) with 6.5-mm rivet
Joint ID 13:	SPR DP 600 (1.6 mm) and 5182-O (2 mm)
Joint ID 16:	RSW 1008 (1.4 mm) and 5182-O (2 mm) with aluminum-clad steel interlayer (1.5 mm)

Static Joint Strength Evaluation

Static tests were performed for three loading configurations for each sample population to derive the overload failure envelope for that population. These three loading configurations are lap shear, cross tension, and coach peel. The results of the static tests were then postprocessed to obtain the peak load, failure displacement, and energy absorption upon failure to validate the proposed energy-based failure criterion. Results from static testing of SPRs of aluminum 5182-O and high-strength steels (HSLA 350 and DP 600) with and without adhesives are compared in Figures 1–4.

The effects of adhesives in SPR joints will be documented in a topical report. The report will include the failure modes of these tests along with an analysis of the static strengths using Weibull probability plots.

Experiments were performed to investigate the effect of rivet length on the static performance of joints. The rivet length of Joint ID 12 (5182-O/DP 600) was increased from 6 mm to 6.5 mm. The same joining parameters were applied (i.e., rivet type, die, pressures). The longer rivet clinches more material and contributes to the performance of the joint. The static results are illustrated in Figure 5.

The effect of piercing direction on the static performance of joints was also evaluated. Joint ID 10 (5182-O/HSLA 350) and Joint ID 11 (HSLA 350/5182-O) are compared in Figures 6 and 7. The same rivet and die design was used to join the two dissimilar materials in each population. It was observed that different piercing directions yield different strength characteristics for the joints.

An annealed aluminum-clad steel interlayer material was used to resistance spot weld 5182-O aluminum with 1008 steel (Joint ID 16). Fatigue, static, and dynamic tests were performed on the RSW joint with the interlayer material. The test data were compared to Joint ID 9 (SPR 1008/5182-O).

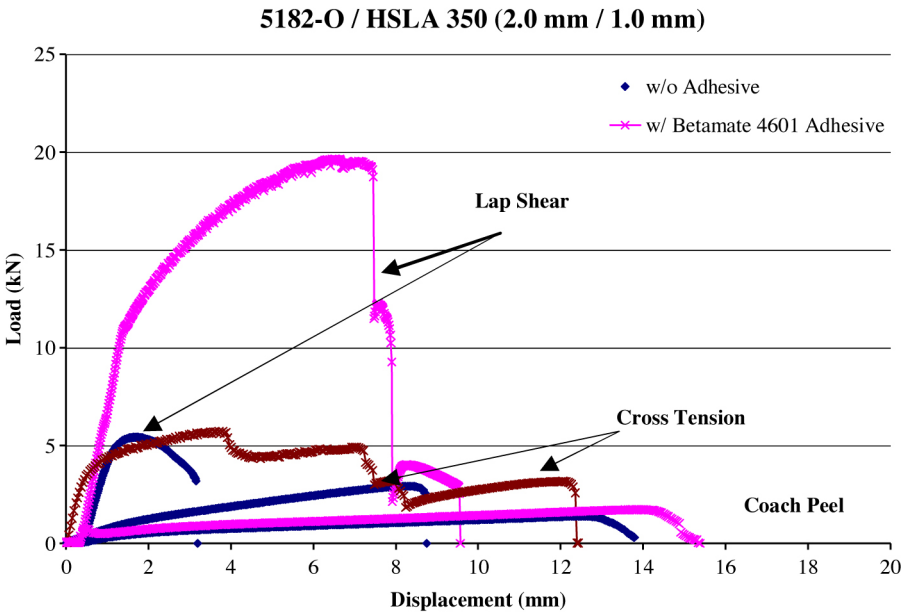

Figure 1. Uniaxial test results for Joint ID 10 and 10A. Results shown are representative of the average peak load observed for the specimen designs tested in each joint population.

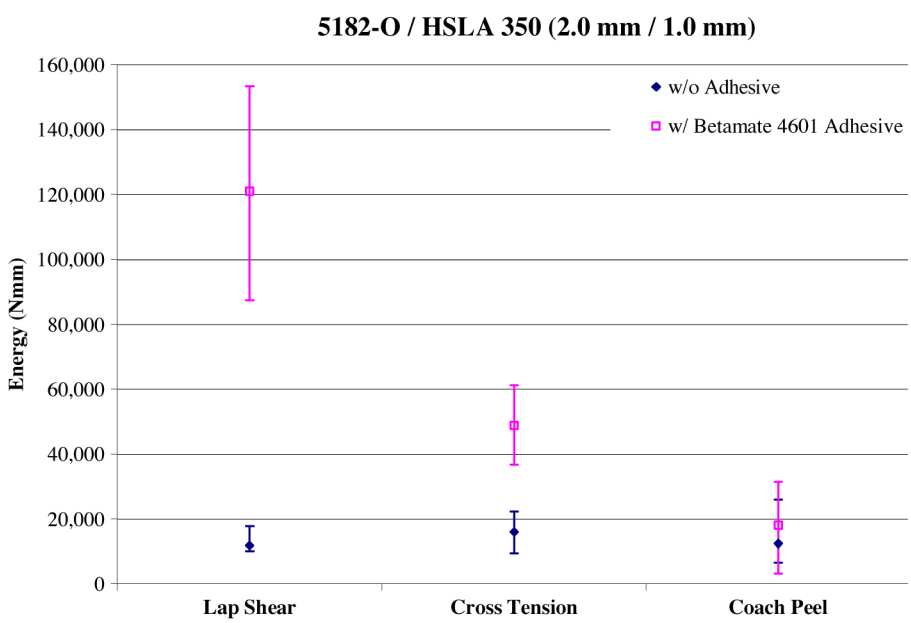

Figure 2. An illustration of the static test energy absorption results for Joint ID 10 and 10A.

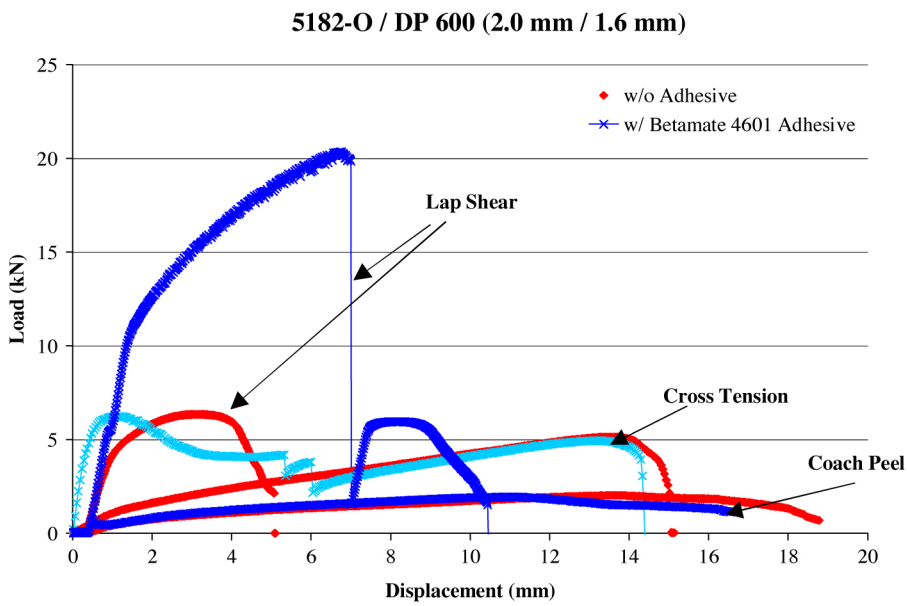

Figure 3. Uniaxial test results for Joint ID 12L and 12A. Results shown are representative of the average peak load observed for the specimen designs tested in each joint population.

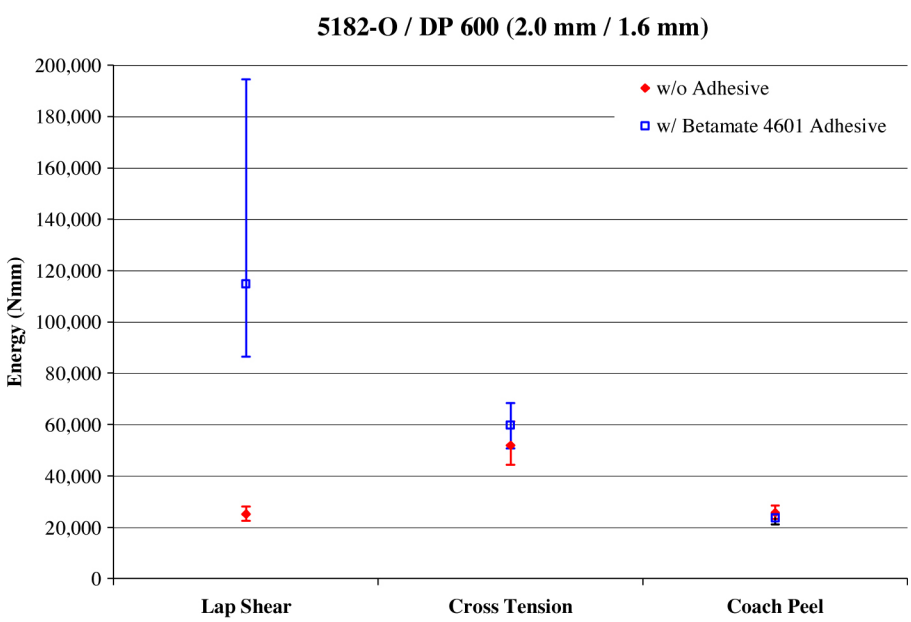

Figure 4. An illustration of the static test energy absorption results for Joint ID 12L and 12A.

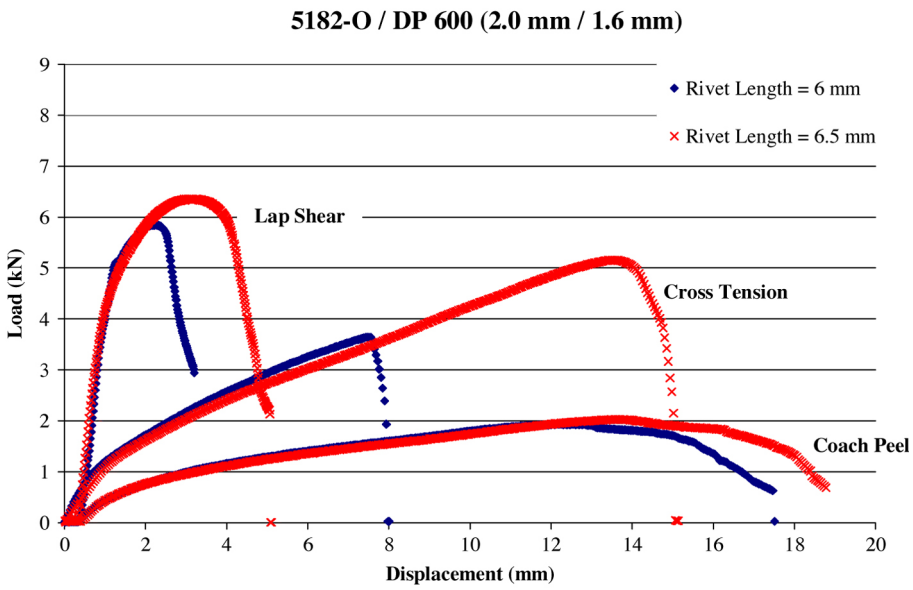

Figure 5. Uniaxial test results for Joint ID 12 and 12L. Results shown are representative of the average peak load observed for the specimen designs tested in each joint population.

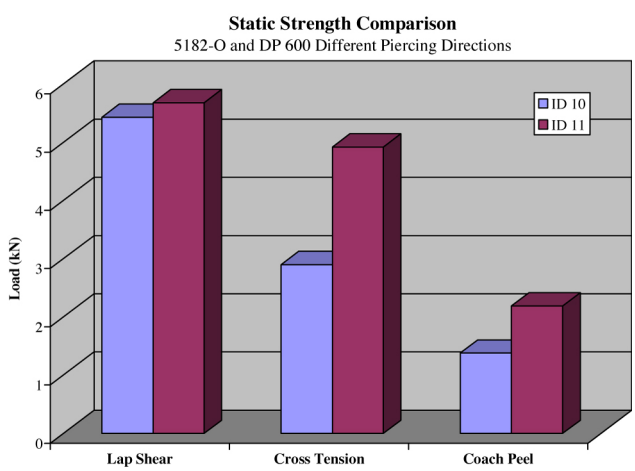

Figure 6. An illustration of the static peak load results for Joint ID 10 and 11. Results shown are representative of the average peak load observed for the specimen designs tested in each joint population.

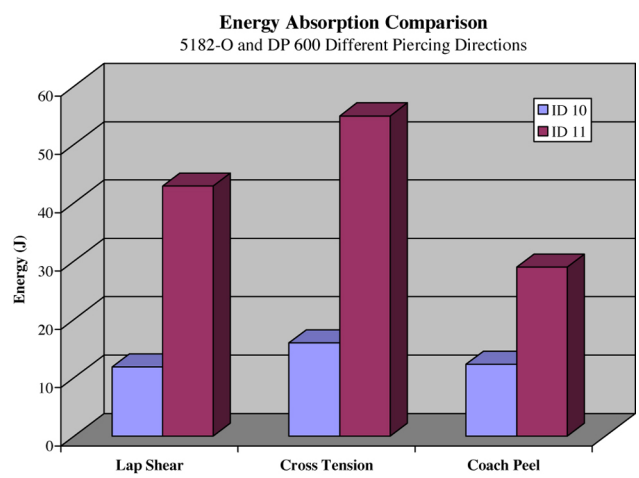

Figure 7. An illustration of the static test energy absorption results for Joint ID 10 and 11. Results shown are representative of the average energy absorption for the specimen designs tested in each joint population.

Figure 8 illustrates the static strength test results for both joint populations.

The development of the interlayer material and utilization of this material to RSW aluminum with steel was documented in a topical report, *Resistance Spot Welds of Aluminum Alloy to Steel with Transition Material—From Process to Performance*. This report characterized the RSW joint from process to performance and compared its performance with Joint ID 9. The report included the failure modes of these tests along with an analysis of the static strengths. These failure modes and static strength data can help the designer of a lightweight vehicle choose the correct material combinations for desired static vehicle performance.

Dynamic Joint Strength Evaluation

Dynamic impact tests of 10 mph and 20 mph were performed on all sample populations under three loading configurations. Example results of cross tension for ID 10A are shown in Figure 9. To determine the dynamic strength accurately, two sets of unique lightweight fixtures were designed for the coupon configurations. These fixtures are rigid, and they connect themselves directly to the piezoelectric load cell, thereby eliminating the possibility of a fictitious load signal resulting from inertia effects. The rigidity, or compliance, of the testing frame was also adjusted prior to the dynamic tests to ensure that the test frame is rigid enough that its natural frequency is much higher than the response frequency of the tested sample. Ringing effect was thus minimized to the greatest extent possible. The dynamic test results were then postprocessed to obtain the peak load, failure displacement, and energy absorption upon failure to populate the failure envelope and to validate the proposed energy-based failure criterion.

Figure 10 illustrates the loading rate effect of Joint ID 11 under cross tension loading condition. It shows that under dynamic loading conditions, displacement to failure decreases with increasing loading rate; however, the peak failure load remains relatively unchanged from the static

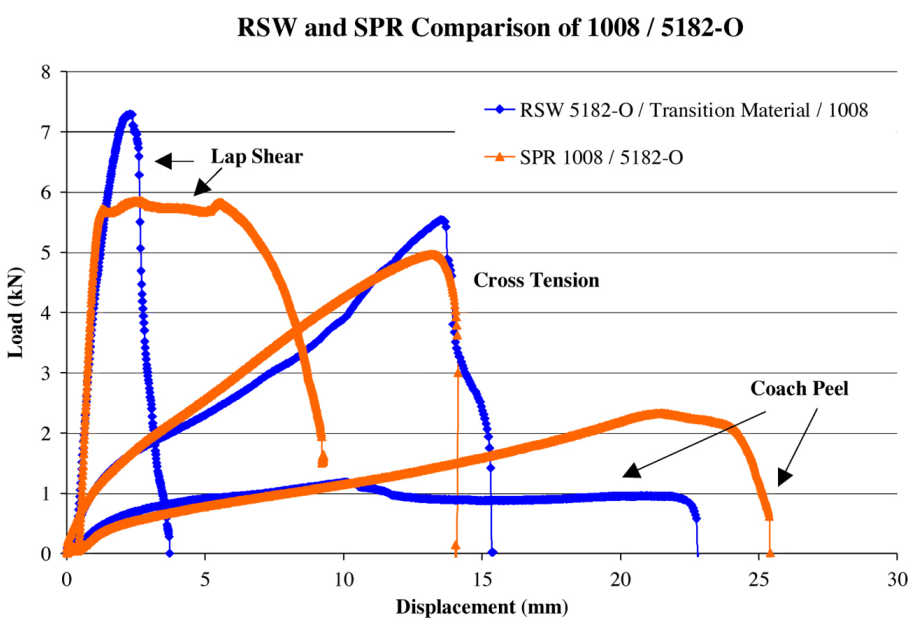

Figure 8. Uniaxial test results for SPR Joint ID 9 and RSW Joint ID 16. Results shown are representative of the average peak load observed for the specimen designs tested in each joint population.

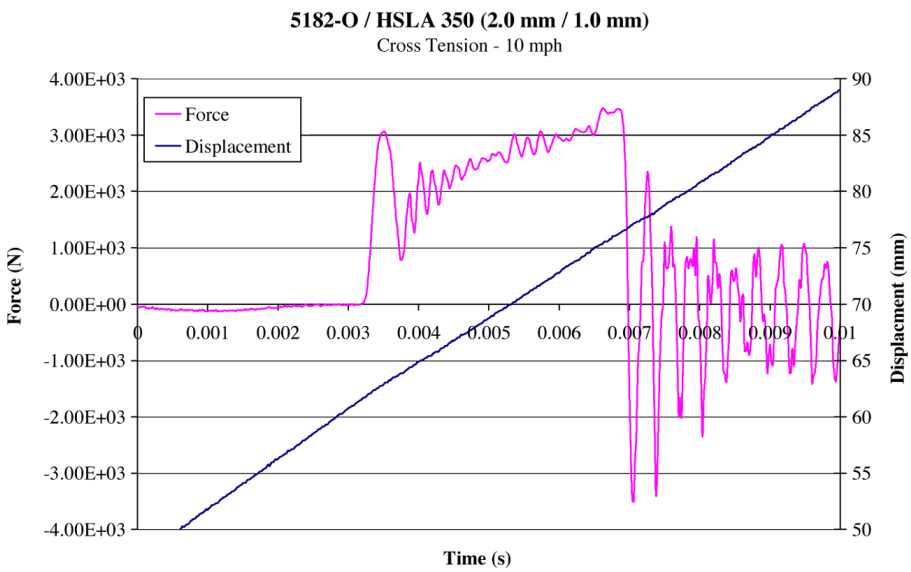

Figure 9. Dynamic test results for Joint ID 10A.

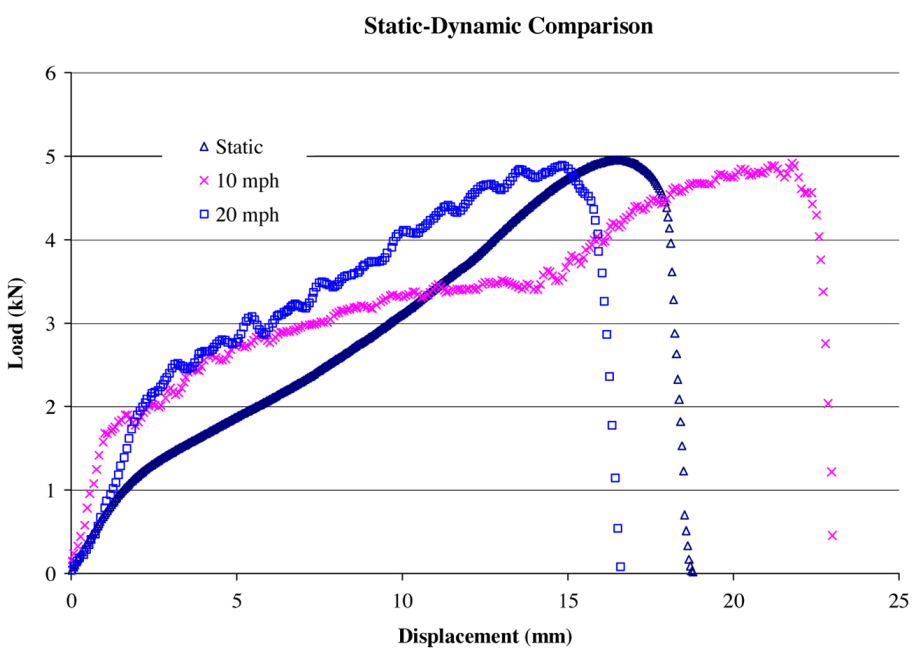

Figure 10. Illustration of the loading rate effect on Joint ID 11 under cross tension loading.

level. Similar conclusions can be drawn for other joint populations with aluminum as the base material. These dynamic results indicate that the total energy absorption for the joint samples decreases with increasing testing velocity. This is because the joints fail in a shorter grip distance due to geometric constraints and inertia effects of the surrounding sheet metal at high loading rates.

The failure modes of these dynamic tests will also be documented in the topical reports. The failure mode and dynamic strength data can help the designer to select materials for desired dynamic performance.

Joint Fatigue Strength Evaluation

Cyclic fatigue tests were performed on all sample populations under a tension-tension ratio of R = 0.1. Fatigue tests were conducted on all specimen designs (lap shear, cross tension, and coach peel). It was found that the coach peel coupons exhibit the lowest fatigue life for the three coupon configurations because of the high stress concentrations for this loading condition. Among the three loading conditions, lap shear had the highest fatigue life. Example results of fatigue data comparing SPR joints with and without adhesives are shown in Figure 11, and fatigue data comparing RSW Joint ID 16 and SPR Joint ID 9 are shown in Figure 12.

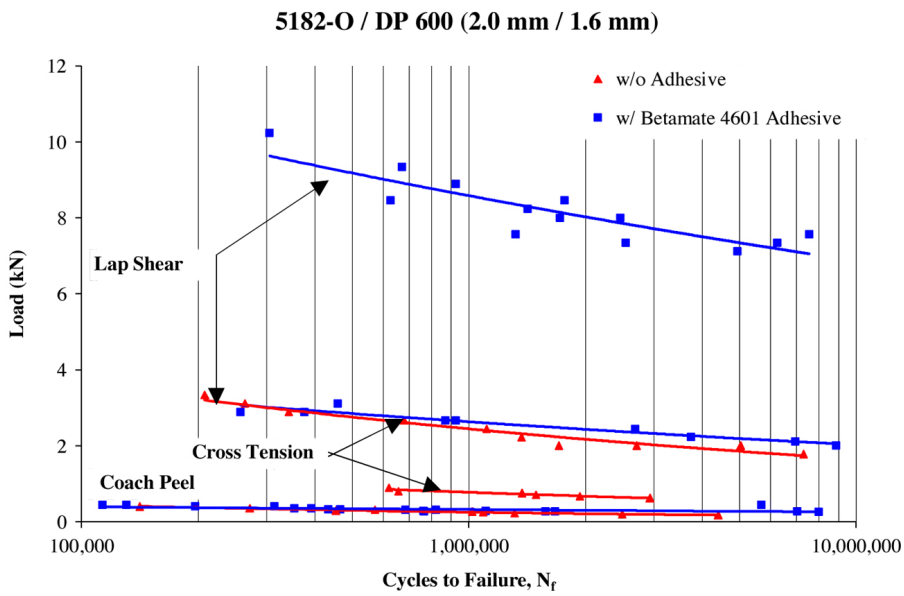

Figure 11. Fatigue test results comparing Joint ID 12L and 12A.

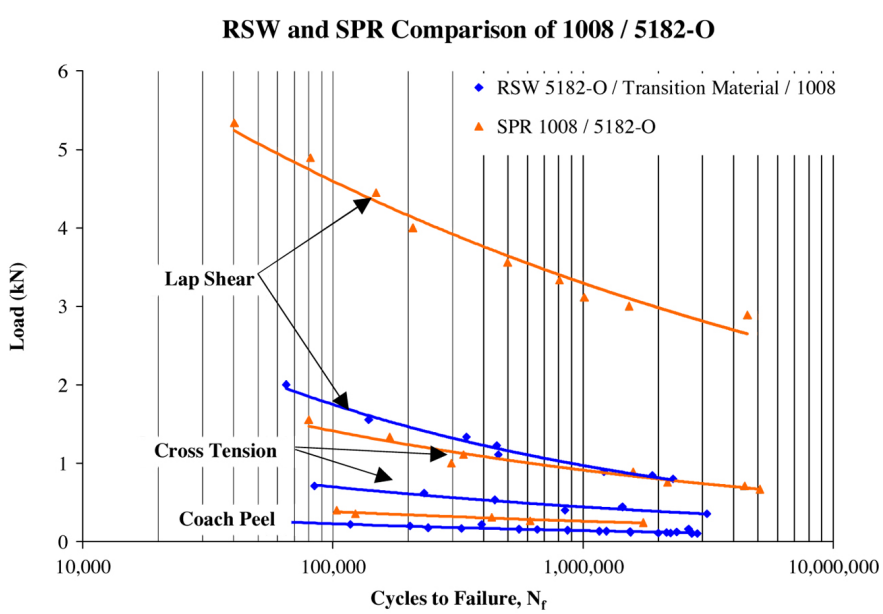

Figure 12. Fatigue test results comparing RSW Joint ID 16 and SPR Joint ID 9.

Joint Corrosion Evaluation

Salt spray corrosion tests were conducted on all current and previous SPR and RSW populations evaluated (with the exception of Joint ID 13 and 16). Specimens were exposed to salt spray/fog for 500 h according to ASTM B117. SEM and EDS were performed to determine whether corrosion was observed in the joints after being exposed to salt spray.

A nontested SPR joint was analyzed to set a baseline for the EDS analysis. It identified the parent substrates, the steel rivet, and the Zn/Sn-Al coating on the rivet. No other significant elements were observed. The same rivet material and rivet coating was used in each varying SPR joint population.

No pitting or crevice corrosion was observed in any of the populations analyzed. However, chloride and increased levels of oxygen were present in all SPR populations tested without adhesive in the joint. No chloride was present in the RSW joints or the SPR joints with adhesive.

Figure 13 is an EDS graph that is representative of the typical elements observed at the rivet interface in all SPR populations analyzed without adhesive. In this particular joint, an EDS analysis was performed at the tail of the rivet where two dissimilar materials met (5182-O and HSLA 350). The presence of chloride and oxygen was observed at the rivet interface in addition to zinc, tin, and aluminum. Chloride and high levels of oxygen were no longer observed at the tail end of the rivet where it is clinched into the bottom material.

Joint CAE

Development of Fatigue Failure Criterion

Fatigue life-vs-load curves tend to have a very large scatter for different material grades, weld sizes, and material thickness combinations. Even for the same joint population, fatigue life-vs-load curves for different coupon configurations are also different. Therefore, it is difficult to cross compare the fatigue performance of different joint geometries and joint populations, and it is even more difficult to apply the fatigue strength measurement from a coupon-level test to a component-level fatigue life prediction. In this project, SIF was chosen to be used as the single parameter to consolidate the fatigue performance curves of different joint populations and different coupon geometries into the fatigue master SIF-life curves. The SIF was chosen because of

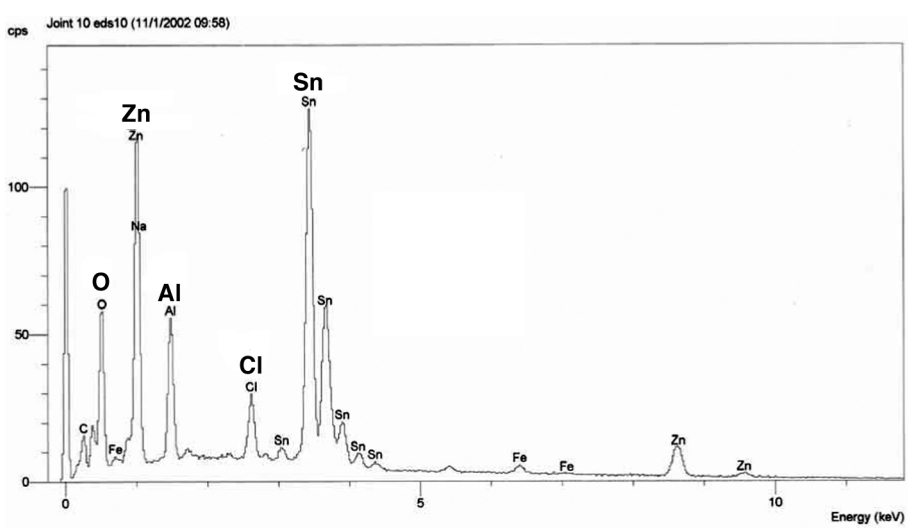

Figure 13. An EDS graph of the rivet interface for Joint ID 10. The EDS graph is typical of the elements observed at the rivet interface in all SPR populations analyzed without adhesive.

its accuracy and computational simplicity in vehicle simulation.

During this reporting period, master SIF-life curves for joints made of different materials and different thickness combinations were also generated using coupon-level fatigue test results under the three different loading conditions. Figure 14 is an example of the master curve for Joint ID 9.

In a component-level fatigue life simulation, the resultant force and moment components for the joint beam element are obtained. The SIF for each joint is calculated based on beam element output, and the corresponding cycle is predicted based on the master SIF-life curve generated.

Development of Overload Failure Criterion

During this reporting period, a force-based failure criterion, Equation (1), was implemented into the dynamic explicit software LS-DYNA. The failure criterion was derived from the static and dynamic test results of different joint coupon configurations.

$$\left(\frac{N_{rr}}{N_{rr_F}}\right)^2 + \left(\frac{N_{st}}{N_{st_F}}\right)^2 + \left(\frac{M_{st}}{M_{st_F}}\right)^2 = 1 \qquad (1)$$

Frontal and side impact simulations were then performed to evaluate the impact performance of spot-welded aluminum and steel hat sections. Failure functions were also monitored for each weld during the deformation processes. It was found that the force-based failure criterion was capable of predicting joint failure due to overloading. However, the force-based failure criterion was not capable of distinguishing between brittle and ductile joint failure. For aluminum and steel rails under the same impact condition with the same joint strength, aluminum rails exhibit better energy management characteristics with more progressive folding and less joint failure, see Figures 15 and 16.

Further study is needed in this area to incorporate the strain rate sensitivity of the weld strength into the dynamic simulation package so that the joint element can be eliminated automatically when the joint forces are outside the corresponding failure

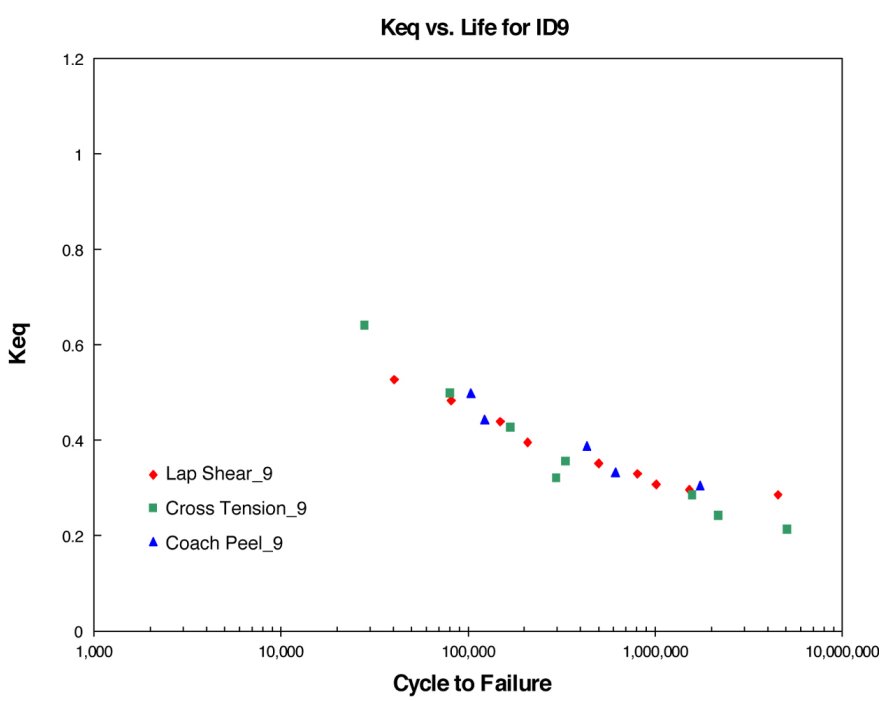

Figure 14. Master SIF curve for Joint ID 9 (SPR 1008/5182-O).

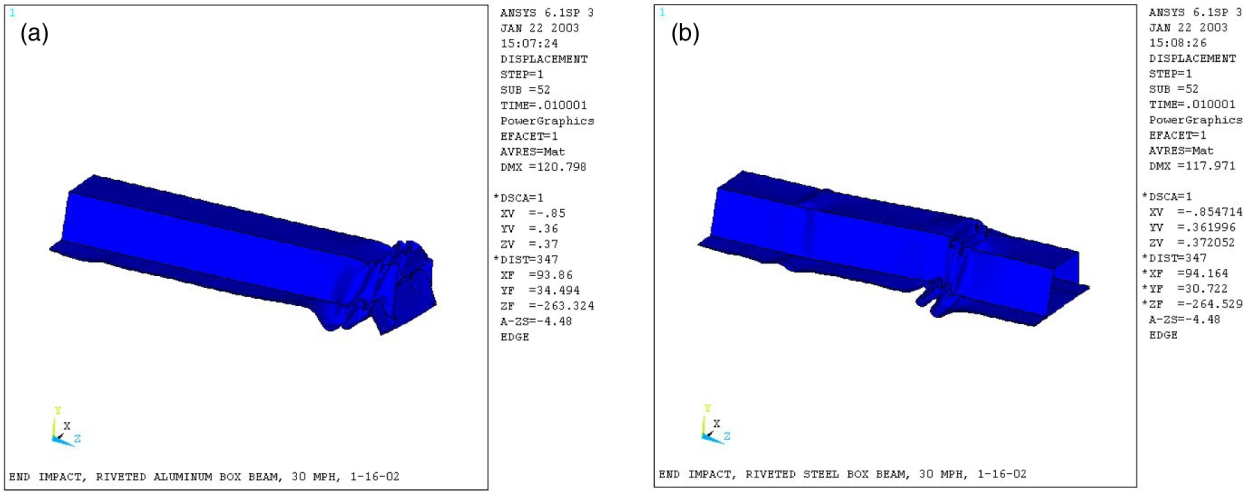

Figure 15. Predicted frontal impact behavior for aluminum and steel hat sections. (*a*) Aluminum hat section; no weld failure predicted. (*b*) Steel has section; two weld failure predicted.

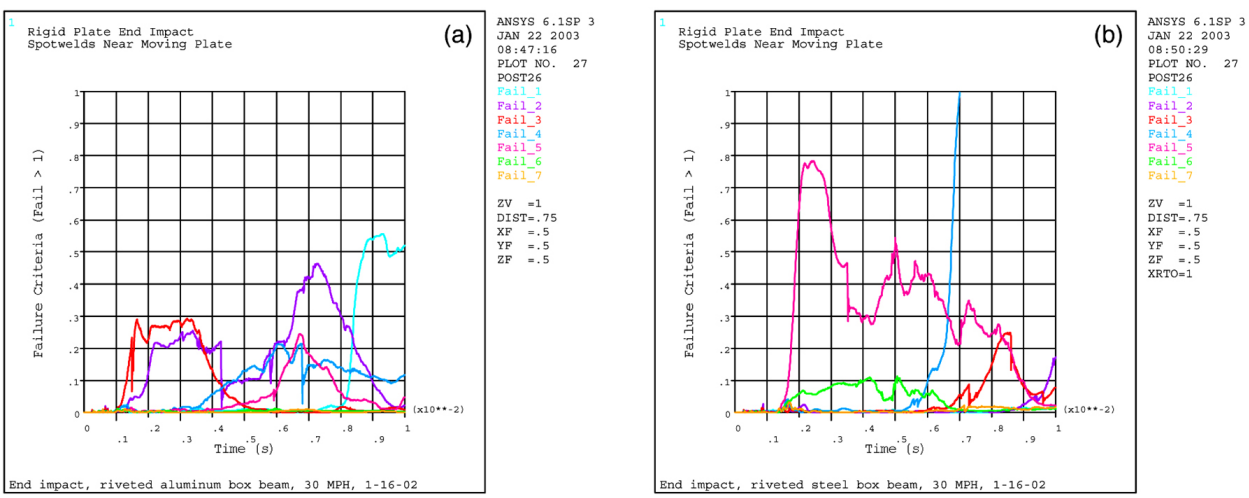

Figure 16. Monitored weld failure functions during impact. (*a*) Aluminum rail. (*b*) Steel rail.

envelope. In addition, more work needs to be done to incorporate the energy-based failure criterion in the simulation package.

Meetings

Project review meetings were held on January 31 and September 19, 2003, at the U.S. Council for Automotive Research. Members of the joining team participated.

Reports

The following topical reports were completed and distributed to the Metals Joining Team:

1. *Performance Comparisons through Weibull Analyses of Self-Piercing Rivets and Resistance Spot Welds Joining Dissimilar Metals*
2. *Resistance Spot Welds of Aluminum Alloy to Steel with Transition Material—From Process to Performance*

3. *Characterization of Fatigue Behaviors of Dissimilar Metals Joints Part I—Experimental Studies*
4. *Effect of Failure Modes on Strength of Aluminum Resistance Spot Welds*
5. *Analytical Strength Estimator for Self-Piercing Rivets*
6. *Lap Shear Coupon Design Sensitivity Study for Self-Piercing Rivets and Resistance Spot Welds*

J. Application of Thread-Forming Fasteners in Net-Shaped Holes

Principal Investigator: Dean M. Paxton
Pacific Northwest National Laboratory
P.O. Box 999
Richland, WA 99352
(509) 375-2620; fax: (509) 375-2186; e-mail: dean.paxton@pnl.gov

Contract Manager: Mark T. Smith
Pacific Northwest National Laboratory
P.O. Box 999, Richland, WA 99352
(509) 375-4478; fax: (509) 375-4448; e-mail: mark.smith@pnl.gov

Technology Area Development Manager: Joseph Carpenter
(202) 586-1022; fax: (202) 586-1600; e-mail: joseph.carpenter@ee.doe.gov
Field Technical Manager: Philip S. Sklad
(865) 574-5069; fax: (865) 576-4963; e-mail: skladps@ornl.gov

---

Contractor: Pacific Northwest National Laboratory
Contract No.: DE-AC06-76RLO 1830

Objective

- To demonstrate concept feasibility of applying thread-forming fasteners (TFFs) into net-shaped hole features in light alloy die castings of aluminum and magnesium for automotive applications.

Accomplishments

- Completed at ELM International design and fabrication of a die casting tool as well as cast aluminum and magnesium nut and washer specimens for testing.
- Obtained from Ford Motor Company and DaimlerChrysler, final machining of nut and washer specimens. They also provided x-radiography of the final machined test specimens.
- Obtained from Bosch Rexroth, a Fastener Tightening and Control System (nut-runner) for driving fasteners into test specimens, which was integrated with the Labmaster Fastener Evaluation Test Cell in use at PNNL.
- Obtained from Textron Fastening Systems, several types of M6 Taptite TFFs for this project as well as standard machine fasteners for comparison.
- Conducted a parametric study at PNNL to evaluate the effects of hole size geometry, fastener coating, and thread engagement depth on clamp load of the joint.
- Performed metallographic examinations of TFFs in cast specimens with net-shaped holes were performed to characterize thread integrity relative to cast specimens with tapped holes and standard machine fasteners.
- Established a broad-based team of contributors for moving forward with the Technical Feasibility portion of this program, including the automotive OEMs, fastener suppliers, assembly equipment suppliers, and manufacturers of cast components.

Future Direction

- Understand and predict casting variation as it applies to the application of TFFs in aluminum castings.
- Optimize fastener design with appropriate coatings for as-cast aluminum and magnesium.
- Understand and control the consequences of in-service reusability and contamination.
- Apply specific assembly process control for component-specific applications.

Introduction

Progress has been made in applying TFFs into machined or stamped holes featured in automotive applications for general assembly. Use of these fasteners eliminated the tapping operation and thereby reduced costs, reduced investment, and improved warranty while delivering better joint properties within an assembly. However, little progress has been made in applying these fasteners into net-shaped holes in as-cast aluminum or magnesium components. Opportunities exist to further reduce costs by using TFFs with net-shaped holes in lightweight castings by eliminating the drilling operation and associated equipment investment without sacrificing joint performance. Potential applications for using TFFs in cast components are numerous and include powertrain (transmissions, engines, and rear axles); chassis (control arms, suspensions); and body structures that utilize large castings (inner doors, liftgates, under-hood attachments, and supports).

The concept feasibility portion of this program to investigate the use of TFFs in net-shaped holes was initiated in 2003. The objectives of the program were to (1) evaluate production die-casting dimensional capabilities to deliver net-sized and shaped holes, (2) demonstrate and characterize the application and use of TFFs for joining (in net-shaped holes), and (3) as required, identify the need for and application of new assembly strategies to support these new joint designs and processes.

Experimental Approach

To perform mechanical testing of TFFs into as-cast net-shaped holes, aluminum alloy A380 nut and washer plates were cast and machined into test specimens. The x-radiography inspections were performed on a sampling of castings prior to final machining to verify structural integrity of the casting. The nut specimens included blind holes with 0.5° and 1.0° draft angles. A photograph and cross-section schematic of these specimens are presented in Figures 1 and 2, respectively. In addition, as-cast nut test specimens were prepared without a preset hole to allow for drilling and/or tapping of holes for comparison testing. A limited number of magnesium alloy AZ91 nut and washer plates were cast and machined into specimens for preliminary testing. Textron Fasteners supplied 6-mm-diam (M6) Taptite fasteners with two coating

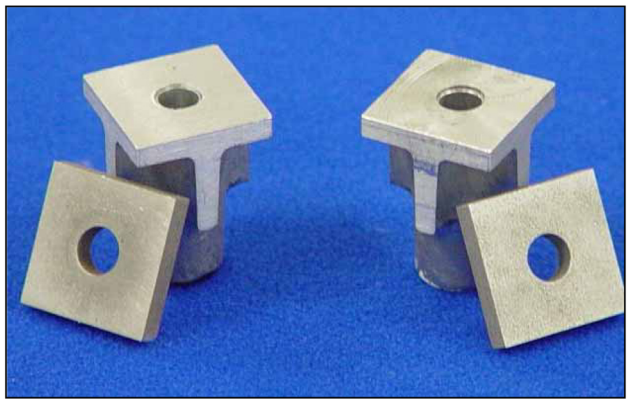

Figure 1. As-cast aluminum nut and washer specimens used for TFF torque-tension mechanical testing.

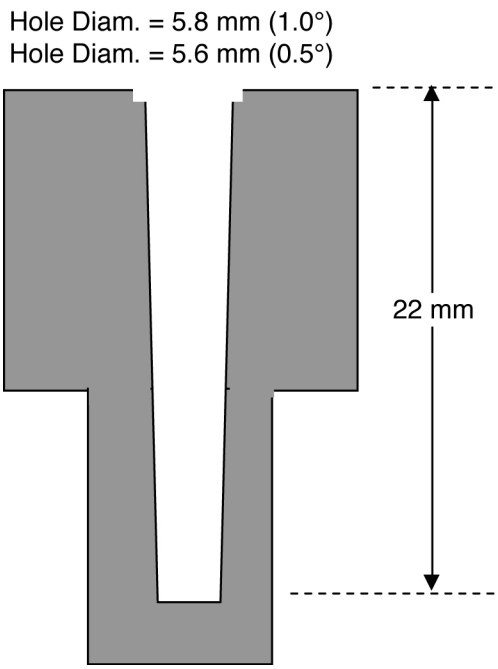

Figure 2. Cross section of nut specimen with blind hole at two draft angles (0.5° and 1.0°).

types: Magni 565, which is an organic coating, and an electroplated zinc coating referred to as S437. Textron also provided standard M6 machine screws coated with both the Magni 565 and S437 coatings for comparison testing. These fastener types were designed for use in aluminum.

The LabMaster Fastener Evaluation Test Cell was used to perform mechanical testing. This unit utilizes a slide-bearing mount for the fastener drive system in addition to mounting for the rotary torque-angle sensor and torque-tension research head. The fastener test system couples with a dc electric nut-runner tool and controller, a rotary torque-angle transducer, a combination thread torque and clamp force transducer, and a computer control system for accurate test reproduction as well as data logging and reporting. The test stand equipment and nut-runner provided by Bosch Rexroth are shown in Figure 3. Individual mounting plates (Figure 4) were machined to size to hold the nut and washer specimens on either side of the load cell. The nut-runner was programmed to drive the fasteners to failure at a

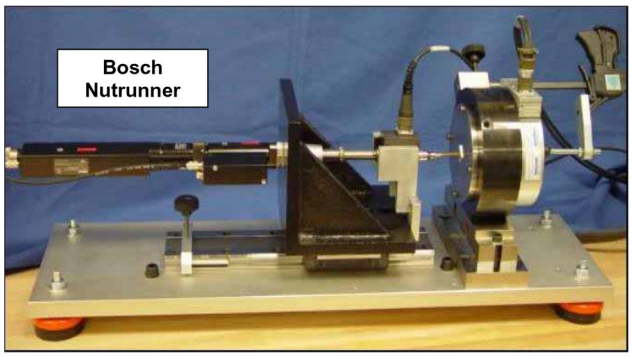

Figure 3. LabMaster Fastener Evaluation Test Cell from RS Technologies with integrated Bosch nutrunner.

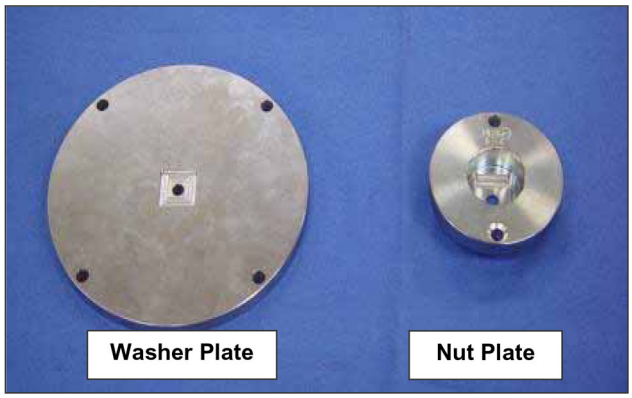

Figure 4. Washer and nut plates used with fastener test stand.

rundown speed of 240 rpm. During testing, the Labmaster software recorded clamp load, input torque, and failure torque-vs-time and angular rotations of the fastener for each test.

To better understand the role of hole geometry and type (net-shape vs drilled) and to compare TFFs to standard machine screws, a parametric study was designed that also included fastener coating type and thread engagement depth. This study was focused on aluminum, although some limited testing was performed on the magnesium specimens. The variables and a symbol for each are listed in Table 1. With two coating types and four hole types, a total of eight combinations are established for each thread engagement depth (e.g., M0518 and S1015).

Table 1. Summary of test matrix parameters

Variable	Description	Symbol
Coating	Magni 565	M
	S437	S
Hole type	0.5° Draft angle	05
	1.0° Draft angle	10
	Drilled hole	DR
	Tapped hole	TP
Depth	18 mm	18
	15 mm	15

Experimental Results

The mechanical testing of installing fasteners into as-cast aluminum specimens was performed during August–September 2003. Initial testing at a thread engagement depth of 18 mm (equivalent to three times the diameter of the 6-mm fastener) showed that failure of the joint occurred by breaking of the fastener adjacent to the top surface of the nut specimen. This result indicates that the input torque applied during tightening of the joint exceeded the strength of the fastener, not the strength of the threads formed in the cast aluminum nut specimen. However, initial testing at a thread engagement of only 15 mm (two and one-half times the diameter of the 6-mm fastener) resulted in failure of the threads in the joint (stripping) rather than failure of the fastener. Failure in this mode does not yield usable data and is attributable to the hole size and draft angle, not specifically to the fastener. Thus, testing at the 15-mm engagement depth was discontinued, and results reported herein will be for the 18-mm depth. Different nut specimens and hole geometry would be required to evaluate two and one-half times thread engagement for specific applications.

Minimum failure torque (Nm) and maximum clamp load (kN) for each combination are shown in Figure 5 and summarized in Table 2. A total of 30 specimens were run at each combination to generate statistically significant data. In general, the minimum failure torque for joints with TFFs was consistent at ~25–26 Nm with the

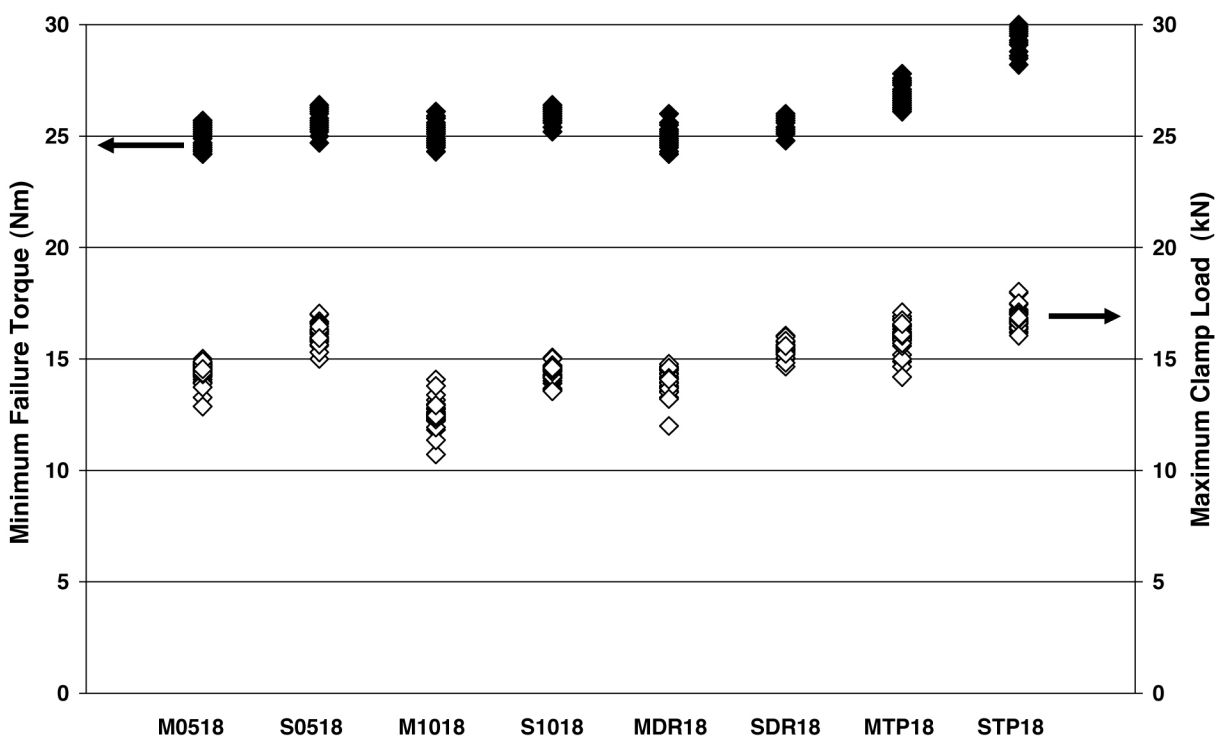

Figure 5. Minimum failure torque and maximum clamp load for cast aluminum alloy A380 test specimens.

Table 2. Summary of maximum clamp load and minimum failure torque for cast aluminum alloy 380 test specimens

Test combination	Maximum clamp load (kN)	Minimum failure torque (Nm)
M1018	12.6	25.1
M0518	14.3	25.1
MDR18	14.0	24.9
MTP18	16.0	27.0
S1018	14.2	25.9
S0518	16.1	25.6
SDR18	15.4	25.3
STP18	16.9	29.6
Nominal standard deviation	<0.5	<0.5

S-coating showing about 1 Nm higher than the M-coating. The tapped holes with machine fasteners showed slightly higher minimum failure torques relative to net-shape holes, and again, the S-coating was higher (29.7 Nm) than the M-coating (27.0 Nm). For maximum clamp load, hole geometry had a consistent effect with the 1.0° draft angle having the lowest clamp load, followed by the drilled holes, and the 0.5° draft angle having the highest clamp load. As with minimum failure torque, the S-coating was consistently higher than the M-coating. The standard deviations for all these measurements were minimal at less than 2–3% of the measured value.

Metallographic Evaluation

Representative fastener test specimens were selected for metallographic evaluation to characterize thread integrity relative to cast specimens with tapped holes and standard machine fasteners. Test specimens that failed by breaking of the fastener were sectioned axially, then mounted and polished for metallographic inspection. Figure 6 shows an optical micrograph of a standard machine fastener in a tapped as-cast aluminum nut specimen. The tapped threads are very clean and consistent along the axial length of the nut specimen and show no signs of significant cracking. Figure 7 is an optical micrograph of a TFF in a cast aluminum nut specimen with 0.5° draft angle. As expected, the threads formed using TFFs are not as clean when compared to a tapped hole with some minor cracking observed in the threads formed by installation of the fastener in the top end of the hole. However, no debris was created during thread-forming, and the clamp loads were acceptable for a M6 fastener. The light regions in the center of the fastener in Figure 7 are surface oxidation of the fastener alloy.

Future Work

The concept feasibility portion of this program was successfully completed in 2003. The results from this effort showed that clamp loads comparable to conventionally drilled holes and tapped fasteners could be achieved with TFFs in net-shaped holes. In addition, a broad-based team of participants was formed, including the automotive original equipment manufacturers (OEMs), fastener suppliers, assembly equipment suppliers, and manufacturers of cast components.

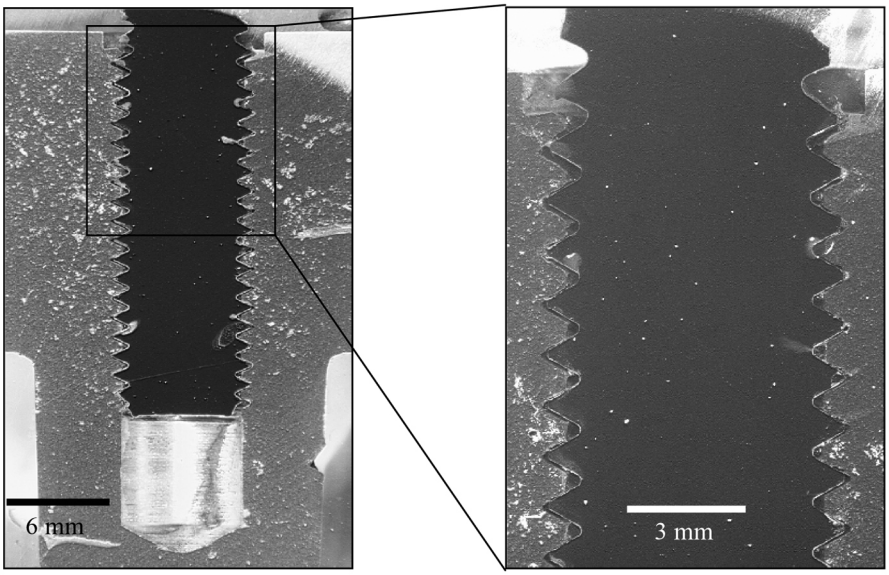

Figure 6. Optical microscopy of a cross section from an M6 standard machine fastener run into an as-cast aluminum nut specimen.

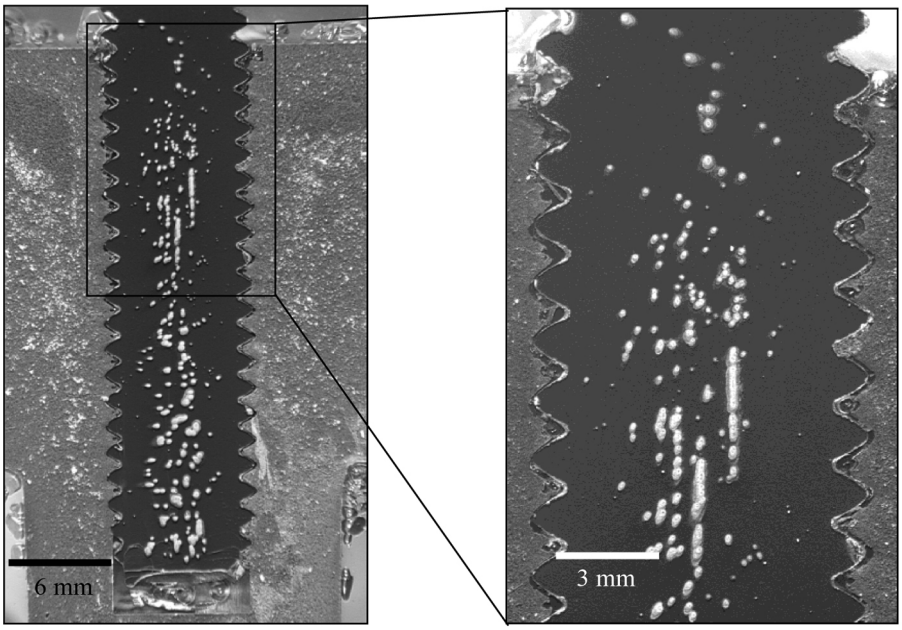

Figure 7. Optical microscopy of a cross section from an M6 TFF run into an as-cast aluminum nut specimen.

However, the application of TFFs in net-shaped holes of lightweight materials is not fully understood. Research and technical development are required to address issues associated with the casting process, thread-forming performance, joint integrity, assembly capability, and the impact to service. The objectives for the proposed technical feasibility portion of this program are as follows:

(1) Startup and Design Phase consists of developing the proof-of-concept experimental design and determining statistical

dimensional variable ranges for a series of die-cast test plates containing net-cast test holes for assembly of the TFFs. Statistical variability parameters will be verified by comparison to measurements taken in the field from production dies and tooling. Initial results from the concept feasibility parametric study will be validated with design and manufacturing engineering input prior to issuing design release for casting and assembly tooling.

(2) Build and Launch Phase will (1) design tooling and cast multiple die-cast test plates containing representative, statistically valid, dimensional variables; (2) install a production-representative automated nut runner system with required instrumentation; and (3) assemble a statistically valid number of TFFs into the multiple die-cast test plates.

(3) Run, Analyze, and Report Phase will characterize the assembly process, joint performance, and variability of fastener assembly parameters as a function of net-cast hole variables. These data will be compared to conventionally drilled and tapped holes. Results will be analyzed and reported along with a recommended assembly torque strategy for net-cast hole TFFs.

K. Nondestructive Evaluation Tools for Evaluation of Laser-Welded Metals

Project Leader: William Charron
Ford Motor Company
24500 Glendale Avenue
Redford, MI 48239
(313) 592-2296; fax: (313) 592-2111; e-mail: wcharron@ford.com

Project Administrator: Constance J.S. Philip
National Center for Manufacturing Sciences
3025 Boardwalk
Ann Arbor, MI 48108-3266
(734) 995-7051; fax: (734) 995-1150; e-mail: conniep@ncms.org

Technology Area Development Manager: Joseph A. Carpenter
(202) 586-1022; fax: (202) 586-1600; e-mail: joseph.carpenter@ee.doe.gov
Field Technical Manager: Philip S. Sklad
(865) 574-5069; fax: (865) 576-4963; e-mail: skladps@ornl.gov

---

Contractor: U.S. Automotive Materials Partnership
Contract No.: DE-FC05-02OR22910

Objectives

- Develop fast, accurate, robust, noncontact nondestructive evaluation (NDE) tools and methodologies to replace current manual destructive testing of laser-welded sheet and structures in zinc-coated and uncoated steel and aluminum.
- Demonstrate accuracy and repeatability of the technologies developed or applied.
- Eliminate the need for highly trained/experienced NDE evaluator.

Approach

- Phase 1: assess state-of-the-art technologies, down-select, performance test using fabricated welded coupons in steel; correlate NDE test results with validation test results; and select technology for Phase 2.
- Phase 2: specify and build a bench prototype from the selected NDE methodology, conduct further validation testing using production laser-welded coupons and production parts in steel and correlate NDE test results with validation test results. Compare destructive test result to NDE test results obtained on production parts.
- Undertake the study of laser-welded coupons in aluminum using an equivalent approach.

Accomplishments

Phase 1:

- Completed original equipment manufacturer (OEM) weld flaw characterization.

- Completed selection of target laser-weld application.
- Defined preliminary NDE system functional specifications.
- Completed initial assessment of NDE state-of-the-art technologies.
- Completed controlled testing of four selected NDE technologies using laboratory-fabricated roof ditch laser-weld coupons.
- Completed analysis of vendor test results.

Phase 2:

- Defined NDE system functional specifications based on roof ditch application and production plant input.
- Selected through-transmission acoustic technology that is suitable for the roof ditch application as well as other weld configurations.
- Evaluated technology using
  - — steel roof ditch samples fabricated on laser-weld production equipment that are complete,
  - — aluminum lap-weld sheet samples fabricated on laser-weld production equipment, and
  - — steel roof ditch production part coupons that are planned.
- Completed analysis test results for steel roof ditch samples and analyses of results for aluminum lap-weld samples and steel production part coupons are projected to be complete by close of CY 2003.
- Monitor prototype build to optimize for roof ditch application.
- Select strategic course of action for prototype implementation and plant trial.

Introduction

Laser welding has been widely accepted by the automotive industry as an industrial process. Uses range from welding of tailor-welded blanks, to transmission component, to airbag inflation modules. The use of lasers continues to increase with some manufacturers considering the use of lasers for welding of the "body in white".

While laser welding is accepted by the automotive industry, cost factors are an issue, particularly with respect to weld discontinuities. With the high speed and high volume of laser, welding coupled with the relatively small critical flaw size, finding these discontinuities can be time-consuming, difficult, and thus, expensive. If not detected before subsequent processing and/or assembly, they could cause failures during processing down line or while in use. For example, porosity in a laser-welded tailor blank can cause failure during a stamping operation, which in turn can damage dies and cause downtime for the press. To forestall this, laser welding must be accomplished with no detrimental weld discontinuities, and the process and product output must be monitored with a high degree of reliability.

A number of systems have been developed to monitor laser welding systems in real time. Generally, these systems examine the byproducts of the laser-to-metal interaction to infer the quality of the weld itself. These process monitoring methods may include examination of the frequency and intensity of the light that is given off, for example, and compare it to those parameters

known to have produced an "acceptable" weld. Most of these monitoring systems use this "training" method as a basis for determining if acceptable welds or unacceptable welds were created by the laser weld process. As of this writing, such systems are being applied in the production environment to gage the process, not as a substitute for weld quality inspection or destructive testing.

The USAMP is exploring NDE tools for use on the weld itself upon completion of the weld process. Of specific interest was the identification of progressive and emerging technologies in NDE. As part of this effort, the AMD 303 project performed phased assessments of NDE technologies, progressively narrowing down the technologies best suited to the production application. From these assessments, specific technology recommendations were reviewed and a technology chosen with the goal being to have a NDE prototype ready for installation in a factory setting by the end of calendar year 2003.

Details of Phase 1 and 2

Phase 1

Phase 1 was the assessment of state-of-the-art technologies, down-selection, testing using fabricated welded coupons, correlation of NDE test results with validation test results, and technology selection. The NDE capability sought was conceptually defined in terms of its functionality, and the laser weld discontinuities that must be detected were characterized.

An initial assessment of NDE technologies from which four technologies were selected for further evaluation, was completed in July 2001. The NDE techniques included in this assessment are identified in Figure 1. Commercial off-the-shelf systems were included along with emerging NDE technologies.

Four technologies were selected for detailed evaluation using a scientifically designed and statistically controlled study. The goal was to determine NDE performance capability using laboratory-fabricated weld samples, simulating laser-welded roof ditch welds (see Figure 2). At this stage of our research, it was not expected that any of the four technologies would prove to be 100% capable. Rather, the goal was to determine which technology offered the best array of detection capabilities and potential for enhancement and configuration as a

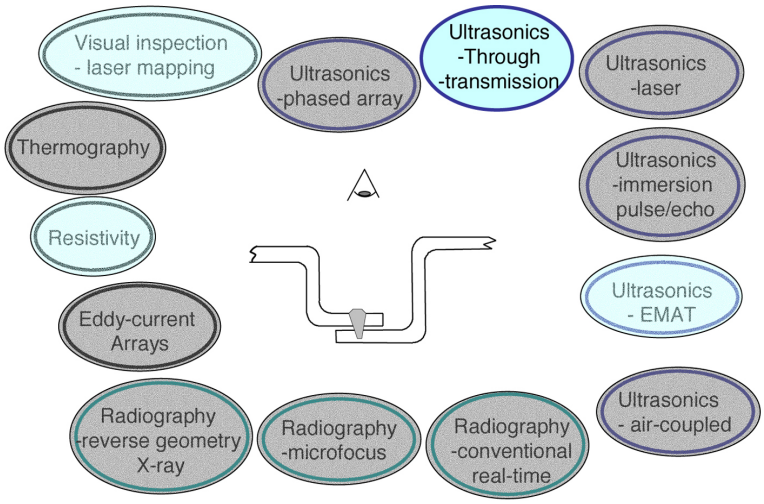

Figure 1. Phase 1 Technology assessment examining the capabilities of 13 technologies/techniques for their suitability to inspect the target weld configuration and the weld discontinuities of interest. Initial analyses identified four techniques, highlighted here, for detailed evaluation.

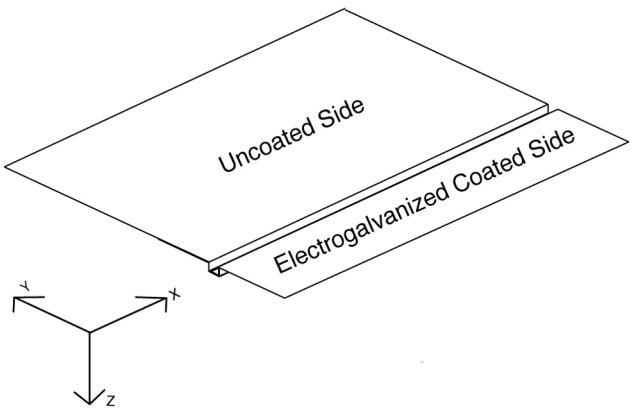

Figure 2. Overall dimensions of roof ditch weld sample: X = 400 mm; Y1 = 202 mm Y2 = 89 mm, overall Y after bending = 287 mm; Z = 12 mm.

prototype suitable for eventual testing in an automotive laser welding production application.

Validation of the laboratory-fabricated roof ditch weld samples in Phase 1 was done using microfocus and conventional radiography and, where appropriate, metallurgical evaluation rather than destructive tear down of the samples. Viewed as too valuable to destroy, the samples were preserved, thereby ensuring our ability to use them in future testing.

Following completion of these evaluations, the AMD 303 Committee undertook an extensive analysis of the data to arrive at an understanding of and consensus on a meaningful comparison of the results. All systems were found to have varying deficiencies:

- excessive false calls;
- missed discrepancies (off-location welds, porosity, lack of fusion);
- tendency to undersize the defects; and
- production suitability deficits.

Concluded in September 2002, this analysis resulted in down-selection to the two most promising technologies for further evaluation and possible prototype development in Phase 2.

Phase 2

The two technologies were found to differ in their capabilities for detecting certain weld discontinuities judged critical by the OEMs and a laser welding system provider. The two NDE systems, based on EMAT and ultrasonic technologies, performed comparably well (albeit on some differing discontinuities), and our conclusions indicated they required either additional development or reconfiguration to perform acceptably well in the OEM production environment. Ultimately, the ultrasonic technology was selected for Phase 2 in-depth evaluation, configuration, and build for the roof ditch weld application. See Figures 2 and 3 for roof ditch weld sample details.

Significant determinants in the decision to focus on the through-transmission ultrasonic technology were its

- demonstrated detection capabilities as they aligned with the production plant detection priorities (see Figure 4);
- demonstrated detection reliability, repeatability, and reproducibility during our testing regimes;
- ease of modification to incorporate additional capability using the pulse-echo ultrasonic technique;
- capability of being mounted on a robot arm or other automation;
- robustness of the device and its near-term prospects for commercialization;
- favorable detection cycle time compared to production cycle time;
- user interface friendliness and ease of training;
- motivation of the vendor to work with the automotive sector; and
- price feasibility for eventual plant purchasing.

Early in 2003, activities were directed at laying a sound statistical and experimental foundation for in-depth evaluations of the

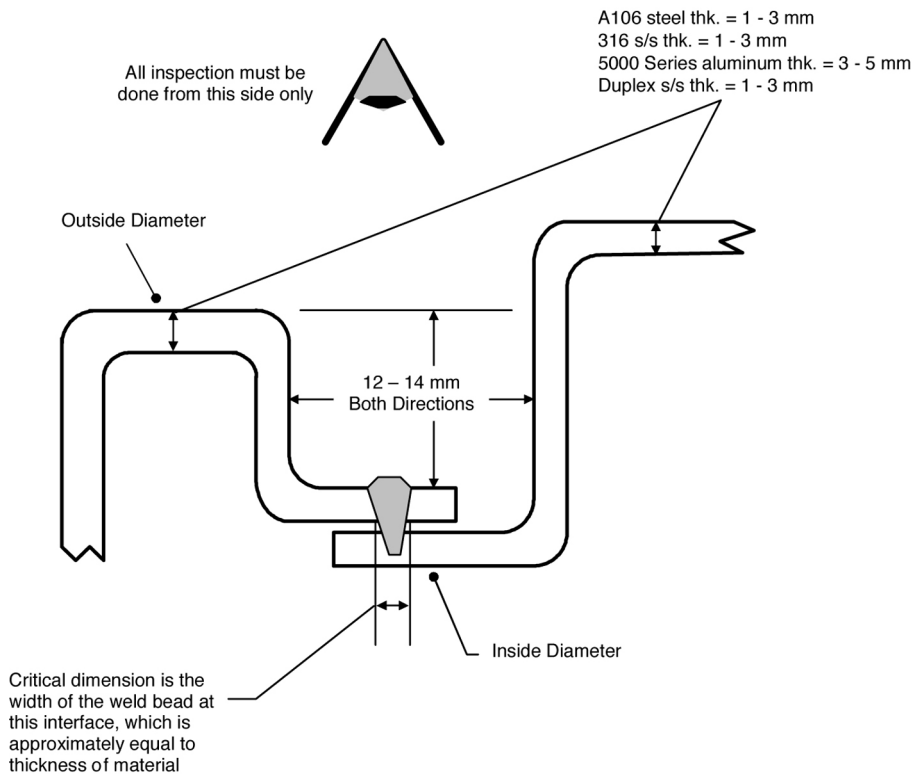

Figure 3. Laser-welded roof ditch joint details.

Discrepancy Detection Requirements

USAMP-AMD

Discrepancy Type	Detection Table			
	NDE-001 Defined	Plant Identified	Through-transmission Ultrasonics	Through-trans plus Pulse Echo
Lack of Fusion	?	?	?	?
Undersize Welds	?	?	?-	?
Underbead Cracks	?			?p*
Crater Cracks	?			?p
Longitudinal Cracks	?			?p
Transverse Cracks	?			?p
Missing Welds Skips	?	?	?	?
Pore, Porosity	?	?	?	?
Inclusions	?			?p
Burn-through & holes	?	?	?	?
Top Sheet Through-cut	?			?p
Undercut or Underfill	?			?p

*p means this detection capability may be possible with the addition of Pulse Echo capability to the UL2000.

Figure 4. Table comparing discrepancy detection requirements and through-transmission ultrasonic device capabilities with and without pulse-echo capability.

ultrasonic device. As part of this process, the AMD 303 team defined and executed:

- Engineering Specifications: NDE-001,
- NDE System Specifications, and
- Coupon Weld Specifications

The coupon test trials were conducted in strict adherence to a detailed test plan jointly defined by Ford, GM, and DaimlerChrysler NDE and statistics experts, in compliance with the specifications defined earlier. The test plan prescribes test regimes for

- calibration,
- RMS variation,
- baseline noise,
- gauge R&R, and
- surface roughness.

To test the device on coupons that are more closely aligned to the target production part than were the laboratory-built coupons in Phase 1, steel roof ditch coupons were fabricated using a production-equal welding cell in parallel with the OEM's laser-welding cell build program for the production plant. Steel roof ditch weld coupons containing known discrepancy sizes and two containing no discrepancies were created with a 4-kW Nd:YAG laser. Discrepancy types were limited to plant-defined priority types and discrepancy sizes ranged from 2.0 to 43.8 mm in length. In addition, lap-weld samples using 5000 series aluminum were fabricated in a production-equal laser welding cell that was configured for aluminum. These samples will be used in evaluating the performance of the through-transmission ultrasonic sensor on aluminum. The aluminum samples contain known defect lengths similar to steel coupons, and our preliminary tests would indicate that the signal obtained should be similar to that seen on the steel weld coupons.

Test trials were conducted on steel roof ditch coupons using a prototype through-transmission ultrasound sensor under the supervision of an independent auditor contracted by AMD 303 (Figure 5). As a result the project team can be assured that the testing regimes were followed as specified and can rely on the integrity of the resulting test data delivered to the team for analysis.

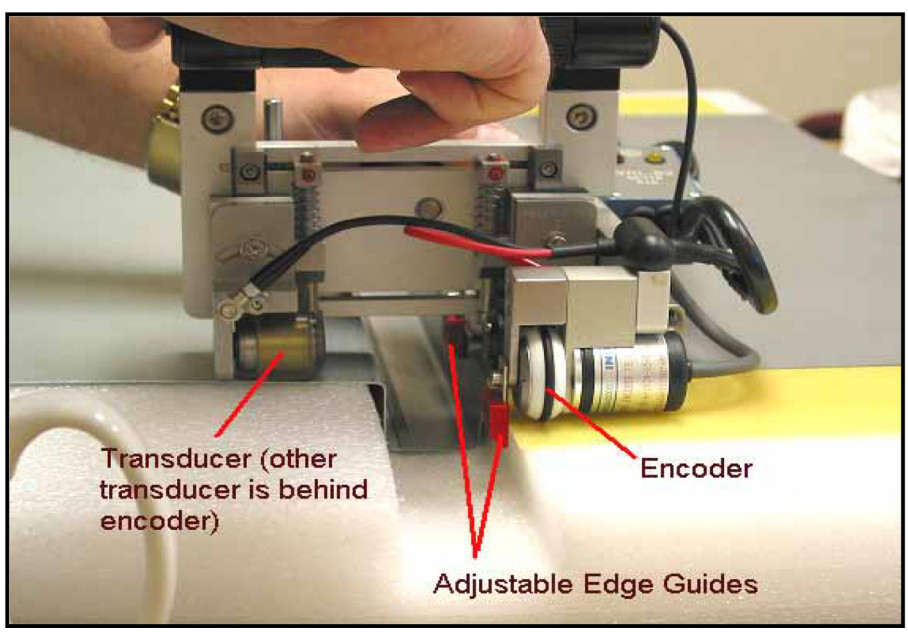

Figure 5. Through-transmission ultrasonic sensor prototype in test run over a steel roof ditch coupon.

Weld coupon validation testing was performed at GM on the steel and aluminum coupons using Immersion Ultrasonic pulse/echo "C-scans". C-scan results by sample are recorded on data sheets for every coupon/sample and later analyzed against the sensor's amplitude signature data outputs by sample upon completion of the testing. At the time of this report, analysis of the steel coupon testing results has been completed. Correlation of ultrasonic signature results with C-scan images can be graphically shown as done here in Figure 6.

Our analysis and findings for steel roof ditch coupons indicate that the through-transmission ultrasonic sensor has the following attributes:

- inspects 100% of weld (continuous),
- detects >99% of lack-of-fusion >8 mm,
- <1 in 10,000 of good welds called bad,
- scans at a speed of 600 mm/min (2 min/roof) at 1-mm resolution,
- monitors and provides feedback to operator if scanning speed is too fast,
- user friendly: red light/green light indicator,
- production-ready,
- can be automated, and
- system was tested with various operators, at various times, and proved to be user friendly and showed good reproducibility.

Testing of the ultrasonic sensor on the aluminum lap-weld samples and analysis of those results will be completed by calendar year end. Additionally, it is planned that production weld coupons will be cut from laser-welded roof ditch production parts and used to test the prototype being built for in-plant trials. Then, based on the analysis of its performance on the production part coupons, the through-transmission ultrasonic sensor will be placed in the target factory for plant tryout. Ultimately during tryout, the performance of the ultrasonic sensor will be correlated with production part tear-down data.

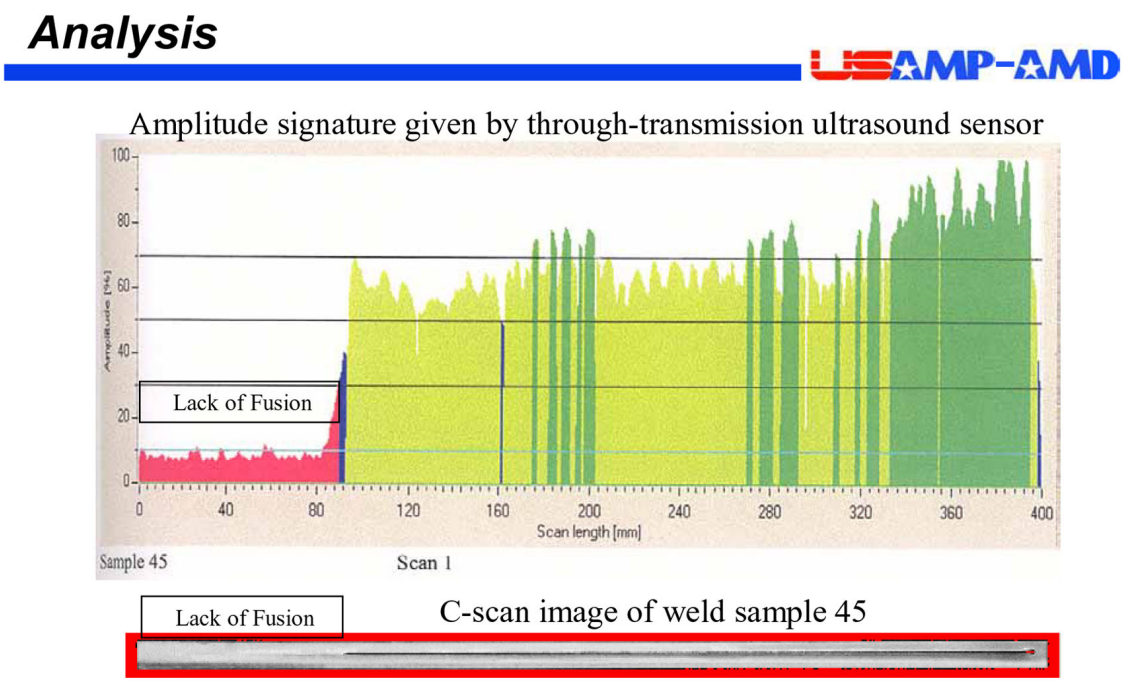

Figure 6. Correlation of the through-transmission ultrasound sensor results against the C-scan images with the area of weld discontinuity, lack of fusion, shown clearly in both images as annotated.

L. Inspection of Spot Welds Using an Ultrasonic Phased Array

Principal Investigator: Deborah Hopkins, Ph.D.
Lawrence Berkeley National Laboratory
1 Cyclotron Road, MS 46A-1123, Berkeley, CA 94720
(510) 486-4922; fax: (510) 486-4711; e-mail: dlhopkins@lbl.gov

Technology Area Development Manager: Joseph Carpenter
(202) 586-1022; fax: (202) 586-1600; e-mail: joseph.carpenter@ee.doe.gov
Field Technical Manager: Philip S. Sklad
(865) 574-5069; fax: (865) 576-4963; e-mail: skladps@ornl.gov

---

Contractor: Lawrence Berkeley National Laboratory
Contract No.: DE-AC03-765F0095

Objective

- Develop an ultrasonic phased-array system that is sufficiently fast, accurate, robust in manufacturing environments, and cost-effective to be suitable for on-line inspection of spot welds used in automotive components.

Approach

- Use state-of-the-art ultrasonic phased-array technology to develop a spot-weld inspection system that can be used by operators with minimal training. Commercially available hardware that has been used to date consists of an electronic controller, several linear probes, and a data-acquisition system.
- Deliver a fully integrated system suitable for deployment and testing in a production environment.
- Develop signal postprocessing algorithms.
- Demonstrate the system's ability to characterize welds with sufficient accuracy and repeatability, and integrate components into a portable system rugged enough for use in a production facility.
- Investigate coupling techniques that would allow existing probes, designed to be used in a water tank, to be used without having to immerse test specimens. A user interface will be required for plant deployment.

Accomplishments

- Evaluated the performance and limitations of existing ultrasonic phased-array systems.
- Conducted a series of laboratory experiments to evaluate the performance of 5-, 10- and 17-MHz phased-array probes for characterization of spot welds in galvanized steel.
- Developed signal-processing algorithms to distinguish between satisfactory, undersized, and defective welds.

Future Direction

- Conduct laboratory experiments to demonstrate the ability of phased-array systems to inspect spot welds with sufficient accuracy and repeatability for the full range of materials and joint configurations used in production.
- Develop automated classifiers to determine weld dimensions and identify defective welds, including cold welds.
- Identify and test coupling techniques that will allow existing probes to be used outside of a water tank.
- Develop a user interface in conjunction with end users to ensure ease of use and reporting of data in the most useful format for inspectors, welding engineers, and plant managers.
- Develop a fully integrated prototype system suitable for deployment and testing in a manufacturing plant.
- Perform large-scale testing and measurement system analysis.

Introduction

Lawrence Berkley National Laboratory (LBNL) previously evaluated the adequacy of commercially available ultrasonic systems for the inspection of spot welds. Although these systems are widely used in European automotive plants, they have not gained widespread acceptance in the United States for a myriad of reasons, including their dependence on trained operators to set system variables and the need to change probes frequently because of the wide range of materials and sheet thicknesses used in production vehicles. Plant managers emphasize the need for intuitive user interfaces and summary reports that can be customized for welding engineers and other plant personnel.

An impediment to implementing new approaches and technology that would advance the state of the art and enable nondestructive spot-weld inspection has been the difficulty of achieving consensus among industry partners on a technology and methodology of choice. LBNL strongly believes that a better approach is to develop platforms that add value immediately, minimize barriers to incorporating emerging technologies at a later date, and are as modular as possible so that they can be easily modified or adapted for new applications. Consistent with that model, the proposed work is to develop a prototype spot-weld inspection platform based on phased-array technology that will be implemented and tested in a manufacturing environment.

Signals from monoprobes, such as those used by the existing commercial systems, are an integrated response over an area, which depends on the diameter of the probe. For these systems, undersized welds and defects are detected by measuring signal amplitudes and comparing them to amplitude gates set by an operator. It has been demonstrated that ultrasonic techniques based only on measurements and evaluation of signal amplitude have poor sizing capabilities. In contrast, a phased-array system allows complex scanning of the acoustic beam through the weld that allows greater accuracy in sizing weld nuggets and provides improved flaw characterization capability.

The current project is making use of an R/D Tech ultrasonic phased-array system loaned to LBNL by the Ford Motor Company. The system consists of an electronic controller, a linear probe, and a data acquisition system. The system is being used to perform laboratory experiments designed to evaluate the performance of existing hardware, determine the optimal probe configuration, and to develop signal-

processing and weld-classification algorithms.

A phased array is a multielement piezoelectric device whose elements are individually excited by electronic pulses at programmed delay times. They have several advantages over conventional ultrasonic probes that derive from the ability to dynamically control the acoustic beam transmitted into the structure under examination. An electronic delay can be applied separately to each electronic channel when emitting and receiving the signal. These delay laws permit constructive and destructive interference of the acoustic wavefront transmitted into the structure, allowing predefined ultrasonic beams to be formed.

For the phased-array system commissioned by Ford, a 5-MHz probe was judged to be sufficient to inspect spot-welded sheets for a range of sheet thicknesses between 1.0 and 3.0 mm. An open question at the beginning of the current project was the adequacy of the 5-MHz probe for the full range of materials and sheet thicknesses currently used in production. Phased-array probes are available up to a frequency of 20 MHz. In general, relatively high-frequency probes provide better spatial resolution than lower frequency probes, but are more expensive.

Initial experiments conducted by Ford and R/D Tech were performed in a water tank, which is impractical for manufacturing applications. To make the transition from a laboratory system where samples are immersed in a water tank to a plant deployable system requires developing coupling strategies that ensure good transmission of ultrasonic waves into the part being inspected without being immersed in water. Experiments performed at LBNL demonstrate that a water-filled column confined by a thin membrane provides the necessary coupling to the part when used in conjunction with ultrasonic gel (Figure 1).

Because the welded test specimens are relatively thin, additional space between the probe and the sample is necessary to have an adequate vertical distance for the electronic beam forming that allows the acoustic energy to be focused at the interface between the sheets.

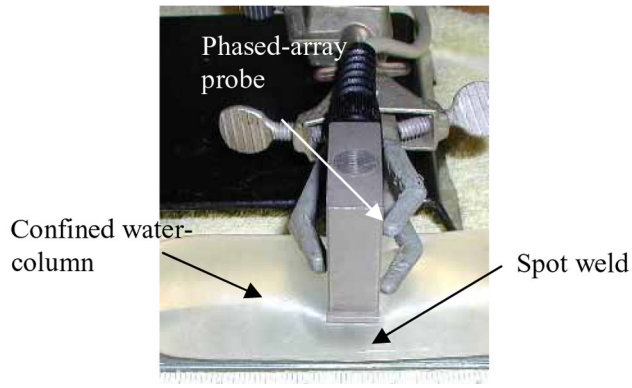

Figure 1. Inspection of spot welds using a phased-array probe with a confined water column for coupling.

Initial experiments were performed with a 5-MHz ultrasonic phased-array probe. The results of these experiments indicate that a central frequency of 5 MHz is too low to inspect welds in the thinnest metal sheets used in the automotive industry (thinner than one millimeter). Therefore, a new suite of experiments was carried out with probes with central frequencies of 10 and 17 MHz, and it is the results obtained with these probes that are presented here. The 10-MHz probe is a 32-element linear probe with a 0.4-mm pitch (distance between two successive elements); the 17-MHz is a 128-element focused probe with a focal distance of 12.5 mm and a pitch of 0.28 mm. Experiments were performed in a water tank or using a confined water column with coupling gel between the probe and the sample. The distance between the probe and samples was held constant at 12.5 mm for all experiments to allow the same focal law to be used. For the results presented here, the samples consisted of spot-welded strips made from 1.4-mm-thick galvanized mild-steel sheet metal.

Phased-Array Inspection Strategy

For the work performed to date, electronic scanning and focusing laws were

combined to inspect the spot welds. Scanning is performed by electronically translating the ultrasonic beam across the sample by firing a specified number of elements in sequence. Focusing is accomplished by applying symmetrical delay laws to the elements. For experiments performed with the 10-MHz probe, eight elements are used at a time, and the acoustic energy is focused at the interface between the two sheets. The beam is then electronically scanned across the weld in steps of one element; for example, elements 1 through 8 are excited to generate the first signal, elements 2 through 9 generate the second signal, and so forth, with elements 25 through 32 generating the last signal. For one spot weld, this results in a total of 25 independent signals.

Fourier-Based Signal Processing

The 25 signals recorded while scanning through the weld are analyzed in the time and frequency domains. Examples of A-scans and their Fourier transforms are shown in Figure 2 for the beam focused inside [2(*a*) and 2(*b*)] and outside the welded area [2(*c*) and 2(*d*)]. The signals displayed in Figures 2(*a*) and 2(*c*) are the moduli of the analytical signals. Note that the

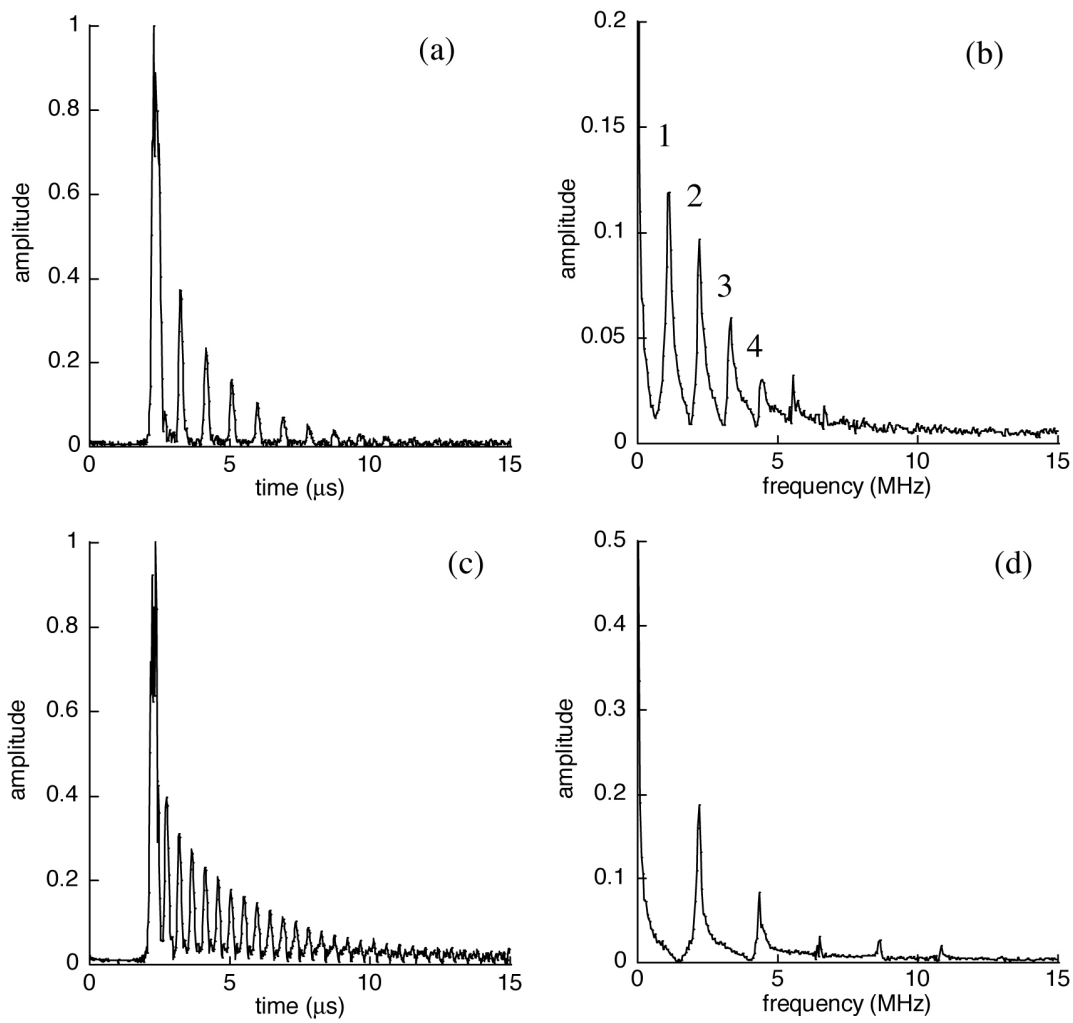

Figure 2. Signal in time recorded with a phased array when the ultrasonic waves are completely transmitted into the second sheet and reflected off the back surface (*a*), compared to signals recorded when waves are totally reflected off the interface between the two sheets (*c*), as occurs outside the welded area, and their respective FFTs [(*b*) and (*d*)].

metallurgical changes in the welded area do not cause a change in acoustic impedance large enough to create a noticeable reflection at the boundary of the weld nugget [see Figure 2(*a*)]. The Fast Fourier Transforms (FFTs) presented here are calculated starting from the first peak after the front-surface echo to minimize the influence of the surface reflection off the top sheet, which does not carry any information about the structure of the weld. The signals in the time domain can be mathematically described as the convolution, $s(t)$, of two functions:

$$s(t) = E(t) \otimes \left[III(t/T)\, e^{-\alpha t} \right] , \qquad (1)$$

where $E(t)$ is the modulus of the ultrasonic reflection; $III(t/T)$ is the Shah function, which is a series of Diracs; $e^{-\alpha t}$ accounts for attenuation; and the symbol $\otimes$ denotes convolution. T is the time interval between the Diracs in the Shah function and is equal to 4d/V for ultrasonic waves propagating into the second sheet, or 2d/V for ultrasonic waves reflected off the interface between the sheets, where d is the thickness of one sheet, and V is the longitudinal velocity in steel. The FFT of $s(t)$, $\tilde{S}(\omega)$, is given by Equation 2:

$$\tilde{S}(\omega) \propto \tilde{E}(\omega) \left[III(\omega T/2\pi) \otimes e^{-(\omega/\alpha)} \right] . \qquad (2)$$

The power spectrum can be described as a succession of peaks with approximately Gaussian decay. Figure 2 shows the signals, $s(t)$ [2(*a*) and 2(*c*)], and the power spectra, $\tilde{S}(\omega)$ [2(*b*) and 2(*d*)], for the two extreme cases of total transmission into the lower sheet and total reflection off the interface between the two sheets, respectively. A first approach to infer weld quality from these data is to identify how many consecutive signals among the 25 are similar to the characteristic signal for total transmission into the lower sheet.

However, fully characterizing the welded area is not as simple as identifying characteristic signals. When scanning at the boundaries of the weld nugget, the source, which is a focused line, begins to be longer than the weld nugget. Because the signal from the linear probe is an integrated response along the line, the signals recorded at the boundary of the weld nugget also contain ultrasonic waves reflected off the interface between the two sheets outside of the welded region; this leads to intermediary peaks in the time domain. The difficulty is in determining the magnitude of these reflections compared to the energy transmitted into the lower sheet through the weld.

As described above, existing techniques using monoprobes distinguish between several weld qualities by setting amplitude thresholds. Classification of the weld depends on whether the amplitude of these intermediary peaks is higher than a threshold set by the operator. This technique works well to a certain extent. However, consider the two signals shown in Figure 3 obtained using a phased array. In both cases, some of the intermediary peaks are higher than the threshold indicated by the horizontal line [3(*a*) and 3(*c*)]. In the first case [3(*a*)], the first intermediary peak has an amplitude higher than the threshold; the following intermediary peaks are quickly attenuated, and their amplitude falls into the noise level. In the second case [3(*c*)], several of the intermediary peaks have amplitudes higher than the threshold. Although these two signals are obviously different in this respect, a classifier based on any intermediary peaks exceeding the threshold would categorize these welds as being the same. This is a problem in general with "hard" classifiers. An alternative approach is to use Fourier analysis. The magnitude of the intermediary peaks is automatically captured in the frequency domain. The higher the energy contained in the intermediary peaks in the time domain, the lower the amplitude of the odd peaks [labeled 1 and 3 in Figure 2(*b*)] in the Fourier domain.

The ratio of the odd peaks to the even peaks is an indication of how much of the total energy is transmitted into the lower sheet.

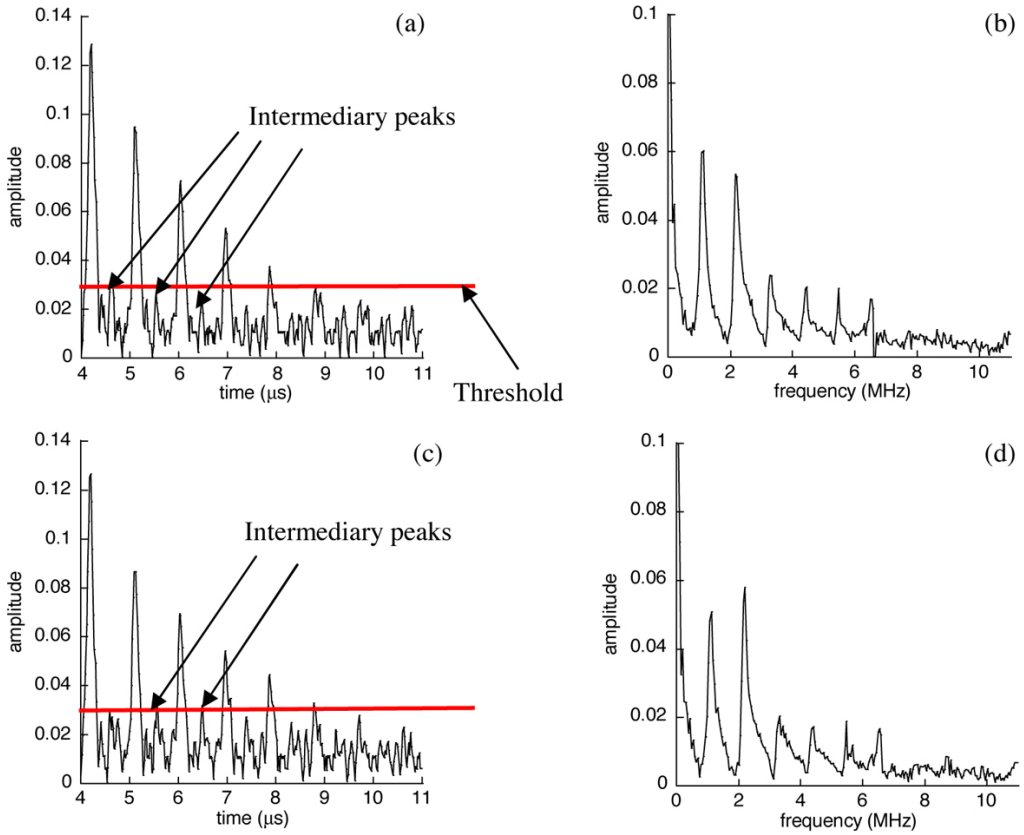

Figure 3. Two phased-array signals recorded when the ultrasonic waves are partially reflected off the interface between the two sheets [(*a*) and (*c*)], and their respective FFTs [(*b*) and (*d*)].

Results Obtained Using A 10-MHz Probe

The industry criterion for evaluating welds is based on the size of the weld button when the welded joint is peeled open. Welds are characterized as undersized when the weld-button diameter is between $2\sqrt{d}$ and $4\sqrt{d}$, and as defective when the diameter is smaller than $2\sqrt{d}$, where d is the thickness of a single sheet. As described above, peak ratios calculated in the Fourier domain are related to the amount of energy transmitted into the second sheet. Peak ratios were calculated for each of the 25 signals that comprise the scans of each weld. The values of the peak ratios, along with pictures of the peeled welds, are shown in Figure 4 for three spot welds with different qualities: satisfactory (a), undersized (b), and defective (c), respectively.

To determine the relationship between characteristic signals and button diameters on peeled samples, the first approach was to estimate the button diameter by counting how many successive signals had peak-ratio values above one, indicative of good transmission into the lower sheet. The distance between two successive signals corresponds approximately to the pitch of the probe, which is 0.4 mm for the 10-MHz probe. Button diameter can thus be estimated by multiplying the number of consecutive signals by the pitch of the probe. For the three welds pictured in Figure 4, the measured and estimated diameters are reported in Table 1.

Comparing the measured and estimated diameters for 150 spot welds indicates that the analysis of peaks in the Fourier domain gives a good indication of the weld quality

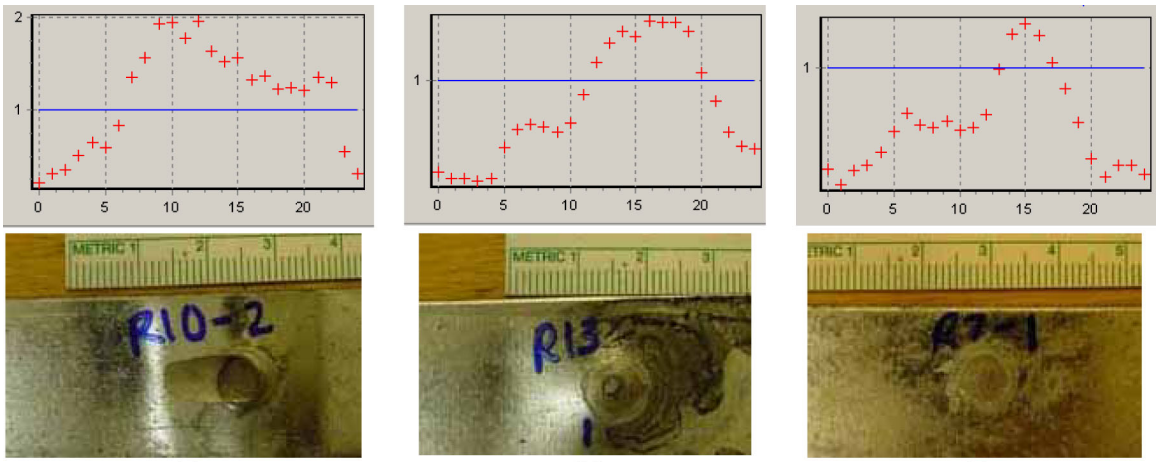

(a) *(b)* *(c)*

Figure 4. Fourier peak ratios (top row) and pictures of the peeled specimens (bottom row) for a satisfactory weld (*a*), an undersized weld (*b*) and a defective weld with no visible button (*c*).

Table 1. Measured and estimated weld-button diameters using only peak-ratio information

Measured diameter, mm	6.4	3.2	0
Estimated diameter, mm	6.0	2.8	1.2

but does not necessarily give an accurate value of the weld-button diameter. Work under way is focused on developing mathematical algorithms to estimate the size of the weld button from the ultrasonic data.

A challenge in identifying defective welds is that they are often characterized by solid, but weak contact between the two metal sheets that allows transmission of the ultrasonic waves into the lower sheet. This is the case for the cold weld pictured in [Figure 4(*c*)]. Other parameters, such as the ultrasonic-wave attenuation and the depth of the surface indentation, are currently being evaluated to determine if they are diagnostic parameters that can be used to provide additional information useful in defining evaluation criteria. Image-processing techniques are also being investigated.

As discussed in the previous section, one of the limitations of using an unfocused linear probe is that each signal is an integrated response along a line. A way around this problem is to use a focused probe. The experiments discussed above were repeated using a 17-MHz focused probe, and the results are discussed in the following section.

Results Obtained Using A 17-MHz Focused Probe

The experiments performed using the 17-MHz focused probe were made in a water-immersion tank because of the difficulty of coupling the focused probe to the confined water column. The probe is shaped to provide a natural focus at a depth of 12.5 mm. For each measurement, 64 out of 128 elements were used, 16 elements at a time. The elements were focused at the interface between the two sheets. The probe was mechanically scanned in the direction perpendicular to the direction of the electronic scan with a step size of 0.28 mm, which is equal to the pitch of the probe. A total of 3216 A-scans were recorded for each weld in approximately 1 s. The data were processed to measure the Fourier-peak ratios described above, as well as to obtain thickness, indentation, and attenuation measurements. The thickness measurement was made between two back-wall echoes assuming a velocity of 5.9 mm/µs.

Images illustrating the Fourier peak-ratio processing are shown in Figure 5 together

with pictures of the weld buttons. The circles superimposed on the Fourier peak-ratio images indicate the measured diameters of the weld buttons. The peak-ratio images [Figures 5(*c*) and 5(*e*)] allow satisfactory and undersized welds to be distinguished according to the size of the area where there is significant transmission of energy into the lower sheet. Although defective welds such as cold welds can result in a large area of ultrasonic transmission into the second sheet, the Fourier peak ratio [Figure 5(*f*)] indicates that the areas of high transmission are relatively sparse and dispersed compared to the well-defined and concentrated areas for the satisfactory and undersized welds.

Other criteria can be used to help distinguish weld quality, such as the indentations on the surface of the sheets caused by the welding electrodes. During the welding process, heat is created at the interface between the electrodes and the metal sheets, leaving indentations on the top and bottom surfaces. The depth of the indentation is

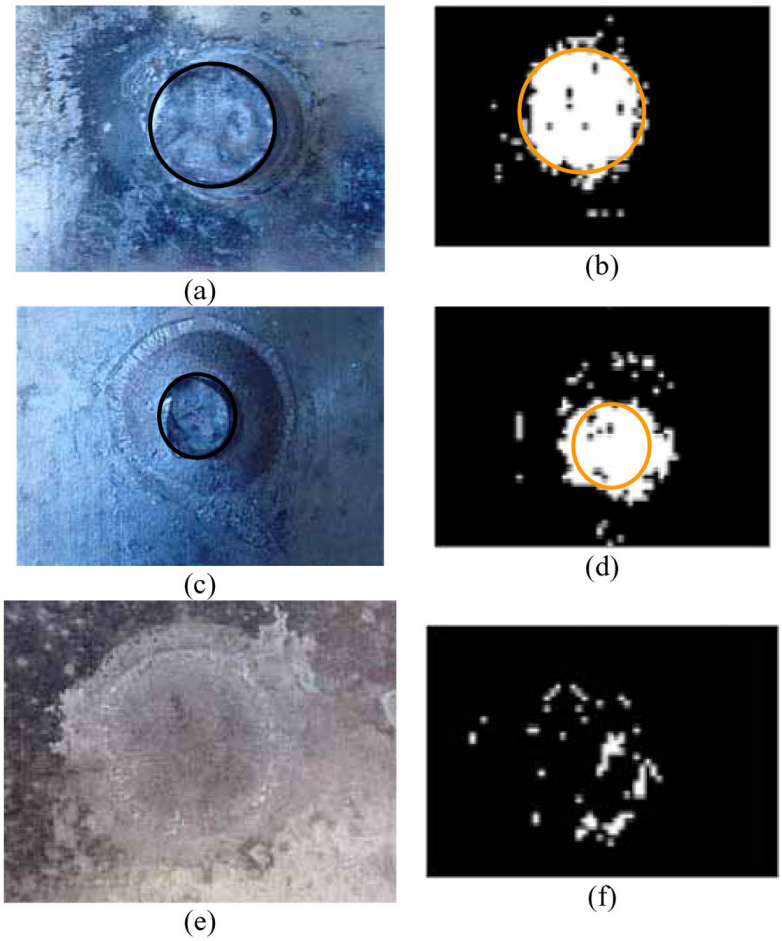

Figure 5. Pictures of the peeled weld buttons (left-hand column) for a satisfactory (*a*), an undersized (*c*) and a cold weld (*e*), and images displaying the Fourier peak ratios (right-hand column) for the same welds (*b*, *d*, *f*). The superimposed black circles on the pictures in the first two rows indicate the measured diameter of the weld button. The same circles are superimposed on the corresponding Fourier peak-ratio images for comparison.

often related to the quality of the weld because it is correlated to the heat created.

A model has been developed to describe the transmissivity of ultrasonic waves through a weld nugget. The model is being used to help understand the relationships between ultrasonic signals and weld quality, which is a necessary step in developing algorithms that will allow automated weld classification based on ultrasonic measurements.

Conclusions

Work to date demonstrates that characterization of spot welds is possible using ultrasonic phased-array technology. Phased arrays have several advantages over monoprobes, including the ability to perform high-resolution scans that greatly increase detection and characterization capabilities. They are also less sensitive to probe placement and provide the ability to inspect a wide array of welds with a single probe. The remaining research challenge is to develop, test, and refine the techniques so that they are suitable for large-scale manufacturing applications. This requires sensor development, integrated real-time diagnostic tools that operate at sufficient speed for assembly-line use, determination of resolution limits and the best diagnostic parameters for specific applications, and demonstration of robustness, accuracy, and cost-effectiveness under realistic operating conditions.

Publications

D. Türler, D. Hopkins, and F. Reverdy, "Nondestructive Evaluation of Spot Welds Using Acoustic and Thermographic Imaging Techniques," Society of Automotive Engineers, Paper No. 03M-160, 2003.

F. Reverdy and D. Hopkins, "Inspection of Spot Welds Using an Ultrasonic Phased Array," to be published in *Review of Progress in Quantitative Nondestructive Evaluation*, **23**, 2003.

D. Hopkins and F. Reverdy, "Model for Deformation, Stress and Contact at Interfaces, and Implications for Ultrasonic Measurements," to be published in *Review of Progress in Quantitative Nondestructive Evaluation*, **23**, 2003.

D. Hopkins, D. Türler, S. Nakagawa, K. Nihei, and G. Neau, "On-Line Nondestructive Inspection Techniques for Lightweight Automotive Structures," Society of Automotive Engineers, Paper No. 00FCC-124, 2000.

G. Neau, D. Hopkins, S. Nakagawa, and K. Nihei, "Complications of Using Resonance-Frequency Shifts to Detect Defective Joints," in *Review of Progress in Quantitative Nondestructive Evaluation*, **19**, D. O. Thompson and D. E. Chimenti, eds., 1999.

D. Türler, "Predicting the Geometry and Location of Defects in Adhesive and Spot-Welded Lap Joints Using Steady-State Thermographic Techniques," in *Proc. SPIE the International Society for Optical Engineering*, **3700**, D. H. LeMieux and J. R. Snell, Jr., eds., 1999.

D. Türler, D. Hopkins, S. Nakagawa, A. Valente, and K. Nihei, "Thermographic and Acoustic Imaging of Spot-Welded and Weld-Bonded Joints," *Review of Progress in Quantitative Nondestructive Evaluation*, **18**, D. O. Thompson and D. E. Chimenti, eds., 1999.

K. Nihei, S. Nakagawa, and D. Hopkins, "Defect Detection Using the Reverberant Wavefield," in *Review of Progress in Quantitative Nondestructive Evaluation*, **18**, D. O. Thompson and D. E. Chimenti, eds., 1999.

D. Hopkins, S. Nakagawa, K. Nihei, and D. Türler, "Imaging Flaws in Adhesive Joints Using Acoustic Techniques and Infrared Thermography," in *Review of Progress in Quantitative Nondestructive Evaluation*, **17**, D. O. Thompson and D. E. Chimenti, eds., 1998.

M. Technical Cost Modeling

Principal Investigator: Sujit Das
National Transportation Research Center
2360 Cherahala Boulevard
Knoxville, TN 37932-6472
(865) 946-1222; fax: (865) 946-1314; e-mail: dass@ornl.gov

Technology Area Development Manager: Joseph A. Carpenter
(202) 586-1022; fax: (202) 586-1600; e-mail: joseph.carpenter@ee.doe.gov
Field Technical Manager: Philip S. Sklad
(865) 574-5069; fax: (865) 576-4963; e-mail: skladps@ornl.gov

---

Contractor: Oak Ridge National Laboratory
Contract No.: DE-AC05-00OR22725

Objectives

- Address the economic viability of new and existing lightweight materials technologies.
- Develop technical cost models to estimate the cost of lightweight materials technologies.

Approach

- Address the economic viability of lightweight materials technologies supported by ALM Technology Area Development.
- Use cost modeling to estimate specific technology improvements and major cost drivers that are detrimental to the economic viability of these new technologies.
- Derive cost estimates based on a fair representation of the technical and economic parameters of each process step.
- Provide technical cost models and/or evaluations of the "realism" of cost projections of lightweight materials projects under consideration for ALM Technology Area Development funding.
- Examine technical cost models of lightweight materials technologies that include (but are not limited to) aluminum sheet; carbon fiber precursor and precursor processing methods; fiber-reinforced polymer composites; and methods of producing primary aluminum, magnesium, and titanium and magnesium alloys with adequate high-temperature properties for powertrain applications.

Accomplishments

- Assessed cost of primary magnesium production for automotive applications.
- Compared life-cycle energy impacts of automotive liftgate inner.
- Assessed comparative cost of alternative manufacturing technologies for the composite-intensive body-in-white (BIW) structures.
- Initiated a new task looking at the lightweighting opportunities for fuel cell vehicles.

Future Direction

- Estimate the lightweighting opportunity toward the early commercialization of fuel cell vehicles.
- Estimate the impacts of the Phase II ALM Technology Area Development for the 2000–2005 period and also aid in the formulation of midterm and long-term goals for the FreedomCAR Program.
- Continue to explore the economic viability of a carbon-fiber composite, intensive BIW part for Focal Project 3 by examining alternative competing manufacturing technologies by specific part type.
- Continue individual project-level cost modeling to identify specific technology improvements and major cost drivers that are detrimental to the economic viability of these technologies.

Cost Assessment of Primary Magnesium Production Technologies

Magnesium use in automobiles has been very limited and occurs mainly in die cast structural products. Even with magnesium's significant lightweighting potential, its cost remains one of the major obstacles in its widespread automotive use. The material cost is one of the key cost components, particularly important at high-production volumes. Primary magnesium currently costs about 1.8 times as much as aluminum, and there have been price swings during the past decade due to supply and demand imbalances. It is important that the competitive magnesium price for the substitution of materials such as aluminum and steel in automotive applications be estimated based on the material density as well as performance. While maintaining the design at equal stiffness, magnesium has maximum weight reduction potentials as high as 62% and 41% for the substitution of steel and aluminum, respectively. Compared to the 2001 magnesium price of $1.25/lb, the competitive magnesium price is estimated to be in the range of $0.78–$1.19/lb for a substitution of existing automotive aluminum components. Current and future production cost estimates (which include both full operating and capital costs) of magnesium were examined to determine the viability of existing production technologies for magnesium's commercial viability as a promising automotive material.

Although the full operating cost of primary magnesium is estimated to be cheaper using electrolytic plants than thermal reduction plants, total production cost is higher for electrolytic plants due to the capital-intensive nature of the process. The current production costs are estimated to be $1.41/lb and $1.31/lb, respectively. With planned electrolytic production capacity increases involving new plants and existing-plant capacity expansions, a substantial decline in the primary magnesium production cost is projected for the year 2009. For electrolytic and thermal reduction plants, the costs in 2009 are projected to be $1.14/lb and $1.27/lb. With these production cost projections and the existing depressed aluminum prices, magnesium will be competitive with aluminum only when the maximum weight reduction potential (i.e., about 40%) is possible in niche automotive applications. A further reduction in primary magnesium production cost may be necessary if aluminum prices do not recover in the future and for applications where this high rate of weight reduction may not be attainable either due to part design and/or manufacturing technology limitations. These production cost estimates further indicate that the average market price of magnesium in recent years has barely recovered its production cost from the depressed market. The industry may be

profitable with the significant, future reductions in projected production costs, strong demand, and consistent supply that precludes price swings observed during the past decade.

Life-Cycle Energy Impacts of Automotive Liftgate Inner

The life-cycle energy comparisons of cast aluminum vs conventional stamped steel liftgate inner used in a DaimlerChrysler minivan were completed. The low-pressure, permanent mold casting process with significantly low tooling cost developed for ultra large automotive components under the recently completed DOE project is used for the cast aluminum part. Using the best available aggregate life-cycle inventory data and a simple spreadsheet level of analysis, energy comparisons were made at both the single vehicle and fleet levels. Analyses were also done to examine how sensitive is the level of analysis (single product vs fleet level) and the assumptions behind each of the major baseline data to determine the most favorable materials with respect to life-cycle energy benefits.

As expected, life-cycle energy impacts of aluminum are lower than steel at a product level—energy savings are estimated to be 1.8 GJ/vehicle (or 1.7 million Btu) as shown in Figure 1. Assuming 10% and 20% penetration rates of this technology in the projected light-duty vehicles of sales of 18.27M and 19.91M by 2010 and 2020, respectively, by the Energy Information Administration, DOE, energy benefits for those years are estimated to be 3289 TJ (3.1 trillion Btu) and 7168 TJ (or 6.8 trillion Btu), respectively. The estimated energy benefits represent only a small fraction of total light-duty vehicles energy use of 17×10^{18} J (16.1×10^{15} Btu) in 2000. In addition to lower estimated energy savings, savings are achievable only after vehicles are retired and recycled. Most energy savings occur at the vehicle operation phase due to improved fuel economy from lightweighting, but the savings are not large

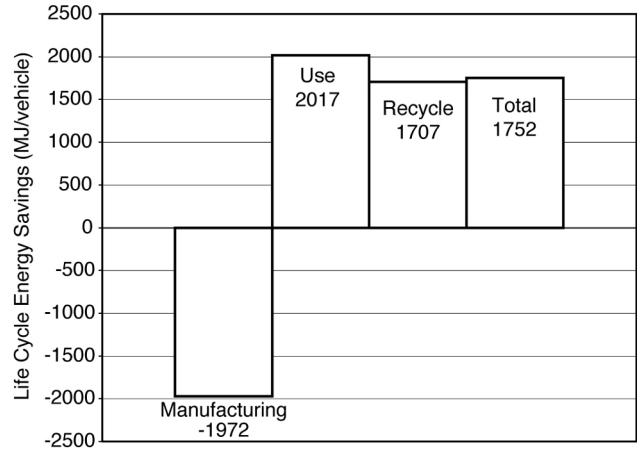

Figure 1. Life-Cycle Energy Savings of Cast Aluminum Liftgate Inner.

enough to annul the effects of high manufacturing energy use. In the first generation, the energy benefits are realized only after 13 years of vehicle operation (close to the standard 14-year vehicle life assumed in the analysis). At the vehicle fleet level with a flat growth rate, it takes longer—about 21 years—for aluminum to achieve life-cycle equivalence with steel.

As with any analysis, results in this study are sensitive to the assumptions made, particularly those regarding the aluminum substitution factor, manufacturing energy, aluminum recycling, and operational fuel efficiency. The number of years aluminum needs to achieve equivalence with steel is quite sensitive to aluminum manufacturing energy and fuel economy. A 25% decrease in aluminum manufacturing energy, which could result from changed assumptions regarding the manufacturing process efficiency and/or recycled content, will change the point at which aluminum achieves life-cycle equivalence with steel by about 6 and 7 years at the vehicle and fleet level, respectively. A 0.30% improvement in fuel economy (compared to 0.20% improvement under the base case), resulting from different fuel efficiency improvement factors due to vehicle weight reduction and/or secondary weight savings, would significantly lower the number from 13 years to 6 years when the benefits can be realized at the vehicle level.

The energy benefits increase significantly with a higher weight reduction potential of cast aluminum liftgate inner (i.e., 35% instead of 21% under the base case), the life-cycle equivalence point at the vehicle level reduces from 13 years to 4 years. The effect of an improvement in the aluminum recycling efficiency is felt only at the vehicle fleet level, by achieving the life equivalence point 2 years earlier than under the base case. Due to relatively low manufacturing energy of steel, results of the sensitivity analysis were not that significant. Because energy benefits at the vehicle fleet level take significantly higher number of years, any parameter that increases the energy usage raises further questions to the viability of aluminum substitution from an energy perspective.

As the race toward the lightweighting by the steel industry continues, a systems approach, instead of part-to-part comparison, is more appropriate in the determination of viability of aluminum substitution from an energy perspective. The extent of lightweighting that aluminum can provide with improved vehicle designs and increasing the recycled content of aluminum will be critical determiners of aluminum's life-cycle benefits. Lastly, a fleet level analysis is appropriate to provide a better indication of the relative environmental merits of alternative products designs and helps in the prediction of time when benefits are realized.

Comparative Cost Assessment of Alternative Carbon-Fiber-Reinforced Composite BIW Manufacturing Technologies

This task continues to focus on the relative cost-effectiveness of competing carbon-fiber-reinforced, polymer composite, BIW manufacturing technologies. The part under consideration is an upper dash panel weighing about 1.9 kg. Of a total of six competing manufacturing technologies under consideration, three are based on the compression molding and long fiber injection processes. The latter process is currently being used by Bayer AG, Dow Chemical Company, and Huntsman. Two carbon-fiber sheet molding compound (SMC) materials for the compression molding process considered are Quantum composites and HexMC by Hexcel Corporation. The former carbon-fiber, sheet molding, SMC material has recently been used in Dodge Viper for the windshield surround, inner door panels, and fender support system applications. Of the three remaining manufacturing technologies, fabric preforms and prepregs besides the programmable powder perform (P4)/structural reaction injection molding process are being considered.

Lightweighting Opportunities for Fuel Cell Vehicles

This ongoing task was initiated to examine the lightweighting opportunities for midsize passenger, direct hydrogen, fuel cell vehicles and to consider whether this would facilitate the early commercialization of fuel cell vehicles. This task will focus on the lightweighting of body structures of a midsize vehicle. Because weight and cost implications are significant not only at this component level but also at the powertrain level and, subsequently, the vehicle level as well, the vehicle level is considered here for the analysis. The current fuel cell powertrain is heavy and expensive, so it is interesting to examine whether at the expense of lightweight BIW materials alone, the fuel cell vehicle penetration rate can be enhanced. The commercial viability of fuel cell vehicles is examined in the context of several advanced lightweight BIW material options alone, as well as in combination with improvements in the fuel cell powertrain. A detailed 35+ vehicle components level automotive system cost model is being used to estimate the lightweighting opportunities for fuel cell vehicles.

N. Springback Compensation in Advanced Sheet Forming Materials

SCP Project Leader: Dr. Chung-Yeh Sa
Technical Manager—Forming & CAE Integration
Global Performance Integration, EPMS
General Motors
6440 E. 12 Mile Rd.,
Warren, MI 48092-3972
(586) 947-0660; fax: (586) 986-8722;
e-mail: chung-yeh.sa@gm.com

Project Technical Chair: Dr. Edmund Chu
Alcoa
100 Technical Drive
Alcoa Center, PA 15069
(724) 337-3853; fax: (724) 337-2255;
e-mail: Edmund.chu@alcoa.com

Contacts

Mr. Laurent Chappuis
Ford Motor Company
VOGO, P.O. Box 1586, Room C-290/B6
Dearborn, MI 48121
(313) 322-4470; fax: (313) 322-4359;
e-mail: lchappui@ford.com

Dr. Manish Mehta, Project Administrator
TRC—NCMS
3025 Boardwalk Dr
Ann Arbor, MI 48108
(734) 995-4938; (734) 995-1150;
e-mail: manishm@ncms.org

Mr. Li Zhang
DaimlerChrysler
CIMS 482-60-15
800 Chrysler Drive
Auburn Hills, MI 48326
(248) 576-3117; fax: (248) 944-6235;
e-mail: lz@daimlerchrysler.com

Dr. Chuan-Tao Wang
General Motors
Mc: 483-520-276
2000 Centerpoint Parkway
Pontiac, MI 48341
(248) 753-4504; fax: (248)753-5006
e-mail: chuan-tao.wang@gm.com

Technology Area Development Manager: Joseph Carpenter
(202) 586-1022; fax: (202) 586-1600; e-mail: joseph.carpenter@ee.doe.gov
Field Technical Manager: Philip S. Sklad
(865) 574-5069; fax: (865) 576-4963; e-mail: skladps@ornl.gov

---

Contractor: U.S. Automotive Materials Partnership
Contract No.: DE-FC05-02OR22910

Objective

- Eliminate die re-cuts and thereby realize significant reductions in the lead time and cost involved in die construction and production tryout.
- Develop a robust, integrated software package, which is capable of accurately and reliably generating optimized die surfaces that compensate for part springback while maintaining formability.
- Have ZERO die re-cuts when forming panels with advanced sheet metals, such as high-strength steel (HSS) and aluminum.
- Demonstrate concept feasibility with
  - a graphical user interface (GUI) tool that can modify the die mesh locally or globally based on predicted springback results and user-specified morphing criteria; and

— numerical simulation modeling results showing minimized deviation from nominal for a part using a newly developed compensation strategy.

Accomplishments

- Implemented new finite-element method (FEM) (manual compensation) code and collaboratively performed iterations to test mesh-based, iterative-based analytic (manual) die compensation techniques and prototype software released by LSTC for porting to common workstations.
- Trained vendor staff and trouble-shooted with the SCP team users to implement and run the new SCP code on a wide variety of materials and geometries for evaluation within the automotive part design/analysis environment.
- Developed geometric compensation method and a software module delivered by ETA to the project team, with GUI pre-/post-processors implemented in DYNAFORM. The software was developed exclusively for use by the U.S. Automotive Materials Partnership (AMP) team.
- Tested manually the robustness of the developed compensation strategies and compared against production part die faces with numerical data developed by the project team (see attached selected examples—each original equipment manufacturer (OEM) tested the code on at least two component geometries):
  - GM: Springback compensation of a DP600 steel rail
  - Ford: Springback compensation of a 6111-T4 aluminum decklid
  - DCX/DCAG: Springback compensation of a HSS load beam outer
  - In addition, T. K. Budd studied a fender outer for an EDDS steel sheet part which has a 0.75-mm thickness and predicted springback of 1.25 mm during draw (before trim); they also developed benchmark information for performing tool re-cuts.
- For all parts, the predicted springback at critical measurement locations on the compensated virtual production dies was within specified tolerance of ±2 mm.

Future Direction

- Submit a proposal to USAMP AMD for research into the Technical Feasibility Phase 2 of the SCP project.
- Demonstrate and validate the new compensation code technology by performing die re-cuts to the numerically compensated shape, with panel tryouts and measurement comparisons.

Introduction

Current manual die compensation is costly and time-consuming, largely trial-and-error. A major gap exists between a "proposed die mesh" and "machinable die face," resulting in countless hours of mesh-to-computer-aided design (CAD) surface smoothing using repetitive human intervention and checking. An average-size stamping die for steel panels requires up to 2 re-cuts; a die for aluminum panels takes up to 4 re-cuts. A typical die re-cut operation (NC Program, machining, checking, benching, spotting) is very costly, requiring several weeks. OEM costs are far higher when die handling, labor, tryout, and panel measurement costs and time are factored, not to mention the overall loss of productivity.

Thus, when working with the newer HSSs and aluminum alloys, the computer-aided engineering (CAE) analysts need a robust technique for generating the new binder and knowledge-based modeling techniques to avoid back draft and perform selective local compensation. The AMD 311 SCP project offers a significant opportunity to compress lead time and productivity in stamping tool development and tryout.

Progress

The technical approach consisted of collaboratively customizing and evaluating commercial FEM software, that would automatically (a) analytically predict, and (b) recommend optimized tool geometry (FEA mesh and CAD surface) and the stamping process, capable of producing panels with the desired final shape after springback. The project utilized the results and deliverables of the completed Springback Predictability Project (SPP, funded by NIST-ATP in 1995–2000), which are incorporated in LS-DYNA, a commercial FEA package available from Livermore Software Technology Corporation (LSTC), a leading software vendor.

Each OEM team member and industrial supplier company collaboratively exercised the FEM code (with the assistance of the software vendors) on at least two (per company) selected automotive sheet panels of HSS and aluminum, and numerically simulated the predicted panel geometry after springback, comparing it with the compensated virtual die.

The results and team progress were tracked and reported via monthly team meetings held at USCAR, augmented by video/teleconferencing and electronic collaboration tools. OEM team members contributed their knowledge of advanced die engineering and massive parallel processing.

The SCP Concept Feasibility Phase 1 project has demonstrated potential to create technology for leadership of the USAMP team that will enable them to

- reduce lead time and cost for hard tools up to 50% in comparison to traditional (manual) approaches;
- accelerate application of advanced metals for weight reduction, such as HSS, advanced aluminum;
- extended project findings in future to magnesium and titanium sheet forming; and
- promote rapid development and implementation of innovative product designs in new vehicles.

Conclusion

The SCP project has demonstrated proof-of-concept with new die compensation software that will help accelerate applications of advanced metals for weight reduction by reducing tool modification costs and lead-time in comparison to traditional approaches. It will also demonstrate new collaboration paradigms in the industry by integrating the product, process and tool design functions.

Future Plans (to be addressed in Phase 2)

In the proposed Technical Feasibility Phase, the technical emphasis of software developments will be on the following areas (as identified from Phase 1 code trials):

- development and evaluation of several additional promising analytic compensation strategies, with down-selection to one method for full-scale code implementation and automation, and its demonstration for a broader variety of parts;
- localized wrinkling must be identified to user criteria and removed before die compensation; and
- the new method and software need to be validated by die recuts to compensated shape and panel forming trials.

Example Automotive Panels Studied in AMD 311 Phase 1

DCX/DCAG HSS Load Beam Outer:

- This is a 1.4-mm gauge HSS 50-ksi galvanneal steel alloy sheet part in production at DaimlerChrysler (Figure 1).
- The initial process FEM simulations indicated that significant local wrinkles and waviness would occur in several locations.
- Application of the new LS-DYNA SCP code indicated that with the first iteration compensation, it was possible to bring the part within the specified ±2-mm tolerance specification.
- OEM conducted simulation and compensated 90% of die geometry to within 0.5 mm.
- It was discovered that local springback deviations greater than 0.5 mm are caused by part wrinkling during draw forming.
- DCX learned that one must minimize wrinkling in the draw die before next iterations are performed.

GM Steel Rail

- Material used was 1.8-mm gauge DP600 dual-phase steel (Figure 2).
- GM used two strategies and performed numerous iterations in each trial to identify issues and gaps for the manual compensation methods.
- All sections were successfully compensated to within 0.5 mm.

Ford Aluminum Decklid

- Material used was 0.9-mm gauge 6111-T4 aluminum sheet (Figure 3).
- The emphasis of the compensation strategy was to evaluate ten different smoothing techniques to generate the compensated die.

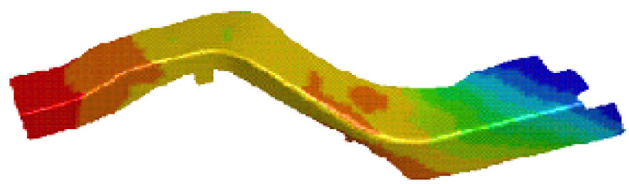

Figure 2. GM steel rail.

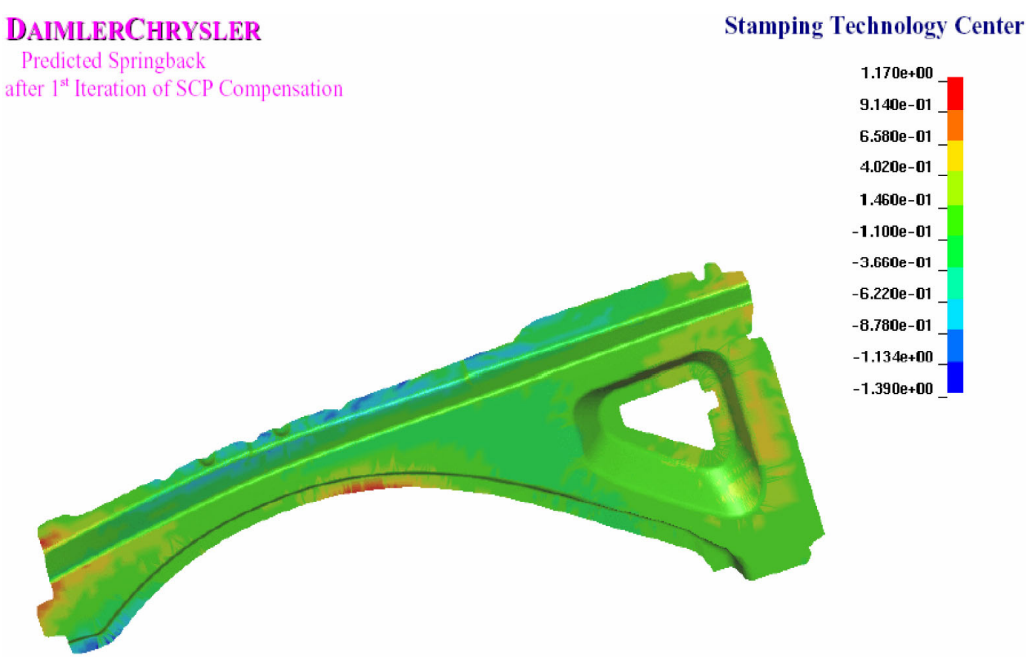

Figure 1. HSS load beam outer.

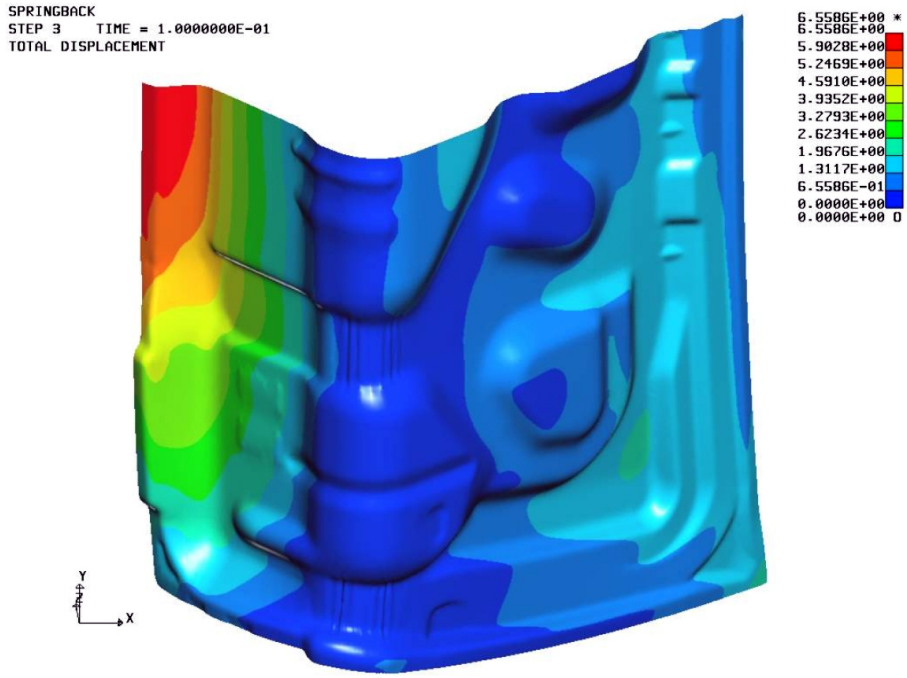

Figure 3. Ford aluminum decklid.

- Good compensated part shape was achieved after one iteration with the right choice of the smoothing method.

Project Team Members

OEM Team: DaimlerChrysler (Auburn Hills and Stuttgart Technical Centers), Ford Motor Company and Volvo Division, General Motors Metal Forming Division (GM-MFD).

Participating Suppliers: (in-kind contributions and project technical guidance): Alcoa, TK Budd, U.S. Steel.

Software Vendors: (under USAMP subcontract for DOE funds): Engineering Technology Associates (ETA), Livermore Software Technology Corporation (LSTC).

8. HIGH-STRENGTH STEELS

A. Modeling of High-Strain-Rate Deformation of Steel Structures

Principal Investigator: Srdan Simunovic
Oak Ridge National Laboratory
P.O. Box 2008, MS 6164
Oak Ridge, TN 37831-6359
(865) 241-3863; fax: (865) 574-7463; e-mail: simunovics@ornl.gov

Technology Area Development Manager: Joseph A. Carpenter
(202) 586-1022; fax: (202) 586-1600; e-mail: joseph.carpenter@ee.doe.gov
Field Technical Manager: Philip S. Sklad
(865) 574-5069; fax: (865) 576-4963; e-mail: skladps@ornl.gov

---

Contractor: Oak Ridge National Laboratory
Contract No.: DE-AC05-00OR22725

Objective

- Develop numerical modeling guidelines to realistically assess the influence that the properties of strain-rate-dependent materials exert in crashworthiness computations.

Approach

- Model dynamic loading problems using diverse combinations of modeling approaches (submodels) that are essential in describing strain rate sensitivity in computational simulations. Submodels examined include finite-element method (FEM) formulations, constitutive materials models, material properties under different strain rates and loading conditions, contact conditions, etc, as well as material property changes caused by component processing.

Accomplishments

- Investigated effects of stress transients for high-strength steel (HSS) and their effects on peak impact force.
- Developed experimental setup for new crashworthiness characterization test based on parallel-plates buckling (test under way at the University of Dayton Research Institute).
- Developed program for analysis of history of strain rate calculations.
- Analyzed history of strain rates in unsymmetric crushing.
- Determined modeling effects on strain rate history in unsymmetric crushing.
- Modeled effects of stress and strain transients on initial impact force.
- Developed framework for modeling stress transients.
- Reviewed literature on Bake Hardening (BH) and proposed a model for FEM analysis.
- Reviewed literature on fracture and damage in impact of HSS.

Future Direction

- Develop new constitutive models for HSS to account for strain rate history and transients.
- Develop new constitutive models for modeling of damage and tearing of HSS during impact.
- Conduct and analyze crush experiments (parallel-plates and tube crush).
- Develop experimental guidelines based on the two tests above.
- Determine optimal FEM formulations for modeling of crushing of rectangular tubes.
- Develop experimental program for crushing of rectangular tubes.
- Develop modeling guidelines rectangular tubes.

Introduction

The objective of the project is to develop numerical modeling guidelines for strain-rate-dependent materials in crashworthiness computations. The scope of the project is to study specific structural problems in automotive impact, develop new experimental and analytical techniques for characterization of strain rate sensitivity of HSS and modeling of complex strain and strain rate histories. The dynamic loading problems are modeled using diverse combinations of modeling approaches (submodels) that are essential in describing strain rate sensitivity in computational simulations. Submodels to be examined include finite-element formulations, constitutive materials models, contact conditions, etc. The trends, influences, and direct effects of employed modeling techniques will be identified and documented. The relative significance of employed sub-models is established, particularly in relation to the strain rate effect resulting from the material constitutive models.

The research project is conducted as a team effort between the ORNL and the Auto/Steel Partnership Strain Rate Characterization Group.

FY 2003 Work Summary

Several important research milestones were completed during FY 2003. First, we investigated modeling of impact of symmetric HSS structures under unsymmetric crushing and developed computer programs for analysis of strain rate histories. The experimental results from drop tower tests were used for comparison with models. The material models were developed based on coupon-level experiments in different experimental apparatus and were used for tube crush simulations. The differences in characteristic material response as a function of strain rate between different steel types were investigated with an objective to develop a unifying approach for HSS constitutive material modeling. The material modeling effects such as strain rate formulations, element formulations, mesh density, and stress transients as function of strain rates and strain rate histories were investigated for their effect on the simulated impact response and compared with experimental results. Modeling guidelines were developed in terms of modifications of constitutive material models and analysis options that yield best agreement with experiments and have sound physical foundation. BH has been identified as an important strengthening mechanism that will be exploited in future car designs with new HSS. Therefore, review of BH literature has been conducted, and a new model has been proposed for incorporation of BH effect in impact simulations.

The new research findings were presented at the 2003 SAE World Congress[1] and United States Congress on Computational Mechanics.[2] The developed models, experimental data and presentations are available

at the project Web site: http://www-cms.ornl.gov/asp. Please contact Srdan Simunovic, simunovcs@ornl.gov for access.

In the following sections, significant research findings during FY 2003 will be described and discussed in the context of their relevance for development of more accurate models for impact simulations.

Strain Rate Sensitivity Modeling of HSS for Unsymmetric Crushing

Strain rate sensitivity of HSS has been mostly analyzed in the context of symmetric deformation of axisymmetric structures. The symmetric axial crushing of tubular specimens has been used as a basic model for crashworthiness analysis in many analytical, semianalytical, and numerical models.[3] The research in the previous year of the project has investigated the history of strain rates during the axisymmetric impact simulations. We have investigated the effects of modeling approaches on strain rate history and the consequence of the modeling assumptions on the required experimental program to support the modeling. The research established for the first time the relation between the FEM modeling approaches and the strain rate history calculations at the level of computational time step. This relation is important because all the strain rate calculations in constitutive models and effects occur at this very fine time scale that is usually several orders of magnitude smaller than the time scale that is usually used to analyze the structural response.

Strain rate history in unsymmetric crush is more difficult to analyze because we cannot make simplifying assumptions of symmetry. For example, in simulation of axially symmetric crushing of circular tubes, symmetry reduces the dimensionality in the problem so that it is sufficient to analyze only a longitudinal strip of a circular tube. When the circular tube crushes in unsymmetric mode, such simplification is not possible. The consequence is that we now have to analyze large areas of the structure, both in longitudinal and hoop direction, and investigate the three-dimensional features of rate history. To enable the strain history analysis, we have developed a computer program that extracts the data from the simulation during its execution, processes it, and stores the process data in a compressed form. Such an approach allows us to reduce the data size by several orders of magnitude and still preserve the needed information. The developed program can also be used in general FEM impact simulation using LS-DYNA3D[4] for detailed investigation of important structural areas that are experiencing complex strain rate histories.

Tube Crush Experiments in Drop Tower

In this project, HSS materials HSLA350 and DP600 were selected for drop tower experiments to investigate the accuracy of the constitutive models based on a piecewise linear plasticity model and various modeling approaches. A test for HSLA350 steel configuration and the final deformed shape are shown in Figures 1 and 2. Force, accelerations, and high-speed photographs are recorded during the experiment.

Force-time traces for two HSLA350 specimens are shown in Figure 3.

The force-time diagram shows the characteristic peak followed by the force plateau associated with progressive tube folding.

Figure 1. Test configuration for HSLA350.

Figure 2. HSLA350 tube at the end of experiment.

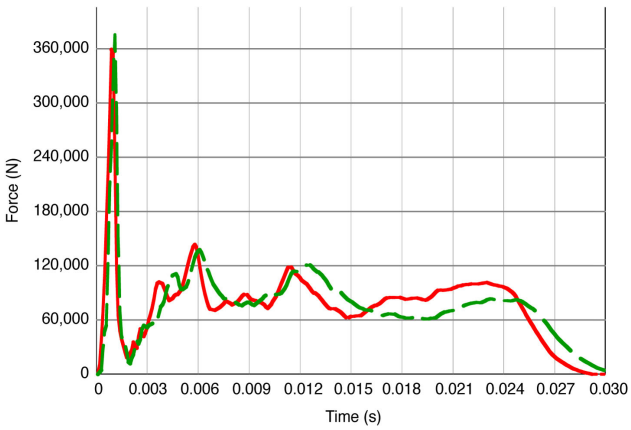

Figure 3. Force history for HSLA350 tubes.

The HSLA350 tubes deformed in an unsymmetric, triangular pattern. The anti-symmetric modes are principal mechanisms of deformation for the tube dimensions and the ranges of imperfections considered.

Impact Simulations and Strain Rate History

Drop tower experiments were simulated using the strain rate sensitive material models described in the previous section. Due to the collapse mode (Figure 4), it is necessary to select a relatively large representative patch of elements to analyze. The selected domain for strain rate history analysis is marked in lighter color in Figure 5. This patch of elements contains a corner of the polygonal collapse pattern for the rate

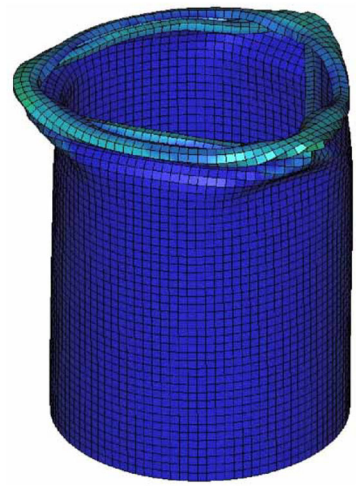

Figure 4. Unsymmetric axial collapse mode of circular tube.

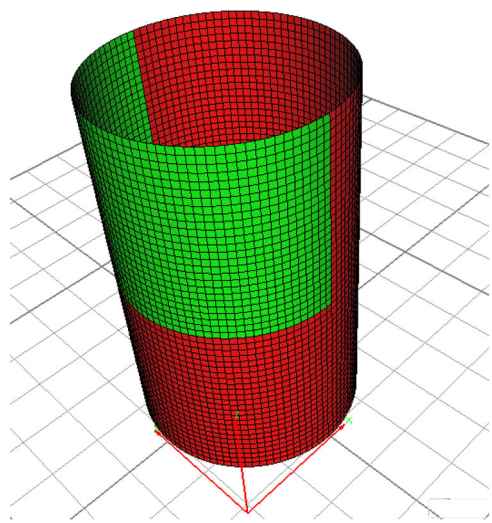

Figure 5. Elements selected for strain rate history analysis.

history. The strain and strain rate history is analyzed for different modeling approaches, and the results were used for determining guidelines for modeling approaches to automotive impact simulations.

Figures 6 and 7 show characteristic results from the simulations. In these figures, the selected domain is unwrapped into a flat surface and strain rates for different time instances are plotted normal to it. Figures depict the sequence of strain rate distributions for increasing time steps. The impact occurs at the NW side of the mesh in the

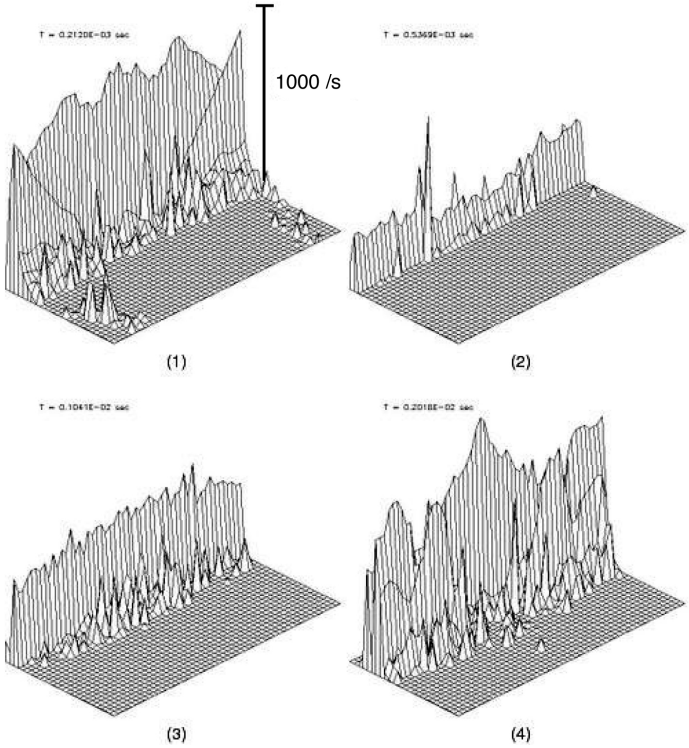

Figure 6. Strain rate history for material model based on total strain rate.

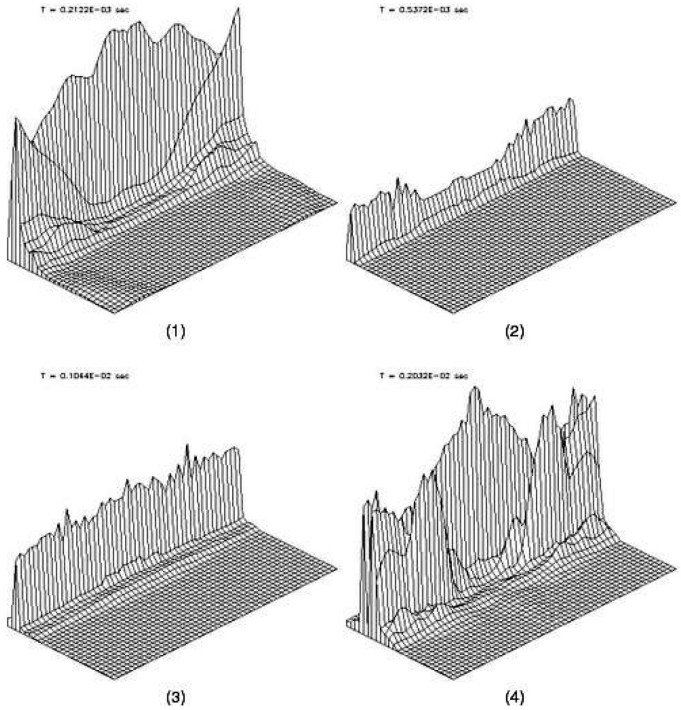

Figure 7. Strain rate history for material model based on plastic strain rate.

image, and rates propagate with time along the tube length, that is, in the SE direction. The white arrow in the figure denotes strain rate magnitude of 1000/s. The material model employed for the analysis is based on total strain rate formulation. The strain rate history in this case exhibits significant oscillations. The elements remain in an elastic state for prolonged periods of time, and then the plastic deformation occurs in bursts that have a very high strain rate that regularly exceed 10000/s.

On the other hand, when the strain rate sensitivity is based on plastic strain rate, the rate history is much smoother with gradual temporal and spatial transitions as can be seen in Figure 7.

In this case, the strain rates rarely reach rates of 1000/s and are well within the range of the available experimental data. The significant implication for modeling is that the material models where strain rate sensitivity is based on total strain rate do not take the advantage of the material data that were gathered with significant expense. When the total rate formulation is used for modeling rate sensitivity, much simpler models can be used that will yield essentially same results. The importance of the cut-off strain rate is also exacerbated because the resulting stresses for the rates exceeding the maximum available rate in the model will be scaled back to those provided for the maximum rate. A discussion about the physical aspects of different modeling approaches is beyond the scope of this document.

A journal publication is under preparation and will be available on the project Web site. Further analysis and discussion on the physical and modeling aspects of the problem are subjects of the journal publication that is in preparation.

The Effect of Stress Transients on Impact Peak Force

Impact experiments with tubes have shown a pronounced force peak for some types of steels that cannot be accounted for with existing strain rate dependent constitutive models. These same steels in coupon-level strain rate experiments show pronounced stress transients with increasing strain rate. These transients are usually discarded in development of constitutive models because presence of softening regions in stress-strain relation brings about significant problems with FEM formulation and uniqueness of the results. However, when strain rate sensitivity is present in the model, and when it is evaluated in certain fashion, these problems are to a large extent eliminated, and stress transients during initial impact and strain rate variations can be taken into account. Figure 8 shows modified stress-strain data where stress transients based on experimental data were added from rate 0.1/s.

When this model is used for simulation of tube crush, an excellent agreement with the initial force peak is found. The comparison of the simulation and the model is shown in Figure 9.

The softening regions of the stress-strain curves do not severely affect the uniqueness of the solution if the material model is based on plastic strain rate. Together with strain rate sensitivity this introduces a characteristic length scale, stabilizes the model evaluation, and alleviates spurious mesh sensitivity.

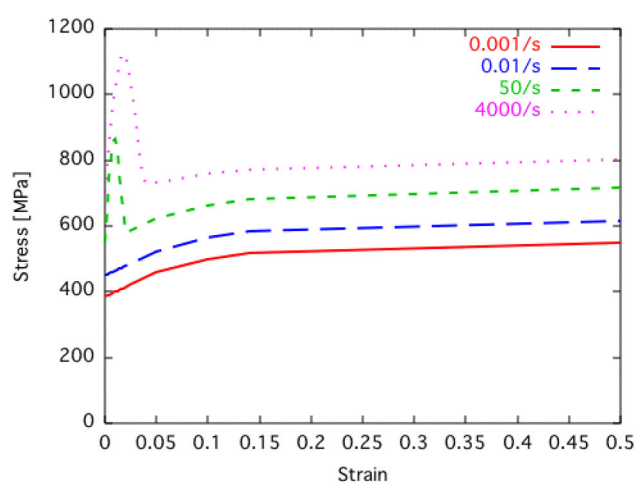

Figure 8. Modified HSLA constitutive model with stress transients.

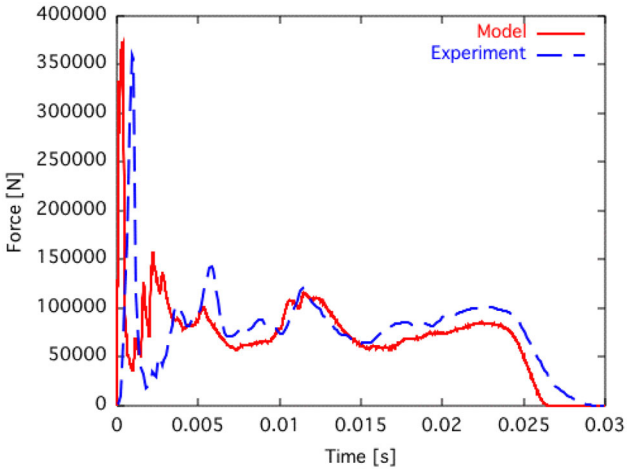

Figure 9. Modified HSLA constitutive model with stress transients.

The stress transients are dependent on strain rate history, and the above treatment is just a first-order approximation of the phenomena. A more fundamental approach is under development that will result in extension of the current strain rate dependent model to account for strain rate history. A journal publication is under preparation to further elaborate on the project developments.

Tube Crushing using Controlled Displacement Equipment

Preliminary tube crush experiments were conducted at the ORNL Test Machine for Automotive Crashworthiness (TMAC) on equipment described in the overall report (7.C). TMAC provides tightly controlled impact conditions that are used for generation of high-quality data for verification and development of new material models and FEM formulations. Tubes made of DP590 and TRIP590 steels were crushed at various speeds. Imperfection was introduced by making the top edge of the tube at a prescribed angle with the actuator, as shown in Figure 10.

The experiments were simulated using an isotropic plasticity and strain rate dependency described by a piecewise linear plasticity model. The simulation was conducted for dual-phase (DP) steel tube under constant crush velocity of the actuator of 0.6 m/s. Tube configuration at 200 ms is shown in Figure 11. The colors in the figure denote magnitudes of plastic strain in the finite elements.

The comparison of deformation features (displacements and curvatures) between the

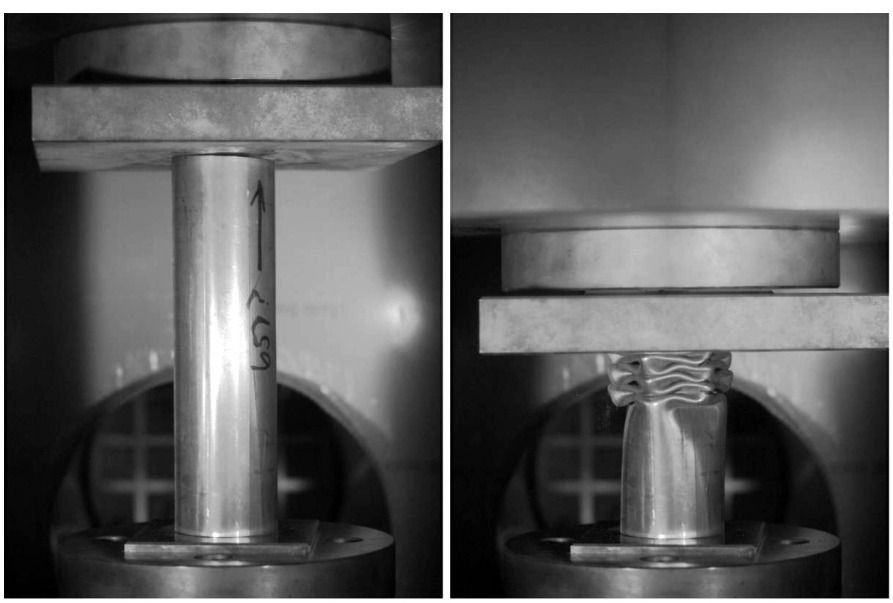

(1) (2)

Figure 10. TMAC tube test.

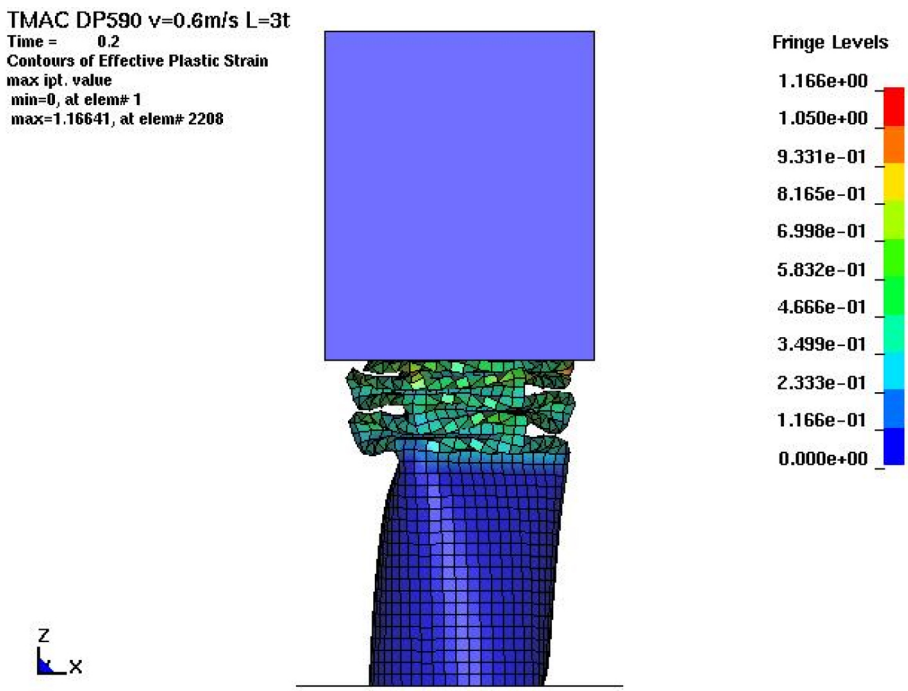

Figure 11. Plastic strain of DP tube at 0.2°s; crush velocity 0.6 m/s.

models and experiments is still ongoing, but the global data can be readily compared. Figure 12 shows the comparison between the experiment and the model. Data have not been filtered.

The model correctly predicts the initial stiffness of the tube, but it fails to achieve experimental peak. The origins of the peak impact force have so far been difficult to isolate because of the coupling between

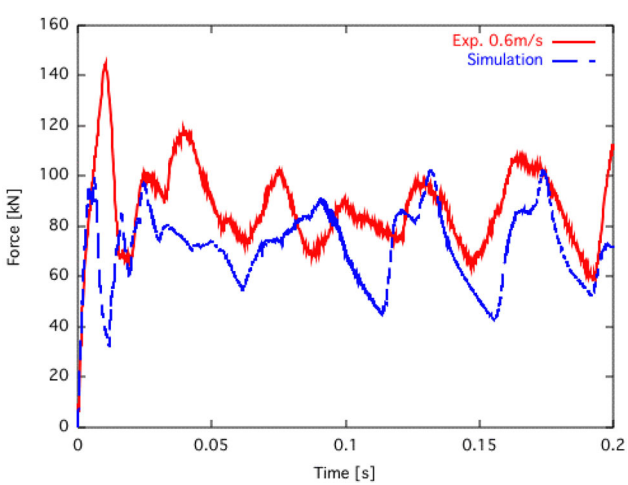

Figure 12. DP tube crush force; crush velocity 0.6 m/s.

the test specimen and testing equipment and inertia of the measurement devices.[5,6] The current results indicate that the peak value is not an artifact of testing but that such force is really experienced by the specimen. The actuator rigidity and inertia together with the measurements from the load washer at different constant loading velocities imply that the origin of the peak force is in the material behavior. The material model would, therefore, have to be modified to include strain rate history effects. Strain rate history effects had been investigated in the past,[7,8] but they have not yet found a wide acceptance in the engineering practice. The experimental data from TMAC can provide necessary information for such material model modifications and further improve predictive capability of the FEM.

Conclusions

The current project concentrates on investigation of different FEM modeling approaches for modeling of impact in HSS structures. The research is performed in collaboration with experimental program on

characterization of HSS under impact. The modeling is also used for development of new high strain rate material and structural characterization tests. The results of the project are used for development of more accurate modeling approaches for automotive design. The research results are also applicable in high strain rate forming operations.

Future Work

The future work on the project will focus on four topics:

1. Support of the strain rate experiments on coupon and component level.
2. Development and validation of material models and modeling techniques.
3. Modeling of HSS rectangular tubes.
4. Development of models and experiments for damage and fracture of HSS in crash.

The remaining most important aspects to address from the modeling of HSS crashworthiness are the methods to model the crush of tubes with rectangular (polygonal) cross section, modeling of damage that the HSS experiences during the deformation, and incorporation of processing into the models.

Acknowledgments

The research was performed at the Oak Ridge National Laboratory (ORNL), which is managed by UT-Battelle, LLC for the U.S. Department of Energy under contract DE-AC05-00OR22725. The drop tower tests were performed at the Vehicle Safety and Crashworthiness Laboratory, General Motors Corporation, Milford Proving Grounds. The tubes for the TMAC experiments were donated by the U.S. Steel Corporation. The support of Auto/Steel Partnership Strain Rate Characterization Team is acknowledged.

Contact

For additional information on details on the research project, please contact

Srdan Simunovic, simunovics@ornl.gov.
Dr. Simunovic is a senior research staff in the Computational Materials Science Group (http://www-cms.ornl.gov) at the Oak Ridge National Laboratory.

References

1. S. Simunovic, P. Nukala, J. Fekete, D. Meuleman, and M. Milititsky, "Modeling of strain rate effects in automotive impacts," SAE Paper 03M-253, 2003.
2. S. Simunovic, P. Nukala, J. Fekete, and D. Meuleman, "Modeling effects on strain and strain rate histories in automotive impact, of strain rate effects in automotive impacts," 7th United States Congress on Computational Mechanics, Albuquerque, New Mexico, 2003.
3. N. Jones, *Structural Impact*, Cambridge University Press, 1989.
4. J. O. Hallquist, "LS-DYNA3D, An explicit finite element nonlinear analysis code for structures in three dimensions," *LSTC Manual*, 1995.
5. J. Singer, T. Weller, and J. Arbocz, *Basic Concepts, Columns, Beams and Plates, Volume 1, Buckling Experiments: Experimental Methods in Buckling of Thin-Walled Structures*, John Wiley & Sons Ltd., 1998.
6. J. Singer, T. Weller, and J. Arbocz, *Buckling Experiments: Experimental Methods in Buckling of Thin-Walled Structures: Shells, Built-Up Structures and Additional Topics*, John Wiley & Sons Ltd., 2002.
7. J. D. Campbell, *Dynamic Plasticity of Metals*, Springer, New York, 1972.
8. J. Klepaczko and J. Duffy, "Strain rate history effects in body-centered-cubic metals," *Mechanical Testing for Deformation Model Development*, ASTM STP 765, R. W. Rohde and J. C. Swearengen, Eds., American Society for Testing and Materials, pp. 251–268, 1982.

B. Enhanced Forming Limits

Project Manager: Pat V. Villano
Auto/Steel Partnership
2000 Town Center Drive, Suite #320
Southfield, MI 48075-1123
(248) 945-4780; fax: (248) 356-8511; e-mail: pvillano@a-sp.org

Project Co-Chairman: John Siekirk
DaimlerChrysler Corporation
Cims 482-28-01, 800 Chrysler Drive
Auburn Hills, MI 48326-2757
(248) 576-1245; fax: (248) 576-2230; e-mail: jfs1@daimlerchrysler.com

Technology Area Development Manager: Joseph A. Carpenter
(202) 586-1022; fax: (202) 586-1600; e-mail: joseph.carpenter@ee.doe.gov
Field Technical Manager: Philip S. Sklad
(865) 574-5069; fax: (865) 576-4963; e-mail: skladps@ornl.gov

---

Contractor: U.S. Automotive Materials Partnership
Contract No.: DE-FC05-020R22910

Objective

- Convert the research results of the Auto/Steel Partnership (A/SP) Enhanced-Forming-Limit Diagram (EFLD) Project Team into an application methodology usable in press shops, and disseminate the resulting application methodology to steel suppliers and users to facilitate the manufacture of lightweight steel vehicles.

Approach

- Study the final research report by the EFLD Project Team to provide the technical foundation for an application methodology applicable to press shop functions.
- Create the application methodology.
- Validate the new application methodology with press shop case studies.
- Prepare reports and materials necessary for training seminars and conduct the seminars.

Accomplishments

- Established a Bead Correction Factor (BCF) to convert from bending and unbending strains generated during sheet metal deformation through draw beads or over sharp tool radii to corrected strains suitable for plotting on existing forming-limit curves (FLCs).
- Published a technology report documenting the creation of the BCF, procedures for using the BCF, detailed computational work sheets for five case studies, and limitations for press shop application on the A/SP open Web site.

- Published a training manual for press shop implementation on the open A/S-P Web site. The manual combined key portions of the technology report with additional instructions on how to use the BCF.
- Conducted seven training seminars for steel suppliers, steel users, tool and die builders, and formability researchers.

Future Direction

- Completed all work on this project.

Introduction

For decades the FLC and circle grid analysis (CGA) have defined the limits of sheet metal deformation from die tryout through production in real world manufacturing and now have been applied to virtual (computer simulation) manufacturing. However, several important areas of the stamping were excluded from these analyses. Sheet metal deformed by bending and unbending through draw beads or over tool radii with radius-to-sheet thickness ratios less than 5 had strain gradients through the sheet thickness and underwent large amounts of strain reversal. The FLC could not be used for forming severity assessment for these modes of deformation. However, severity analyses of these deformation modes become especially important for utilizing high-strength steels, thickness reductions, and other weight reduction opportunities.

The A/SP conducted and successfully completed an extensive research program entitled "Enhanced Forming Limit Curves" (EFLC) to study the forming severity of bending and unbending sheet steel. Their complete research report and additional data spreadsheets can be downloaded from their open Web site www.a-sp.org. The last phase of this program—transformation of the research results into usable press shop procedures—was completed in 2003.

Project Details

The project to develop press shop procedures was conducted as a consecutive series of five tasks. Completion of all tasks meant original equipment manufacturers (OEMs), steel companies, tool and die shops, and others involved in forming sheet metal were capable of implementing a simple press shop floor severity assessment for the bending and unbending forming modes.

Task 1: Convert research results to an application methodology suitable for press shop implementation.

The research program utilized measurement of FLCs before and after bending and unbending deformation. The height of the FLC after bending and unbending was higher than the FLC of the as-received steel. Thus the name of the project team was EFLC. While an excellent research tool, increasing the allowable amount of stretch before failure by cold working the metal through a draw bead would be difficult to explain and even harder to implement in the press shop.

However, the research showed that only 40% of the deformation going through draw beads actually affected the stretchability of the sheet steel. Rather than creating many different EFLCs for different amounts of bending and unbending strain within a given stamping, a BCF was created that corrected (reduced) the level of the measured strain by 60% before plotting the data on the FLC (Figure 1).

The BCF is proportional to the thickness strain created by the draw bead and/or tool radius. Because strain correction factors already were utilized by many stampers to correct strain severity readings measured on the outer fiber plane of a single bend, the BCF was deemed a reasonable and suitable tool for the press shop.

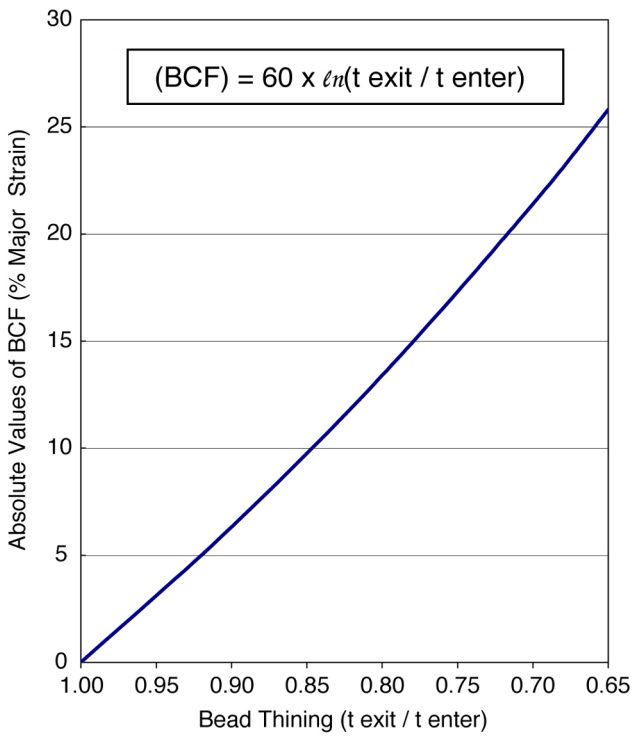

Figure 1. The BCF shown as a function of the thinning through the draw bead.

The computed BCF (a negative number) is added to the measured major strain and then plotted on the FLC as shown in Figure 2.

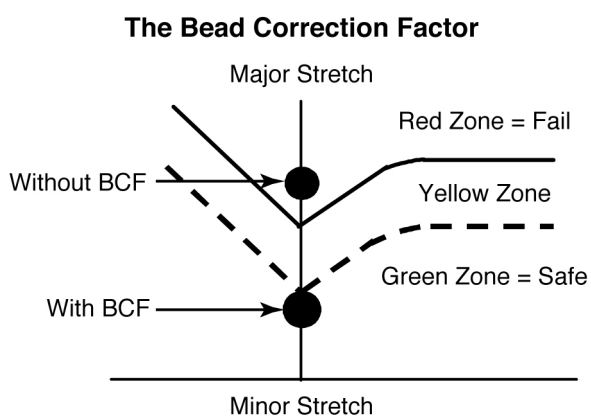

Figure 2. Forming-limit diagram (FLD) showing the effect of the BCF in lowering forming severity.

Task 2: Conduct press shop trials.

Task 2 was a very important milestone for completion of this project. The BCF procedure developed in Task 1 was applied to actual stampings in various press shop environments, including die build, die buyoff, and production. The first goal was to validate the analysis procedure on production stampings instead of the special test pieces created during the research phase. The second goal was to acquire case studies useful for the subsequent training phase of the project. From the group of stampings studied, five were selected for inclusion in the formal reports because of their special benefit for validation and training.

Case study 1 was a hood outer measured at final die buyoff. Figure 3 shows location C that had not undergone bending and unbending through the draw bead and therefore was analyzed using the traditional FLC. The strain at location C was only 35 strain percent major strain (direction of arrow) and 0 strain percent minor strain (perpendicular to arrow). However, this strain was located above the FLC line, and failure was predicted.

Figure 3 shows that location B of the stamping that had undergone bending and unbending through the draw bead, but had not torn.

The strain at location B was 47 strain percent major strain and 0 strain percent minor strain, which had a major strain one-third higher than the tear at location C. When the BCF was applied to location B, the

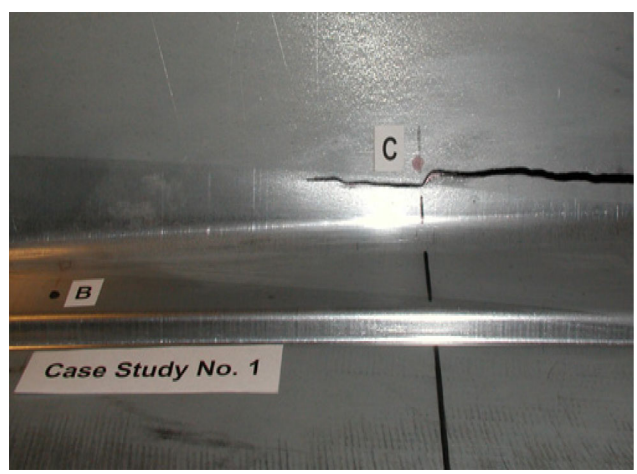

Figure 3. Hood outer stamping highlighting two measurement areas.

major strain was reduced from 47 strain percent to 24 strain percent. The severity was now in the green zone. This change in severity is illustrated in Figure 2.

Case study 2 was a fender at press show. The day before the show the fender passed all tests and evaluations. On press show day, however, the fender split (Figure 4) with engineers and die buyoff staff present.

The measured major strain was 58 strain percent, which was well above the 35 strain percent strain allowed by the FLC. Subtracting the computed BCF of 19 strain percent, a corrected major strain of 39 strain percent was obtained. Even after the BCF was applied, the strain was still above the 35 strain percent allowed by the FLC, and failure was predicted. The resultant tear indicates that the BCF is a reasonable compensation factor and will correctly predict failures in steel pulled through draw beads.

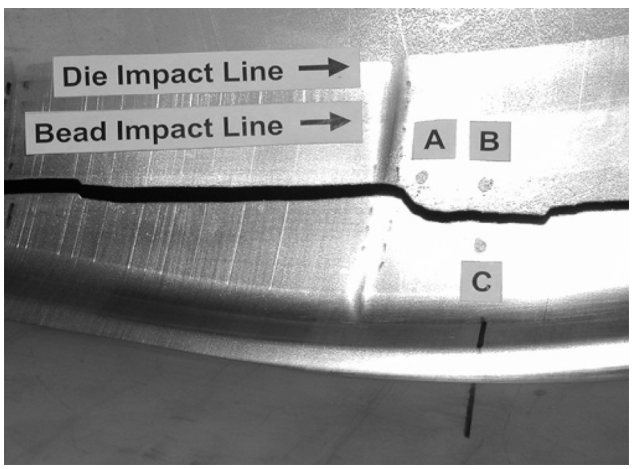

Figure 4. Fender showing severe split in metal pulled through a draw bead.

Case study 4 was a hood outer panel that had been in production more than a year (Figure 5).

When production was started on this hood, the major strain was 51 strain percent and well above the 36 strain percent allowed by the FLC. However, no tears had been encountered during die tryout or die buyoff. The company was aware of the EFLC project and therefore made the decision to release the tooling for production. During the year

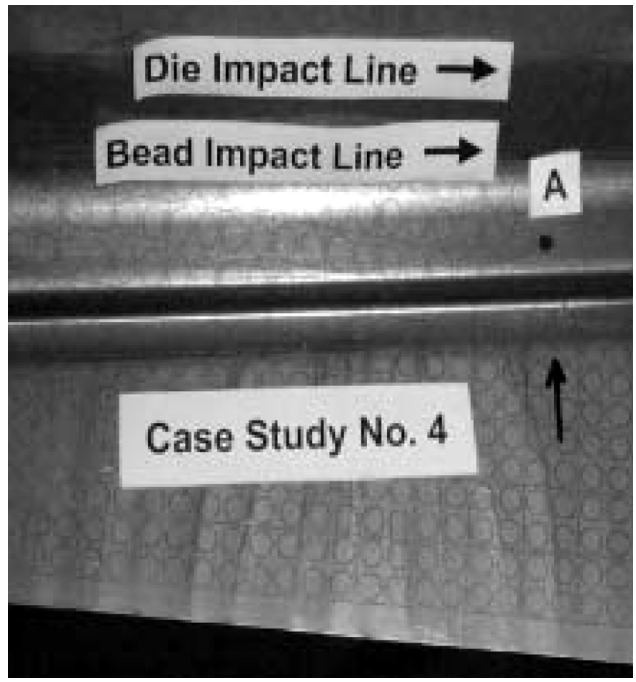

Figure 5. Hood outer panel evaluated after one-year of production.

of production, no tears had been encountered. The gridded panel was given to the EFLC team for evaluation.

The BCF was computed to be 22 strain percent, thereby reducing the corrected major strain to 29 strain percent. While the corrected major strain did not fall below the 26 strain percent major strain level required by green zone or the minimum safety margin, the corrected major strain was well below the 36 strain percent failure level. The decision to go ahead with production of the panel was a valid decision based on the procedure developed by this project.

Task 3: Prepare and publish a report describing and justifying the application methodology.

An extensive report, entitled *Enhanced Forming Limit Diagram—Project Team Technology Report*, was prepared to describe the key results from the research report and their conversion to the BCF methodology acceptable to the press shop. The technology report describes in detail a step-by-step procedure for conducting the analysis and an illustrative calculation. Five case studies are

described with complete calculation worksheets and discussion of results. Finally, suggested applications and their limits are presented. The complete Technology Report is downloadable from the A/S-P open Web site www.a-sp.org and is listed under the "Enhanced Forming Limit Diagrams" heading.

Task 4: Prepare and publish a training manual for use in press shops.

While the technology report described in Task 3 above could be used in the press shop, that report contained extensive reference to research procedures and results, as well as great detail. The technology report serves the engineering community but would be confusing for press shop application. Therefore, the project was expanded to include preparing and publishing an additional document, entitled *Training Manual—Enhanced FLC Project*. This manual contains only the press shop procedures and suggested applications for the BCF, summary of the five case studies, and all computational work sheets. The complete training manual is downloadable from the A/SP open Web site www.a-sp.org and is listed under the "Enhanced Forming Limit Diagrams" heading.

Task 5: Conduct training seminars on the application of the BCF technology.

A total of seven training seminars were conducted at different locations. In attendance were representatives from the automotive OEMs, steel companies, tool and die shops, and sheet metal forming research groups. A copy of the training manual was given to each attendee. The concept of the BCF was well accepted by the attendees. In many instances, steps to implement the BCF were initiated by various companies.

Summary

Bending and unbending sheet metal through draw beads and/or over a tool radius with a radius to sheet thickness ratio less than 5 can generate significant amounts of strain. Because these forming modes have both large gradients of strain through the sheet thickness and one or more strain reversals, these strains do not reduce subsequent stretching as much as a uniform through-thickness elongation. Therefore, a BCF must be applied to bending and unbending strains before their severity can be assessed by the FLC.

The completion of this project resulted in a technology report and a training manual, both downloadable from the A/SP Web site www.a-sp.org. Both contain the application methodology, five case studies with complete computational work sheets, and suggested press shop applications. To disseminate this information, seven training seminars were conducted.

C. High-Strength Steel Stamping Project

Program Manager: Jack Noel
Auto/Steel Partnership
2000 Town Center, Suite 320, Southfield, MI 48075-1123
(248) 945-4778; fax: (248) 356-8511; e-mail: jnoel@a-sp.org

Co-Chairman: James Fekete
General Motors Corp.—Metal Fabricating Division
100 Kirts Blvd., Troy, MI 48007-5001
(248) 696-1176; fax: (248) 696-1101; e-mail: jim.fekete@gm.com

Co-Chairman: Changqing Du
DaimlerChrysler Corporation
800 Chrysler Drive, Auburn Hills, MI 48326
(248) 576-5168; fax: (248) 576-7910; e-mail: cd4@dcx.com

Technology Area Development Manager: Joseph Carpenter
(202) 586-1022; fax: (202) 586-1600; e-mail: joseph.carpenter@ee.doe.gov
Field Technical Manager: Philip S. Sklad
(865) 574-5069; fax: (865) 576-4963; e-mail: skladps@ornl.gov

---

Contractor: U.S. Automotive Materials Partnership
Contract No.: DE-FC05-02OR22910

Objectives

- Determine how to accurately predict and control the amount of springback and other deviations from the desired stamping geometry for parts made from high-strength steel (HSS) and advanced HSS (AHSS) prior to the construction of the production tooling.
- Identify part designs and manufacturing processes that will reduce springback and other part distortions and recommend them to design and manufacturing engineers.

Approach

- Enhance HSS stamping springback predictability through finite-element analysis (FEA).
- Improve HSS stamping springback control by developing knowledge of part design geometries that affect flange springback and die processes that control springback.

Accomplishments

- Studied the effects of alternate stamping processes on springback reduction.
- Identified processes to control springback, sidewall curl, and panel twist.
- Built and/or modified tooling for stretch-forming processes of AHSS autobody structural components.

- Established that stretch-forming processes are intended to neutralize the residual stresses that cause springback and sidewall curl. Good results have been shown for HSLA 350 and DP 600. The results with DP 780, DP980 and Trip 800 have been less successful due to the inability to achieve a locked metal condition with simple two-bend lock steps. It is expected that a more complex four-bend lock step will provide the desired results with the higher strength materials.
- Discovered another process showing promise, which is the double-pressure pad form and flange die. This process requires a high-pressure hydraulic cushion that can be programmed for various control features. A die with this type of pressure pad has been designed for this project group and is being built for further experimentation with the higher strength steels. Much higher holding pressures are required for the new grades of AHSS than with current materials.
- Controlled springback by modified panel geometry. Effective use of stiffening beads, ribs, and darts is being recommended to product designers. Springback control experiments were conducted using tooling designed to replicate actual production stamping die processes. These experiments confirmed the importance of optimizing part geometry and the stamping process to reduce residual stress, flange springback, and part-to-part variation. Stampings were made with HSS, AHSS, and tailor-welded blanks. Parts were measured and data were recorded and analyzed. Results will be published in hard copy and on the Auto/Steel Partnership (A/SP) Web site.
- Determined that tooling wear is a major concern due to the higher die pressures and the material strength. This project group is working with the Tribology Project Group to find suitable die surface materials and lubricants. Vapor deposition of chromium nitride on cast iron has shown early promise.

Future Direction

- Complete the construction of the new prototype die and programmable hydraulic cushion. This die is designed as a master die set and pressure system that will accept subdie inserts to produce a variety of structural parts and/or stamping processes.
- Continue wear testing of die materials and die surface treatments with the support of the Tribology Group.

Introduction

Owing to the mechanical properties of HSS, the springback after forming and the geometric dimensional control of the stamped parts has been a critical issue in stamping tool construction and in stamping production. Because the actual dimensions of HSS stampings off the tooling are unpredictable with current tools and technology, the average die face remachining may be four to six times normal and result in 2 to 3 months of lost tryout time.

Computer simulation technology has been widely applied in the stamping industry and has been recognized as a common virtual stamping tool to identify formability issues and evaluate solutions before the actual stamping dies are made. Although computer simulation provides accurate prediction for splits and buckles, experience has shown that computer simulation data have not been reliable in predicting the amounts and modes of the springback, twist, or sidewall curl.

Springback and other distortions in HSSs must be controlled by innovative stamping processes that neutralize residual stresses from the metal deformation. These processes will involve some type of stretch forming to give the stamping "shape set." The work of this project group is to determine the most effective means of researching and applying

these processes. Computer simulation is also being analyzed to improve the data input for accurate formability prediction.

Progress Toward Meeting Deliverables

To assess the accuracy of the current forming/springback simulation technology, a full-scale fender rail stamping die was used (see Figure 1). A lockstep was added to the die to provide sidewall stretch. Two different HSS materials, HSLA 50KSI and DP 600, were used to stamp fender rails and the finished panels measured. Optimum stamping die processes inputs were established through comparison of simulation output with actual stamping die results. Springback control experiments were conducted using tooling designed to replicate actual production stamping die processes. These experiments confirmed the importance of optimizing part geometry and the stamping process to reduce residual stress, flange springback, and part-to-part variation. Parts were measured, and data were recorded and analyzed. Results will be published in hard copy and on the A/SP Web site.

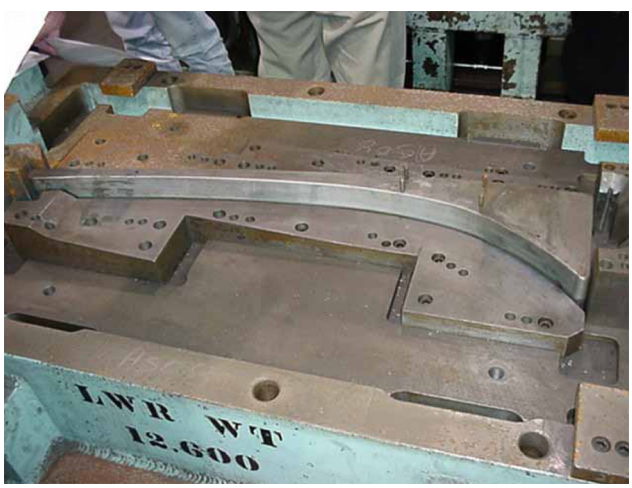

Figure 1. Full-scale fender rail stamping die (lower-half).

Project Status

Currently, the project group is focused on building a research master die with subdie inserts (see Figure 2) to produce various automotive structural components by a variety of processes. This master die will have the necessary higher holding pressures and controlled processes required for working the higher strength materials. A programmable hydraulic pressure cushion will be the main component of this system, which will provide the means of stretch forming the metal and controlling springback. This tooling is scheduled for completion in the first quarter of 2004.

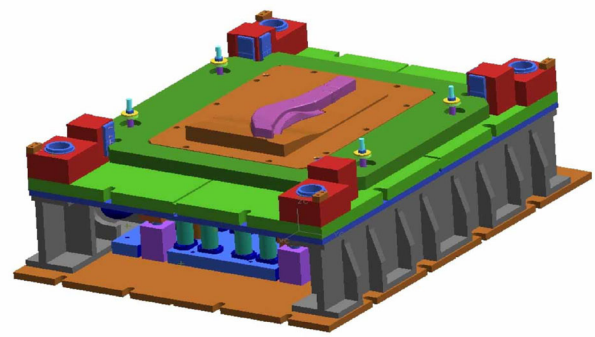

Figure 2. Research master die with subdie inserts.

Future Work

Further attempts at successful stampings of DP 780, DP 980, and TRIP 800 will be conducted on typical automotive underbody structural members with the new tooling and processes. These materials, in lighter gauges than currently employed, will assist the weight reduction goals of other project groups in the A/SP.

D. High-Strength Steel Joining Technologies Project

Project Manager: Thomas D. Mackie
Auto/Steel Partnership
2000 Town Center, Suite 320, Southfield, MI 48075-1123
(248) 945-4781); fax: (248) 352-1740); e-mail: tmackie@a-sp.org

Project Co-Chairman: James Dolfi
Dolfi AWS LLC
16883 Shrewsbury, Livonia, MI 48154
(734) 427-8117; fax: (734) 427-1827; e-mail: dolfi@www.net.com

Co-Chairman: Philip Coduti
Ispat Inland Inc.
3001 East Columbus Drive, Mail Code MC9-000
East Chicago, IN 46312
(219) 399-6111; fax: (219) 399-6562; e-mail: phil.coduti@ispat.com

Technology Area Development Manager: Joseph A. Carpenter
(202)586-1022; fax: (202) 586-1600; e-mail: joseph.carpenter@ee.doe.gov
Field Technical Manager: Philip S. Sklad
(865) 574-5069; fax: (865) 576-4963; e-mail: skladps@ornl.gov

---

Contractor: U.S. Automotive Materials Partnership
Contract No.: DE-FC05-02OR22910

Objective

- Facilitate the increased use of the advanced high-strength steels (AHSSs) in the Auto/Steel Partnership (A/SP) lightweighting projects through the development of weld parameters and weld schedules that will produce quality welds in 12 grades of these advanced steels.

Approach

- Evaluate weld lobe under peel test conditions to determine the optimum welding time and current. Properties such as hardness, tensile shear, metallographic, impact, and fatigue will be evaluated.
- Evaluate weld bonding of three of the AHSSs and compare to straight welded joints. Properties of tensile shear, impact, and fatigue will be considered.
- Document fracture characteristics of these welds and compare to the weld strengths in the development of a standard for partial-thickness fractures.
- Evaluate (Phase II) the weldability of different grades of HSS to each other, and different thicknesses to each other (nine combinations of dual-phase and martensitic steels, 1.5-mm to 2.0-mm thickness, as recommended by the A/SP Lightweight Structures Group). Determine the welding parameters to produce optimum welds and statistically test welds produced at these parameters. Tensile shear, impact and fatigue will be evaluated.

- Evaluate an ongoing project that addresses the effect of tempering welds made with dual-phase and transformation-induced plasticity (TRIP) steels, an AISI/EWI project also in concert with the DOE.
- Secure the various material grades in sufficient quantities to complete the welding and the tests.
- Write the test plan and procedures for the project (Statement of Work).
- Weld coupons and test accordingly.
- Report results.
- Develop a Standard of Acceptance for welds with inner-facial fractures that meet the strength requirements of welds or pull the traditional nugget.

Accomplishments

Weld Lobe Study:

- Established procedure for weld lobe study, testing, and machine characterization.
- Characterized two machines, scissor gun and C gun regarding rigidity and weldability.
- Secured the samples for all 12 materials, at 200 ft^2 each, at Roman Engineering, Inc. Material sheared into coupons and welded for weld lobe study, tensile shear, impact, and fatigue testing.
- Completed weld lobe study on all 12 materials.
- Completed impact tests and microhardness traverse tests on all 12 materials.
- Designed, produced, and tested fatigue test coupons.
- Designed, produced, and tested weld bonded coupons.
- Performed tensile shear on ten material iterations.

EWI/AISI Temper Study:

- Secured five materials for phase 1 work.
- Developed posttempering diagrams.
- Evaluated initial spike tempering.
- Designed process robustness study.

LWFS Weldability Study:

- Ordered materials.
- Developed weld and test program (using weld window).
- Secured welding source.
- Secured prototype build source.
- Received some materials and proceeded to weld coupons.

SWSG MIG/Laser Weld Study:

- Ordered materials.

- Developed test program.
- Selected welding source.

Introduction

The use of AHSS is integral to the steel industry effort to lightweight automotive components while not sacrificing strength or raising costs, an issue with the use of other lightweight materials. Development of welding parameters and the physical testing of the new steels are necessary to qualify these steels for various automotive applications. Extensive work has been completed on the spot welding of mild steels during the Intelligent Resistant Welding Project of the Auto Body Consortium, and various A/SP welding and bonding projects. This study is an in-depth investigation of the weldability and mechanical property improvements using the AHSSs.

Discussion

The Welding Technology Task Force started in about 1990 as an investigative technical committee of the A/SP with the purpose of better understanding production resistance welding processes and increasing electrode life. In about 2000 the Adhesive Bonding group combined with the Welding group to form the Joining Technology Group. When the Lightweighting Structures was formed, all the specific technology groups became "enablers" to the Lightweighting group. The Lightweighting group was charged with the task of using the AHSSs extensively for rails, bumpers, and frames.

Because of strong lightweighting incentives and desire to use the lightest and strongest steels available, coupled with the advancement of dual-phase, complex phase, martensitic and TRIP steels, there is a need to know how to weld the new steels, and how to cope with partial facial fractures.

When the AISI Ultralight Project (ULSAB) showed that considerable weight could be saved by using HSSs, and then AHSSs came on the scene, the Welding committee was given the task of improving the weldability and permitting use of the AHSS in the new designs. When the A/SP was revamped to concentrate on lightweighting issues, Welding was combined with Adhesive Bonding to form the Joining Technologies Group, and Joining became an enabler to the Lightweighting Team.

The projects studied over the years and completed follow:

- Weldability Test Standard Manual (1994–1995)
- Electrode Weld Mechanisms (1995–1997)
  - Hot Dip Galvanized (HDG) Steels (1997)
  - Galvannealed Steels (1996)
  - Finite Modeling of Electrode Tip (1995)
- HSS Weldability (1998–2000)
- IRW Effort (1997–2000)
- Design of Experiments-Coated Steel (1998–2000)

The first project listed, was to develop a qualification procedure that could be accepted by the industry and avoid duplicate or triplicate testing of materials for weldability. This test procedure was developed by the Welding team and accepted by the AWS and SAE under D 8.9 standard. Coupon geometry and electrode shape were evaluated and established in the standard test. Today this is a widely used standard.

One of the early projects was a study of electrode weld mechanisms and electrode wear on both galvanized and galvannealed steels. This study was led by Edison Welding Institute and Michigan Technological University in an effort to study electrode wear mechanisms and increase electrode life. It was found that aluminum content in the

HDG coatings in excess of 0.2% caused a rapid decrease in electrode life. It was also determined that electrode life decreased sharply as expulsion occurred, which was related to excessive current. Truncated cone electrodes also proved to be the best.

One of the studies led by Battelle Institute, was "Finite Modeling of the Electrode tip," adding to the electrode wear mechanism information. Photographic studies during the welding process, by Michigan Technological University, showed graphically what was happening at the electrode tip.

In 1998, investigation of the weldability of the traditional HSSs 50 ksi and over, such as high-strength low-alloy (HSLA), HSS, and Bake Hardenable (BH) was started. A Design of Experiments was proposed and completed using these steels, looking for a way to increase electrode life and to make the process robustness on the production floor. The aspect ratio (a measure of the size and roundness of the weld nugget) proved to be a measure of process robustness. When welds exceeded an aspect ratio of 2.0, the process becomes erratic. In this case the electrode should be redressed and welding continued. The current was also kept to a level just below "weld expulsion," to keep the process in control.

Four welding projects that are enablers to the Lightweight Front Structures Group are

1. Weld lobe study,
2. EWI/AISI temper study,
3. LWFS weldability study, and
4. SWSG MIG/laser weldability.

The **weld lobe study** involves the weldability of 8 different AHSS steels in 13 coating combinations, which may used in AHSS designs. Using two different weld guns (C gun and pedestal gun), and three hold times (16, 22, and 28 cycles), welds were made and peel tested.

Shown below is the materials matrix to be evaluated: All the steel was 1.5 mm thick and welded to itself.

Grade:
High Strength Low Alloy—HSLA HD—1.5 mm
High Strength Low Alloy—HSLA GA
Dual Phase 600—DP-600 GA
Dual Phase 600—DP-600 HDG
Dual Phase 600—DP-600 CR
Dual Phase 980—DP-980 CR
Recovery Annealed 830—RA-830 HDG
Recovery Annealed 830—RA-830 CR
Martensitic 1320—MS-1320 CR
Transformation-Induced Plasticity—TRIP-600 CR
Transformation-Induced Plasticity—TRIP-800 EG

The process of investigation involved:
1. secure materials and shear and weld coupons,
2. determine best schedule for three hold times on both guns at a current below expulsion (peel testing at each level), and
3. perform property tests and chart results.

Making welds along the power curves at 16, 22, and 28 cycles, the parameters that produced 6-mm welds were recorded. Then tested welded coupons were made on this schedule for tensile, impact, hardness, metallographic, and fatigue.

Figure 1 shows the welding curves and resultant welds produced along them.

Figure 2 shows the impact data comparison of the first six steels tested:

Impact test coupons were made and tested on the IRW impact machine developed during the IRW study, and tested at the University of Toledo.

Fatigue tests were made and evaluated by the Fatigue Team of ASP for nine of the material iterations. The Fatigue Team had already tested the mild steel and some of the traditional HSSs as base metal. Figure 3 shows the load amplitude for the various materials using a tensile shear coupon. There is very little difference in all these steels for tensile shear. Cross tension tests showed much more variability. Microhardness tests were made at each level.

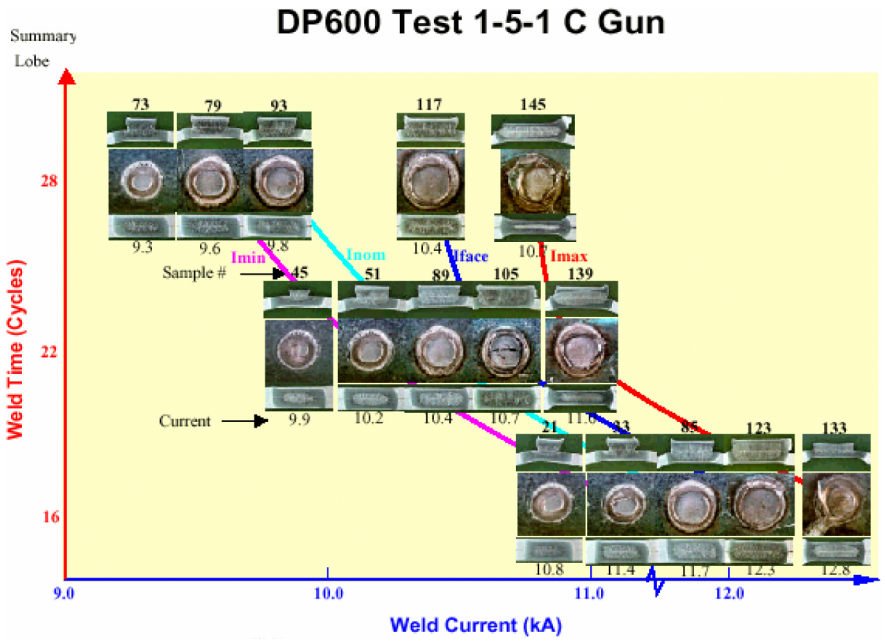

Figure 1. Welding curves and welds produced.

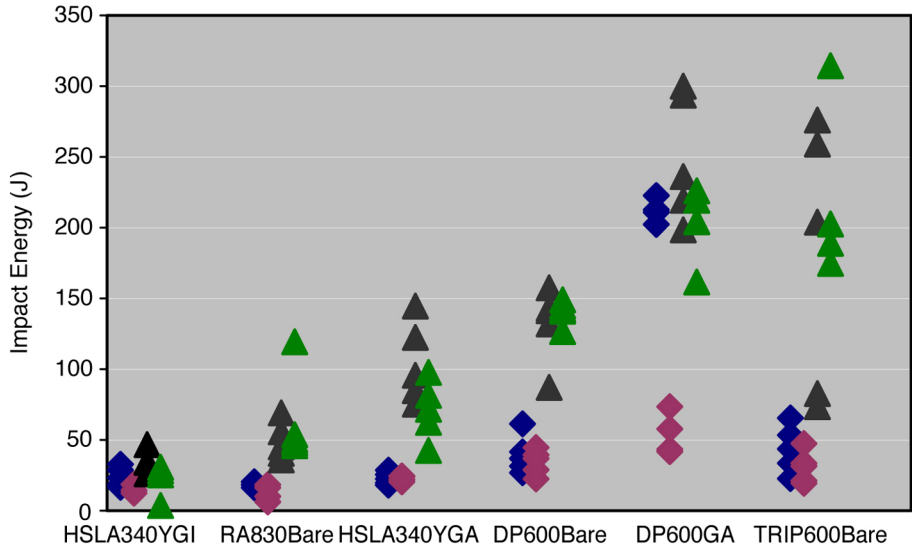

Figure 2. Impact data comparison of first six steels.

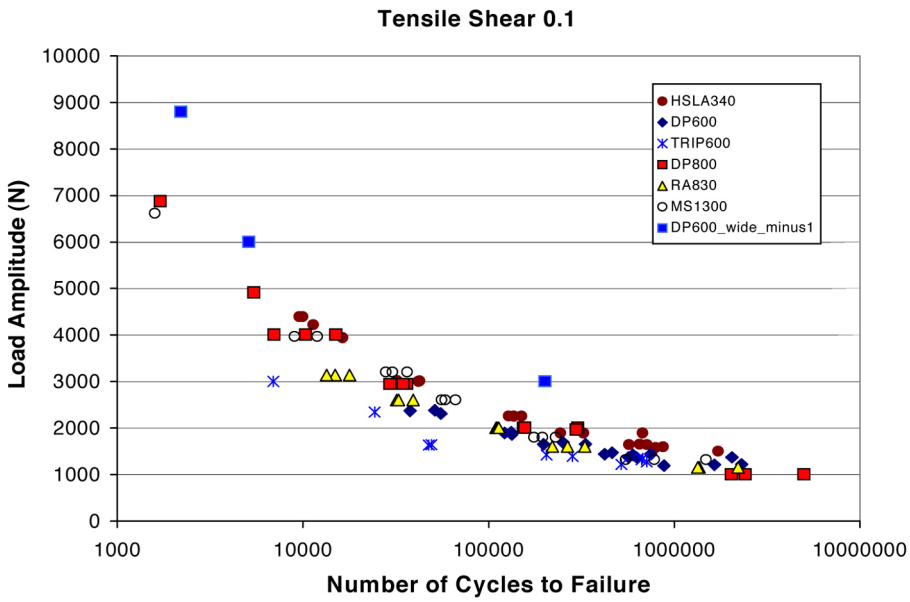

Figure 3. Load amplitude vs cycles to failure.

Involved in this study was the use of weld bonding on three of the materials and comparing test data of weld-only vs weld-bonded. The materials are DP-600 GI, DP-600 GA, and HSLA 340 GI. The results show about a 50% increase in lap-shear tensile for weld bonding over weld only.

An acceptance criteria document in the form of a fracture classification chart, which would discriminate between good and bad welds, was drafted. This is confidential information, not for publication yet.

The **EWI/AISI Temper project** was one where AISI and EWI were cooperating with the DOE to evaluate a fallback position, by welding and posttempering or spike tempering AHSS welds to produce ductile welds and possibly reduce any partial facial fractures. The Partnership assumed the involvement of AISI, and proceeded to evaluate the work and its feasibility to the use of AHSS. Six AHSS materials were compared, with tempering curves developed.

The process here was to

1. secure material, shear and weld;
2. develop tempering diagrams during welding;
3. detail the spike-tempering region; and
4. study for process robustness.

The materials matrix for this project is shown below:

Grade:
Dual Phase—DP-600 1.6 mm to Self
Dual Phase—DP-800 1.0 mm to Self
Dual Phase—DP-980 1.6 mm to Self
TRIP—TRIP 600 1.6 to Self
TRIP—TRIP 800 1.6 to Self
Martensitic—MS-1300 1.0 to Self

The Lightweight Front Structure Project

A weldability program was intended to evaluate nine particular AHSS for use as the Lightweight Front Structures Project (8.I). In this case, a weld window would be determined for each material or combination, and the "sweet spot" of optimum welds was chosen. A statistical number of welds were made using these parameters, with testing for tensile strength, impact, hardness, and fatigue for each iteration.

The materials matrix for the Lightweight Front Structures Group (resistance welding):

Grade:
DP-980 1.0 to Self
DP-800 1.0 to Self

DP-800 1.2 to Self
DP-800 1.4 to Self
DP-800 1.4 to DP-800 2.0
DP-800 1.2 to DP-800 2.0
DP-800 1.4 to DP-800 1.4 to DP-800 2.0 (triplicate)

The test process would be to

1. secure materials and shear and weld coupons,
2. using a weld window, determine best weld schedule,
3. make 25 samples for statistical test, and
4. perform tensile shear, impact, hardness, and fatigue.

Several new materials were suggested as designs progressed to make lightweight rails; consequently, this added to the program. Several tests have been completed for the martensitic steels and DP 800.

SWSG MIG\Laser Project

The latest project to be incorporated is the weldability of AHSS using GMAW welds and laser welds and modified MIG and Laser processes. Obviously, this is a different joining process than RSW, but it is used extensively in frame, bumper, and rail construction.

Many of the same AHSS materials will be evaluated by these fusion-welding processes. The test process for this project will be

1. secure materials and shear coupons,
2. weld coupons by various MIG and laser processes,
3. test by bend test and tensile, and
4. record results and use parameters to weld prototype parts.

These four welding projects will be contributing to the knowledge base to understand and improve weldability, and the effect upon the properties of the welded coupons and the welded assemblies. Weldability is characterized by the welding schedules and subsequent use of these schedules to make prototype parts like rails, bumpers, and frames.

By determining proper weld schedules for each material and stack-up, a starting point to weld prototype parts and establish schedules for the production floor has been determined. The welding source will also be closely involved with the Prototype builder to make parts as early as March 1, 2004. This database of weld schedules for many combinations, gives the designer a wider choice for material combinations to feed into his design models.

The deliverables from these four projects will include

1. welding schedules for a variety of material combinations,
2. welding validation on prototype parts,
3. property values on a variety of welded combinations, and
4. acceptance criteria for the production floor.

In the next few months, both laboratory and prototype build data are forthcoming. Most of these welding efforts will conclude this year, with the exception of some of the MIG and laser work due to funding restraints.

E. Sheet Steel Fatigue Characterization

Program Manager: Gene Cowie
Auto/Steel Partnership
2000 Town Center, Suite 320, Southfield, MI 48075-1123
(248) 945-47798; fax: (248) 356-8511; e-mail: gcowie@a-sp.org

Chairman: Benda Yan, Ph.D.
Staff Research Engineer, Product Applications
Ispat Inland Inc.
3001 E. Columbus Drive, East Chicago, IN 4312
(219) 399-6922; fax: (219) 399-6562; e-mail: bxyan@ispat.com

Technology Area Development Manager: Joseph Carpenter
(202) 586-1022; fax: (202) 586-1600; e-mail: joseph.carpenter@ee.doe.gov
Field Technical Manager: Philip S. Sklad
(865) 574-5069; fax: (865) 576-4963; e-mail: skladps@ornl.gov

---

Contractor: U.S. Automotive Materials Partnership
Contract No.: DE-FC05-02OR22910

Objectives

- Compile the test data generated in the previous phases of the program into a user-friendly database so that it can be used in all phases of design and structural analysis of sheet steel vehicle bodies.
- Investigate the fatigue life of joints formed by spot welding and weld bonding (a combination of welding and adhesive bonding).
- Explore the parameters for testing metal inert gas (MIG) and laser-welded joints.

Approach

- Investigate spot welding, a fusion process in which the metal being joined is melted and re-solidified to form an alloy with a distinctly different microstructure from that of the metal(s) that are joined. In addition, the weld nugget, or button, may contain discontinuities, which can become sites at which fatigue cracks form. The amount and type of discontinuities are affected to a considerable extent by the welding process. The microstructures of the joined metals are also refined in the area adjacent to the weld, which is known as the heat affected zone (HAZ).
- Investigate adhesive bonding that introduces an entirely different material into the load path, which must adhere to the metals being joined and resist fatigue failure at the areas of contact and within the adhesive.
- Investigate these previously unknown, or at best little known, factors that are expected to improve durability and facilitate modeling and simulation. Therefore, the testing was conducted on a variety of steel grades and coatings.

Accomplishments

- Defined parameters of the database and engaged a contractor to perform the work. The database has been constructed and is being evaluated by team members. Work is expected to be complete in early 2004.
- Selected 22 combinations of steel grade and coating. Of the combinations, 17 were spot welded, with 8 completed and 9 in process. Two of the combinations were weld bonded, and both have been completed. Three of the combinations were bonded, with all three in process.
- Contacted several consultants and invited them to present proposals for fatigue testing MIG welds.

Introduction

In the era when vehicle mass was not a drawback and, in fact, was sometimes considered an advantage, the primary concern in body design was rigidity. More recently, the need to reduce body mass to comply with mandated corporate average fuel economy (CAFE) while improving the levels of occupant protection in a crash caused design engineers to reexamine design procedures and materials. High-strength steels, judiciously selected and applied, emerged as potential low-cost (compared with aluminum and plastics), reliable materials for meeting these mandates. As structural components are optimized and thinner gauge, higher strength materials are assessed, fatigue life of the component and the areas where loads are transferred become considerations. To assess the performance of a component in the design phase, the fatigue characteristics of the base material and the areas where loads are transferred must be known. This project has completed a significant amount of testing of various grades of steel and is currently addressing joining methods most commonly used in vehicle bodies made from sheet steel.

Details

The three participating auto companies have been investigating the fatigue characteristics of spot welds, but there remains a need for a joint effort to evaluate the fatigue characteristics of spot welded and weld bonded joints. The effort began in the 2002 fiscal year with presentations by key researchers on the current state of the work at DaimlerChrysler Corporation, Ford Motor Company, and General Motors Corporation. Based on these presentations, the Sheet Steel Fatigue Project Team was able to develop parameters for a test program that would produce results beneficial to all three companies. Early in the planning, the Auto/Steel Partnership (A/SP) Joining Technologies Team was consulted, and it was agreed that Joining Technologies would prepare the samples to be tested. This interaction ensured that the samples would be joined using procedures that were properly controlled and in adherence to the best current practices in sheet metal joining.

The following test parameters were developed and agreed on in the planning stage:

1. There will be two modes of testing: tensile shear and coach peel.
2. Weld fatigue performance is independent of metal thickness for mild steels and high-strength low-alloy (HSLA) grades; therefore, tests on these grades will utilize only one metal thickness (1.6 mm).
3. Because no such data are yet available for advanced HSS, several grades in this class will be tested at two thicknesses (1.6 mm and 0.7 mm).
4. Testing will be done at two R ratios: 0.1 and 0.3. R is the stress ratio, defined as the ratio of the minimum stress to the maximum stress in the test cycle.

Maximum and minimum values are algebraic, with tension designated as positive and compression negative.

5. Eight steel grades will be tested.
6. Testing will include both spot welded and weld bonded joints.

Eight testing laboratories known to have capabilities in this type of testing were invited to submit proposals. Two were selected to perform the work: The University of Missouri in Columbia, Missouri, and Westmoreland Mechanical Testing and Research, Inc. in Youngstown, Pennsylvania.

As the testing progressed, and results were analyzed, the following tests were added for comparison purposes.

1. Testing at specified R ratios means that the maximum and minimum loads are constant throughout the test. This process is valuable for establishing baseline data. However, in the real world, loads can be expected to vary. For this reason, two sets of spectrum loading tests, run at predetermined load variations, were scheduled.
2. Two tests are in progress on samples with a different welding schedule that produced a smaller weld button.
3. Three tests were scheduled with samples joined by adhesive bonding only.
4. At the request of the Joining Technologies Team, three tests were scheduled using wide samples (125 mm vs the standard 38 mm). The wider samples minimize twisting of the weld under load.

Preliminary analysis of results received to date indicate that the fatigue performance of a spot weld is independent of the materials being welded. This is thought to be due to the melting and resolidifying processes (see Approach, above), which make material properties, coating, and welding paremeters insignificant contributors to fatigue performance.

Continuing Work

During the next 6 months, raw data received from the testing sources will be processed into a format useful for engineering analysis and compiled into a Web-enabled database. The anticipated date for uploading the database to the Web is April 30, 2004.

F. Strain Rate Characterization

Project Manager; Pat V. Villano
Auto/Steel Partnership
2000 Town Center Drive, Suite #320
Southfield, MI 48075-1123
(248) 945-4780; fax: (248) 356-8511; e-mail: pvillano@a-sp.org

Chairman: James Fekete
General Motors Corporation-Metal Fabricating Division
100 Kirts Blvd., Troy, MI 48007-5001
MC-483-610-116
(248) 696-1176; fax: (248) 696-1240; e-mail: jim.feteke@gm.com

Srdan Simunovic
Oak Ridge National Laboratory
P.O. Box 2008, MS 6164, Oak Ridge, TN 37831-6359
(856) 241-3863; fax: (865) 574-7463; e-mail: simunovics@ornl.gov

Technology Area Development Manager: Joseph A. Carpenter
(202) 586-1022; fax: (202) 586-1600; e-mail: joseph.carpenter@ee.doe.gov
Field Technical Manager: Philip S. Sklad
(865) 574-5069; fax: (865) 576-4963; e-mail: skladps@ornl.gov

---

Contractor: U.S. Automotive Materials Partnership
Contract No.: DE-FC05-95OR22363

Objectives

- Develop new experimental setups for characterization of crashworthiness and strain rate sensitivity of high-strength steels (HSSs).
- Replicate impact conditions that occur in automotive impact by simpler and more manageable experiments.

Accomplishments

- Developed experimental setup procedures for new crashworthiness characterization test based on parallel-plates buckling (procedure was developed at the University of Dayton Research Institute).
- Developed and conducted constant-velocity crash experiments on circular tubes made of dual-phase (DP) and transformation-induced plasticity (TRIP) steels.

Future Direction

- Conduct and analyze crush experiments on coupon level (parallel-plate impact test).
- Develop experiments for characterizing strain and strain rate history in tubular components (circular and rectangular tube crush tests).

- Provide high-quality data for material and finite-element method (FEM) modeling development.

Introduction

Crashworthiness characterization of HSS[1] requires testing of materials and structures under increased strain rates, large plastic strains, and large displacements that are characteristic of actual impact events. Aside from providing a physically quantitative measure of crashworthiness, the experiments also provide benchmarks for verification of FEM models that are used for automotive design and analysis. Typical crashworthiness experiments involve crushing of tubular objects, such as circular or rectangular tubes.[2] Due to a combination of relatively high velocities and force levels required for progressive crushing, the experiments are usually conducted in inertia-based equipment, such as drop towers or impact sleds. For example, in a drop tower the drop height and the drop mass can be adjusted to generate desired crush force and length. However, there are practical limits on the mass and the velocity that can be used in a drop tower. The kinetic energy of the impact must be such that it can be expended in the deformation of the specimen and the safety restraints in order not to damage the testing equipment. Vibrations of the falling mass are practically impossible to eliminate, and the lateral forces are not easily measured, nor controlled. The velocity of impact cannot be kept constant and gradually reduces from the onset of impact.

The objective of this project is to develop and conduct coupon- and component-level experiments for characterization of crashworthiness of HSS. The project will also provide high-quality data for development of material and structural FEM models, and, therefore, enable more accurate modeling and design of lightweight crashworthy vehicles.

Design of Experiments

Parallel-Plate Impact Test

A new coupon-level test based on parallel-plate drop tower test by Tam and Calladine[3] has been developed for the servo-hydraulic testing machine. The University of Dayton Research Institute (UDRI) was contracted to perform high-strain-rate double-hinge buckling tests as part of Auto/Steel Partnership (A/SP) work to develop structures for the automotive industry that will improve passenger safety in crashes. Results from drop tower tests were used to develop a model of energy absorption. The results from the test will be used for characterization of material under impact and bending. The tests are currently under way at the UDRI.

The test is developed with the objective to replicate deformation history of automotive structures made of polygonal tubular components that occurs during impact. The simplicity of the specimen allows for analytical extraction of data and simple correlation with the FEM experiments. The instrumentation includes strain gages and a high-speed camera that will be used to correlate the measurements. The initial fixture design with the specimen and the specimen after the test are shown in Figures 1 and 2.

Due to the problems with obtaining symmetric deformation that is crucial for interpreting the data from the experiments, several modifications were made to the preparation of the specimens and the fixture. Current specimen design is shown in Figure 3.

Up to eight strain gages are used to record strain history for a test. Gages are arranged as seen in Figure 4, with gages 4, 5, and 6 placed back-to-back with 1, 2, and 3. If desired, the location of gage 8 can be changed after the first few tests. The strain

Figure 1. Double-plate test fixture.

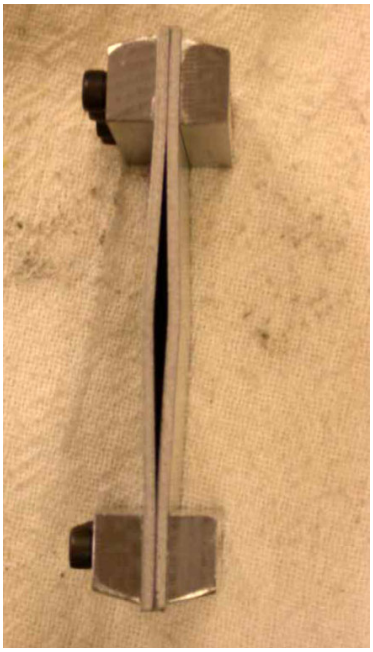

Figure 3. Specimen design.

Figure 2. Double-plate specimen after impact.

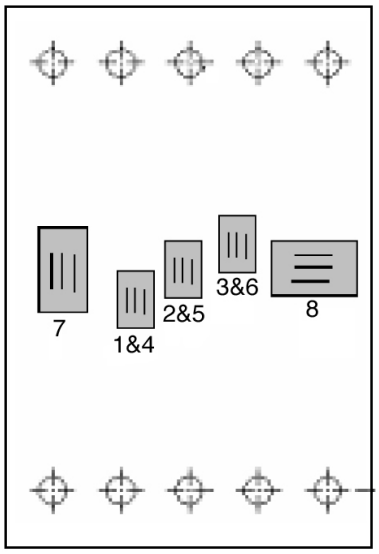

Figure 4. Strain gage location.

gage equipment will be calibrated to record up to 10% strain, or 20% strain, as appropriate. Some of the gages may be set to record a smaller scale on some of the tests to capture the onset of yielding. Strain gages are applied in accordance with procedures published by the manufacturer.

Results from the latest successful test setup are shown in Figure 5. The increasing numbers below the photographs denote the relative time sequence.

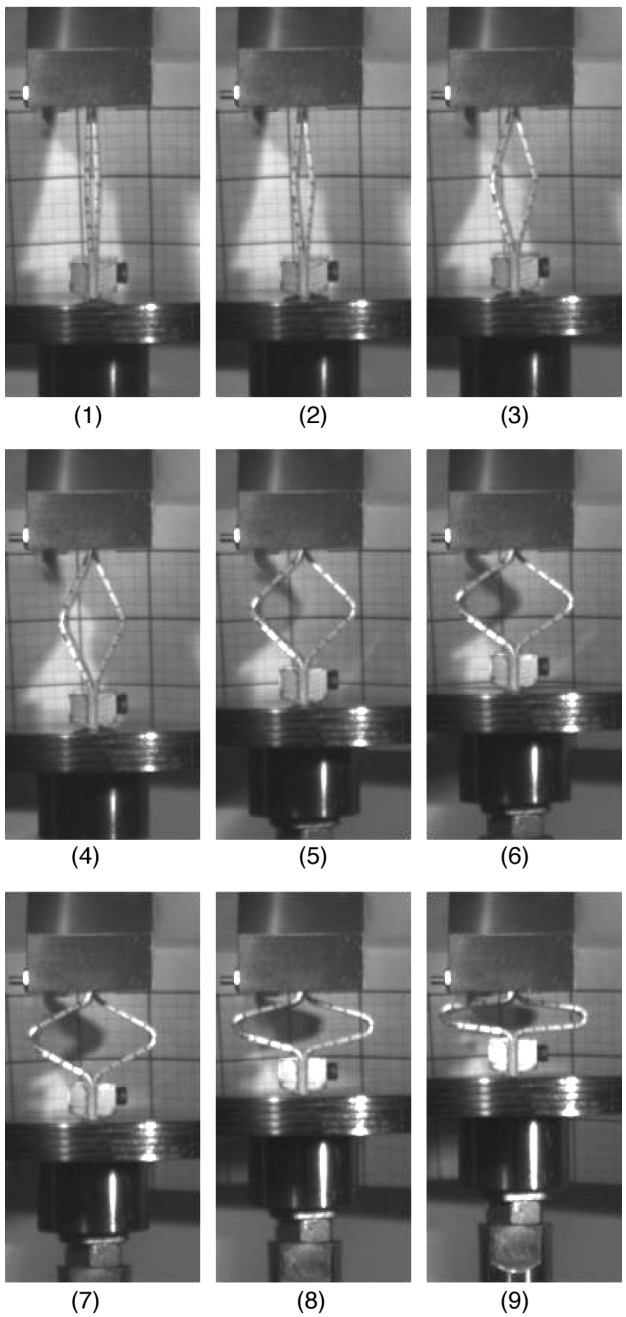

Figure 5. Double-plate test.

Data from the test are used to develop information about material rate sensitivity and deformation during early impact and formation of plastic hinges. The data are also used for correlation with and modification of the computational FEM models.

Tube Crush Experiments

To improve experimental investigations of the material and structural behavior for automotive impact, the Oak Ridge National Laboratory (ORNL) and the ACC of USCAR have developed a new integrated virtual and physical test system for hydraulic, high-force, high-velocity crashworthiness experiments of automotive materials and structures. This unique system, the test machine for automotive crashworthiness (TMAC), permits controlled, progressive crush experiments at programmable velocity profiles and high-force levels. More details about the TMAC system can be found on http://www.ntrc.org and in 7.C.

The tube crush experiments were conducted at the National Transportation Research Center user facility in Oak Ridge, Tennessee. The TMAC system is shown in Figure 6.

The ability to control displacement (velocity) and large lateral stiffness of the machine allows for strain history measurements[4] that are not practical in drop tower equipment. The test setups have been developed and will be reported in forthcoming publications. The current document deals only with global measures, such as loads and displacements and their comparison with the simulations.

The test specimens were provided by the U.S. Steel Corporation. Two materials were tested:

(a) DP600 600-MPa steel, and
(b) TRIP 600-MPa steel

Tube diameter was 70 mm (2.75 in.). The tubes were made by the ERW method. Tube

Figure 6. Test machine for automotive crashworthiness.

thickness was 1.6 mm in both cases. Basic material properties along the circumference of the tubes are shown in Table 1.

Table 1. Material properties

Test direction	Location (0° weld)	Yield (MPa)	Tensile (MPa)	Total elongation (50 mm)
Dual-phase 600 1.6 mm				
L	0	573	666	15.5
L	90	453	635	23.8
L	180	459	625	22.2
T	0	419	638	18.8
T	180	410	649	24.0
Trip 600 1.6 mm				
L	0	676	795	17.5
L	90	465	640	30.1
L	180	480	635	31.4
T	0	466	648	16.1
T	180	414	638	30.0

In the table, L and T denote directions along the length and circumference of the tube, respectively. Test tubes were cut to length of 0.254 m (10 in.). The base of the tube was restrained by a steel insert mounted on the supporting plate of the machine. The drawing of the insert is shown in Figure 7.

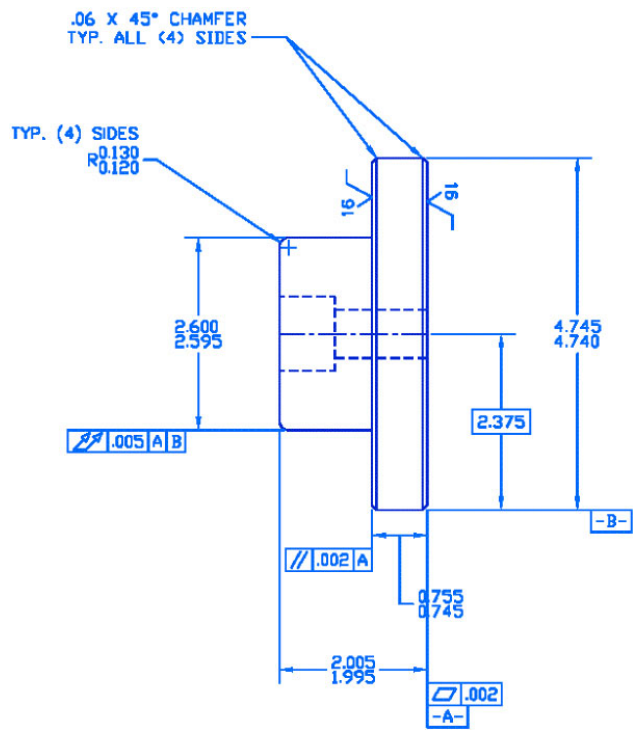

Figure 7. Tube insert.

Because of the high imperfection sensitivity of circular tubes[5,6] it was necessary to incorporate crush initiators into the tubes in order to generate a repeated folding mode. The various modes and magnitudes of imperfections were considered using FEM models to determine the controlling factors for tube fold formation. It was determined that the tube top height imperfection (or equivalently the loading plate angle) has dominant influence on tube crush for the practical imperfection ranges already present in the tubes. This finding was in agreement with experiments reported in the literature.[7] Therefore, the tubes were cut at an angle of 2° to initiate folding at the predetermined location and mounted in the equipment as shown in Figure 8.

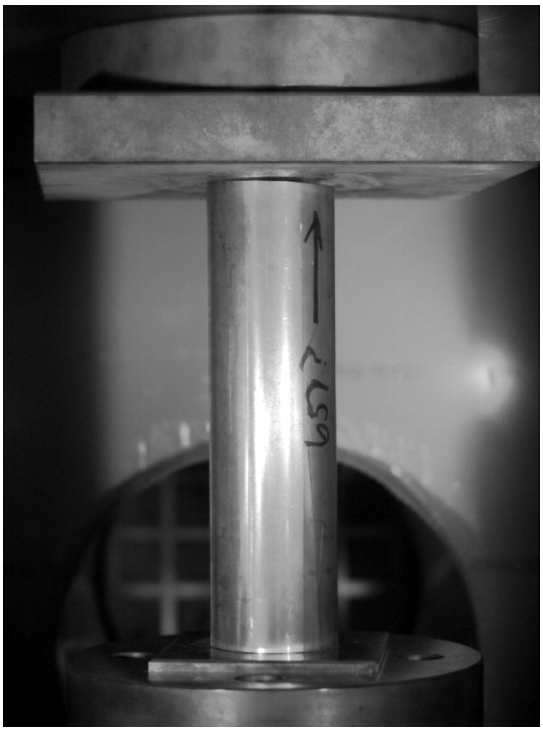

Figure 8. Experimental setup and initial tube imperfection.

Several loading velocities were considered. The tubes were crushed under effectively quasi-static mode, and under constant actuator velocities of 0.6 m/s, 1 m/s, 2 m/s, 4 m/s and 6 m/s. The tests were recorded with a high-speed camera. Typical sequence of deformations for crush velocity of 2 m/s and DP steel is shown in Figure 9.

The tube force was measured by a set of load cells and a load washer. The data from load sensors, displacement trace, and high-speed camera are synchronized and together provide comprehensive information about the progressive crush, and crashworthiness. This information can be taken advantage of for developing FEM modeling guidelines because we can now easily compare displacements, collapse modes and forces between the models and experiments. The ongoing research involves investigations of different measurement techniques in crashworthiness characterization.

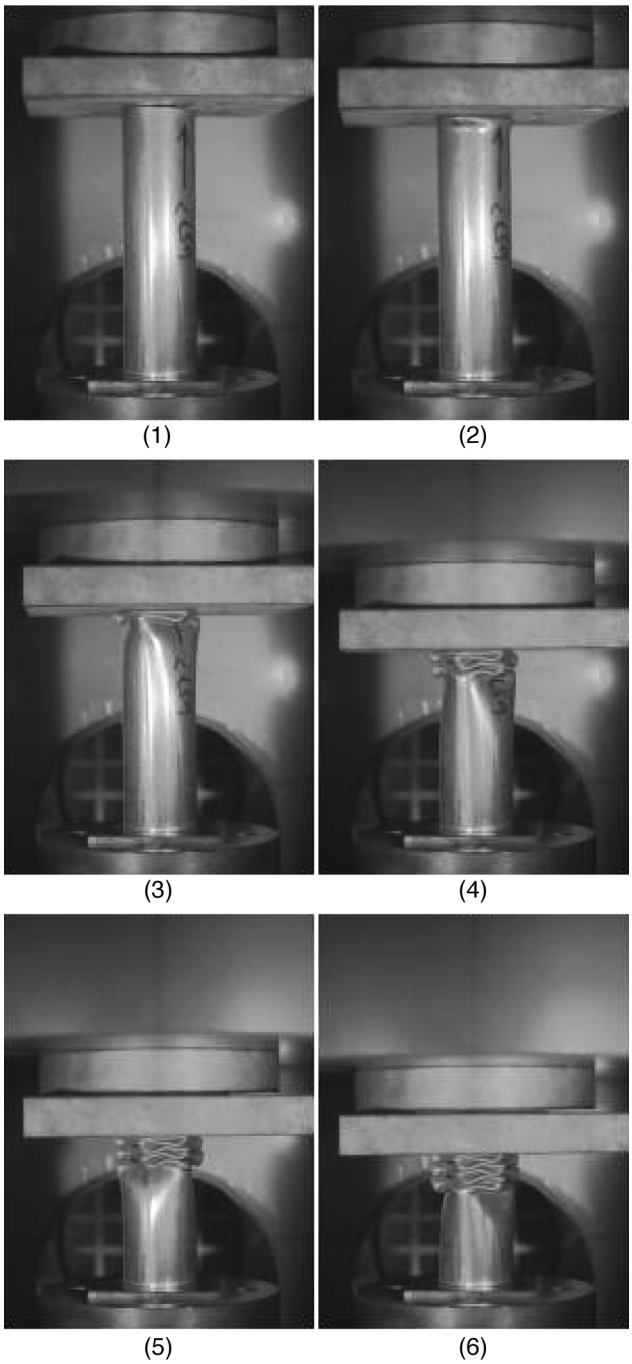

Figure 9. Crush sequence for 2-m/s loading velocity.

Conclusions

Two new experimental setups have been developed for characterization of crashworthiness of HSS. The experiments are

based on hydraulic-based testing systems. The systems provide unique tightly controlled testing environments for structural and material characterization. The experimental data are also used for validation and evaluation of modeling approaches, and for development of modeling guidelines for HSS materials and structures under impact loads.

Acknowledgments

The tubes for experiments were donated by the U.S. Steel Corporation. The support of Auto/Steel Partnership Strain Rate Characterization Team is acknowledged.

Future Work

The future work on the project will focus on four topics:

1. Conducting parallel-plate experiments for HSS under three loading speeds.
2. Conducting circular tube crush experiments in TMAC.
3. Measurement of strain and strain rate histories in parallel-plate and tube crush experiments.
4. Development of experimental setup for crushing of rectangular tubes in TMAC.

References

1. "Constitution and Properties of Steels," ed. F. B. Pickering, *Materials Science and Technology*, vol. **7**, VCH, New York, 1992.

2. N. Jones, *Structural Impact*, Cambridge University Press, 1989.

3. L. L. Tam and C. R. Calladine, "Inertia and strain-rate effects in a simple plate-structure under impact loading," *International Journal of Impact Engineering*, **11**(3), 349–377 (1991).

4. M. Avalle and G. Belingardi, "Experimental evaluation of the strain field history during plastic progressive folding of aluminum circular tubes," *International Journal of Mechanical Sciences*, **39**(5), 575–583 (1997).

5. J. Singer, T. Weller, and J. Arbocz, "Basic Concepts, Columns, Beams and Plates," *Volume 1, Buckling Experiments: Experimental Methods in Buckling of Thin-Walled Structures*, John Wiley & Son Ltd., 1998.

6. J. Singer, T. Weller, and J. Arbocz, *Buckling Experiments: Experimental Methods in Buckling of Thin-Walled Structures: Shells, Built-Up Structures and Additional Topics*, John Wiley & Son Ltd., 2002.

7. A. Copa, "Effect of end conditions on buckling of cylindrical shells under axial compression impact," in *Test Methods for Compression Members*, ASTM Tech. Pub. No. 419, pp. 115–136, 1966.

G. Advanced High-Strength Steel Tailor-Welded Blank Project

Project Manager: Jack Noel
Auto/Steel Partnership
2000 Town Center, Suite 320
Southfield, MI 48075-1123
(248) 945-4778; fax: (248) 356-8511; e-mail: jnoel@a-sp.org

Co-Chair: Aleksy Konieczny
U.S. Steel Group, a unit of USX Corp.
5850 New King Court, Troy, MI 48098-2692
(248) 267-2541; fax: (248) 267-2581; e-mail: akonieczny@uss.com

Co-Chair: Mariana Forrest
DaimlerChrysler Corporation
2730 Research Drive, Rochester Hills, MI 48309
(248) 838-5256; fax: (248) 838-5338; e-mail: mgf@daimlerchrysler.com

Technology Area Development Manager: Joseph A. Carpenter
(202) 586-1022; fax: (202) 586-1600; e-mail: joseph.carpenter@ee.doe.gov
Field Technical Manager: Philip S. Sklad
(865) 574-5069; fax: (865) 576-4963; e-mail: skladps@ornl.gov

---

Contractor: U.S. Automotive Materials Partnership
Contract No.: DE-FC05-02OR22910

Objective

- Investigate the manufacturability and formability of high-strength steel (HSS) and advanced high-strength steel (AHSS) tailor-welded blanks.
- Demonstrate that these products can be used to produce automotive components of significantly lower mass. The application of high-strength low-alloy (HSLA) steels and advanced high-strength steels (AHSS) offer the potential for further weight reduction. However, uncertainty exists regarding the weld processes for these products and the resultant ductility of the weld and heat-affected zone. Develop manufacturing techniques and validate to assure reliable, high-volume HSS and AHSS tailor-welded blanks.

Accomplishments

- Fatigue tested laser welds in AHSS tailor-welded blanks (see Figures 1–3). DP 600-MPa and DP 800-MPa material tests have been completed (see Table 1).
- Defined some product design and manufacturing process modifications for control of springback and side-wall curl on tailor-welded blank stampings of different strengths.
- Evaluated benefits of hybrid laser/arc welding processes for AHSS tailor-welded blanks.

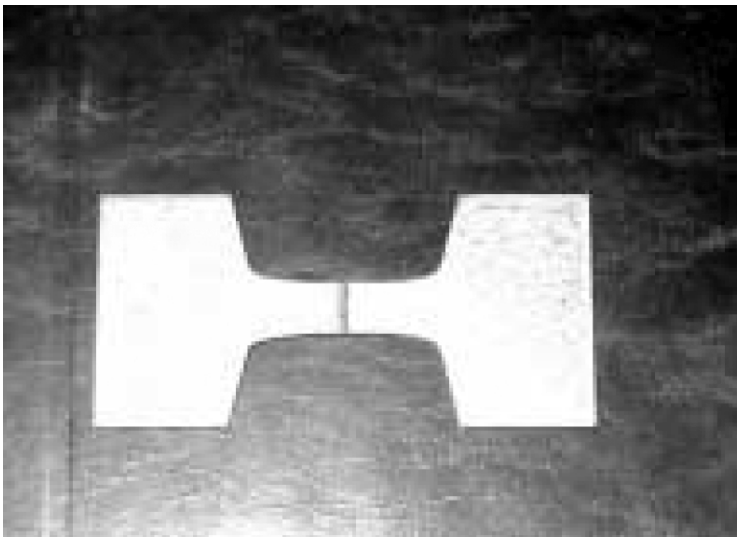

Figure 1. Tailor-welded blank fatigue test specimen.

Figure 2. Fatigue test specimen mounted in test machine grips with an antirotation guide.

Figure 3. A test specimen mounted in the MTS test machine with an antibuckling guide.

Table 1. Tailor-welded blank combinations for tension-compression fatigue tests

DQ 1.6 mm to DP 800 1.2 mm	T-C	Laser
DQ 1.6 mm to DP 600 1.2 mm	T-C	Laser
DP 800 1.6 mm to DP 800 1.2 mm	T-C	Laser
DP 600 1.5 mm to DP 600 1.2 mm	T-C	Laser
DP 600 1.5 mm to DP 800 1.2 mm	T-C	Laser
DP 800 1.6 mm to DP 600 1.2 mm	T-C	Laser
DP 800 1.6 mm to DP 800 1.2 mm	T-C	Laser
DP 600 1.2 mm to DP 600 1.2 mm	T-C	Laser
DP 600 1.2 mm to DP 600 1.2 mm	T-C	Mash

Future Direction

- Expand the fatigue testing for other HSS grades.
- Continue evaluation of hybrid laser processes as well as formability and fatigue testing of test specimens from these processes.
- Continue to work on the control of springback and other distortions resulting from residual stresses in tailor-welded blanks stampings made with materials of different tensile strengths.

Introduction

Tailor-welded blanks have gained acceptance in the automotive industry as a means of part integration or elimination, thereby simultaneously reducing tooling cost and weight. The application of HSLA steel and AHSS, such as dual-phase and TRIP steel, offer the potential for further weight reduction. Optimum weld processes for the high-strength tailored blanks and the resultant ductility of the weld and heat-affected zone must be validated to assure reliable, high-volume HSS and AHSS tailor-welded blanks.

The project group intends to demonstrate that AHSS tailor-welded blanks can be used to produce automotive structural components of significantly lower mass.

Progress Toward Meeting Deliverables

Fatigue testing planning was done in conjunction with the Sheet Steel Fatigue Project Group, the Joining Technology Group, and the Lightweight Front End Structures Project. As they defined the materials they would use for tailor-welded blanks in the motor compartment rails, the Tailor Welded Project Group has determined the required fatigue test procedures and has procured quotes for this work. Fatigue testing of Dual Phase 600- and 800-MPa laser-welded specimens has been completed. Specimens were tested for tension-compression fatigue at the University of Waterloo in Ontario, Canada. Reverse bending fatigue testing was done at the University of Illinois at Urbana-Champaign. Although results were favorable in both tests, further testing with a baseline 350-MPa HSS and other AHSS is necessary for good comparative fatigue test data. More of these specimens will be tested in the near future.

Hybrid laser/arc welded processes for possible improvement of the weld structure were evaluated at Fraunhofer USA in Plymouth, Michigan. Test specimens were produced to further evaluate fatigue, formability, and physical characteristics of this type of weld.

Springback control for tailor-welded blanks of different strength levels is being addressed by manufacturing process and product design modifications. The work to study the effect of these modifications on springback on tailor-welded blanks of different strength levels has been conducted at Ronart Industries in Detroit, Michigan. Recommended modifications have been provided to the automotive group members for future AHSS product design guidelines.

Project Status

The project is currently focused on improving the weld characteristics of AHSS tailor-welded blanks to assure reliable formability and fatigue properties. Laser-welded and hybrid/laser test specimens are being evaluated and the results documented by Fraunhofer USA for reference by automotive product and manufacturing engineers.

Future Work

In addition to planned fatigue testing and evaluation of alternate joining processes for tailor-welded blanks, the project group will keep product designers and manufacturing engineers in the automotive community appraised of innovative applications of this process at domestic as well as at foreign manufacturers.

H. Tribology

Project Manager: Pat V. Villano
Auto/Steel Partnership
2000 Town Center Drive, Suite #320
Southfield, Michigan 48075-1123
(248) 945-4780; fax: (248) 356-8511; e-mail: pvillano@a-sp.org

Project Chairman: Alan Pearson
General Motors Corporation
Metal Fabricating Division
1450 Stevenson Hwy., Mail Code 480-992-415, Troy, Michigan 48083
(248) 528-4706; fax: (248) 528-4764; e-mail: alan.pearson@gm.com

Technology Area Development Manager: Joseph Carpenter
(202) 586-1022; fax: (202) 586-1600; e-mail: joseph.carpenter@ee.doe.gov
Field Technical Manager: Philip S. Sklad
(865) 574-5069; fax: (865) 576-4963; e-mail: skladps@ornl.gov

---

Contractor: U.S. Automotive Materials Partnership
Contract No.: DE-FC05-02OR22910

Objectives

- Conduct stamping simulation tests to study the effects of tribological conditions on the stamping performance of Advanced High Strength Steels (AHSS). Stamping performance in this project is defined as minimizing die wear and maximizing dimensional stability. The understanding of the contribution of lubricants to errors in springback prediction when using finite-element analysis (FEA) will also improve dimensional performance.
- Include these ultimate benefits:
  - Improve test procedure to simulate springback and die wear.
  - Improve control of springback and die wear.
  - Optimize lubricant/die combinations for AHSS.
  - Maintain common lubricants between automotive companies and steel suppliers.
  - Conduct a study to examine wear rates of different die materials.

Approach

- Compare the die wear rate with various HSS and lubricants.
- Correlate other process indicators such as restraining force, temperature, and contact area to wear on the draw beads.
- Correlate the data with the friction test results from Phase 1.
- Build on the extended knowledge gained in Phase 1 and Phase 2. Phase 2 established a baseline of wear data from three sheet steel materials, and two lubricants, with one die material.

Accomplishments

- Completed Phase 1 report "Enhanced Stamping Performance of High Strength Steels with Tribology."
- Completed Phase 2 report "Effect of Stroke Length and Penetration on Die Wear."
- Used steel coils of galvanneal-coated AKDQ, HSLA340, and DP600 supplied by partnership companies. The material is used in the wear tests for Phase 3.
- Collected data for the eight test conditions.

Future Direction

- Develop wear rate model to predict die life.
- Gather wear test data to substantiate model.
- Correlate model with production data as AHSSs come into production.

Introduction

Historically, lubricants are used in forming sheet metal stamping to reduce friction, improve formability, minimize die wear, and provide corrosion protection. The projected increase in the use of AHSSs places a greater emphasis on understanding the process parameters associated with die wear such as heat buildup and die scoring and dimensional stability caused by springback variation. The contribution of interfacial friction to springback variation is not known. AHSSs may require different lubricant and/or die materials to minimize the friction and die wear.

In an attempt to reduce weight, automotive manufacturers are using thinner, higher strength steel panels. Several issues are associated with stamping parts from these steels. The springback of HSS panels results in reduced process capability and greater variations in the vehicle assembly. The higher strength of the steels means that dies will be subjected to higher contact pressure and greater wear. Wear in the draw beads will affect the restraining force and will result in greater variation as well as down time for repairs.

This project will examine how springback and die wear are affected by lubricant and die material with AHSSs. The test simulates the forming of several thousand parts. Changes in process conditions and physical wear on the die are evaluated.

Tribology tests are used to collect data and measure responses such as friction, or restraining force, temperature, contact area, springback, and wear. These responses are related to actual stamping practices, an important step in quantifying the problem and implementing possible solutions.

Background

Phase 1 of this study examined how springback and wear are affected by lubricant and die material with AHSSs. The results presented here outline the results of testing in Phase 1 of the study.

Tribology tests were used to collect data and measure responses such as friction (for restraining force), temperature, contact area, springback, and wear. These responses can be related to actual stamping practices, an important step in quantifying the problem and implementing possible solutions.

Some of the most significant findings included

- significant increase in springback and part temperature with HSSs,
- large difference in friction and wear with dry film lubricants, and

- significant effect on friction and wear from choice of sheet coating.

The broad scope of this study examines the effect of lubricants and die material on formability and die life with coated and AHSSs. In Phase 1, bench tests were used to compare friction and springback results with a broad range of lubricants, die materials, and sheet steels. The data from these tests provided limited information on die wear in production of metal stampings. Because die wear is difficult to measure without extended testing, a modified drawbead tester was developed and constructed and has shown to be effective in producing measurable die wear over thousands of strokes.

Phase 2 studied the effects of bead penetration and stroke length on die wear in the newly developed die wear test. The materials selected for phase 2 were originally intended to be AKDQ, HSLA, and DP600. However, availability of the latter two materials delayed the project to the point where it was decided to use the available material (AKDQ-45/45 galvanneal) as a baseline.

Six coils of material were run through the die wear test (DWT), using three bead penetrations and two stroke lengths. Because coil length was constant, the different stroke length meant that different numbers of strokes were run for each stroke length. The short stroke (50 mm) resulted in 16,000 strokes per coil, while the long stroke (100 mm) resulted in 8,000 strokes per coil. Wear was quantified by weight loss measurements. The large amount of material sliding over the die meant that even under the lowest wear condition weight loss was significant. The 60% and 80% penetration showed similar weight loss trends, that is, higher weight loss with the long stroke length and fewer strokes. Conversely, the 100% penetration showed more weight loss with the greater number of strokes and short stroke length.

These trends were attributed to contact phenomena, which are highly dependent on penetration. The lowest penetration had a single band of wear on the entry side of the bead. With 80% there were two bands of wear, entry and exit. And with the 100% penetration there was a continuous, less severe, band of wear from entry to exit. The concentrated wear with 60 and 80% penetration means that boundary contact is predominant and the lubricant is less effective with long sliding distances. The distributed contact with the 100% penetration allowed lubricant to become entrapped thereby providing protection on the longer strokes.

Continuously measured force and temperature data indicated that temperature and force increase linearly with penetration. It was also found that temperature increased with the number of strokes (after an initial, unexplained, decrease with 60% penetration).

Phase 1 findings show that temperature and pull force will become more important factors with HSLA and DP600 AHSSs. These materials will be studied in the next phase of die wear testing.

The Phase 2 results and analysis show that stroke length and penetration are powerful factors in die wear and must be carefully controlled in future experimentation. Because wear patterns are dependent on penetration, penetrations should be selected to model production practices rather than laboratory practices (DBS). Similarly stroke length in the future wear testing should be controlled to ensure that test parameters model production. In addition, Phase 2 could have an immediate impact on implementation of AHSS. Because bead wrap decreases with AHSS, the effect on die wear patterns and subsequent die wear may be the same as reducing penetration.

Die Wear Test Procedure

This test is a modification of the DBS using coil-fed continuous sheet strip (see Figure 1). The concept of pulling continuous strip through drawbeads to measure wear had been considered by Dr. John Schey and Greg Dalton as early as 1989. Their first DBS

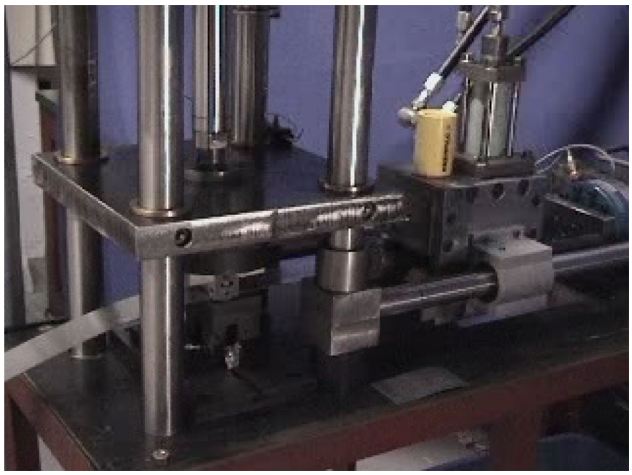

Figure 1. Die wear test.

design allowed for strip feed. This technique has been used at University of Darmstadt with some success. Die temperature and restraining force are measured throughout the test, while die wear is measured upon completion of the test.

Test Parameters

It is recommended that the following parameters be controlled (fixed or varied):

- Process: speed, lubricant type, lubricant amount, pull length, bead penetration;
- Die: surface finish, material, geometry, temperature; and
- Sheet: thickness, width, surface finish, and coating.

Analysis

The following outputs will be measured in the wear test:

- Restraining force,
- Contact area,
- Temperature,
- Bead wear, and
- Thinning.

Redundant Responses

This analysis includes redundant responses in all tests with the hope of identifying the most effective means (analytically and economically) of evaluating the tribological effect on die wear.

The temperature, change in bead geometry, and restraining force will be reported throughout the test from the male bead. The bead will be examined under optical and scanning electron microscopes to determine wear severity.

The data will be compiled and analyzed for cause and effect using statistical analysis. Where trends appear, statistical significance will be tested.

Experimental Methodology

Variable	Wear test
Sheet	AKDQ, HSLA, DP600
Coating	Galvanneal
Die	G3500, G3500—ion nitride, G3500—chromium nitride
Lubricant	Mill oil (1.2–1.6 g/m^2)
Total	8 tests

Test Matrix

Test	Surface treatment	Sheet
1	Flame hardened	AKDQ
2	Flame hardened*	HSLA
3	Chromium nitride	HSLA
4	Ion nitride	HSLA
5	Flame hardened	DP600
6	Chromium nitride	DP600
7	Ion nitride	DP600
8	Best performer	DP600

*Repeated.

Analysis of data will include statistical analysis of the appropriate test responses.

Test Methodology

TribSys, Inc., will conduct experiments to evaluate die wear on drawbeads under the following conditions:

1. A 2-in.-wide strip will be pulled through a set of three beads. The center bead will be used to evaluate wear.
2. Lubricant is mill applied, and weight is measured during testing.

3. For each condition, 500 m of strip will be pulled through the beads. Wear is evaluated by reduction in volume and temperature. Other measurables such as strip condition, vibration (noise), and forces may be included.
4. Results are analyzed using statistical analysis and subjective methods (scanning electron microscope/surface roughness). Analysis of wear will be presented in a report.

Deliverables

- Statistical analysis of data from experimental matrix: restraining force, temperature, contact area, and die wear.
- Tribological analysis of restraining force, temperature, contact area, die wear results with "hypotheses" on cause and effect.
- Ranking of die treatments from best to worst with respect to antiwear properties.
- Summary report in electronic format presented to the A/SP.

Results and Discussion

The type of wear differed with flame-hardened (FH) and chromium nitrided (CrN) displaying abrasive wear. With abrasive wear, die material is removed as the sheet slides over it under the forming pressure. Abrasive wear leads to die geometry changes that can affect part shape and process control. The CrN showed the least wear with little difference between the HSLA and DP600. The ion nitrided (IN) surface treatment showed signs of adhesive wear. With adhesive wear, the sheet adheres to the die and causes buildup of sheet material on the die surface. This buildup caused sheet surface damage and affected restraining force and part stability.

Die temperatures generally rose until steady state was reached (several hundred parts) after that point temperatures either rose or fell depending on die wear type. With abrasive wear temperatures rose, while with adhesive wear temperatures decreased. The CrN showed lower internal die temperatures and higher strip exit temperatures than the FH dies.

Springback as measured by the curl in the strip was greatest with the higher strength materials (Figure 2) and greatest with lower restraining force (Figure 3). Wear scars were most evident on the center bead at the entry and on the exit bead. Wear differences were visible with the naked eye (see Figure 4).

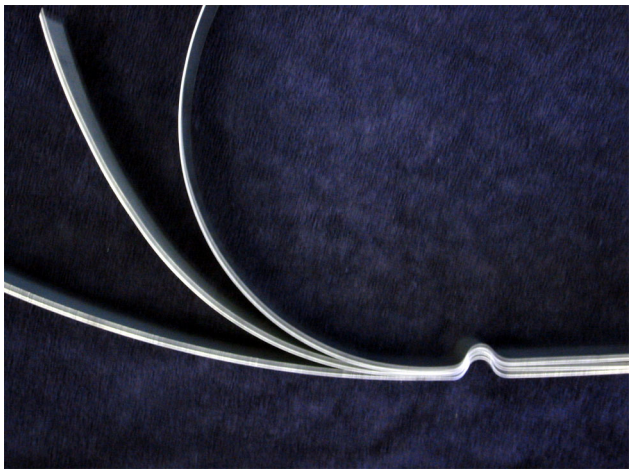

Figure 2. Strip curl of IF, HLSA, DP600 with FH dies.

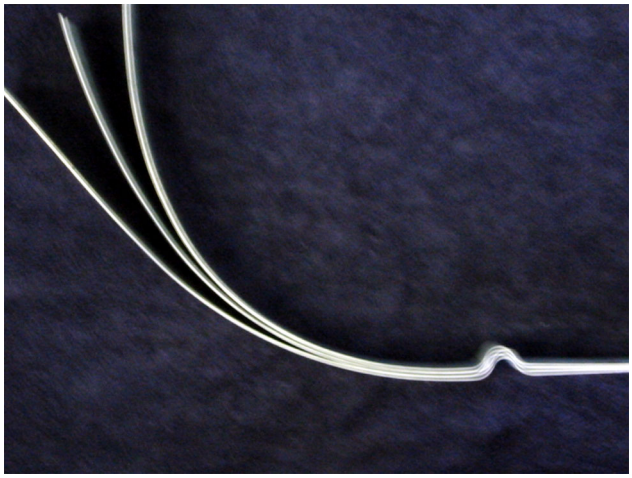

Figure 3. Strip curl with IN, FH, CrN—HSLA sheet.

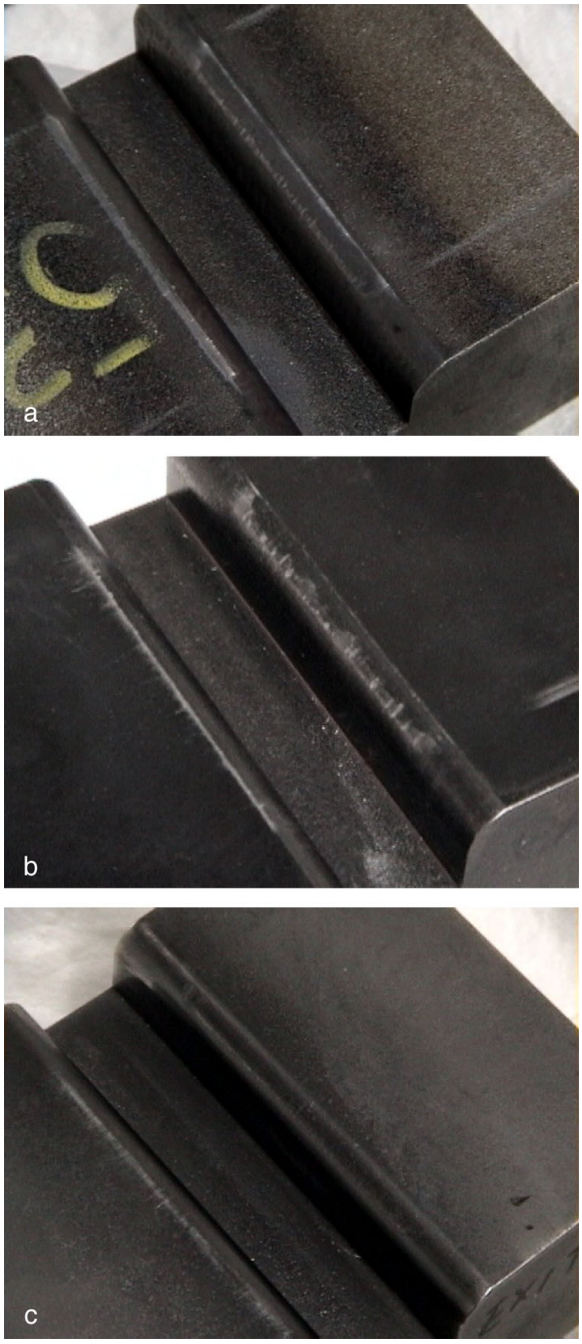

Figure 4. Die wear with (*a*) FH, (*b*) IN, (*c*) CN dies.

Conclusions

1. The die wear test was used to produce continuous die wear data in a coil-fed drawbead arrangement. Preliminary analysis of the data shows that wear type differs with surface treatment and that wear rate increases with increasing sheet strength.
2. As expected from theory and models, springback increases with increasing sheet strength and with reduced retraining force.
3. The CrN surface treatment resisted abrasive wear and showed no signs of adhesive wear with the galvanneal coating.
4. Die temperatures and strip exit temperatures were highly dependent on die surface treatment, die wear, and sheet type.

I. Lightweight Front Structures

Project Manager: Pat V. Villano
Auto/Steel Partnership
2000 Town Center Drive, Suite #320
Southfield, MI 48075-1123
(248) 945-4780; fax: (248) 356-8511; e-mail: pvillano@a-sp.org

Co-Chairman: John Catterall
General Motors Corporation
Body Systems Center
2000 Centerpoint Parkway, Mail Code 483-510-2F6 05F1-RED, Pontiac, MI 48341
(248) 753-3314; fax: (248) 753-3619; e-mail: john.1.catterall@gm.com

Co-Chairman: Jody Shaw
5850 New King Court, Troy, MI 48098-2608
(248) 267-2608: fax: (248) 267-2581; e-mail: jrshaw@uss.com

Technology Area Development Manager: Joseph Carpenter
(202) 586-1022; fax: (202) 586-1600; e-mail: joseph.carpenter@ee.doe.gov
Field Technical Manager: Philip S. Sklad
(865) 574-5069; fax: (865) 576-4963; e-mail: skladps@ornl.gov

---

Contractor: U.S. Automotive Materials Partnership
Contract No.: DE-FC05-95OR22910

Objectives

- Benchmark, develop, and document proven solutions that will balance the interaction of material, manufacturing, and performance. The initial phase of the study focused on the automotive front-end system solutions that address high-volume manufacturing and assembly. Example solutions will be manufactured and physical testing will be performed to evaluate the Advanced High Strength Steel (AHSS) designs.
- Use the AHSS solutions to provide choices and consequences that address real world challenges faced in the vehicle development process. A comprehensive knowledge-base design tool will be developed that capitalizes on a set of robust AHSS automotive design guidelines relating choices to consequences.

Approach

- Redesign an existing Front Rail System from a donor vehicle utilizing AHSS (DP800 and above) to save at least 20% mass.
- Manufacture and test the AHSS designed rail system to compare performance with the conventional design it replaces.
- Conduct analytical and physical testing on the original and newly redesigned rail system.
- Draw comparisons and document recommended practices.

Accomplishments

Phase 1 Deliverables

- Completed Phase 1 Engineering Report and posted it on the Auto/Steel Partnership (A/SP) Web site and made available on CD Rom.
- Ensure that related Hyper-view animated crash files are also available on CD ROM.
- Ensure that Windows version of Proteus (knowledge base tool) is available.
- Ensure that a complete "project roll-out" communications package is available.

Phase 2 Deliverables

- Complete preliminary subsystem design.
- Complete competitive benchmarking study.
- Complete rail concept development.
- Complete initial validation of NCAP and IIHS models.
- Complete enhanced crash model report.
- Completed Concept 1 Final Design—Modified baseline vehicle.
- Completed Concept 2 Final Design—Stamped Rail Design.
- Completed Concept 3 Final Design—Hydroform Rail Design.

Future Direction

- Select final design.
- Generate a "response surface."
- Obtain the final optimized design of rail and bumper.
- Generate CAD data for manufacturing of new rail and bumper designs.
- Develop soft tools for rail and bumper subassemblies.
- Assemble the donor vehicle with new rail and bumper subassemblies.
- Conduct NCAP crash testing of the donor vehicle with new rail and bumper subassemblies.
- Correlate the vehicle crash test data with analytical results.
- Update Proteus (knowledge base tool) with the findings of this project.
- Publish a final report detailing all the findings of this project.
- Develop a "project roll-out" communications package.

Phase 1 Results

In Phase 1 of the project, optimized designs were obtained for two different configurations of the original ultralight steel auto body (ULSAB) vehicle.

The baseline ULSAB vehicle consisted of a front end that could accommodate a 3.1-L V6 engine package and had 195/60 R15 wheels and tires. The baseline ULSAB vehicle

also consisted of the same front-end overhang as the original ULSAB vehicle.

The "Best" solution obtained from the knowledge base had the following features: Double 5-star NHTSA/Overall Good IIHS, 12-kg mass reduction compared to the original ULSAB, $69.00 cost reduction, Extensive use of DP800 and DP1000 steels, and mass of structure plus bumper plus cradle 223.3 kg vs 235.3 kg for original ULSAB.

The upgraded ULSAB vehicle consisted of a front end that could accommodate a 3.8-L V6 engine package and had 205/60 R16 wheels and tires. The upgraded ULSAB vehicle had 50 mm less front-end overhang than original ULSAB vehicle. The upgraded vehicle was also 180 kg heavier than original vehicle.

The "Best" solution obtained from the knowledge base had the following features: Double 5-star NHTSA/Overall Good-Acceptable IIHS, 16-kg mass increased compared to original ULSAB, $15.00 cost increase, Extensive use of DP800 and DP1000 steels, and mass of structure plus bumper plus cradle 251.3 kg vs 235.3 kg for original ULSAB.

Because of the increased vehicle weight and geometric compromises, the mass of the upgraded ULSAB vehicle was increased by 28 kg compared to the optimal solution from the baseline ULSAB vehicle. Furthermore, to achieve fully optimized lightweight vehicles, it will be necessary to address the packaging and geometry compromises as well as utilizing advanced materials.

When vehicles become lighter, power trains can become more compact because of lower power demands. Also, if bigger tires and wheels are desired, track width changes should be considered to reduce the impact to the main rails.

Phase 2 Results

The objective of this phase is to benchmark, develop, and document proven solutions that will balance the interaction of material, manufacturing, and performance. The initial phase of the study focused on the automotive front-end system solutions that address high-volume manufacturing and assembly.

The preliminary design of a subsystem was developed to simulate the NCAP performance of a full vehicle finite-element model, in the first 40 ms. The subsystem predicted accurately the full vehicle response in the first 40 ms of the NCAP load case and achieves a 50% reduction in the simulation time. The subsystem achieved the same crush pattern for rail and bumper, as in the full vehicle. The subsystem would assess various rail and bumper concepts in the Lightweight Front-End Structure Project.

A benchmarking study was undertaken to examine rail designs and architectures of competitive vehicles with good NCAP and IIHS performance. The knowledge from this study was very useful in designing AHSS rails for the donor vehicle in Phase II of the Lightweight Front-End Structure Project. A total of 14 competitive vehicles were benchmarked for rail design and architecture.

Various rail concepts were developed for the Phase II donor vehicle by employing AHSS materials. The concepts developed in this study would be further developed into concrete designs and be evaluated for performance, cost, and manufacturability. The most feasible design would be eventually prototyped, assembled into the donor vehicle, and tested for NCAP performance. Three concepts were developed during the course of this study:

Concept 1: Existing Rail Architecture

- Minimum modifications to the current rail design
- Providing design direction
- Filling holes and removing notches
- Reducing flange width
- Tailor-welding DP800T rails
- AHSS materials
- Gauge change

- New bumper: Bumper 3 design from Phase I study

Concept 2: Best Stamped Design

- Improved performance and mass savings
- Hexagonal rails
- Modification of rail curvatures in side view (XZ) and plan (XY) view
- Modification of rail extension
- Possibility of tying rails to rocker and cradle

Concept 3: Best Hydroformed Design

- Alternative to stamped design
- Integration of parts
- Hexagonal/octagonal rails
- Reduction of welding
- Mass reduction by elimination of flanges
- Superior material properties
- Improved crush

New Bumper Design

- Designed to contribute to high-speed crash events
- DP1000T 1.0 mm thick
- Two-piece stamped design
- Feasibility confirmed with bumper supplier
- Common in all the three designs

Regression analysis of the response surfaces obtained from the NCAP DOE Study of Concept 1 resulted in a design with 11 kg (28%) mass reduction and NCAP performance at par with that of the baseline. However, the IIHS performance of the design was inferior to the baseline. The intrusions could be reduced by increasing the gauges appropriately, but it will result in a mass penalty and would not meet the 20% mass reduction target.

A new straighter load path through the existing packaging envelope was developed. This load path would be used by concepts 2 and 3. Requirements to package an engine mount inside the left-hand rail would be eliminated in both the concepts.

A clearance requirement of 10 mm would be set for the worse-case component set. Tailor-welded DP800T rails would be utilized to eliminate reinforcements. Full system optimization would be undertaken to optimize for mass.

Both concepts show potential for the same mass savings of well above the 20% target. Deficiency in stamped design in IIHS was due to lack of development in the kick-down area. Modifications in the stamped design would lead to similar IIHS response as that of the Hydro-Formed concept. Figure 1 shows the three concepts.

Conclusion

One concept will be selected based on the selection criteria set by the project team. A decision will be forthcoming along with a plan and schedule to complete Phase 2 in FY 2004.

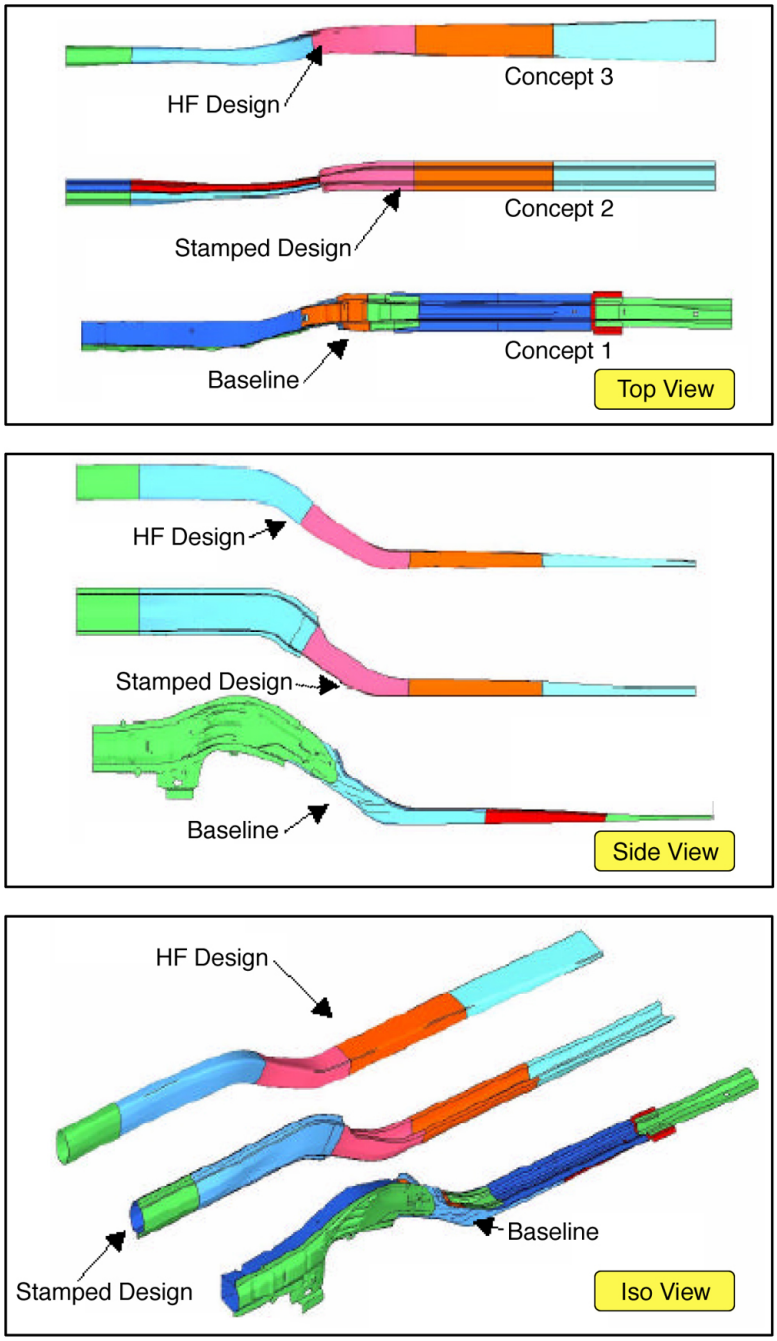

Figure 1. Rail designs: top, side, and isoview.

Appendix A. ACRONYMS AND ABBREVIATIONS

ADFG	advanced drive file generation
A/SP	Auto/Steel Partnership
ABP	acrylobenzophenone
ACC	Automotive Composites Consortium
AES	auger electron spectroscopy
AFS	American Foundry Society
AHSS	advanced high-strength steel
AKDQ	aluminum killed draw-quality
Al	aluminum
ALCOA	Aluminum Company of America
ALM	Automotive Lightweighting Materials
ALTC	Automotive and Light Truck Committee
AMD	Automotive Metals Division
AN	acrylonitrile
ANL	Argonne National Laboratory
APAW	aluminum plasma arc welding
APC	American Plastics Council
AS	adaptive simulation
ASTM	American Society for Testing and Materials
BCC	body-centered cubic
BCF	Bead Correction Factor
BH	Bake Hardening
BHF	blank holder force
BIW	body-in-white
CAD	computer-aided design
CAE	computer-aided engineering
CAFE	corporate average fuel economy
CGR	circle grid analysis
CD	compact disk
CFC	carbon-fiber composite
CHIP	CIP/sinter/HIP
CIP	cold isostatic pressing
CLM	cast light metals
COV	coefficient of variability
CP	cold pressed
CRADA	cooperative research and development agreement
CWRU	Case Western Reserve University
DAQ	data acquisition
DCB	double cantilever beam
DNS	double notch shear
DOE	U.S. Department of Energy
DOE	design of experiment
DP	dual phase

DPF	direct powder forging
DSC	dispersion strengthened copper
DQSK	drawing quality special-killed
E	experimental
EDS	energy-dispersive spectroscopy
EDX	energy dispersive x-ray
EFLC	enhanced forming limit curve
EDS	electron dispersive x-ray spectroscopy
EFLD	enhanced forming limit diagram
EGN	exfoliated graphite nanostructure
ELV	end-of-life vehicle
ENF	end-notch flexure
EMF	electromagnetic forming
FBL	feedback linearization
FCVT	FreedomCAR and Vehicle Technologies
FE	finite element
FEA	finite-element analysis
FEM	finite-element method
FLC	forming-limit curve
FLD	forming-limit diagram
FP2	Focal Project 2
FP3	Focal Project 3
FY	fiscal year
GASP	grazing angle surface polarimeter
GM	General Motors
HDG	hot dip galvanized
HDPE	high-density polyethylene
HIP	hot isostatic pressing
HSLA	high-strength low-alloy
HSS	high-strength steel
HTML	High Temperature Materials Laboratory
HVSC	Huron Valley Steel Corporation
ICS	Industrial Ceramic Solutions
IF	interstitial free
IFU	University of Stuttgart
IIW	International Institute of Welding
IR	infrared
IRDI	Industrial Research and Development Institute
ISRM	intermediate strain rate machine
ITP	International Titanium Powders, Inc.
ITP	Industrial Technologies Program
LANL	Los Alamos National Laboratory
LBNL	Lawrence Berkeley National Laboratory

LCCF	low-cost carbon fiber
LFI	long fiber injection
LIBS	laser-induced breakdown spectroscopy
LLDPE	linear low-density polyethylene
LLNL	Lawrence Livermore National Laboratory
MA	methylacrylate
MAP	microwave-assisted plasma
MIG	metal inert gas
MIT	Massachusetts Institute of Technology
MMB	mixed-mode bending
MMC	metal matrix composite
MMCC	metal matrix cast composites
MPCC	magnesium powertrain cast components
NAT	N. A. Technologies
NCC	National Composites Center
NCF	noncrimped fabric
NDE	nondestructive evaluation
NDT	nondestructive test
NWR	nuclear magnetic imaging
NRCAN	Natural Resources of Canada
NTRC	National Transportation Research Center
ODS	oxygen dispersion strengthened
OEM	original equipment manufacturer
OFC	oxygen-free copper
OPT	optimization
ORNL	Oak Ridge National Laboratory
P4	programmable powder preform process
P&S	press and sintering
PAN	polyacrylonitrile
PC	personal computer
PE	polyethylene
PID	proportional integral derivative
PM	powder metallurgy
PMC	polymer matrix composite
PMPRA	powder metallurgy particle-reinforced aluminum
PNNL	Pacific Northwest National Laboratory
PP	polypropylene
PPS	poly (phenylene sulfide)
PRA	particle-reinforced aluminum
PVB	polyvinyl butyral
PVC	polyvinyl chloride
R&D	research and development
RH	relative humidity
ROI	return on investment

ROM	read-only memory
RSW	resistance spot welding
RT	room temperature
RUC	representative unit cell
RVE	representative volume element
SA/RD	sales and administrative/research and development
SAE	Society of Automotive Engineers
SAMPE	Society for the Advancement of Material and Process Engineering
SCMD	structural cast magnesium development
SEA	specific energy absorption
SEM	scanning electron microscope
SHT	solution heat treatment
SIF	stress-intensity factor
SIMS	secondary-ion mass spectroscopy
SLS	single-lap shear
SMC	sheet molding compound
SNL	Sandia National Laboratories
SOM	solid-oxygen-conducting membrane
SPR	self-piercing rivet
SRIM	structural reaction injection molding
STL	sound transmission loss
TCM	technical cost model
TDM	Troy Design and Manufacturing
TEM	transmission electron spectroscopy
TGA	thermo-gravimetric
TMAC	Test Machine for Automotive Crashworthiness
TRIP	transformation-induced plasticity
TWB	tailor welded blank
ULSAB	ultralight steel auto body
UM	University of Michigan
USAMP	U.S. Automotive Materials Partnership
USCAR	U.S. Council for Automotive Research
UT	University of Tennessee
UTS	ultimate tensile strength
UV	ultraviolet
XPS	x-ray photoelectron spectroscopy
YSZ	yttria-stabilized zirconia